

PIC-SOL 209/5
August 1964



ARMY • NAVY • AIR FORCE • ARPA • AEC • NASA

PROCEEDINGS OF THE FOURTH PHOTOVOLTAIC SPECIALISTS CONFERENCE

VOLUME I

**RADIATION EFFECTS ON SOLAR CELLS AND
PHOTOVOLTAIC DEVICES**

2 June 1964

Held at the NASA-Lewis Research Center
Cleveland, Ohio

FOREWORD

Maintaining an interest in the photovoltaic area, the Interagency Advanced Power Group (IAPG) has published for the second year the proceedings of the Photovoltaic Specialist's Conference. The content of these proceedings - a vital link in the information exchange activities of the IAPG - is of particular concern to the members of the Solar Working Group.

This year's conference, the fourth, was co-sponsored by the IEEE, AIAA, and the NASA-Lewis Research Center. Facilities for meetings and other arrangements were the responsibility of NASA-Lewis Research Center.

Presentations are included in the order in which delivered at the conference and have been prepared from papers submitted to the Power Information Center (PIC) through the IEEE. Where papers have been authored by more than one person, cover sheets bear the name of the person who actually gave the presentation.

Transcriptions of the discussion periods following each presentation and the panel on Thin Film Solar Cells were prepared and edited by Dr. Potter of NASA-Lewis Research Center and his staff. Mr. Robert Hamilton, of IDA, prepared the panel discussion on Sunlight Simulators. These efforts are gratefully acknowledged and noted as a significant contribution to the proceedings.

Inclusion of a paper in these proceedings in no way precludes later publication in professional society journals.

PROCEEDINGS OF THE FOURTH PHOTOVOLTAIC SPECIALISTS CONFERENCE

Date: 2-3 June 1964

Place: NASA-Lewis Research Center
21000 Brookpark Road
Cleveland, Ohio

Attendance

The following represents, to the best of our knowledge at the time of publication, a list of those who attended one or both days conference sessions:

IAPG Members Present:

Brancato, E. L.	NRL
Hamilton, Robert C.	IDA-Observer
Lubarsky, Bernard	NASA-Lewis
Scott, Walter C.	NASA-Hq.
Smith, Arvin A.	JPL
Swain, James R.	NASA-Ames
Wise, Joseph	USAF-APL
Zoutendyk, John A.	JPL

Government:

Bernatowicz, Daniel	NASA-Lewis
Blue, James	NASA-Lewis
Brandhorst, Henry	NASA-Lewis
Broder, Jacob	NASA-Lewis
Campbell, Francis J.	NRL
Canal, Albert P.	NRL
Cherry, William R.	NASA-Goddard
Corcoran, Charles	NASA-Lewis
Corrigan, Francis R.	NASA-Lewis
Cunningham, Brian T.	NASA-Goddard
Dallas, Tom	NASA-Lewis
Dawson, John R.	NASA-Langley
Duncan, Charles	NASA-Goddard

Evans, John C.	NASA-Lewis
Ewashinka, John	NASA-Lewis
Fang, Paul	NASA-Goddard
Fessler, Ted	NASA-Lewis
Geiger, Felix	NASA-Goddard
Haynes, G.	NASA-Goddard
Hess, W.	NASA-Goddard
Johnston, Phillip A.	NASA-Ames
Kaminski, Gerald	NASA-Lewis
Lambert, Robert J.	NRL
Mandelkorn, Joseph	NASA-Lewis
Massie, Lowell D.	USAF-APL
Moeckel, Wolf F.	NASA-Lewis
Plauche, F. M.	NASA-Houston
Potter, Andrew E.	NASA-Lewis
Reetz, Arthur	NASA-Hq.
Ritchie, Donald W.	JPL
Schach, Milton	NASA-Goddard
Schalla, Rose	NASA-Lewis
Schwartz, Larry	NASA-Lewis
Silverman, Jerry	USAF-Hanscom Field
Smith, Al	NASA-Lewis
Spakowski, Adolph	NASA-Lewis
Statler, R. L.	NRL
Thaller, Larry	NASA-Lewis
Ulman, Robert P.	NASA-Lewis
Waddel, R. C.	NASA-Goddard
Yasui, Robert K.	JPL

Nongovernment:

Adams, Frank	Bendix Research Labs.
Addis, R. R., Jr.	RCA Labs.
Allen, Walter	Johns Hopkins Univ.
Augustine, Frank	Clevite Corp.
Babcock, Richard	Westinghouse Res. Labs.
Bachner, R. L	Solar Systems, Inc.
Bachwansky, P.	EOS
Baker, J. K.	General Electric
Bean, Kenneth E.	Texas Instruments, Inc.
Belt, Roger	Harshaw Chemical Corp.
Beltz, Robert B.	IT & T Corp.
Blake, A. H.	Dow Corning Co.
Blumer, J.W.	Libby-Owens Ford Glass Co.
Boer, Karl	General Instrument Corp.
Bourke, R. C.	Allison Div. - GMC
Bucci, Nick	Westinghouse

Cain, O.	Dow Corning Corp.
Cavanaugh, L.	Pratt & Whitney
Chamberlin, R. R.	National Cash Register
Chidester, L.G.	Lockheed M & S Co.
Cole, R. L.	Texas Instruments, Inc.
Colehower, E. W.	Martin Co.
Currin, C. T.	Dow Corning Co.
Cusano, D. A.	General Electric
Denney, Joseph	TRW-Space Technology Labs.
Deshotels, W. J.	Clevite Corp.
Dickie, D.	Harshaw Chemical Corp.
Downing, R. G.	TRW-Space Technology Labs.
Dunkerly, W. C.	Hughes Aircraft
Epstein, Arnold	Monsanto Co.
Fischell, Robert E.	Johns Hopkins University
Gault, J.	International Rectifier
Goldstein, Bernard	RCA Labs.
Gordon, G. D.	RCA Labs.
Gorton, H. C.	Battelle Memorial Institute
Gummel, Herman	BTL
Hadley, C.P.	RCA Labs. - Mountaintop
Hangen, N.R.	RCA Labs. - Mountaintop
Harmon, Henry D.	RCA Labs. - Princeton
Harvey, D. J.	Harshaw Chemical Corp.
Hicks, John M.	Westinghouse
Hietanen, J. R.	Clevite Corp.
Hill, E.	Harshaw Chemical Corp.
Holloway, H.	Philco Corp.
Holmes-Siedle, A. G.	RCA Astro
Hui, William L. C.	RCA Astro
Julius, R. F.	Aero Geo Astro Corp.
Kaufman, Wm.	General Instrument Corp.
Kaye, S.	EOS
King, W. J.	Ion Physics Corp.
Klischies, G.	International Rectifier
Krause, A. J.	Westinghouse
Kuzminski, H. W.	RCA L'bs. - Mountaintop
Larin, Frank	Bendix Research Labs.
Lee, A. C.	TRW-Space Technology Labs.
Lodi, E. A.	Lockheed M&S Co.
Loferski, J. J.	Brown University
Luft, Werner	TRW-Space Technology Labs.
Maher, Michael	Aero Geo Astro Corp.
Menetrey, W. R.	EOS
Mihm, F. J.	Heliotek
Miller, E.	Grumman Aircraft Engineering Corp.
Miluschewa, Sima	RCA-Princeton

Ming-Duo Tang	Westinghouse
Mir Vilayet Ali	Fairchild
Ogle, T. C., Jr.	Libby-Owens Ford Glass Co.
Oman, Henry	Boeing Co.
Pastel, C. A. J.	Bureau D'Analyse et DeRecherche Appliquees
Pearson, Gerald L.	Stanford University
Peden, J. C.	General Electric
Pelto, Wm. V.	IT & T Corp.
Perkins, David M.	RCA Labs. - Princeton
Perlman, S. S.	RCA Labs. - Princeton
Prince, M. B.	EOS
Ralph, E. L.	Heliotek
Rappaport, Paul	RCA Labs. - Princeton
Reynard, D. C.	Lockheed M&S Co.
Richards, J. L.	Philco
Rosen, J. M.	Texas Instruments, Inc.
Ross, Bernd	Hoffman Electronics
Rosenzweig, W.	BTL
Rubin, Irwin	International Rectifier Corp.
Rupprecht, George	Tyco Labs.
Santopietro, Richard	Brown University
Schwartzburg, M.	Republic Aviation
Sheng, W. T.	Aerospace Corp.
Shirland, Fred	Clevite Corp.
Skarman, T. S.	National Cash Register
Smith, K. D.	BTL
Stevenson, R. D.	Douglas Aircraft Co., Inc.
Stone, Louis E.	Eagle-Picher Research Co.
Stonebraker, E. A.	Westinghouse
Stroup, R. F.	Texas Instruments, Inc.
Taylor, E.	TRW
Tarneja, K. S.	Westinghouse
Van Lint, V.	General Atomics
Vineyard, Raymond	Texas Instruments, Inc.
Weiner, Paul	RCA-Astro
Werth, J. J.	General Motors Corp.
Wolf, Guenther	Tyco Labs.
Wolf, Martin	Heliotek
Wysocki, J.	RCA Labs. - Princeton
Zehner, D.	Westinghouse

IAPG Secretariat:

Ashleigh, Robert F.	Secretary, Solar Working Group IAPG
Williams, F. Karl	Asst. Secretary, Solar Working Group IAPG

VOLUME I

TABLE OF CONTENTS

PART A. RADIATION EFFECTS ON SOLAR CELLS

Radiation Damage to Solar Cells on Relay I and II R. C. Waddel, NASA-Goddard Space Flight Center	A-1
The Effects of Low-Energy Electron Irradiation on the Surface Properties of Silicon Solar Cells R. F. Santopietro, Brown University	A-2
Low-Energy Proton Bombardment of Silicon Cells J. J. Wysocki, RCA Laboratories	A-3
Results of Low-Energy Proton Irradiations of Solar Cells E. A. Lodi, Lockheed Missiles and Space Co.	A-4
The Energy Dependence of Electron Damage in Silicon R. G. Downing, TRW-Space Technology Laboratories	A-5
Effects of Impurities on Radiation Damage of Silicon Solar Cells Joseph Mandelkorn, NASA-Lewis Research Center	A-6
The Electrical Characteristics of Irradiated Silicon Solar Cells as a Function of Temperature B. T. Cunningham, NASA-Goddard Space Flight Center	A-7
Radiation Resistance of Webbed Dendritic Solar Cells R. V. Babcock, Westinghouse Electric Co.	A-8
Effects of Shielding on Electron Damage to Solar Cells F. J. Campbell, Naval Research Laboratory	A-9
High-Energy Radiation and Solar Cell Shields G. A. Haynes, NASA-Langley Research Center	A-10

PIC-SOL 209/5

PART B. PHOTOVOLTAIC DEVICES

- Current Status of Drift Field Solar Cells B-1
P. H. Fang, NASA-Goddard Space Flight Center
- Solar Cells Produced by Ion Implantation Doping B-2
W. J. King, Ion Physics Corporation
- Photovoltaic Effect and Surface States on Silicon - B-3
Metal Interfaces
G. Rupprecht, Tyco Laboratories, Inc.
- Single Crystal Gallium Phosphide Solar Cells B-4
A. S. Epstein, Monsanto Co.
- Effect of Thickness on Short Circuit Current B-5
Martin Wolf, Heliotek
- Solar Cell Performance at High Temperatures B-6
Jacob Broder, NASA-Lewis Research Center
- Effect of Antireflection Coatings and Coverglasses on B-7
Silicon Solar Cell Performance
E. L. Ralph, Heliotek
- Design of Optically Reflective Electrodes for Germanium Cells B-8
John Werth, General Motors Corporation

PIC-SOL 209/5
Section A-1

N6L-29153

RADIATION DAMAGE TO SOLAR CELLS ON RELAY I
AND RELAY II

Presented by

Ramond C. Waddel

NASA Goddard Space Flight Center

Greenbelt, Maryland 20771

RADIATION DAMAGE TO SOLAR CELLS ON RELAY I
AND RELAY II

Ramond C. Waddel
Goddard Space Flight Center
Greenbelt, Maryland

Introduction

Solar cell radiation damage experiments on spacecraft can provide empirical information on the relative merits of various solar cells bearing shields of different thicknesses. They also are useful in testing our ability to predict solar cell damage in orbit. [This paper reports on the results of solar cell radiation damage experiments on board Relay I and Relay II, both of which are active at this writing, and indicates the degree of agreement between predictions of radiation damage, based on laboratory damage studies and flux data, and that observed in the spacecraft experiments.]

Orbits

Some orbit parameters of Relay I and Relay II are given in Table I. Note that perigees and apogees bracket the "inner belt" of trapped particles centered at about 3000 Km. The higher perigee of Relay II would be expected to make this orbit somewhat more damaging than that of Relay I. The results here reported are characteristic of these orbits, but certain generalities may be inferred.

Solar Cells

The solar cells are listed in Table 2, together with the nature and thickness of shields. The "REV, Si" cells on Relay I were designed to make them very radiation damage sensitive, the front surface being about one diffusion length thick. Shrinking of this length with damage would then leave large numbers of photon produced carriers at a distance from the junction greater than the diffusion length, with consequent rapid drop in cell output. The conventional silicon cells were of about 1 ohm-cm base resistivity. They were selected for uniformity of spectral response and efficiency and are believed to be representative of good commercially available products. The gallium arsenide cells are of interest because, on theoretical grounds at least, this material is potentially more efficient and has a greater radiation damage resistance than silicon. The gallium arsenide cells used in these experiments were actually less efficient than the silicon P/N and N/P cells.

All cells were mounted on an aluminum panel whose dimensions were about 4.0 by 5.3 by 0.125 inches. Each cell was loaded to approximate short circuit conditions by a resistor selected to give an initial voltage of about 165 millivolts in space sunlight. The maximum output of each cell, during spin, was computer corrected to normal illumination, 25°C, and mean earth-sun distance. These corrected voltages were normalized with respect to initial undamaged values and averaged. From 12 to 18 observations of a given cell type and shield were used in determining each data point.

Results, Relay I

The results from the first 387 days of observations of the Relay I radiation damage experiments are shown in Figure 1. Solar cell damage in laboratory studies using a constant intensity and energy beam of particles shows degradation, in these log-linear coordinates, as an initial horizontal section bending into a section having approximately constant negative slope. The responses of the shielded cells in Figure 1 show these general characteristics. The responses of the unshielded cells fall in a step-wise fashion during the first few orbits as the spacecraft passed through a fairly well defined region in which highly damaging particles were trapped. This region was at about 30° south latitude at an altitude of 6,100 Km.

The N/P, 0 cells (N on P silicon cells with 0 mils of shield) and the GaAs, 0 cells degraded similarly to about the 50% point, after which the latter cells fell rapidly. It has been pointed out that when cells degrade below about the 50% level the internal resistance rises so much because of majority carrier depletion that currents drawn, even by a zero resistance load, are not truly "short circuit" currents.

The N/P, 0 cells show rapid degradation at about 40 days and 130 days, for reasons unknown. The shielded cells all show plateaus from about 65 to 90 days in orbit, followed by a decline at about 17% per decade of time.

It is obvious that the order of merit for the shielded cells, under the given test conditions, is N/P, 60; N/P, 30; P/N, 60; and P/N, 30. When judged at the 75% level the N/P, 60 cells last about 10 times longer than P/N, 60 cells. Also the N/P, 60 cells last about 2.4 times longer than the N/P, 30 cells. At a degradation rate of 17% per decade of time the useful lifetime of 30 mil shielded silicon N/P cells may be increased by a factor of 2.4 by (a) doubling the shield thickness, or (b) increasing the number of N/P, 30 cells by about 7%.

Figure 2 shows the responses of the "REversed" cells on Relay I. All of these cells show initial increases in response followed by a maximum and eventual fall. The time of maximum increases with the shielded thickness.

These results were unexpected, and, as yet, unexplained. It is suggested that a drift field was built up under the action of trapped particles. This drift field may initially have increased the collection efficiency (initially low) before a damage mechanism dominated and caused the observed final decline in response. This type of cell thus did not provide the high damage sensitivity that was intended. In the Relay II experiment they were replaced by GaAs cells, as Table 2 indicated.

Results, Relay II

Figure 3 shows results of the Relay II radiation damage experiment for the first 72 days in orbit. Note the similarity to Relay I results of Figure 1. The step-wise damage of the unshielded cells and the cross-over of the P/N, 0 and GaAs, 0 responses are common to both experiments. The maximum for the N/P, 0 cells in Figure 3 at about 10 days is undoubtedly real, being exhibited by all 3 cells of this type. It may be noted in Figure 1 that a maximum for these Relay I N/P, 0 cells may also have actually occurred at about 10 days, but was not evident because of lack of data between one and 13 days (because of spacecraft malfunction). Annealing or drift field mechanisms may have caused the maxima.

Figure 4 shows results for the Relay II shielded cells. It is striking that the 3 mil shielded GaAs cells (GaAs, 3) appear nearly as damage resistant as the much more heavily shielded cells of this type, or of silicon. This indicates that the principal damaging agent for unshielded cells was either protons of energy less than about 3 Mev or electrons of energy less than about 0.1 Mev. However, it is known that 0.1 Mev electrons cause practically no damage to solar cells, so low energy protons must here be the principal damaging agent.

Because of the small amount of damage that is shown in Figure 4, the only generality to be drawn with certainty concerning order of merit is that, of the six types shown, the P/N, 60 cells are inferior. The shielded GaAs cells appear to be as good as, or better than, the N/P, 60 cells.

Selected numerical results from the Relay I and Relay II radiation damage experiments are shown in Table 3. Underlined values are for Relay II. It is evident that the Relay II orbit is considerably more damaging than that of Relay I. Also, extrapolations like that which indicates that it would take 18,000 days (50 years) for N/P, 60 cells to degrade to the 50% level must be viewed with caution.

The numerical results of the Relay I and Relay II radiation damage experiments, discussed above, are of interest to designers of solar cell power supplies. Certainly a design involving a type of cell here reported on, and for an orbit similar to that of Relay (or Telstar) which counts on solar cell lifetimes much different than those here reported should be viewed with suspicion.

Predictions, Unshielded Cells

A second use for the data here reported is to attempt to predict them from other considerations. Only when such observations can be predicted with satisfactory accuracy can the design of solar cell power supplies be considered to be on a sound engineering basis.

Figure 5 shows (as heavy data points) the early behavior of the P/N, O cells on Relay I, together with the results of a detailed prediction.

Preliminary work indicated that the only possibility of accounting for the very rapid degradation of bare cells was to ascribe it to low energy protons. Both silicon and gallium arsenide cells show a proton damage susceptibility which rises rapidly at low energies. Leo Davis, of Goddard Space Flight Center, has made measurements of the distribution of this type of particle and (in a private communication) provided the writer with a detailed prediction of the cumulative low energy proton flux encountered by Relay I during the first 11 hours of orbit. Under certain assumptions, this flux was converted to equivalent 4.6 Mev protons. The damage data of Cherry and Slifer (NASA TN D-2098) using protons of this energy and solar cells similar to those flown in orbit, was then combined with the orbital proton flux to predict cell response as a function of time. This prediction is shown in Figure 5 as the curve with uncertainty bars. It is seen that fair agreement is obtained, with predicted response being somewhat higher than that observed. The predicted and observed times of occurrence of the first and second damage steps are not in disagreement. These steps occurred as the spacecraft passed through the south latitude extension of the low energy proton distribution, whose main part is above Relay apogee.

Figure 6 shows predicted and observed results for the N/P, O cells on Relay I. The agreement is again fair, with predicted responses somewhat lower than observed.

Predictions, Shielded Cells

Since unshielded cells are so damage sensitive, the above exercise with such cells is instructive, but academic. Prediction of the behavior of shielded cells is of immediate engineering interest.

The 30 and 60 mil shields used on Relay I silicon cells exclude the low energy protons which evidently damaged the unshielded cells. Damage by protons and electrons of higher energy was thus considered. Information on such particles has been accumulated in the form of the GSFC P1 proton grid and the GSFC E8 electron grid in a fashion suitable for computer use.

The Relay I spacecraft was "flown" by computer through each of these two grids for five, two day intervals. The cumulative fluxes were tabulated by 1 $\frac{1}{4}$ second steps. These proton and electron fluxes were averaged, modified under certain assumptions concerning particle spectra, damage susceptibility as a function of particle energy, angle, and shielding and used to calculate the response of the P/N, 60 and N/P, 60 cells after 300 days in orbit. Cherry and Slifer damage rates were again used. The results are shown in Table 4.

It is evident that the predicted responses under proton or electron damage are somewhat less than those observed. A solar cell power supply designed under such conditions would be unnecessarily "over-designed" from a radiation damage standpoint.

Future Work

Anyone attempting to make predictions of orbital damage will find a need for (1) up-to-date computer grids of proton and electron distributions in space and energy, (2) more laboratory studies of solar cell damage as a function of cell type, particle type and energy (particularly low energy protons) with complete V/I curves evaluated under a space-sunlight simulator, and (3) some method, of either empirical or theoretical origin, for taking into account the modifications that a shield imposes on particle energy and angular distribution. Further, (4) improved orbital damage experiments should be conducted with solar cells, in which promising cell types, shields, and adhesives should be explored and in which full V/I cell characteristics are measured as the cells degrade. Finally, (5) a continuing effort must be made to improve our understanding of the solid state physics of the radiation damage process in semiconductors.

Conclusions

Among the conclusions which may be drawn from the data of the Relay I and Relay II solar cell radiation damage experiments are:

- (a) The results from the Relay I and Relay II damage experiments, where comparable, are similar.
- (b) Unshielded silicon (1 ohm-cm) and gallium arsenide solar cells degrade to the 75% initial short circuit current response level in less than one day. The order is silicon P/N, gallium arsenide, and silicon N/P.
- (c) Shields equivalent to 3 mils of Corning 0211 glass, or greater, extend time to 75% initial response by at least a factor of 100, compared to unshielded cells.

(d) From Relay I results the times in orbit for N/P (60 mil. 7940 shield), N/P (30), P/N (60) and P/N (30) solar cells to degrade to the 75% initial response level are 480, 197, 47, and 32 days, respectively.

(e) Heavily shielded N/P silicon cells last about 10 times as long as similarly shielded P/N cells.

(f) Silicon N/P cells with 60 mil silica shields last about 2.4 times as long as similar cells with 30 mil shields.

(g) The degradation rate of the heavily shielded silicon cells is about 17% per decade of time, in the severe damage region.

(h) Tentative results from Relay II indicate that gallium arsenide cells with 3 and 12 mil glass shields are about as damage resistant as the silicon N/P cells with 60 mil silica shields, judged at the 90% response level. Gallium arsenide cells with 30 and 60 mil silica shields appear considerably more damage resistant than silicon N/P cells with 60 mil shields.

(i) Predicted damage to the unshielded silicon cells on Relay I agreed fairly well, in amount and time, with observed damage. The damage was evidently caused by protons whose energies were a few Mev.

(j) For the 60 mil shielded silicon N/P and P/N cells the damage predicted by considering the available information on trapped electrons and protons, together with laboratory determined damage curves, was considerably greater, for both electrons and protons, than that observed.

(k) The supposedly damage susceptible "reversed" cells did not behave as expected.

(l) The more conventional solar cells showed several interesting anomalies, including a maximum in the response curve for the N/P, 0 cells around 50% response, at 10 days in orbit.

Acknowledgements

I acknowledge the assistance of a number of colleagues, including L. Slifer for damage panel procurement and testing, J. Albus for the solar aspect sensor, J. Schaffert for circuitry, J. Bourne for data processing, and D. Brown for liaison with the Communications group.

TABLE I
ORBIT PARAMETERS

Parameter	Relay I	Relay II
Apogee (Km)	7439	7414
Perigee (Km)	1321	2088
Inclination (Deg)	47.5	46.3
Period (Min)	185.1	194
Zero Time, GMT	1962 Yr, 348 Day, 00 Hr, 00 Min, 00 Sec.	1964 Yr, 21 Day, 21 Hr, 42 Min, 00 Sec.

TABLE II
RELAY RADIATION DAMAGE SOLAR CELLS

Cell Type	Shield Mils, (C.R.t.No.)	No.of Cells on Relay I	No.of Cells on Relay II
P/N, Si	0	3	3
P/N, Si	30, (7940)	3	3
P/N, Si	60, (7940)	3	3
N/P, Si	0	3	3
N/P, Si	30, (7940)	3	3
N/P, Si	60, (7940)	3	3
REV, Si	0	3	0
REV, Si	30, (7940)	3	0
REV, Si	60, (7940)	3	0
Ga As	0	3	2
Ga As	3, (0211)	0	2
Ga As	12, (0211)	0	4
Ga As	30, (7940)	0	2
Ga As	60, (7940)	0	2

TABLE III

TIMES IN ORBIT AT WHICH VARIOUS SOLAR CELLS
FELL TO GIVEN PERCENT INITIAL VALUES

Output (%)	P/N, 0 (Days)	P/N, 30 (Days)	P/N, 60 (Days)	N/P, 0 (Days)	N/P, 30 (Days)	N/P, 60 (Days)	Ga As, 0 (Days)
90	(0.033) <u>0.044</u>	(3.2) <u>2.5</u>	(5.7) <u>5.0</u>	0.14 <u>0.16</u>	34 <u>16</u>	50 <u>30</u>	(0.06) <u>0.044</u>
75	(0.044) <u>0.062</u>	32 <u>25</u>	47 <u>50</u>	0.33 <u>0.39</u>	197 x	(480) x	0.25 <u>0.18</u>
60	0.17 <u>0.18</u>	128 <u>(150)</u>	300 <u>(360)</u>	1.6 <u>1.2</u>	(1800) x	(4000) x	0.66 <u>0.34</u>
50	(0.28) <u>0.30</u>	(470) x	(1200) x	17 <u>4.5</u>	(7200) x	(18000) x	1 <u>0.49</u>

() = Estimated.

n.nn = Relay II, others Relay I

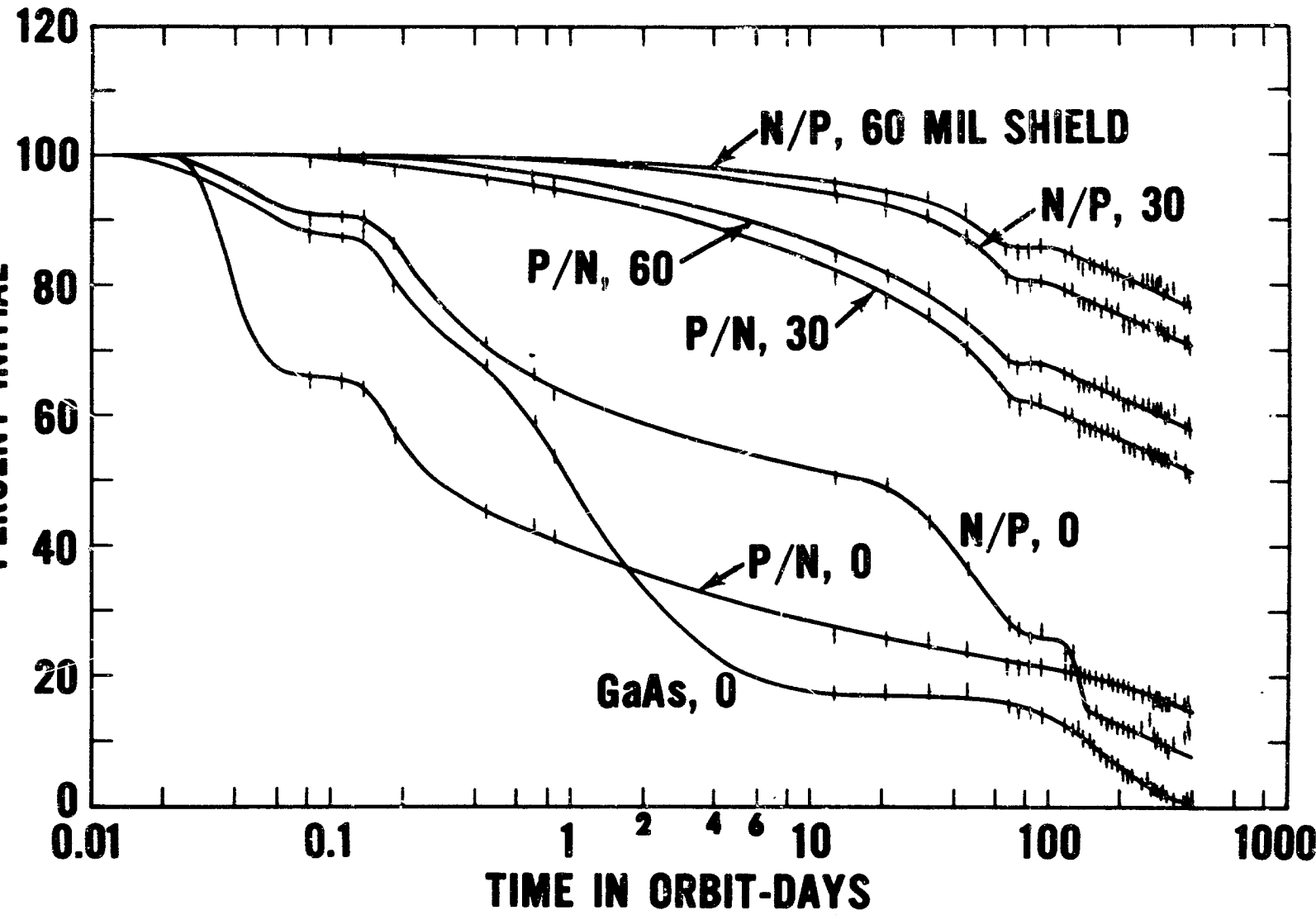
TABLE IV

PREDICTED AND OBSERVED SOLAR CELL RADIATION
DAMAGE AFTER 300 DAYS IN ORBIT, RELAY I

Cell Type	Shield Mils, (Cat.No.)	Radiation Info. Source	Predicted Response (%)	Observed Response (%)
P/N, Si	60, (7940)	GSFC P1 Proton Grid	56	60
N/P, Si	60, (7940)	GSFC P1 Proton Grid	75	79
P/N, Si	60, (7940)	GSFC E8 Electron Grid	47	60
N/P, Si	60, (7940)	GSFC E8 Electron Grid	75	79

RELAY I RADIATION DAMAGE EXPERIMENT

TT-T-V
CORRECTED SHORT CIRCUIT CURRENT
PERCENT INITIAL



PIC-SOL 209/5

Figure 1 - Relative short circuit current vs. time for the silicon and gallium arsenide cells on Relay I.

RELAY I SOLAR CELL DAMAGE

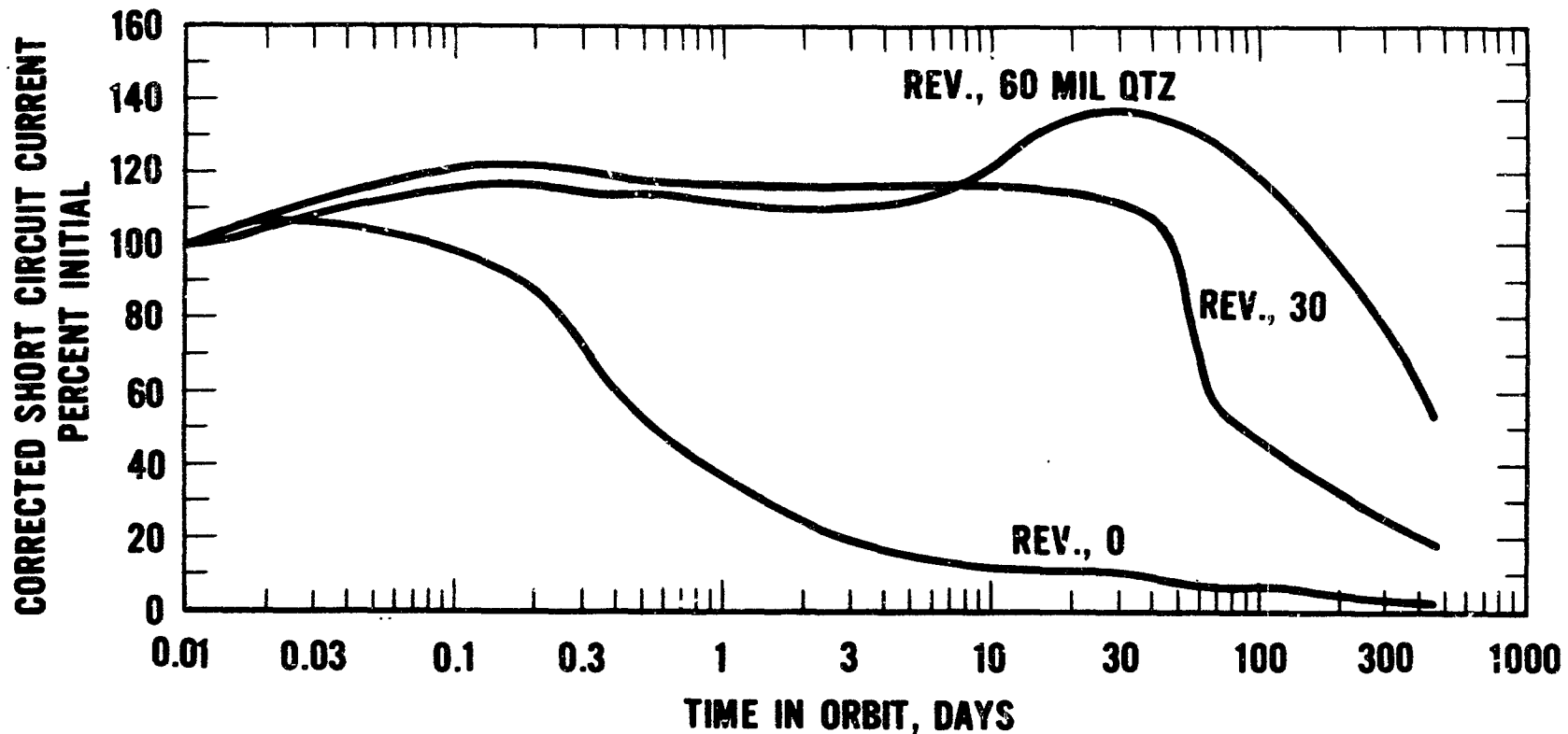


Figure 2 - Relative short circuit current vs. time for the special "reversed" cells on Relay I.

RELAY II RADIATION DAMAGE EXPERIMENT

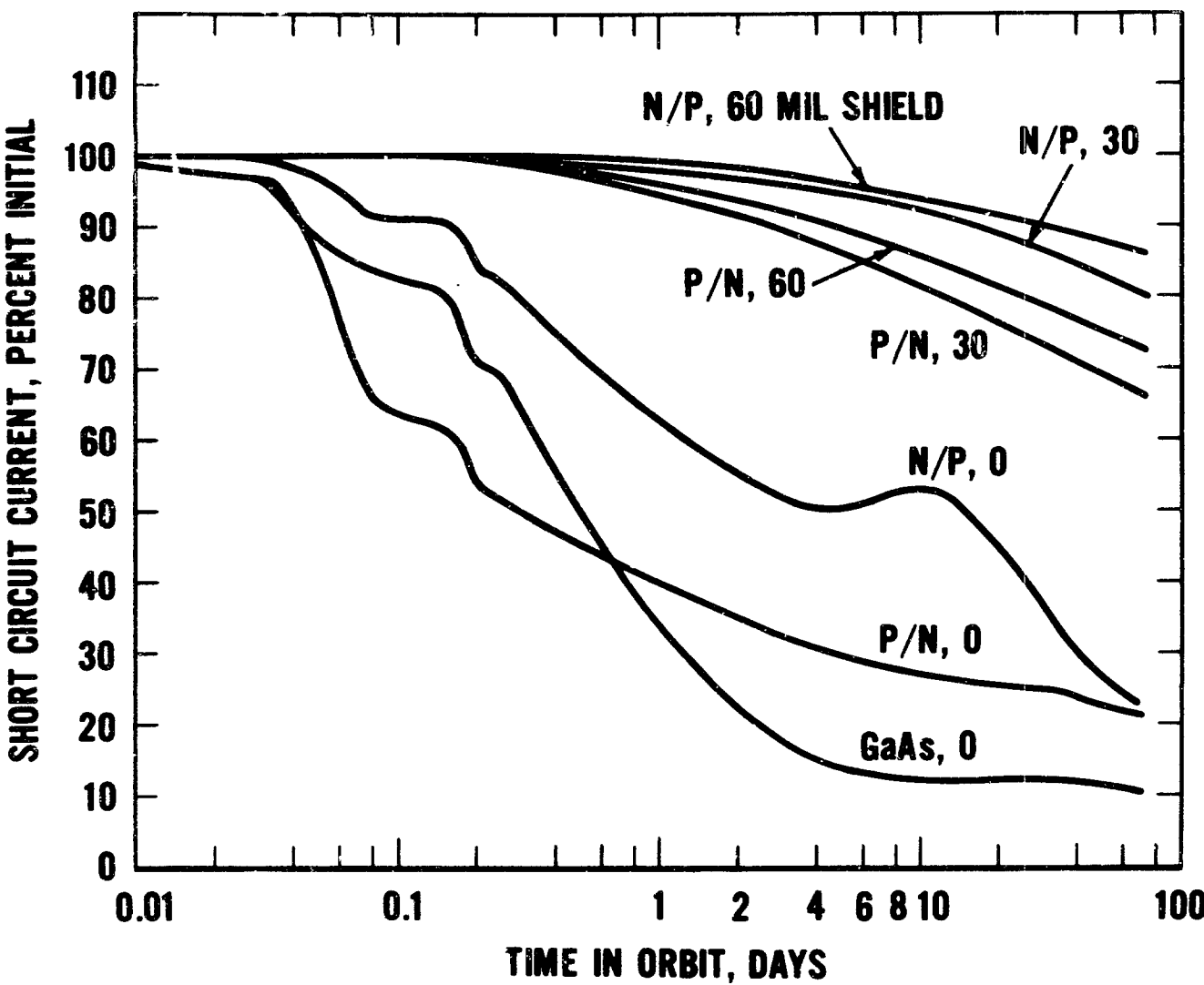


Figure 3 - Relative short circuit current vs. time for certain cells on Relay II.

RELAY II RADIATION DAMAGE EXPERIMENT

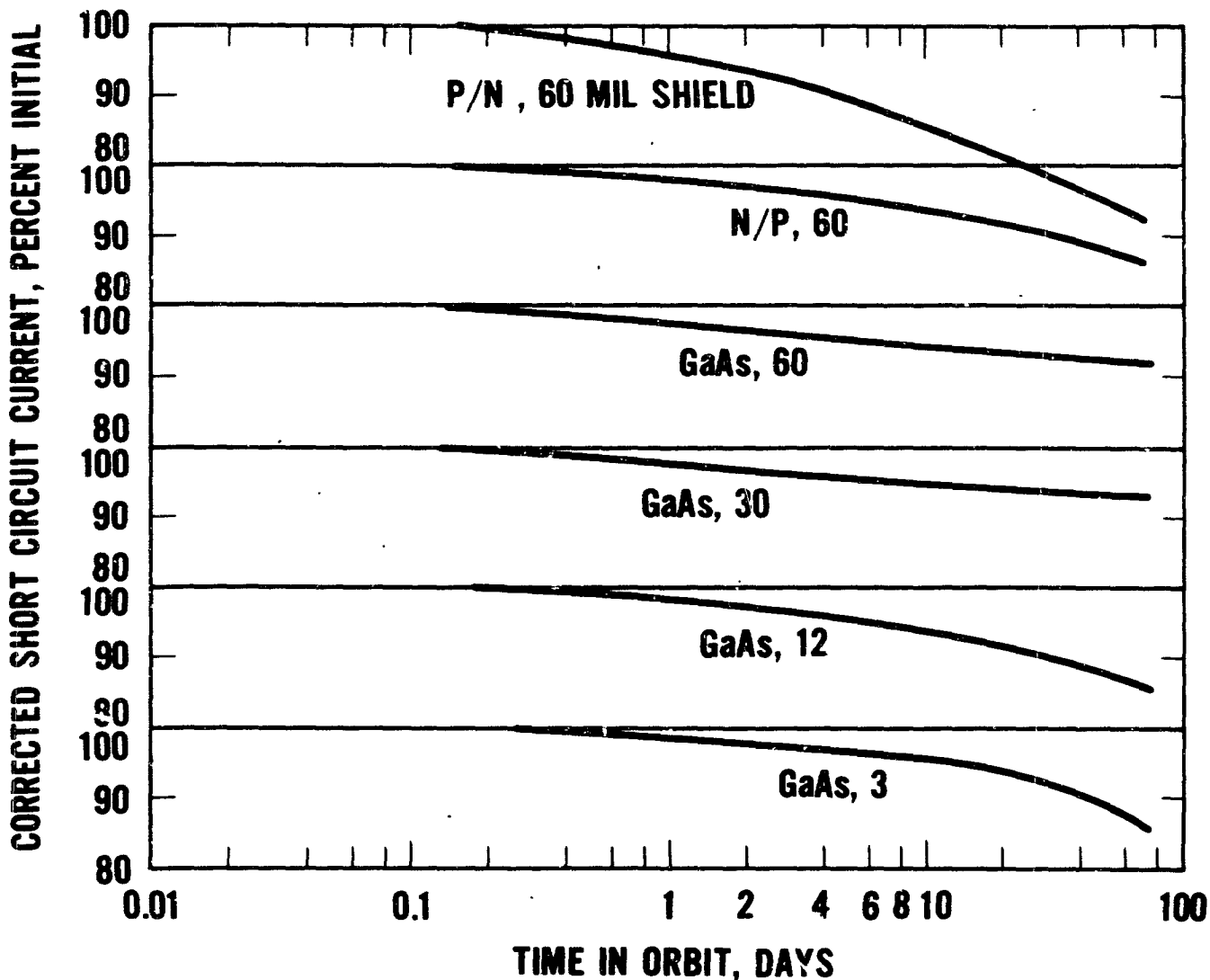


Figure 4 - Relative short circuit current vs. time for certain shielded cells on Relay II.

RELAY I RADIATION DAMAGE EXPERIMENT

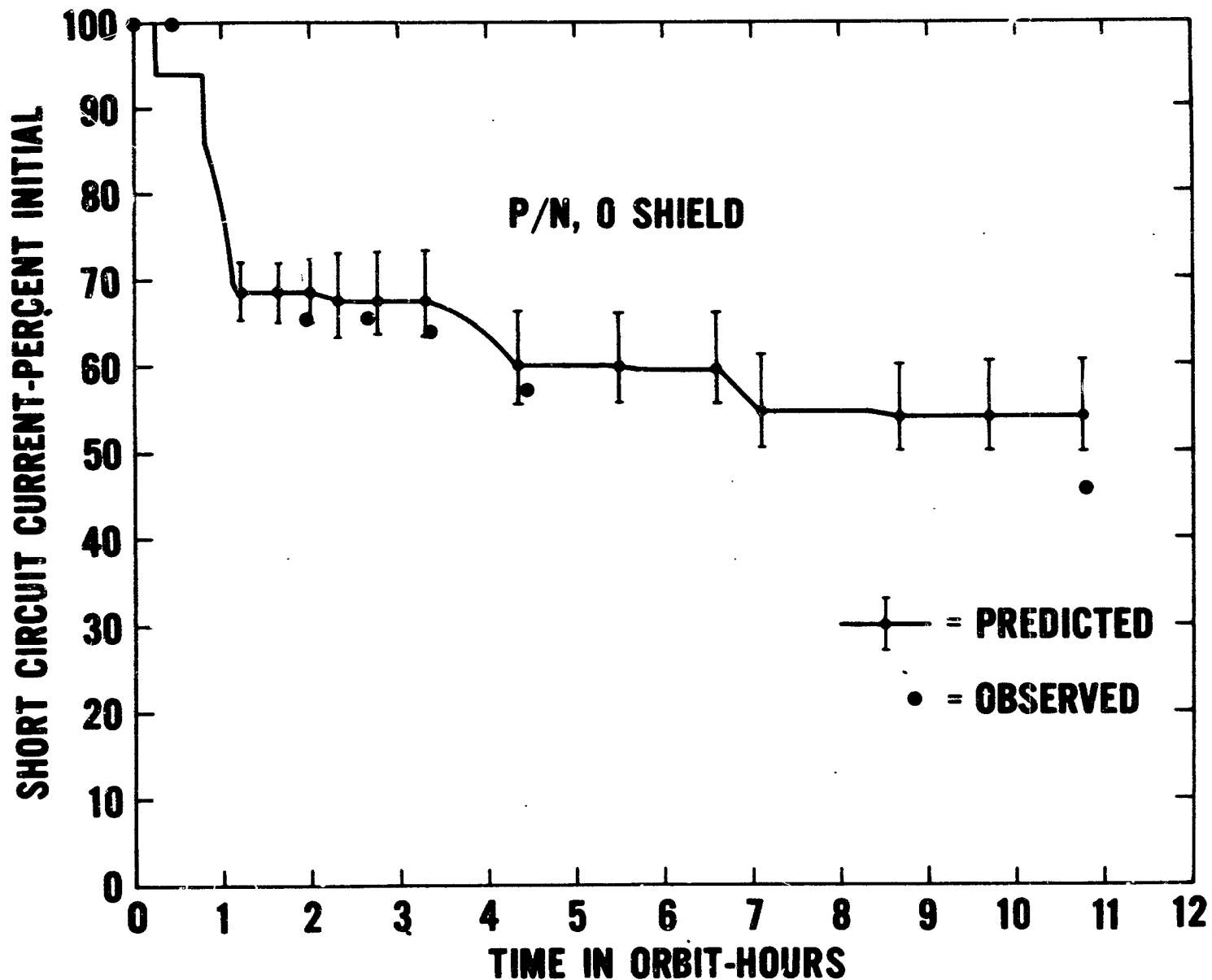


Figure 5 - Comparison of predicted and observed damage to P/N solar cells on Relay I.

RELAY I RADIATION DAMAGE EXPERIMENT

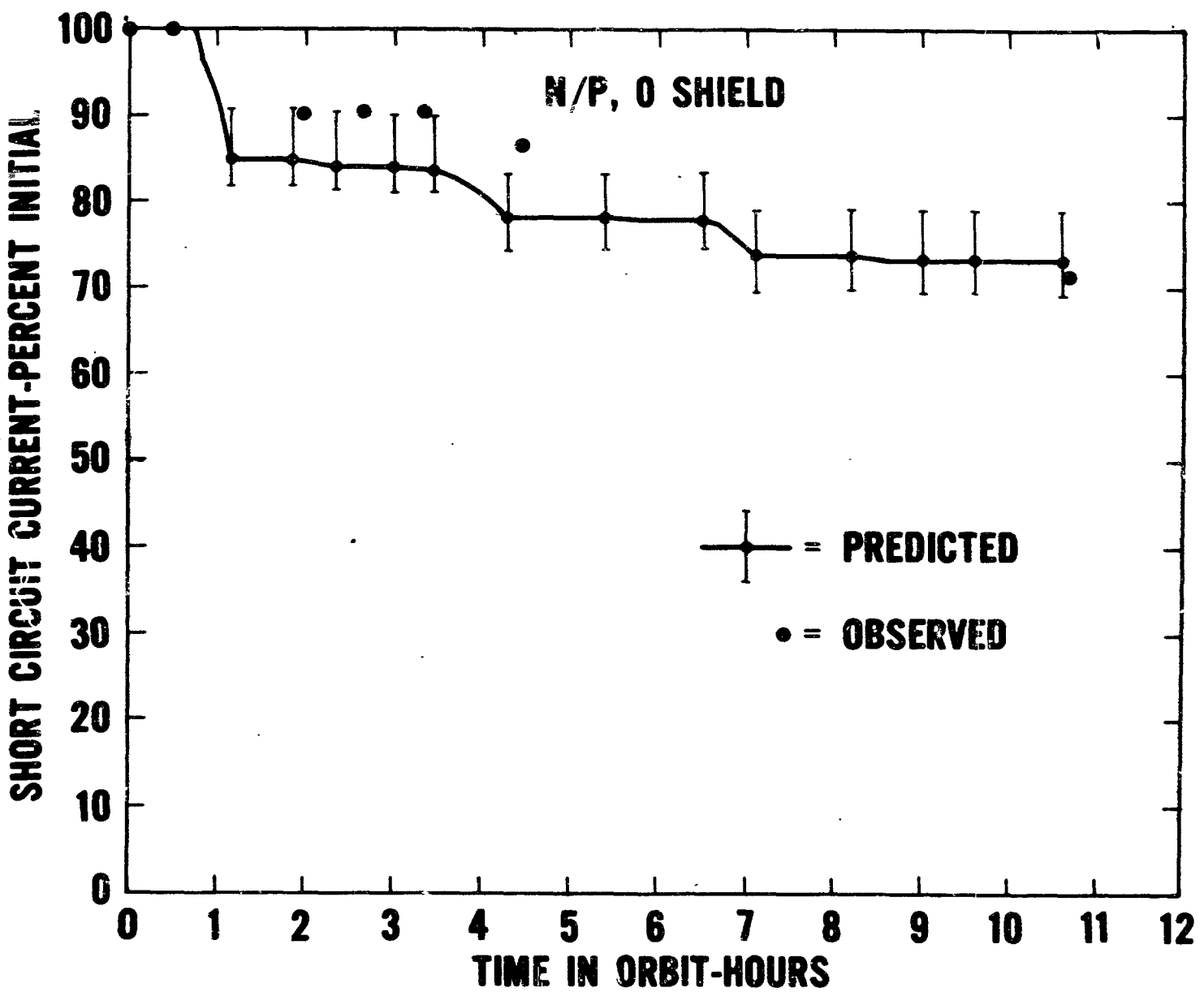


FIGURE 6. Comparison of predicted and observed damage to N/P solar cells on Relay I

DISCUSSION

LOFERSKI - BROWN UNIVERSITY: What was the arrangement on the so-called reversed silicon cells?

DR. WADDEL: I am embarrassed to say that I have forgotten this. Does Dr. Wolf from Heliotek recall this? (In the discussion which followed, it appeared that the front, or thick layer of the cell was n-type.)

ROSS - HOFFMAN ELECTRONICS CORPORATION: I have two questions. First, what were the results of your lifetime experiments? Did you find a one-to-one correlation to your degradation as recorded on power? And, second, what was the basis for your prediction?

DR. WADDEL: I believe you refer to the experiment in which the minority carrier lifetime of the diodes was monitored. We cut some of these diodes open. They were standard Texas Instrument LN649 diodes. We found that they were inherently shielded by about 20 mils of glass. The carrier lifetime curves for these diodes, when normalized so that they could be put on the same sort of scale that the normalized solar cells were, oscillated in the region of the 30 mil shielded p-on-n silicon solar cell. The effect was certainly in the expected direction. The carrier lifetime definitely and grossly shrunk with time; secondly, the degree of the effect lay between that for the unshielded and a 60 mil shielded silicon solar cell.

Now, I will answer the second part of your question concerning the basis for my prediction. We will consider the prediction for the heavily shielded solar cells, which are of greatest interest. The computation group flew, in effect, the spacecraft for five 2-day intervals through the Relay I orbit, and evaluated the cumulative flux of protons of energy greater than 30 Mev and the cumulative flux of electrons of energy greater than 0.2 Mev. From these figures I could calculate an average electron and proton flux. Concerning protons, I extended the 30 Mev cutoff point down to $16\frac{1}{2}$ Mev which is the nominal cutoff point for protons in a 60 mil shield, by the use of a relation by McElwain which concerns the shape of the spectra. This gave me a new number for the proton flux. I then inserted factors; the factor of a half for infinite rear shielding, a factor of one-third for obliquity, and an important factor extending the consideration of $16\frac{1}{2}$ Mev protons to 4.6 Mev protons using the inverse energy damage curve. This finally gave the predicted proton flux down to 4.6 Mev protons, a certain number of them in 300 days. We then used damage relations obtained by Mr. Cherry and Mr. Slifer to predict the damage. I don't think I can go through all the rest of it. I must say that these tests are not exact, and as some of you have observed, if I had done much worse on the prediction, I would have been considered incompetent and if I had done a lot better I would have been considered a scoundrel.

WEINER - RCA: What was the base resistivity of the cells you used?

DR. WADDEL: They were 1 ohm centimeter cells.

N64-29154

THE EFFECTS OF LOW ENERGY ELECTRON IRRADIATION ON THE
SURFACE PROPERTIES OF SILICON SOLAR CELLS*

Presented by

R. F. Santopietro

Division of Engineering

Brown University

Providence, R. I. 02912

2 June 1964

*Research reported herein is supported by Harry Diamond Laboratory under DA-49-186-AMC-12(X).

ABSTRACT

Both p/n and n/p silicon solar cells were irradiated by electrons whose energy was below the threshold for bulk radiation damage. The photovoltaic effect produced by strongly absorbed (0.365μ) and penetrating (1.02μ) light was measured during the course of irradiation. It was found that the surface recombination velocity of the n-type surface decreased while that of the p-type surface increased with increasing flux. It was also found that as the pressure of the ambient decreased, the surface recombination velocity experienced appreciable changes. The experimentally observed changes were used to predict changes in the output of a solar cell which could be attributed to radiation-produced surface effects.

Ans

THE EFFECTS OF LOW ENERGY ELECTRON IRRADIATION ON THE
SURFACE PROPERTIES OF SILICON SOLAR CELLS*

R. F. Santopietro and J. J. Loferski
Division of Engineering
Brown University
Providence, R.I.
(02912)

INTRODUCTION

When a semiconductor surface is subjected to irradiation by high energy particles, its structure can experience changes which will be reflected in changes in the electrical properties of the surface. The structural changes can be of various forms. For example, the radiation can dislodge either host lattice or impurity atoms (like those deposited by an etchant) from the surface. It can change the ionization state of atoms adsorbed on the surface. It can ionize atoms of the ambient gas in which the surface is immersed and thereby increase or decrease the probability of adsorption of ambient gas atoms on the surface. These changes in surface composition can change the conductivity of the surface layer even to the extent of changing conductivity type. They can change the work function of the surface as well as the lifetime of minority carriers at the surface, i.e. they can cause changes in the surface recombination velocity s .

Consequently, those parameters of a solar cell which are functions of s will also change. These include the short circuit current and the reverse saturation current of the junction.

Such changes in photovoltaic cell parameters are always observed during the course of studies of the effects of radiation on the bulk properties of cells. Since the surface changes usually saturate after the elapse of some irradiation time, the usual procedure is to ignore the initial changes and to attribute them to "surface" changes. The purpose of this investigation is to examine the changes in silicon photovoltaic cell properties which can be attributed to irradiation of the surface.

EXPERIMENTAL PROCEDURE

The optical absorption constant of silicon rises rapidly as the energy of the photons is increased above the energy gap (1.1eV at 300°K). Thus, the absorption constant is about 10^2 cm^{-1} for $\lambda = 1.03\mu$ and $2 \times 10^5 \text{ cm}^{-1}$ for $\lambda = 0.365\mu$. Consequently, the response of a silicon photovoltaic cell to 0.365μ light will be a strong function of the surface recombination velocity.¹ On the other hand, only a small fraction of the hole-electron pairs produced by 1.03μ light are produced in sufficient proximity to the surface to be affected by s . This difference in sensitivity to s was the basis of the experimental technique used in this investigation.

Figure 1 shows the experimental arrangement. Electrons from a Van de Graaff accelerator enter the irradiation chamber through a 0.001" aluminum window which serves to diffuse the beam and to separate the vacuum of the Van de Graaff from the ambient in the irradiation chamber. The electron beam energy is initially 140 KeV (which is below the threshold for bulk damage of 165 KeV), but after passing through the window the average energy decreases by about 15 KeV and of course the beam is no longer monoenergetic.

The photovoltaic solar cells (either Heliotek p/n or RCA n/p cells) were mounted on a water cooled copper block. The cells, which had a solar energy conversion efficiency of about 10%, had no anti-reflection coatings or cover glass. Prior to insertion in the irradiation chamber, the cells were first washed in boiling acetone, then in de-ionized double distilled water and dried.

A system of mirrors and shutters made it possible to direct light of either of two wavelengths onto the sample as shown in the drawing. The 0.365μ light was produced by combining a low pressure Hg arc and a Type 18A Wratten filter. The 1.03μ light was produced by an incandescent light combined with an interference filter. Spectral purity of these two sources was checked by passing the light through a Perkin Elmer monochromator.

The intensity of the two wavelengths was adjusted so that the open circuit voltage V_{oc} was low enough to keep the i-V characteristic in the linear region. The i-V characteristic was measured with a Kintel dc meter whose output was compared to that of a Leeds and Northrup Type K3 potentiometer. Figure 2 shows a typical i-V characteristic; its intercept with the current axis yields I_s while its slope is equal to $(\lambda I_o)^{-1}$.

The effect of irradiation was determined by recording an initial i-V characteristic with each of the two wavelength sources, exposing the sample to a predetermined electron flux and then repeating the measurement of the i-V characteristic. The characteristic was recorded rapidly enough so that recovery was negligible during the measurement.

The electron beam current received by the sample was determined by direct measurement of the current incident on the electrically insulated sample.

EXPERIMENTAL RESULTS

a) Effect of ambient pressure only.

Figure 3 shows V_{oc} as a function of time for a p/n cell exposed to 0.365μ light in a forepump vacuum. Similar behavior was observed when the cell was illuminated by 1.03μ light in a diffusion pump vacuum (about 10^{-5} mm Hg). This decrease in V_{oc} was traced to an increase in the reverse saturation current I_o , which in turn means that s increased. Since solar cells mounted on satellites must operate in the ultrahigh vacuum of outer space, their spectral response and power output probably experiences some change. Note that Figure 3 shows V_{oc} for a low illumination level. When the incident light corresponds to solar intensity, the changes in V_{oc} will of course not be as great as those observed in this experiment because V_{oc} is a logarithmic function of I/I_o at high light levels.

b) Irradiation of p/n cells.

Figure 4 shows relative changes in V_{oc} vs. integrated flux for both wavelengths of light for a sample placed in a diffusion pump vacuum (about 10^{-5} mm Hg). These data were collected only after the vacuum induced changes described above had reached saturation. The initial electron beam energy was 140 KeV. Note that the V_{oc} produced by both lights decayed by approximately the same amount. The fact that the 1.03μ response seemed to decay more rapidly in the run shown in this figure is not significant because repeat runs on this same sample resulted in some cases for which the 0.365μ response decayed more rapidly. From this behavior, it is clear that the changes in V_{oc} are dominated by changes in I_o .

Figure 5 shows how V_{oc} can be cycled by exposing it to the electron beam, interrupting the beam and allowing the cell to recover in vacuum. Note that V_{oc} never returned to its original value and that the relative changes in V_{oc} were different in the two cycles shown in this figure. Here again the behavior for 1.03μ and 0.365μ light is essentially the same so that the changes of V_{oc} must be attributed to changes in I_o .

Figure 6 shows I_o and I_s for 0.365μ and 1.03μ light plotted as a function of electron flux for a fresh cell, i.e. one which has not been exposed to any irradiation. Note that during this run I_s for the 0.365μ light increased initially by about 20% and then decreased. On the other hand, I_s for the 1.03μ light remained essentially constant throughout the run. Finally, I_o first decreased by about 30% and then increased.

Figure 7 shows the same three parameters plotted versus integrated flux when this same p/n cell went through a second cycle after it had been allowed to recover in the vacuum overnight. This time, the initial increase in I_s for 0.365μ light is absent and this parameter decreases by about 20%. Here again I_s for 1.03μ remains constant. Finally, I_o increases by about 20%.

Since I_s for 0.365μ light is approximately an inverse function of surface recombination velocity s while I_o is approximately proportional to s , it is reasonable to conclude that the behavior shown in Figures 6 and 7 can be attributed to changes in s .

c) Irradiation of n/p cells.

Figure 8 shows I_s for 0.365μ and 1.03μ light plotted versus flux for a fresh n/p cell placed in a diffusion pump vacuum. Here again the electron energy was initially 140 KeV. Note that I_s for 0.365μ light increases by about 40% and saturates at this higher value. The response to 1.03μ light remains constant.

Figure 9 shows these same two parameters for the same cell after overnight recovery in the vacuum. This time I_s for 0.365μ increases by 30% while I_s for 1.03μ remains constant. Note that the final point in Figure 9 corresponds to an integrated flux which is about 50% larger than the maximum value given for the p/n cell. No decrease in I_s for 0.365μ light was observed even after it is increased irradiation.

CORRELATION OF EXPERIMENTAL RESULTS AND THEORY

The experiments described above indicated that s changed as a result of low energy electron irradiation. It should, therefore, be possible to correlate these results with theoretical calculations of the response of photovoltaic cells to light of these two wavelengths. The continuity equation with appropriate boundary conditions was solved for a cell with the same geometry as the photovoltaic cells used in this study (junction depth, 1μ).

Figure 10 shows a plot of the collection efficiency Q_p vs s for $a = 2 \times 10^5 \text{ cm}^{-1}$ and for two plausible values of τ in the diffused region (10^{-8} and 10^{-9} sec). The parameter Q is proportional to I_s so that an experimentally observed change in I_s can be related to a certain change in s through curves like those in Figure 10. To be specific, consider the case of irradiation of an n/p cell. As is evident from Figure 9, an n/p cell experiences a 30% increase in I_s before the surface changes saturate. Suppose that the saturation corresponds to a value of Q_p which is close to the maximum in Figure 10, i.e. let it correspond to a value of $s = 10^4 \text{ cm/sec}$. Then according to the figure, the value of s at the beginning of irradiation would have been about $2 \times 10^5 \text{ cm/sec}$. Wolf¹ has published curves of Q_p vs λ for $s = 10^5$ and 10^4 cm/sec and $\tau = 10^{-8} \text{ sec}$. If his calculations are combined with the Johnson's air mass zero solar spectrum, it is possible to calculate the short circuit current which this cell would deliver prior to ($s = 10^5 \text{ cm/sec}$) and after irradiation induced saturation of s ($s = 10^4 \text{ cm/sec}$). Such a calculation yields the result that I_s (and also the maximum power) would increase by about 10%. The same sort of computation for a p/n cell leads to the conclusion that I_s would decrease by about 10% in that case.

AN ESTIMATE OF THE EFFECT OF VAN ALLEN BELT ELECTRONS

From Figures 6-9, the flux needed to cause a saturation of s is about $2 \times 10^{15} \text{ electrons/cm}^2$. These irradiations were performed by electrons with $E_B < 140 \text{ KeV}$. If it is assumed that the changes are functions of integrated flux only, i.e. that they are independent of the particle energy, it becomes possible to estimate the time needed for a cell to reach saturation when it is exposed to the Van Allen radiation flux. It has been estimated that the integrated electron flux with $E_B > 20 \text{ KeV}$ is as high as $10^{10} \text{ particles/cm}^2 \text{ sec}^2$.² Using this flux value, it would take a few days for the surface effects in the cells to attain saturation.

DISCUSSION OF THE EXPERIMENTAL RESULTS

The experiments described in this paper show how the surface properties of photovoltaic cell change during radiation but they do not indicate the mechanism underlying these changes. Further experiments on devices whose construction favors better control over the semiconductor surface are in progress, but even at this stage the following preliminary observations are worthy of note.

- 1) If the pressure in the irradiation chamber is nearly atmospheric, the amount of surface change decreases sharply, i.e. it appears that the surface changes require simultaneous irradiation in a vacuum.
- 2) One run was made at liquid nitrogen temperature. The amount by which the surface changes is even greater in this case.
- 3) It is possible that I_o changes because of edge effects around the periphery of the cell. Preliminary experiments designed to reduce the role played by such edge effects have tended to rule out this possibility.
- 4) The changes produced when a cell is placed in a vacuum in the absence of radiation are not affected by ultraviolet light at least not for uv intensities delivered to the specimens from the low pressure Hg arc.

BIBLIOGRAPHY

1. M. Wolf, Proc. IEEE, 51, 674-93, May 1963.
2. G. E. Mueller and E. R. Spangler, "Communication Satellites," p. 49, John Wiley & Sons, New York, 1964.

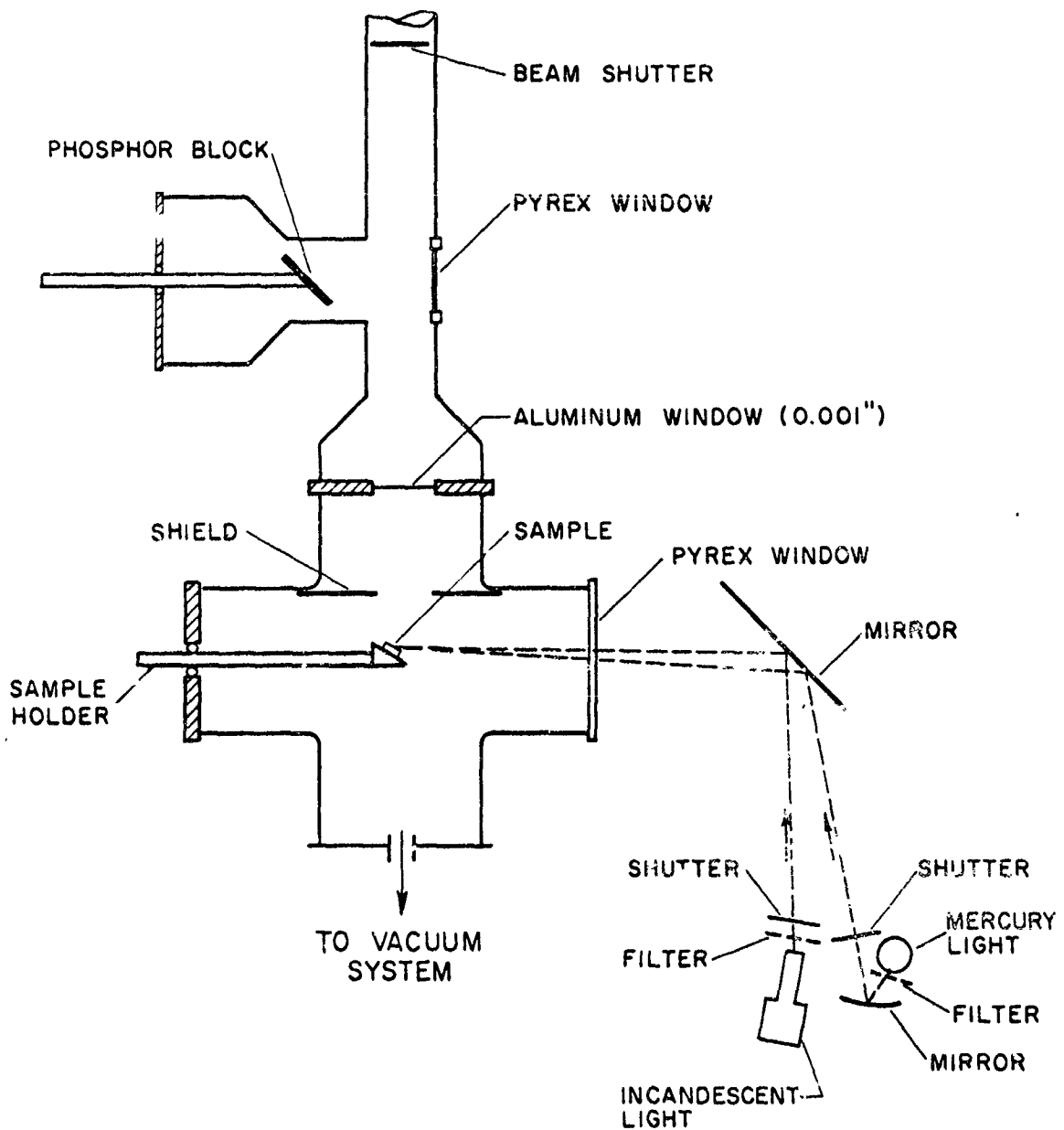


FIG. 1 EXPERIMENTAL ARRANGEMENT

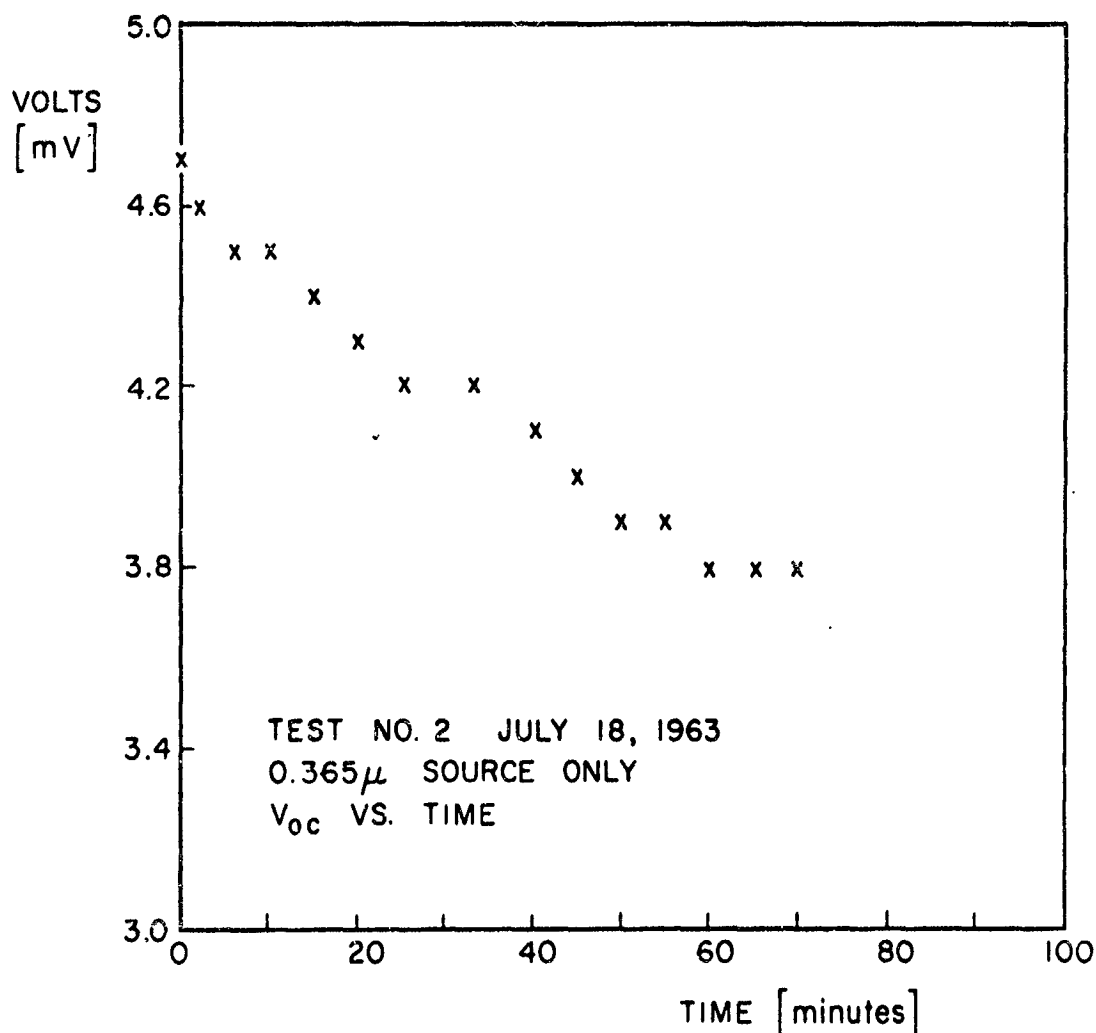


FIG. 2

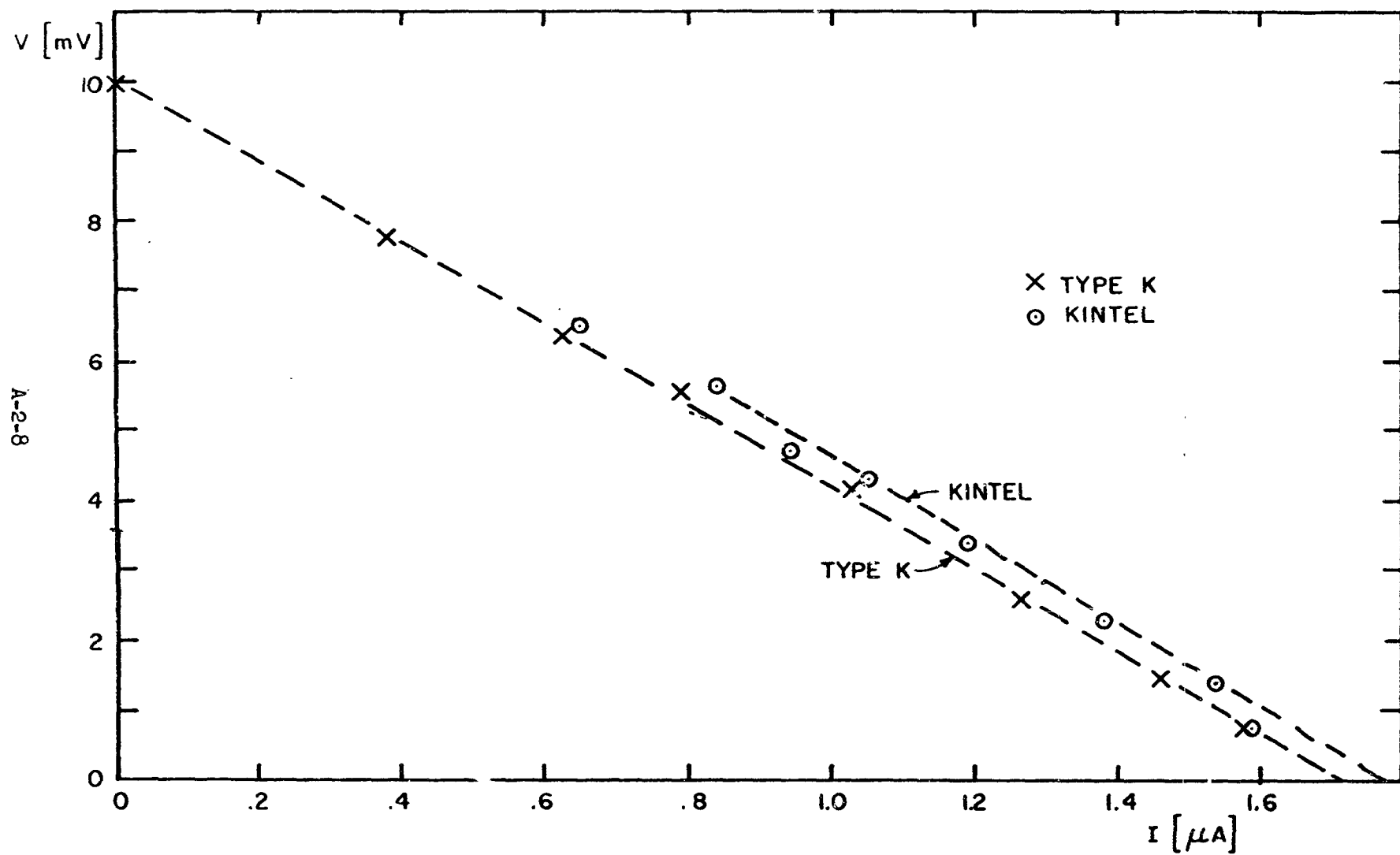


FIG. 3 I-V CHARACTERISTICS OF P/n SOLAR CELL UNDER 1.036μ LIGHT

A-2-9

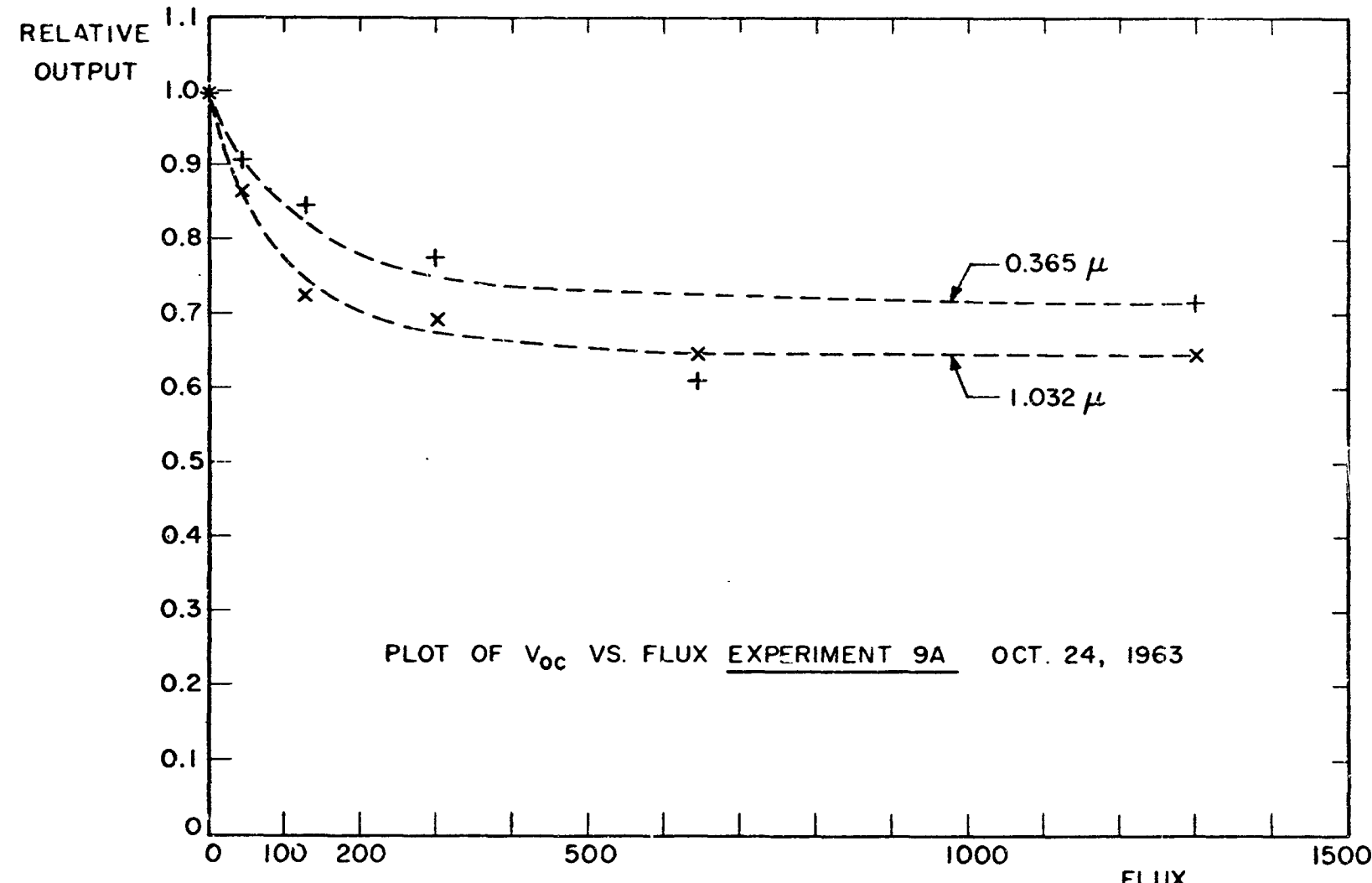


FIG. 4

A4-2-10

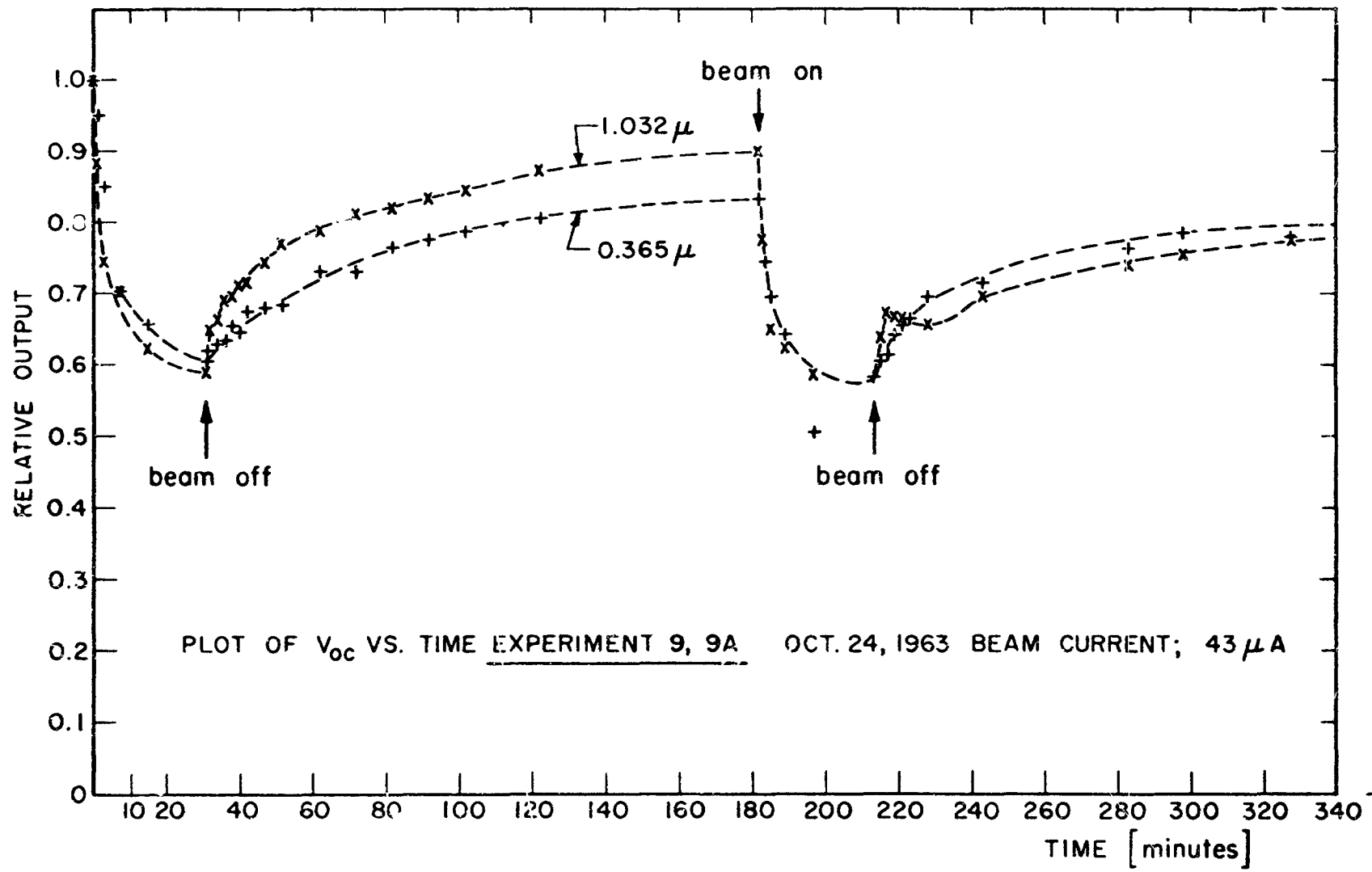


FIG. 5

A-2-11

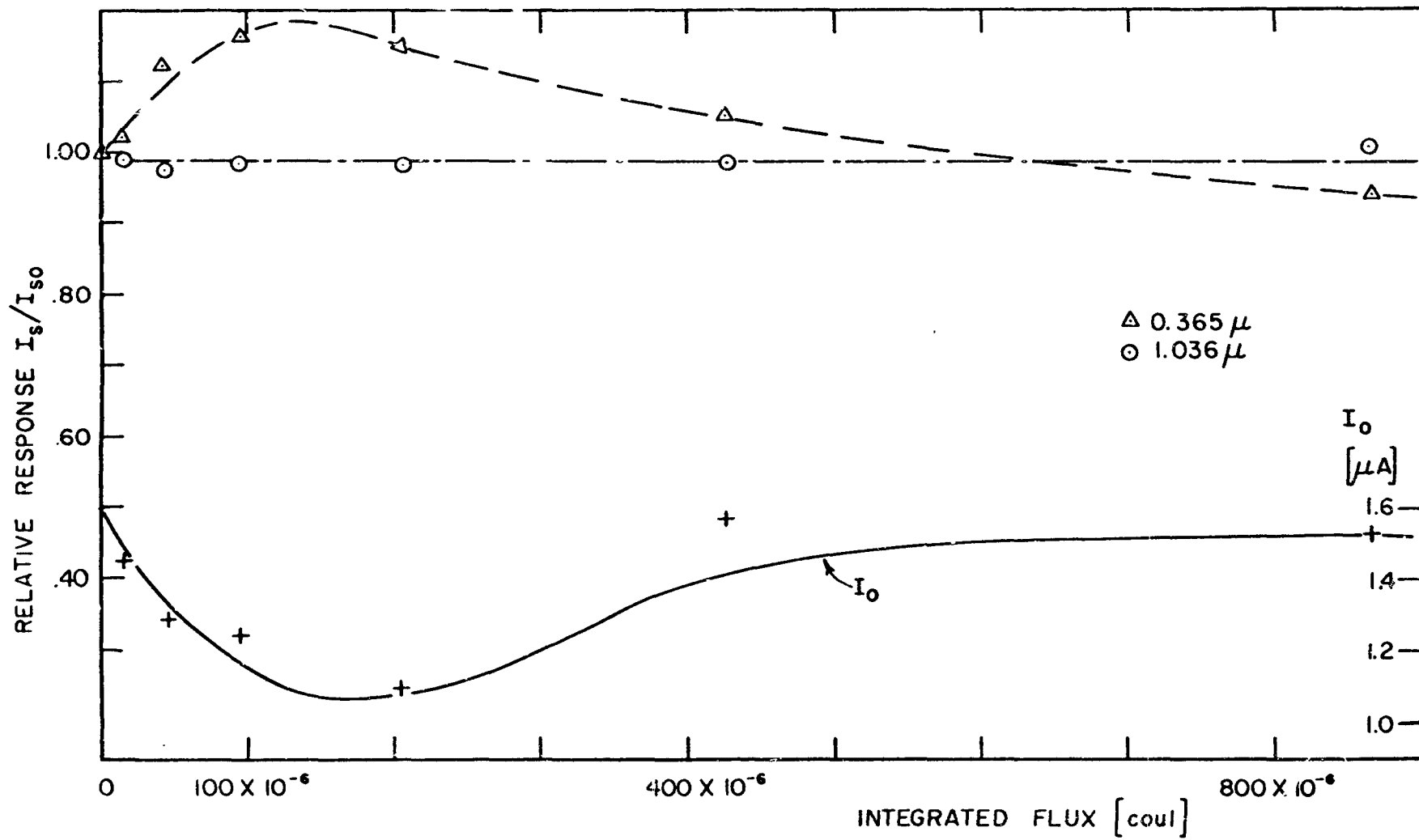


FIG. 6 P/n SAMPLE (NEW)

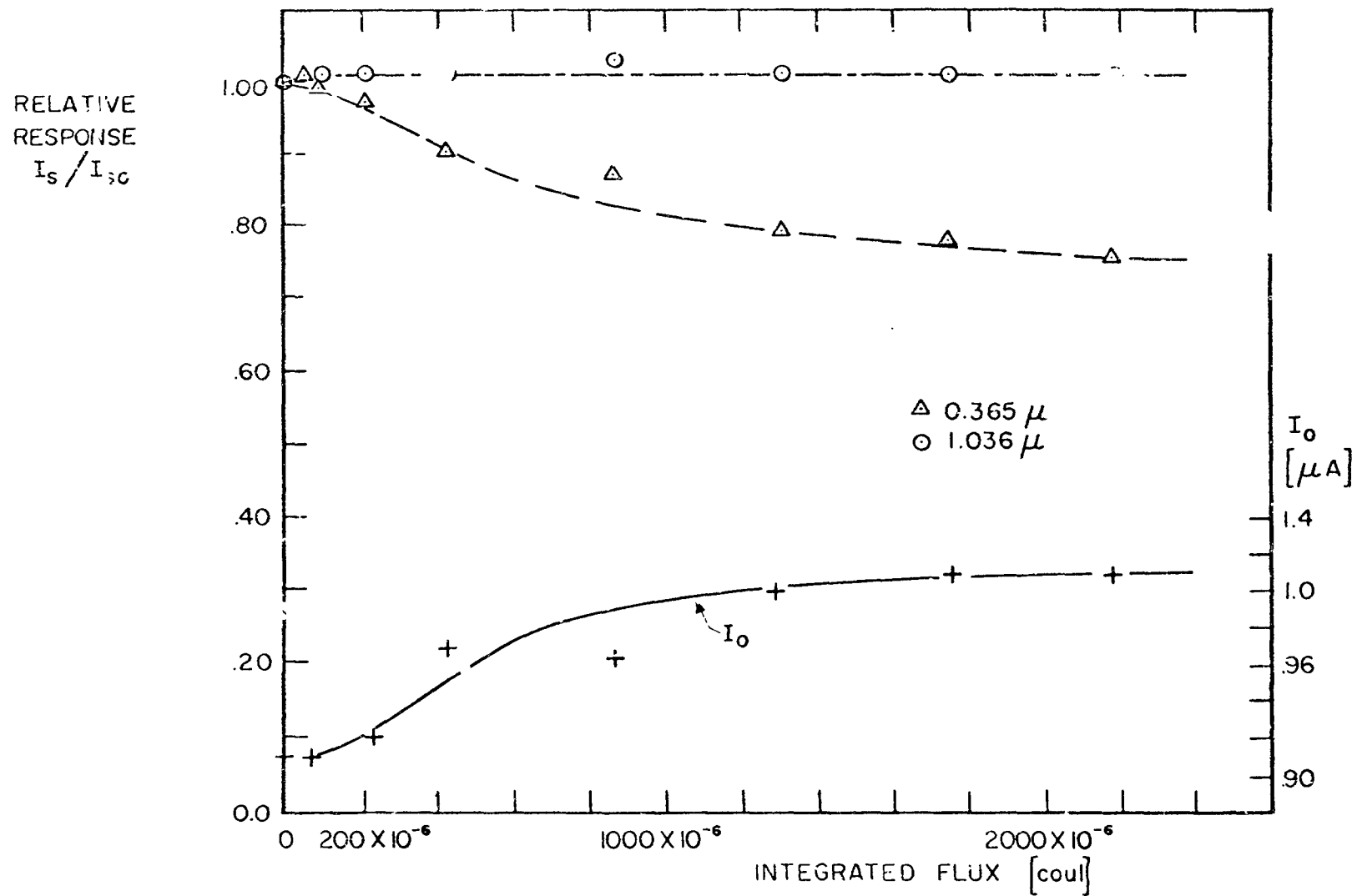
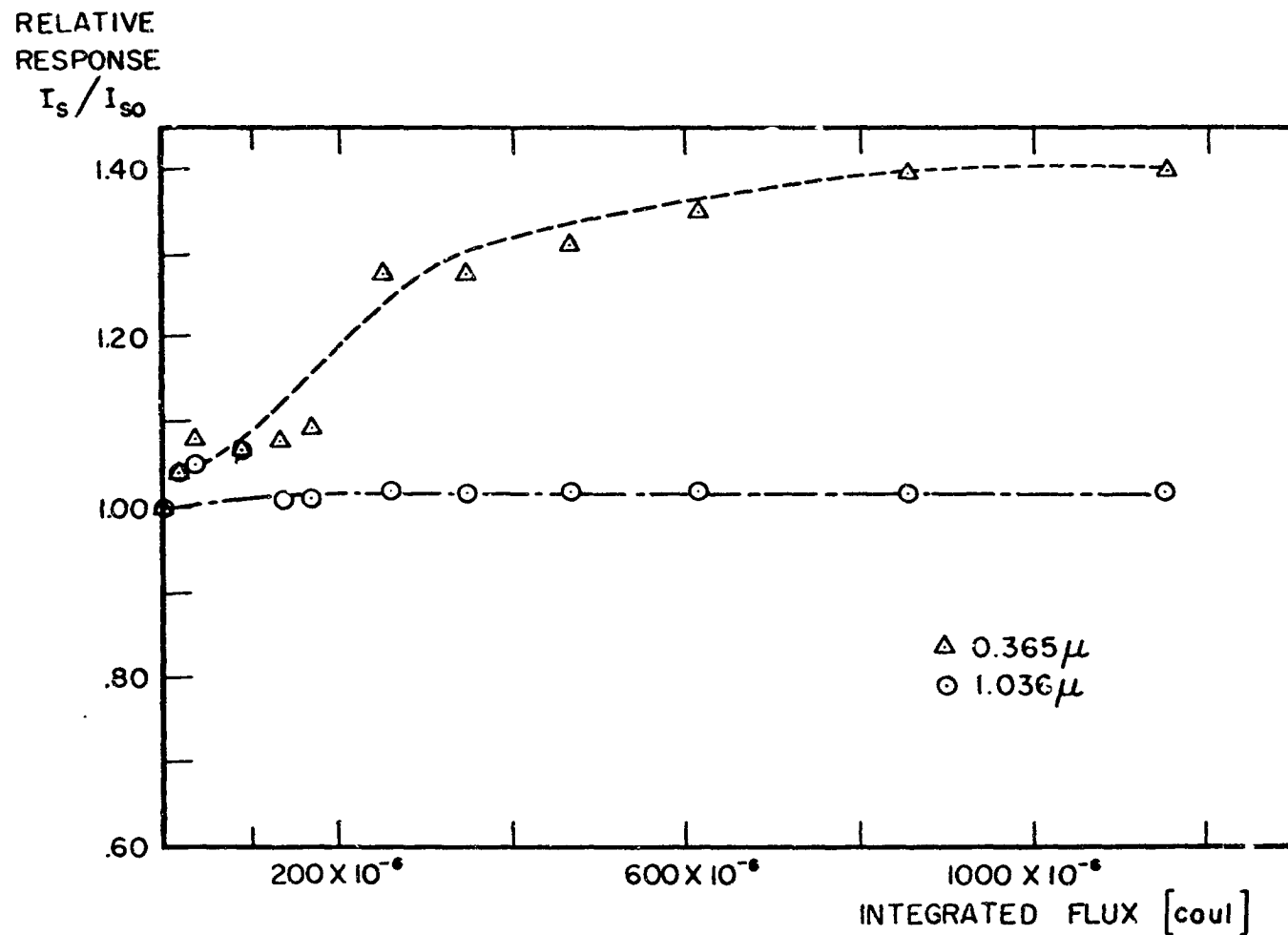


FIG. 7 P/n SAMPLE (OLD)

A-2-13



IG. 8 n/P SAMPLE (NEW)

A-2-14

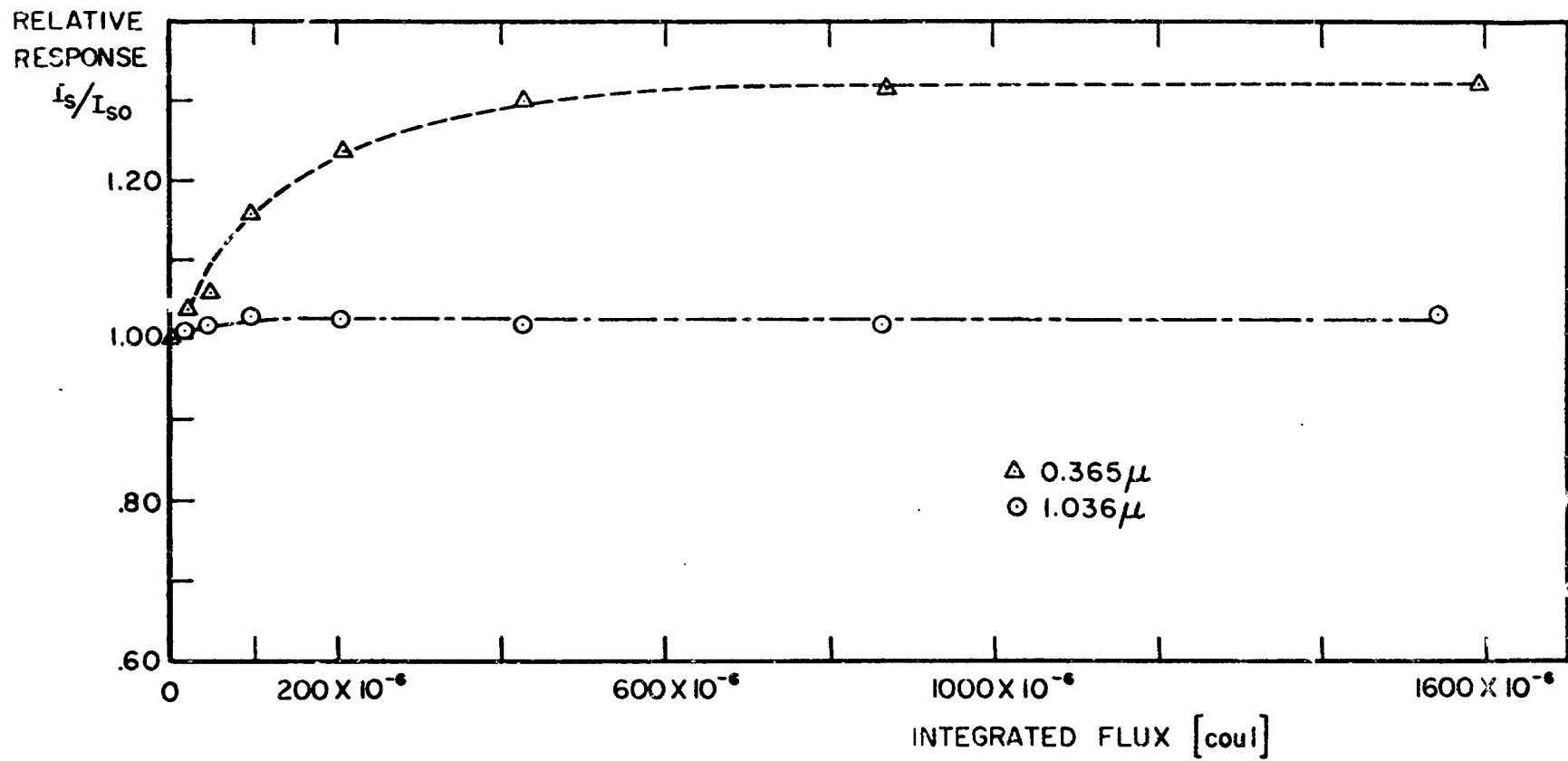


FIG. 9 n/p SAMPLE (OLD)

A-2-15

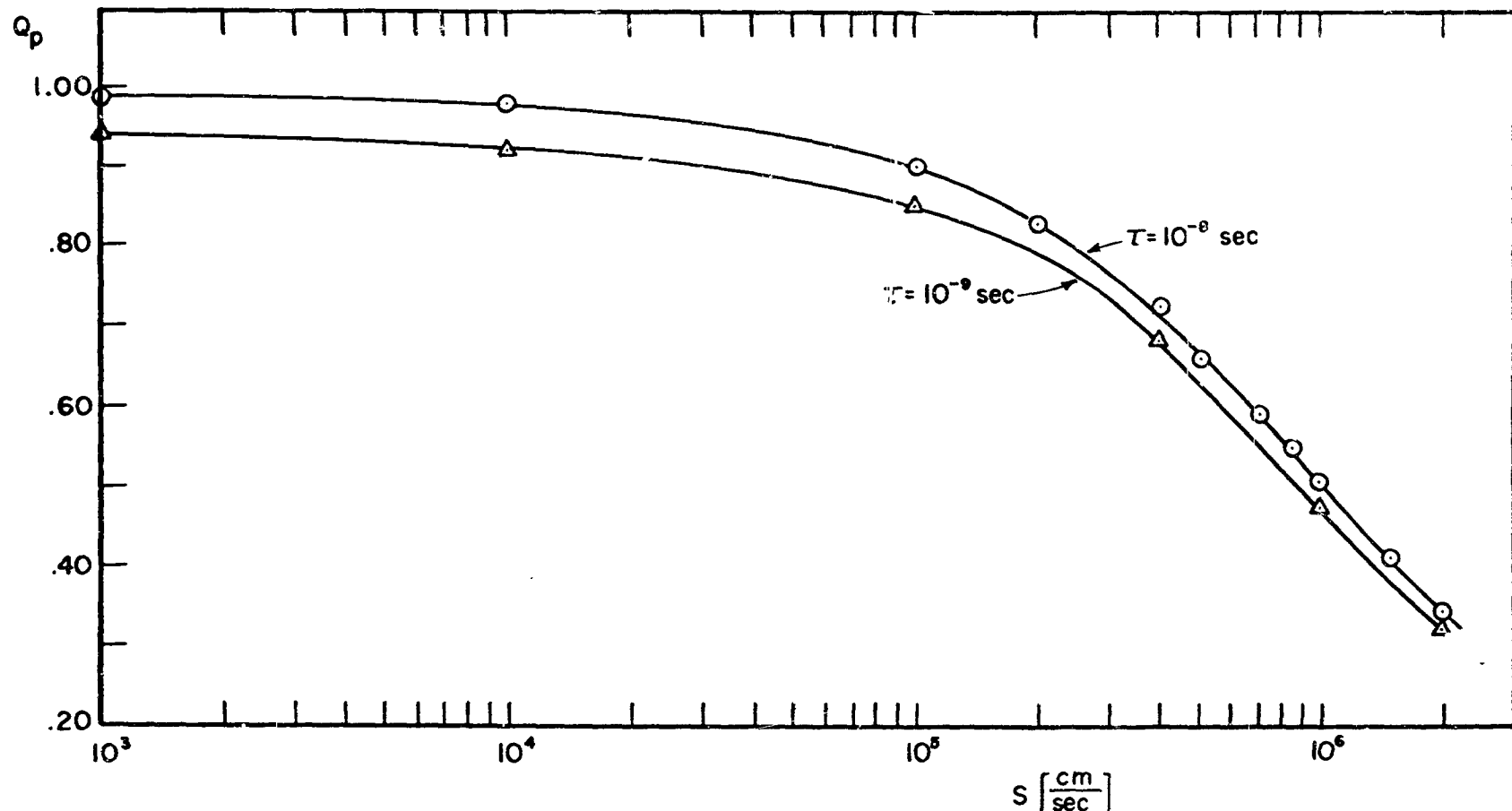


FIG. 10 Q_p VS. S

Page intentionally left blank

DISCUSSION

MILTON SCHACH - GODDARD SPACE FLIGHT CENTER: Did you measure reflectance before and after?

MR. SANTOPIETRO: No.

PAUL RAPPAPORT - RCA: Were you able to separate how much I_s changed with the UV radiation? And also, do you have any ideas as to why I_o changes because of surface effects?

MR. SANTOPIETRO: First, you said that I_s will change from the ultraviolet. The ultraviolet generated I_s is strongly dependent on the surface, so that when that changes, I_s from the ultraviolet will change.

RAPPAPORT: I know that, but it looks to me as if you might be able to account for your change solely on the basis of a change in I_o .

MR. SANTOPIETRO: Well, I_o is also determined by I_s .

JOE LOFERSKI - BROWN UNIVERSITY: There were checks made of what the effect of ultraviolet radiation alone would be on the surfaces. We found that ultraviolet radiation alone did not cause any changes in I_s or I_o . As far as why I_o should be changing, it turned out that it is in part dependent upon surface recombination velocity. When we undertook these experiments, we thought we could look only at the open circuit voltage, and not have to worry about I_o . But evidently this is not the case for this particular solar cell structure. I_o does depend on the surface recombination velocity, rather strongly.

QUESTION (NO NAME): Your plots for the p-on-n cell show that I_o apparently decreased, then increased with the radiation. Do you have an explanation for this?

MR. SANTOPIETRO: This occurred only in fresh cells. The preparation technique we used was to wash the cells in acetone, then distilled water, dry them, put them in vacuum, wait for the vacuum changes to stop, and then begin to irradiate. Only on the first irradiation was the increase in I_s in the ultraviolet observed and the decrease in I_o . If the same cell was allowed to recover, and then irradiated again, I_o increases while I_s decreases. So the I_o changes only in one direction after the initial irradiation.

MARTIN WOLF - HELIOTEK: It appears that the effect observed here could explain Dr. Waddel's observation on the solar cells.

ROSS - HOFFMAN ELECTRONICS CORP: I wonder if one really can explain the large changes Dr. Waddel observed in thick cells, that is cells as thick as

PIC-SOL 209/5

10 mils of silicon between the surface and the junction by means of surface recombination effects. I don't think that these thick cells would be effected by surface recombination.

REPLY (NO NAME): We did a calculation for the effect of surface recombination on 4 mil thick cells. We found that the collection efficiency in the thick region was quite dependent on the surface recombination velocity at the surface farthest from the junction.

N64-29155

LOW-ENERGY PROTON BOMBARDMENT OF SILICON CELLS*

Presented by

J. J. Wysocki

RCA Laboratories

Princeton, N. J.

2 June 1964

* Research reported herein is sponsored by NASA-Goddard Space Flight Center under contract number NAS5-3788.

LOW-ENERGY PROTON BOMBARDMENT OF SILICON CELLS

J. Wysocki, J. Loferski* and E. Davison
RCA Laboratories
Princeton, N. J.

Introduction

At last year's conference, the effects of low-energy protons on GaAs and Si cells was discussed.¹ It was shown, for example, that the short-circuit current of GaAs and the open circuit voltage of Si cells were the most easily damaged solar cell parameters. A subsequent experiment confirmed these results.

While the behavior of the GaAs cells was well understood, it was not clear why the Si cells behaved as they did.¹ For example, from a study of the behavior of the short-circuit current as shown in Fig. 1, it is observed that the current is unaffected until a flux of $10^{11} - 10^{12}$ p/cm² has been accumulated, after which the current falls rapidly. The fall-off approaches 50% per decade, reminiscent of the degradation observed in GaAs cells. Furthermore, particles of higher energy are more damaging, contrary to arguments based on Rutherford scattering. The behavior of the other cell parameters, on the other hand, is typified by the results shown in Fig. 2. While the current has the behavior alluded to, the open-circuit voltage, and consequently, the power drops steadily with flux. The voltage falls at a rate of approximately 20% per decade.

The behavior of the current and voltage is recognized to be quite different from that observed in higher energy irradiation, where the current degrades at a rate of approximately 20% per decade and the voltage is insensitive to irradiation. The results considered here are the current and voltage behavior of the Si cells.

Model

The model is based on the following features. First, the range of low-energy protons is small in Si. It varies from 1.8μ for 185 KeV protons to 6.8μ for 530 KeV particles. In our experiments, the cells were inclined at 45° with respect to the beam; consequently, the effective ranges (so to speak) are only 1.3-4.9μ. Secondly, most of the carriers are generated by light in, and collected from, the base region, a consequence of the absorption mechanism in Si.

*Brown University, Providence, R. I.

The model is shown in Fig. 3. The proton range is the distance X_1 plus the anti-reflection thickness and junction depth. Irradiation introduces a damage region in the base adjacent to the junction. We inquire how this damage layer, X_2 , effects the response of the solar cell.

The behavior can be computed by solving the continuity equation with appropriate conditions at the various boundaries. The following assumptions are made. First, the protons introduce damage uniformly over the region X_2 . The lifetime in the material beyond X_2 , however, is not affected. Secondly, fields generated by the lifetime gradient are negligible.

Results

Although the solution for all wave lengths is easily obtained, we restrict our discussion to the case of penetrating radiation. The effective diffusion length in the base L^* is shown in Fig. 4 as a function of the reciprocal diffusion length in the damage region X_2 . The curves were computed for a cell with a total coating and junction thickness of 0.4μ and an initial diffusion length of 100μ . Observe the behavior is a strong function of proton energy, or more properly, proton range. The effective diffusion length is independent of L_1 to a certain point and then falls rapidly. As the proton range increases, the rapid drop occurs at larger values of L_1 . Since L_1 is some function of flux, perhaps $\phi^{-1/2}$, this figure implies the effective diffusion length (hence short-circuit current) will be almost independent of flux up to a certain value and then fall rapidly. This was the observed behavior, as shown in Fig. 5. These data were obtained from electron-voltaic and spectral response measurements. The 185 KeV data shows little variation with flux up to 10^{13} p/cm^2 . The higher energy data shows the trend expected on the basis of the physical model; the diffusion length changes little and then rapidly with flux.

A comparison of the computed degradation and the experimental values at a flux of $4 \times 10^{12} \text{ p/cm}^2$ is shown in Fig. 6. The computed curves are based on the values of L_1 shown, namely 2.5 and 3.3μ . No correction for relative introduction rates were made in the computations. The qualitative comparison is reasonably good.

When an attempt is made to correct the computations for an introduction rate governed by Rutherford scattering, the comparison between experiment and theory is somewhat poorer as shown in Fig. 7. For the correction, it was assumed that $L_1 \propto (\sigma v)^{-1/2}$ where σv , the defect introduction rate, varies approximately with the reciprocal of proton energy.² If this theoretical argument is pursued, the proton energy at which Rutherford-type behavior (i.e. varying inversely with proton energy) becomes evident is 4-6 MeV for cells irradiated at 45° with respect to the beam, and 3-5 MeV for cells irradiated normal to the beam.

Implications and Conclusion

The form and energy dependence of the current degradation has thus been predicted. The difference in current and voltage behavior follows directly. The open-circuit voltage depends critically upon the lifetime in the vicinity of the junction through the dark current. From the onset, low-energy protons reduce the lifetime in regions close to the junction without reducing collection from the base. As irradiation proceeds, the lifetime becomes too small and the short-circuit current falls rapidly. In this sense, Si cells approach the exponential behavior ordinarily seen in GaAs.

Since the proton range is small, the junction depth and thickness of the anti-reflection coating become important parameters in the results. Slight variations in either will lead to large differences in behavior, contributing to scatter in the data.

FIC-SOL 209/5

1. J. Wysocki & J. A. Baicker, "Radiation Damage in Solar Cells", Trans. Photovoltaic Specialist's Conf. Vol. 1 (1963).
2. F. Seitz and J. S. Koehler, "Displacements of Atoms during Irradiation" in Solid State Physics (Academic Press Inc., N. Y. 1956), Vol. 2.

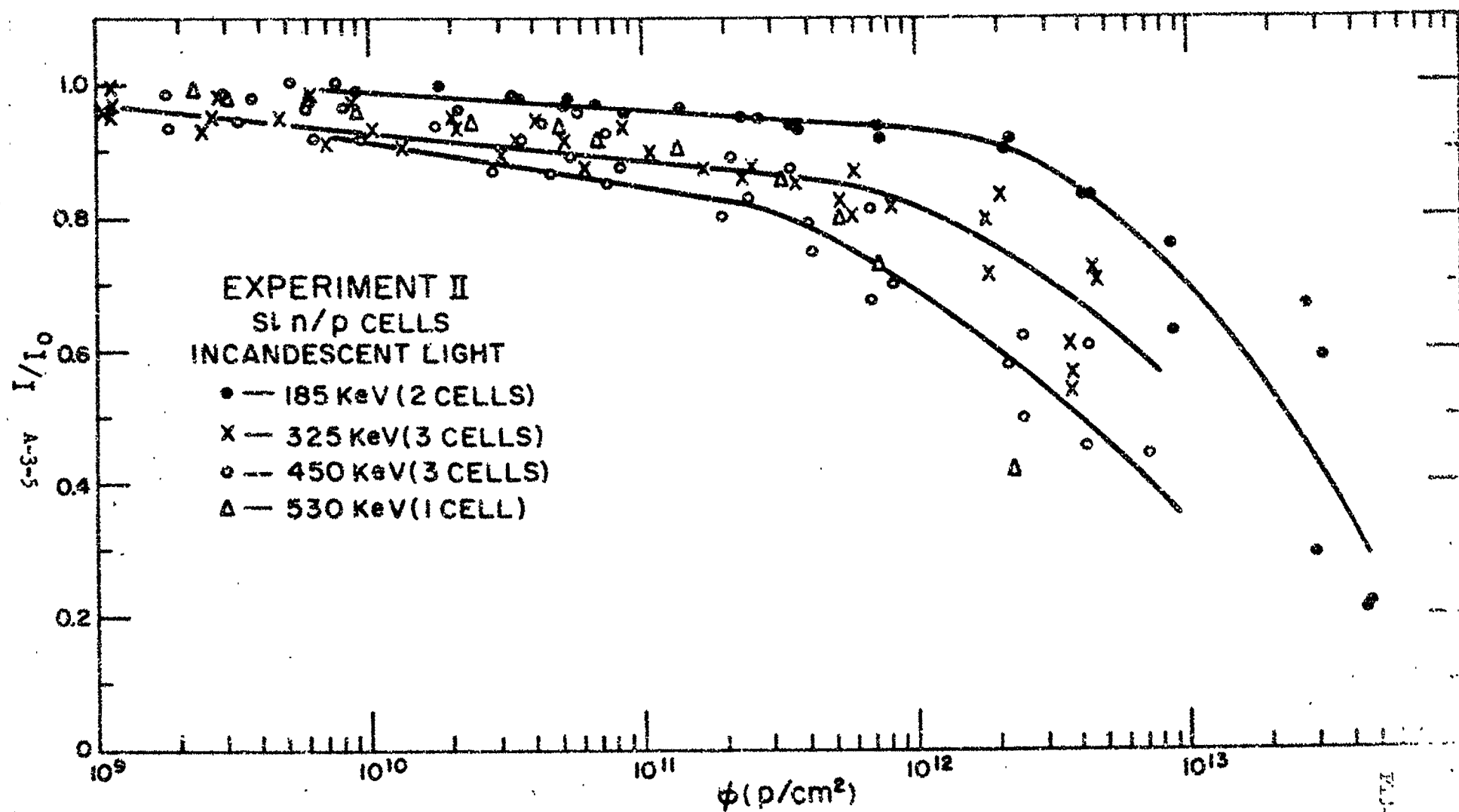


Fig. 1 I/I_0 vs. ϕ FOR Si n/p CELLS

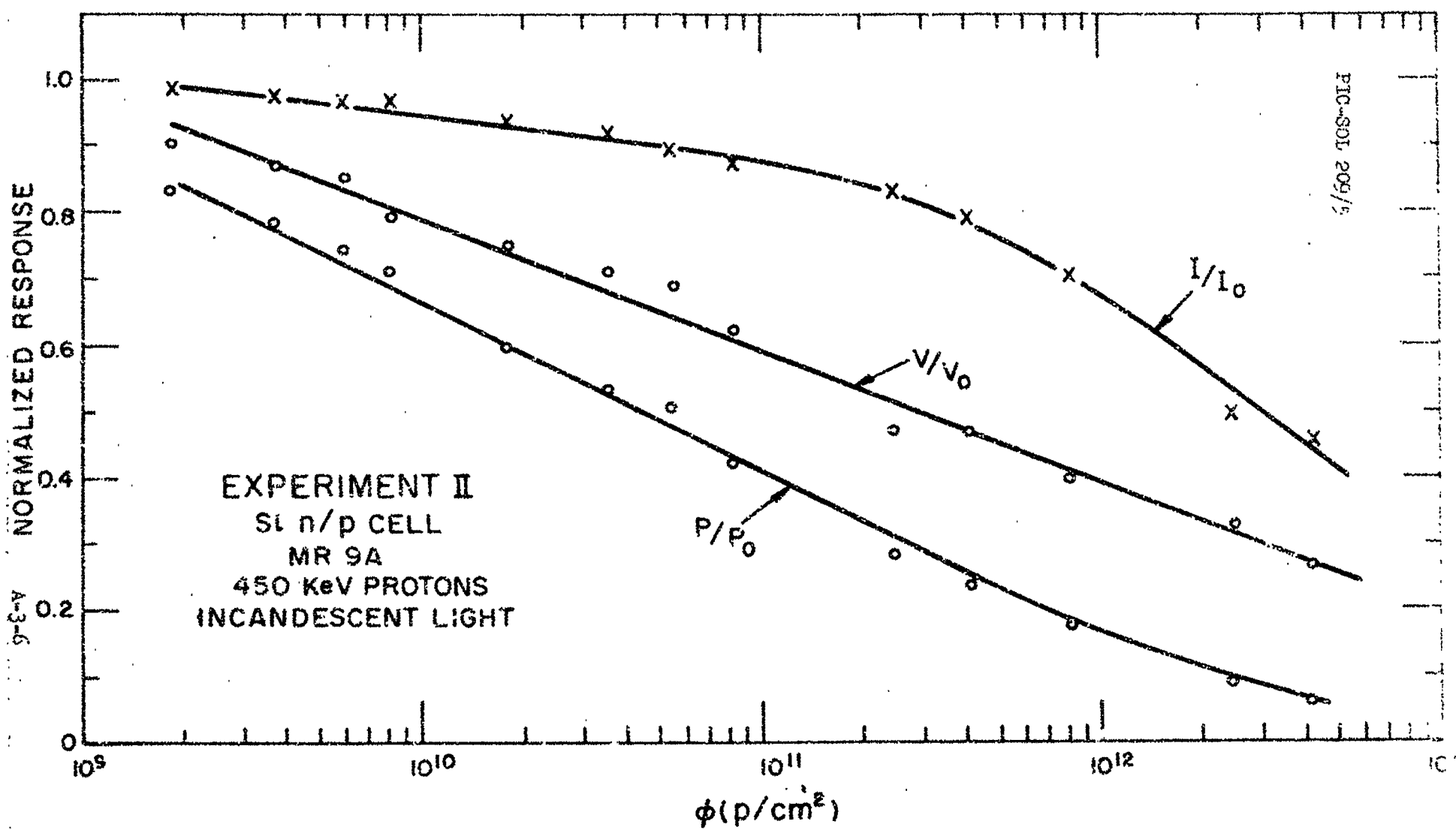


Fig. 2 NORMALIZED RESPONSE OF Si n/p CELLS vs. FLUX

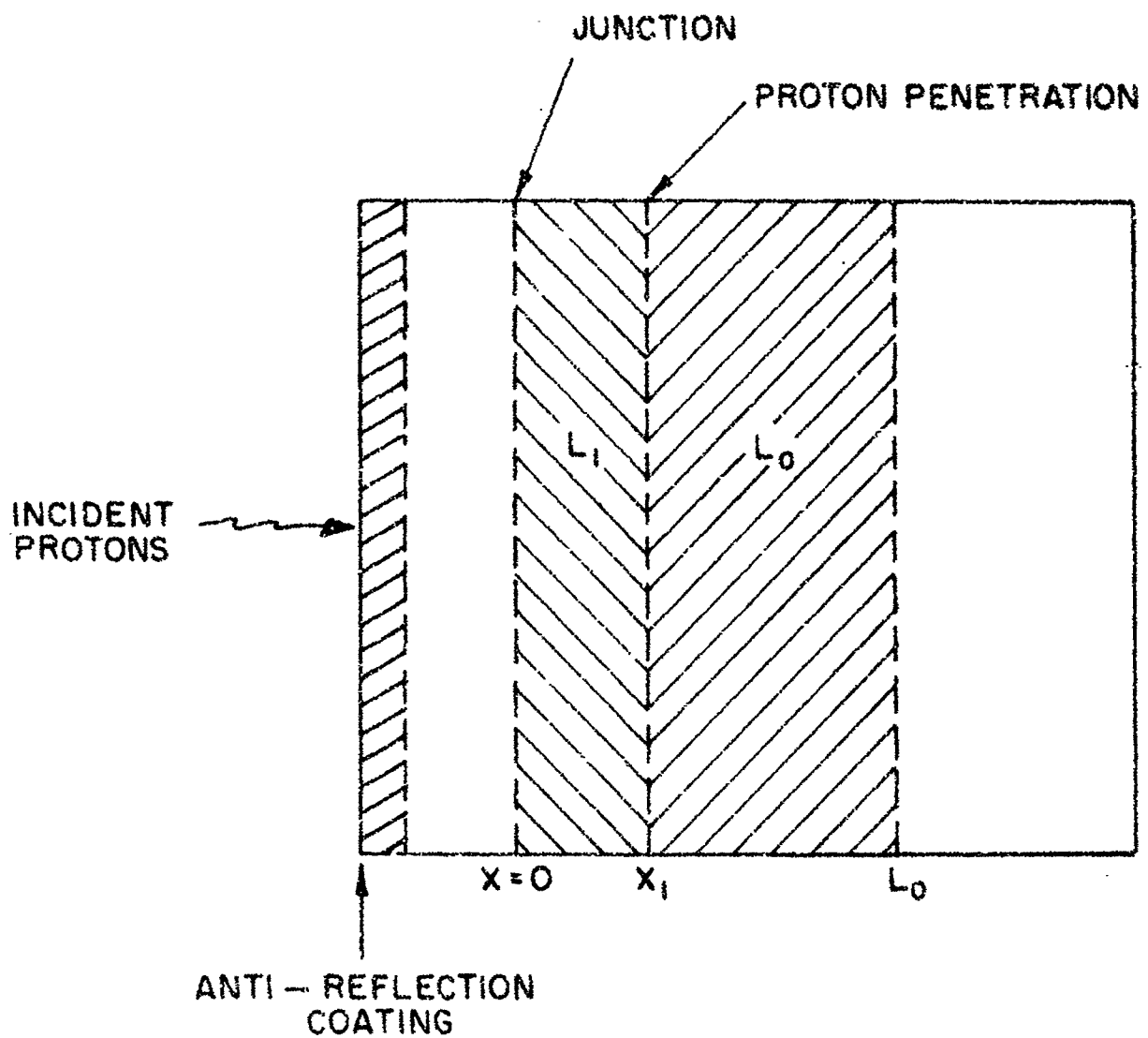
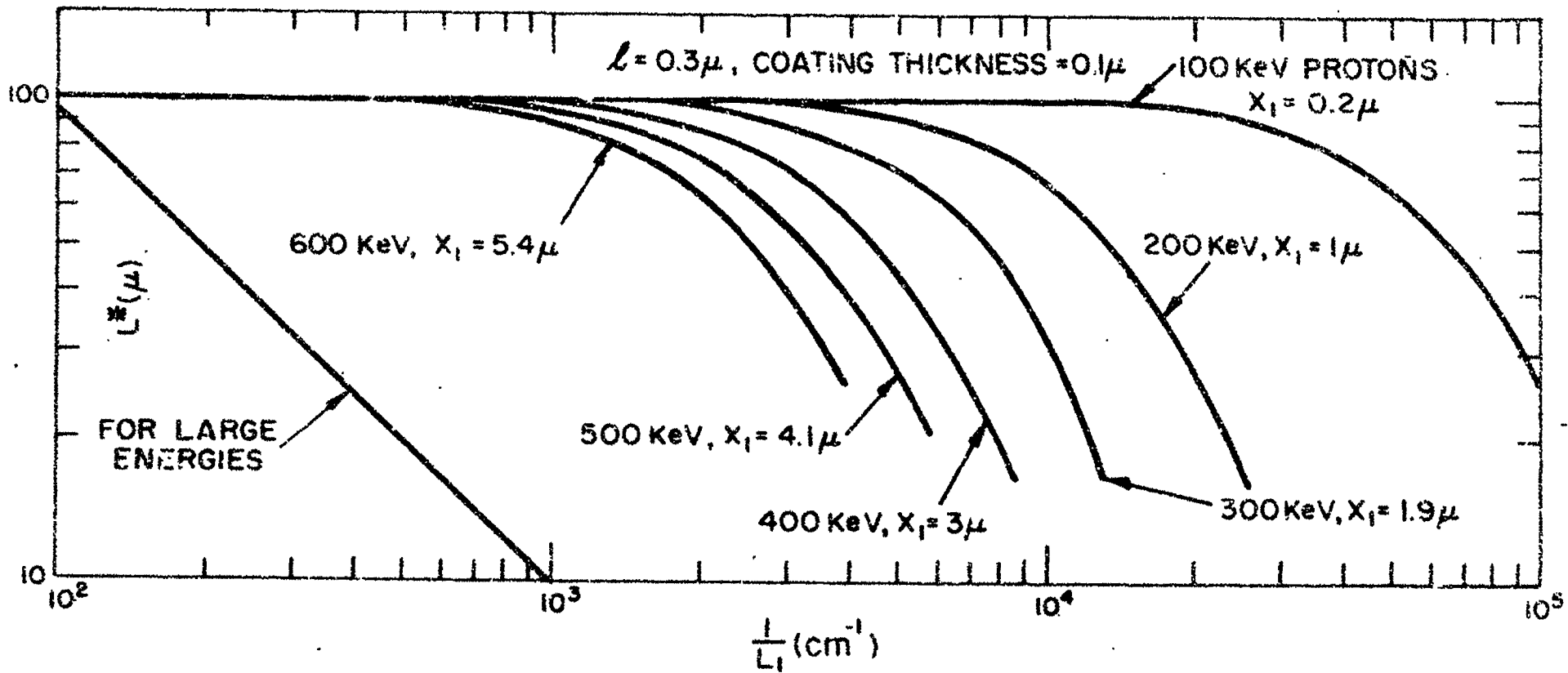


Fig. 3 Model of Junction

A-3-8

Fig. 4 L^* vs. $\frac{1}{L_1}$

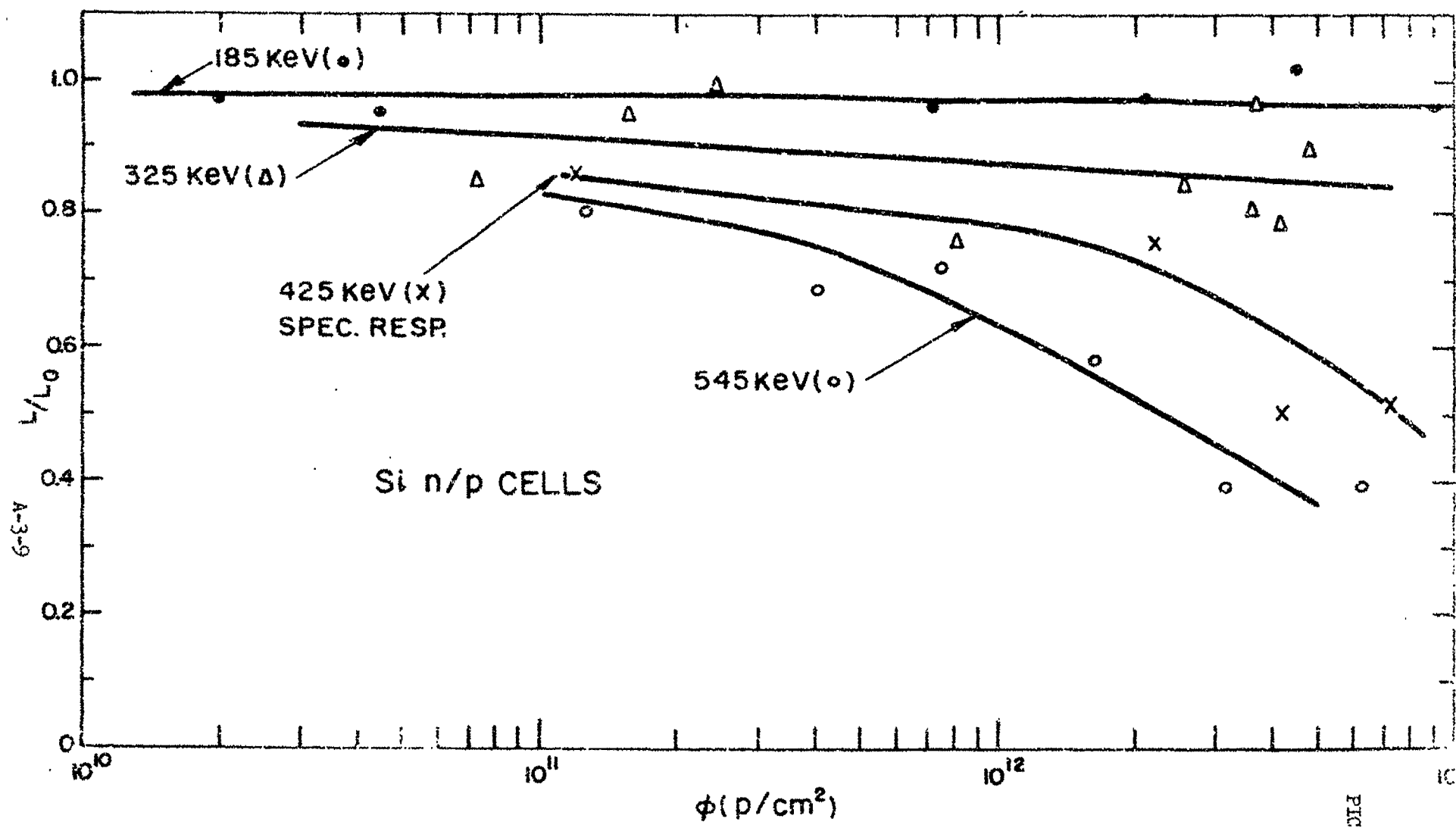


Fig. 5 L/L_0 vs ϕ

FIG-SOL 209/5

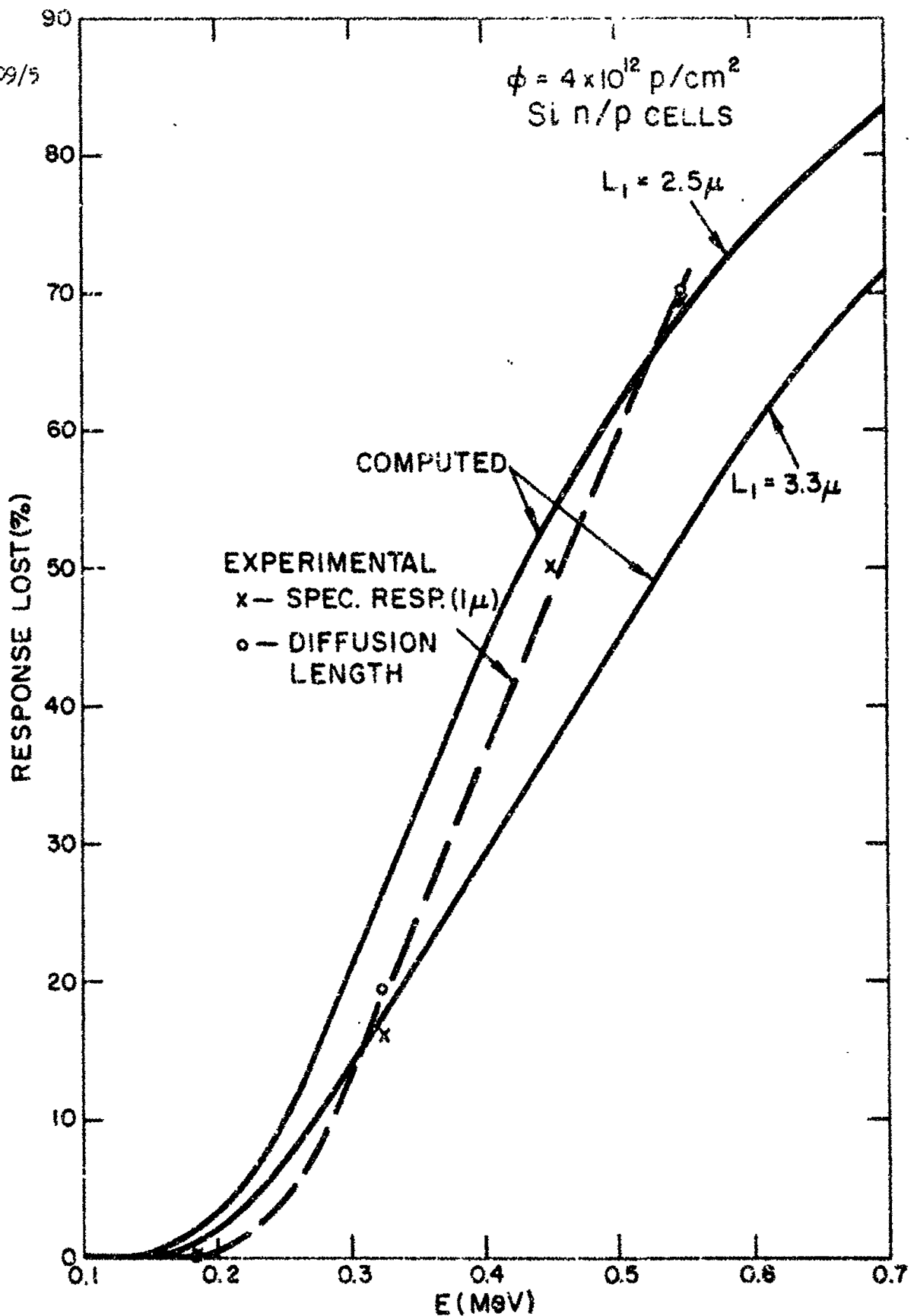


Fig. 6 Response Lost vs Proton Energy

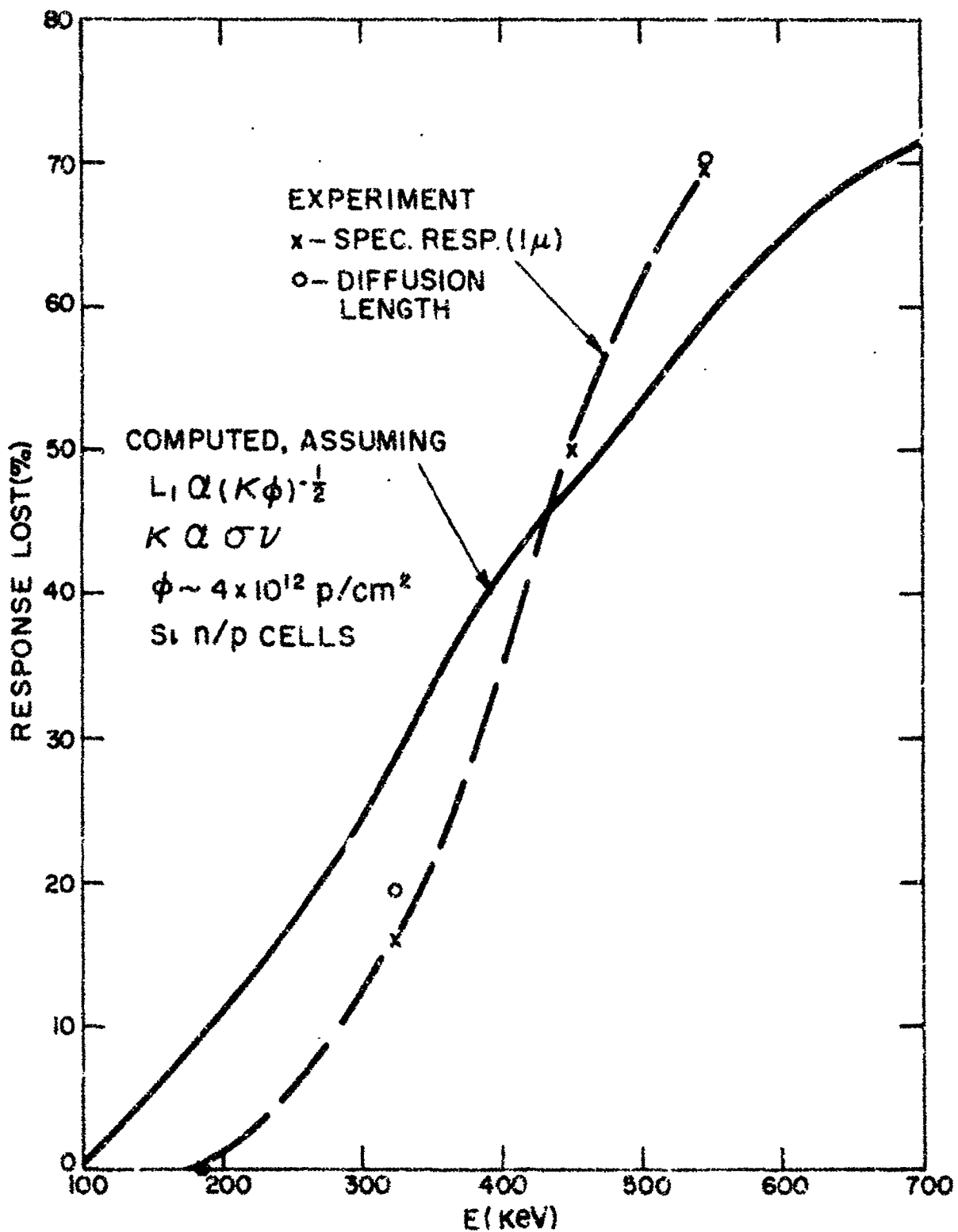


Fig. 7 Comparison of Computed and Experimental Degradation in Response

Page intentionally left blank

DISCUSSION

PAUL RAPPAPORT - RCA: I think that some of the results of our proton experiments can be used to explain Dr. Waddel's Relay observations on unprotected solar cells. In Dr. Waddel's experiment the device that was down the most after a large irradiation was the gallium arsenide cell. The device that was down the next most was the silicon n-on-p cell. The best device after very large irradiation was the p-on-n cell. This is somewhat different than the results we're used to for protected solar cells. This qualitatively can be explained by the fact that the front layer of the cell is the most important part of the cell to get damaged. The reason that the p-on-n is the best is that the p-type material has a better damage characteristic than the n-type material. Hence for an unprotected p-on-n cell, where the radiation damage is chiefly the front part of the cell, you would expect the p-on-n cell to be the best, which was the case in the Relay experiment.

MR. WYSOCKI: I don't think that's what Waddel's experiments showed. The p-on-n was always the worst. On second thought, it would depend on the energy. If the energy were sufficiently high, so that the radiation penetrates into the base, then you would expect and indeed we found that the n-on-p cell was better.

PAUL RAPPAPORT - RCA: At the very high fluxes the unprotected silicon p-on-n was the best and the unprotected gallium arsenide was the worst. The reason that gallium arsenide is worst is because its response depends almost completely on the front layer. Dr. Waddel's results show that only 3 mils of glass protection will completely change this result. I think that this is very good evidence that the low energy protons are causing these results.

EPSTEIN - MONSANTO: Do you have any idea what element in the p layer of the gallium arsenide might cause the degradation with proton damage?

MR. WYSOCKI: In gallium arsenide the response is almost entirely due to regions near the surface. The range of the protons is roughly a factor of 2 less in GaAs than it is in silicon. As a result, the protons preferentially damage those regions which you depend upon for response. I don't know whether or not there are any specific impurity effects on damage.

PIC-SCL 209/5
Section A-4

N64-29156

RESULTS OF LOW-ENERGY PROTON IRRADIATIONS
OF SOLAR CELLS

Presented by

E. A. Lodi

Lockheed Missiles and Space Company
Palo Alto, California

2 June 1964

79156

ABSTRACT

The main purpose of this study was to observe the damage effects produced in silicon and gallium arsenide solar cells by protons in the energy range, 100 to 500 kev. In order to study these effects and to obtain accurate flux measurements, several refinements were made over a previous experiment¹ completed in April 1962. One of the major refinements was that of modifying the Lockheed 3-Mev Van de Graaff accelerator so that it could produce protons with energies as low as 100 kev. The importance of this energy range was indicated in the previous experiments and was firmly established and extended in the present experiment.

Several interesting and unexpected results were found for N/P type silicon solar cells. For example, the N/P cells exhibited a levelling-off in the degradation of the open-circuit voltage for large time-integrated fluxes of 130-kev protons. At 200 kev the short-circuit current displayed a double reversal in degradation. At 300 kev the degradation rate of the short-circuit current at large time-integrated fluxes was higher than it was for higher energy protons. The experiment also confirmed Wysocki's² observation that gallium arsenide solar cells degrade rapidly when irradiated with 200- and 500-kev protons.

Also included in this paper is a comparison of the low-energy proton results with previous results obtained at Lockheed using 1-, 3-, and 12-Mev protons.

Check

-
1. Lodi, E. A. and D. L. Crowther, "Some New Results from Low-Energy Proton Irradiations of Silicon Solar Cells", *Applied Physics Letters* 2, 1 (1963).
 2. Wysocki, J. J., "Radiation Properties of GaAs and Si Solar Cells", *Jour. Appl. Phys.* 34, 2915 (1963).

RESULTS OF LOW-ENERGY PROTON IRRADIATIONS OF SOLAR CELLS

by

E. A. Lodi, J. De Pangher, and E. B. Pearson
Lockheed Missiles and Space Company
Palo Alto, California

Introduction

Our interest in studying radiation damage to solar cells irradiated with low-energy protons stems from the fact that the data^{1,2} are rather sparse in this energy range and there is information^{3,4} indicating high intensities of low-energy protons in the space radiation environment. Although the injected electron belt of July 1962 severely increased the radiation hazards in space, the electrons did not replace protons as the predominant particles in damaging N/P solar cells. In fact, our studies of the space radiation environment show that protons are at least, if not more, damaging than electrons for most orbits.⁵

Experimental Arrangement

Test Cells and Illumination Source

The dimensions of all the test cells were nominally 1 cm x 2 cm. The cells were soldered to copper mounts which were mounted one at a time on a brass rod used to position the particular cell chosen for irradiation in the evacuated irradiation chamber. Each cell also had a wire lead soldered to the surface contact. The cells were irradiated one at a time and the proton beam was interrupted periodically to allow current-voltage curves to be measured.

-
3. Bame, S. J., J. P. Conner, H. H. Hill, and F. E. Holly, "Protons in the Outer Zone of the Radiation Belt," J. Geophys. Res., Vol. 68, p. 55, 1963.
 4. Freeman, J. W., "Detection of an Internal Flux of Low-Energy Protons or Ions Trapped in the Inner Radiation Zone," J. Geophys. Res., Vol. 67, p. 921, 1962.
 5. Calculated by E. A. Lodi at Lockheed using in-flight experiments, and particle fluxes calculated by a 7090 computer program, Orbital Flux Code, developed by W. H. Harless at Lockheed.

Two different illumination sources were used in the experiment. A tungsten lamp source filtered by two inches of water was used when the solar cell was in the irradiation chamber. The Lockheed sun simulator⁶ was used only for pre-irradiation and post-irradiation tests which were made in another building. The light intensity employed with the sun simulator was 140 mw/cm^2 of simulated outer space sunlight. The intensity of the tungsten light source at the solar-cell position was adjusted by moving this light source until a standard solar cell gave the same value of the short-circuit current at normal incidence, as it did previously with the Lockheed sun simulator. In the case of the tungsten light source, the angle of incidence of the light on the test cell was 45° .

Electrical Measurements

The circuitry used to measure the response of the solar cell is displayed in Fig. 1. The X-Y plotter recorded all of the current-voltage curves obtained before, during, and after the irradiations. To avoid any drift in the plotter during the experiment two calibrated voltage sources were used periodically to check the calibration of the voltage and current axes.

Proton Scattering

The proton beam was scattered with a gold foil to reduce the beam intensity to tolerable values and to obtain a larger exposure area for irradiating solar cells. The thickness of the gold foil used in the experiment was about 10^{-5} cm. In the energy range, 100 - 500 kev, a proton loses about 20 kev in passing through the gold at normal incidence. From this fact it can be easily shown that the proton energy experienced by a solar cell irradiated at a scattering angle of 45° can be as much as 28 kev below the primary proton energy.

Figure 2 depicts the arrangement for: (1) collimating the proton beam to strike a $1/8$ in. diameter circular area on the gold foil, (2) irradiating the solar cell with protons scattered through 45° , (3) monitoring the transmitted beam with a Faraday cup, (4) illuminating the solar cell at an angle of incidence of 45° with the light from the tungsten lamp, and (5) counting the scattered protons at the detector positions of 45° and 120° . A pressure of at least 10^{-5} torr was maintained in the irradiation chamber

6. This simulator was built by the Solid State Physics Group at Lockheed. Their calibration of the simulator indicates less than 10% deviation from Johnson's spectrum in intensity as a function of the wavelength.

during the experiment. Two silicon surface barrier detectors,⁷ one at 45° and the other at 120°, were required to count the protons over the energy range desired and over a wide range of counting rates. Complete separation of noise from 130- kev proton pulses was possible only with the 45° detector. This separation was not possible with the 120° detector because of the poorer energy resolution present in it. Thus the discriminator in the 120° detector circuit had to be raised above the noise level. The 120° detector was calibrated against the 45° detector whose counts were calculated to yield the time-integrated flux at the solar cell. At the highest irradiation rates the count rates in the 45° detector were too high to be counted; consequently, the proton irradiation upon it was interrupted by closing a shutter in the detector tube and then the 120° detector with its lower rates were used for monitoring the irradiation flux. The poorer energy resolution obtained with the 120° detector is caused by the fact that the extreme path length of the protons in the gold foil is about 2.1 times as large for the 120° detector as it is for the 45° detector. The collimators in front of each detector both had diameters of 0.1 in. and both were located 100 cm from the gold foil. According to calculations based on the Rutherford scattering law the ratio of the 45° count rate to the 120° count rate has the value 27, while actual measurements of the count rates gave values from 22 to 28. Measurements obtained with this detection system showed that the Faraday-cup monitor was a nonreproducible monitor for the very thin gold foil that had to be used; consequently, complete reliance was placed on the two solid state detectors in determining the proton fluxes at the solar cell.

Figure 3 shows a block diagram of the electronics system used for amplifying, measuring, and recording the proton pulses in the two detectors. By gating the 400-channel pulse height analyzer and observing the part of the pulse height spectrum selected by the two discriminators they could be visually set to give the best signal-to-noise ratios in the two counting systems. Rather wide discriminator pulses of 10-microsecond duration were employed to insure coincidence of discriminator pulses with the corresponding pulses that were being analyzed. An analysis of the data obtained from the two detectors over a wide range of counting rates showed that the dead time of the systems was the same as the time duration of the discriminator pulse. The data were corrected for dead-time loss in determining the time-integrated fluxes.

7. Obtained from the Oak Ridge Technical Enterprises Corporation in Oak Ridge, Tennessee.

Modification of the Lockheed 3-Mev Van de Graaff Accelerator

The normal energy span of the Lockheed Van de Graaff accelerator is 0.8 to 3.0 Mev. To extend the lower energy limit the most extensive modification of the accelerator required removing the standard 3-Mev corona-point-control mechanism and in permanently installing a deeper penetrating mechanism⁸ normally used with a 5-Mev Van de Graaff accelerator. Other modifications consisted in shorting out a fraction of the accelerator column, in using a Hall effect device to measure the magnetic field strength in the analyzing magnet at low-field strengths instead of the usual proton-moment gaussmeter, and in using the molecular H_2^+ beam instead of the usual atomic H^+ beam to obtain a further reduction of the proton energy. For one particular fraction of the accelerator column which was shorted out, a voltage span of 0.2 to 1.2 MV resulted and led to a proton-energy span of 0.1 to 1.2 Mev. A different shorting fraction is required for a different energy span and requires the opening of the Van de Graaff pressure tank to make the change. Actually the lowest proton energy operating point, 150 kev, used in this experiment was set by noise⁹ in the solid state detectors and full use of the accelerator energy range was not employed.

Results

The results are separated into two parts. The first part covers the 130- to 500- kev proton irradiations. These results are displayed in Figs. 4-10. The second part is concerned with the comparison of these results and those obtained with 1-, 3-, and 12- Mev protons. These comparisons are given in Figs. 11-14. Table I shows the comparison, before and after irradiation, of the maximum-power degradation of the cells as obtained with the LMSC sun simulator and with the tungsten-water light source.

Figures 4-7 display the degradation of the relative maximum power as a function of the time-integrated flux for silicon solar cells with proton energies of 130, 200, 300, and 500 kev respectively. At each energy, results are given for P/N and N/F type cells and they show that N/P type cells are more radiation resistant than P/N type cells, as was expected. This fact becomes more and more evident with increasing proton energy. Also included in Fig. 7 are results for a 10 ohm-cm N/P solar cell. These results show that at 500 kev, the 10 ohm-cm N/P cell is no more radiation resistant than 1 ohm-cm N/P cells. This observation is in good agreement

-
- 8. Purchased from the High Voltage Engineering Corporation in Burlington, Massachusetts.
 - 9. Weller, J. F. and R. L. Statler, "Low-Energy Proton Damage to Solar Cells", IEEE Trans. Nucl. Sci. NS-10, 66 (1963).

with the results of the Naval Research Laboratory¹⁰ using 4.65-Mev protons, which differs from the results of electron damage and very high energy proton damage. Figure 8 shows the degradation of the relative maximum power of GaAs solar cells as a function of the time-integrated flux for 200- and 500- kev protons. By comparison, as the irradiation proceeds, the GaAs cells degrade as fast as N/P silicon solar cells for 500- kev protons but considerably faster for 200- kev protons. Figures 9 and 10 show the changes in the current-voltage profiles as a function of the time-integrated flux for N/P cells with 130- and 200- kev protons. The curves for 130- kev protons (see Fig. 9) are numbered to show successive measurements taken with increasing time-integrated flux. The ordering of numbers is regular as observed along the current axis but shows a reversal in open-circuit voltage after the time-integrated flux corresponding to curve (7) is exceeded. On the other hand, for 200- kev protons (see Fig. 10), the ordering is regular as observed along the voltage axis but shows a double reversal in short-circuit current after the time-integrated flux corresponding to curve (5) is exceeded. That is, the short-circuit current initially degrades and then not only stops degrading but increases substantially and then degrades once again. At the higher energies, 300 kev, 500 kev, 1 Mev, 3 Mev, and 12 Mev, no such reversals in the degradation have been observed. Figure 11 gives the comparison of the degradation rate of the short-circuit current as a function of time-integrated flux for N/P cells over the proton energy range of 130 kev to 12 Mev. There are several interesting observations one can make from this comparison. First of all, there is the transition region between 130 and 300 kev where the slope of the short-circuit current degradation changes drastically. Within this transition region are the unexpected results of the 200- kev proton irradiation of N/P cells, as described previously. Another observation is the difference in the slopes of the degradation curves of short-circuit current over the entire proton energy range. This result is emphasized by observing that the 3- and 12- Mev degradation curves cross the 1 Mev degradation curve and appear as though they will cross the 300 and 500 kev degradation curves with sufficient flux. Figure 12 gives the same information as Fig. 11 except that it is for P/N type cells. The most important aspect of Fig. 12 is the similarity to Fig. 11 with respect to the relative slopes of the degradation curves for corresponding proton energies (except at 200 kev where the P/N type cell has already gone through the transition region). Figure 13 displays the degradation of the open-circuit voltage versus time-integrated flux for the proton energy range, 130 kev to 12 Mev.

10. Weller, J. F. and R. L. Statler, "Low-Energy Proton Damage to Solar Cells", IEEE Trans. Nucl. Sci. NS-10, 66 (1963).

The significant point here is that the results indicate that the degradation of open-circuit voltage is approximately independent of the proton energy in this energy range. Further tests are clearly indicated to extend this result into larger time-integrated fluxes for all proton energies. Table 1 gives a comparison of the maximum-power degradation as observed using the LMSC sun simulator and the tungsten-water light source. For P/N silicon solar cells the results indicate that the damage appears greater with the tungsten-water source than with the sun simulator. For N/P silicon solar cells at the two lowest proton energies this is not the case. It is only at proton energies of 300 kev and greater that the N/P cells appear more damaged under the tungsten-water light source. For the two GaAs solar cells Table 1 shows that the damage is not as severe with the tungsten-water light source as it is with the sun simulator. These results clearly indicate that care should be taken whenever results from experiments using a tungsten light source are used for outer space sunlight conditions. It should be emphasized that any interpretations derived from Table 1 are subject to error because of annealing of damage observed at low energies and also because of the variance of total fluxes at which the comparisons are made.

Acknowledgments

Thanks are due Dr. A. Andrew and Mr. D. L. Crowther of the Environmental Effects Group for their advice and encouragement in planning the experiment and to Mr. H. H. Chung of the same group for assisting in the experiment. Thanks are also due Dr. L. F. Chase and his Van de Graaff group for responding to our suggestions of extending the lower energy limit of the accelerator and for providing part of the counting equipment needed for operating the two solid state detectors.

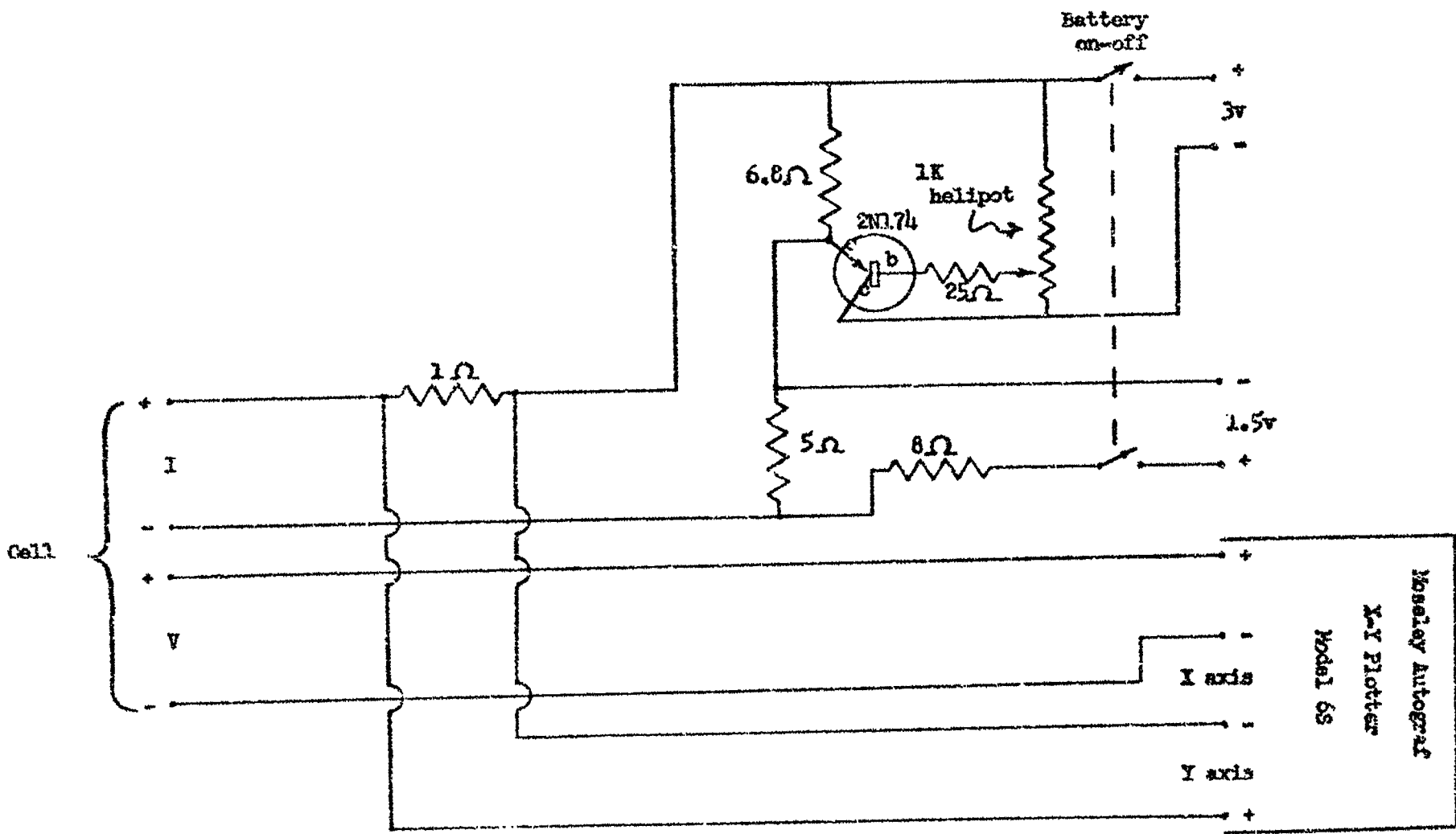


Fig. 1 Schematic Diagram of Circuit Used to Record Current-Voltage Curves of Solar Cells

PIC-SOL 209/5

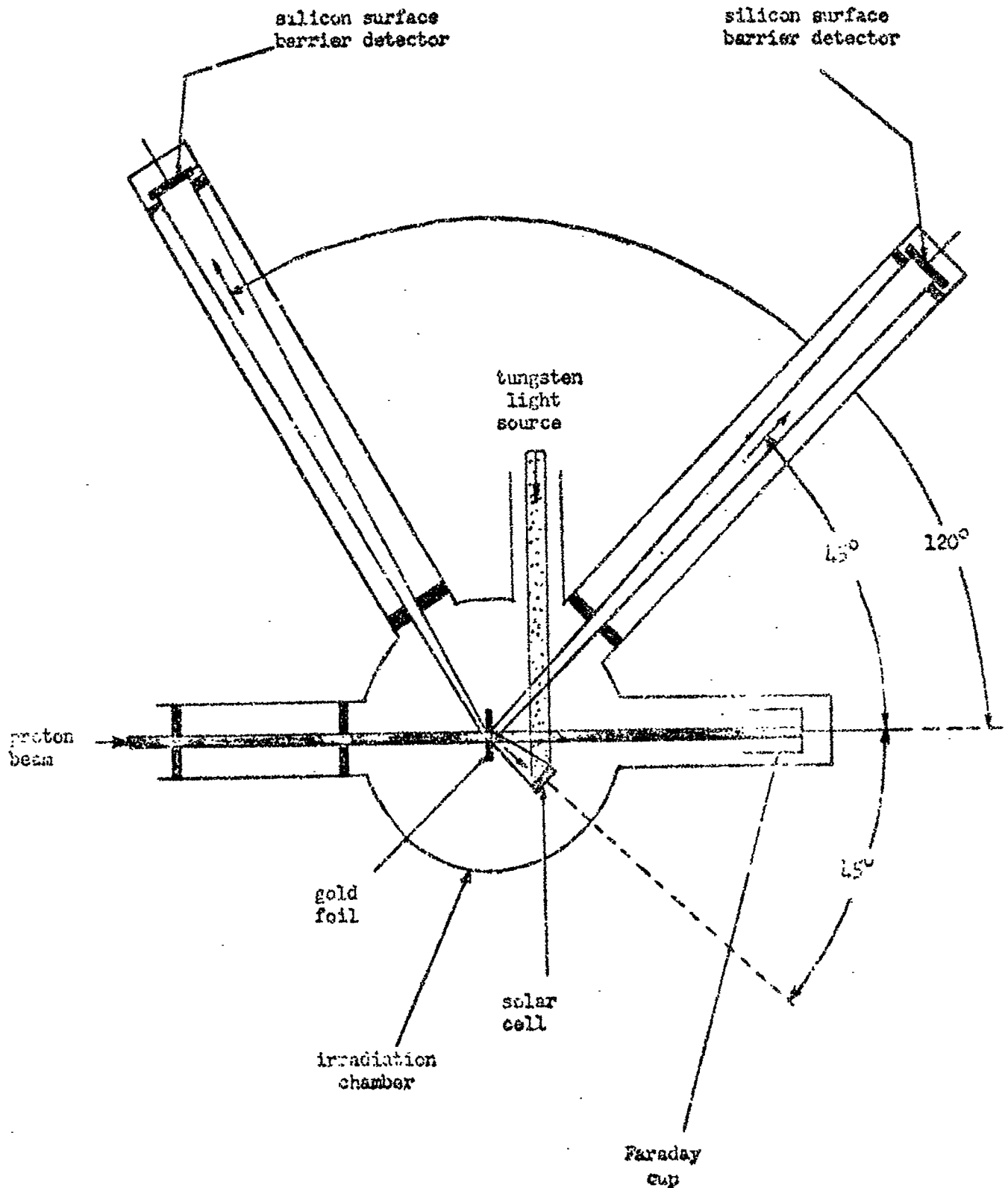


Fig. 2. Irradiation chamber and monitoring system.

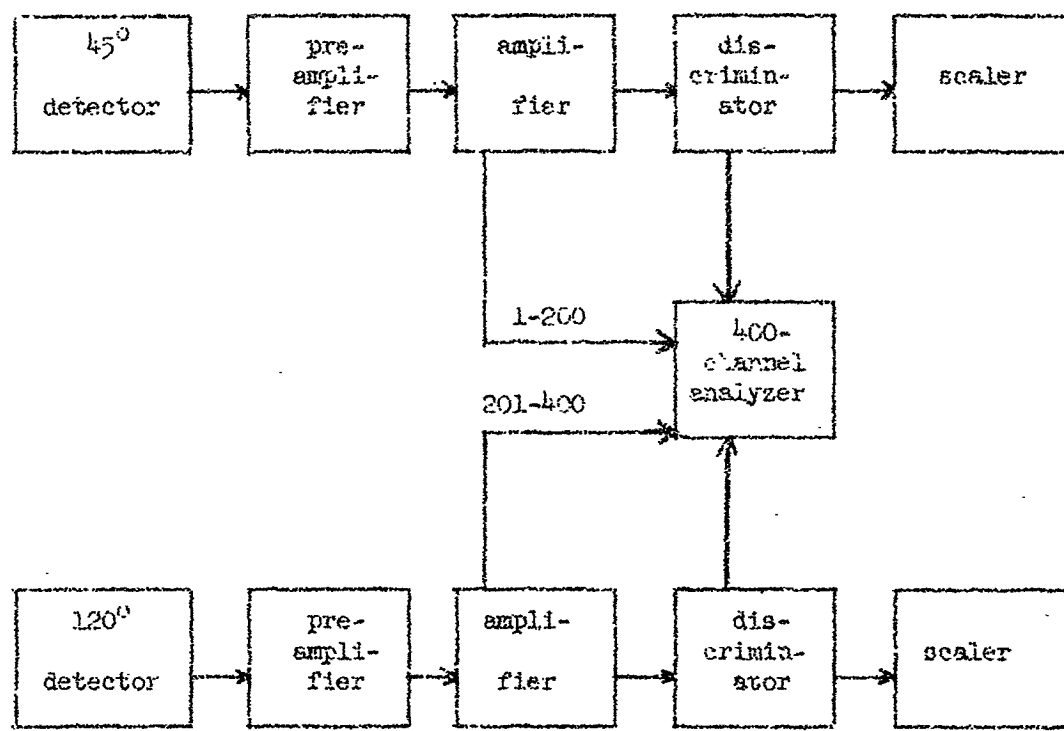
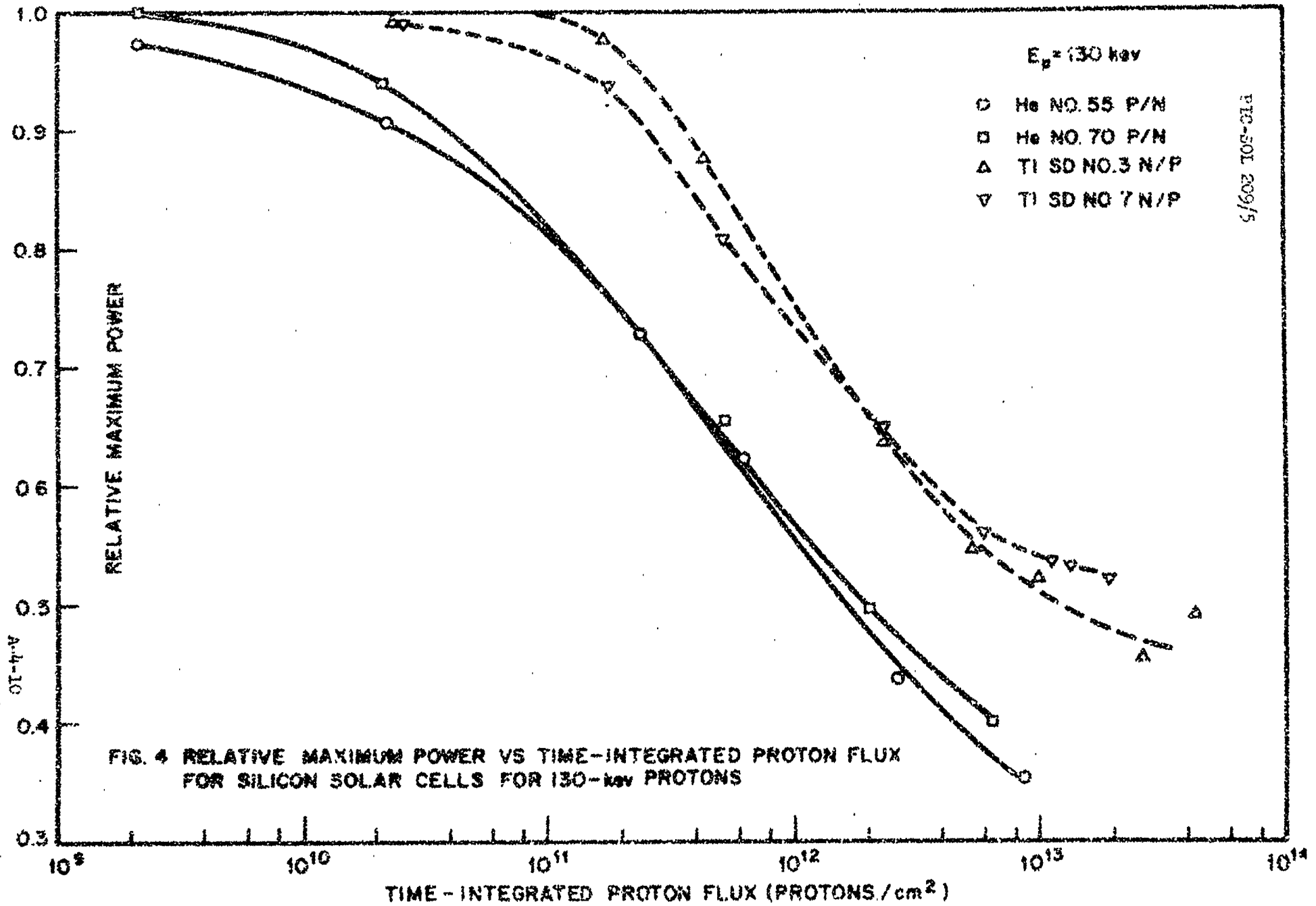


Fig. 3. Block diagram of electronics used in the proton-monitoring system.



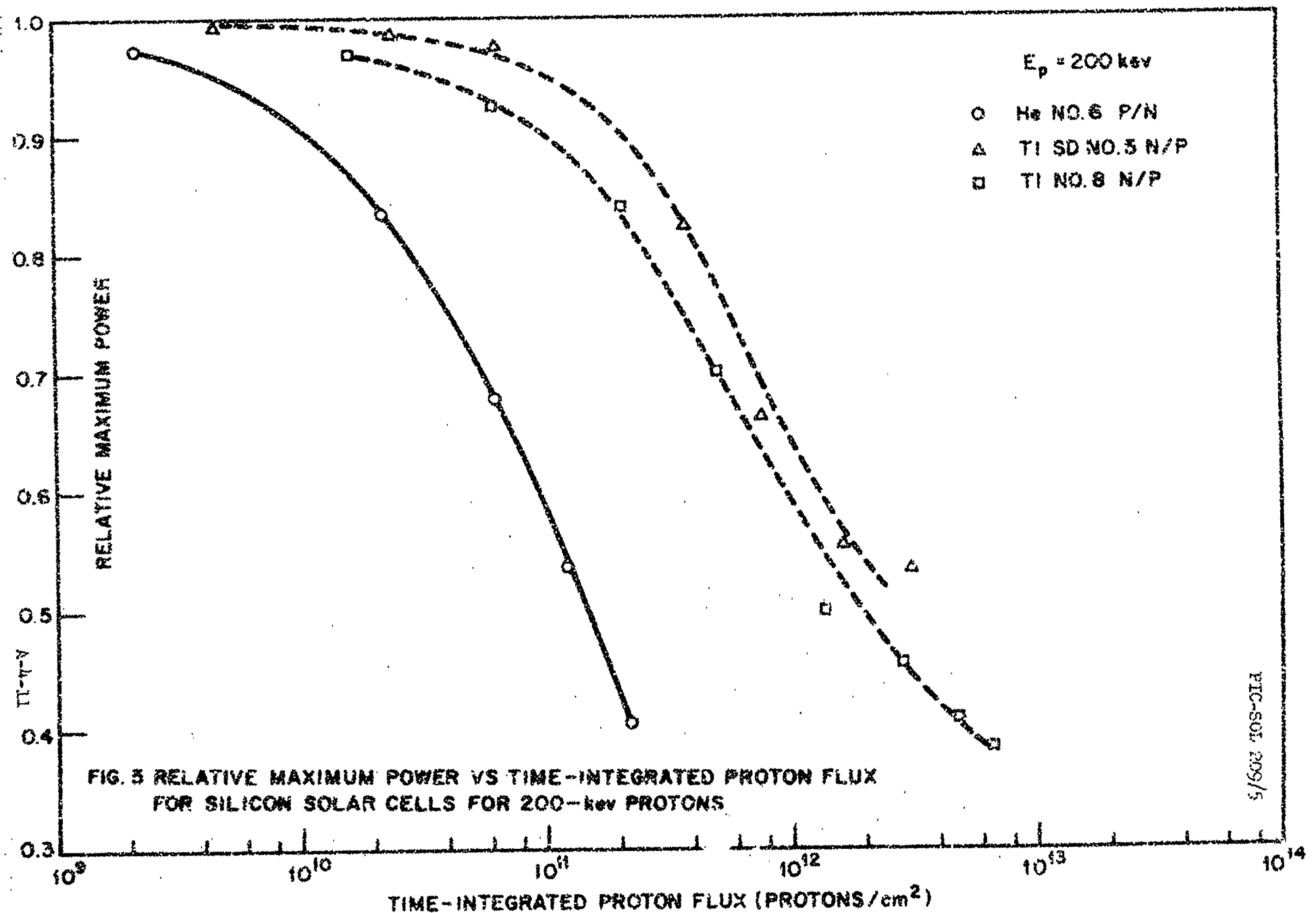
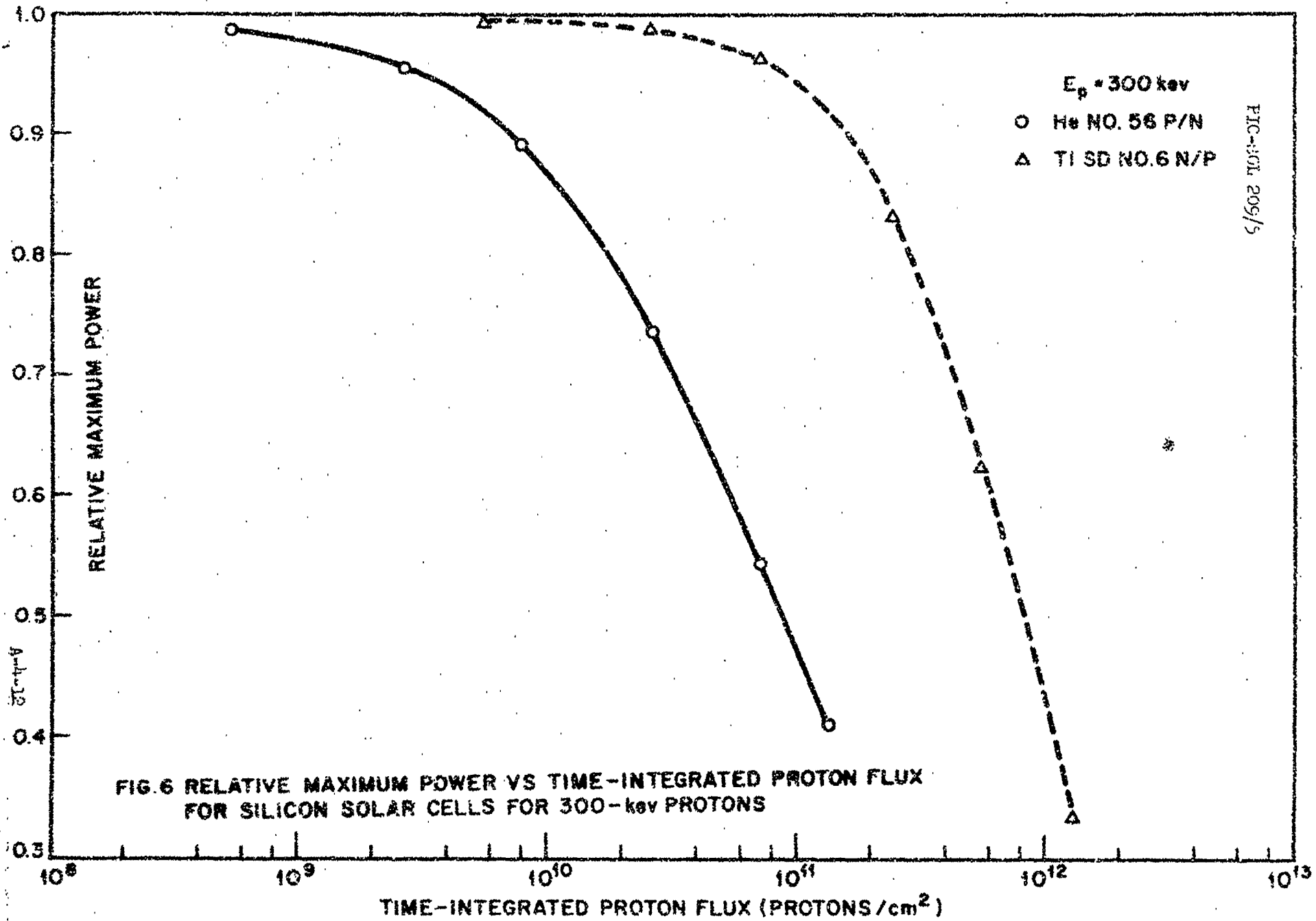


FIG-532 6/6/65



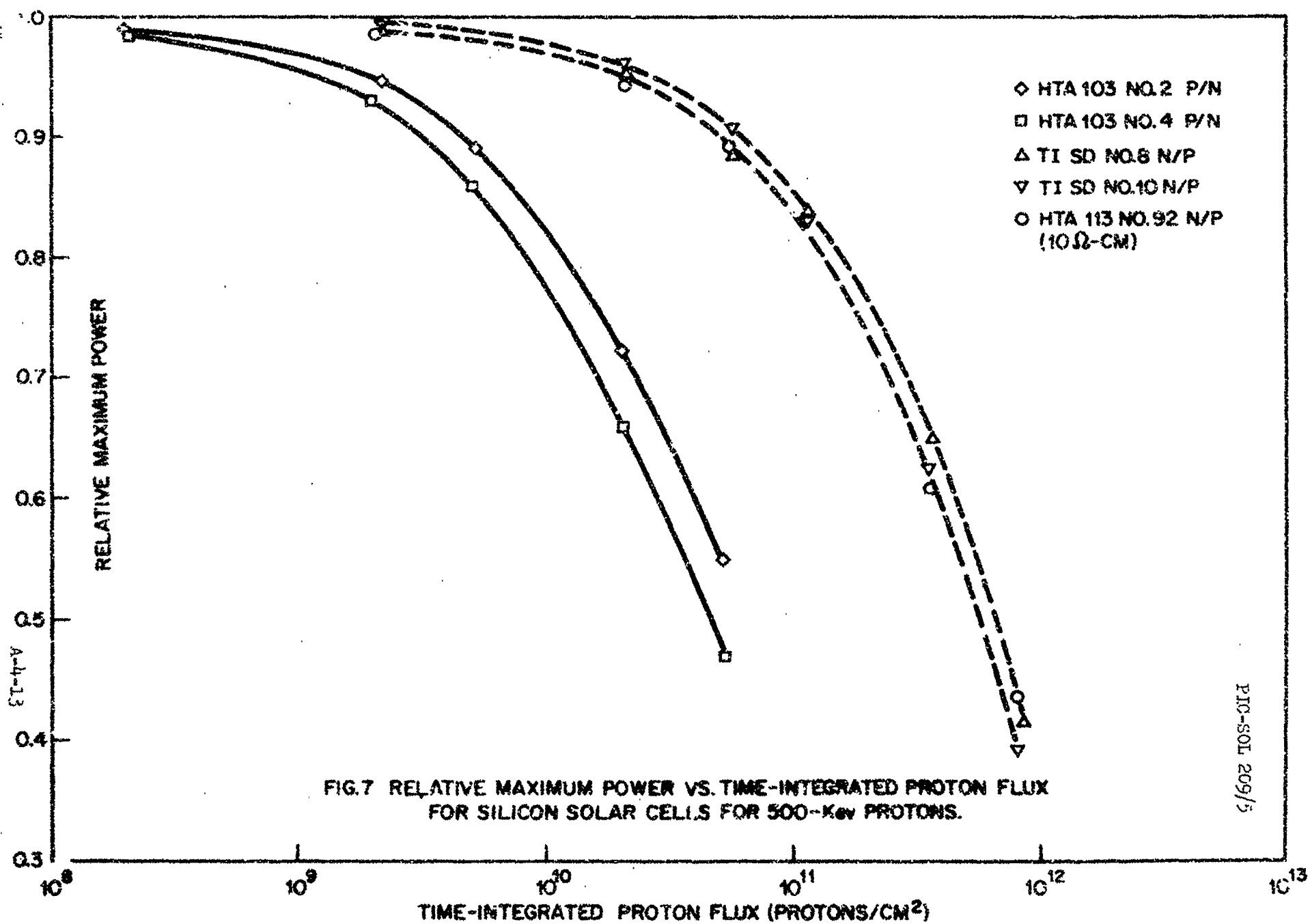


FIG. 7 RELATIVE MAXIMUM POWER VS. TIME-INTEGRATED PROTON FLUX
FOR SILICON SOLAR CELLS FOR 500-Kev PROTONS.

PIC-SOL 209/3

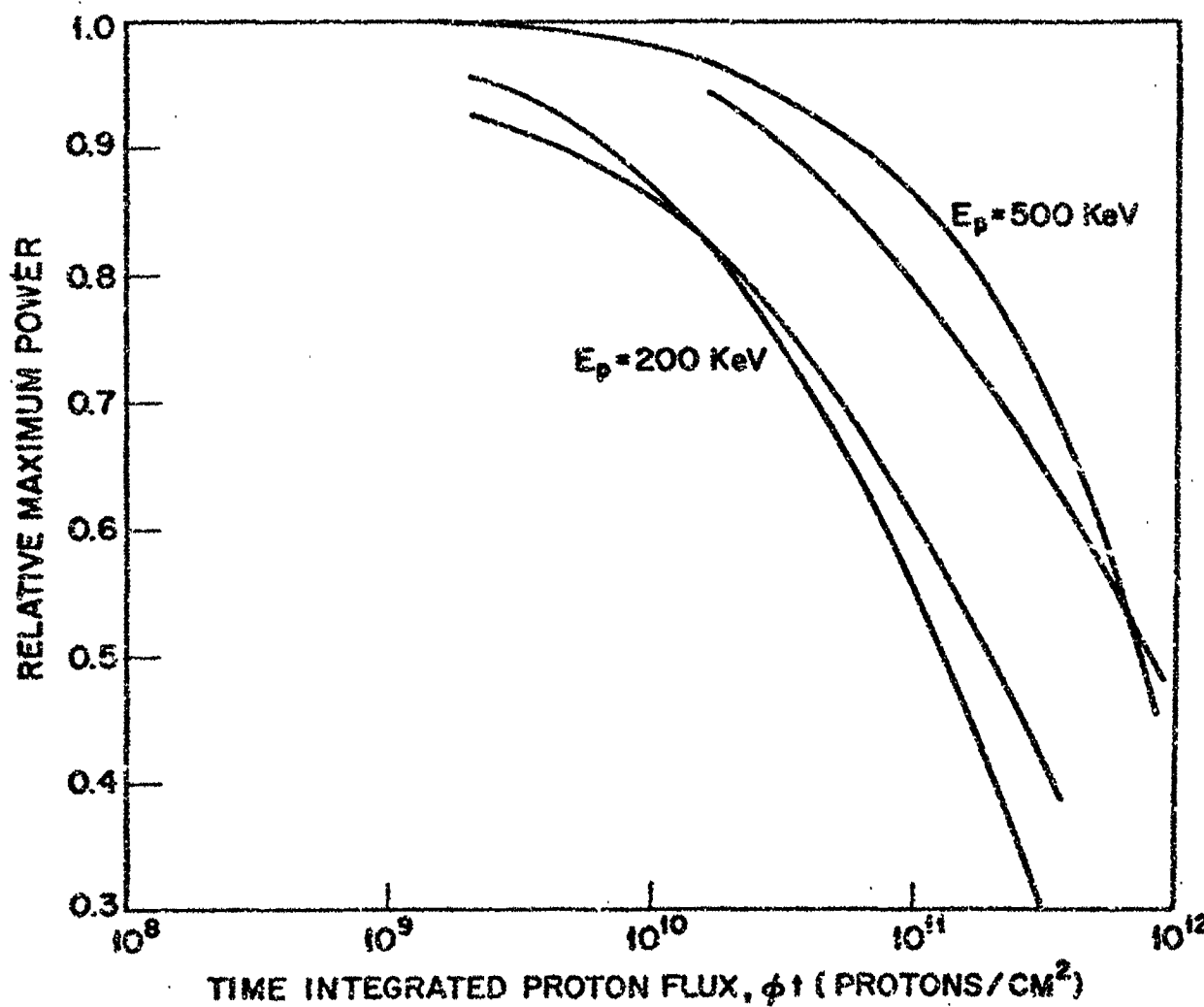


FIG. 8 RELATIVE MAXIMUM POWER VS TIME INTEGRATED FLUX
FOR GaAs SOLAR CELLS FOR 200-AND 500-KeV PROTONS)

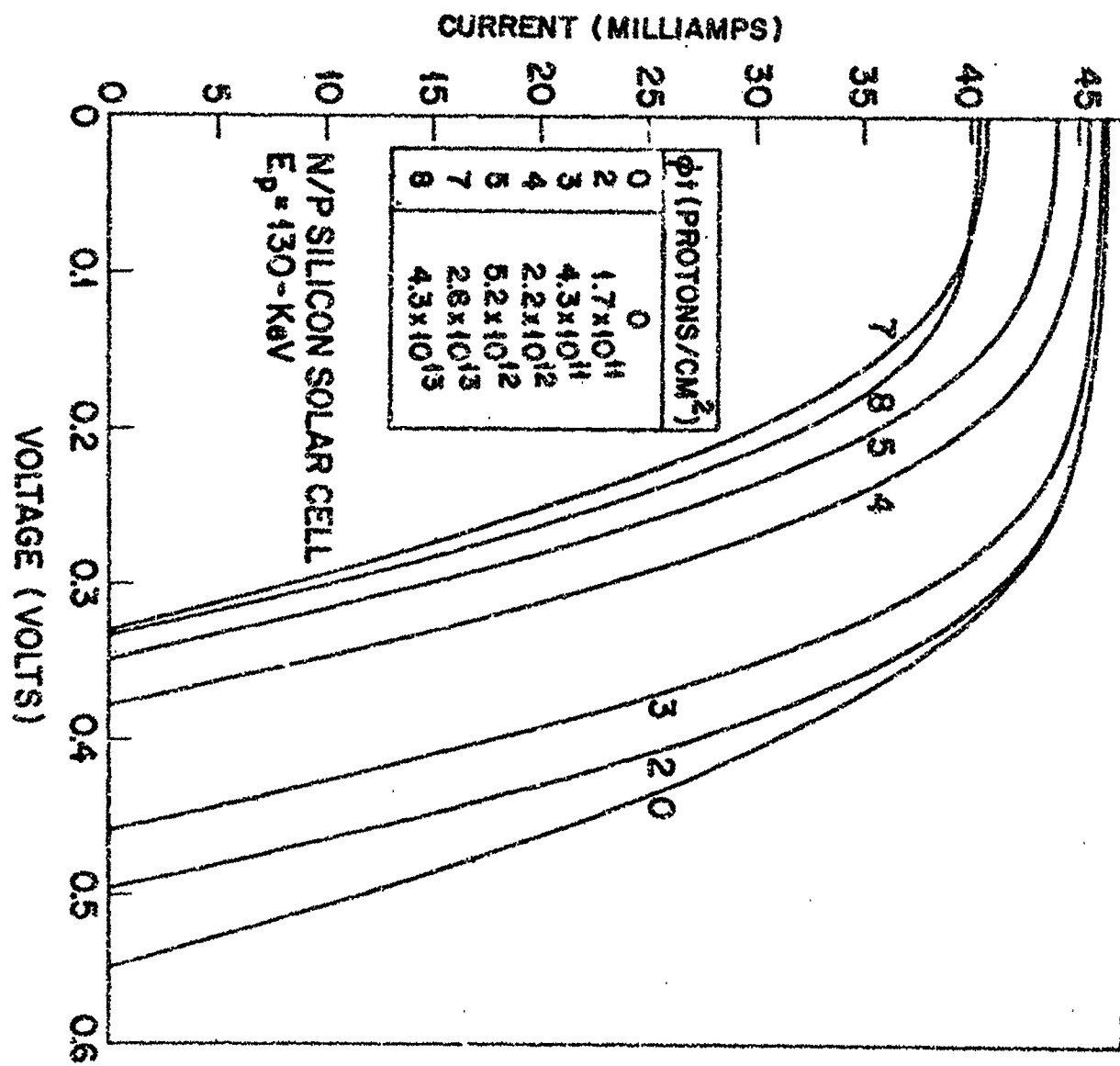


FIG. 9 THE EFFECT OF 130-KEV PROTON IRRADIATION
ON CURRENT-VOLTAGE PROFILES

A-4-16

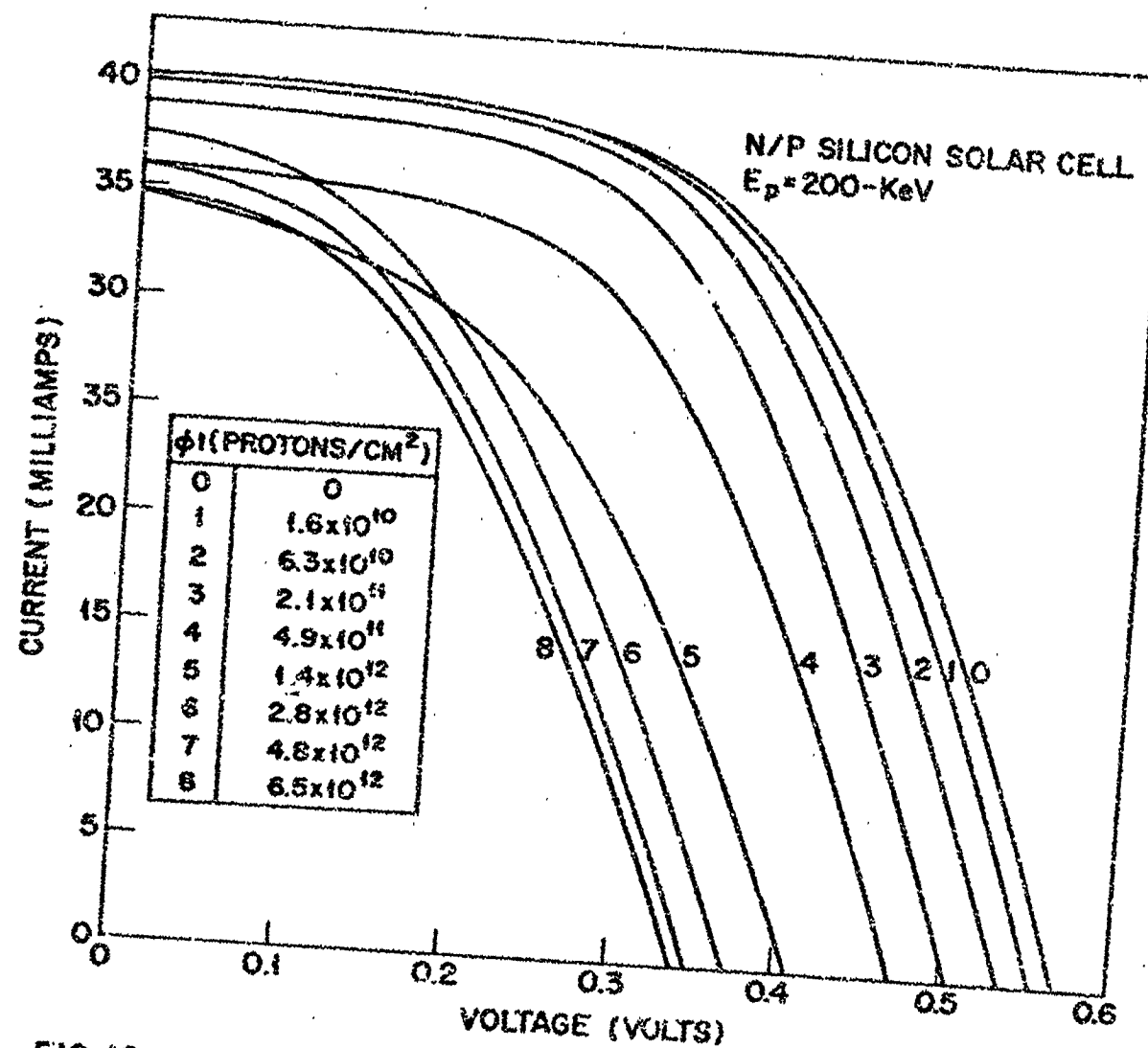


FIG. 10 THE EFFECT OF 200-KeV PROTON IRRADIATION
ON CURRENT - VOLTAGE PROFILES

A-4-17

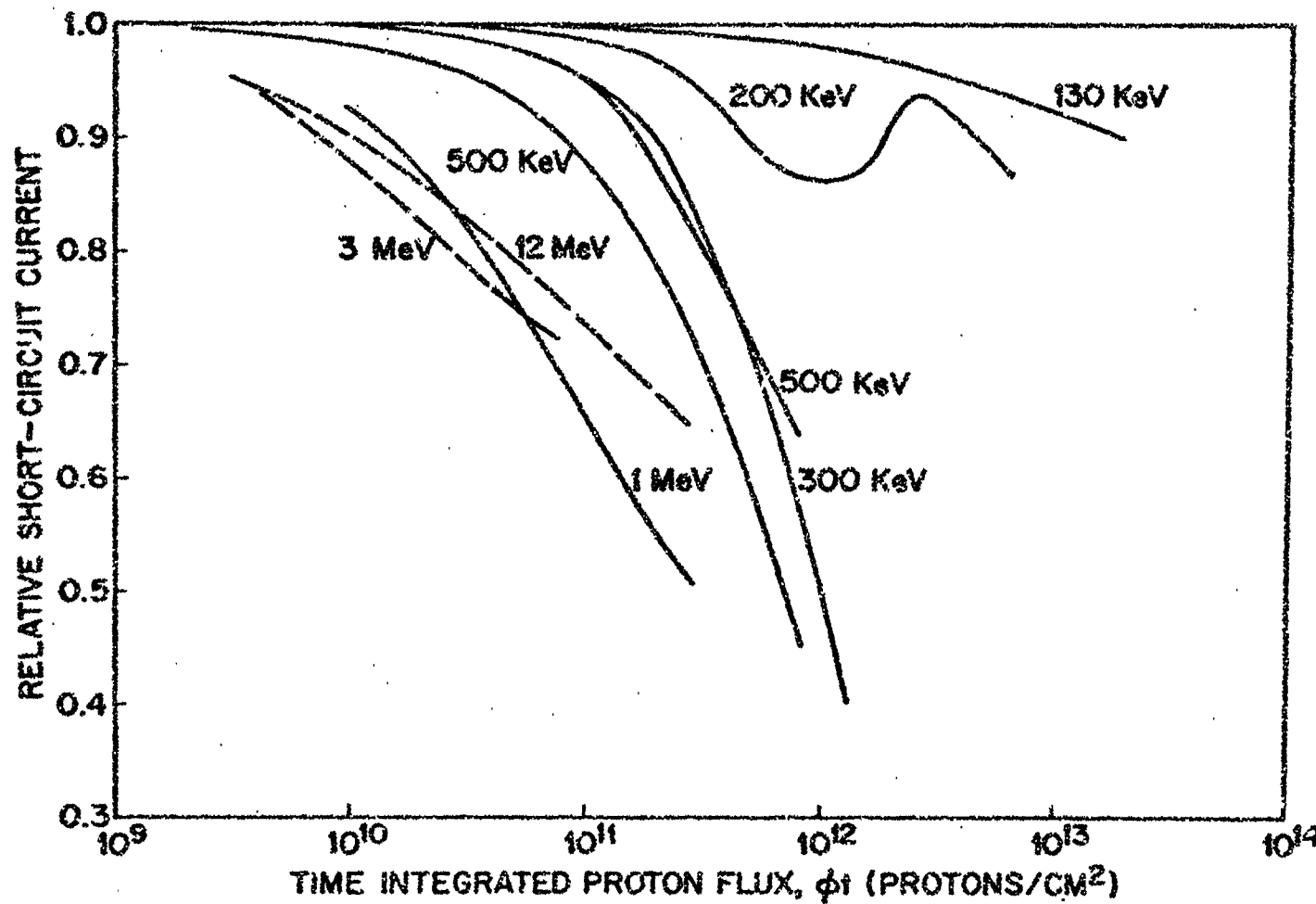


FIG. 11 RELATIVE SHORT-CIRCUIT CURRENT VS TIME INTEGRATED FLUX FOR N/P SILICON SOLAR CELLS IN THE PROTON ENERGY RANGE 130-KeV TO 12-MeV

209/5

A-4-18

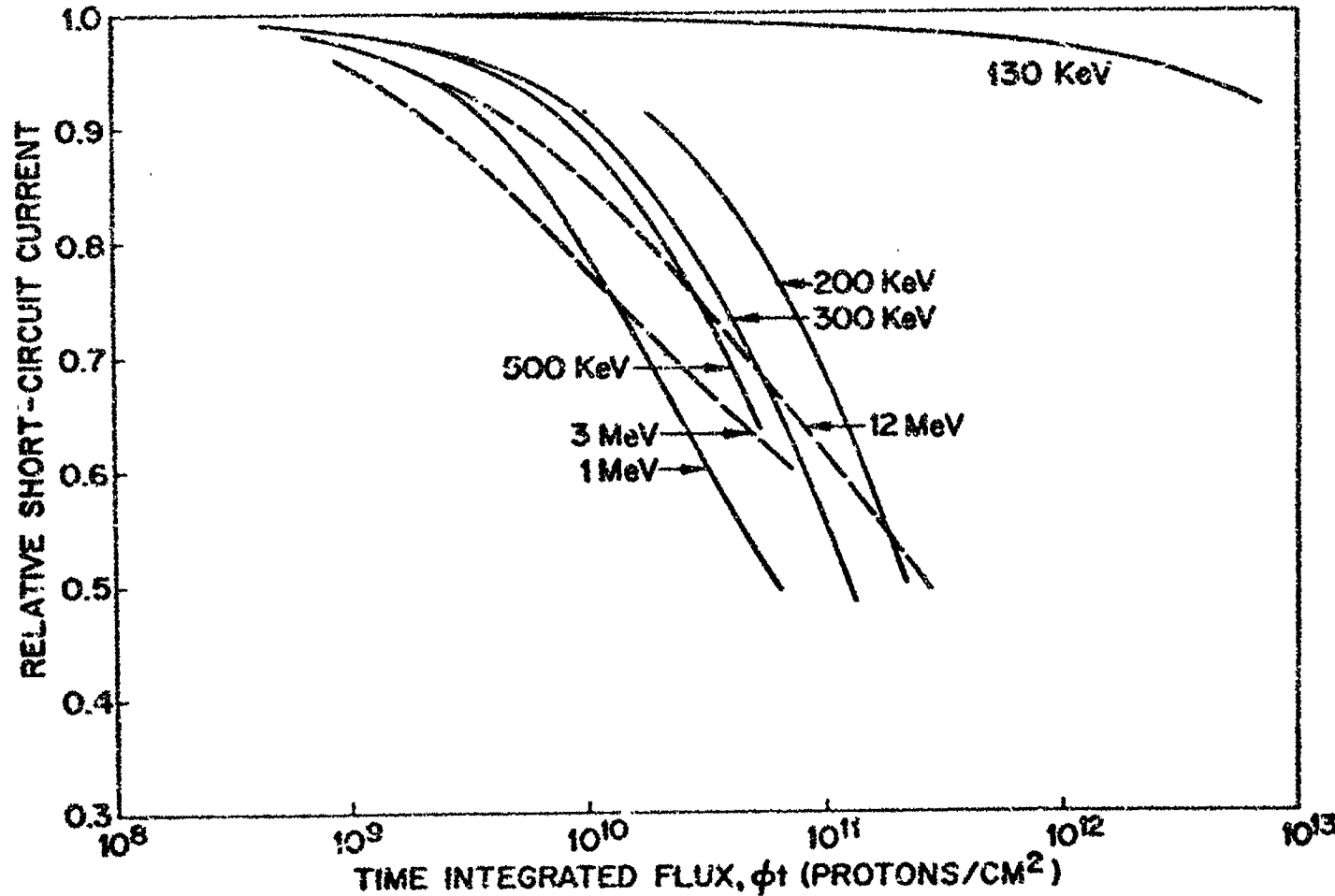


FIG. 12 RELATIVE SHORT-CIRCUIT CURRENT VS TIME INTEGRATED FLUX
FOR P/N SILICON SOLAR CELLS IN THE PROTON ENERGY RANGE
130-KeV TO 12-MeV

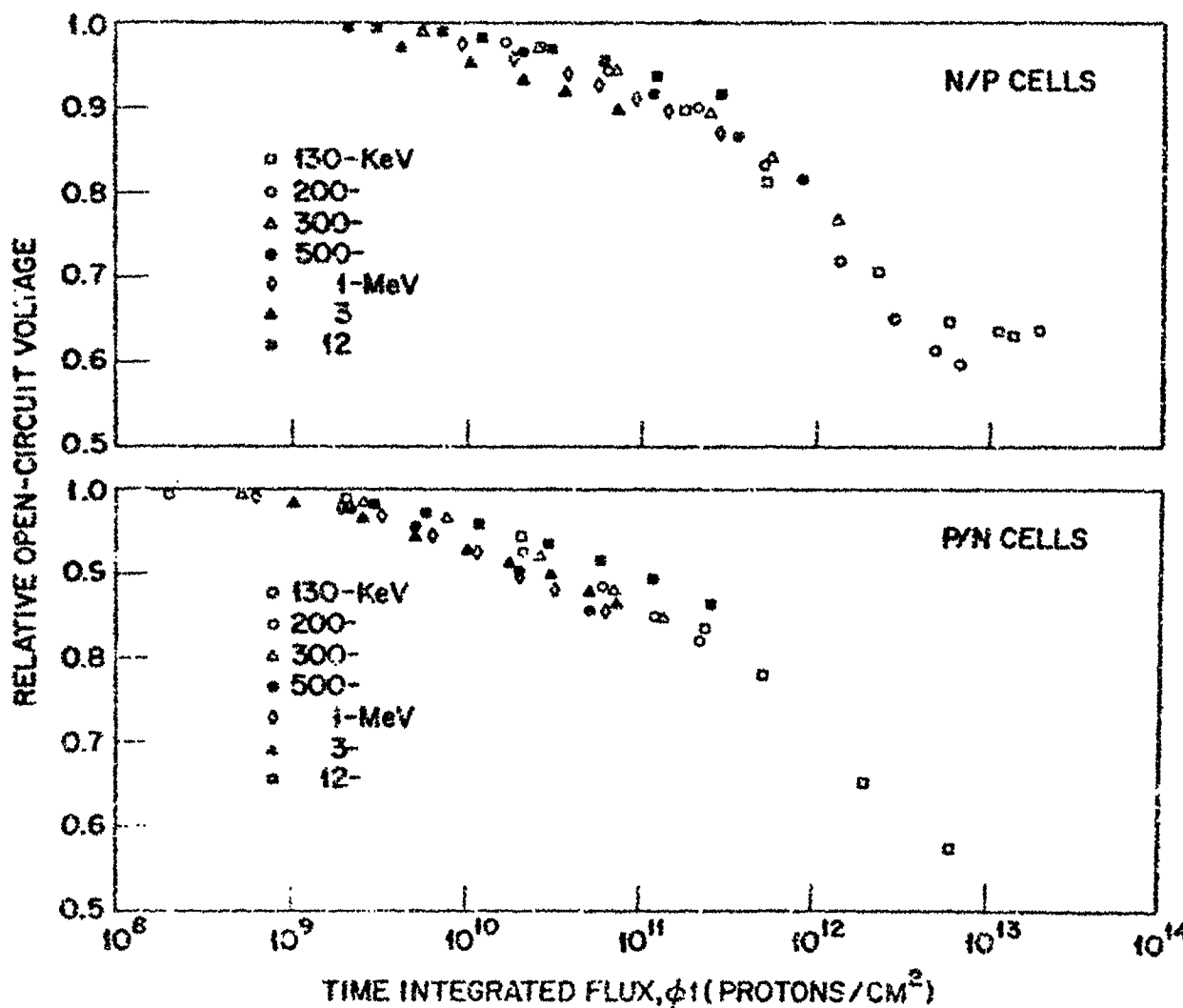


FIG. 13 RELATIVE OPEN-CIRCUIT VOLTAGE VS TIME INTEGRATED FLUX
FOR SILICON SOLAR CELLS IN THE PROTON ENERGY RANGE
130-KeV TO 12-MeV

Table 1.

Comparison of the Results Obtained With the LMSC Sun Simulator and the Tungsten-Water Light Source*

(Note: Only one representative cell for each case is presented)

(Note: P/P_0 = ratio of maximum power to initial maximum power)

Cell	Type	Proton Energy (MeV)	ϕ_t ($p/cm^2/sec$)	LMSC Sun Simulator P/P_0	Tungsten-Water P/P_0
He #70	P/N	.13	6.4×10^{12}	.424	.401
He #60	F/N	.20	2.2×10^{11}	.490	.406
H #56	F/N	.30	1.4×10^{11}	.507	.409
ETA 103 #4	P/N	.40	5.2×10^{10}	.574	.471
H #1A	P/N	1.0	6.5×10^{10}	.529	.392
H #4A	P/N	3.0	5.2×10^{10}	.612	.450
H #2167	P/N	12.0	2.7×10^{11}	.570	.426
<hr/>					
TI SD #3	N/P	.13	4.2×10^{13}	.394	.489
TI #8	N/P	.20	6.5×10^{12}	.352	.386
TI SD #6	N/P	.30	1.3×10^{12}	.396	.335
TI SD #10	N/P	.50	8.1×10^{11}	.479	.391
TI #2	N/P	1.0	2.8×10^{11}	.537	.424
TI #4	N/P	3.0	7.2×10^{10}	.709	.619
TI #14	N/P	12.0	2.8×10^{11}	.690	.623
<hr/>					
GaAs #201	F/N	.20	3.5×10^{11}	.374	.364
GaAs #203	P/N	.50	8.5×10^{11}	.453	.484

*Care should be taken with any interpretation of these data due to annealing of damage observed at the low energies¹.

DISCUSSION

MR. WYSOCKI - RCA: If you extend my model to higher energies, assuming that there is a Rutherford introduction rate, then you find that the shift in the curve comes at around 3 Mev.

LOFERSKI - BROWN UNIVERSITY: What types of cells did you use in your experiments? Which ones showed the double reversal?

MR. LODI: Unfortunately, we didn't have exactly the same types of cells all the way through. These experiments were done over a number of years, and quite a variety of cells were represented. However those particular ones were the newest type of n-on-p 1 ohm-cm., approximately 0.5 micron junction depth.

LOFERSKI - BROWN UNIVERSITY: Did all the n-on-p cells show this double reversal?

MR. LODI: We irradiated two such cells. Only one was bombarded to a large enough dose to show this double reversal. The other was not bombarded to as large a dose, but showed a definite tendency to go up to a second peak.

QUESTION (NO NAME): Under what light sources were the short circuit currents measured and would a different light source have given you different results? Also, when you showed the open circuit voltage, was this under a constant light source or was the light source adjusted for maximum short circuit current conditions?

MR. LODI: First of all the IV curves were plotted using a tungsten lamp with a water filter. We have also results for before and after using a Lockheed sun simulator. However, the actual curves as a function of integrated flux were taken at the facility in vacuum using a water filtered tungsten lamp. The energy was kept constant for all the cells. The lamp was set from a standard cell, and was then checked intermittently to be sure that the standard cell output was constant. The sun simulator does show some indication that at high energies the output under sunlight is greater than under the tungsten light. For lower energy protons the results are either that outputs under tungsten and sunlight are the same, or sunlight output is a little less than tungsten output.

PIC-S-L 203/5
Section A-5

N64-29151

THE ENERGY DEPENDENCE OF ELECTRON DAMAGE
IN SILICON

Presented by

R. G. Downing

TW Space Technology Laboratories

One Space Park

Redondo Beach, California

2 June 1964

THE ENERGY DEPENDENCE OF ELECTRON DAMAGE IN SILICON

R. G. Downing, J. R. Carter, J. M. Denney
TRW Space Technology Laboratories
Redondo Beach, California

Introduction

Because of the importance of electrons in the energy range of 1 Mev and above, a series of experiments were conducted in February and March of 1963 to compare the experimentally observed electron energy dependence with theoretical predictions based on classical relativistic Coulomb scattering laws and simple displacement theory. These experiments, conducted at the General Atomic linear electron accelerator facilities in San Diego, indicated that p on n silicon solar cells and gallium arsenide solar cells agreed quite well with the theoretical predictions^{1,2}. However, n on p silicon solar cells were observed to exhibit damage rates greatly in excess of those predicted by theory as a function of increasing electron energy. Although the data obtained in these initial experiments confirmed the steep energy dependence of electron radiation damage for n on p silicon solar cells, the data were not adequate for accurate power supply design calculations due to lack of sufficient statistical data and lack of information on the dependence of this effect on base material resistivity. In addition, an insufficient number of specimens were obtained for laboratory study in the determination of the energy levels and defect mechanisms responsible for the observed departure from existing theory.

Due to the increasing use of the more radiation-resistant n on p high resistivity silicon solar cells in the construction of satellite solar cell power supply systems, a third series of experiments were performed in May 1964 at the General Atomic linear electron accelerator facilities. The objectives of this third series of experiments were: (1) to obtain statistically significant and accurate data on the energy dependence of electron radiation

damage, (2) to determine the effect of resistivity on the damage rate and energy dependence, and (3) to obtain added specimens and information for further analysis of the energy levels and defect mechanisms responsible for electron radiation damage in silicon. The purpose of this paper is the presentation of the results of these experiments. The next section describes the conduct of the experiments; Section III presents the results and analysis of the data, and Section IV presents the conclusions based on the data obtained in this series of experiments.

Description of Experiments

In this section a description of the experiments and experimental techniques will be presented. Subjects to be covered include the description of the test specimens, the measurements performed before, during, and after the experiments, the beam diagnostics used to determine the radiation environment, and the techniques used to analyze the data and determine the energy dependence of the damage characteristics.

Test Specimens

The test specimens consisted of both p on n and n on p silicon solar cells and bulk n-type and p-type silicon material. The p on n silicon solar cells used in this experiment were commercial, off-the-shelf Hoffman 0.2 to 2.0 ohm-cm cells of nominal 9 per cent efficiency. These cells are from the same lot of cells that were used in the previous two high energy electron experiments and, hence, serve as a comparison with previous experiments. The n on p silicon solar cells were specially constructed devices in which base material resistivity was controlled and selected to within plus or minus 5 per cent for the reduction of data scattering due to variations about nominal resistivity. The resistivities were actually measured after the final diffusion prior to the application of contacts. The resistivities used for the n on p cells were 1.3, 3.3, and 10.6 ohm-cm. In addition, some 21 ohm-cm n on p silicon solar cells were tested at 1 Mev but were not available for the higher energy experiments. Several n on p 1.2 ohm-cm

Western Electric cells from the same lot used in the previous experiments were included in the experiments for comparison with previous data and also for comparison with the 1.3 ohm-cm n on p Hoffman solar cells.

In addition to the solar cells, 150 ohm-cm p-type and 100 ohm-cm n-type silicon were included. These specimens were pre-cut to the conventional six arm bridge configuration for post-irradiation measurements of Hall effects. These measurements of Hall effects, in addition to measurements of diffusion length versus temperature on the solar cell specimens, are analyzed to obtain information on the energy levels and defect mechanisms induced as a function of electron energy.

Measurements

A large number of measurements were performed on all specimens prior to, during, and after the irradiations. Some measurements were performed during the actual conduction of the irradiation at the linac site. Other measurements, such as minority carrier diffusion lengths and Hall effects, which could not be conducted at the linac site were performed at the STL laboratories immediately after completion of the irradiations. The complete series of measurements will be described in this section.

Minority carrier diffusion lengths were measured on each solar cell before and after irradiation. These measurements were obtained using the STL 1 Mev Van de Graaff. This technique for diffusion length measurement has been described in the literature³ and consists of relating the observed steady state short circuit current produced with ionizing radiation to the minority carrier diffusion length of the bulk material. Minority carrier lifetime can be obtained from this measurement using the diffusion coefficient, D, of the carriers in the material of interest. With these diffusion length measurements, a commonly used damage constant, known as a K value, is obtained with the following equation:

$$\frac{1}{L^2} = \frac{1}{L_0^2} + K \frac{T}{I} \quad (1)$$

which reduces to

$$K = \frac{1}{\Phi} \cdot \frac{1}{L^2} - \frac{1}{L_C^2} \quad (2)$$

The principal requirement for this K value to be meaningful is that a log-log plot of diffusion length versus integrated flux exhibit a -1/2 slope. If this condition is not met, then different K values will be obtained on any given cell depending upon the integrated flux chosen to calculate the K value. Therefore, preliminary experiments are always conducted with the 1 Mev STL Van de Graaff on a given lot of cells before performing an off-site experiment to insure that the cells follow these characteristic degradation equations based on simple displacement theory.

Minority carrier diffusion lengths were also measured indirectly at the linac site through the established relation between short circuit current and minority carrier diffusion length for a given lot of cells. This relationship between short circuit current and minority carrier diffusion length is established for any given lot of cells with the 1 Mev Van de Graaff before proceeding to an off-the-site experiment. Minority carrier diffusion length values obtained with this indirect technique are then compared with minority carrier diffusion lengths measured directly after the completion of the experiments. In addition, all cells irradiated at the higher electron energies are checked for injection level dependence of the minority carrier diffusion length over a range extending from approximately one-sun illumination down to the limits imposed by minimum Van de Graaff beam currents and signal-to-noise levels. This injection level range covers approximately six orders of magnitude. Although it is predicted by Hall, Shockley-Read recombination statistics that minority carrier lifetime, and hence minority carrier diffusion length, must exhibit injection level dependence, the injection level region in which this dependence occurs is important in the analysis of the data to insure that measurements made at different injection levels be comparable.

I-V characteristics were obtained on all solar cells with a 2800°K unfiltered tungsten illumination source. The approximate sunlight equivalent intensity of this illumination source is 110 to 130 mw/cm². Due to the differences between the spectral content of solar illumination and 2800°K tungsten illumination and the spectral differences in various types and manufacturers' solar cells, it is not possible to maintain constant absolute intensity on the light table and at the same time specify constant sunlight equivalent illumination. Therefore, this illumination source is absolutely calibrated and this calibration has been maintained over the last four years for purposes of comparing data on a large number of different experiments. As a result, the actual sunlight equivalent intensity will vary between different types of cells depending upon their initial diffusion lengths and surface characteristics. The choice of the 2800°K tungsten illumination is based on its ease of reproducibility and maintenance over a long period of time and the fact that it amplifies the base region diffusion limited portion of the solar cell output which is most directly affected by charged particle irradiation, and minimizes differences due to variations in surface characteristics due to the lack of short wavelength energy in the tungsten spectrum. Although no solar illumination measurements were obtained on these cells, previous measurements obtained in a large number of experiments allow reasonable predictions of performance under solar illumination based on the tungsten illumination data.

From the I-V characteristics which are obtained after each individual radiation exposure, plots of short circuit current density, J_{sc} , versus integrated electron flux are obtained. These short circuit current densities are expressed in terms of ma/cm² for a 90 per cent active area device. Hence, devices with different grid structures than those of the standard device with a 1 mm wide collector strip running the long edge of the cell are normalized to this configuration. Once again, this normalization to a standard device is necessary in order to perform meaningful comparisons of data on different types of cells irradiated over the years in different experiments. For example,

short circuit current density in terms of ma/cm^2 for a $1 \times 2 \text{ cm}$ cell with the collector strip located along the length of the cell would be obtained by simply dividing the observed short circuit current by a factor of two, whereas short circuit current density for a cell with the collector strip located along the short edge would be obtained by dividing the observed short circuit current by a factor of 2.11. The I-V curves are also used to obtain degradations of open circuit voltage and maximum power output as a function of integrated flux.

In order to obtain a damage constant from the plots of short circuit current degradation versus integrated flux for comparison with K values and for determination of energy dependence, a value known as the critical flux is determined. Critical flux was defined several years ago as integrated flux required to reduce the short circuit current 25 per cent. This amounted to a reduction in short circuit current under 2800°K tungsten illumination from $25 \text{ ma}/\text{cm}^2$ initial to $19 \text{ ma}/\text{cm}^2$ for a cell with a minority carrier diffusion length of 100 microns under an illumination of approximately $110 \text{ mw}/\text{cm}^2$ sunlight equivalent. During the past few years, however, typical minority carrier diffusion lengths have been observed to range from 175 microns to 225 microns. Since the normal condition is for the minority carrier diffusion lengths to degrade to equal values independent of original values for a given resistivity and type of material, the definition of critical flux as integrated flux required to produce a short circuit current of $19 \text{ ma}/\text{cm}^2$ has been retained, even though it now represents more than 25 per cent degradation under tungsten illumination for current state-of-the-art solar cells. This approach allows meaningful comparison of data obtained on current state-of-the-art devices and data previously obtained over the past several years where original output characteristics were somewhat lower due to lower minority carrier diffusion lengths. Since K in Eq. (2) is inversely proportional to integrated flux, the reciprocal of the critical flux is plotted versus energy for comparison with K values. As in the case previously discussed with minority carrier diffusion length measurements, specimens from each individual lot of cells are irradiated with

1 Mev electrons prior to any off-the-site irradiations to insure that the slope of the short circuit current degradation characteristic follows the $6.25 \text{ na/cm}^2\text{-decade}$ slope characteristic of normal solar cells illuminated under these conditions.

After completion of the series of experiments at the linac site, further measurements were performed in the laboratory to delineate the energy levels responsible for the observed degradations. Hall effects measurements on the p-type and n-type specimens are performed on specimens irradiated at each energy at several integrated fluxes to determine the energy levels responsible for majority carrier trapping. In addition, minority carrier diffusion length versus temperature measurements are obtained using the Van de Graaff to illuminate a solar cell placed in a cryostat. From these data, dependence of minority carrier lifetime on temperature is obtained. This technique has the advantage over direct measurements of minority carrier lifetime with pulsed techniques in that the effects of trapping levels are removed due to the steady state conditions of the measurement as opposed to the conventional transient techniques for measuring minority carrier lifetime. These data are then analyzed using Hall, Shockley-Read statistics in an effort to fit the observed slopes with the particular energy level responsible for minority carrier recombination.

Dosimetry

In order to obtain quantitative, accurate data, particular attention was given to measurements of beam energy, distribution, and intensity. Electron beam energy was determined by General Atomic personnel with a calibrated steering magnet. This magnet had been previously calibrated through a series of range-energy relationships to within plus or minus 2 per cent. Magnet current was supplied by a regulated power supply insuring a constant magnetic field through the steering magnet. Any appreciable drift or change in beam energy due to operating characteristics of the accelerator would result in loss of beam at the port where the experimental apparatus was located. Corrections were applied for energy loss of the

beam in traversing the exit port window and air in the determination of the energy incident upon the test specimens.

Beam spreading was accomplished with quadripole focusing magnets and air scattering to produce a beam spot large enough to accommodate the test specimens. Polarcid film was used to determine beam position and distribution over the beam area and to position the test specimens. The Polaroid film was used as a coarse indicator of beam distribution, and solar cell degradation as a function of position was used as a more accurate determination of beam distribution. The quadripole magnets were driven with regulated power supplies and found to be quite stable. Due to the small diameter of the accelerator drift tubes, however, there was a practical limit to the maximum beam spot size that could be produced in the drift tubes. To obtain further defocusing, the experimental apparatus was located a sufficient distance from the exit port window to take advantage of small angle air scattering for further improvement in beam size and distribution. Particular distances between the experimental apparatus and the beam exit port window were determined by the energy of the beam and ranged from six inches to three feet. In all of the experiments the beam area exceeded 25 cm^2 at half of the peak intensity. Only the center 4 cm^2 of the total beam was used for sample irradiation wherein intensity gradients were less than 5 per cent.

Electron intensity was monitored with a Faraday cup of conventional design. The inner sensing chamber was constructed of copper 50 Mev thick and was mounted in a larger evacuated chamber which was fore pumped and trapped to a pressure of less than 10^{-3} Torr. The bottom or target area of the Faraday cup contained a $\frac{1}{4}$ Mev thick aluminum plate to reduce the back-scattered electron component to a minimum. In addition, a copper back-scatter shield was utilized to reduce the back scatter solid angle a factor of ten. Additional back scatter control was exercised through the application of grid bias directly above the entrance aperture to the inner sensing chamber. Application of grid voltage from -400 to +400 volts indicated that the low energy back-

scattered component had been reduced to less than 2 per cent and further that forward scattering from the 0.005 inch aluminum vacuum window of the Faraday cup was less than 1 per cent. Calculations of the high energy back-scatter component for the geometry and materials used here indicate an error of less than 1 per cent for this component. An estimate of the over-all accuracy of the Faraday cup is a maximum error of less than 5 per cent. Comparisons of beam current with apparatus utilized by General Atomic personnel were in agreement to within better than 3 per cent. The output of the Faraday cup was fed directly to an integrating amplifier system which measured both current and integrated charge to an accuracy of 1 per cent. This type of instrument is ideal for accepting high impedance inputs such as Faraday cups since it presents essentially zero input impedance to the Faraday cup and eliminates errors due to leakage currents.

Experimental Techniques

The test specimens were mounted in the central 4 cm² area on thin aluminum plates. These plates in turn were placed in a jig indexed directly in front of the Faraday cup, and integrated flux measurements were obtained simultaneously with the irradiation of the test specimens. Each group of specimens was exposed to a predetermined integrated flux and removed for post-irradiation measurements, then re-inserted in the beam for further irradiations. When a sufficient number of irradiations had been performed to define a straight line function of the degradation of the short circuit current with the logarithm of the integrated flux, the specimens were removed and stored for later post-irradiation measurements. A minimum of four specimens of each individual type was tested at each energy in an alternating sequence such that if serious accelerator or equipment changes occurred, the data would exhibit corresponding deviations. In the event deviations or unexpected behavior occurred, machine characteristics would be examined and, if necessary, an adequate number of additional cells would be tested to determine if the deviation were machine-produced or were caused by deviations in the test specimens themselves, such as deviations in resistivity.

Beam alignment and distribution were continuously checked throughout each series of experiments at any given energy by Polaroid film. In addition, beam energy measurements were performed utilizing the calibrated steering magnet before and after each series of runs to determine any deviation of beam energy throughout any given series of irradiations.

Pre-irradiation Experiments

As mentioned in previous sections, a complete series of 1 Mev electron radiation degradations were performed on sample cells from each lot of cells prepared for the high energy experiments. The purpose of these irradiations was twofold: (1) to acquire degradation characteristics in the energy range from 0.4 to 1.0 Mev for each particular group of cells and (2) to qualify the groups of cells as to linearity and slope of both the short circuit current and minority carrier diffusion length degradation characteristics. The experimental conditions utilized on the 1 Mev STL Van de Graaff experiment are much simpler than those required at the higher energies and further are described in detail elsewhere⁴. In essence, the accuracy with which beam energy, distribution, and intensity can be determined with this machine is better than plus or minus 2 per cent. For these reasons and also because of the ready availability of this machine for further calibrations and checks as required, all data are normalized and analyzed to 1 Mev data where necessary or desirable.

Experimental Results

Separate linac experiments were conducted at four energies: 40.0 Mev, 16.4 Mev, 6.4 Mev, and 2.7 Mev. Included with these data and experimental results are additional data obtained on the STL Van de Graaff at 1.0 Mev, 0.6 Mev, and 0.4 Mev. The resulting electron energy dependence of the radiation damage is determined by utilizing both K values and reciprocal critical fluxes. The K values were obtained from diffusion length measurements with the Van de Graaff accelerator and with the calibrated light source. The reciprocal critical flux determinations were acquired from short circuit

current degradation characteristics. In addition, several energy levels were obtained from both resistivity dependence of the radiation damage and Hall effects measurements on bulk silicon. Additional measurements of minority carrier diffusion length dependence on temperature are currently underway, but these experiments and the subsequent data analysis are not completed at the time of the writing of this paper and, therefore, are not included here but will be considered in detail in future reports. The remainder of this section will be devoted to the presentation of the experimental data and the results of the subsequent data analysis.

Degradation of Solar Cell Output Characteristics

The inclusion of all the raw data obtained in this series of experiments is beyond the scope of this paper; however, these data will be presented in a later NASA Report, Contract NAS5-3805, under which this work was sponsored. Typical data plots will be included, however, to illustrate the type of data obtained and the techniques utilized in their analysis. The final results of the analyses of these data are summarized in Table I. Included in Table I are the values of critical flux, reciprocal critical fluxes, and K values for each cell type at each energy studied. It is from these data that subsequent plots of damage coefficients versus energy were obtained.

Shown in Figure 1 are typical diffusion length degradation curves as a function of electron integrated flux at 1.0 Mev for several types of cells. It should be noted that the data points fit the -1/2 slope, shown as a solid line, quite accurately resulting in a meaningful K value in the qualification of these cells to simple displacement theory as given by Eqs. (1) and (2) in the previous section. Figure 2 presents a typical I-V characteristic versus integrated electron flux at 16.4 Mev. This figure is typical of the actual raw data obtained at the linac site and is the source of subsequent plots of short circuit current density (J_{sc}), open circuit voltage (V_{oc}), and maximum power output (P_{max}) versus integrated electron flux. Shown in Figure 3 is a typical plot of J_{sc} degradation versus integrated flux for cells irradiated

with 2.7 Mev electrons. Note that a minimum of four cells and sometimes six cells of each given type are shown on the curve. The scatter among each individual group of cells is typically less than plus or minus 2 per cent. A standard slope of $5.25 \text{ ma/cm}^2\text{-decade}$ fits all the data quite well. The degradation slope under equivalent sun illumination would be approximately $4.5 \text{ ma/cm}^2\text{-decade}$ for $1 \times 2 \text{ cm}^2$ cells having an active area of 1.8 cm^2 . The Φ_c values shown in Table I are the integrated fluxes required to produce a J_{sc} of 19 ma/cm^2 on plots of this type. A shift in cell type or energy simply represents a lateral shift of the characteristic slope as shown in Figure 3 to the appropriate Φ_c value indicated in Table I. The initial J_{sc} values for these cells lie in the 27 to 29 ma/cm^2 range with corresponding initial minority carrier diffusion lengths in the 175 to 225 micron range.

Shown in Figure 4 and Figure 5 are plots of K versus E and Φ_c^{-1} versus E for the p on n cells tested in this series of experiments. Also shown in these figures are some data obtained in a previous series of experiments. The solid line shown in Figure 4 is identical to the solid line shown in Figure 5 and is determined by a best fit to both the K values and the Φ_c^{-1} values, jointly. The dashed line shown in Figures 4 and 5 represents predictions based on classical Coulomb scattering and simple displacement theory. As is observed, the fit of the experimental data with the predicted energy dependence is reasonably good. It is interesting to note that the high energy tail observed in previous experiments is not evidenced here and was, therefore, most probably due to data scattering through resistivity variances or undetected shift in machine characteristics in the previous experiment.

Figures 6 and 7 show the energy dependence of the K values and the Φ_c^{-1} values for the n on p silicon solar cells tested. The solid lines drawn through the data points are identical in both figures in shape as well as separation. The good fit of the sets of lines to the data indicates agreement in the energy dependence as obtained by K values with that obtained by Φ_c^{-1} values. Further, each line in the set of lines is parallel to each other, indicating that the energy dependence of the degradation of

silicon solar cell characteristics is independent of base material resistivity in this energy range. Shown in both Figures 6 and 7 at 16.4 Mev are data on the older Western Electric cells of the type used in previous experiments. These cells have a resistivity of 1.2 ohm-cm, and therefore are comparable with the 1.3 ohm-cm Hoffman cells. The K values indicate essentially identical values confirming that reproducibility is obtainable with materials from different sources processed at different times by different manufacturers. The agreement is not quite as good in Figure 7 on the basis of Φ_c^{-1} values, but this is anticipated on the basis that manufacturing techniques are continuously improving surface characteristics and over-all collection efficiencies which in turn affect the Φ_c^{-1} values. The dashed curve shown in Figures 6 and 7 indicates the predicted energy dependence based on relativistic Coulomb scattering and simple displacement theory. As evidenced in previous experiments, n on p cells and, hence, p-type silicon depart radically from this relationship since damage rates at 40.0 Mev are approximately a factor of 30 greater than those observed at 1.0 Mev as opposed to a factor of three as predicted by theory.

In all the K values presented in the previous figures, measurements of the dependence of the minority carrier diffusion length on injection level were performed. No injection level dependences of consequence were observed in the carrier density range covered in these experiments, i.e., from one sun illumination level to approximately 10^{-6} sun illumination level. It is anticipated, however, that measurements at higher injection levels would indeed indicate injection level dependences as predicted by Hall, Shockley-Read recombination theory; however, the geometry and characteristics of these solar cells are such that appreciably higher injection levels cannot readily be obtained.

The typically observed degradation in V_{oc} as a function of integrated electron flux, material type, and resistivity is shown in Figure 8. Data scatter of approximately 5 to 10 mv is inherent in these data since solar

cell cooling is provided by blowing ambient laboratory air over the specimens, and the temperature of the ambient air routinely varies 4°C to 5°C depending upon ambient heat loads and time of day. There are several interesting features which appear in these data. The observed degradation fits a straight line with a slope of approximately 40 mv/decade reasonably well in all cases regardless of cell type and resistivity. This degradation rate is considerably in excess of that observed by simply lowering the illumination level an amount corresponding to short circuit current degradation or sliding the original I-V characteristics downward on the current axis to the appropriate short circuit current value. The observed additional degradation in V_{oc} is most likely due to radiation-induced changes in the saturation current I_o and possibly the constant, A, which appears in the exponent of the diode equation. The initial values of V_{oc} and subsequent absolute values of V_{oc} as a function of integrated flux show the anticipated decrease with increasing resistivity. Not observed here, however, are increases in the degradation rate for the higher resistivity material. Actually, this lack of increased degradation rate for the higher resistivities is not surprising at the exposure levels used for these experiments. For example, an exposure of approximately $2 \times 10^{15} e/cm^2$ at 1.0 Mev would be required to introduce active defect concentrations equal to 10 per cent of the original majority carrier concentration in 20 ohm-cm p-type silicon. Since defect concentrations of this magnitude or greater would be required to produce resistivity increases, and hence additional open circuit voltage degradations, the absence of this effect in Figure 8 is expected. Additional exposures beyond $2 \times 10^{15} e/cm^2$ should result in an increase in V_{oc} degradation rates for the higher resistivity cells but adequate beam time for these longer exposures was not available in this series of experiments.

Figure 9 illustrates the effect of resistivity on maximum power output degradation as a function of integrated flux for a random selection of I-V characteristics. These data were obtained by correcting the appropriate I-V

characteristics to equivalent 1.0 Mev integrated fluxes under solar illumination of approximately one sun intensity using a short circuit current degradation rate of $4.5 \text{ mA/cm}^2 \text{-decade}$ as determined by previous experiments⁴. As observed in Figure 9, the maximum power output degradation as a function of integrated flux is noticeably improved at higher resistivities even though the decreased voltages obtained at higher resistivities detracts from the increased radiation resistance of the short circuit current. The large amount of scatter evident in these data is due to the random selection of points and is indicative of what may be anticipated in the actual design of solar cell arrays using large numbers of commercially available solar cells.

Radiation Induced Energy Levels in Silicon

The Hall, Shockley-Read recombination statistics predict, for a given recombination energy level, the dependence of minority carrier lifetime degradation on base material resistivity. Using diffusion length degradation data and appropriate diffusion coefficients for p-type material resistivities of 1.3, 3.3, 10.6, and 21.0 ohm-cm, an energy level of $E_c - E_g = 0.17 \text{ ev}$ fits the recombination statistics equations quite well as shown in Figure 10. Additional measurements of dependence of minority carrier lifetime on temperature are currently underway to verify this energy level; however, sufficient data are not available at the time of the preparation of this paper. The resulting fit for the 0.17 ev level is in agreement with data previously obtained by Wertheim⁵ but is not in agreement with data obtained by Baicker⁶. Using the defect introduction rate of this level as determined by Hall measurements on n-type silicon, an electron capture cross section of the order of 10^{-15} cm^2 is obtained which is also in agreement with data reported by Wertheim⁵. This fit of the 0.17 ev level to the n on p solar cells irradiated as a function of electron energy would imply that the defect introduction rate of this level should exhibit the same energy dependence as previously shown through K values and ξ_c^{-1} values. However, Hall measurements on n-type silicon obtained in previous experiments indicate

that the defect introduction rate of this level as a function of electron energy closely follows the theoretical predictions of a factor of three increase from 1.0 to 40.0 Mev rather than a factor of 30 increase as implied by the analysis of the data with Hall, Shockley-Read recombination statistics. It is evident, therefore, that a basic inconsistency exists in the results of the analysis of the data as presented here. Since the Hall measurements yield a direct indication of energy level, whereas the analysis through the use of Hall, Shockley-Read recombination statistics requires assumption of single level recombination and empirical curve fitting, the results of the analysis based on recombination statistics are suspect. In addition, resistivity dependence data were obtained only over one order of magnitude wherein far more confidence would exist in the results if data were obtained over three or four orders of magnitude variation in resistivity. Further the assumption of single level recombination may quite easily be an oversimplification of the situation inasmuch as many workers have obtained data which cannot be reasonably fit under the assumption of single level recombination models. In any event, considerable additional effort will be required to clarify this existing inconsistency.

Acquisition of Hall data on the p-type and n-type silicon irradiated in this series of experiments is not at this time complete. Data acquired to date, shown in Figure 11, indicate that the defect introduction rate dependence of the $E_t - E_v = 0.3$ ev defect level in 150 ohm-cm p-type silicon does not follow the theoretical predictions. The data shown in the figure indicate that the defect introduction rate is a factor of 10 higher at 40.0 Mev than at 1.0 Mev in disagreement with theory which predicts approximately a factor of three and also in disagreement with the observed factor of 30 from K and Φ_c^{-1} values. If the acquisition and analysis of further data support the energy dependence as shown in Figure 11, it would imply that this level, commonly referred to as the divacancy energy level⁷, does not predominantly control the recombination process in either n-type or p-type silicon. Preliminary results from the analysis of the Hall measurements on the 100 ohm-cm n-type

silicon, though not yet complete, confirm previous measurements⁸ in previous experiments that the defect introduction rate of the 0.17 ev level is relatively insensitive to incident electron energy and appears to follow simple displacement theory and relativistic Coulomb scattering laws.

Summary and Conclusions

The primary objectives of this series of experiments were: (1) to obtain statistically significant and accurate quantitative data on the energy dependence of electron radiation damage in silicon, (2) to determine the effect of resistivity on the damage rate and energy dependence, and (3) to obtain data on the energy levels and defect mechanisms responsible for electron radiation damage in silicon. The first two objectives were accomplished resulting in an accurate energy dependence function over the practical range of interest from 0.4 Mev to 40.0 Mev. Estimation of solar cell radiation damage and subsequent power supply degradation in space for n on p cells of any resistivity can be performed with the results of these experiments to an accuracy better than the knowledge of the radiation environment in space. It was also observed that the shape of the energy dependence curve of electron radiation damage in p-type silicon is independent of resistivity and, therefore, the difference in the absolute damage rates for any energy over the range of resistivities from 1.0 to 21.0 ohm-cm can be predicted quite accurately. As a result of these findings, it will be possible to do any further testing on n on p solar cells at 1.0 Mev and extrapolate the damage characteristics to other electron energies. This technique has several advantages in that the conduct of experiments at 1.0 Mev is an expedient and economical task and, further, the large number of 1 Mev Van de Graaff accelerators currently in operation relative to the higher energy linear accelerators renders this technique available to a large number of organizations.

The practical importance of the observed steep energy dependence for n on p solar cells lies in the integration of this energy dependence relationship

with the fission beta energy spectrum of the artificial electron radiation belt. The result of the folding of the n on p silicon solar cell energy dependence with this fission electron energy spectrum is an increase in the predicted damage rate of approximately a factor of three over that predicted on the basis of the theoretical energy dependence as characterized by p on n solar cell response. Though the energy dependence of the more radiation resistant n on p cells is a much steeper function than the p on n cells, extrapolation of the damage rate versus energy characteristics indicates that the n on p cell will remain superior to the p on n cell in radiation resistance to electron energies of beyond 1 Bev. Hence, even though the n on p cells suffer more rapidly increasing degradation under higher energy electrons than do p on n cells, their absolute sensitivity to radiation will always remain superior to the p on n cells at any electron energy of practical interest.

The data obtained on the energy levels responsible for the observed degradation of minority carrier lifetime do not yet form a consistent picture. The fit of the $E_c - E_r = 0.17$ ev energy level to the resistivity dependence of the degradation of minority carrier lifetime in p-type silicon is not consistent with defect introduction rate versus electron energy measurements obtained through Hall effects in n-type silicon. In addition, Hall measurements on p-type silicon indicate defect introduction rate dependence on electron energy which is different than either the observed response of p-type or n-type silicon minority carrier lifetime degradation energy dependences. Data acquisition and analysis are continuing in this area, and it is hoped that future results will aid in clarifying the situation. Once it is possible to pin down the energy levels responsible for minority carrier recombination, it will be possible to hypothesize models of the defect structure and subsequently establish theoretical equations to explain the observed energy dependences. Although adequate models and equations do not exist at this time, it appears evident that the energy dependence is not controlled by the primary event of the displacement of a silicon atom.

from the lattice site by an incident high energy electron. The mechanism must, therefore, be related to either characteristics of secondary progeny displacement or motion of the defects to sites wherein stable defect configurations and, hence, active energy levels are formed.

REFERENCES

1. J. M. Denney, R. G. Downing, G. W. Simon, and W. K. Van Atta, "Charged Particle Radiation Damage in Semiconductors, VI: The Electron Energy Dependence of Radiation Damage in Silicon Solar Cells," Report No. 8653-6019-KU-000, Contract No. NAS5-1851, (13 February 1963), TRW Space Technology Laboratories, Redondo Beach, California.
2. J. M. Denney and R. G. Downing, "Charged Particle Radiation Damage in Semiconductors, VIII: The Electron Energy Dependence of Radiation Damage in Photovoltaic Devices," Report No. 8653-6025-KU-000, Contract No. NAS5-1851, (15 July 1964), TRW Space Technology Laboratories, Redondo Beach, California.
3. R. Gremmelmaier, Proceedings of the IRE, 46, 1045, (1958).
4. J. M. Denney, R. G. Downing, W. L. Hoffnung, and W. K. Van Atta, "Charged Particle Radiation Damage in Semiconductors, V: Effect of 1 Mev Electron Bombardment on Solar Cells," Report No. 8653-6018-KU-000, Contract No. NAS5-1851, (11 February 1963), TRW Space Technology Laboratories, Redondo Beach, California.
5. G. K. Wertheim, "Electron Bombardment Damage in Silicon," Physical Review (June 1958), Vol. No. 110, No. 6, p. 1272.
6. J. A. Baicker, "Recombination and Trapping in Normal and Electron Irradiated Silicon," Physical Review (1 February 1963), Vol. No. 129, No. 3, p. 1174.
7. G. D. Watkins and J. W. Corbett, "Electron Paramagnetic Resonance of Defects in Irradiated Silicon," Discussions of the Faraday Society (1961), No. 31 (87).
8. J. A. Carter and R. G. Downing, "Charged Particle Radiation Damage in Semiconductors, VII: Energy Levels of Defect Centers in Electron and Proton Bombarded Silicon," Report No. 8653-6021-KU-000, Contract No. NAS5-1851, (15 February 1963), TRW Space Technology Laboratories, Redondo Beach, California.

TABLE I
 $\frac{f_c}{f_c}$ and K Values as a Function of Energy of Solar Cell Type

	f_c (electrons/cm ²)	f_c^{-1} (cm ² /electron)	K (electrons ⁻¹)	E (Mev)
CEG	4.90×10^{13}	2.04×10^{-14}	2.00×10^{-9}	0.4
OUMX	1.75×10^{15}	5.70×10^{-16}	7.35×10^{-11}	
OUMY	2.43×10^{15}	4.20×10^{-16}	5.50×10^{-11}	0.6
OUOX	4.55×10^{15}	2.20×10^{-16}	3.30×10^{-11}	
CEG	9.25×10^{12}	1.08×10^{-13}	8.00×10^{-9}	
OUMX	6.00×10^{14}	1.67×10^{-15}	2.50×10^{-10}	
OULMY	9.60×10^{14}	1.04×10^{-15}	1.48×10^{-10}	1.0
OUOX	1.90×10^{15}	5.30×10^{-16}	8.33×10^{-11}	
OUCY	2.90×10^{15}	3.50×10^{-16}	5.30×10^{-11}	
CEG	4.35×10^{12}	2.30×10^{-13}	1.77×10^{-8}	
OUMX	1.54×10^{14}	6.50×10^{-15}	1.17×10^{-9}	
OUMY	2.27×10^{14}	4.40×10^{-15}	7.80×10^{-9}	2.7
OUOX	4.32×10^{14}	2.30×10^{-15}	4.45×10^{-10}	
CEG	2.90×10^{12}	3.45×10^{-13}	3.11×10^{-8}	
OUMX	5.90×10^{13}	1.70×10^{-14}	2.62×10^{-9}	
OUMY	9.00×10^{13}	1.11×10^{-14}	1.72×10^{-9}	6.4
OUOX	1.80×10^{14}	5.55×10^{-15}	9.92×10^{-10}	
CEG	2.65×10^{12}	3.80×10^{-13}	3.70×10^{-8}	
OUMX	2.85×10^{13}	3.50×10^{-14}	4.15×10^{-9}	
OUMY	4.55×10^{13}	2.20×10^{-14}	3.47×10^{-9}	16.4
OUOX	9.10×10^{13}	1.10×10^{-14}	1.84×10^{-9}	
MWM	1.28×10^{13}	7.80×10^{-14}	5.04×10^{-9}	
CEG	2.38×10^{12}	4.20×10^{-13}	4.15×10^{-8}	
OUMX	2.10×10^{13}	4.75×10^{-14}	8.30×10^{-9}	
OUMY	3.08×10^{13}	3.15×10^{-14}	5.61×10^{-9}	40.0
OUOX	6.00×10^{13}	1.67×10^{-14}	2.79×10^{-9}	

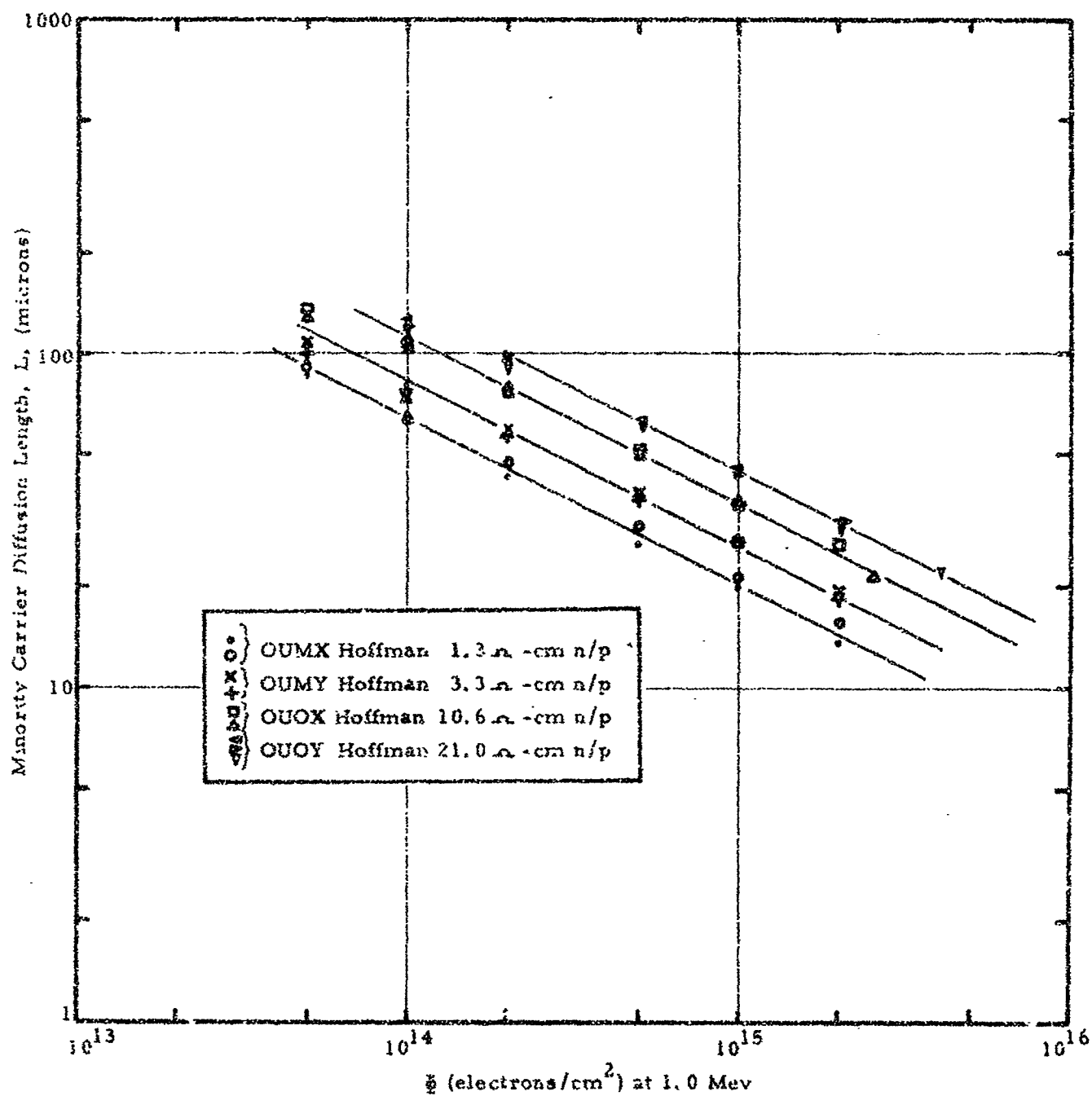


Figure 1. TYPICAL MINORITY CARRIER DIFFUSION LENGTH DEGRADATION DATA

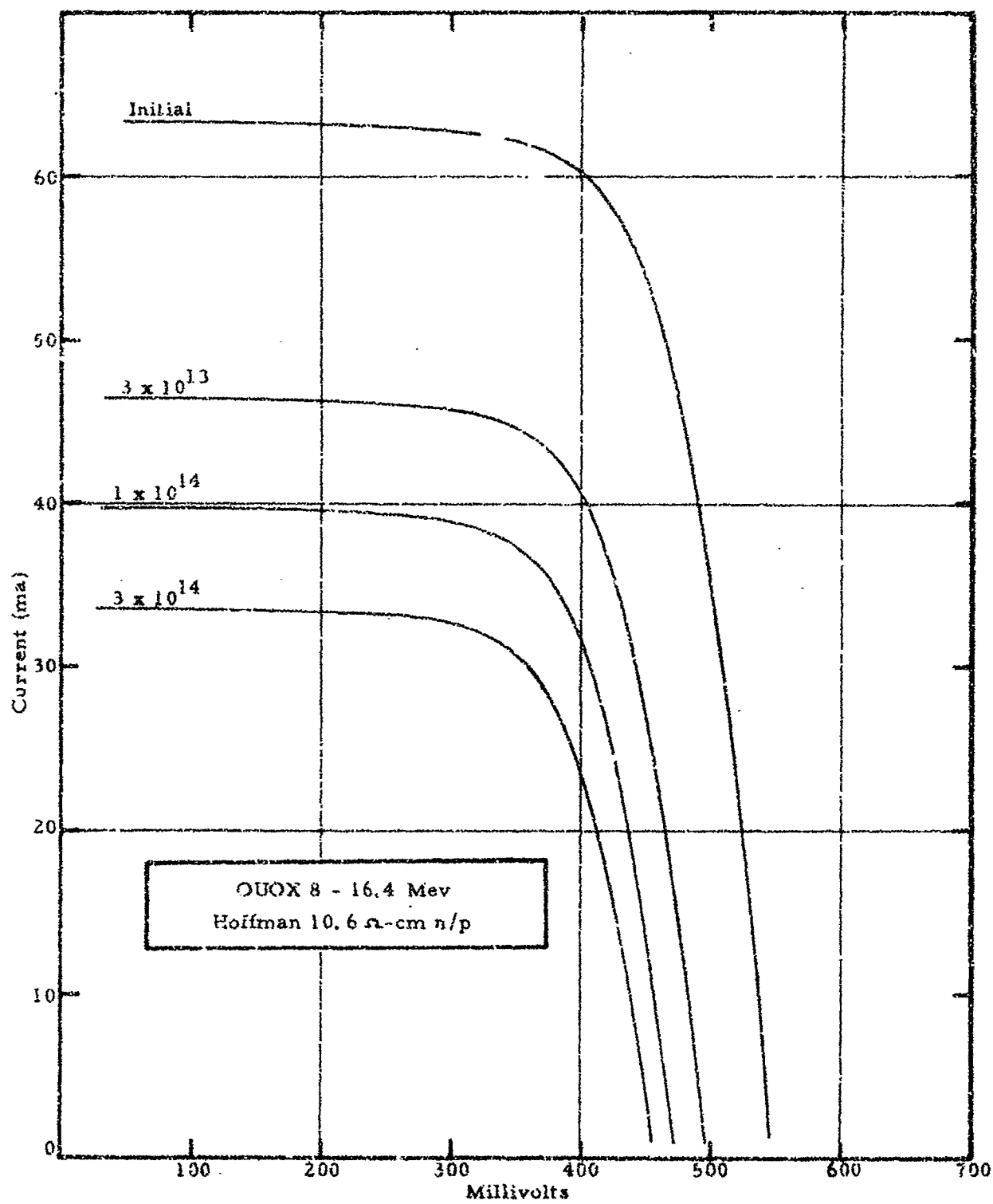


Figure 2. TYPICAL I-V CHARACTERISTIC DEGRADATION DATA

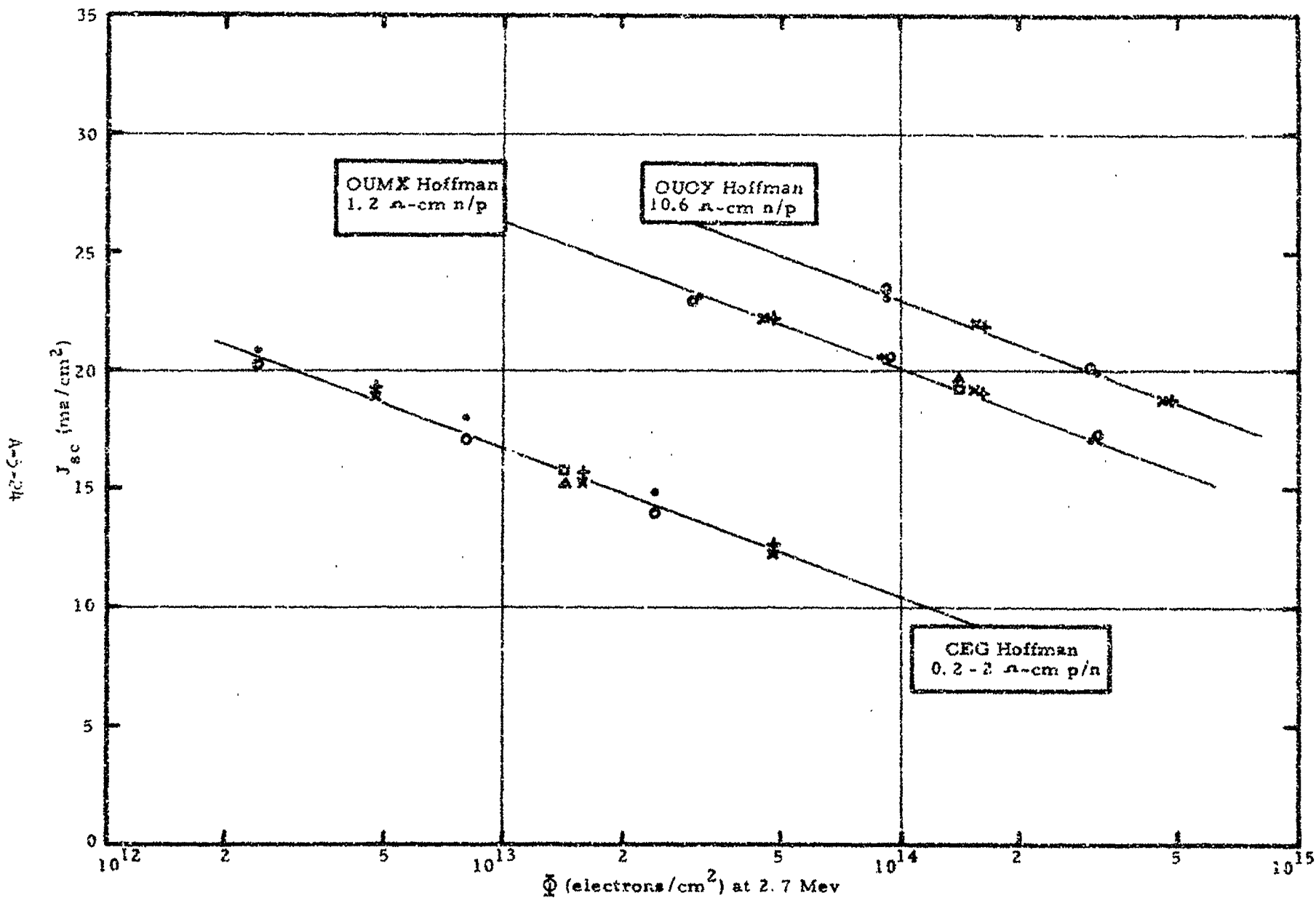


Figure 3. TYPICAL SHORT CIRCUIT CURRENT DEGRADATION DATA

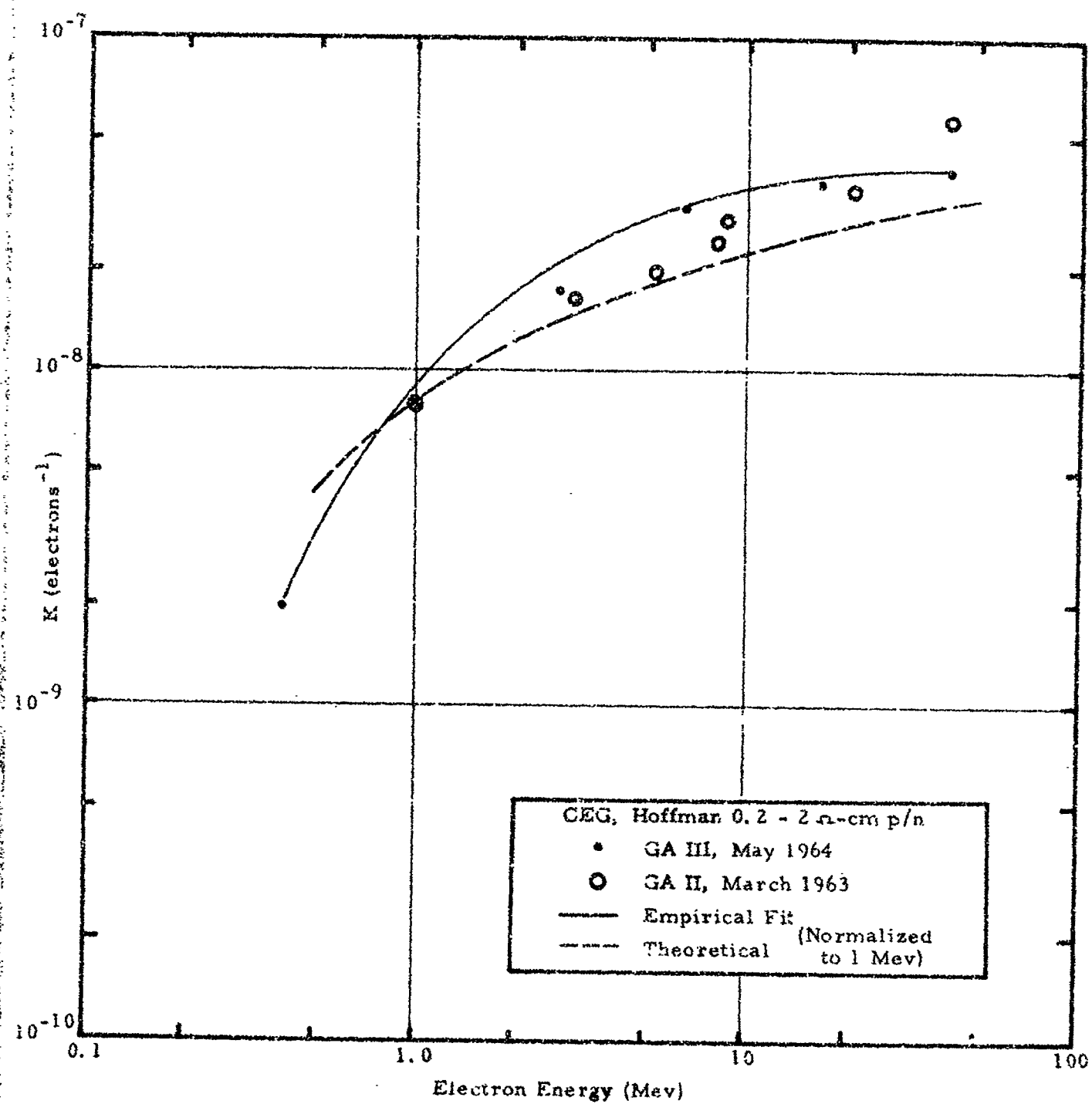


Figure 4. ELECTRON ENERGY DEPENDENCE OF K VALUES FOR P ON N SILICON SOLAR CELLS

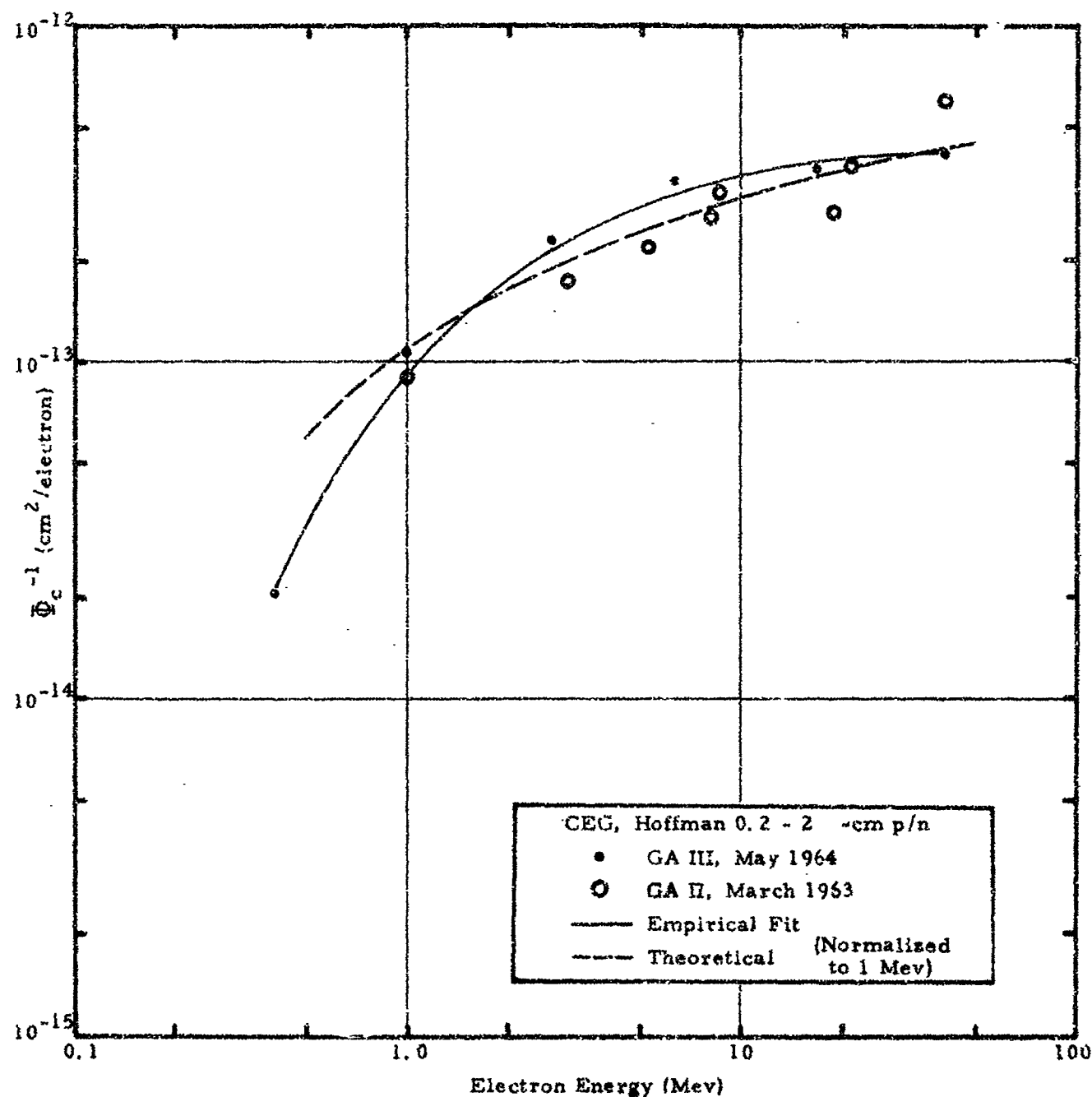


Figure 5. ELECTRON ENERGY DEPENDENCE OF Φ_c^{-1} VALUES FOR P ON N SILICON SOLAR CELLS

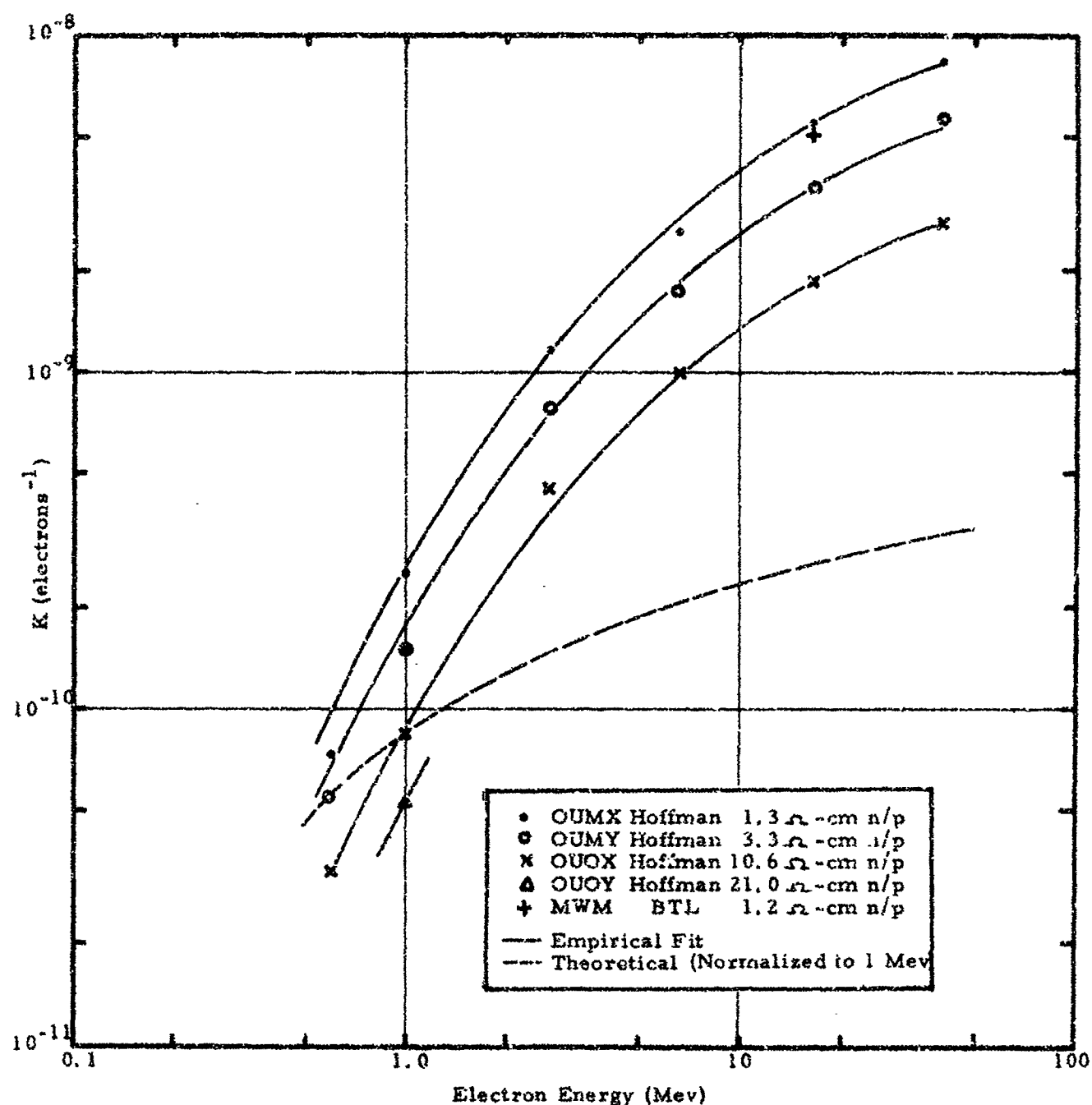


Figure 6. ELECTRON ENERGY DEPENDENCE OF K VALUES FOR N ON P SILICON SOLAR CELLS

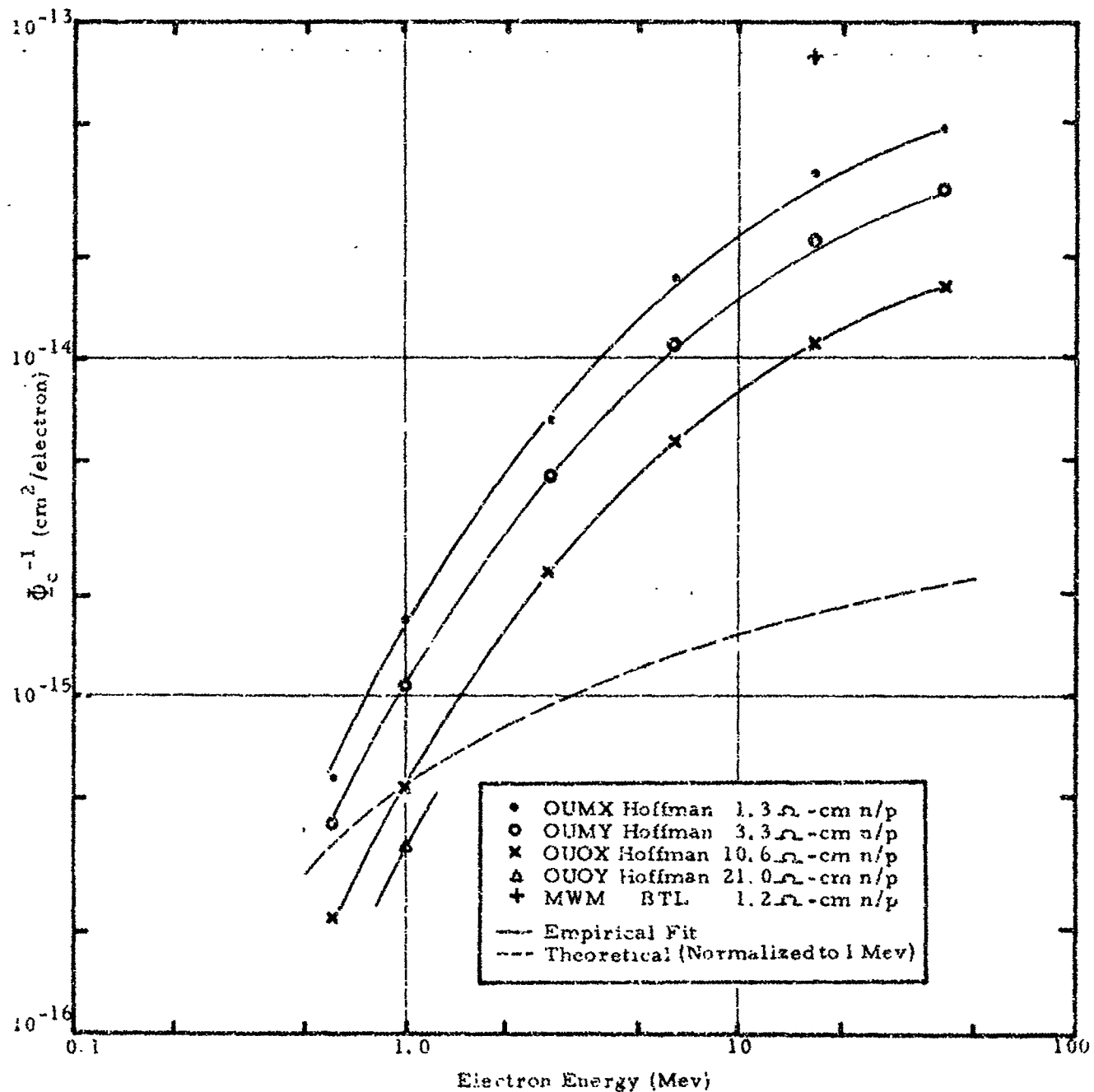


Figure 7. ELECTRON ENERGY DEPENDENCE OF Φ_c^{-1} VALUES FOR N ON P SILICON SOLAR CELLS

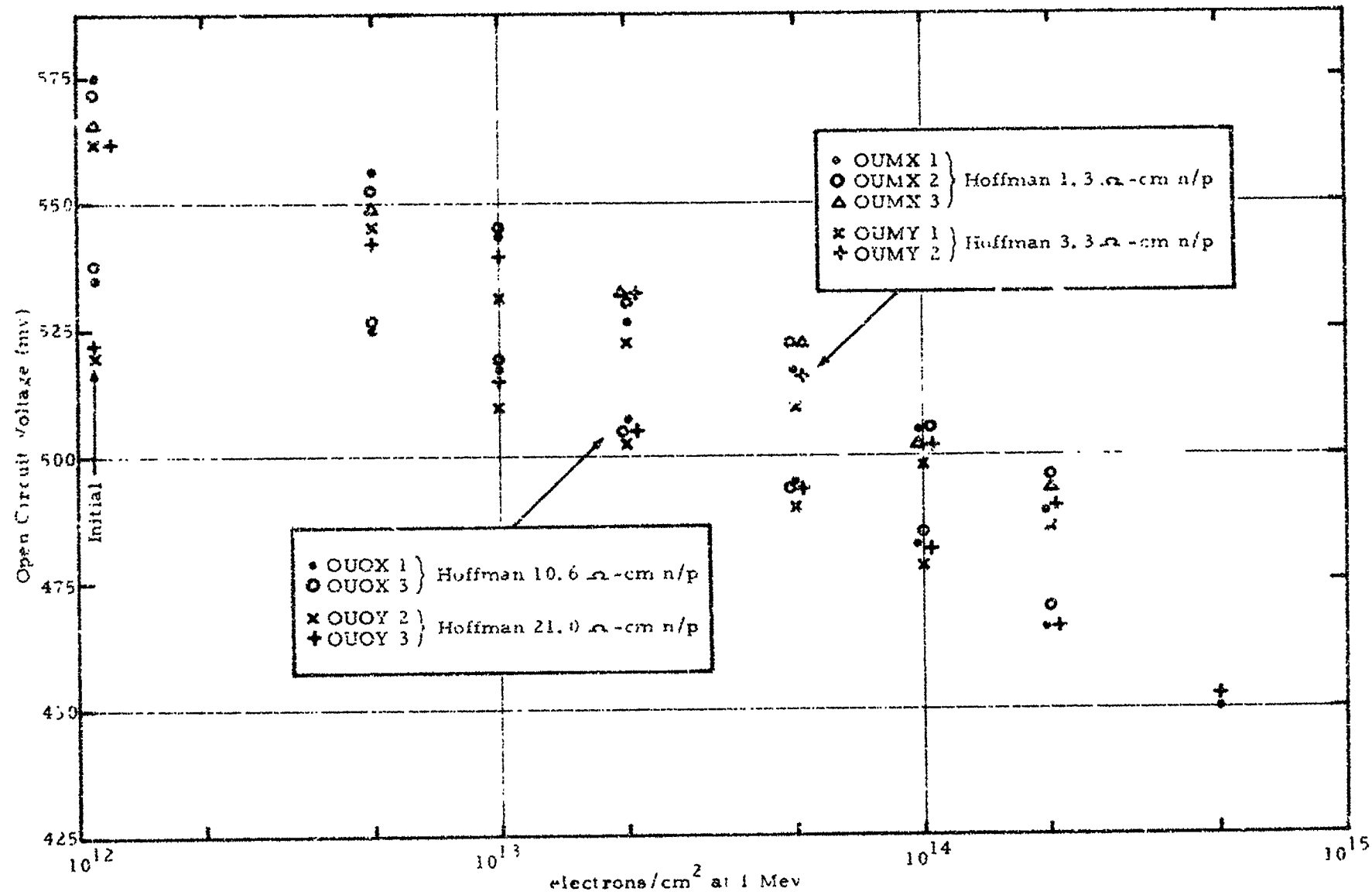


Figure 6. DEGRADATION OF OPEN CIRCUIT VOLTAGE AS A FUNCTION OF RESISTIVITY

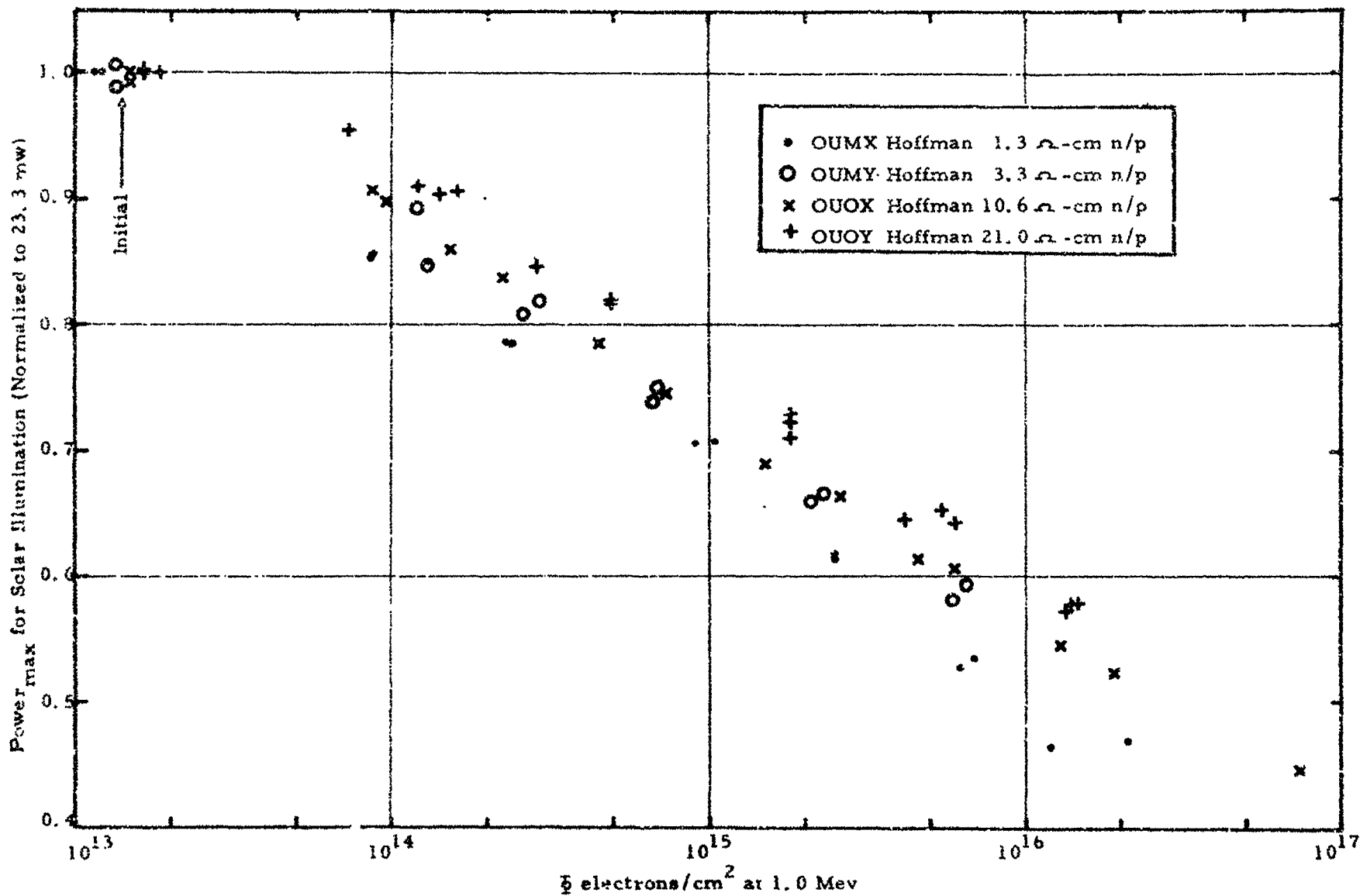


Figure 9. DEGRADATION OF MAXIMUM POWER UNDER SOLAR ILLUMINATION AS A FUNCTION OF RESISTIVITY

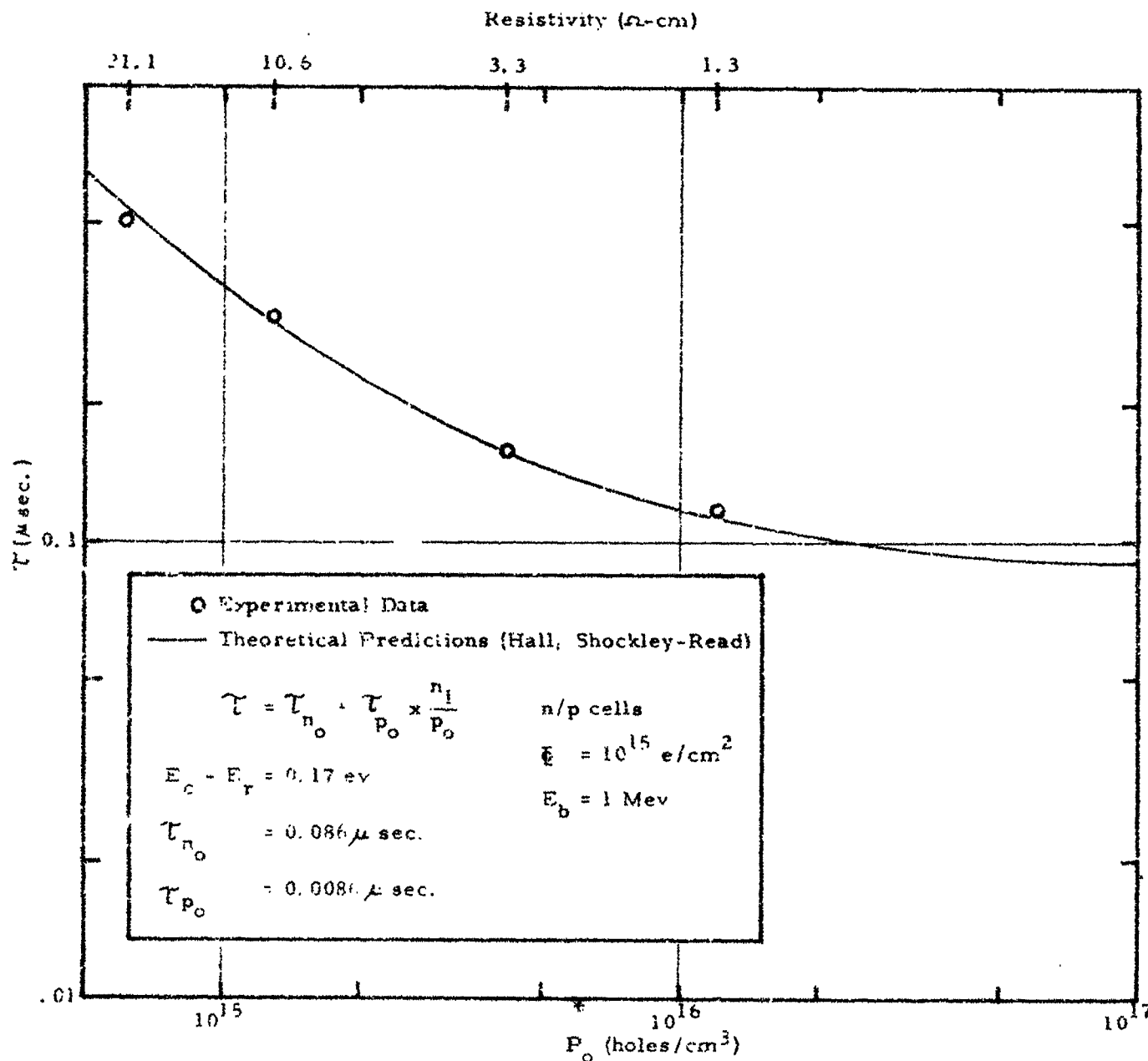


Figure 10. DEPENDENCE OF MINORITY CARRIER LIFETIME DEGRADATION ON RESISTIVITY

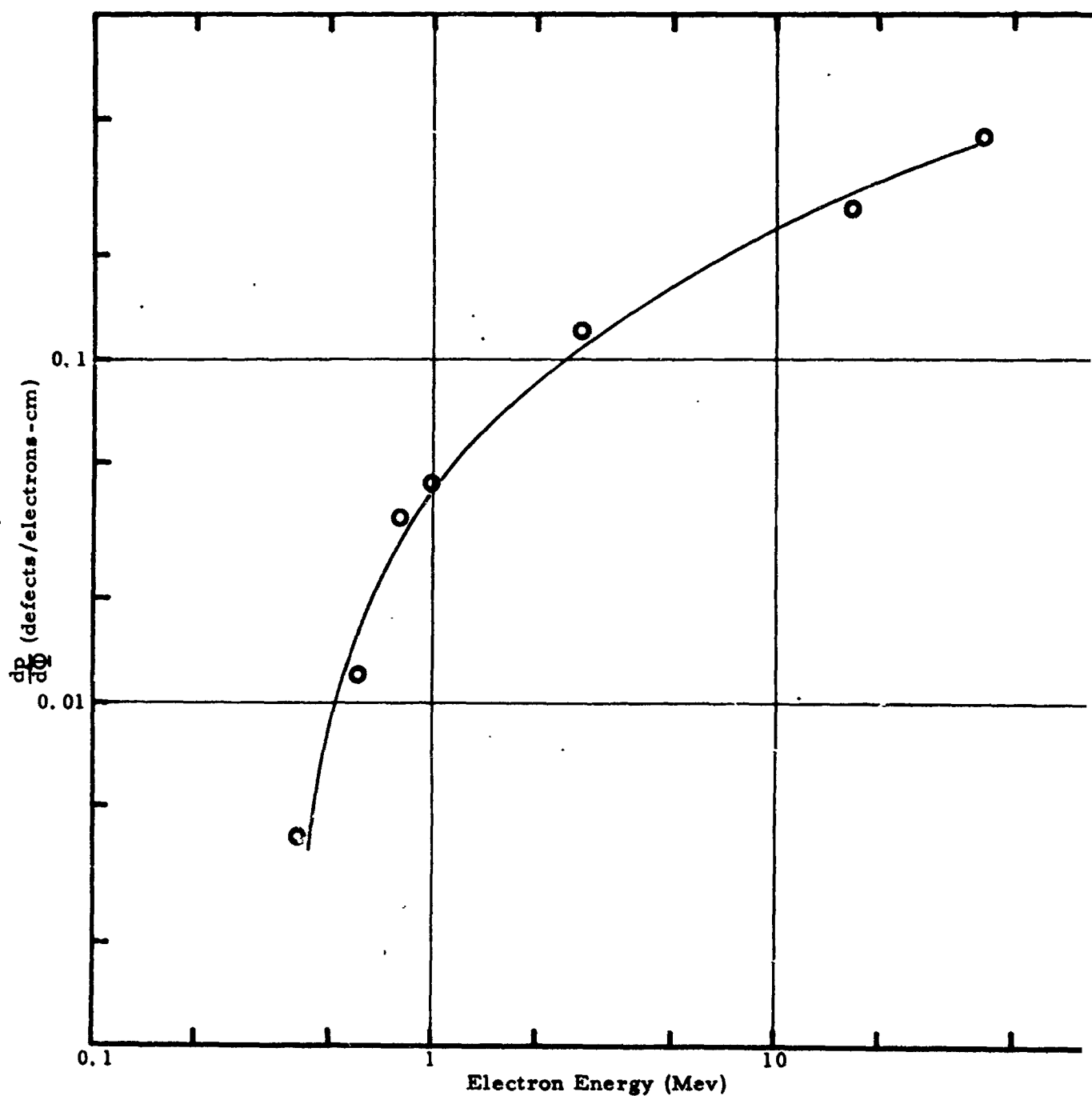


Figure 11. ELECTRON ENERGY DEPENDENCE OF THE $E_t - E_v = 0.3$ ev DEFECT LEVEL IN 150 OHM-CM P-TYPE SILICON

DISCUSSION

LOFERSKI - BROWN UNIVERSITY: Concerning the lifetime measurements, did you make any measurements versus temperature or was it just versus resistivity?

MR. DOWNING: We initiated last Sunday some lifetime measurements versus temperature, or rather diffusion length versus temperature. The first data started coming out Monday before I left. Preliminary analysis indicated that it was going to fit the level 0.17 ev below the conduction band better than it would fit the other level at 0.19 above the valence band.

ADAMS - BENDIX: At what energies did you go to too high an injection rate for your bombardment? Did you change the machine?

MR. DOWNING: The General Atomic machine is a Linac, which by nature is a pulse machine and has a duty cycle of approximately 1000. So for average currents of a one-to-ten microamperes you're talking about currents of milliamperes. At these peak currents we discovered that the cells go into saturation.

QUESTION: At what energy was it that you had to start using the Linac?

MR. DOWNING: From 2.7 up. That would be 2, 6, 16, and 40 Mev. roughly. The 1 Mev and below points were all obtained on the STL Van Der Graaf, which is a d-c machine.

PIC-SOL 209/5
Section A-6

N64-29158

EFFECTS OF IMPURITIES ON RADIATION DAMAGE
OF SILICON SOLAR CELLS

Presented by:

Joseph Mandelkorn

NASA-Lewis Research Center

Cleveland, Ohio 44135

EFFECTS OF IMPURITIES ON RADIATION DAMAGE
OF SILICON SOLAR CELLS

by Joseph Mandelkorn, Lawrence Schwartz, Robert Ulman,
Jacob Broder, and Harold Kautz
Lewis Research Center
National Aeronautics and Space Administration
Cleveland, Ohio

and Richard Statler
Naval Research Laboratory

The effects of some impurities on the radiation damage of silicon solar cells are described in reference 1. The study of radiation damage behavior of modified boron-doped cells led to the conclusion that boron atoms in silicon participate in the creation of recombination centers.

To substantiate this conclusion, gadolinium atoms were substituted for boron atoms in the base region of n-on-p solar cells. Figure 1 shows plots of minority-carrier diffusion-length variation as a function of 1 Mev electron flux for gadolinium-doped cells. The plot for 50-ohm-cm cells appears to be composed of three distinct regions. The central region of the plot in the dose range 4×10^{15} to 1.5×10^{16} 1 Mev electrons/cm² has a slope of zero. Vacancies are definitely being generated in the cell material in this dose range. Yet, there is no measurable change in base region diffusion length or in cell short-circuit current. The other two regions of the plot differ from each other as well as from the central region in slope. It is emphasized that for plots of the type shown only the general shape and the values of diffusion length measured for specific doses are significant. The slopes between measured points have been assigned arbitrarily. The general shape of the plots suggests that the rate of introduction of damage is a function of bombardment dose as well as impurity content.

The plot for the 18-ohm-cm cells has the same three-region appearance as that for the 50-ohm-cm cells. The central region has a small negative slope, however. At a dose of 1.2×10^{15} 1-Mev electrons/cm², the diffusion length preserved in the 18-ohm-cm cells was higher than that in the 50-ohm-cm cells. This situation is not unusual. The gadolinium used to dope the 50-ohm-cm cell material was of lower purity than that used to dope the 18-ohm-cm cell material. Electrically inactive impurities are known to affect the formation of recombination centers in silicon¹. The density of recombination centers in high-resistivity base material solar cells is strongly influenced by the concentration of electrically inactive impurities in the dose range that includes 10^{15} 1-Mev electrons/cm². For higher dose ranges, the concentration of electrically active impurity, gadolinium in this case, dominates

recombination center formation. Thus the 50-ohm-cm cells preserve longer diffusion lengths for doses above 4×10^{15} 1-Mev electrons/cm².

Figure 2 shows the effects of bombardment on diffusion lengths of 130- and 12-ohm-cm indium-doped cells. Again the plots have a three-region appearance. The values of diffusion length preserved in the 130-ohm-cm cells far exceed those of the 12-ohm-cm cells for any specific bombardment dose. This is similar to the comparative damage behavior of 10- and 100-ohm-cm boron-doped cells.¹ The values of diffusion length preserved in the 130- and 12-ohm-cm indium-doped cells are, however, lower than those preserved in 100- and 10-ohm-cm boron-doped cells, respectively. As will be discussed, there is a dependency of rate of formation of recombination centers on the specific electrically active impurity element as well as on its concentration.

Although not shown, the bombardment-damage behavior of 5- and 12-ohm-cm gallium-doped cells results in similar three-region plots. Analysis of the plots for the various types of cells indicates that the slope of the central region increases with increasing concentration of electrically active impurity. A study is underway to obtain data on the behavior of bombarded 50-ohm-cm cells containing various dopants. It is expected that the completely flat region observed in the 50-ohm-cm gadolinium plot of figure 1 will not occur for 50-ohm-cm boron-doped cells, whereas 50-ohm-cm aluminum-doped cells are expected to surpass the performance of the 50-ohm-cm gadolinium cells.

Figure 3 contains a formula expressing a hitherto accepted relation between the diffusion length L retained in a bombarded semiconductor material and the total flux ϕ of atomic particles. The damage constant K contains the various factors that determine the behavior of the sample material in its specific environment. Figure 3 also shows plots of diffusion length versus bombardment flux for a number of high-resistivity cell types. It is evident that none of the plots conform with the formula. This lack of conformity was first noted for high-resistivity boron-doped cells.¹ The 20-ohm-cm boron-doped cell plot is shown as a straight line. However, the extreme left of figure 3 also shows that values of diffusion length for high-resistivity boron-doped cells show appreciable scatter at a dose of 10^{15} 1-Mev electrons/cm². The slope of any high-resistivity-cell plot is strongly dependent on electrically inactive impurity content in the dose range extending to 5×10^{15} 1-Mev electrons/cm². The concentrations of electrically inactive impurities vary with purity of dopant source, material growth processes, section of silicon ingot from which the wafer was cut, and cell fabrication processes. Valid comparison of the effects of electrically active impurities on radiation damage can be made only at doses exceeding 5×10^{15} 1-Mev electrons/cm². In this dose range, the superiority of aluminum-doped cells is evident from the plots shown.

The variability between types of cells is a result of impurities rather than the inconsistency of measurements as shown in Table I.

TABLE I. - UNIFORMITY OF POST BOMBARDMENT DIFFUSION

LENGTHS OF LEWIS CELLS

[1 Mev electron bombardment.]

Cell	Dose, e/cm ²			
	1.2×10 ¹⁵	4.8×10 ¹⁵	1.5×10 ¹⁶	4.1×10 ¹⁶
Diffusion length L, μ				
a22-3-8	83	36	29	18.4
9	83	36	29	18.5
10	78.5	36	30	18.9
11	80	37	29.5	18.7
b14-32-1	45.5	19.7	18.5	14.3
2	45.5	19.9	18.2	14.3
3	44.5	20.4	18.1	14.0
4	43	19.8	18.1	14.0
6	44.5	19.7	18.3	13.9
7	45.4	19.7	18.5	13.9

a 130-ohm-cm indium-doped.

b 17-ohm-cm aluminum-doped.

Materials and processes were rigidly controlled for the cells shown. The result is good uniformity of diffusion lengths obtained for each type of cell throughout an entire series of bombardments.

Figure 4 presents further data on the two types of cells considered in table I. The cells were bombarded and their diffusion lengths measured at the Bell Telephone Laboratories (BTL).

A definite decrease in the rate of introduction of recombination centers occurs for both the 130-ohm cm indium and the 17-ohm-cm aluminum cells in the dose ranges 2×10^{14} to 8×10^{14} , and 3×10^{15} to 1.2×10^{16} 1-Mev electrons/cm². The fluxes at which diffusion lengths were measured at BTL were slightly lower than those for which values of diffusion lengths were shown in previous figures. The values of diffusion length determined from extrapolation of the points shown in figure 4 are in very good agreement with the data presented earlier in this report. The change in slope of the plots in the dose range 3×10^{15} to 1.2×10^{16} would appear more pronounced if the plots had included measured values at 4×10^{16} 1-Mev electrons/cm².

The plots closest to the bottom of figure 4 illustrate bombardment behavior of 1-ohm-cm cells. Two groups of cells having different values of unbombarded diffusion lengths are compared. After bombardment to a small dose of 10^{14} 1-Mev electrons/cm², the differences in diffusion lengths preserved in each group are insignificant.

Unlike 1-ohm-cm cell behavior, high-resistivity cells, which have longer values of original diffusion length, preserve their superiority to bombardment doses greater than 10^{15} 1-Mev electrons/cm². Longer original diffusion lengths in high-resistivity cells are indicative of low concentrations of electrically inactive impurities in the base region of such cells. Consequently, the rate of introduction of recombination centers is slower in such cells even at doses that are equivalent to those that cells could experience after a year or more in the Van Allen belt. The preservation of long diffusion lengths in fabricated high-resistivity cells is therefore of significance in obtaining high-radiation-damage resistance in practical applications.

From analysis of the characteristics of modified cells, we find that impurities influence diffusion-length degradation, carrier removal rate, open-circuit voltage, and junction characteristics of cells. It is, therefore, impossible to predict characteristics of cells from mere knowledge of the resistivity of the base material. We are advancing the following concepts to explain our observation:

- (1) Bombardment-generated vacancies are mobile at room temperature.
- (2) Mobile vacancies may be captured by impurity atoms or other vacancies, forming impurity-vacancy or vacancy-vacancy configurations.
- (3) Specific configurations so formed can have trapping-center or recombination-center behavior.
- (4) The terminology for the variables involved in formation of configurations involving capture of mobile vacancies can be patterned in a fashion similar to carrier capture terminology. Equations showing the relations of variables will also be similar to those for carrier capture. Variables are
 - (a) Specific impurity element, its electronic state and concentration in the lattice
 - (b) Concentration of generated mobile vacancies
 - (c) Localized lattice imperfections
- (5) Types of configurations:
 - (a) Impurity-single vacancy, impurity-multiple vacancy, and vacancy-vacancy clusters can occur.

- (b) The concentration of compound vacancy configurations is significantly determined by the density of generated mobile vacancies as well as the variables previously considered.
- (c) When compound vacancy configurations exist because of instantaneous local generation of high densities of mobile vacancies, redistribution occurs with time at room temperatures.

Based on these concepts it is possible to explain impurity effects on junction characteristics,¹ changes in damage-introduction rate with bombarding-particle energy and with bombardment dose, differences between proton and electron damage introduction, and room-temperature annealing of proton-bombarded cells. Further data establishing the validity of these concepts and information on the behavior of high-resistivity solar cells under proton bombardment will be published in an NASA report.

The study of impurity effects has led to the design and fabrication of improved cells. With regard to the preservation of diffusion length in the base region of solar cells after bombardment, the optimum base-region material should contain the minimum achievable concentration of electrically active impurity. However, the power output of the solar cell depends upon base-region parasitic resistance as well as upon base-region diffusion length. Base parasitic resistance increases with decreasing electrically active impurity concentration. Furthermore, the open-circuit voltage of cells decreases with decreasing electrically active impurity concentration, while the temperature coefficient of power output increases.² From investigation of these effects, we have concluded that the optimum concentrations of electrically active impurity in solar-cell material correspond to material resistivities in the 10- to 20- $\Omega\text{-cm}$ range. In the past year, more than two hundred 10- to 20- $\Omega\text{-cm}$ solar cells have been fabricated and analyzed at the Lewis Research Center. As a result of this effort, the following important advantages stemming from use of 10- to 20- $\Omega\text{-cm}$ silicon for solar cells have become apparent:

Application advantages:

- (1) Extremely shallow junction cells with very good junction characteristics have been made with excellent yields by using 10- $\Omega\text{-cm}$ -silicon.
- (2) Cells as made in (1) had better curve power factors, much higher short and long wavelength response, and higher efficiencies than 1- $\Omega\text{-cm}$ cells.
- (3) Considerably higher long wavelength response and higher efficiencies are preserved in bombarded 10- $\Omega\text{-cm}$ cells as compared with 1- $\Omega\text{-cm}$ cells.

(4) The 10-ohm-cm cell degradation with temperature is such that the 10-ohm-cm cell is still superior to the 1-cm cell at temperatures up to 100° C.

Production advantages:

(1) Material rejection is low. Original minority carrier lifetime in 10-ohm-cm material exceeds that preserved after subjecting the material to diffusion processing. This is usually not true for 1-ohm-cm material.

(2) Distributions of characteristics of 10-ohm-cm cells are tighter because of the superior properties of 10-ohm-cm material and because of the better and controllable junction characteristics attainable by using 10-ohm-cm material.

(3) Special low-cost super blue coatings can be applied to the 10-ohm-cm cell.

The benefits to be realized from use of the 10- to 20-ohm-cm material and the characteristics of 10- to 20-ohm-cm cells justify application of such cells at temperatures up to 100° C in nonradiation environments. In a radiation environment, the efficiencies preserved in 10- to 20-ohm-cm cells are sufficiently higher than those of 1-ohm-cm cells so that the 10- to 20-ohm-cm cell (hereafter referred to as 10-ohm-cm cell) is definitely superior to the 1-ohm-cm cell in power output at 100° C.²

Since the specific impurity element added to the silicon material to reduce its resistivity to the 10- to 20-ohm-cm range will influence all the characteristics of the cell, we have investigated the use of aluminum, indium, gallium, or boron for doping silicon in this resistivity range. The results show that aluminum is the most desirable impurity element.¹

Approximately 50 aluminum-doped 17-ohm-cm cells have been fabricated. A specification for the characteristics of such cells is shown in table II.

TABLE II. - CHARACTERISTICS OF SUPER BLUE 10-OHM-CM CELL

[Application: For power supplies exposed to atomic radiation.]

V_{OC} , 0.54 V	Grid fingers, 10
I_{SC} , 62-65 mA	Thickness, 0.008 - 0.020 in.
Area, 1.8 cm ²	"n" value, <2
P_{out} , 24 MW min. ^a	I_R , max, 20 μ A for 0.6 V bias
Efficiency, 9.5% min. ^a	R_C , 0.25 - 0.4 ohm
CPF, 70%	L, 150 - 200 μ
$I_{0.4-0.6}$, 26 mA ^b	Coating, super blue
$I_{0.4-0.6}$, 40%	Dopant, aluminum
I_{SC}	T_{coeff} , 0.53 %/°C

^aOuter space equivalent

^b $I_{0.4-0.6}$, outer space current for 0.4 - 0.6 μ region of solar spectrum.

The cells are made by a standard diffusion process³ at temperatures of approximately 800° C. The sheet resistance of the diffused layer must be kept at or below 200 ohm/square, and this determines the diffusion times, which are approximately 30 minutes. Ten grid fingers on the top surface of the cell permit attainment of curve power factors of 70 percent for the maximum value of sheet resistance cited. Experiments have revealed that the equivalent outer-space currents of these cells are not appreciably decreased for a base-region thickness of 0.008 inch. The thicknesses of the cells can therefore range from 0.008 to 0.020 inch depending on application requirements. Minority carrier diffusion lengths of 200 microns are obtainable in fabricated cells of this type with the optimized low-temperature diffusion process used. The low-temperature short-time diffusions also result in extremely shallow junctions which have better "n" junction characteristic values and lower diode reverse currents I_R than obtained for deeper junctions in 1-ohm-cm material. In addition, the high short wavelength response achieved coupled with a special super blue antireflective coating results in collecting 40 percent of the cell short-circuit current from the 0.4 to 0.6 micron region of the solar spectrum. The significance of this super blue behavior in preservation of efficiency of the cells after bombardment is illustrated in reference 4. The high short and long wavelength collection of the cells results in their equivalent outer-space short-circuit currents being higher than those normally obtained for 1-ohm-cm cells despite the extra gridding on the cell surfaces.

The open-circuit voltages of the cells are 0.54 volts, which is the common value of this parameter for 10-ohm-cm cells. The efficiencies for a 1.8-cm² area (main contact subtracted) range from 9.5 to 10.5 percent. The spread in efficiencies is small because of the uniformity of long wavelength collection under the solar spectrum, the reproducibly good junction characteristics, and the controls used in the fabrication process, which are achievable using 10- to 20-ohm-cm material.

From a series of bombardments of these aluminum-doped cells and of 1-ohm-cm high blue and 10-ohm-cm super blue boron-doped cells, data have been compiled on power outputs and efficiencies preserved after irradiation. The data are shown in figure 5. Power outputs and efficiencies were measured for the 1- and 10-ohm-cm boron-doped cells using a filter wheel simulator.⁴ Efficiencies are predicted for the aluminum-doped cells based on measurements of initial characteristics and measurement of post-bombardment diffusion lengths. It was not possible at the time of bombardment to make measurements of the short-circuit currents of these cells under the simulator. However, the aluminum-doped cells were equal or superior to the 10-ohm-cm super blue boron-doped cells in all characteristics and preserved longer diffusion lengths after bombardment than did the 10-ohm-cm super blue boron-doped cells. The predictions are therefore believed to be reliable.

Based on approximately 12 bombardments of the cells with 10-Mev protons and a series of electron bombardments, we have made approxima-

PIC-SOL 209/5

tions of anticipated lifetimes of various types of cells in a Telstar I orbit with Telstar I solar-cell shielding. An arbitrary lifetime of 1 has been assigned to the p-on-n cell in figure 6.

The data of Waddell⁵ and of Rosenzweig⁶ of a comparative damage of p-on-n and 1-ohm-cm n-on-p cells result in assignment of comparative lifetime of 6x to the 1-ohm-cm Telstar cell. Comparison of the data on Lewis aluminum-doped super blue cells with Telstar-type cells results in assigning a factor of 25x to the Lewis cell.

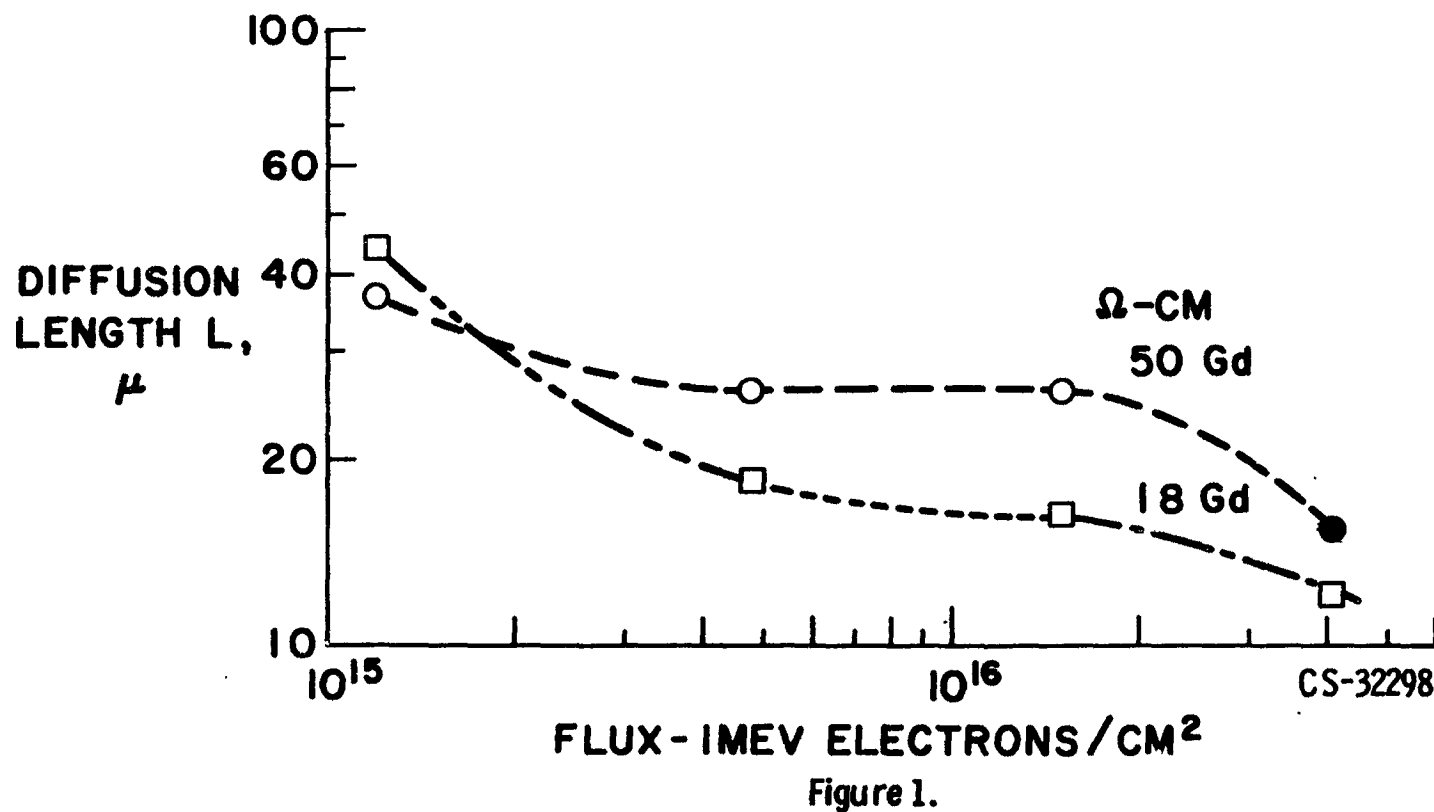
It must be emphasized that the full potential of the Lewis cell has not been realized as yet. The possibility of the inclusion of chlorine in the aluminum-doped silicon as well as the further elimination of detrimental electrically inactive impurities could result in a factor of perhaps 60x for the Lewis cell.

REFERENCES

1. Mandelkorn, J., et al.: Jour. Appl. Phys. 35, June 1964, p. 2258.
(Also available as NASA TM X-52007.)
2. Broder, J., et al.: "Solar Cell Performance at High Temperatures," these proceedings.
3. Mandelkorn, J., McAfee, C., Kesperis, J., Schwartz, L., and Pharo, W.: J. Electrochem. Soc. 109, 313, 1962.
4. Mandelkorn, J.: "A Filter Wheel Solar Simulator," these proceedings.
5. Waddell, R. C.: "Radiation Damage to Solar Cells on Relay I and II," these proceedings.
6. Rosenzweig, W., Gummel, H. K., and Smits, F. M.: Bell System Tech. J. 42, 399, Mar. 1963.

DIFFUSION LENGTH VS ELECTRON FLUX FOR GADOLINIUM-DOPED CELLS

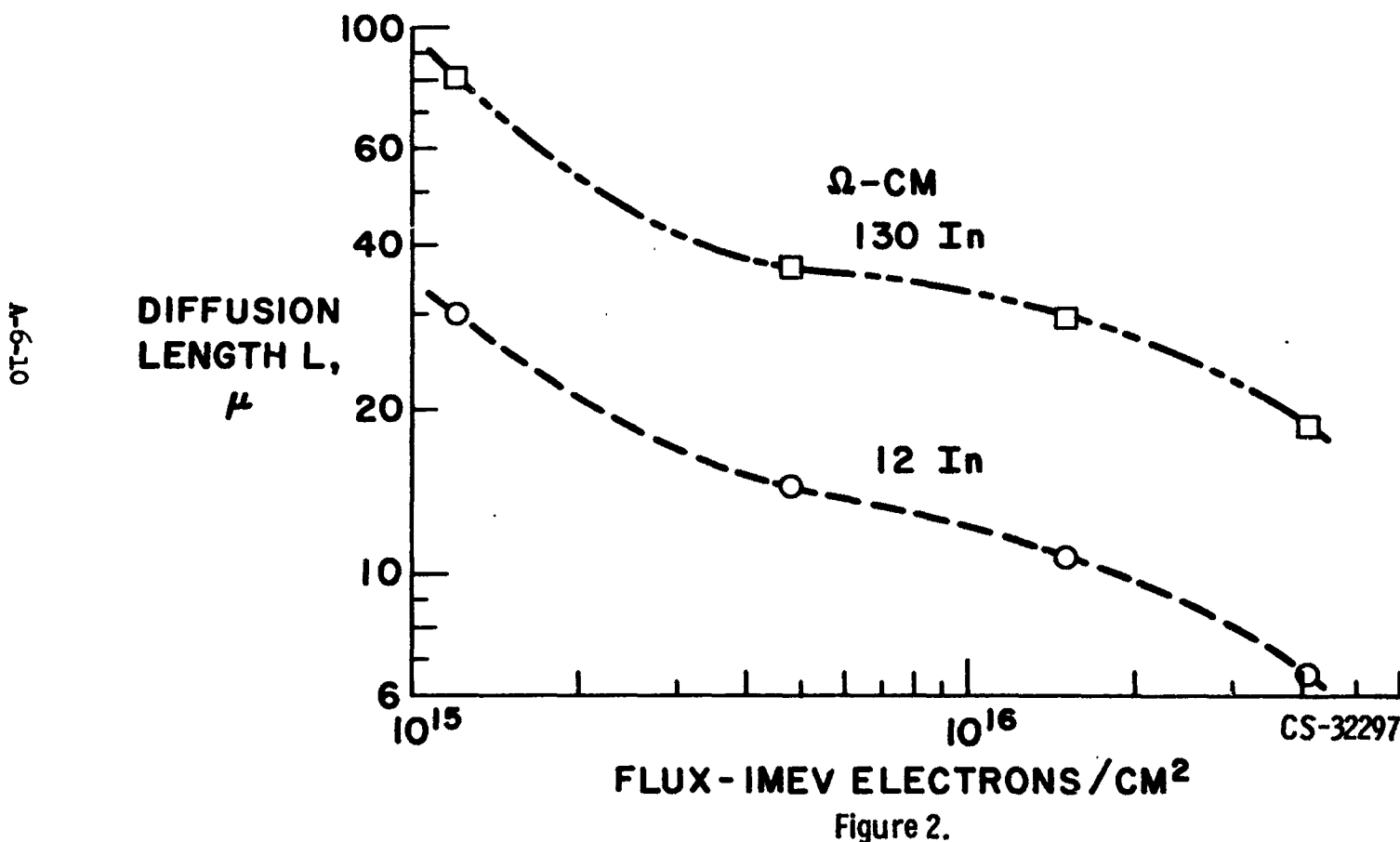
A6-6



PIC-SOL 209/5

Figure 1.

DIFFUSION LENGTH VS ELECTRON FLUX FOR INDIUM-DOPED CELLS



EFFECTS OF IMPURITIES ON POST BOMBARDMENT DIFFUSION LENGTH

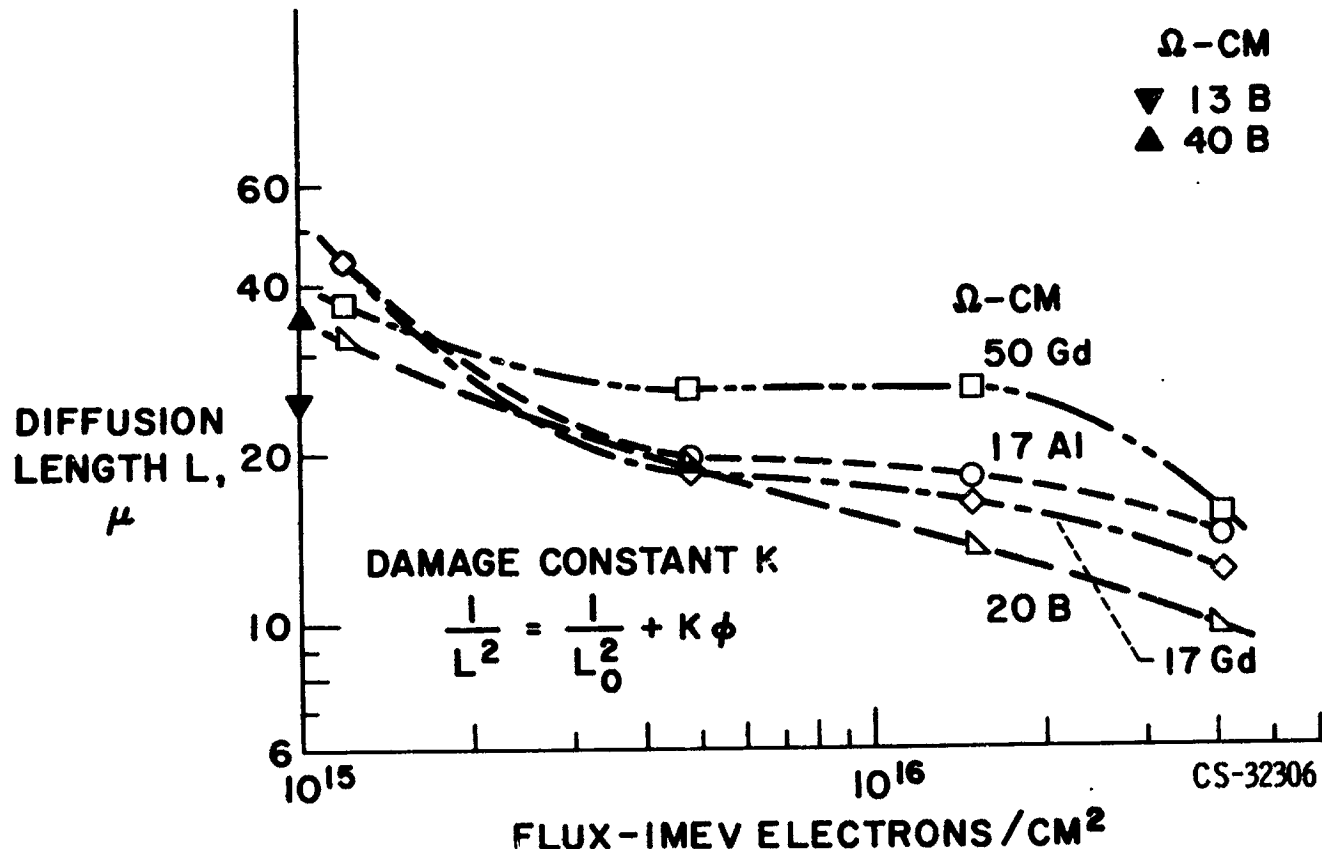


Figure 3.

PIC-SOL 209/5

DIFFUSION LENGTH VS ELECTRON FLUX

A-6-12

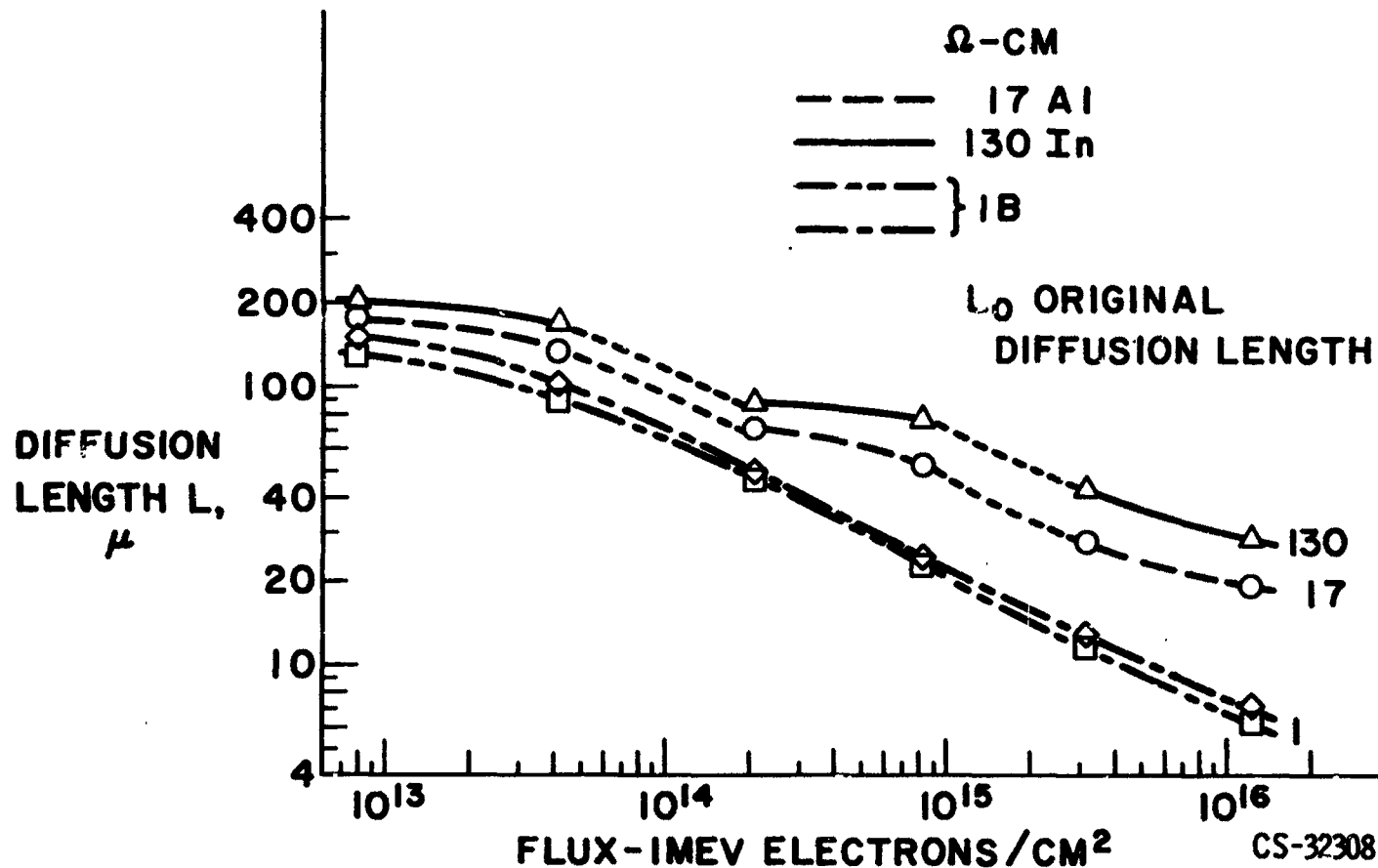


Figure 4.

MAXIMUM POWER OUTPUT VS ELECTRON FLUX

A-6-13

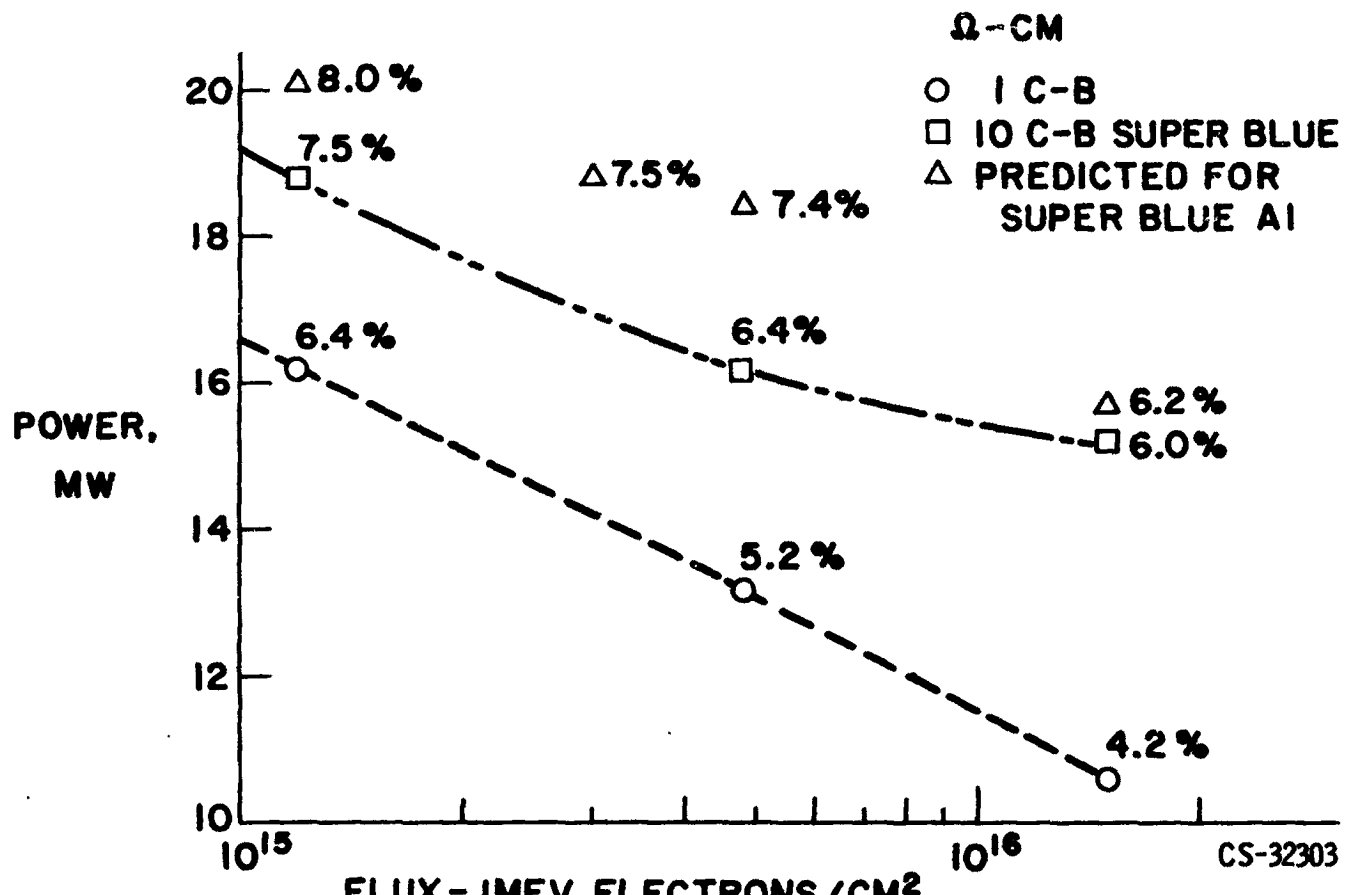


Figure 5.

PIC-SOL 209/5

COMPARATIVE LIFETIME IN VAN ALLEN BELT

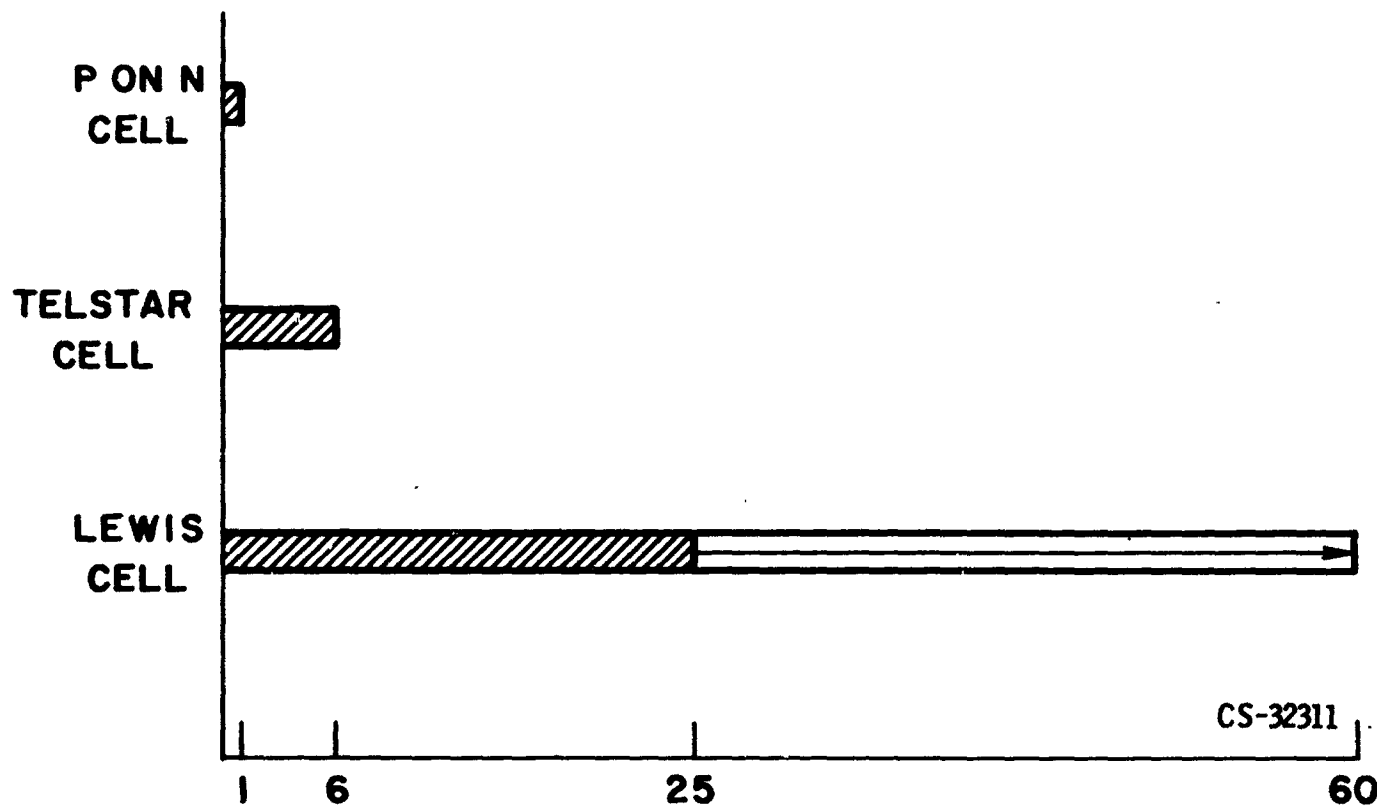


Figure 6.

DISCUSSION:

LODI-LOCKHEED: Could you just mention the range of proton energies that you bombarded with?

MR. MANDELKORN: We used only 10 Mev protons. This I feel is a high enough energy so that the data of Rosenzweig would apply in comparison.

CHIDESTER - LOCKHEED: You predict an 8% degradation at the end of one year. Is this with no protection?

MR. MANDELKORN: This is with shielding as on the Telstar I and in the Telstar I orbit. This uses the equivalent flux of 6×10^{12} per day as given in recent publications by the Bell Telephone Laboratory.

LOFERSKI - BROWN UNIVERSITY: About these gadolinium cells, do I understand that you are not advocating them very strongly? I have some other questions about them. For example, why did you use gadolinium in the first place, why not europium, lutecium, or some of the other rare earths? How did you know how much gadolinium there was in these cells, and also, how about resistivity of these cells of the gadolinium doped material? Were they measured on finished cells or raw material, or where did these figures come from?

MR. MANDELKORN: The high resistivity gadolinium doped material was made at the Signal Corps, two years ago. The cells made from it were not evaluated until we had come here. The 18 ohm cm. gadolinium doped material was made here, using much purer gadolinium. The resistivity was fairly uniform throughout the ingots. As we mentioned in the TM we had great difficulty in bringing the resistivity down below 20 ohm centimeters. We are also experimenting with other impurities. The reason we selected aluminum is because industry states that they do not feel that it would be difficult to prepare 10 ohm-cm. aluminum doped material. That's why we are at this time specifying aluminum. What we will specify in the future I am not at liberty to state.

LOFERSKI - BROWN UNIVERSITY: How do you know how much gadolinium there is in your crystals? How do you know that the resistivity is controlled by the gadolinium? Have you analyzed the material for gadolinium content?

MR. MANDELKORN: This is a very good question, and what we can state here is that we have dumped large quantities of gadolinium into silicon melts. We have not been able to bring the resistivity down below 18 ohm centimeters. This indicates to us that if there are any foreign impurities in the gadolinium, they are not electrically active.

QUESTION (NO NAME): I think to ask the question more directly, have you made any mass spectrographic analyses of your materials?

MR. MANDELKORN: We have not made mass spectrographic analyses. However, we have used the highest purity indium, aluminum and gallium obtainable in six nines purity. We don't feel that there is any possibility of their being some other electrically active impurity in those cells.

WEINER - RCA-ASTRO: Were the temperature characteristics of the cells measured under the simulator?

MR. MANDELKORN: The short circuit current of these cells do not vary to any extent with temperature for unbombarded cells. The diffusion lengths are so high, that the collection under the solar spectrum is not influenced even if the lifetime goes up to some limited extent with the temperature changes. As a result, the power outputs are not affected by changes in current. We have actually measured temperature characteristics, and Jack Broder will go into this in a later paper.

WEINER - RCA: Did you indicate that for bombarded cells, 10 ohm centimeter material was still superior to the 1 ohm centimeter material?

MR. MANDELKORN: Yes.

WEINER - RCA: This implies that for unbombarded cells, 10 ohm centimeter material is better than 1 ohm centimeter material.

MR. MANDELKORN: We recommend the 10 ohm centimeter cell up to temperatures of 100°C. We feel that you can make 10 ohm centimeter cells which have efficiencies of approximately the same order as the 1 ohm centimeter cells. Then it's a question of production yields. We feel that you can get higher yields of high efficiency cells from 10 ohm-cm. material than you can from 1 ohm-cm material. Since the temperature coefficient is not bad compared with 1 ohm centimeter cells, we feel that they are competitive up to temperatures of 100°C. However, above 100°, as will be seen in a later paper, we cannot recommend 10 ohm centimeter cells.

TARNEJA - WESTINGHOUSE: On the 10 ohm centimeter cells, did you measure your junction depth? You said they were shallow.

MR. MANDELKORN: I'm sorry, I wish we could measure junction depth on the type of cells we make. On the standard 875°, 30-minute diffusion which we published several years ago, the junction depth is 0.5 microns. On these cells the diffusion is made at approximately 800° and the junction depth is so shallow that we don't even bother to try and measure it.

TARNEJA - WESTINGHOUSE: Would you speculate on the surface concentration?

MR. MANDELKORN: I would speculate only on one thing. Sheet resistance. The sheet resistance of the cells as we make them is 150 ohms per square.

RAPPAPORT - RCA: Now, I'm somewhat confused as to the difference between the changes of damage resistance with resistivity, which I think we all recognize, and the changes with dopants. One of the crucial experiments I'd like to see is what the power output versus flux looks like for a 10 ohm centimeter boron doped and 10 ohm centimeter aluminum doped cell, where the resistivity has been accurately measured. Do you have that comparison?

MR. MANDELKORN: Yes, on the last slide I had a super blue 10 ohm centimeter boron doped cell depicted. This is not a cell normally available in industry because it has a super blue coating and a shallow junction. This slide compares a super blue 10 ohm centimeter boron with a super blue 17 ohm centimeter aluminum doped cell.

RAPPAPORT - RCA: The resistivities are not the same.

MR. MANDELKORN: Well, I can't give it to you in any other form. We have values of diffusion lengths for 10-20 ohm centimeter boron doped materials, and although as I mentioned there is scatter, in general the aluminum diffusion lengths are considerably higher. I will be glad to show some of the things we have at the Wednesday night meeting. We have a tremendous amount of data on annealing the cells and on the Denney effect. We have proton bombardment damage data for 1000 ohm centimeter cells, which shows that at fluxes of 3×10^{11} of 10 Mev electrons, 1000 ohm centimeter cells are virtually undegraded in terms of diffusion length. We have considerable amounts of data that would answer that, and I will be glad to show this data at the Wednesday night meeting.

RAPPAPORT - RCA: Unfortunately, many of us won't be here Wednesday night. The important data is power output versus flux. Diffusion length is a very fine scientific measurement but it doesn't tell the story for solar cells, especially when you go to very high resistivities.

MR. MANDELKORN: I agree with you, Paul, in fact I also think and I hope you agree with me that the short circuit current degradation of cells does not tell the entire story. Eventually all comparisons of cells based on short circuit currents and diffusion lengths have to finally be put behind comparisons based on power output. I emphasize this, the last slide showed measurements of power output under valid solar simulation.

PRINCE - EOS: What is the super blue coating?

MR. MANDELKORN: I'm glad it didn't come up before. When we are cleared to present information on this type of coating, we will discuss it with industry. At the moment we are not cleared to present this information.

ROSS - HOFFMAN ELECTRONICS CORPORATION: I believe that the segregation coefficient of aluminum is rather high. The nice thing about making boron-doped

PIC-SOL 209/5

ingots is that you get a reasonably good yield of material. I don't believe that's true of aluminum, is it?

MR. MANDELIKORN: Contrary to expectations the growth of aluminum should be much better or at least as good. Since it has such a high segregation coefficient, we find that most of the aluminum remains in the melt throughout. It's as if you are growing from an infinite source, and we get very high uniformity both radially and axially. We feel that this is a point of superiority which you do not achieve with boron.

PIC-SOL 209/5
Section A-7

N64-29159

THE ELECTRICAL CHARACTERISTICS OF IRRADIATED SILICON SOLAR CELLS
AS A FUNCTION OF TEMPERATURE

Presented by

Brian T. Cunningham

NASA-Goddard Space Flight Center

Greenbelt, Maryland 20771

2 June 1964

29159

ABSTRACT

The electrical characteristics of N/P (less than one ohm-cm to a nominal 10 ohm-cm base resistivity) and P/N (one ohm-cm) silicon solar cells irradiated with 1 Mev electron flux to a level of 10^{16} electrons/cm² have been obtained through a temperature range of -100 degrees Centigrade to +125 degrees Centigrade. The information was obtained using a tungsten light source in conjunction with a 3-centimeter water filter. Correction techniques are described to convert the spectral and intensity distributions to the air mass zero operating environment. Curves are presented which relate the power, voltage, temperature and 1 Mev electron flux level in a manner useful to the solar power supply designer.

and

SUMMARY

Satellite solar power supplies are subject to degradation from temperature and hard particle radiation. When the power supply is operating in the constant voltage mode, it is essential to choose the optimum operational voltage per cell for the space environment.

Post-irradiation electrical measurements were made on N/P (less than 1 ohm-cm to a nominal 10 ohm-cm base resistivity) and P/N (1 ohm-cm base resistivity) state-of-the-art (1962) silicon solar cells. These cells had been irradiated at room temperature with 1 Mev electrons at various flux levels up to 10^{16} electrons/cm². The electrical characteristics of the cells were determined for the entire temperature range between -100°C and +125°C, using a tungsten light source with a 3 cm water filter. Spectral and intensity corrections can be made to obtain air mass zero equivalent outputs.

The measurements clearly show the superiority of the 10 ohm-cm N/P cell for all solar power supplies subject to appreciable amounts of irradiation. Families of curves were developed which relate the solar cell power, operational voltage, temperature and 1 Mev flux level. These curves will aid the designer in the selection of the optimum operational voltage per cell. They can be directly applied when the solar power supply is operating in the constant voltage mode and adapted through cross-plotting to a peak power or constant load system. Selection of too high an operational voltage per cell, combined with a low estimate of either solar array temperature or hard particle irradiation, can be disastrous for the power system.

THE ELECTRICAL CHARACTERISTICS
OF IRRADIATED SILICON SOLAR CELLS
AS A FUNCTION OF TEMPERATURE

by

Brian T. Cunningham, Robert L. Sharp

and Luther W. Slifer

Introduction

Numerous studies have been conducted to determine the effect of electron irradiation on silicon solar cells. In order to extend the knowledge already gained in this area, an investigation was undertaken to determine the electrical characteristics of irradiated silicon solar cells as a function of temperature. Consultation with individuals familiar with satellite environments indicated that a temperature range of -100°C to +125°C would be appropriate for study.

During October and November 1962, silicon N/P and P/N state-of-the-art solar cells were purchased from nine different manufacturers. All the cells received had a photovoltaic area of approximately 1.8 cm². Since no particular requirement was placed on base resistivity, the cells received from the producers varied from less than 1 ohm-cm to approximately 10 ohm-cm, depending on the manufacturer's production methods. The voltage current (E-I) characteristics of these cells were measured in sunlight and under tungsten illumination at, or near, room temperature. Some cells from each manufacturer were set aside for thermal and mechanical tests and thirty cells from each manufacturer were forwarded to the Naval Research Laboratory, Washington, D.C. for irradiation. Fifteen of these cells were irradiated with 1 Mev electrons

in dosages varying from 10^{11} to 10^{16} electrons/cm². The room temperature characteristics of these irradiated cells were obtained (1) and these same cells were then made available for the temperature effects study described here.

Equipment

The experimental equipment used to collect the data is shown in Figures 1 and 2. The unit consists of a 9" diameter aluminum temperature-controlled chamber sealed off on one end by a 3 cm thick, circulating water, cooling bath contained by 1/4" thick plexiglass walls. The water bath also served as a filter for the tungsten source by cutting out a large amount of the undesirable infrared. The other end of the chamber was fitted with an aluminum temperature control block shown in Figure 2. The unit contains both a 340-watt, nichrome wire heater and a cooling spiral of 1/4" aluminum tubing for the transfer of liquid nitrogen. The front of the temperature control block is a 1/2" thick heat sink and acts as a base for the 1/8" thick copper plate on which the cells are mounted.

The light source used in the investigation was a 300-watt tungsten filament, reflector flood bulb. The bulb was calibrated for color temperature and was operated at 2800°K in the cylindrical light chamber shown in Figure 1. The entire assembly was constructed so as to prevent stray light from affecting the test. The bulb platform was mounted on a worm screw so that the intensity of illumination on the cells could be adjusted by moving the source closer to or further away from the cells under test. All surfaces exposed to the light source were coated

with optical quality black paint to prevent reflections which would disturb the uniformity of illumination. After assembly the entire 6.5 square inch area of the temperature control block was checked for illumination uniformity, using a standard solar cell as a detector and found to be uniform within 2%. The uniformity of illumination on the cells is considered better than this because they were mounted in the central 3 square inches of this area.

When in operation, the temperature chamber was evacuated to 35 microns of mercury in order to prevent any frost accumulation on the cells at the low temperatures. Temperatures were measured using three copper-constantan thermocouples calibrated over the temperature range of the tests to an accuracy of $\pm 1^{\circ}\text{C}$. An attempt was made to determine the cell junction temperature as closely as possible. To this end, the thermocouples were placed on the top (on the contact strip) and on the bottom of the cells, first to determine if a temperature gradient existed, and second, to find out what its magnitude might be. The data collected led to somewhat inconclusive results and further work is being performed in this area. The thermocouple outputs were initially measured with a potentiometer. Later a deflection type pyrometer was employed, which gave results nearly as accurate as those from the potentiometer with a great saving of time. At the extremes of the temperature range, an accuracy of $\pm 5^{\circ}\text{C}$, including errors due to temperature gradients on the cells, was obtained. This accuracy improved to within $\pm 1^{\circ}\text{C}$ as room temperature was approached.

The solar cell electrical characteristics were measured by varying the load resistance across the cell from 1 ohm to 2500 ohms. The current flowing with the 1 ohm load across the cell is, by accepted definition, short circuit current, I_{sc} , while the voltage across the 2500 ohms is considered to be open circuit voltage, V_{oc} . The complete I-V characteristics were recorded on an X-Y plotter to obtain a permanent record.

Procedure

I-V characteristics were obtained for all cells, using both sunlight and the filtered tungsten source. For the sunlight measurements, the sun intensity was monitored with a 15-junction normal incidence pyrheliometer. The solar cell short circuit current was measured in collimated sunlight and then linearly normalized to the short circuit current for a sunlight intensity of 100 mw/cm². These normalized current readings were compared to the short circuit current readings obtained from measurements made on the cells at room temperature using the tungsten light source. The latter measurements were made with the illumination set at 100 milliwatts/cm² "sunlight equivalent." To accomplish this, a standard solar cell with a known short circuit current at 100 milliwatts/cm² sunlight input was used in setting the illumination level from the tungsten light source so that the same short circuit current was obtained.

Mounting of the cells was initially accomplished by heating a pre-tinned copper plate to the solder melting point. Four solar cells were then placed on the plate and the unit was removed to a cool heat sink as quickly as possible. Results using this system were poor. First,

electrical measurements before and after mounting indicated changes in short circuit current up to 4%; and secondly, cells under test would occasionally shatter when undergoing temperature changes. To alleviate this problem, a conductive epoxy was used to bond the cell to the test plate. Curing of the epoxy at 60°C had no measurable effect on the electrical characteristics of the cells; neither was any additional series resistance evident. The epoxy held throughout the test temperature range and no cracking of the cells was observed after institution of its use.

Cells to be tested were selected at random in groups of four and mounted on the copper plate. The cells were then placed in the chamber and the illumination was adjusted to give the "pre-chamber installation" short circuit current value from the cells. The chamber was then evacuated and the temperature lowered to -110°C. Because of the comparatively large heat sink, it was found suitable to simply let the temperature drift upward while readings were taken at the desired temperature intervals. In most cases, all four I-V curves could be obtained with a variation of only $\pm 2^\circ\text{C}$ of the nominal measuring point. I-V curves were then analyzed for short circuit current, open circuit voltage, maximum power, and power at specific voltages.

Results and Discussion

The data obtained from the measurements and its analysis and interpretation will be presented in four parts. The first three parts present individual electrical parameters, i.e., short circuit current, open circuit voltage and maximum power as a function of temperature and

irradiation. The final section shows the interrelationship of power, voltage, temperature and flux (P , V , T and Φ) in the manner considered most useful to the solar power supply designer.

It should be noted that the electrical parameters in the ensuing analysis are presented in absolute terms and are therefore subject to criticism from a "representative sampling" viewpoint. In defense of this approach it can be said:

1. All the available irradiated samples were temperature-tested.
2. Wherever more than one sample was available (i. e., non-irradiated cells and those irradiated to 10^{16} electrons/cm²), favorable comparisons were obtained between similar cells throughout the temperature range.
3. There is a favorable comparison between the results obtained during these tests and earlier results obtained with a larger number of samples at room temperature.

For these reasons, it is felt that the results are, in reality, representative of large samples and the information sufficiently reliable to be extended to this application.

Short Circuit Current

The initial room temperature measurements showed that for non-irradiated cells under tungsten light, essentially the same readings were obtained as in sunlight regardless of manufacturer. However, for N/P solar cells irradiated with dosages greater than 10^{13} electrons/cm², the percent change as seen under tungsten light became significantly

different, depending upon manufacturer, from that seen under sunlight. It should be recalled that in the N/P category several different base resistivity cells were under evaluation, ranging from less than 1 ohm-cm to more than 10 ohm-cm. Results of an earlier investigation⁽¹⁾ show that the higher base resistivity cells are less susceptible to radiation damage from 1 Mev electrons at room temperature. For P/N solar cells a significant difference in the results under the two light sources was observed for dosages greater than 10^{11} electrons/cm². The percent change in short circuit current for solar cells due to irradiation of 10^{16} electrons/cm² as measured using tungsten and sunlight is shown in Table I.

Table I

**Comparison of Sunlight and Tungsten Sources
for Measurement of Short Circuit Current
on Irradiated Solar Cells**

Solar Cell Nominal Base Resistivity	Type	Percent Change in I_{sc} after 10^{16} electrons/cm ²	
		Tungsten Light (100 mw/cm ² sunlight equivalent)	Sunlight (100 mw/cm ²)
10 ohm-cm	N/P	37	26
1 ohm-cm	N/P	49	37
<1 ohm-cm	N/P	57	40
1 ohm-cm	P/N	76	63

These results show the extent to which the degradation in the long wavelength end of the response of the solar cells due to electron irradiation⁽²⁾ is to be considered when analyzing data obtained from measurements on

irradiated cells using a source other than sunlight. In the interpretation of the information presented here, it must be emphasized that tungsten operating at 2800°K is a "red" source, that is, the spectrum reaches a maximum near 1.0 micron (in the infrared region), while the sun is a "blue" source and peaks near 0.46 micron (in the blue). Since electron irradiation degrades the red end of the solar cell spectral response, radiation degradation appears worse under tungsten light than under sunlight.

As shown in Figure 3, the short circuit current does not change linearly with temperature; however, it is worthwhile to compare the change observed over the entire temperature range with respect to irradiation. The average short circuit current coefficient for a non-irradiated cell is $50.8\mu A/{}^{\circ}C$, while for a cell irradiated to 10^{16} electrons/cm² it increases to an average of $69.8\mu A/{}^{\circ}C$ over the range -100° C to +100° C . This average is derived from data taken on all manufacturers' cells.

Short circuit current degradation as a function of irradiation has been adequately covered in an earlier report.⁽¹⁾ Since the results of the present study do not add to the data already presented except as previously mentioned, no further discussion need be given on this parameter.

Open Circuit Voltage

Open circuit voltage degradation as a function of flux level is shown in Figure 4 for both N/P and P/N solar cells. The N/P degradation points at each flux level represent an average of five different cells,

while the P/N points at each level represent a single cell. The latter data should therefore be treated cautiously. Within the limits of the experiment no appreciable difference in radiation degradation of the open circuit voltage was observed between N/P cells of different base resistivities.

As shown in Figure 5, it was found that open circuit voltage, for both irradiated and non-irradiated (control) cells, decreased linearly with temperature over the entire test range. The average coefficient of open circuit voltage change with temperature was $-2.34 \text{ mv}/{}^{\circ}\text{C}$. The extremes were $-2.16 \text{ mv}/{}^{\circ}\text{C}$ and $-2.60 \text{ mv}/{}^{\circ}\text{C}$. Since the variation noted appeared between individual cells of the same manufacturer rather than being manufacturer-dependent, it is probably due in large part to experimental error, but effects of real differences between cells (base resistivity effects, for example) are not considered negligible. For this reason, the average of $-2.34 \text{ mv}/{}^{\circ}\text{C}$ is considered the appropriate choice for power supply design calculations. The temperature coefficient was also found to be independent of the level of irradiation as shown in Figure 5. Figure 6 depicts the percent change in open circuit voltage as a function of the percent change in short circuit current for both sun-light and tungsten sources at different irradiation levels for a nominal 1 ohm-cm solar cell. Figure 7 is a similar curve except that the cell has a nominal 10 ohm-cm base resistivity. The purpose of presenting these figures is to emphasize the fact that the degradation of open circuit voltage with irradiation must be considered in the design of a solar power supply.

Figure 8 shows the variation in peak power as a function of temperature and irradiation for a typical set of N/P cells under investigation. Peak power is somewhat meaningless to the power supply designer without reference to temperature, voltage and irradiation level, so no attempt will be made at this point to present detailed variations from one type of cell to another. In a later section of this report, curves will be presented which will allow the designer to determine peak power, taking into consideration the temperature and irradiation levels of interest. Specific values of radiation degradation of peak power at room temperature have been reported earlier.⁽¹⁾ Comparison between results obtained with tungsten light and sunlight as sources for measurement is given in Table II.

Table II

**Comparison of Sunlight and Tungsten Sources
for Measurement of Peak Power
on Irradiated Solar Cells**

Solar Cell Nominal Base Resistivity	Type	Percent Change in P_{max} after 10^{16} Electrons/cm ²	
		Tungsten Light (100 mw/cm ² sun- light equivalent)	Sunlight (100 mw/cm ²)
10 ohm-cm	N/P	50.2	41.3
1 ohm-cm	N/P	58.2	47.6
<1 ohm-cm	N/P	65.2	47.4
1 ohm	P/N	85.5	78.0

P, V, T, and Φ Curves

In order to relate the appropriate solar cell electrical parameters for the power supply designer, curves have been drawn in the manner

of Figure 9. These curves relate power (P), "operational" voltage (V), temperature (T), and flux level (Φ). The origin of this data is the set of I-V characteristic curves which were obtained during this investigation for temperatures between -100°C and $+125^{\circ}\text{C}$ in increments of 25°C . The power at each "operational" voltage is determined and the results are then combined to form the family of P, V, T, and Φ curves. In Figures 9, 10, and 11, the 1 Mev electron flux level and the operational voltage have been held constant so that it is possible to evaluate the effect of cell type and base resistivity on power output. As shown in Figure 9, where the cells have not been exposed to any hard particle irradiation, all the manufacturers' cells lie in a relatively narrow range. For the power supply designer, the P/N cell is the most appropriate choice here due to its higher open circuit voltage, which gives it a higher power over a wider temperature range. In Figure 10, irradiation has progressed to 10^{13} electrons/cm² and all cells with the exception of the severely degraded P/N cell lie in a close range of power output over the temperature range. Hence, if hard particle irradiation equivalent to the damage done by 1 Mev electrons at 10^{13} electrons/cm² were anticipated, the designer would be able to use most effectively the highest efficiency (as measured at room temperature) non-irradiated N/P cell available. Some cross-over will be noted at the higher temperatures; however, it is too early, in terms of irradiation, to see any distinct advantage of base resistivity. Progressing to 10^{16} electrons/cm², in Figure 11, there is a distinct advantage to the higher base resistivity cells. This advantage

becomes less evident as the operational voltage is increased, and in fact, in extreme cases (high temperature) the 1 ohm-cm cell is the more desirable. The reason for this is the higher initial open circuit voltage of the 1 ohm-cm cell relative to the 10 ohm-cm cells among the cells under investigation. However, the solar cell would be operating in an extremely precarious and inefficient region of the P, V, T, and Φ curve in order to achieve any advantage of this characteristic. Figure 12 depicts this extreme situation on an expanded power scale and shows the 10 ohm-cm, 0.40 volt curve dropping inside the 0.40 volt, 1 ohm-cm curve. The 0.45 volt curves of this figure would have the same relationship if complete data were available for this region and hence are shown as such by extrapolation of the 0.45 volt, 10 ohm-cm curve. It should be kept in mind that choosing too high an operational voltage, combined with a low estimate of operating temperature, would be disastrous for the power supply because the curves have a steep slope relative to increasing temperature after the peak is achieved. In consequence of the foregoing, the next series of figures (13-21) present the available P, V, T, and Φ curves for the N/P, 1 and 10 ohm-cm cells only. (Although the 10 ohm-cm solar cell has been shown to be more radiation resistant and the preferred choice for the power supply designer in almost all circumstances, the 1 ohm-cm curves are presented because of continued use of this type of cell on solar power supplies.) These figures will directly aid the power supply designer who is designing a constant voltage supply (the most common in satellite use) in determining the most desirable operating voltage once he knows the 1 Mev electron flux

equivalent and the operating temperature of the cell. Also, since these curves are derived directly from the I-V curves, they can be used (through cross-plotting) for any other mode of operation. The curves presented for irradiated cells, if used "as is," allow for a considerable margin of safety in that the source used in the investigation was tungsten.

In order to be useful to the spacecraft solar power supply designer, the data obtained during this investigation will have to be corrected to reflect the air mass zero operating environment. Also, extrapolations are necessary to reflect solar cell conversion efficiency improvements made by manufacturers since this project was initiated.

To correct the tungsten air mass 1 equivalent data (i.e., all P, V, T, and Φ curves in this report) to the air mass zero operating environment, both spectral and intensity adjustments must be made. Tungsten, as was indicated earlier, exaggerates I_{sc} damage seen on irradiated cells. To evaluate this difference, I_{sc} measurements were made under both tungsten light and sunlight on all cells. The results were then normalized to 100 mw/cm² and 30°C. The ratio of the short circuit currents under the two illumination conditions was obtained for each group of cells and is shown in Figure 22 for the 1 and 10 ohm-cm samples. Measurements indicate that this ratio holds, within experimental limits, throughout the temperature range. If the power value, on any of the P, V, T, and Φ curves is multiplied by this factor, taken at the appropriate flux level, the result is a sunlight air mass one, 100 mw/cm² value. The air mass zero intensity adjustment is made by obtaining the ratio of energy, in the solar cell response region, of the sunlight air mass zero

spectrum to the sunlight air mass one spectrum, weighted according to the spectral response of the cells. This ratio has been determined⁽³⁾ to be 1.17.*

The solar cell efficiency improvement correction is made by obtaining an I-V curve of the new non-irradiated cell at some convenient temperature and illumination condition. Similar information is extracted from the appropriate (1 or 10 ohm-cm) F, V, T, and Φ curve for the same temperature and illumination conditions. A ratio of the currents of the old and new cell at the constant voltage point of interest is then extracted from this data. All of the power values on the P, V, T, and Φ curves at this particular voltage can then be multiplied by this ratio to obtain a good estimate of the output from the improved cell. This correction may be applied only to cells which are similar, in terms of dopants, base resistivity, etc., to the ones under investigation in this report. Fortunately, most of the cells being used on today's power supplies fall into this category. The result of this correction will still yield a slightly conservative power figure in that additional improvements have been made in both the series resistance and open circuit voltage of the newer cells.

To summarize the above conversions:

$$P_2 = P_1 \left(\frac{I_s}{I_1} \right) \left(\frac{M_0}{M_1} \right) \left(\frac{I_2}{I_1} \right) \quad (1)$$

*Different values ranging between 1.17 and 1.23 are in common use. The value 1.17 was chosen here because it represents a properly conservative approach to extrapolations.

where

P_2 = Power of the improved solar cell at air mass zero at the given conditions of temperature and irradiation.

P_1 = Power as measured under the tungsten air mass one equivalent conditions. This value is taken directly from the P , V , T , and Φ curves presented herein.

I_s = Sunlight short circuit current after irradiation at a given temperature and 100 mw/cm^2 .

I_T = Tungsten short circuit current after irradiation at the same temperature as I_s (see Figure 22).

M_0 = Air mass zero energy in the solar cell response region weighted by the solar cell response.

M_1 = Air mass one energy in the solar cell response region weighted by the solar cell response.

I_1 = Current of the lower efficiency (old) cell at the desired operational voltage and some comparative temperature.

I_2 = Current of the higher efficiency (new) cell at the same operational voltage and temperature and under the same illumination conditions as I_1 .

The use of the P , V , T , and Φ curves and the corrections described above are best illustrated with the aid of a design procedure description.

In this example, the solar array operating conditions have been predicted to be 0°C with a 1 Mev equivalent flux of $10^{15} \text{ electrons/cm}^2$ at end of mission.

1. The 10 ohm-cm cell is chosen due to the high 1 Mev flux equivalent. The P, V, T, and Φ curve which fits these conditions is found in Figure 20.
2. The optimum operational voltage is determined from Figure 20. In this case 0.45 volt is nearly optimum. (If more detail is required, power-voltage curves can be constructed from the given data.)
3. Correct the power at this voltage to reflect the air mass zero operating environment and the efficiency improvement on the newer cells using equation (1).

Conclusions

The following conclusions regarding the characteristics of 1962 state-of-the-art silicon solar cells bombarded under low level illumination and room temperature conditions by 1 Mev electrons have been obtained.

1. Post-irradiation measurements in the temperature range from -100°C to $+125^{\circ}\text{C}$ show N/P solar cells to be decidedly more radiation resistant than the 1 ohm-cm P/N cells.
2. Post-irradiation measurements in the temperature range from -100°C to $+125^{\circ}\text{C}$ show the nominal 10 ohm-cm N/P solar cells to have greater radiation resistance than the lower, 1 ohm-cm and less than 1 ohm-cm nominal base resistivity cells.
3. No single cell type (N/P or P/N; 1 ohm-cm or 10 ohm-cm base resistivity) can be chosen as the best cell (for power supply use)

for the entire range of irradiation from 0 to 10^{16} electrons/cm², the entire range of temperature from -100°C to +125°C, and the entire range of operating voltages. This results primarily from the fact that significant differences exist in the open circuit voltages of the various types of cells. However, the following generalizations can be made:

- a. Prior to irradiation, P/N cells have better electrical power generating characteristics than N/P cells and the difference is most significant for higher operating voltages (above 0.35 volt/cell) and higher temperatures (above 50°C). This is primarily because of the higher open circuit voltage of the P/N cells.
- b. After nominal irradiation (equivalent to 10^{13} electrons/cm²), the overall higher radiation degradation rate of the P/N cells results in the loss of the advantage at the higher operating voltages and higher temperature conditions and also results in a disadvantage under low voltage and low temperature conditions. The amount of radiation is still not sufficient to produce a distinction between base resistivities in the N/P cells.
- c. After extensive irradiation (equivalent to 10^{16} electrons/cm²), the P/N cells are significantly poorer than any of the N/P cells under all conditions of temperature and operating voltage. The difference in radiation sensitivity is sufficient to clearly show the nominal 10 ohm-cm cells to be better than the nominal 1 or less than 1 ohm-cm cells except at the higher temperatures and higher voltages.

4. Degradation of open circuit voltage as a function of both 1 Mev electron flux and increasing temperature has a significant effect on the choice of operating voltage for a solar power supply.
 - a. The percentage degradation of open circuit voltage in sunlight with irradiation is roughly 1/2 the percentage degradation of short circuit current.
 - b. Open circuit voltage varies linearly with respect to temperature between -100 and +125°C for both irradiated and non-irradiated silicon solar cells.
 - c. The temperature coefficient of open circuit voltage is constant for any cell but varies from cell to cell. The average value is -2.34 mv/°C.
 - d. Irradiation does not appreciably affect the temperature coefficient of open circuit voltage in the temperature range from -100°C to +125°C.
5. Degradation of short circuit current with 1 Mev electron flux is significant, but variation with temperature is relatively unimportant.
 - a. Short circuit current increases but does not increase linearly over the temperature range from -100 to +100°C.
 - b. In general, the average temperature coefficient of short circuit current increases with increasing radiation. For non-irradiated 1 X 2 cm cells, the average coefficient is $50.8 \mu A/^\circ C$ and for cells irradiated to 10^{16} electrons/cm², it is $69.8 \mu A/^\circ C$.

6. Peak power generally decreases linearly above -50°C. Below -50°C, peak power is observed to increase, decrease and not change, depending on the cell. In most cases the change at temperatures below -50°C is small.
7. The P, V, T, and Φ curves represent a convenient aid to the solar power engineer, particularly in the design of constant voltage power supplies, but also in the design of power supplies operating in other modes. These curves show that at less than 10^{13} electrons/cm² the degradation is essentially the same for all N/P cells regardless of base resistivity. They also show that at irradiation levels above 10^{13} electrons/cm², the use of higher base resistivity cells is desirable.

BIBLIOGRAPHY

1. William R. Cherry and Luther W. Slifer, Jr., Solar Cell Radiation Damage Studies with 1 Mev Electrons and 4.6 Mev Protons, NASA-Goddard Space Flight Center, Greenbelt, Md., May 27, 1963.
2. William C. Cooley and Robert J. Janda, Handbook of Space Radiation Effects on Solar Cell Power Systems, Washington, D.C., Office of Scientific and Technical Information, NASA, 1963, p. 28.
3. Solar Cell Measurements, Hoffman Electronics Corporation, Semiconductor Division, El Monte, California, May 1960.

PIC-SOI, 209/5

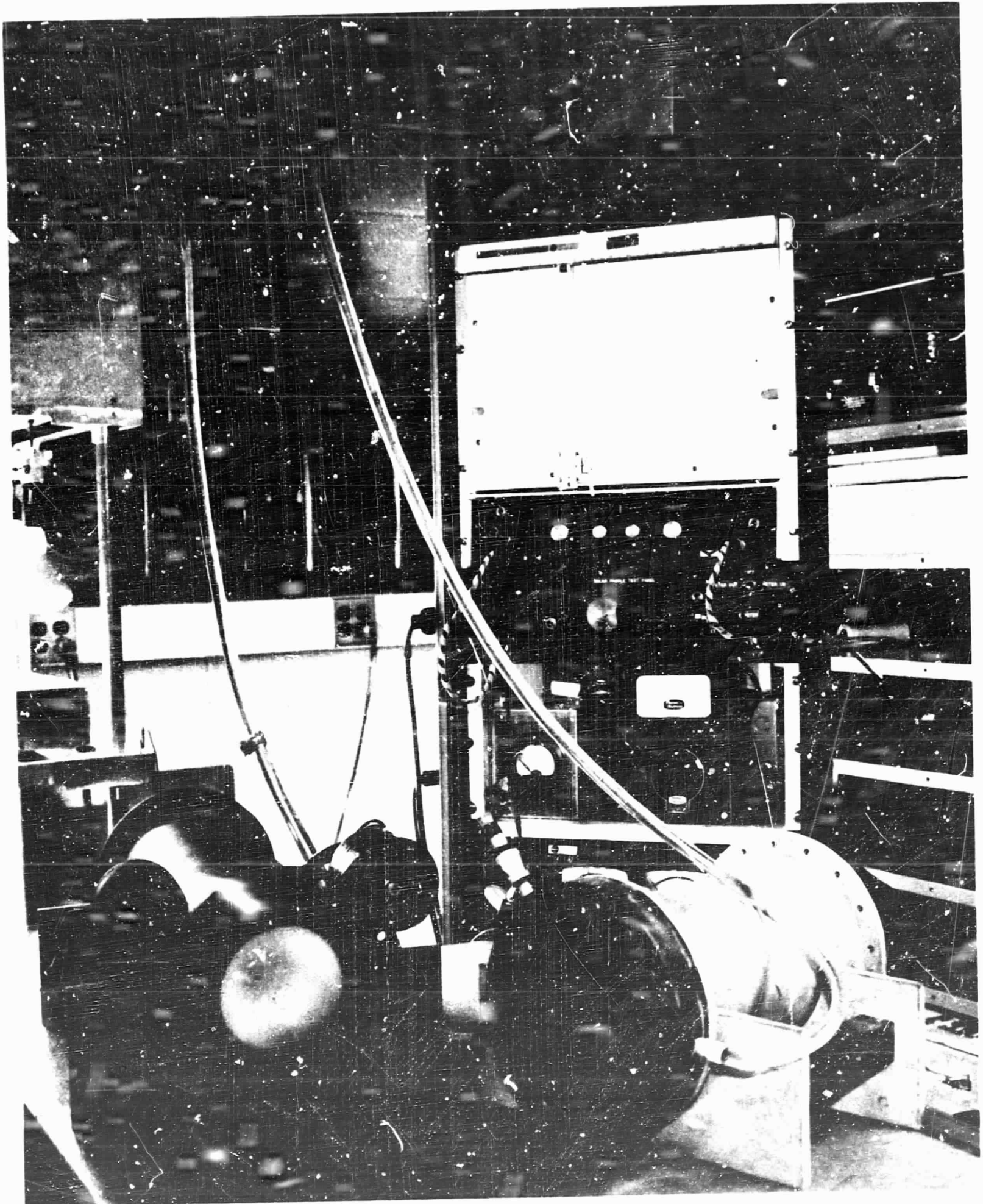
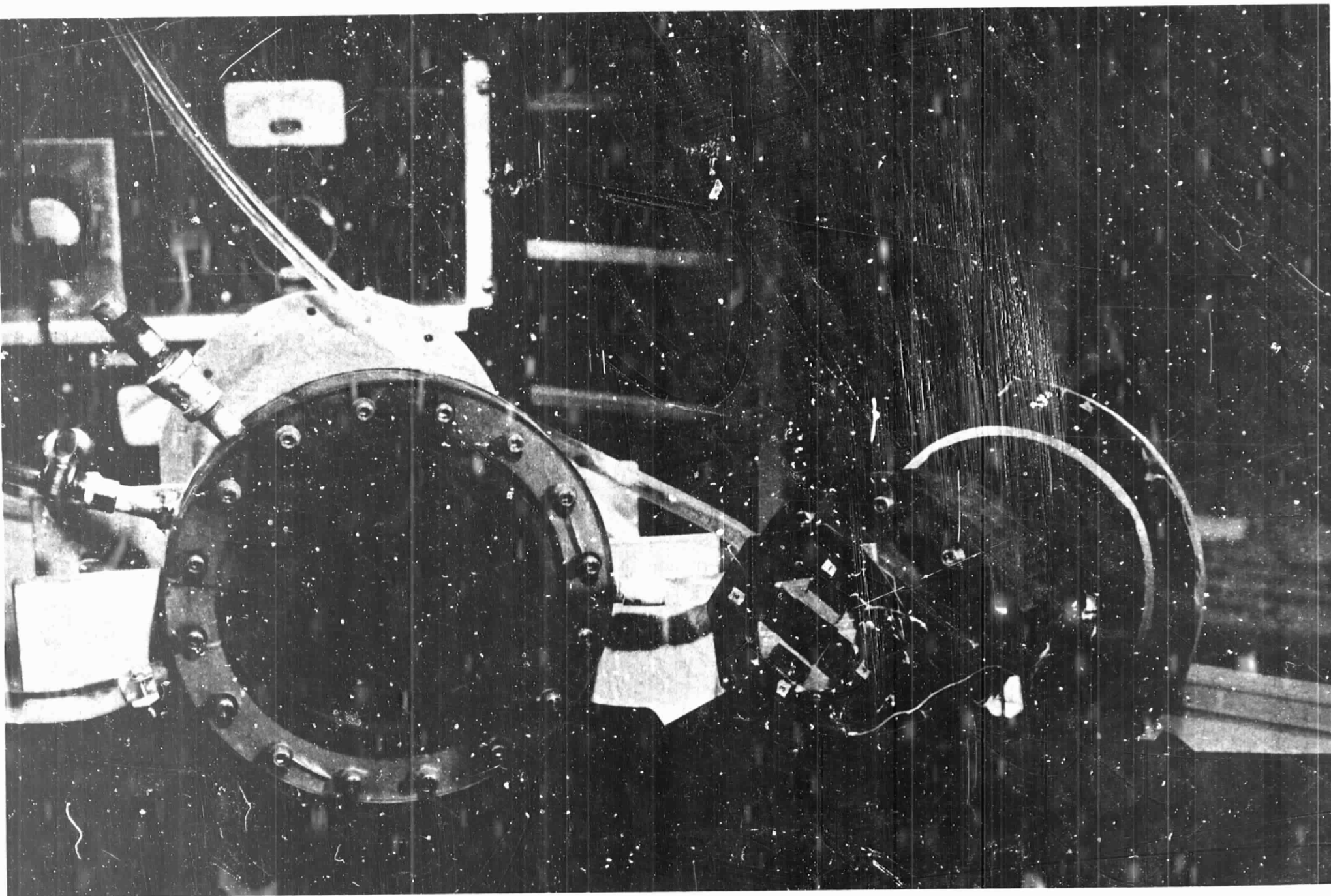


Figure 1 - Test Equipment

A-7-20



A-7-21

Figure 2 - Temperature Control Block and Chamber

PIC-SOL 209/5

**FIGURE 3. EFFECT OF TEMPERATURE AND IRRADIATION
ON SHORT CIRCUIT CURRENT
(TYPICAL CELLS)**

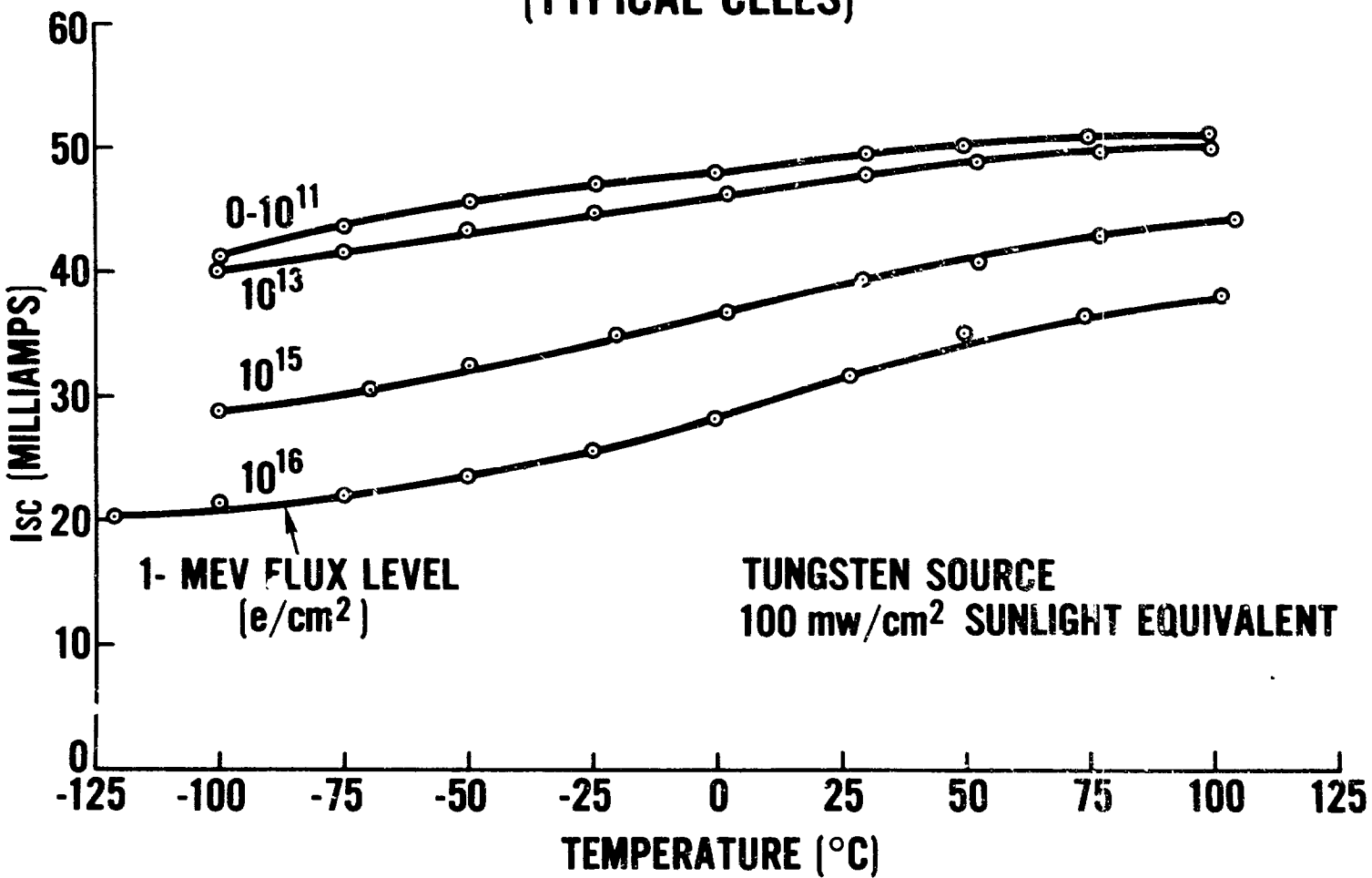
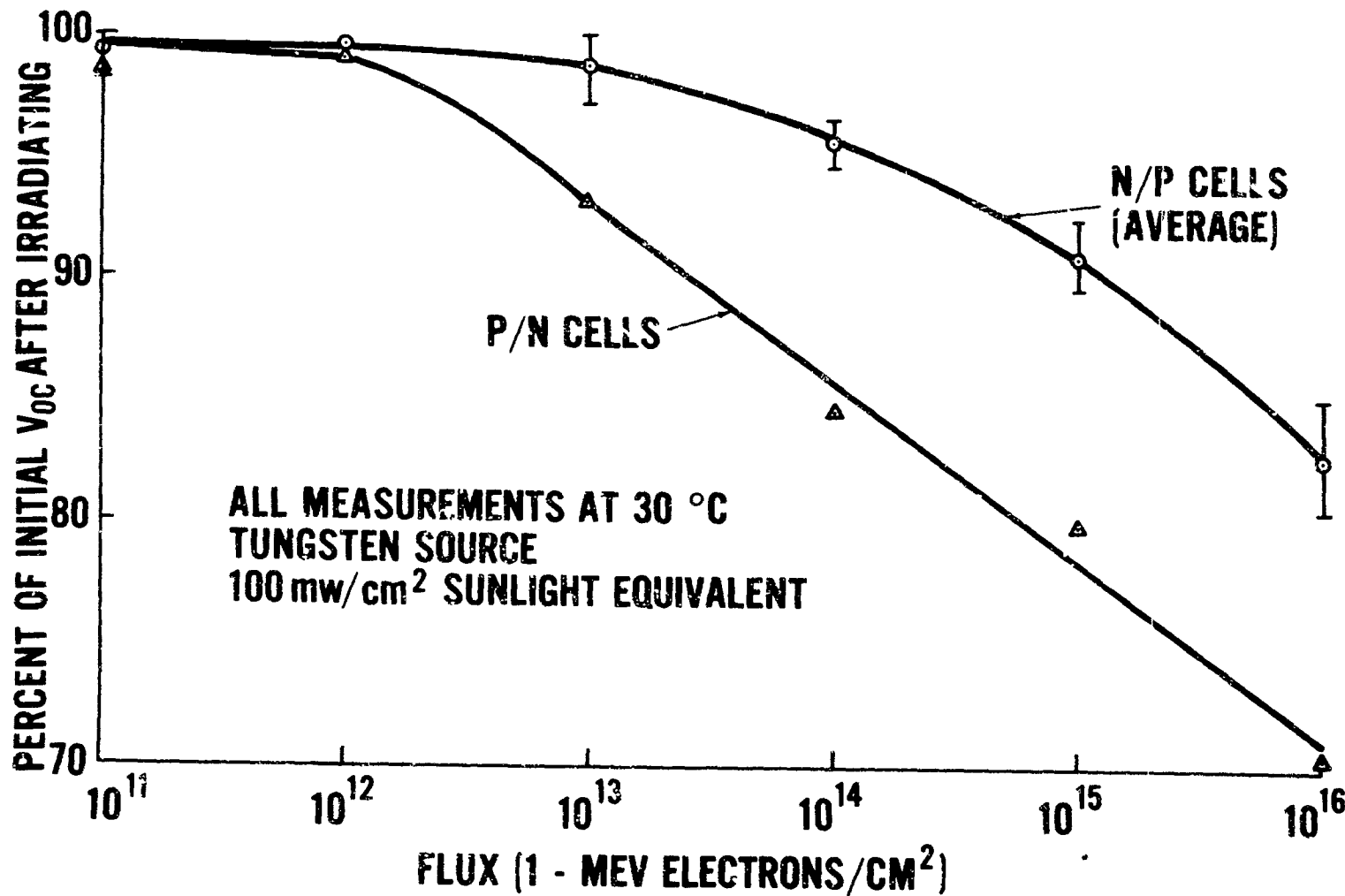
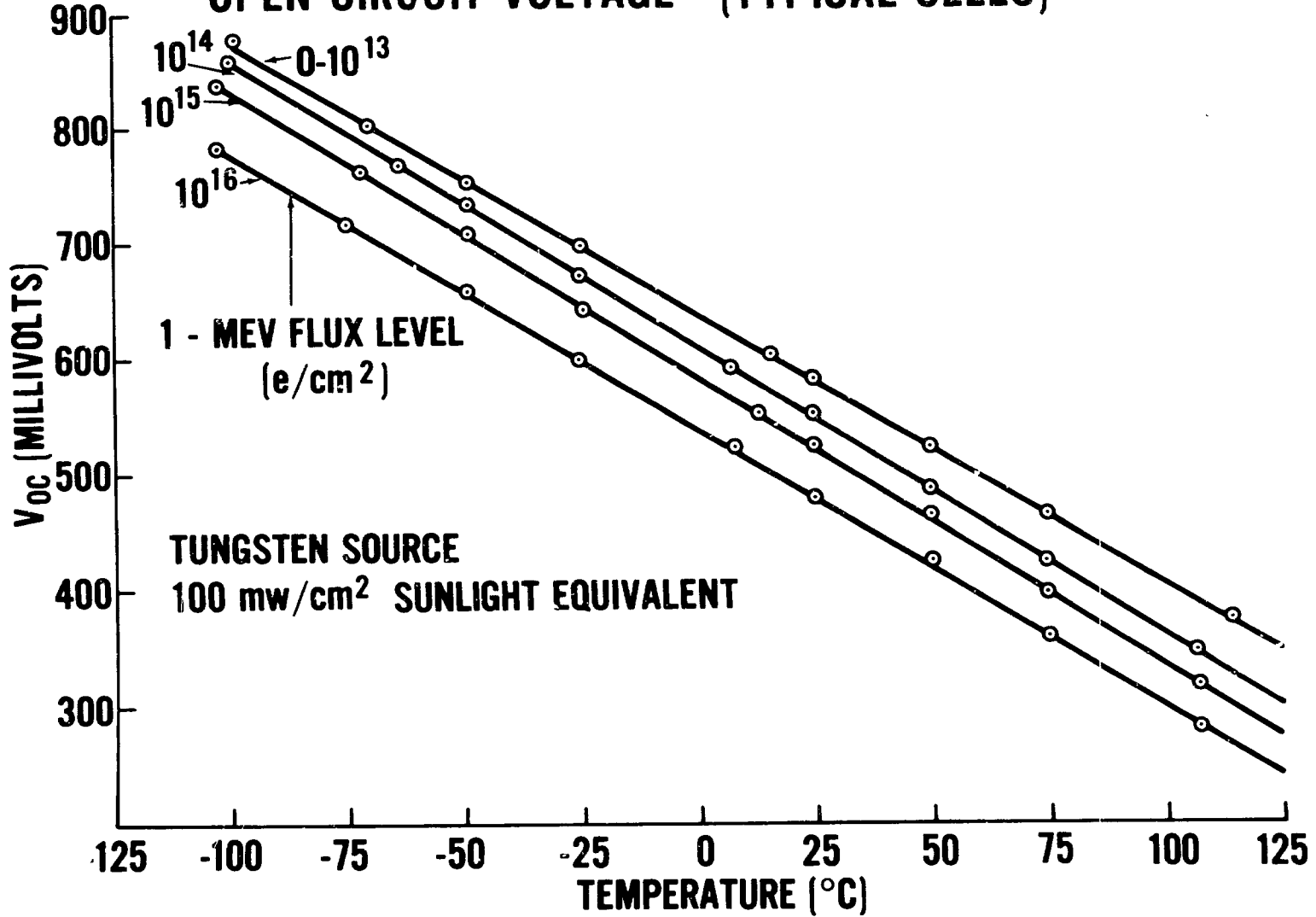


FIGURE 4. DEGRADATION OF OPEN CIRCUIT VOLTAGE



**FIGURE 5. EFFECT OF TEMPERATURE AND IRRADIATION ON
OPEN CIRCUIT VOLTAGE (TYPICAL CELLS)**



**FIGURE 6. COMPARISON OF OPEN CIRCUIT VOLTAGE DEGRADATION
TO SHORT CIRCUIT CURRENT DEGRADATION FOR
NOMINAL 1-OHM-CM CELLS**

A-7-25

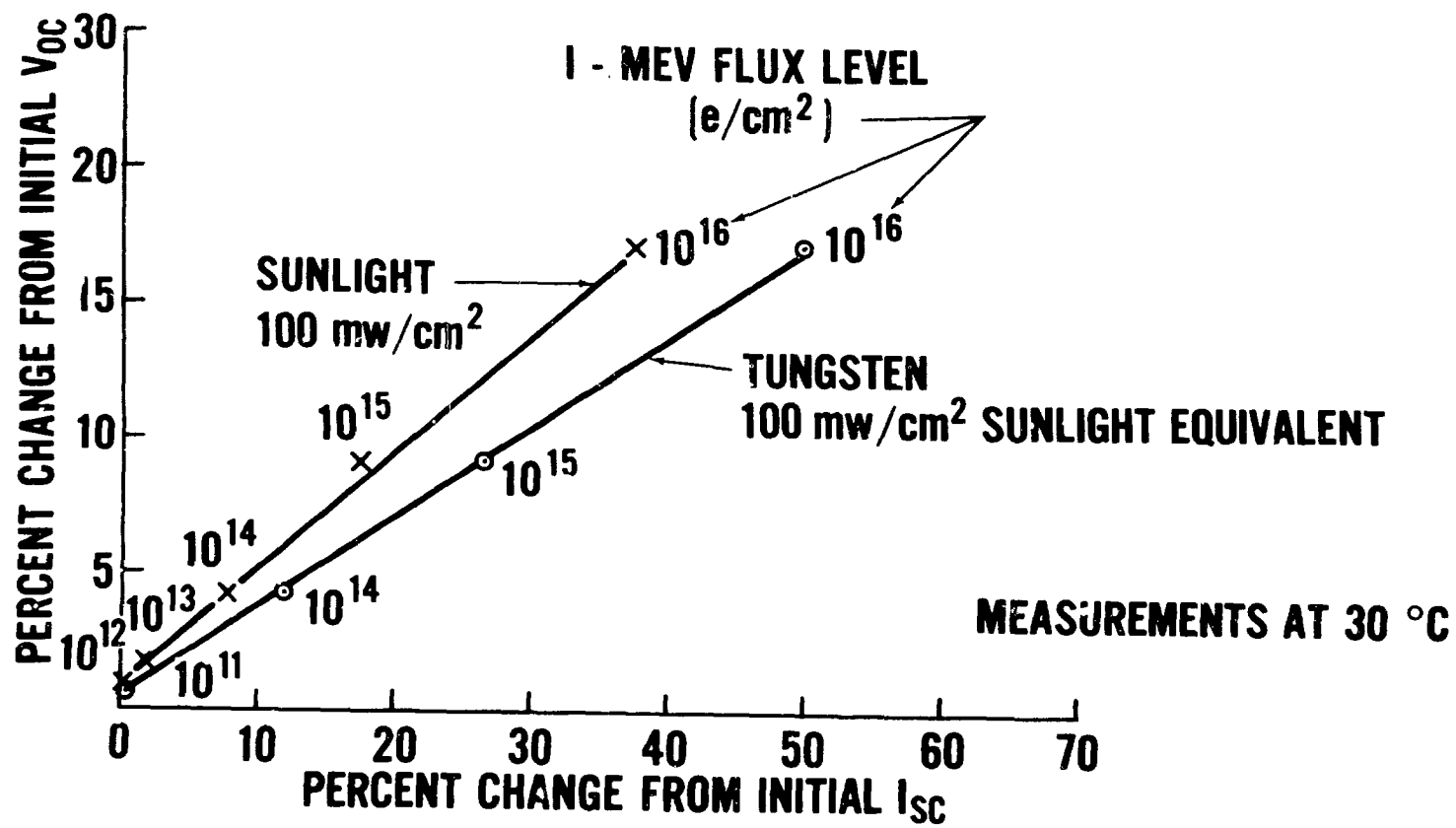


FIGURE 7. COMPARISON OF OPEN CIRCUIT VOLTAGE DEGRADATION
TO SHORT CIRCUIT CURRENT DEGRADATION FOR
NOMINAL 10 OHM-CM CELLS

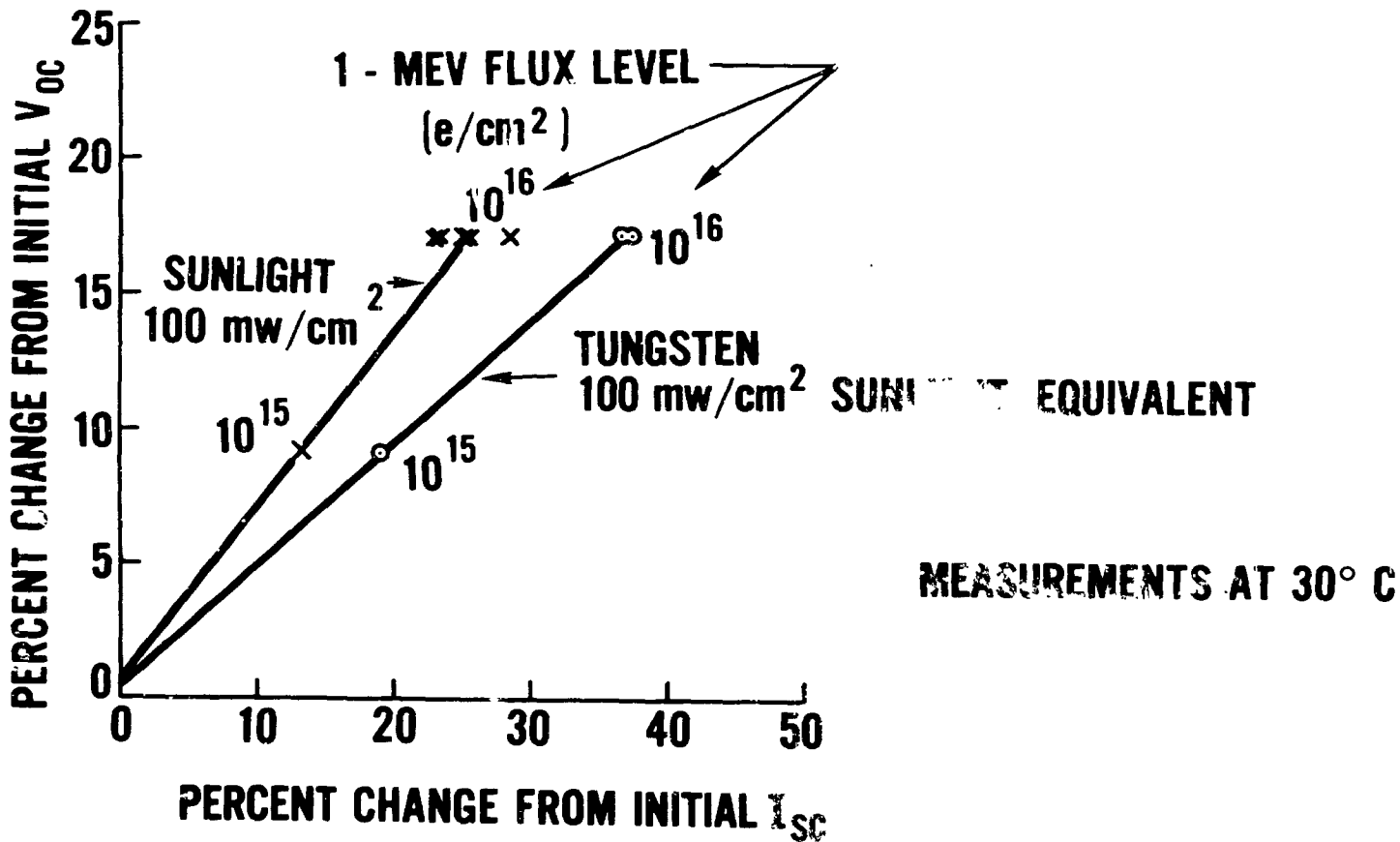


FIGURE 8. EFFECT OF TEMPERATURE AND IRRADIATION ON PEAK POWER (TYPICAL CELLS)

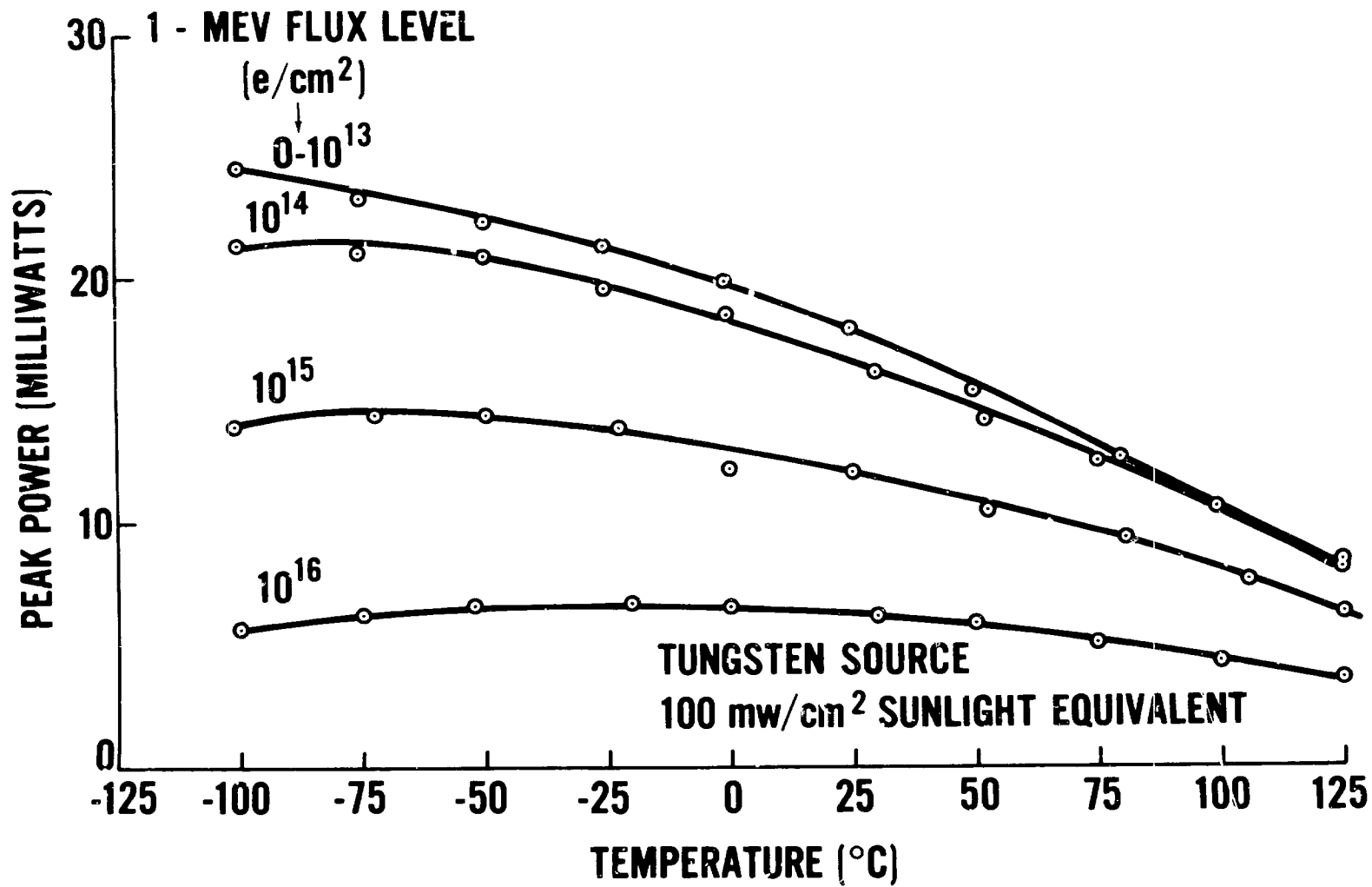
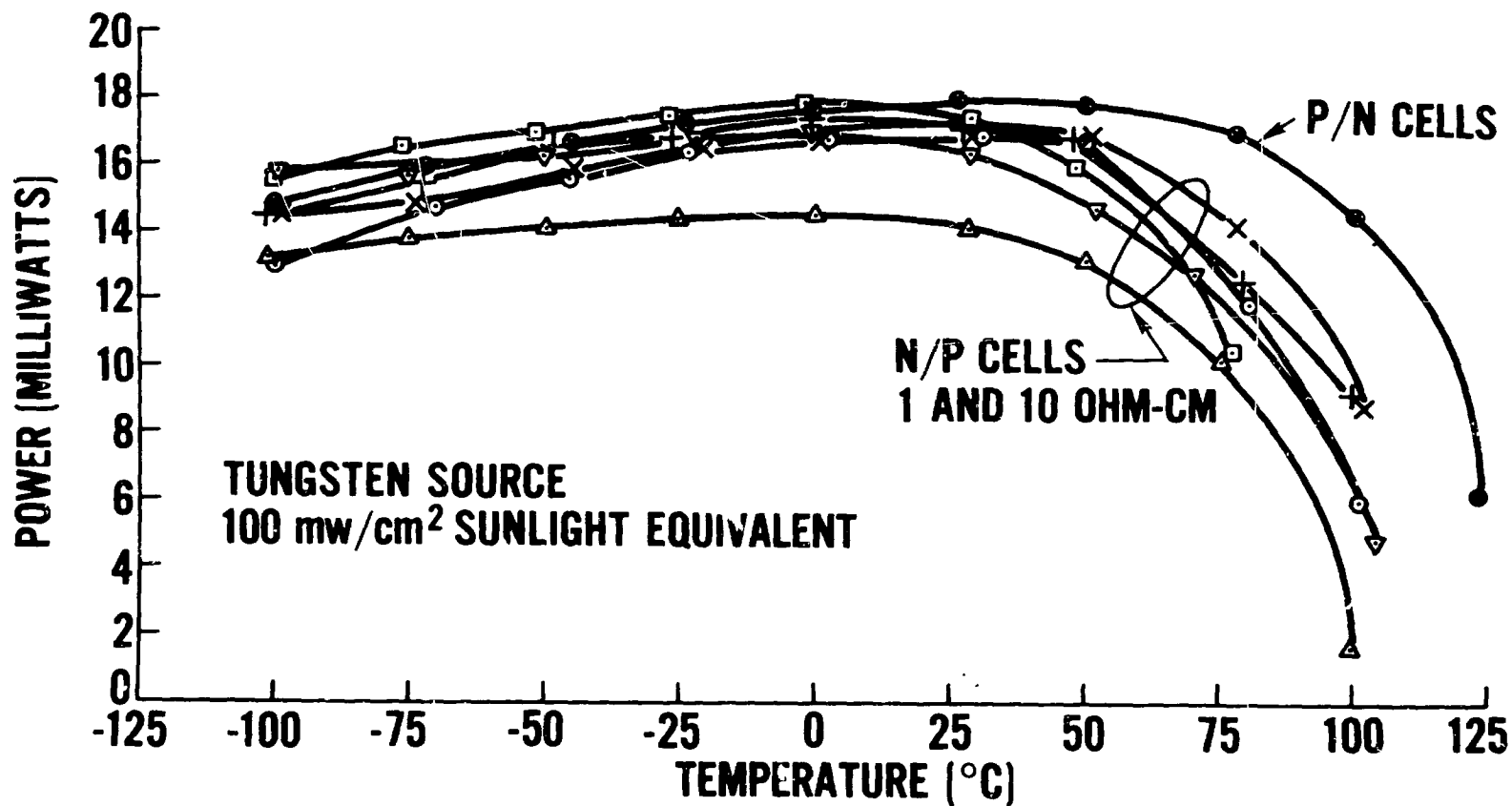


FIGURE 9. COMPARISON OF POWER OUTPUT FOR NON-IRRADIATED SOLAR CELLS AT 0.35 VOLTS



**FIGURE 10. COMPARISON OF POWER OUTPUT AT 0.35 VOLTS
FOR SOLAR CELLS IRRADIATED WITH 1 MEV
ELECTRONS TO 10^{13} ELECTRONS/CM²**

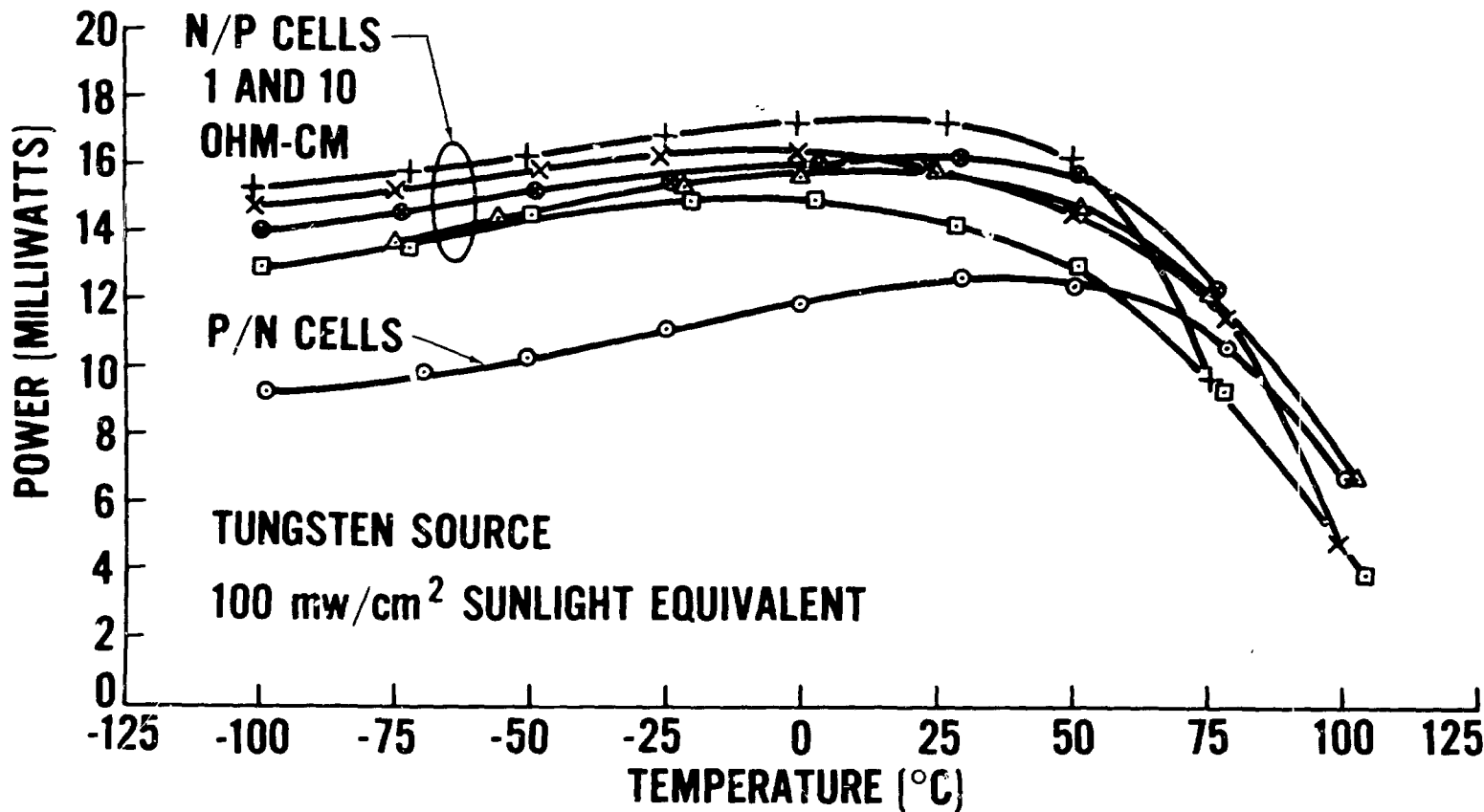


FIGURE 11. COMPARISON OF POWER OUTPUT AT 0.35 VOLTS FOR SOLAR CELLS IRRADIATED WITH 1 MEV ELECTRONS TO 10^{16} ELECTRONS/CM²

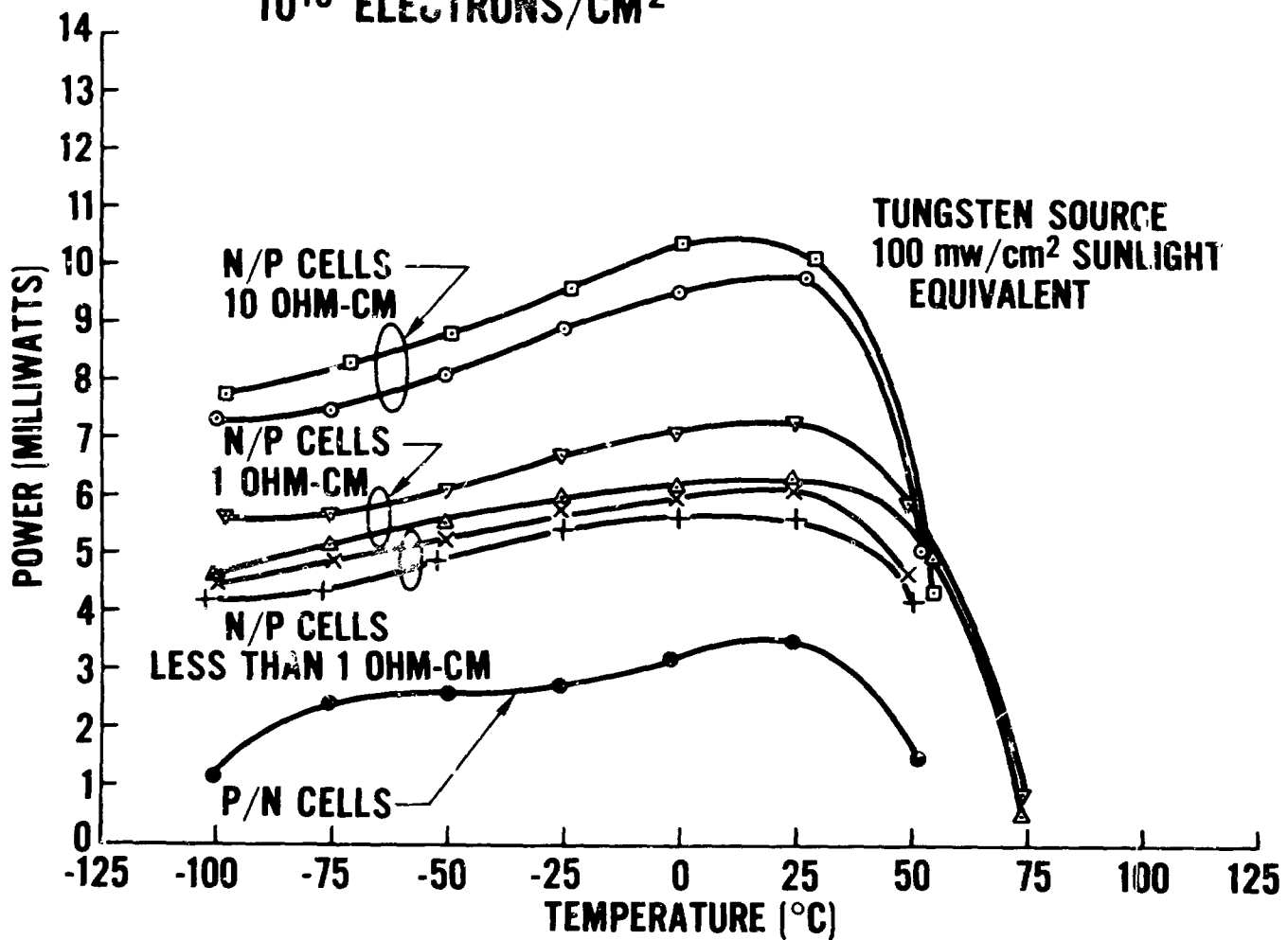
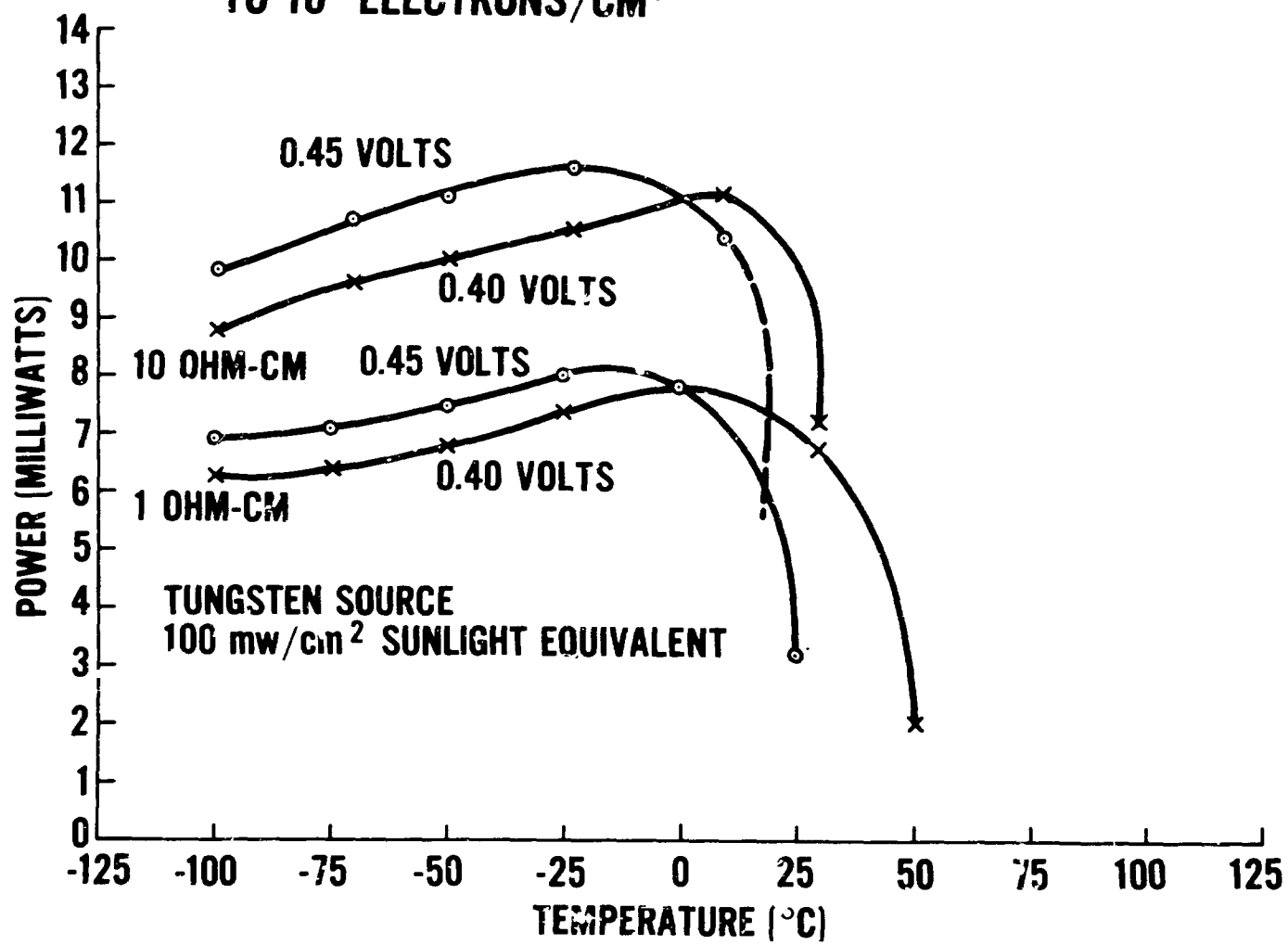
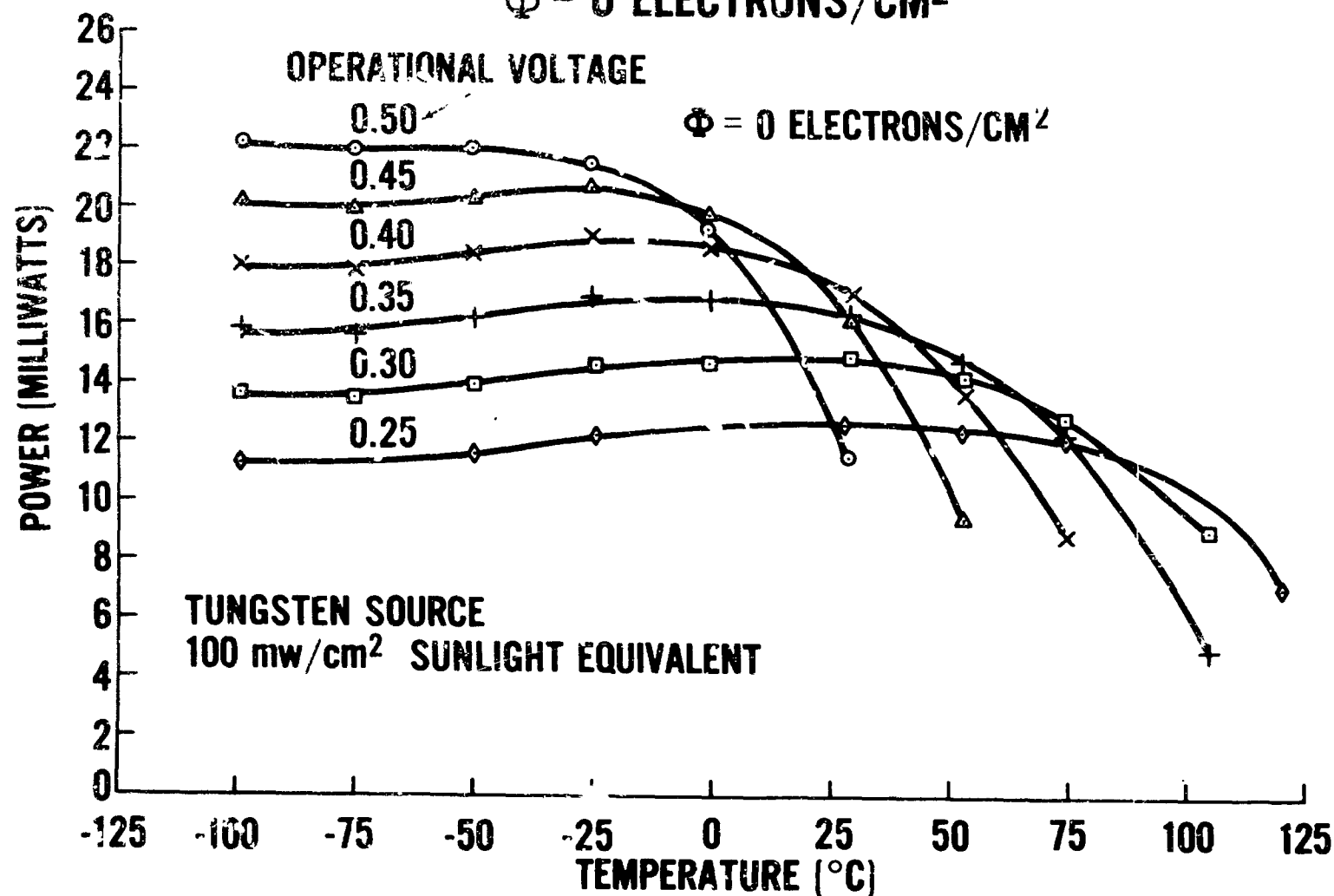


FIGURE 12. COMPARISON OF 1 AND 10 OHM-CM SOLAR CELL POWER OUTPUT AT 0.40 AND 0.45 VOLTS AFTER IRRADIATION TO 10^{16} ELECTRONS/CM²



A-7-31

FIGURE 13. P,V,T, Φ CURVES FOR A 1 OHM-CM N/P CELL WITH
 $\Phi = 0$ ELECTRONS/CM²



**FIGURE 14. P,V,T, Φ CURVES FOR A 1 OHM-CM N/P CELL WITH
 $\Phi = 10^{13}$ ELECTRONS/CM²**

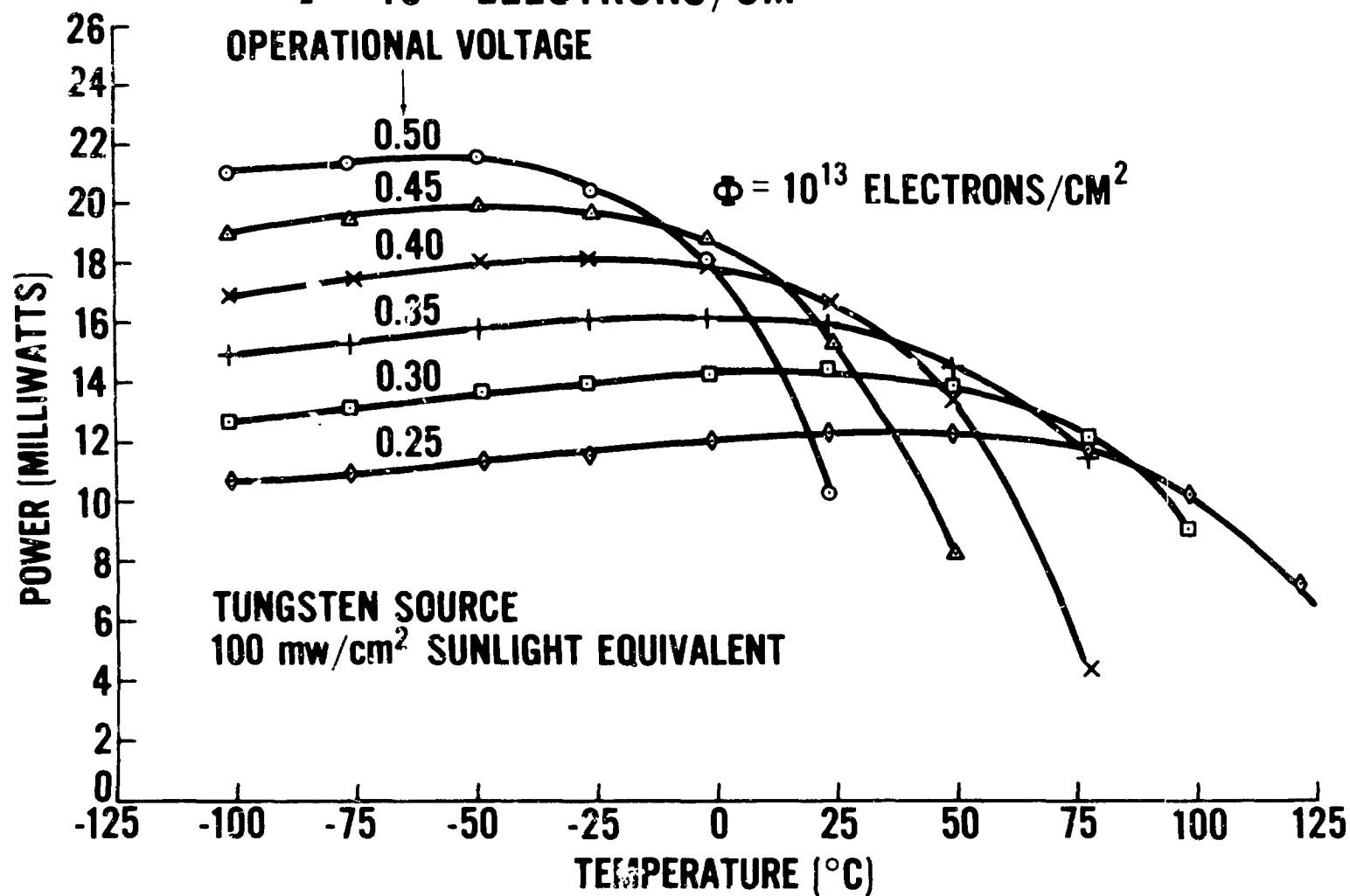


FIGURE 15. P,V,T, Φ CURVES FOR A 1 OHM-CM N/P CELL WITH
 $\Phi = 10^{14}$ ELECTRONS/CM²

PIC-SOL 209/5

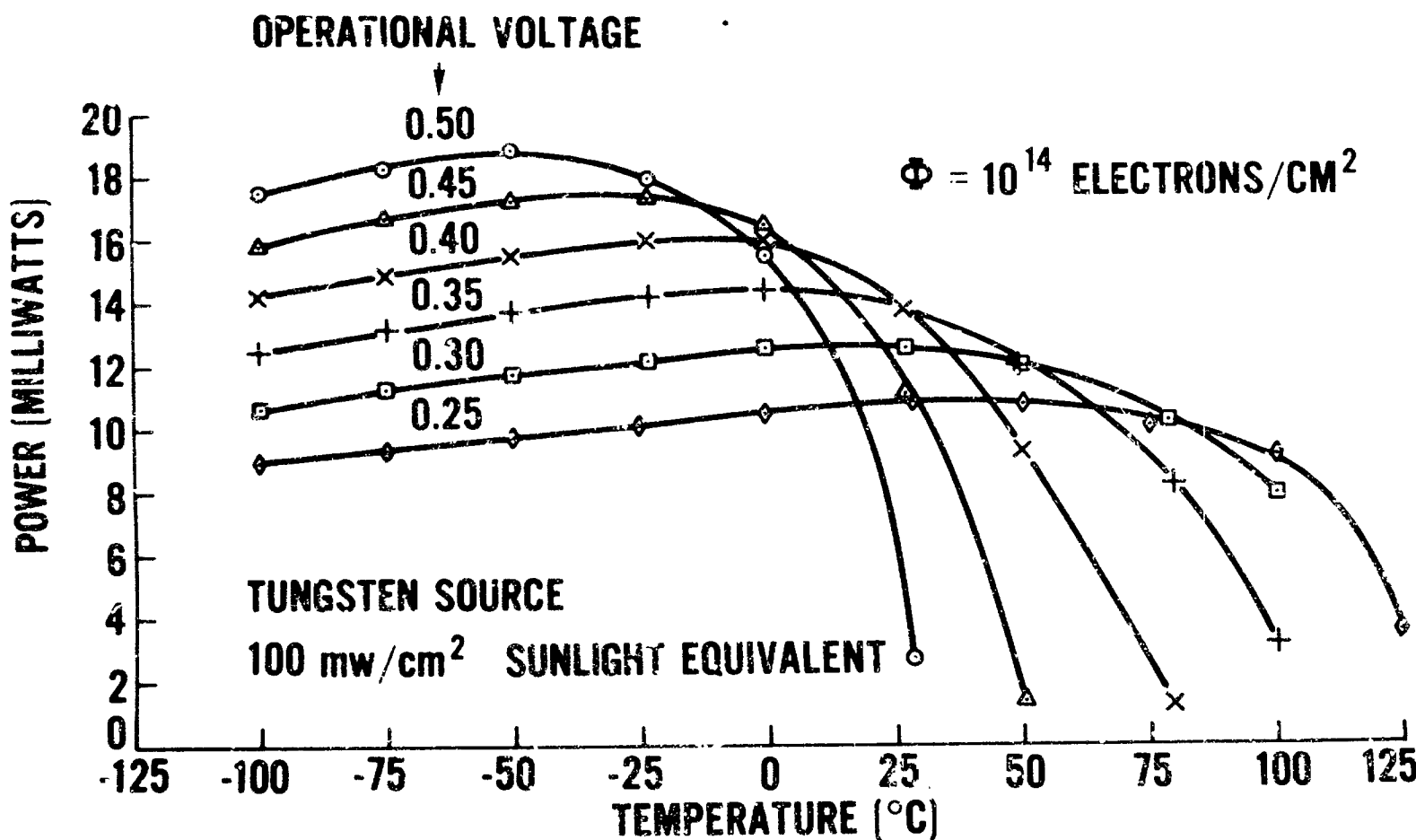


FIGURE 16. P,V,T, Φ CURVES FOR A 1 OHM-CM N/P CELL WITH
 $\Phi = 10^{16}$ ELECTRONS/CM²

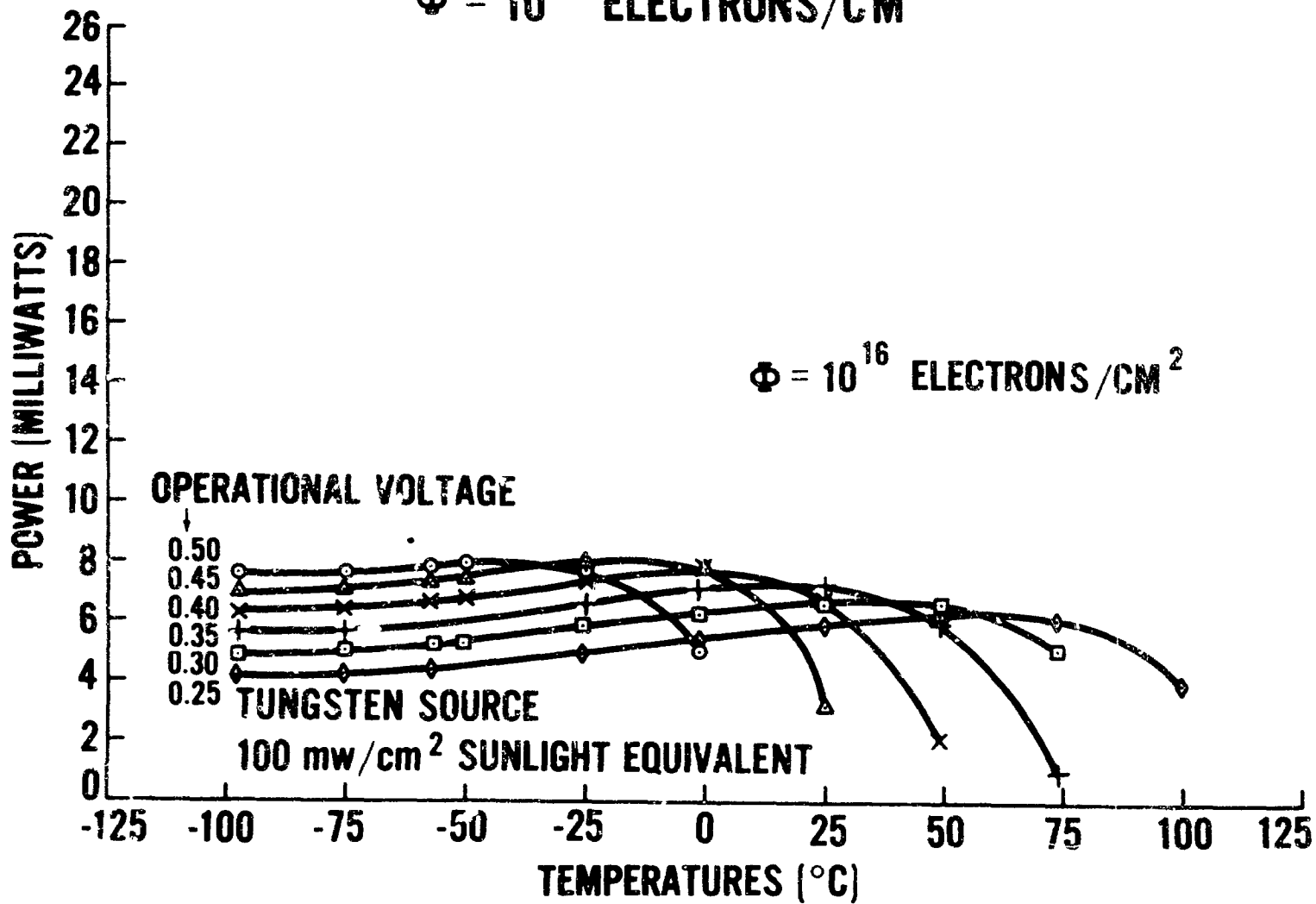
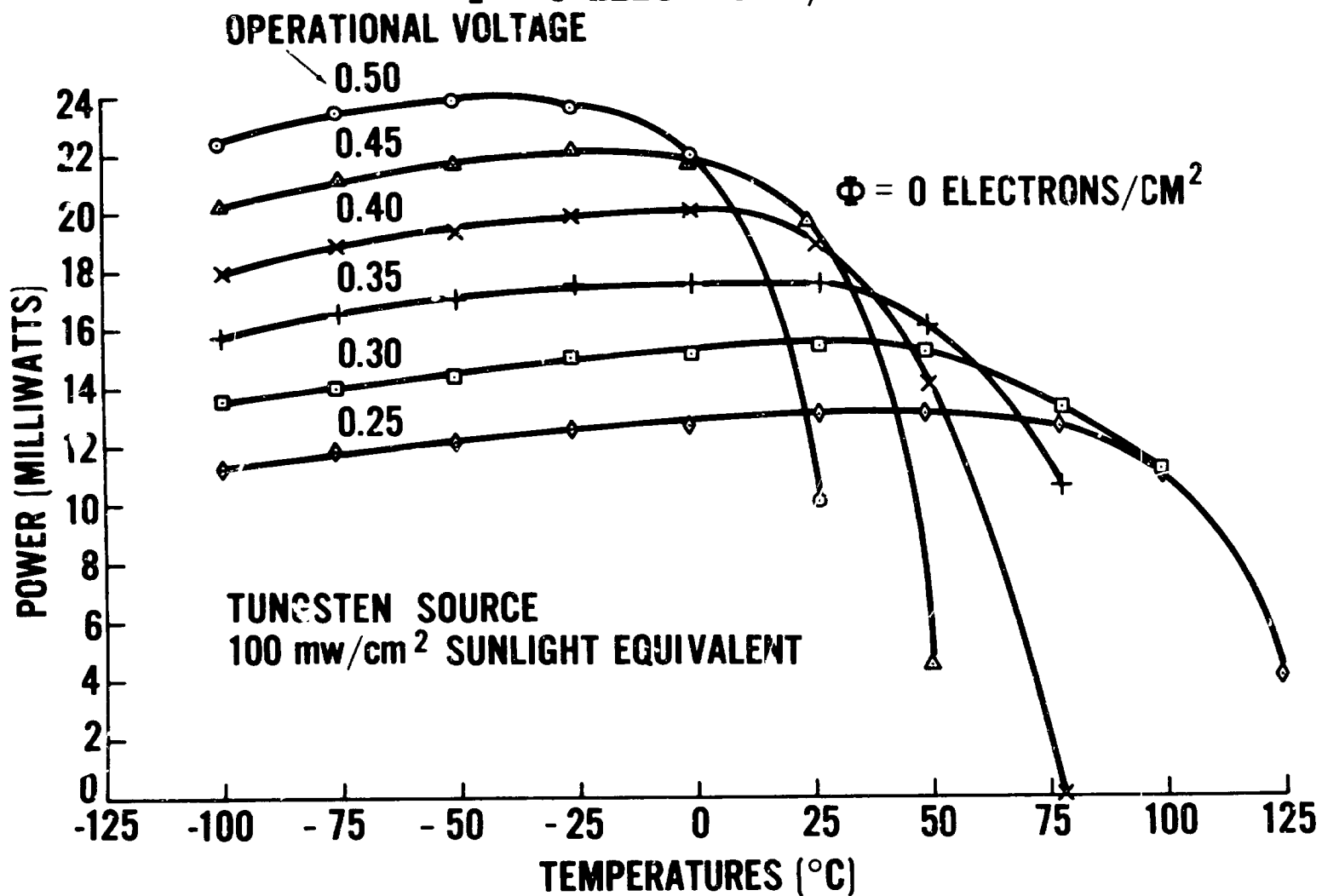


FIGURE 17. P,V,T, Φ CURVES FOR A 10 OHM-CM N/P CELL WITH
 $\Phi = 0$ ELECTRONS/CM²



**FIGURE 18. P,V,T, Φ CURVES FOR A 10 OHM-CM N/P CELL WITH
 $\Phi = 10^{12}$ ELECTRONS/CM²**

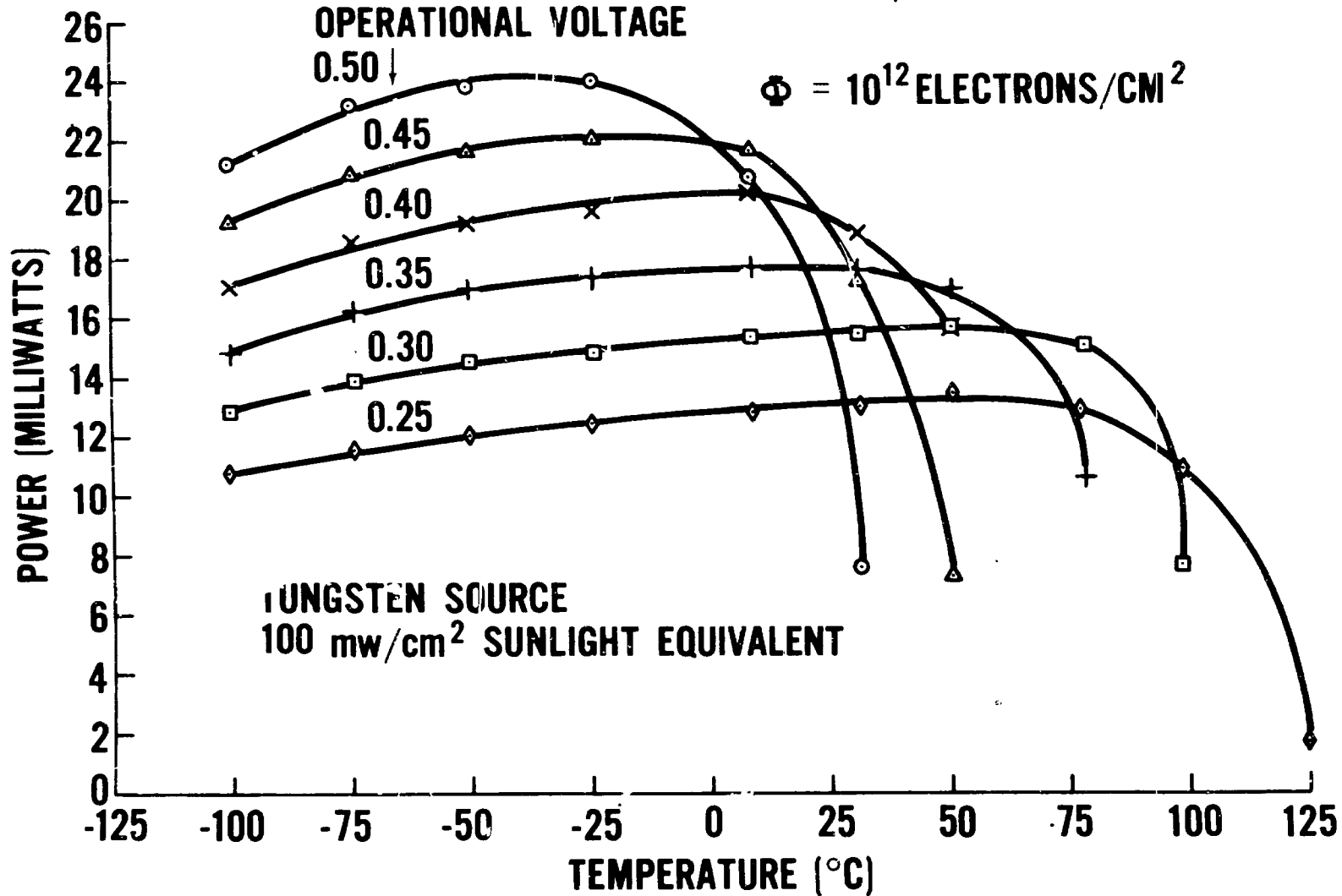


FIGURE 19. P,V,T, Φ CURVES FOR A 10 OHM-CM N P CELL WITH
 $\Phi = 10^{13}$ ELECTRONS/CM²

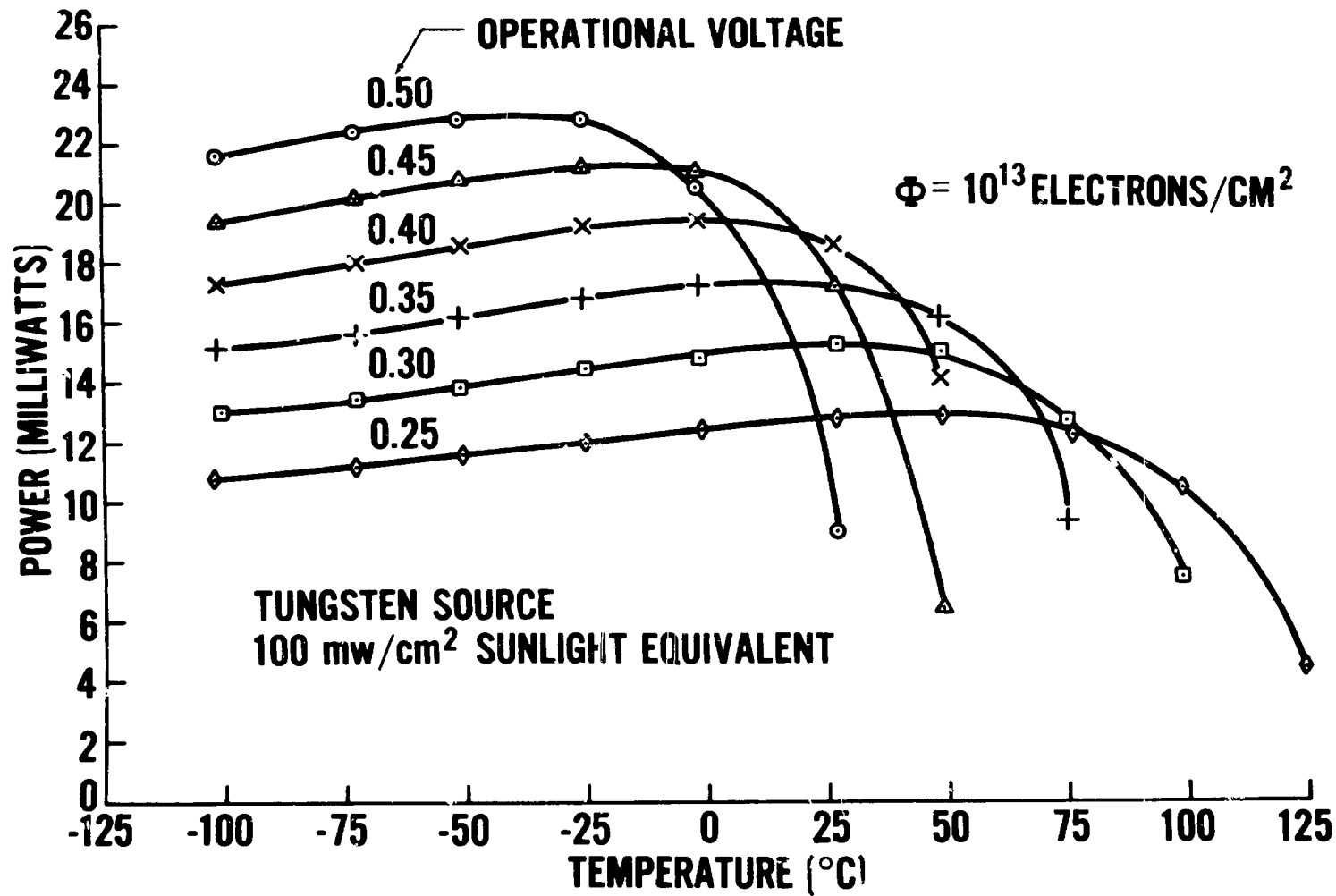
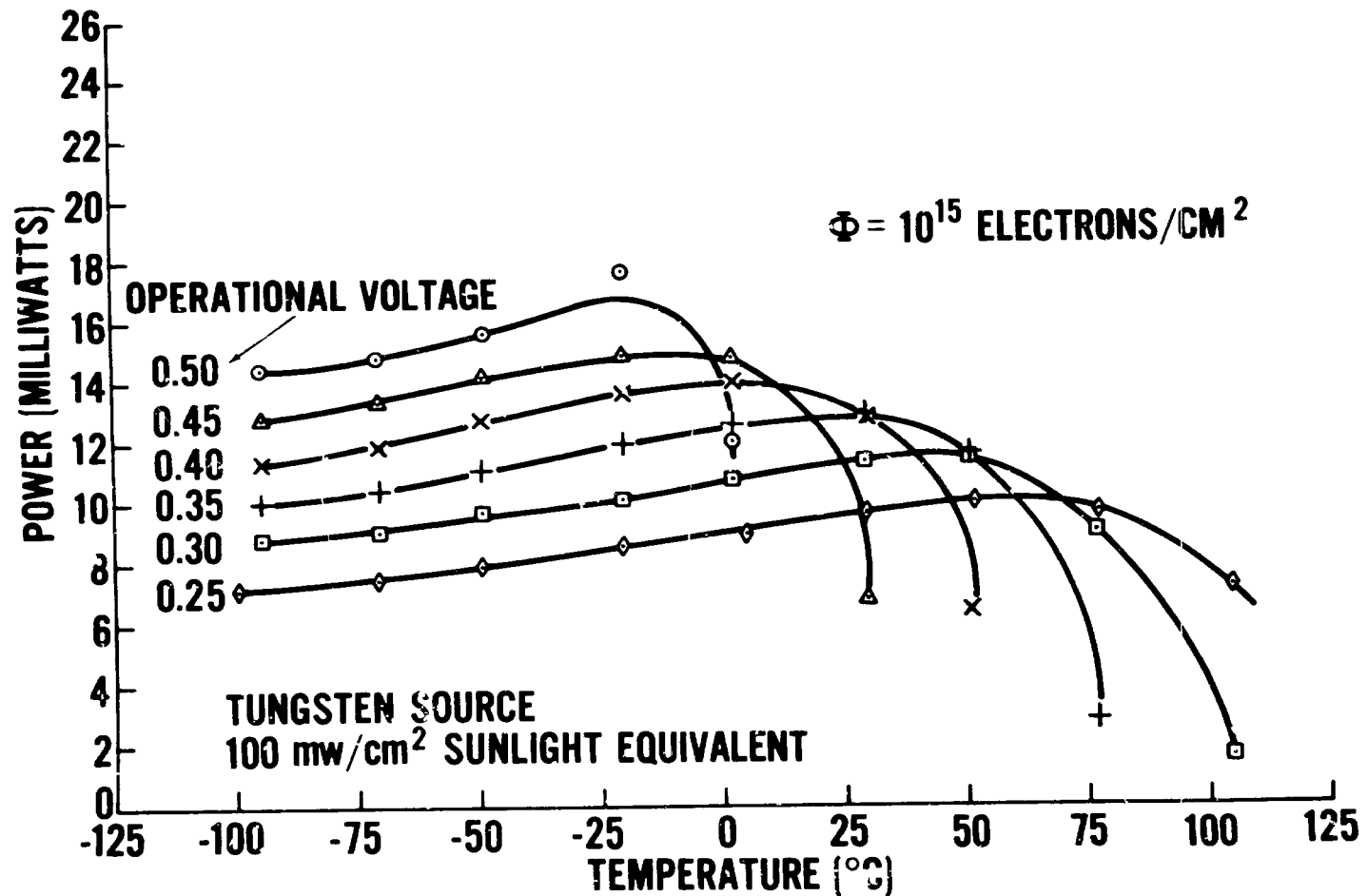


FIGURE 20. P,V,T, Φ CURVES FOR A 10 OHM-CM N/P CELL WITH
 $\Phi = 10^{15}$ ELECTRONS/CM²



**FIGURE 21. P,V,T, Φ CURVES FOR A 10 OHM-CM N/P CELL WITH
 $\Phi = 10^{16}$ ELECTRONS/CM²**

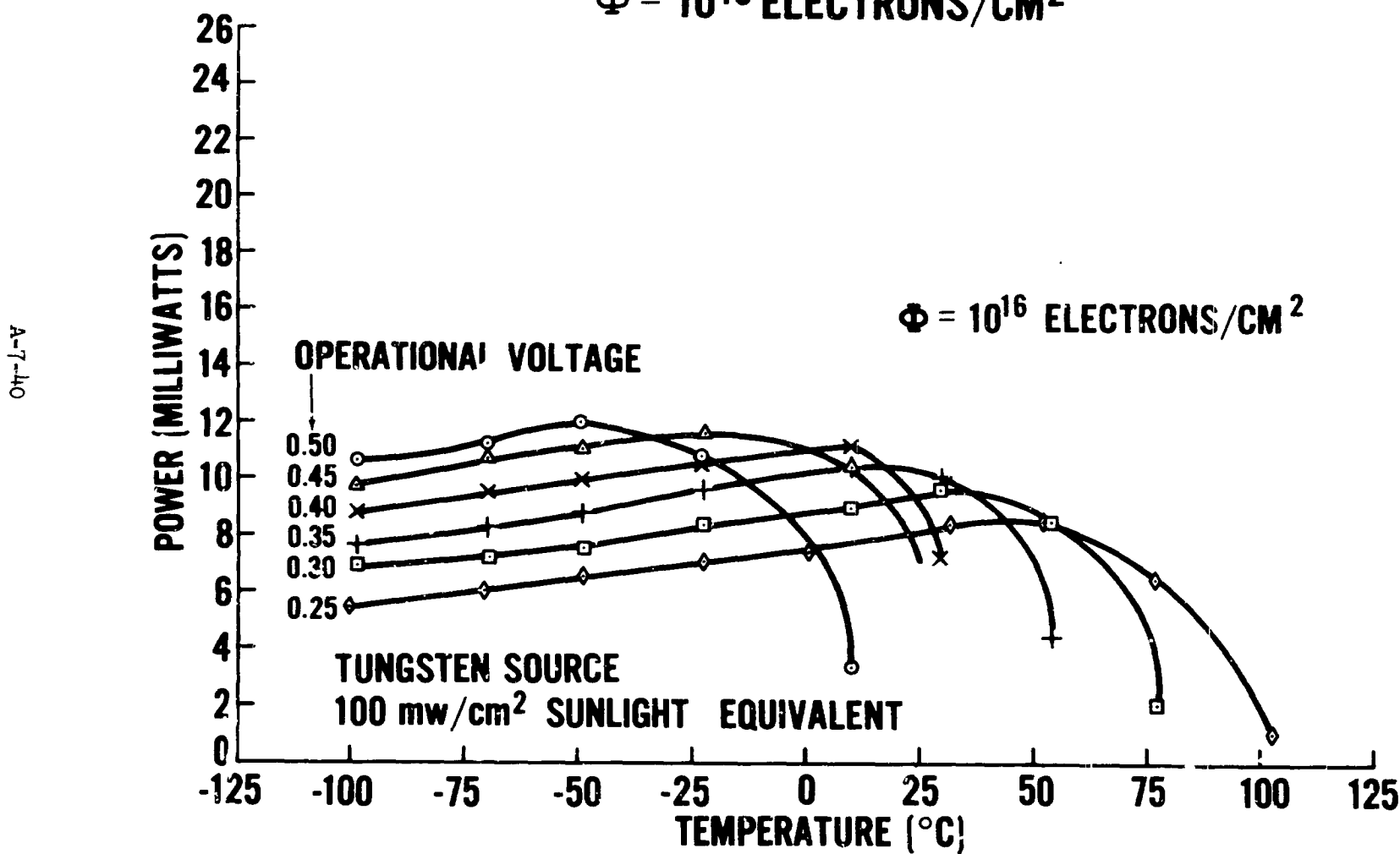
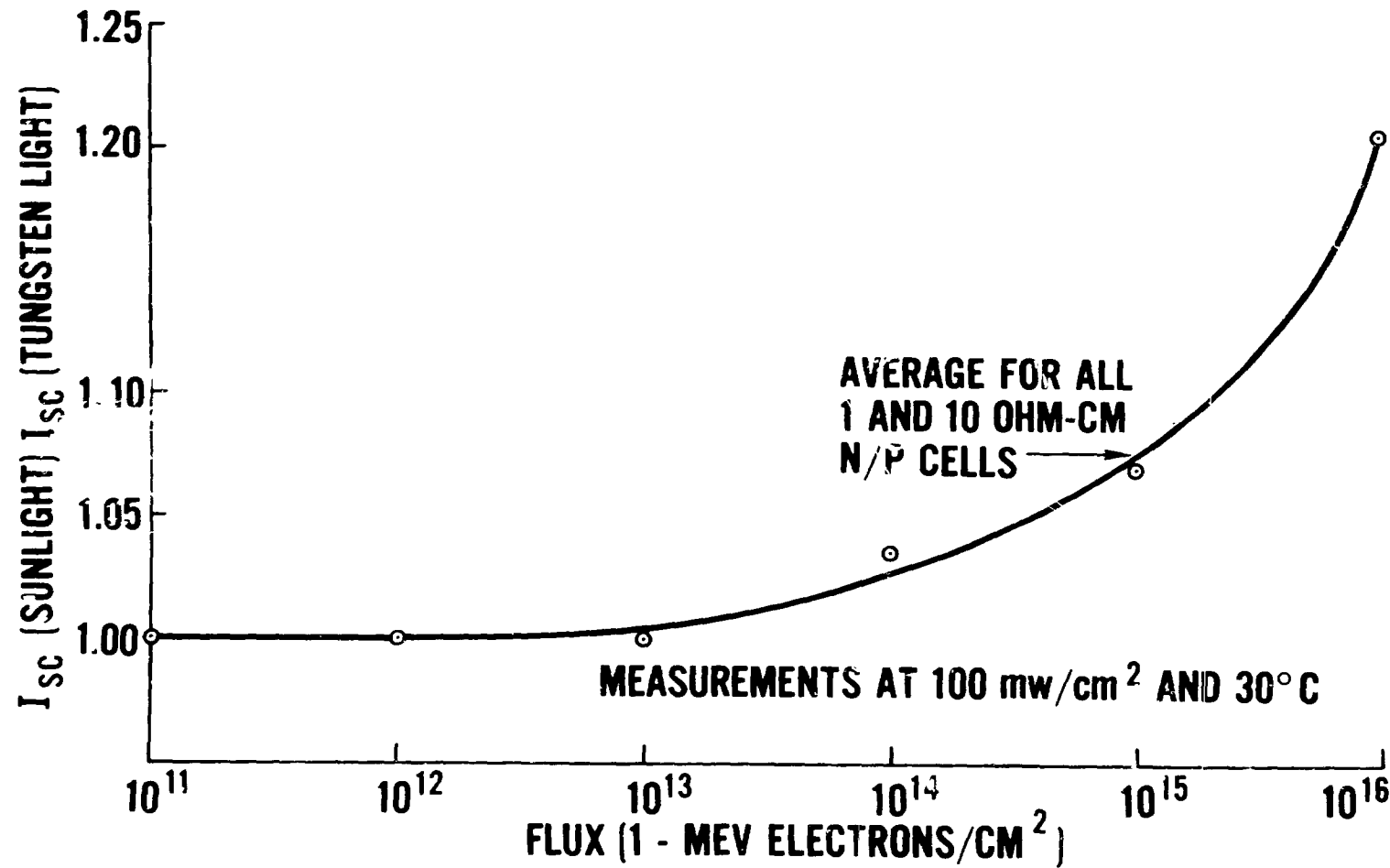


FIGURE 22. RATIO OF SHORT CIRCUIT CURRENT IN SUNLIGHT
TO SHORT CIRCUIT CURRENT IN TUNGSTEN
LIGHT - AFTER DEGRADATION



DISCUSSION

LOFERSKI-BROWN UNIVERSITY: Was there anything special about the impurity in these cells?

MR. CUNNINGHAM: No, these were standard flight quality units which we bought from the leading manufacturers. One comment that I would like to make here is that the choice of .35 volts to evaluate these cells is somewhat arbitrary. It happens to be a point where we were evaluating an array. If you choose some other voltage, higher or lower, what would happen is that the cross over point which you noted for 10 ohm centimeter and the 1 ohm centimeter cell would shift to the left or right depending on whether or not it was a higher or a lower voltage. I think that this is what Mr. Mandelkorn had in mind when he said that he didn't recommend the 10 ohm centimeter above 100°C. This is the cross over point, where you can't buy any more with the higher base resistivity cell.

HARMON-RCA: From your results, I gather that you did not notice any increase in short circuit temperature sensitivity with radiation. I've seen other results in which there was approximately a 200-300 per cent increase of temperature dependence of short circuit current with radiation damage.

MR. CUNNINGHAM: You mean the temperature coefficient of the short circuit current? Well of course whenever you use tungsten light you come under suspicion when you start quoting short circuit temperature coefficients. In an attempt to evaluate this, we made sunlight measurements on several of the cells. We found that the agreement was pretty good, in other words, the temperature coefficient was affected very little by the nature of the light source. We decided that tungsten is a pretty good light source for this kind of measurement.

HERMAN GUMMEL-BELL TELEPHONE LABS.: You did quote some numbers for the temperature coefficient. At what temperatures are the curves not straight lines?

MR. CUNNINGHAM: Between -50° and +50°, they seem to be straight lines.

HICKS-WESTINGHOUSE: Did you notice anything peculiar about your VI curves? We've done some similar temperature measurements, and we noticed that on some cells it appeared as if a nonlinear resistance had been inserted into the cell.

MR. CUNNINGHAM: Yes, we did. Where it would show up is in a plot of peak power versus temperature. We observed peculiarities but we could not pin them down. Above ~50°C the power increased, decreased, or didn't change

at all, although these variations were very small.

JOE LOFERSKI-BROWN UNIVERSITY: What happened when you reversed your temperature cycle and went up in temperature and then down in temperature? Were there any hysteresis effects?

MR. CUNNINGHAM: We didn't take the chance in going up, we went down first and then came up. It is something that we're going to try shortly.

ROSS-HOFFMAN ELECTRONICS: I wonder if you saw any effects of annealing in your studies?

MR. CUNNINGHAM: On the short circuit current plots that you saw, the short circuit current at higher temperatures appeared to taper off. This is just the opposite of what you would expect if annealing were occurring, so I can't really say that we did see any annealing.

MARTIN WOLF-HELIOTEK: The short circuit current curves are very sensitive to the spectral distribution of the light and must be interpreted with care. If you use a different sunlight simulator, you will probably get different short circuit current data. A zero temperature coefficient or negative temperature coefficient could be obtained, depending on the spectral distribution of the light.

N64-24160

PIC-SOL 209/5
Section A-8

RADIATION RESISTANCE OF WEBBED DENDRITIC
SOLAR CELLS

Presented by

R. V. Babcock

Westinghouse Electric Corporation

Pittsburgh, Pa., 15235

2 June 1964

Radiation Resistance of Webbed Dendritic
Solar Cells

K. Tarneja
J. Hicks
R. Babcock
E. Stonebraker

Westinghouse Electric Corporation

This report concerns a two part^{(1), (2)} program undertaken by Westinghouse, for the Flight Vehicle Power Branch of the AF Aero Propulsion Laboratory, to maximize the radiation resistance of silicon webbed dendritic solar cells. This is part of a larger effort which includes development of efficient fabrication techniques and power supply design.

The initial contract, concluded at the end of 1963, called for the development of dendritic cells, by conventional diffusion techniques, which showed the maximum resistance to 2 MeV electrons. The current work extends this study to include various drift field structures; it utilizes 1 MeV electrons as a standard of comparison and will later consider other particle types and energies. We are concurrently studying the effect of a vacuum environment on radiation damage rates. These three subjects will be discussed in turn, after a word about dendritic solar cells.

It is possible to pull a pair of dendrites from a silicon melt in such a way that a web of silicon of a chosen width and thickness freezes between the dendrites. This process, developed by Westinghouse, can be controlled to grow silicon blanks 1 cm wide, of the optimum thickness.

for solar cells, and of arbitrary length. At present we cut off sections 30 cm in length, trim away the dendrites to reduce leakage current, then proceed with diffusion and contacting. For radiation damage testing, smaller cells 1 x 2 cm in area are used.

These dendritic cells were not expected to differ markedly in radiation resistance from cells of similar composition produced in other ways; their promise lies in the elimination of silicon wastage and extra fabrication steps, which should permit lower costs, and in increased reliability due to fewer interconnections.

Radiation Resistance of Conventionally Diffused Dendritic Cells

Our approach was to fabricate many series of solar cells under closely controlled conditions, systematically varying several parameters in order to determine the structure which provided maximum resistance to damage by 2 MeV electrons. Toward the end of this study several irradiations with 1 MeV electrons were also made to provide a basis for converting the results to the 1 MeV electron damage rates which seem to have become the standard for comparing solar cell damage. The parameters varied were base resistivity type, magnitude of base resistivity, diffusion depth, and temperature during irradiation.

Some 1200 inches of dendrite were pulled for this program from five charges of polycrystalline silicon. Junctions were formed by vapor diffusion with BCl_3 or P_2O_5 , followed by acid etching and application of gridded contacts by photoresist techniques and electroless nickel plating. Soldered aluminum base plates provided thermal contact to the heat sink during irradiation. From each dendrite five cells were made, and the most uniform three were selected for irradiation. Dislocation density, resistivity, sheet resistance and diffusion depth were measured for each dendrite. Oxygen content was determined periodically.

Nine cells were irradiated at a time by placing them, and a Faraday cup of special design, on a belt which conveyed them repeatedly through a beam of 2 MeV electrons. In this way each cell, and the Faraday cup, received an equal integrated flux, which was constant over the cell area

to a few percent. Periodically, irradiation was halted and all cells were evaluated at 27°C. Dark I-V curves, I-V curves under 3400°K tungsten light at 140 mW/cm², and I-V curves under the same light source filtered through 1/2 inch of plexiglass and 3 cm of de-ionized water, were taken. The intensities stated refer to solar illumination; i.e., the intensity was adjusted until two calibrated solar cells gave the same power output which they would deliver under 140 mW/cm² ground level solar illumination. Also, spectral response curves were determined before and after irradiation.

Efficiencies at the maximum power point were calculated from the light curves. All data given in this paper refer to the filtered light source. Such a filtered light source provides an apparent rate of degradation in efficiency which is closer to the rate seen in sunlight than to the rate seen in unfiltered tungsten light, although this effect is empirical and is not based on any close similarity to the solar spectrum. In all cases, the two light sources gave the same indication as to which of two cell types was more resistant to damage.

The typical effect of damaging radiation on solar cells is illustrated by Figure 1, which shows I-V curves for an 8 Ω-cm P/N cell measured after exposure to different electron fluxes. One sees a decrease in short circuit current which also, by shifting the power curve upward, accounts for about half of the observed decrease in open circuit voltage. An increase in the load resistance corresponding to the maximum power point is also apparent. When efficiencies are calculated from these curves, one sees the typically logarithmic decrease in efficiency with electron flux shown in Figure 2.

Unfortunately, there is no single method of abstracting one value from a curve such as this which gives a just comparison among the radiation damage rates for all types of cells. One measure which has been used is the slope of the logarithmic decrease in efficiency; i.e., the % decrease in efficiency caused by a factor of ten increase in the total electron flux. This is very deceiving because both N/P and P/N cells eventually exhibit similar slopes, but the N/P cells do not begin to show logarithmic

degradation until they have received about ten times greater integrated fluxes. Another common measure is the electron flux at which the efficiency has fallen to 75% of its initial value. This method discriminates against a cell which has a high initial efficiency because of a low initial concentration of recombination centers. A given number of radiation induced recombination centers will cause a greater fractional decrease in efficiency for this cell than for a cell with lower initial efficiency. This second method is meaningful, however, if one can compare only cells with equal initial efficiencies. This we were rarely able to do. A third method which is of particular value to the satellite designer, who must design for a certain minimum power level toward the end of his mission, is to specify the efficiency after exposure to a particular flux.

In Table I the results of the investigation are summarized by the latter two methods, and by one other; the electron flux required to reduce the efficiency to 6%. The particular electron flux chosen as a criterion is $10^{15}/\text{cm}^2$. Initial efficiencies are also shown. The third and fourth columns in Table I show a distinct reciprocity--a high initial efficiency tends to reduce the apparent resistance of the cells as indicated by flux at 75% of initial efficiency. In the latter two columns, high initial efficiency should tend to increase the apparent resistance to 2 MeV electrons. Although each line in Table I represents the average of from three to nine cells, the data appears to scatter badly because of the effect of variations in initial efficiency. However, when the effects of the initial efficiencies are considered, the results become fairly clear.

The effect of diffusion depth appears to be minor, and an optimum value of 0.5μ was chosen, rather arbitrarily. N/P cells are seen to resist roughly 3 times as much 2 MeV electron flux as P/N cells, and the optimum values of base resistivity lie in the range $10-15\Omega \text{ cm}$. If short circuit current density is considered instead of efficiency, the damage rate continues to decrease with increasing resistivity up to the highest resistivity tested. The maximum in damage resistance of N/P cells actually

occurs because of series resistance losses, and could be shifted to higher resistivities by constructing thinner cells. The 20 Ω -cm cells reported here were 7 mils thick.

From Table I the optimum structure is taken to be 13 Ω -cm N/P, with a diffusion depth of 0.5μ . This is quite similar to the findings of the many investigators who have studied damage rates of cells fabricated from Czochralski grown silicon. To obtain a direct comparison we tested optimum dendritic cells together with cells made from Czochralski grown material of the same type and resistivity. The results for the Czochralski cells are also shown in Table I, and are quite similar to the results for dendritic cells.

The effect of ambient temperature on the formation of radiation defects was found to be unimportant. Cells of the optimum structure were irradiated at -80, -30, 27 and 75°C , and no significant differences in damage rates were seen. Since it was possible that low temperature defect structures were annealing during measurement, one set of cells was maintained at -30°C during irradiation and measurement. Again, there was no effect on the damage rate.

The variation of efficiency with temperature over the range -80°C to $+75^{\circ}\text{C}$ for the optimum cell type is shown in Figure 3. The increase in efficiency at low temperatures over the room temperature value is not as great as should be expected, probably because of the series resistance.

Oxygen contents of the silicon dendrites were measured by vacuum fusion. With the exception of one n-type sample, oxygen concentrations were in the range 0.006 to 0.011 wt.%. Since this was about six times as great as the oxygen content of the Czochralski grown crystal which provided cells with virtually identical damage rates, the variation of oxygen content among the several dendrites was presumed to be unimportant.

The investigation was concluded with a comparison of 1 MeV and 2 MeV electron damage rates. Figure 4 shows this data for the optimum dendritic cells and for a matching set of Czochralski cells. For the dendritic cells, a given decrease in efficiency required six times as much electron flux at

1 MeV as at 2 MeV. For the Czochralski cells the factor was 3-4 A similar experiment with P/N dendritic cells gave a factor of 2-1/2 - 3-1/2. This should be compared to the results of Denney and Downing, (3) who found (for the flux required to reach a particular short circuit current) a factor of about 4 in N/P cells and about 1-1/2 in P/N cells.

Drift Field Structure

This work is an extension of the search for an optimum radiation resistant dendritic cell to include drift field structures. Several speakers at last year's Power Sources Conference discussed the possibility of improving radiation resistance by suitably controlling the concentration gradients in the base region. This would produce an electric field which by speeding charge collection would tend to offset the decrease in carrier lifetime.

Two fabrication methods are being investigated to provide the desired graded base structures--diffusion techniques and epitaxial growth techniques.

1. Diffused graded base solar cell structure:

Solar cell fabrication in this case consists of boron diffusion into P-type silicon webbed dendrites to obtain a graded base followed by phosphorus diffusion for formation of the N/P junction. Efficiencies as high as 8% have been achieved in these cells.

2. Epitaxial graded base solar cells:

Two epitaxial techniques were also used to form graded base structures. One was to deposit a high resistivity, epitaxial grown layer onto a low resistivity, silicon webbed dendrite base and establish the desired gradient by out-diffusion techniques. The second method was to deposit the graded epitaxial layer by controlled doping during epitaxial growth. After this structure was obtained, N/P junctions 1/2 micron deep were formed by phosphorus diffusion. After diffusion and post-diffusion cleaning of these blanks, grid structure contacts were put on the diffused surface and the back surface using either Ni-plated or Ag-Ti evaporated and alloyed contacts, followed by dip soldering. Figure 5 shows the structure designed for epitaxial graded base solar cells. Efficiencies as high as 9% have been achieved.

We do not yet have satisfactory direct measurements of the fields or concentration gradients in these cells. The best evidence of their drift field structure is the behavior of their spectral response under γ -radiation. Figure 6 shows the spectral response curves of cells of these two types before and after irradiation with 4×10^{16} and 7×10^{16} 1 MeV electrons/cm². For comparison, spectral response curves of an optimum non-graded base cell before and after irradiation with 1.4×10^{16} e¹/cm² are also shown. The response to long wavelength light, and therefore the collection of carriers from deep in the base region, is preserved as well or better in the graded base structures, despite the greater electron flux received. The short circuit currents are maintained correspondingly well, as shown in Figure 7. Here, and in Figure 8, the dashed lines represent one particularly good group of cells which we have not yet been able to reproduce. The other lines show the average for all cells of each of the three types. Figure 8 shows efficiency versus 1 MeV electron flux for the same groups of cells. Here, the advantage of the graded base cells is less obvious because damage to the open circuit voltage is beginning to have an effect. It is clear that the graded base cells will prove more resistant than the conventionally diffused cells, and that much work must still be done to optimize their resistance.

Effect of Vacuum

Most of the recent evaluations of silicon solar cells have been done in air. Mr. Joseph Wise, of the AF Aero Propulsion Laboratory, brought to our attention some recent work⁽⁴⁾ that indicates two to three orders of magnitude decrease in the flux necessary to degrade solar cells when they are irradiated in vacuum rather than in air. Some earlier work by Loferski and Rappaport⁽⁵⁾ in 1958 indicates more rapid damage to a factor of about 30 in vacuum. Their finding was noted but not investigated further, possibly because the predictions of solar cell life in space at that time appeared to give a comfortable margin of safety. Because of the more intense radiation fields now known to be present, however, it is necessary to resolve the question. The accumulated satellite experience

with solar cell power supplies surely precludes any general order of magnitude effect, but any accelerated damage due to vacuum environment could be very costly.

An apparatus was designed to simultaneously evaluate pairs of solar cells, one in vacuum and one in atmospheric air. The cells are simultaneously irradiated with 1 MeV electrons, receiving identical flux densities.

Irradiations to date have employed a vacuum no better than about 1×10^{-4} Torr, with the air in the "atmospheric" chamber being continuously changed to eliminate ozone build-up. Cell efficiency is measured at 27°C, with water-filtered 3400°K tungsten light. The intensity is the same on each cell at about 120 mw/cm².

Representative results for several types of cell are displayed in Figures 9 through 12. Each pair of cells had the same initial efficiencies. The first three plots of efficiency vs flux density show no difference between air and vacuum. Figure 12, for two 10 Ω-cm P/N cells from the same supplier, shows that the air irradiated cell consistently required 5 times the flux for equivalent degradation, for flux densities exceeding about 4×10^{14} el/cm². This difference was due to degradation of open-circuit voltage, rather than short-circuit current density. A repetition of this last experiment showed a similar enhancement of the damage rate in vacuum, but the effect was less clear. Further study of this phenomenon is clearly needed.

Future work will employ a better vacuum and the experimental survey of cell types will continue. We also hope to develop apparatus that allows both irradiations and efficiency measurement in vacuum, without interruption.

References

1. See Tech. Doc. Report No. APL-TDR-64-20 for a full report of work performance under contract AF 33(657)-10527.
2. See also current reports under contract AF 33(615)-1049.
3. J. M. Donney and R. G. Downing, "Charged Particle Radiation Damage in Semiconductors, VIII: The Electron Energy Dependence of Radiation Damage in Photovoltaic Devices," TRL Report 8653-6025-KJ-000, Contract No. NAS 5-1851, p. 15 (July, 1963).
4. W. King, "Report on P/N Junction Formation Techniques" Ion Physics Corp., Burlington, Mass., report under AF Aero Propulsion Laboratory contract AF 33(615)-1097.
5. J. Loferski and P. Rappaport, "The Effect of Radiation on Silicon Solar Energy Converters," RCA Review, pp. 536-554, December, 1958.

Diffusion Depth (μ)	Resistivity ($\Omega\text{-cm}$)	initial efficiency (%)	electron flux @ 75% of init. (10^{13} el/cm^2)	efficiency @ 10^{15} el/cm^2 (%)	electron flux @ 6% eff. (10^{13} el/cm^2)
<u>P/N Cells</u>					
0.4	1	11.7	1.9	4.3	22
0.6		13.2	1.5	4.4	33
0.9	↓	10.3	1.5	3.6	8.5
0.6	1	13.2	1.4	4.5	33
	5	12.4	4.6	5.6	85
	8	10.5	13	5.8	120
↓	24	9.0	42	5.9	95
<u>N/P Cells</u>					
0.3	1	9.6	25	6.0	120
0.5		9.4	30	5.8	120
1.0	↓	9.7	40	6.3	90
0.5	1	9.4	30	5.8	120
	5	9.7	40	7.1	330
	10	8.1	170	6.4	170
→	13	9.3	150	7.0	370
↓	21	8.9	90	6.5	200
dendritic 0.5	13	10.1	40	6.6	170
Czochralski 0.5	13	11.3	25	7.1	270

Table I. Effect of resistivity, resistivity type, and diffusion depth on resistance to damage by 2 MeV electrons. Each listing is the average of 3 to 9 cells. The horizontal arrow shows the structure chosen as optimum. The last two lines compare cells of dendritic and Czochralski grown silicon, each having the chosen optimum structure.

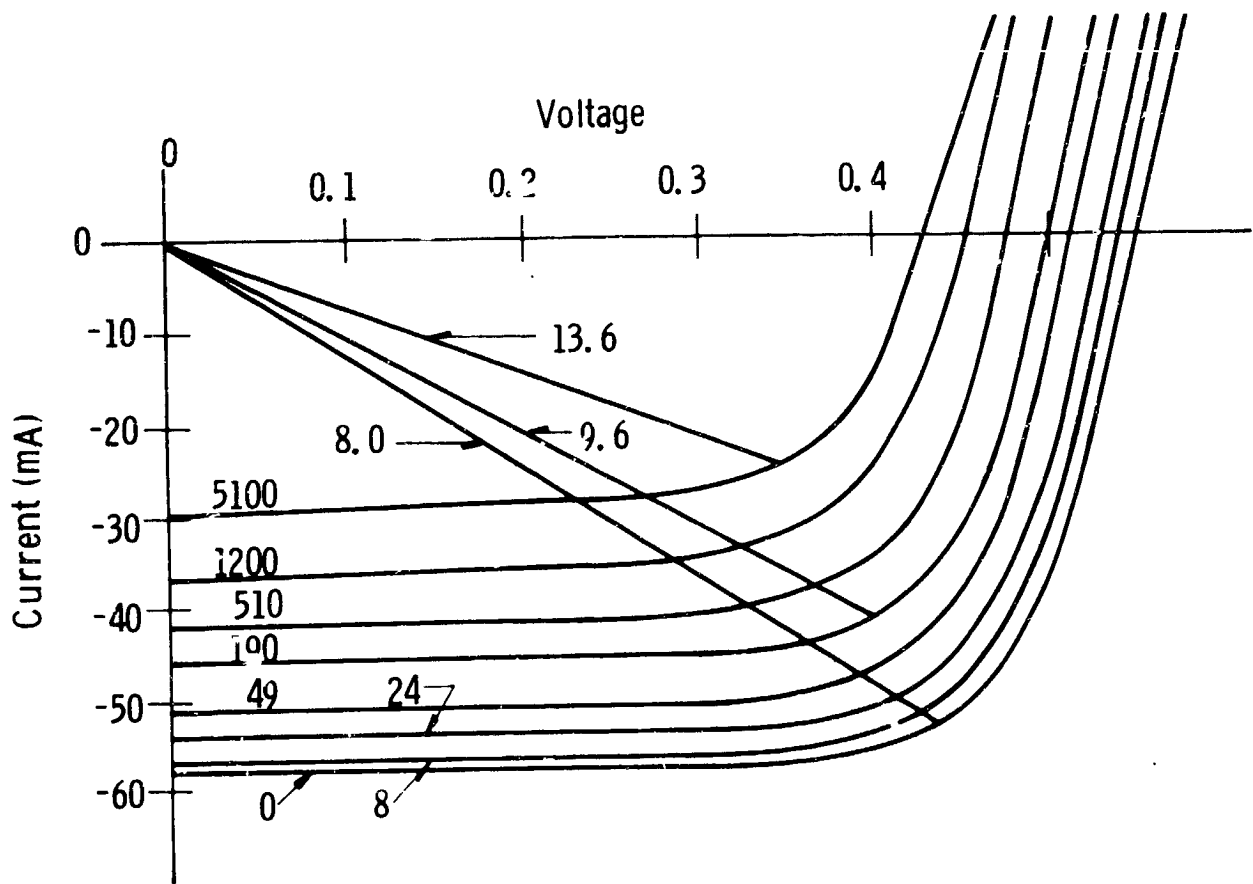


Fig. 1—Current voltage characteristics of $8.4 \Omega\text{-cm}$ P/N cell with 0.5μ diffusion depth, tested after exposure to different fluxes of 2 MeV electrons. Cells were tested at 27°C with filtered 3400°K tungsten light at an intensity equivalent to 140 mW/cm^2 sunlight. Electron fluxes are shown for each curve in units of 10^{13} el/cm^2 . Numbers attached to the oblique lines are source impedances of the cell, in Ω , after exposure to the electron flux indicated.

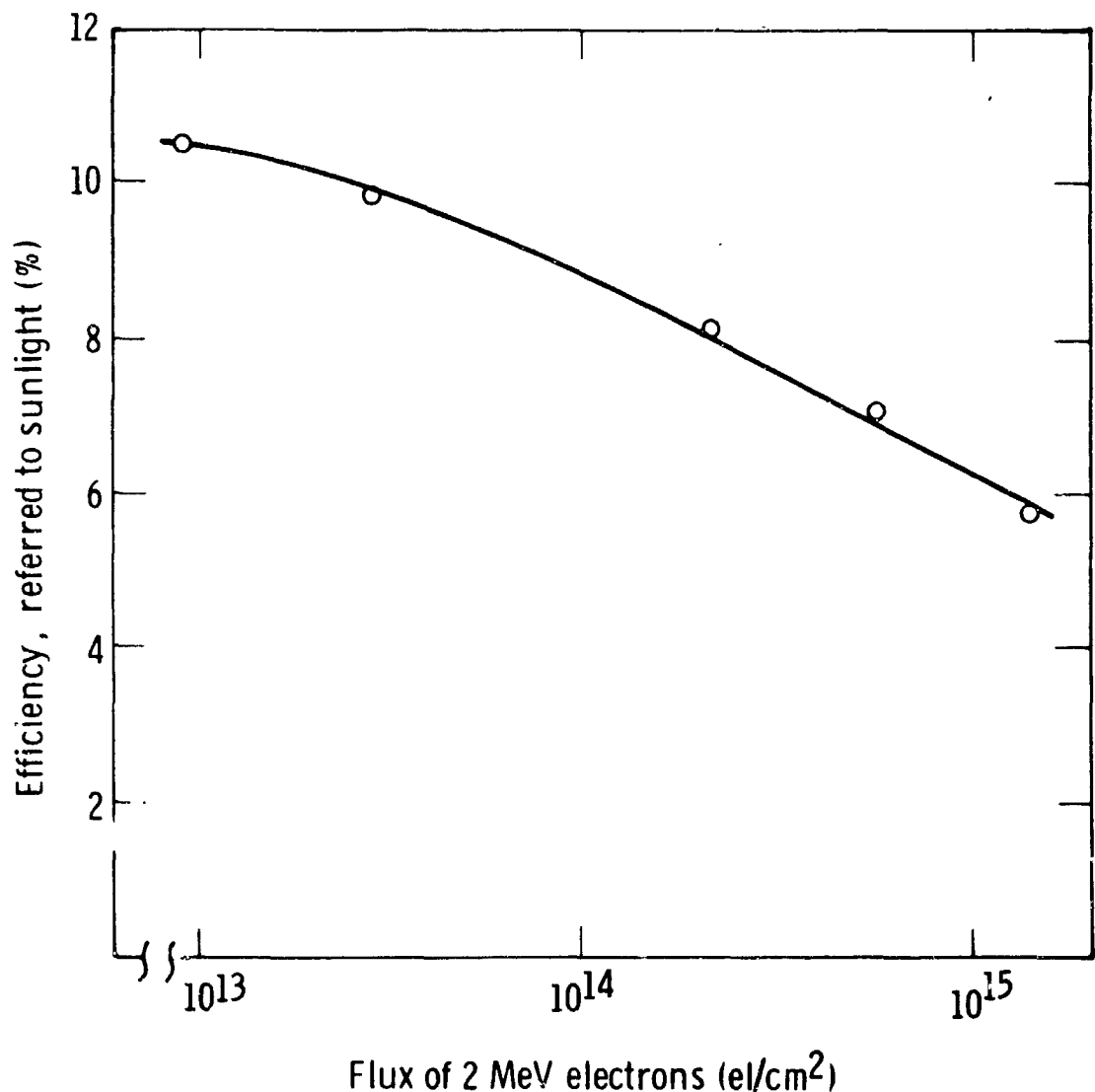


Fig. 2—Decrease of efficiency with 2 MeV electron flux, for an $8.4 \Omega\text{-cm}$ P/N cell with 0.5μ diffusion depth. Cells were tested at 27°C with filtered 3400°K tungsten light at an intensity equivalent to $140 \text{ mW}/\text{cm}^2$ sunlight.

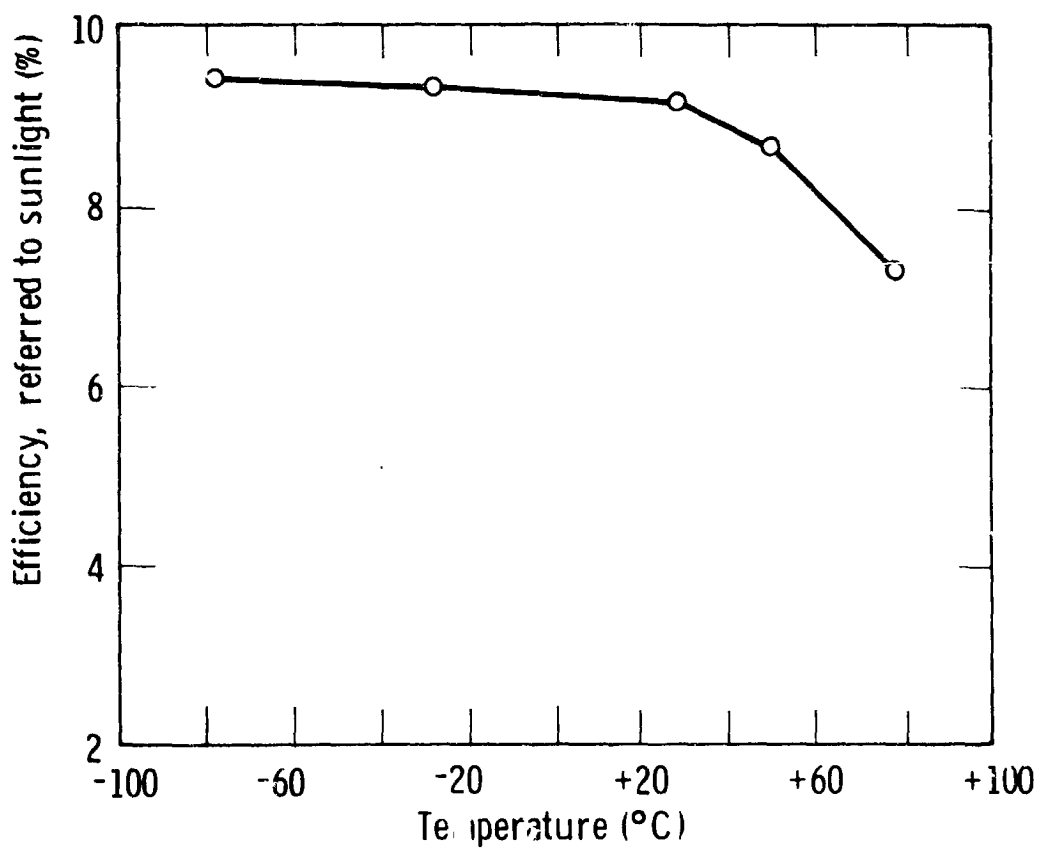


Fig. 3— Variation of efficiency with temperature for a dendritic solar cell of optimum structure ($13 \Omega\text{-cm}$ N/P, with 0.5μ diffusion depth). Cells were tested with filtered 3400°K tungsten light at an intensity equivalent to 140 mW/cm^2 sunlight.
Note the suppressed zero on the vertical scale.

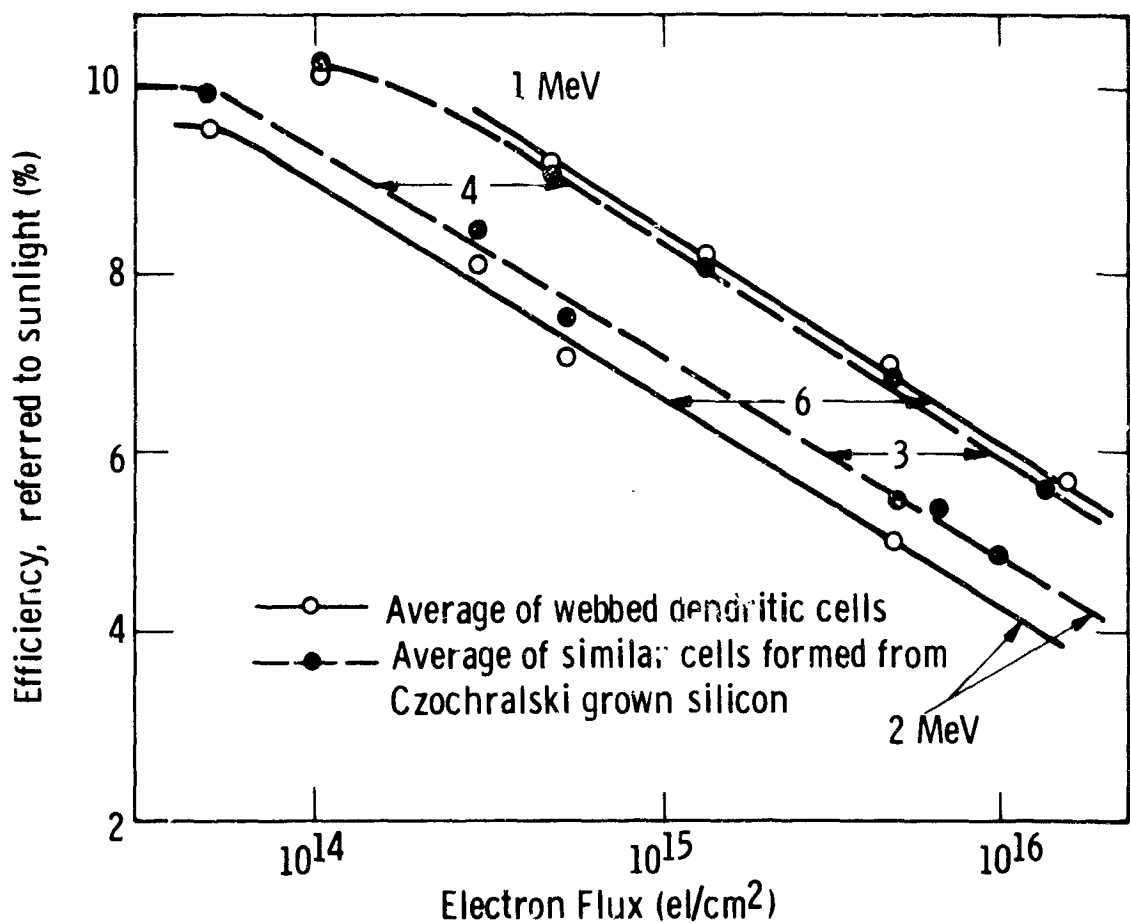


Fig. 4- Variation of efficiency with 1 MeV and 2 MeV electron flux for N/P solar cells of optimum design. Cells were tested with filtered 3400°K tungsten light at an intensity equivalent to $140 \text{ mw}/\text{cm}^2$ sunlight.

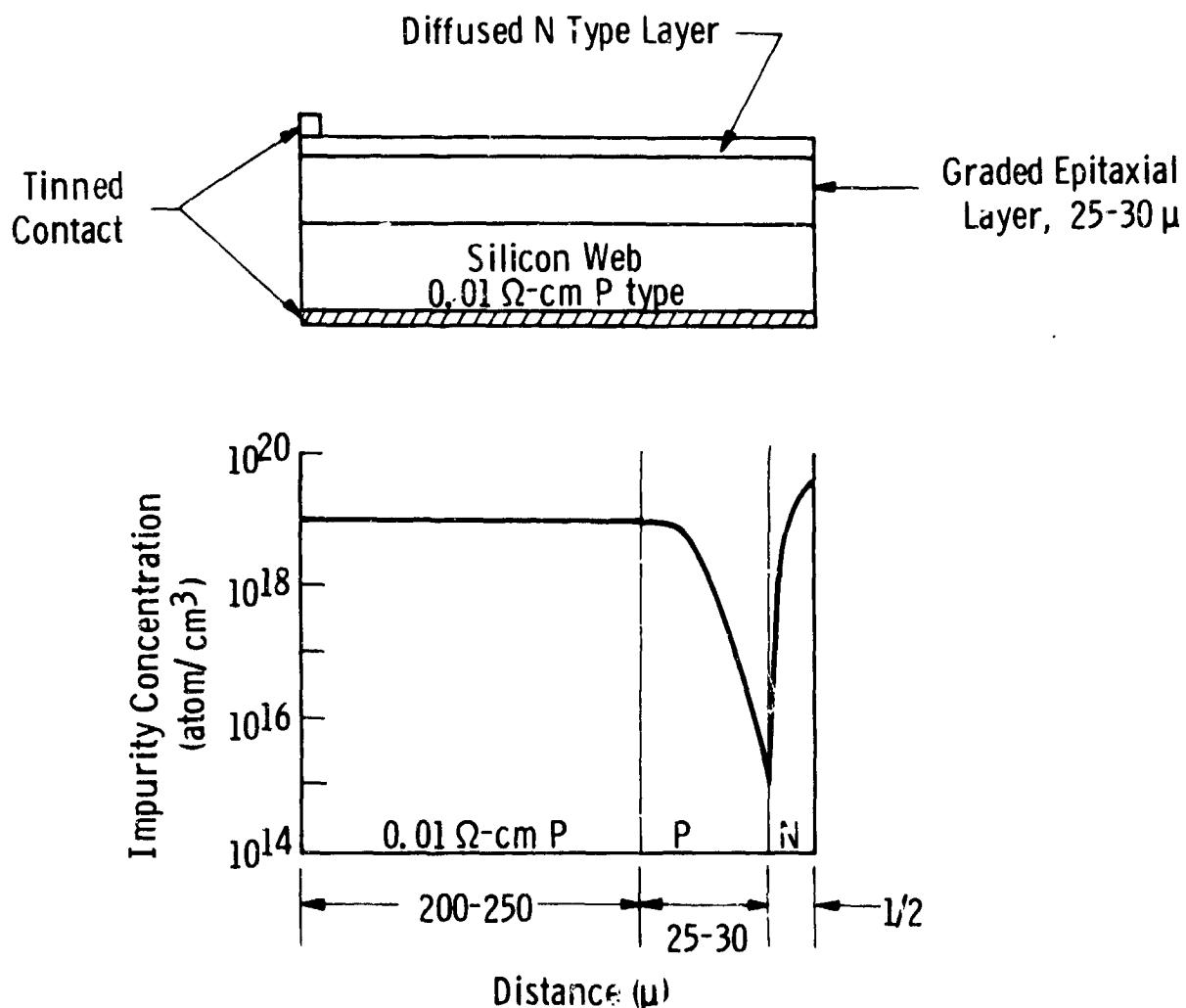


Fig. 5—Planned structure and concentration profile for initial epitaxial drift field solar cells.

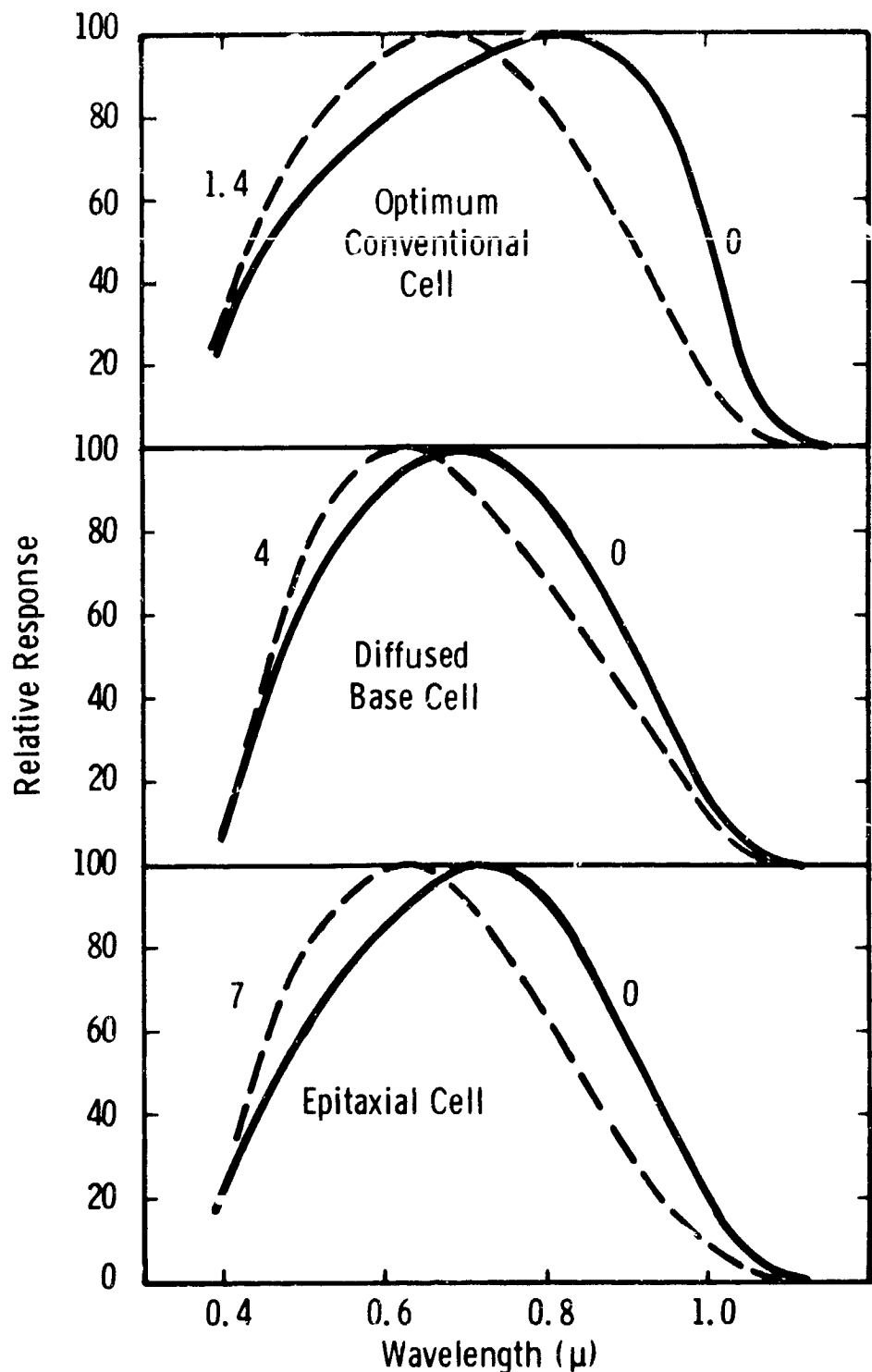


Fig. 6—Effect of 1 MeV electron irradiation on spectral response curves of three types of cell made from webbed dendritic silicon. The number attached to each curve is the electron flux received in units of 10^{16} el/cm².

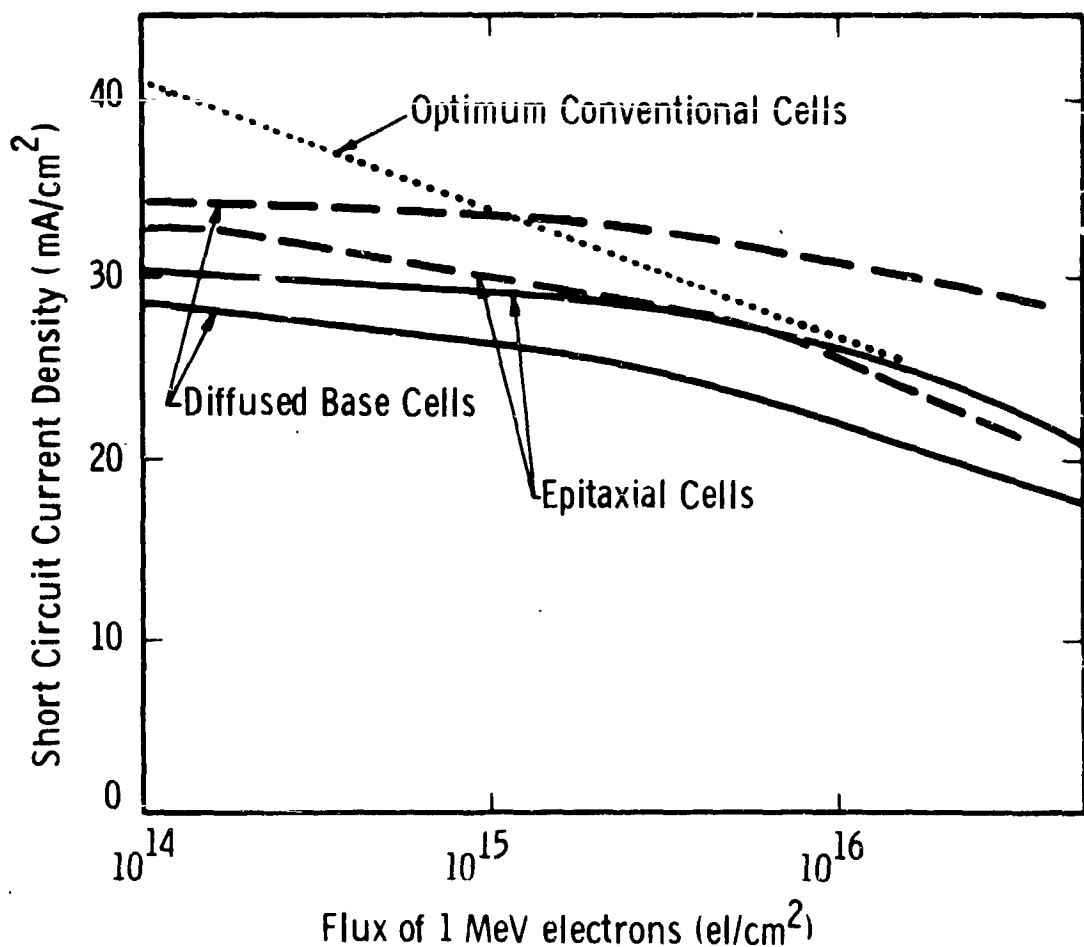


Fig. 7—Decrease of short circuit current density with 1 MeV electron flux, for three types of cells made from webbed dendritic silicon. The solid lines show the average of all cells tested; the dashed lines represent the best group of cells.

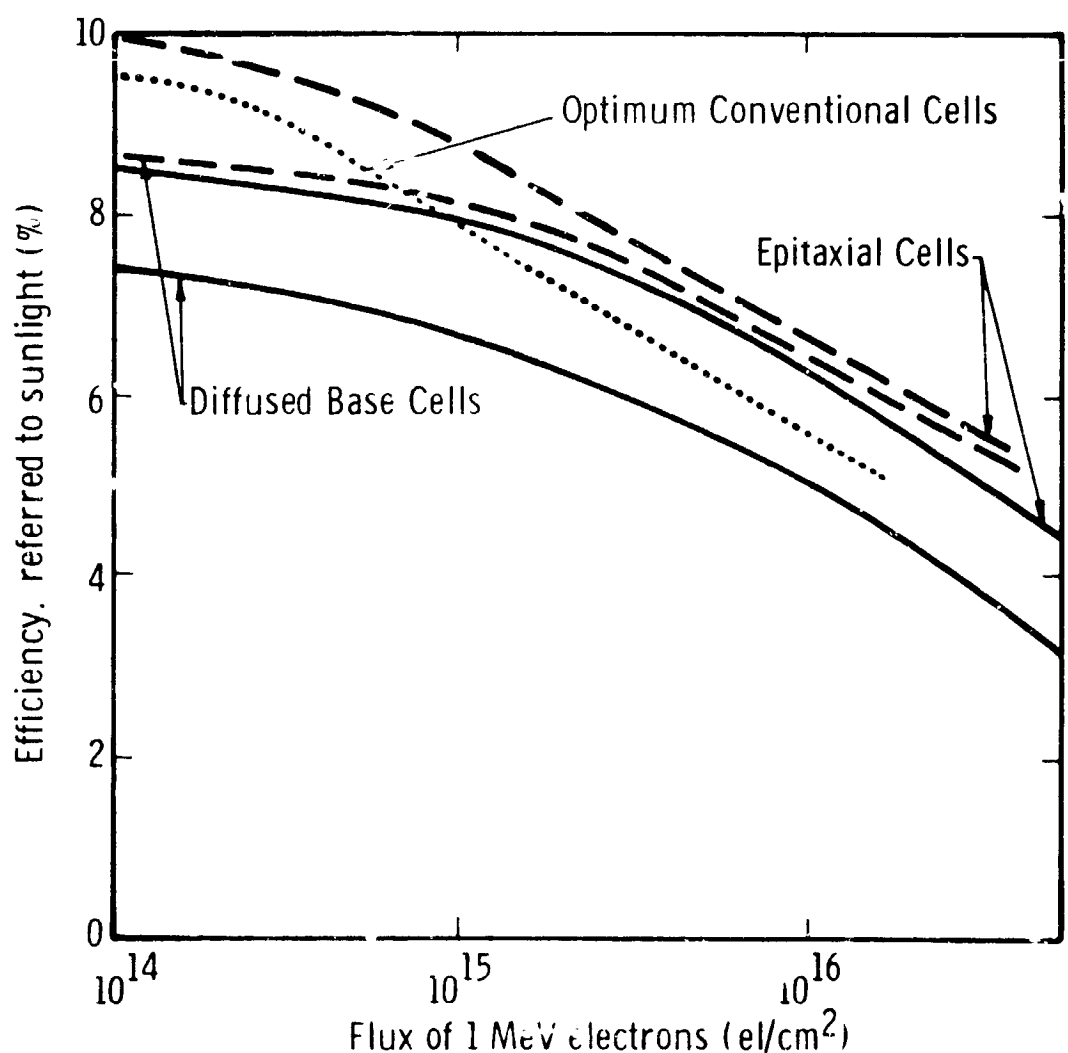


Fig. 8—Decrease of efficiency with 1 MeV electron flux, for three types of cells made from webbed dendritic silicon. The solid lines show the average of all cells tested; the dashed lines represent the best group of cells.

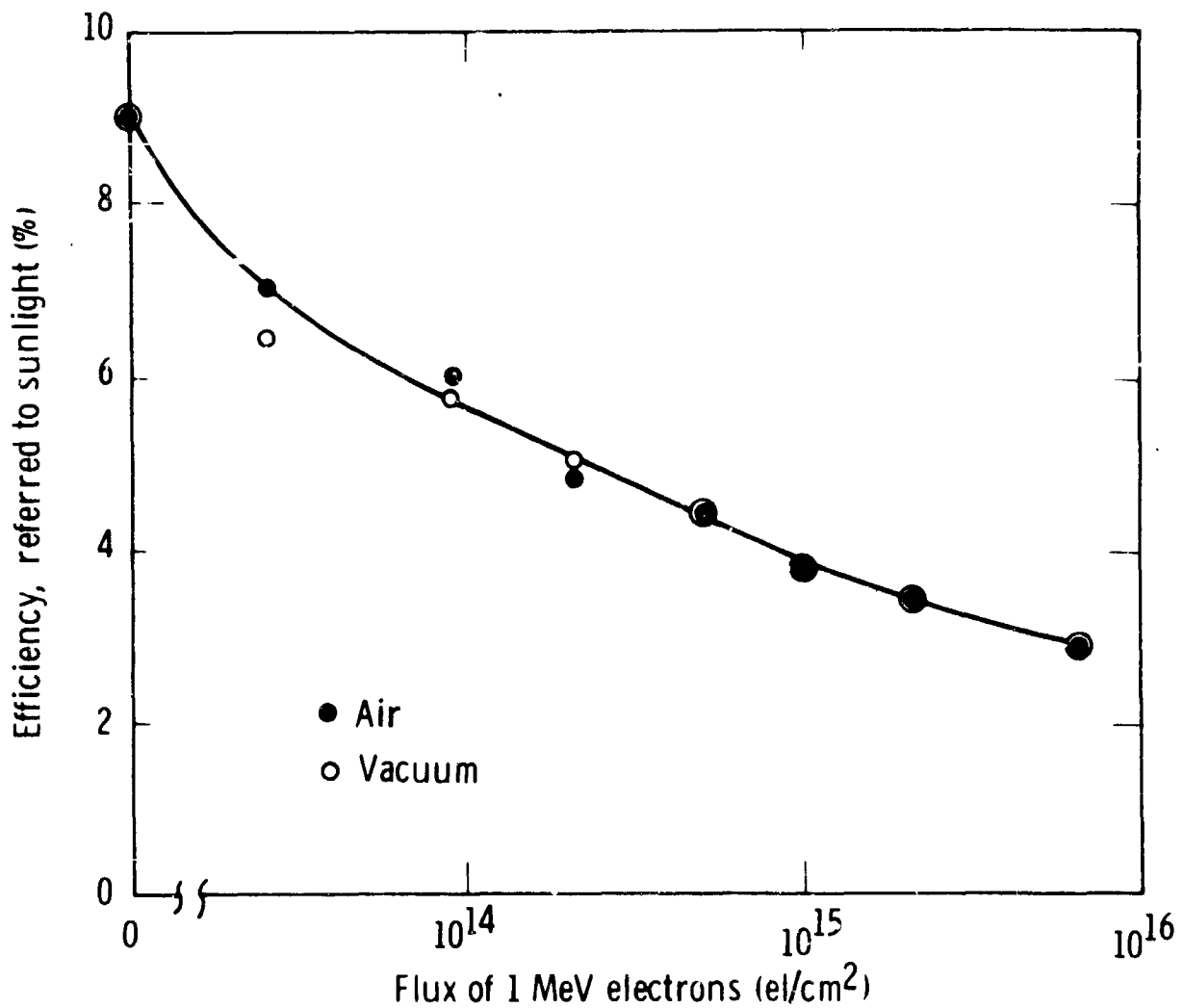


Fig. 9—Decrease of efficiency with 1 MeV electron flux, for $1 \Omega\cdot\text{cm}$ P/N silicon solar cells, irradiated in air and in vacuum ($\sim 10^{-4}$ torr). Cells were tested in filtered 3400°K tungsten light at an intensity equivalent to $140 \text{ mW}/\text{cm}^2$ sunlight.

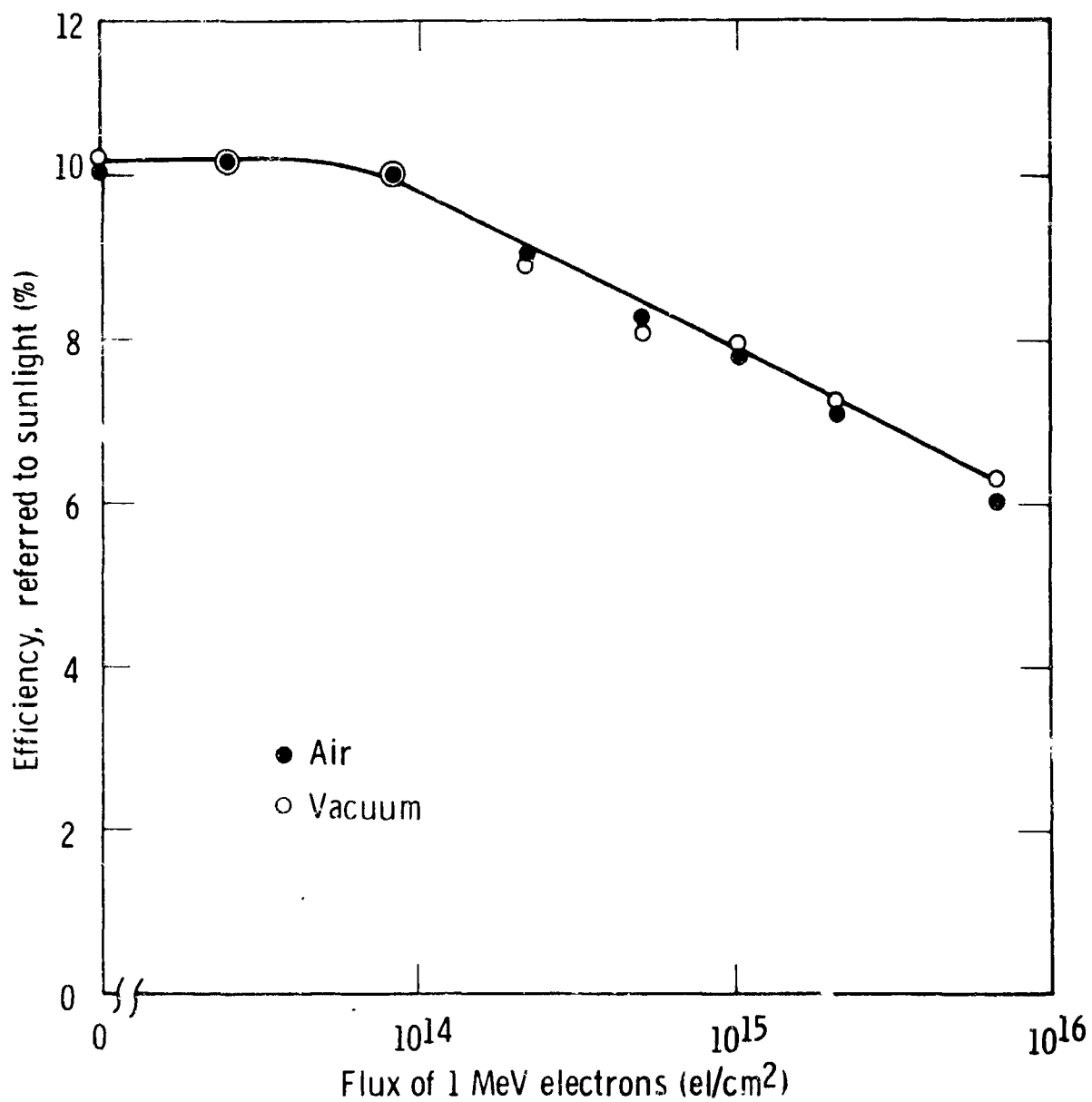


Fig. 10—Decrease of efficiency with 1 MeV electron flux, for $10 \Omega\text{-cm}$ N/P silicon solar cells, irradiated in air and in vacuum ($\sim 10^{-4}$ torr). Cells were tested in filtered 3400°K tungsten light at an intensity equivalent to $140 \text{ mW}/\text{cm}^2$ sunlight.

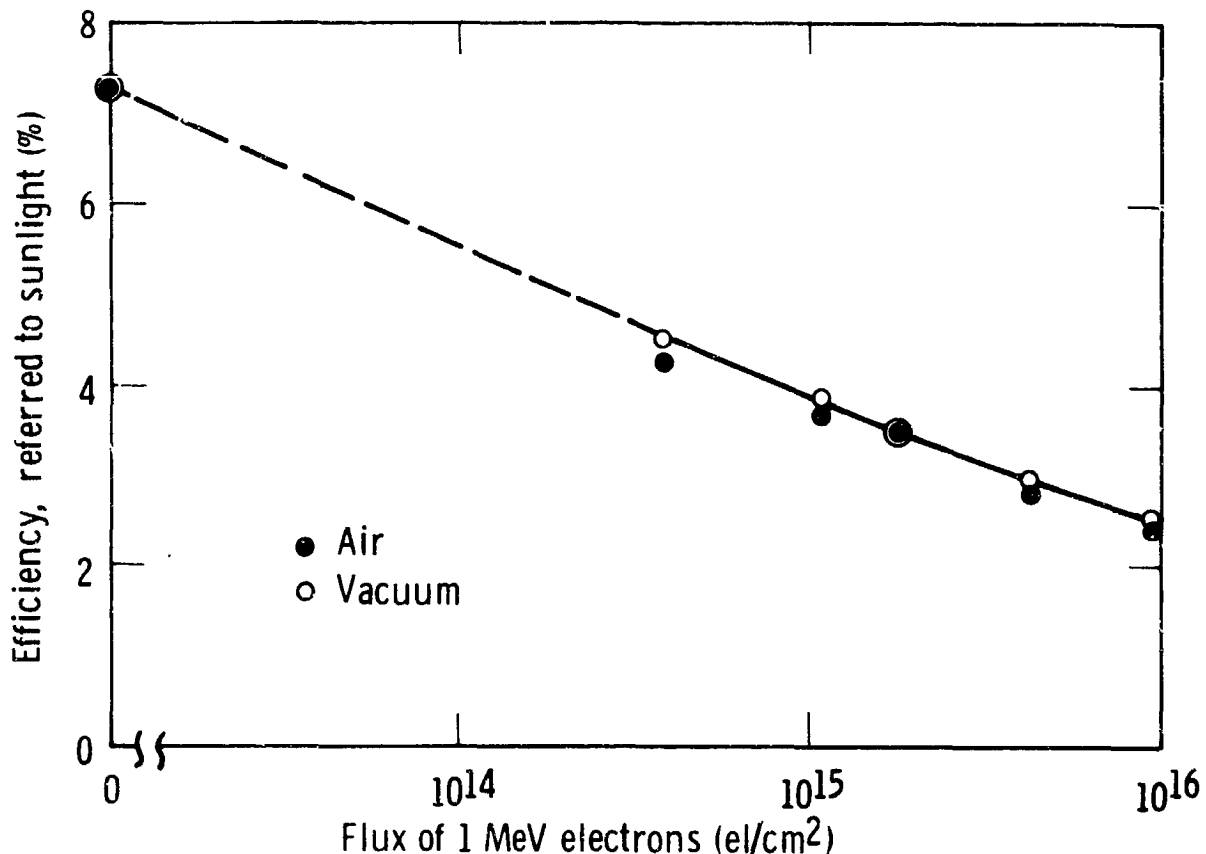


Fig. 11—Decrease of efficiency with 1 MeV electron flux, for 1 $\Omega\text{-cm}$ P/N silicon solar cells, irradiated in air and in vacuum ($\sim 10^{-4}$ torr). Cells were tested in filtered 3400 $^{\circ}\text{K}$ tungsten light at an intensity equivalent to 140 mW/cm^2 sunlight.

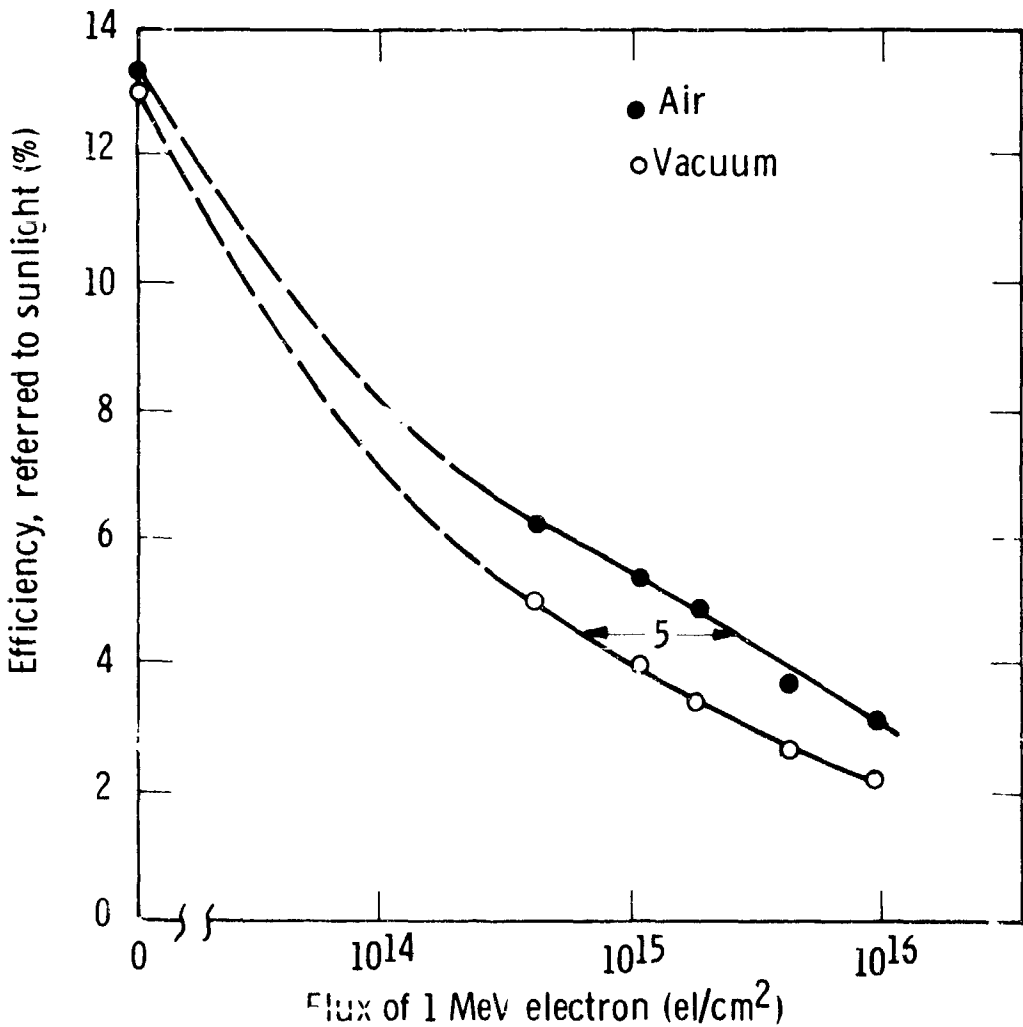


Fig. 12—Decrease of efficiency with 1 MeV electron flux, for $10 \Omega\text{-cm}$ P/N silicon solar cells, irradiated in air and in vacuum ($\sim 10^{-4}$ torr.). Cells were tested in filtered 3400°K tungsten light at an intensity equivalent to $140 \text{ mW}/\text{cm}^2$ sunlight.

DISCUSSION

MANDELKORN - NASA, LEWIS: Can you explain what you mean when you say efficiency referred to sunlight?

MR. BABCOCK: We take standard solar cells, which are unfortunately not as blue as I would like them, determine their short circuit current at 140 milliwatts per square centimeter sunlight, and then adjust our 3400°K tungsten illumination so that the calibrated cells give the same short circuit current. That's what we mean by referred to sunlight.

JOE LOFERSKI - BROWN UNIVERSITY: Can you say something about this vacuum versus air business? In an earlier paper we discussed the effect of radiation on surfaces and it appeared there that the response to infrared radiation did not change. It is the response to ultraviolet or violet radiation that is readily changed by radiation. An incandescent source like the one you are using is rich in the infrared and will not show the changes, or at least they will be suppressed.

MR. BABCOCK: Of course the situation is very different when you are looking at the surface.

JOE LOFERSKI - BROWN UNIVERSITY: What I mean is that in sunlight perhaps the differences between vacuum and air are greater because of the greater amount of violet and blue in the sunlight as compared with the incandescent tungsten lamp light source.

MR. BABCOCK: Of course the use of tungsten light is only an empirical dodge which does very little to simulate sunlight. I don't know how much of an effect this difference would make.

RALPH - HELIOTEK: You mentioned a lot of leakage in the dendrites on either side of the web. What kind of leakage was this, and how much of the dendrite did you have to remove?

MR. BABCOCK: The dendrites are trimmed mainly to get a uniform width for the cell and the reason we cannot make the cell with the dendrite on is due to the nonuniform width of the material as it is grown, rather than leakage. Leakage is not as important as I might have given you to understand.

ROSS - HOFFMAN ELECTRONICS: What is your actual degradation rate in percentage per decade? It seems to be a little faster than 20 per cent and that worries me a little bit.

MR. BABCOCK: For a p-on-n cell in a decade it goes from 8.6 to 6 percent which is about 30 percent per decade. Yes, that is high. But I also have data for an n-on-p cell. (A lengthy pause followed, which the chairman interrupted and closed the discussion).

PIC-SOL 209/5
Section A-9

1164-29151

EFFECTS OF SHIELDING ON ELECTRON DAMAGE
TO SOLAR CELLS

Presented by

F. J. Campbell

Naval Research Laboratory

Washington, D. C. 20390

2 June 1961

EFFECTS OF SHIELDING ON ELECTRON DAMAGE TO SOLAR CELLS

F. J. Campbell
R. J. Lambert

Radiation damage is not just a function of the solar cell degradation--the entire assembly must be considered in an analysis of the performance of the power supply. In Figure 1 is shown the common form of this assembly. The solar cell is covered with a sheet of glass, which serves as a shield against surface erosion, and when necessary it is thick enough to attenuate some of the incident particle radiation encountered in the Van Allen belts. On the outer surface of the glass is an anti-reflection coating which serves to increase the amount of light transmitted through the glass. On the inner surface a selective reflecting filter is applied which rejects ultraviolet energies which do not photo-activate the solar cell. This reduces internal heating and provides some protection against degradation of the adhesive used to bond the shield to the solar cell.

Based on the radiation exposure anticipated for the particular orbit, the designer of a satellite's solar cell power supply must evaluate the required thickness and composition of glass required to provide radiation protection (maintaining an optimum in the balance of cost, weight efficiency, and solar cell life) and select the most stable and effective adhesive. For example, in the design of the power supply for SYNCOM II, preflight calculations were based on the assumption that at the orbiting altitude of 22,300 miles, there would be insignificant damage due to particle radiation. The solar cells used are Hoffman p/n cells covered with OCLI 6-mil thick microsheet shields, containing the anti-reflecting coating and a "blue" filter, bonded together with Furane 15-E epoxy adhesive.

Previous experiments have been reported on electron, proton, and UV degradation studies of microsheet glass and 15-E adhesive which illustrated the changes in spectral transmittance observed in these and many other materials.¹ Notably, the first effect is a decrease in transmittance at the blue end of the spectra, which proceeds to fall further with increasing dose.

To determine exactly what effect this darkening has on the solar energy conversion efficiency of the solar cell assembly used on SYNCOM II, a study was conducted by irradiating the individual components with 1-Mev electrons and measuring the individual parameters by various methods. The specimen components obtained from the power supply contractor's assembly line for this study were as follows:

- (1) Bare solar cells (p/n)

(2) OCLI covers (6-mil microsheet) bonded to fused silica bases with adhesive 15-

(3) Same shields bonded to matching solar cells with adhesive 15-E

(Two specimens of each component were irradiated for each data point. A third specimen was measured each time as a control check on the instruments.) The irradiation degradation of the individual components should then equate as follows:

$$\underline{1} + \underline{2} \text{ (equivalent decrease in response due to darkening)} = \underline{3}$$

Irradiations with 1-MeV electrons were obtained with a Van de Graaff accelerator. To ensure uniformity of exposure, all specimens were mounted on the perimeter of an aluminum wheel which rotated at 10 rpm under the beam tube so that the circular path of each specimen passed through the axis of the beam tube on each revolution. Irradiations were conducted at different flux densities for each decade increment so as to maintain a reasonable time control. Exposure time varied from 80 seconds for $10^{12} e/cm^2$ to 122 minutes for the final dose of $10^{15} e/cm^2$.

Spectral transmittance through the cover glasses was obtained over the range of wavelengths from 0.35 to 1.2 microns with a Beckman IR-4U, double-beam, recording spectrophotometer. The spectra following accumulated doses of 10^{13} , 10^{14} , and $10^{15} e/cm^2$ are shown in comparison to the unirradiated spectra in Figure 1. At 10^{12} there was no change from the original spectra.

One of the methods used for measuring solar cell performance and the comparative degradation was with I-V curves obtained under illumination from a 2800°K tungsten light source through a water filter. The percent degradation in short-circuit current calculated from these measurements at successive dose increments are given in Table 1.

This conventional method did not, however, provide sufficient information to calculate the effect on performance due to irradiation damages to the glass and adhesive. Since this degradation is predominantly in the visible light region, in order to accurately determine the effect of degradation on the efficiency of the solar cell, it is necessary to determine changes in the cell's response with respect to the sun's spectrum rather than by the common method of tungsten source illumination. The relative spectra of these two sources are illustrated in Figure 2. Such a means of measuring this response and presenting it on a recorder has recently been developed at the Naval Research Laboratory.² Briefly, the original instrument provided a curve of relative spectral response at constant incident energy at all wavelengths. Recent modifications in instrumentation have made it also possible to multiply this response by Johnson's curve to obtain a curve representing

the relative solar response versus wavelength actually obtained from the solar cell or the shielded cell assembly in operation on a satellite's power supply. The resulting solar response curve obtained by this method is illustrated in Figure 3. If the curve of the degraded cover glass and adhesive were superimposed on this figure, it becomes apparent that an important region of the sun's spectrum has been attenuated. This effect is illustrated by the several curves in Figure 4, which were obtained with the NRL instrument. The solar response curves of the irradiated specimens are presented relative to the unirradiated specimens. An electronic integrator that will read out relative integrated response while the curve is being recorded has been recently added to the computer circuit.

These curves can be very helpful in design calculations for a power supply when the information is tabulated for calculations as in Table 2. Then, by multiplying the selected integrals under the curve of the relative solar response of an unirradiated bare solar cell by the average percent attenuation in this integral due to the cover glass and adhesive, the net decrease in short circuit current can be calculated. In this example, it is about 7%. By the same procedure with a normalized curve of the irradiated bare cell and the values of percent attenuation versus wavelength of the irradiated glass and adhesive, the effective radiation damage can also be calculated. Examples of these calculations are given in Table 3. The 6-mil thickness of glass provides very little attenuation of 1-Mev electrons, so the shielding effect is not taken into consideration in these calculations.

As a final check on this method, the same set of solar cell specimens was measured under the xenon-tungsten solar simulator at the Applied Physics Laboratory, Johns Hopkins University. This light source closely simulates Johnson's curve. Calculated radiation degradation of solar cells and the complete assemblies obtained from these measurements is compared to those obtained by the other methods in Table 4. Table 5 lists the calculated decrease in short-circuit current due to the attenuation of the cover materials before and after irradiation. Here the differences in results by the various methods are obvious. With the tungsten source, degradation of solar cells is accentuated since it is loss of response to longer wavelengths that is most affected, while the change due to degradation of the cover materials is undervalued. For a realistic analysis of degradation, either of the other methods described will provide practical results that will give a closer estimation of the effects of radiation on the performance of a shielded solar cell power supply.

REFERENCES

1. Campbell, F. J., "Effects of Space Radiation on Solar Cell Cover Materials," Proc. of Photovoltaic Specialist's Conf., Vol. II, July 1963.
2. Lambert, R. J., "Automatic Computation and Plotting of Spectral Response Data," Report of NRL Progress, Feb. 1964.

Table 1

Effects of 1 Mev Electron Irradiations on
Short-Circuit Current of p/n Solar Cells
(Tungsten Light Source)

Dose (electrons/cm ²)	% Decrease in I _s	
	Bare Cells	Covered Cells ⁺⁺
10 ¹²	5.7	7.4
10 ¹³	19.2	23.6
10 ¹⁴	39.8	44.6
10 ¹⁵	60.4	62.2

* Covered with 6-mil microsheet and 15-E adhesive

Table 2

Radiation Effects on Bare and Covred Solar Cells by
 Calculated Integrations of Solar Response Curves
 (Figure 4)

Wavelength Increment microns	Relative Solar Response per Increment			
	Before Irradiation		After Irradiation ($10^{15} e/cm^2$ - 1 Mev electrons)	
	Bare	Covered	Bare	Covered
.41 - .43	50	36	41	34
.43 - .47	146	122	158	117
.47 - .50	183	174	186	156
.50 - .60	814	770	910	638
.60 - .70	937	898	671	599
.70 - .80	952	909	438	393
.80 - .90	844	780	223	204
.90 - 1.0	622	572	52	46
1.0 - 1.1	313	203	8	5
1.1 - 1.2	23	18	0	0
Sum	4894	4482	2687	2192

Decrease due to Radiation Exposure

$$\text{Bare Cells: } \frac{(4894 - 2687) \times 100}{4894} = 45.1\%$$

$$\text{Covered Cells: } \frac{(4482 - 2192) \times 100}{4482} = 51.1\%$$

Decrease due to Cover Materials

$$\text{Before Irradiation: } \frac{(4894 - 4482) \times 100}{4894} = 8.4\%$$

$$\text{After Irradiation: } \frac{(2687 - 2192) \times 100}{2687} = 18.4\%$$

Table 3

Calculation of Decrease in I_{sc} Attributed to Light Attenuation by Cover Materials on SYNCOM II Solar Cell Assemblies as Determined from Normalized Solar Response Curves of Bare Cells and Spectral Transmittance of Covering

A-9-6

Wavelength Increment microns	Before Irradiation			After Irradiation ($10^{15} e/cm^2 - 1 \text{ Mev electrons}$)		
	Solar Response	% Attenuation	Decrease in Response	Solar Response	% Attenuation	Decrease in Response
.41 - .43	60	20	12	51	31	16
.43 - .47	146	14	20	221	25	55
.47 - .50	183	8	15	240	18	43
.50 - .60	814	6	50	949	15	142
.60 - .70	937	6	60	874	11.5	100
.70 - .80	952	6	60	573	9	51
.80 - .90	844	6	52	287	8.5	24
.90 - 1.0	622	7	44	69	9	6
1.0 - 1.1	313	7	22	6	8	0
1.1 - 1.2	23	6	1	0	7.5	0
Sum	4894		336	3270		437

Decreases due to Cover Materials

Before Irradiation: $\frac{336 \times 100}{4894} = 6.9\%$

After Irradiation: $\frac{437 \times 100}{3270} = 13.4\%$

Table 4

Comparison of Electron Damage to Solar Cell Assemblies as Determined by Various Methods

(Total Dose = 10^{15}e/cm^2 - 1 Mev electrons)

Method	% Degradation of I_{sc}	
	Bare Cell	Covered Cell
NRL Spectral Response Instrument Calculated (Table 2) Integration	45.1	51.1
Electronic Integration	47.2	51.0
APL Solar Simulator	42.8	48.2
Tungsten Light Simulator	60.4	62.2

Table 5

Decrease in I_{sc} Attributed to Light Attenuation by
Cover Materials on SYNCOM II Solar Cell Assemblies
as Determined by Various Methods

Method	Before Irradiation	After Irradiation ($10^{15} e/cm^2$ - 1 Mev electrons)
NRL Solar Response Instrument		
Calculated Integration	8.4%	18.4
Electronic Integration	6.2	12.8
Calculated from Attenuation Spectra	6.9	13.4
APL Solar Simulator	8.0	16.3
Tungsten Light Simulator	5.6	9.2

A-9-9

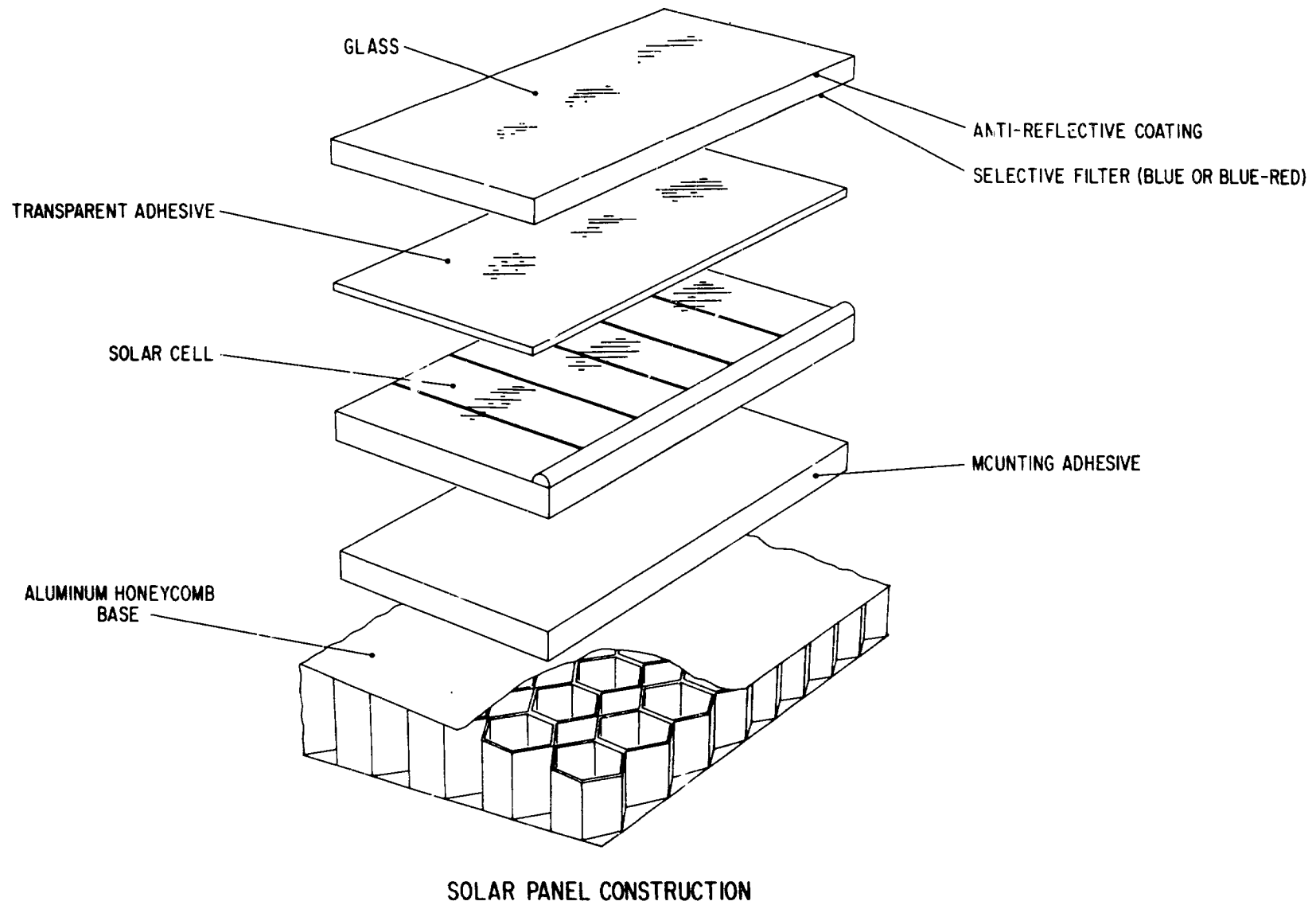


Figure 1

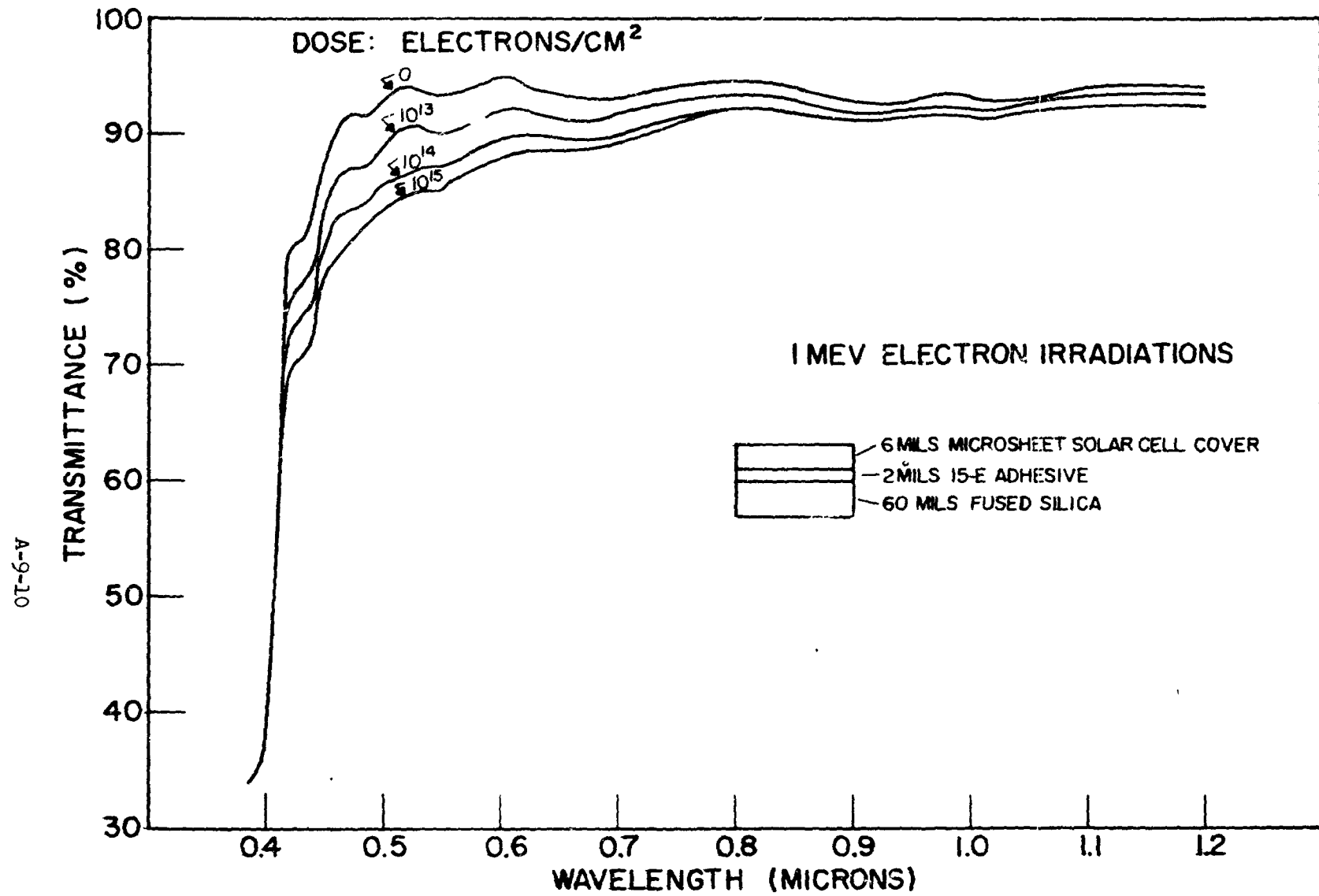


Figure 2

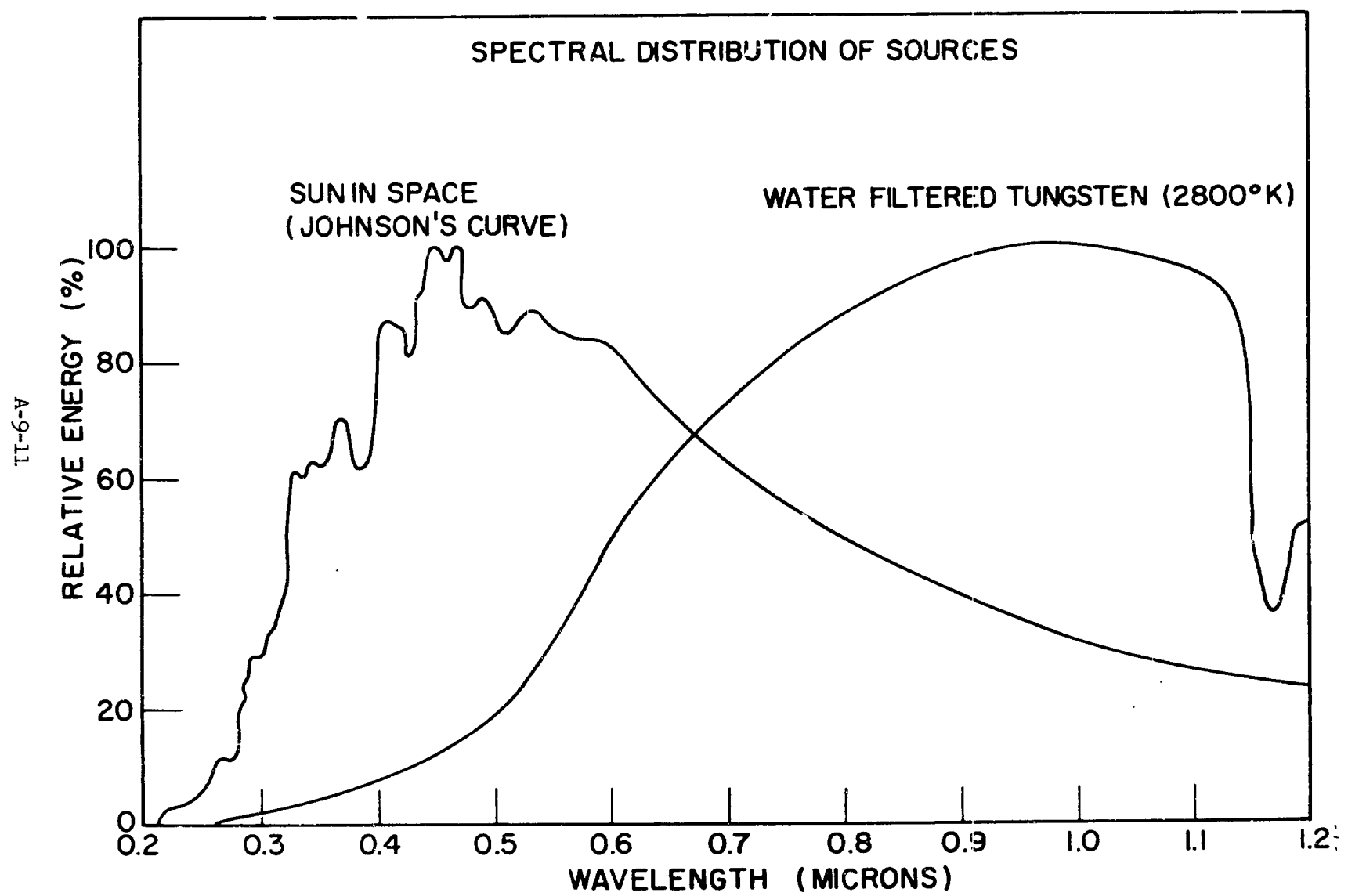


Figure 3

A-9-12

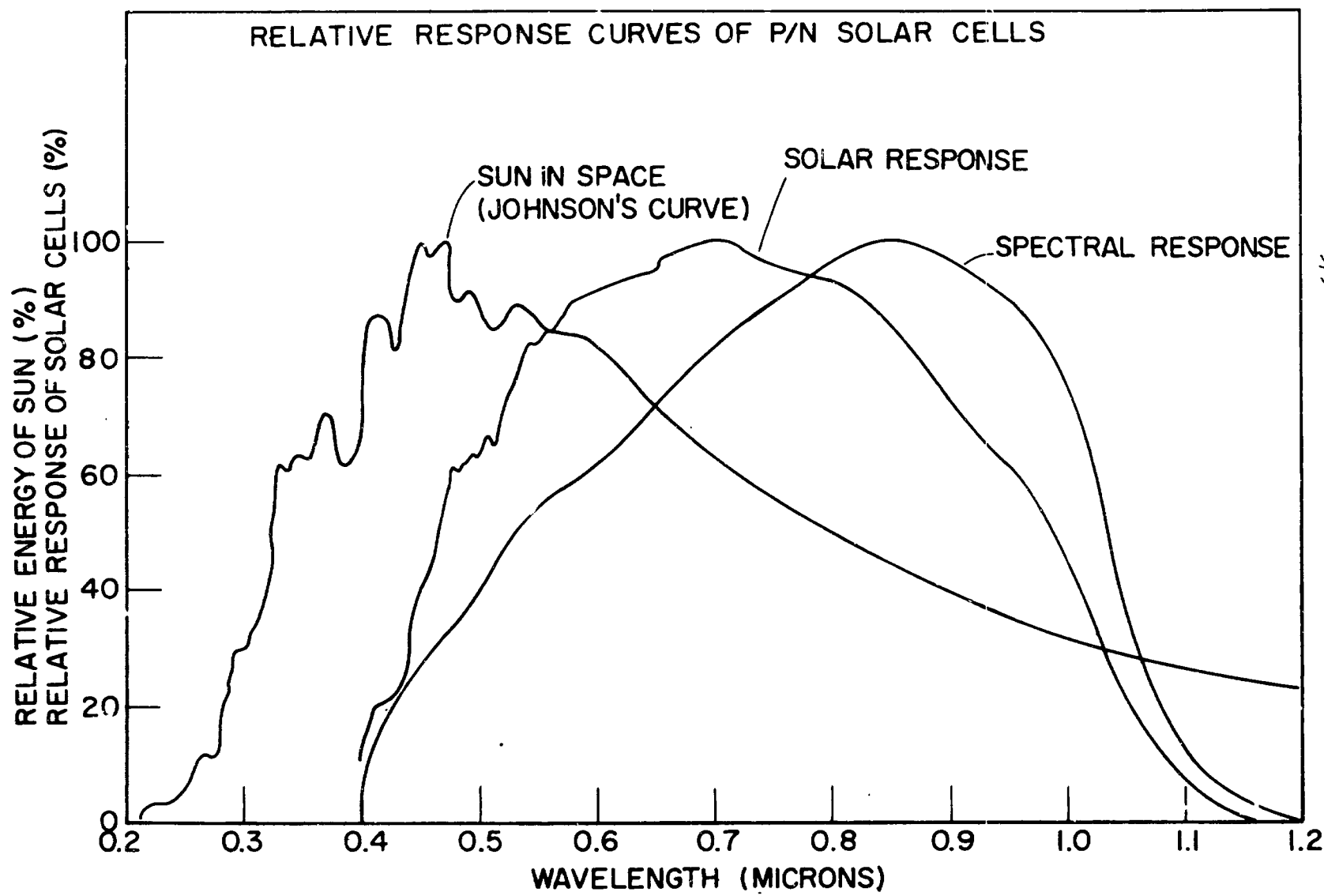


Figure 4

A-9-13

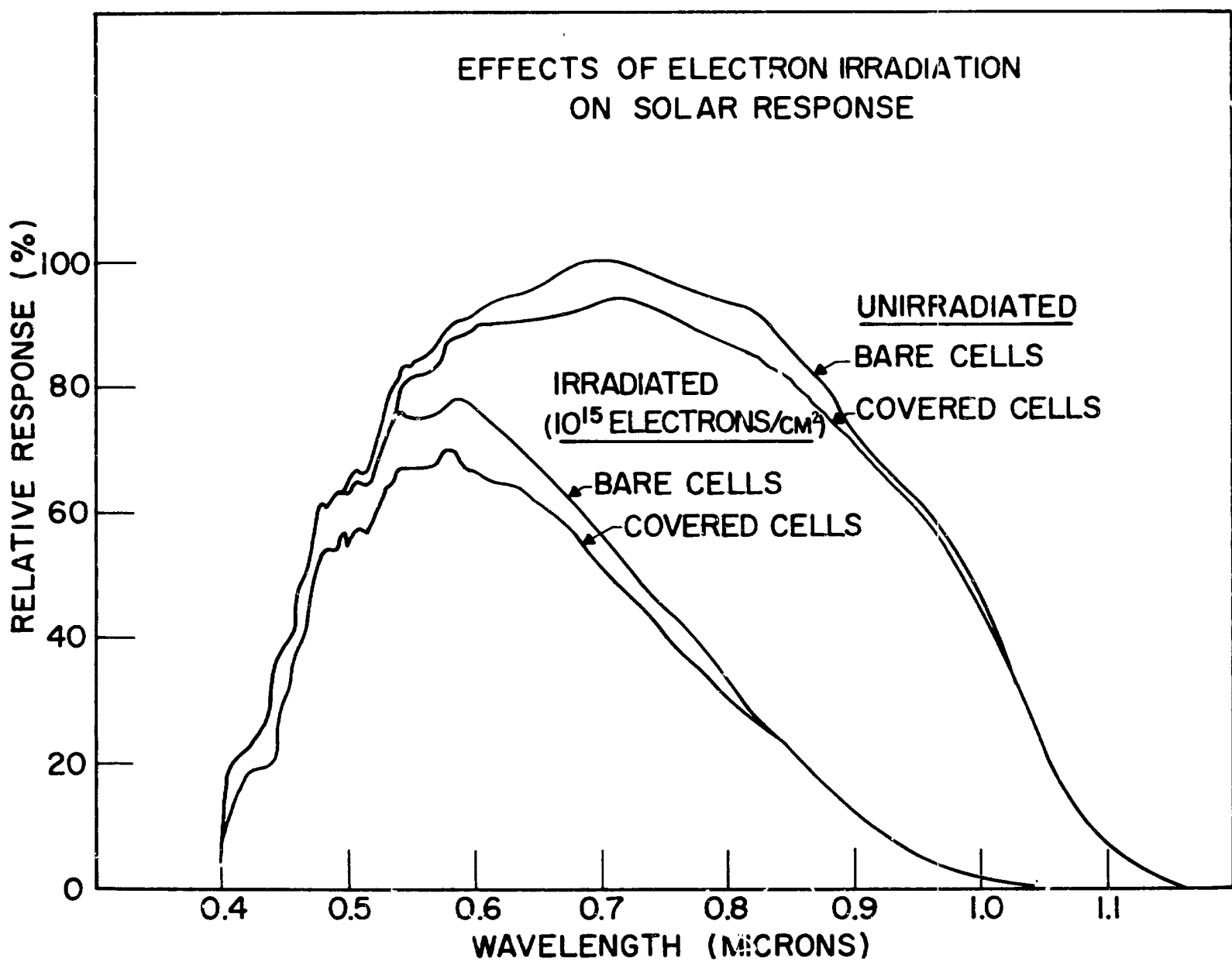


Figure 5

Page intentionally left blank

DISCUSSION

WEINER - RCA-ASTRO: Could you distinguish between the amount of damage to the 0211 and the purine 15E?

MR. LAMBERT: In this experiment there was no separation of the two. However, in previous reports that we have made we showed that purine 15E does degrade in transmission quite considerably. I believe our data was carried out to a dose of 10^{16} electrons per square centimeter.

WEINER - RCA-ASTRO: We have run some tests of the effect of radiation on various materials for the Nimbus application. Our transmission curves are more optimistic than those we have published in the past. We have some slides of this that we would like to show. The first slide shows two different transmission curves taken of the cover glass with a given piece of apparatus, and shows some of the variability found when you try to repeat experiments. The curves on the next slide are a little more interesting. These are transmission curves for a purine 15E coated six-mil 07940 cover glass. We have one curve at 10^{14} , one for 10^{15} , and two for 10^{16} representing two different samples. They are in general agreement with the data given by Campbell up to 10^{15} . But for the 10^{16} case we don't show a depression of the entire curve, but rather a sort of wedge-shaped deterioration at the shorter wavelengths. This curve is for another adhesive, X74, on the same cover glass. You can see that the effect of damage is much greater. If we take these absorption curves and the spectral response curves of reference unbombarded silicon cells and multiply them together we find that the response of the 15E combined unit is very little affected past a dose of 10^{15} . This is not the case for X74 where there is considerable degradation. We have more data which we will be glad to discuss in private with anyone who is interested.

CHERRY - NASA-GODDARD: I want to say that Fred has done a great deal of work on investigating different cover glasses and adhesives under electron, proton, and ultraviolet radiations. There is an NRL publication that has a great deal of this information in it. This publication is available by contacting Fred Campbell.

HIGH-ENERGY RADIATION AND SOLAR CELL SHIELDS*

N64-29162

By

Gilbert A. Haynes

NASA-Langley Research Center

Langley Station, Hampton, Va.

June 1964

*Not presented at the conference, but contributed for publication.

HIGH-ENERGY RADIATION AND SOLAR CELL SHIELDS

By Gilbert A. Haynes*

NASA Langley Research Center

INTRODUCTION

Particulate radiation such as that found in the earth's radiation belts poses a serious problem to some components of earth orbiting satellites. Solar cells are especially subject to radiation damage and often require shielding. Shields for the light-sensitive side of solar cells must, of course, be transparent. The transparency of many materials is affected by radiation, particularly by the high-energy electrons typical of the artificial radiation belt. Presented in this paper are data covering the effect of electron radiation on the optical transmission of a number of transparent materials which could be used as solar cell covers. Most samples were irradiated with 1.2 Mev electrons; however, some irradiation was also done with 0.30 and 2.4 Mev for comparison.

For accurate prediction of solar cell performance in a radiation environment, the effectiveness of the shielding material must be known. Data needed to compute shielding effectiveness are scarce, particularly for electrons when using relatively thick materials other than aluminum. Data are presented comparing the degradation of unshielded solar cells with that of cells shielded with various thicknesses of synthetic fused silica, using 2.4 Mev electrons.

APPARATUS AND TEST PROCEDURE

The particle accelerators used were 1 and 3 Mev dynamitrons located at Langley and Lewis Research Centers, respectively.

Pre- and post-irradiation tests on the optical transmission of the shield samples were made using a Beckman DK-1 spectrophotometer and a wide-band transmission monitor consisting of a solar cell, a tungsten light, and a readout instrument. The resolution of the spectrophotometer was about 10 angstroms maximum, and the repeatability was within 2 percent. The wide-band tests were repeatable within 0.5 percent. Visible appearance was also observed. The shielding materials tested were: synthetic sapphire, synthetic fused silica, fused quartz, micro-sheet, nonbrowning lead glass, high-density lead glass, nonbrowning lime glass, and solex.

Measurements were made of the solar cell short circuit current before and after irradiation using unfiltered tungsten light at 2800° K color temperature and 116 mw/cm^2 intensity. All tests were made with the shields off to eliminate any effects of the radiation damaged shields. Spectral response measurements were made on each cell (unshielded) before and after irradiation using a set of narrow band-pass interference filters.

*Aerospace Technologist.

RESULTS AND DISCUSSION

Irradiation of Transparent Materials

The materials chosen for testing had an optical transmission of 85 percent or better in the solar cell response band. The thickness of each sample was such that it approached or exceeded the penetration depth of the irradiating electrons in material. Penetration depths were computed from the range-energy curve in figure 1 (ref. 1). The penetration depth in silica (SiO_2) is 0.086 inch for 1.2 Mev electrons. Using range-energy curve for aluminum, the penetration depth in sapphire (Al_2O_3) is 0.051 inch.

Results are presented for a sample of most materials tested. A number of transparent shielding materials were tested at 1.2 Mev. A description of a sample of each material and results of wide-band transmission tests on each are given in table I. All samples in this table were irradiated with $2.7 \times 10^{15} \text{ e/cm}^2$ except the starred sample which was irradiated with $1.0 \times 10^{17} \text{ e/cm}^2$. The thickness of most of these samples exceeds the range of electrons in the material.

The sapphire sample listed is synthetic annealed crystalline sapphire and has a purity of 99.99+ percent. Synthetic fused silica is a material manufactured by a vapor deposition method where SiCl_4 is oxidized at high temperatures. Materials produced by this method may contain as little as 0.2 ppm impurities. Fused quartz is manufactured by fusing natural quartz crystals at high temperatures. By this method purities of 99.8 percent have been obtained in commercially available quartz. Corning No. 8362 is a cerium doped lead glass, and Corning No. 8365 is a cerium doped lime glass. Cerium tends to inhibit radiation darkening of glass and also enhances recovery from discoloration. Corning No. 0211 or micro-sheet is a fire-polished drawn glass available in thickness from 0.006 to 0.026 inch. Solex is a heat absorbent glass with a large iron content.

The wide-band transmission results indicate that a dose of $2.7 \times 10^{15} \text{ e/cm}^2$ causes no measurable damage over the solar cell response region in sapphire or synthetic fused silica. A heavy dose ($1.0 \times 10^{17} \text{ e/cm}^2$) will cause less than 2 percent damage in synthetic fused silica (starred sample). Only two of the nine kinds of fused quartz tested are represented. These are a slightly damaged sample and a heavily damaged sample. Other types tested that lost less than 7 percent in wide-band transmission were Amersil Infrasil, GE 105, and GE 106. GE 104 lost less than 1 percent in transmission at the listed dose.

The samples of Corning No. 8363 and No. 8365 did not change in transmission in the solar cell response band. However, the sample of Corning No. 8362 developed electron discharge patterns or Lichtenberg Figures (ref. 2) after a dose of about $7.4 \times 10^{14} \text{ e/cm}^2$. Such imperfections cause attenuation of light being transmitted by the sample; thus, a loss in transmission was seen. The densities of these materials are relatively high so the penetration depth of electrons in them is less than in quartz.

The sample of Corning No. 0211 listed was 0.026 inch thick. By virtue of its thinness the majority of the incident electrons were transmitted. There were samples of this material irradiated that were only 0.006 inch thick. These samples lost only about 2 percent in wide-band transmission. The solex tested exhibited good radiation resistance.

Figures 2 through 5 show the spectral transmission of some of the materials before and after irradiation. Figure 2 represents sapphire. At a dose of $2.7 \times 10^{15} \text{ e/cm}^2$ no change occurred in the transmission. However, after a dose of $1.0 \times 10^{17} \text{ e/cm}^2$ a very small decrease in ultraviolet transmission occurs. Sapphire also developed a slight discoloration.

Figure 3 represents synthetic fused silica before irradiation and after several doses. Notice that at a dose of $1.0 \times 10^{15} \text{ e/cm}^2$ the transmission degradation is primarily in the ultraviolet. But as the dose increases the degradation extends into the visible. Associated with the visible transmission degradation is a slight bluish visible coloration. The depth of this discoloration in the material appears to approximate the penetration depth of 1.2 Mev electrons in SiO_2 .

Figure 4 represents a lightly damaged sample of fused quartz. There is degradation of transmission in the UV, and visible regions with some degradation in the infrared. Notice that an absorption maximum appears to be centered at 0.55μ . Damage to other types of fused quartz differed in degree only from that shown in the figure. The absorption maximum and the spectral range of the damage were characteristically the same. Associated with this absorption maximum in the visible is a discoloration that is proportional to the degree of absorption. It varies from a faint brownish color for the lightly damaged samples to a deep purple for the heavily damaged samples.

Figure 5 represents Corning No. 8363 high-density lead glass. A dose of $2.7 \times 10^{15} \text{ e/cm}^2$ causes very little damage in the region of the spectral cut-off for the sample. The transmission decrease in the solar cell response region is minute thus explaining negligible wide-band transmission loss for this sample. Even less damage occurred in Corning No. 8365. The Corning No. 8362 sample showed a substantial decrease in spectral transmission. However, this decrease was not due to discoloration but to electron discharge patterns as discussed earlier.

Most of the damage to Corning No. 0211 occurs in the visible region. This material has a spectral cut-off at approximately 0.35μ . It also had a brownish visible appearance after irradiation.

Figure 6 shows damage versus flux curves for several materials. These curves show that damage to materials is nonlinear, and the damage occurs at relatively low fluxes as pointed out by curves c and d.

It is believed that the impurities in the materials are the main cause of discoloration or absorption in the visible. Damage to UV transmission is thought to be caused by defects in the atomic structure of the material (refs. 3 and 4). These theories are borne out in the quartz tests. The very pure synthetic fused

silica degraded relatively little while the less pure fused quartz degraded substantially. There are exceptions in the cases of the cerium doped glasses, and Solex which have high impurity contents.

Shown in table II is a tabulation of the relative effects of 2.4, 1.2, and 0.30 Mev electrons on the wide-band transmission of four materials. Not all materials were irradiated at all energies. However, from data in the table the damage to the optical transmission of the materials appears to be more energy dependent than flux dependent. Notice that for sapphire the extremely large dose of 1.0×10^{17} at 1.2 Mev causes no wide-band transmission damage while at one-tenth the dose with 2.4 Mev electrons the transmission degrades. There is a similar occurrence for all of the samples listed.

Solar Cell Shielding Tests

Figure 7 shows the degradation vs. integrated flux for typical N/P cells both unshielded and with synthetic fused silica shields of several thicknesses. The atmospheric density satellite (12-foot sphere) cells were covered with 1/8-inch shields. The Explorer XVI power cell trays had 3/16-inch covers. The aspect sensor on S-55C satellite will use a 1/4-inch synthetic fused silica cover.

The parameter shown in the figure is short circuit current. It was measured using a tungsten light source and the data corrected for space sun (air mass = 0). The 2.4 Mev energy was the highest available at the time and it is reasonably typical of the artificial belt electrons. This energy has a practical range of 1.1 gm/cm^2 in SiO_2 (corresponding to 0.197 inch of synthetic fused silica).

From the figure it can be seen that the shields substantially increase the critical flux f_c (flux required to produce 25 percent damage). A 1/8-inch shield increases f_c by a factor of 6.4 over that for a bare cell; a 3/16-inch shield increases f_c by a factor of 48 or more; and a 1/4-inch shield increases f_c by a factor of over 1000. These factors are considerably larger than those deduced from data given by Marshall and Ward for electron transmission of aluminum foils (ref. 5). Possibly a large number of the straggling electrons had energies too low to be effective in damaging the cells.

CONCLUSIONS

1. Sapphire was found to be practically unaffected by radiation in the spectral response region of solar cells.
2. Synthetic fused silica is damaged primarily in ultraviolet transmission, thereby it is an excellent material for use as solar cell covers.

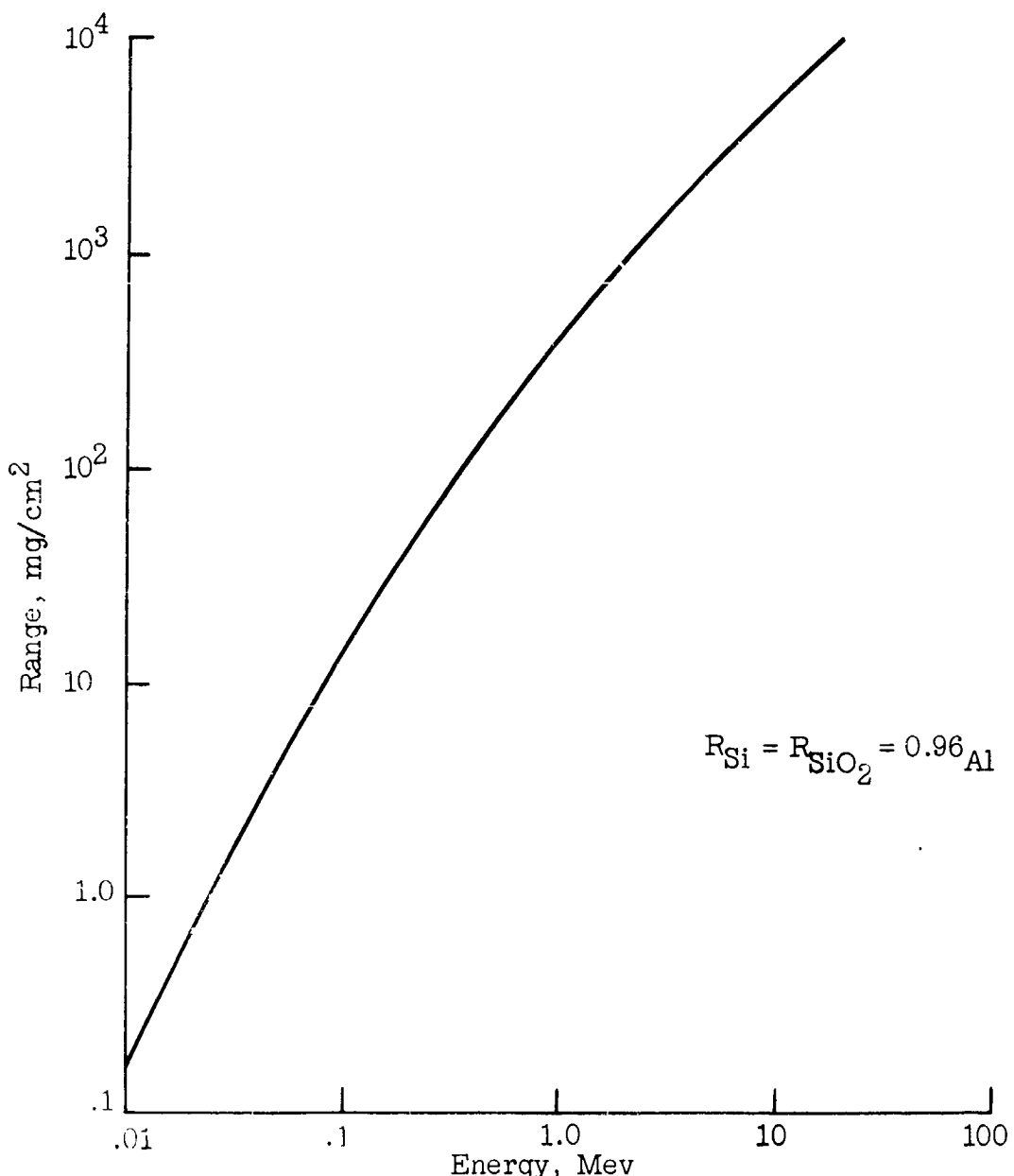
TABLE I.- EFFECT OF 1.2 MEV ELECTRONS ON SEVERAL MATERIALS

[Dose 2.7×10^{15} e/cm²]

Manufacturer	Trade name	Type	Wide-band transmission loss, percent
Linde Company	Sapphire	Annealed sapphire	0
Corning Glass Works	Corning No. 7940	Synthetic fused silica	0
Dynasil Corp.*	Dynasil Optical Gr.	Synthetic fused silica	1.5
Amersil Quartz Division, Engelhard	Amersil Optical Gr.	Fused quartz	1.8
Amersil Quartz Division, Engelhard	-----	Fused quartz	41.6
Corning Glass Works	Corning No. 8362	Nonbrowning lead glass	2.4
Corning Glass Works	Corning No. 8363	High-density lead glass	0
Corning Glass Works	Corning No. 8365	Nonbrowning lime glass	0
Corning Glass Works	Corning No. 0211	Drawn glass	7.6
-----	Solex	Heat absorbent glass	2.7

TABLE II.- COMPARISON OF SEVERAL MATERIALS IRRADIATED WITH
ELECTRONS OF SEVERAL ENERGIES

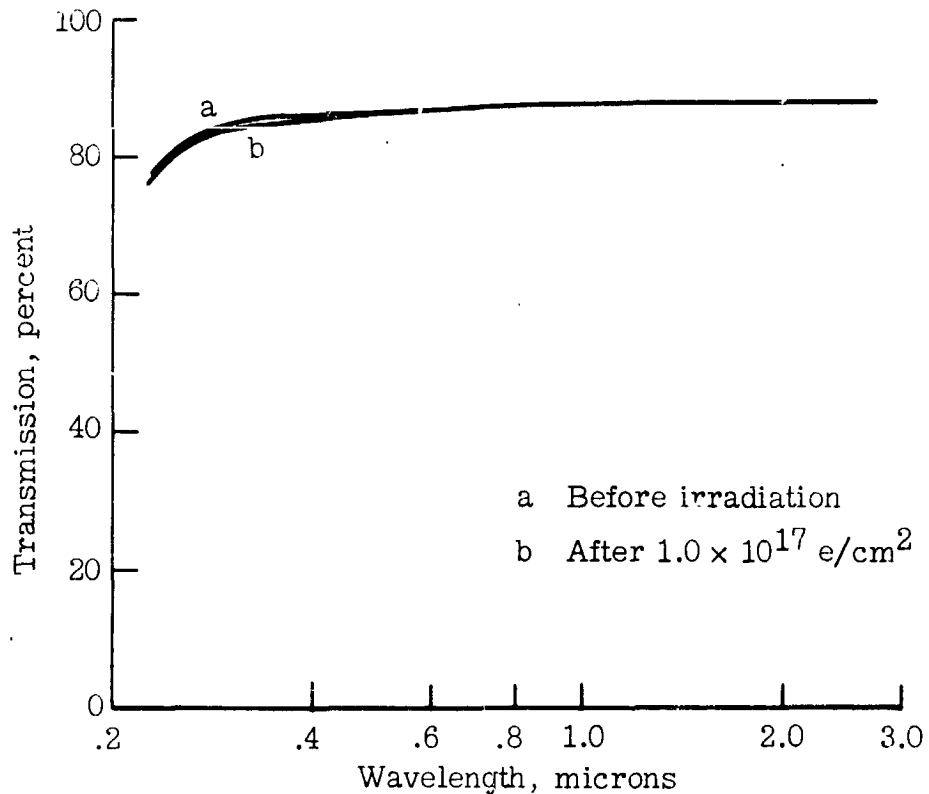
Trade name	Thickness, in.	Energy, Mev	Electron flux (e/cm^2)	Wide-band transmission loss, percent
Annealed sapphire	0.120	2.4	1.0×10^{16}	0.9
	0.080	1.2	1.0×10^{17}	0
	0.040	0.30	2.7×10^{15}	0
Synthetic fused silica	0.250	2.4	1.0×10^{16}	3.9
	0.125	1.2	1.0×10^{17}	1.5
	0.125	0.30	2.7×10^{15}	0
Fused quartz	0.0935	1.2	2.7×10^{15}	30.0
	0.0935	0.30	2.7×10^{15}	5.3
Corning No. 0211	0.026	1.2	2.7×10^{15}	7.6
	0.026	0.30	2.7×10^{15}	3.2



NASA

Figure 1.- Range-energy relationships for electrons in aluminum.

A-10-7



NASA

Figure 2.- Transmission of annealed sapphire before and after irradiation with 1.2 Mev electrons.

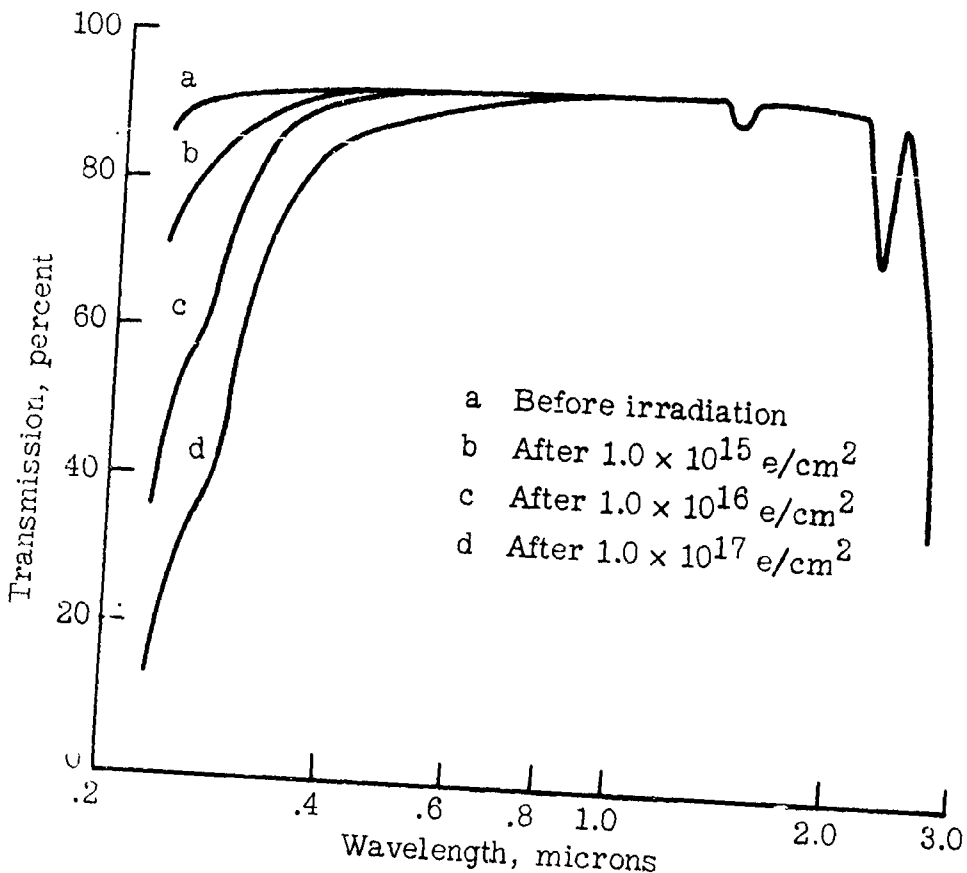
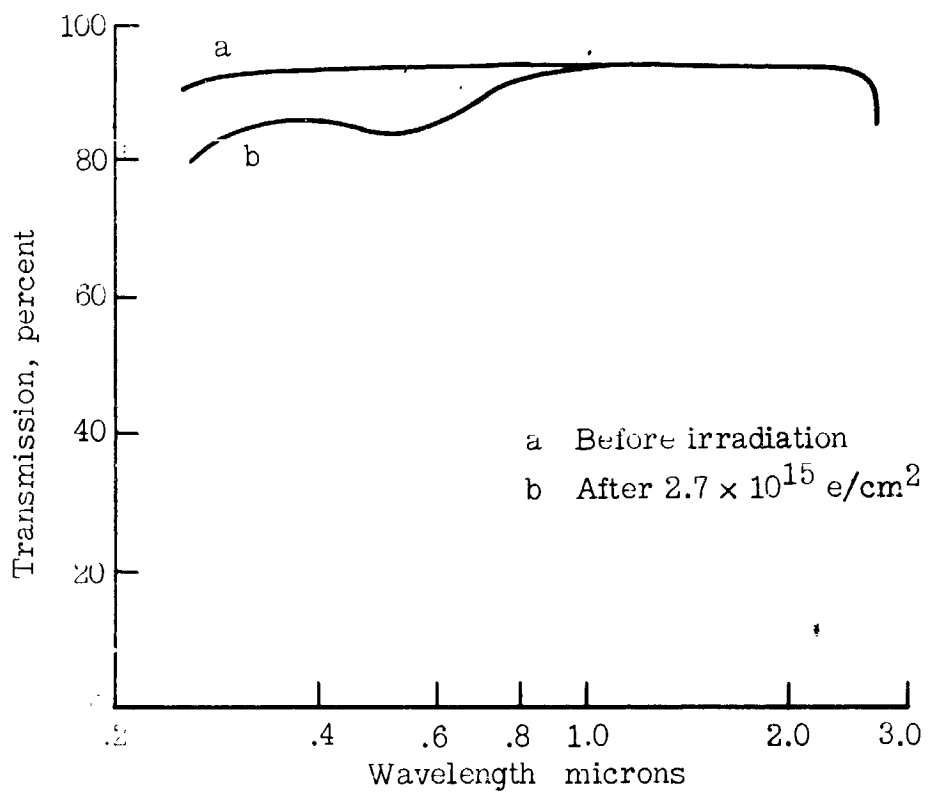


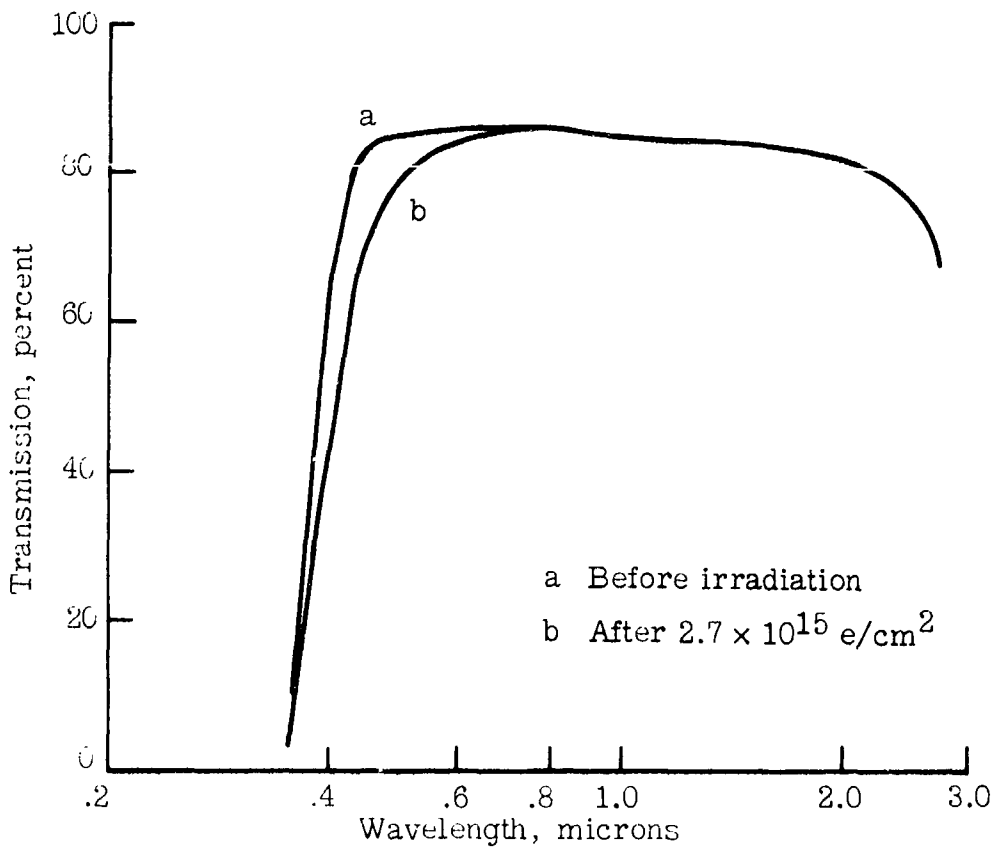
Figure 3.- Transmission of synthetic fused silica before and after irradiation.

NASA



NASA

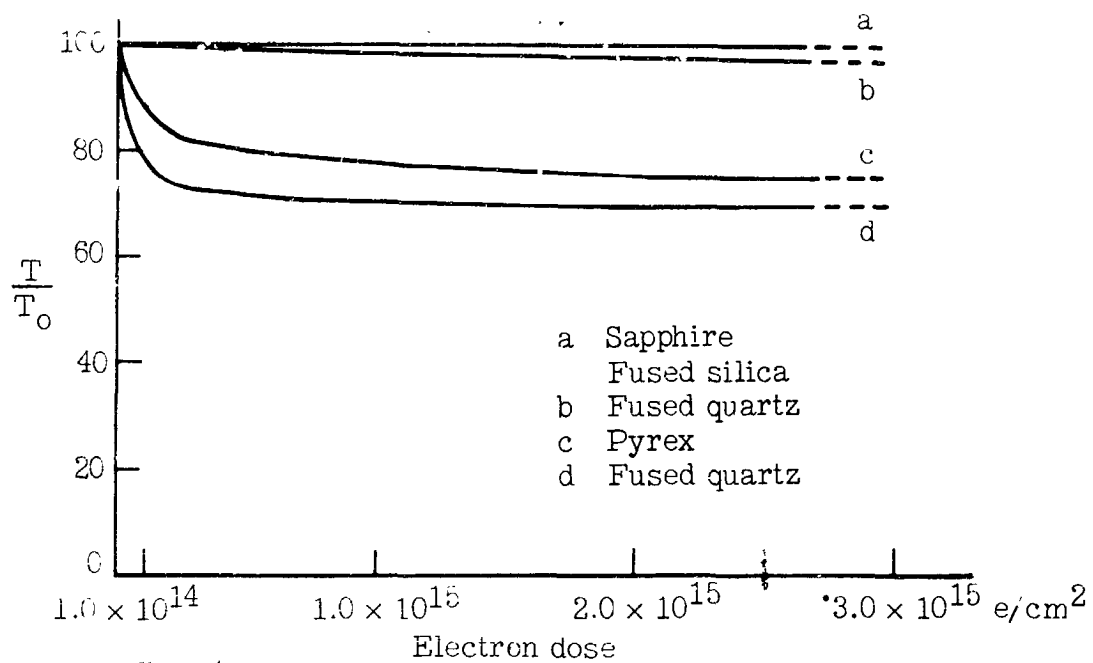
Figure 4.- Transmission of fused quartz before and after irradiation with 1.2 Mev electrons.



NASA

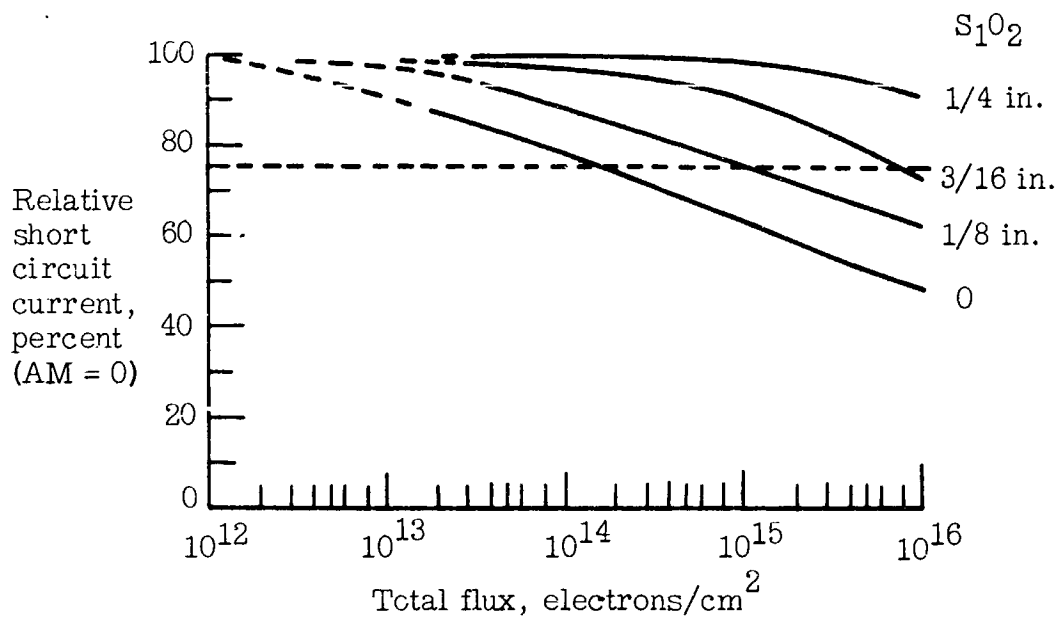
Figure 5.- Transmission of Corning number 8363 before and after irradiation with 1.2 Mev electrons.

A-10-11



NASA

Figure 6.- Damage vs. flux curves for 1.2 Mev electron irradiated materials.



NASA

Figure 7.- Damage rates of N/P solar cells with and without shields
- 2.4 Mev electrons.

N61-29163

CURRENT STATUS OF DRIFT FIELD SOLAR CELLS

Presented by

P. H. Fang

NASA-Goddard Space Flight Center

Greenbelt, Maryland

2 June 1961

Current Status of Drift Field Solar Cells

Presented by
P. H. Fang
NASA-Goddard Space Flight Center
Greenbelt, Maryland

Introduction of Radiation Damage Problems

The electrical power used in space exploration-except for some missions of short duration where ordinary batteries are used-is derived from photovoltaic solar cells, in particular, Silicon (Si) solar cells made of single crystal Si with a np junction, near but beneath the surface of the incident sunlight. With optimization of the junction polarity (np versus pn) and the base resistivity of Si, the power of the solar cells deteriorated to 75% of the original value in a matter of hours in space. With a protective glass shield, however, the deterioration rate is of the order of weeks and months, depending on the orbits of the satellite. Therefore, the search for solar cells with high resistivity to radiation damage continues to be important.

Some recent attempts have been made to use different materials other than Si, as described in the work of Wysocki, Perkins (GaAs), Aldrich (CdTe), Deshotels and Augustine, Chamberlin and Skarman, Schaefer and Statler, and Brandhorst (CdS), Werth (Ge) of the present Proceedings of Photovoltaic Specialist Conference, and Webb ($\text{GaAs}_{1-X}\text{P}_X$) of the 1963 Proceedings; or on using Si with different doping impurities, as reported by Mandelkorn. The consideration of replacing Si by other materials involves multitudes of problems and is not likely to become decisive for at least another five years or so. On the other hand, we cannot readily evaluate or appreciate the effect on the radiation resistivity of different impurities, mainly because the physical evidences are either not known or not shown as yet.

The present paper reports yet another attempt to improve the radiation resistance by a modification of Si solar cells. Before entering into specificities, we would like to make a phenomenological division of solar cells into two categories: (1) Films and (2) Bulk.

In this picture, single crystal GaAs solar cells and the modified Ga(As,P) solar cells belong to the first category, because of their direct transition mechanisms confined to the generation of hole-electron pairs in shallow regions of the order of a few microns. Si films or the type of Si cells considered by Wolf and Ralph in the present Proceedings also belong

to the first category in spite of the fact that Si has an indirect-band transition. The reason is the following: Si has a wide region of spatial dispersion of photons whose energy is larger than the band gap. Thus, the geometrical thickness of the film type of solar cells is smaller than the reciprocal of the attenuation coefficient of the usable and available photons. Of course, CdS and CdTe film solar cells belong to the first category.

At present, Si single crystals are a unique example of the second category.

These two categories of solar cells behave differently in their radiation properties and are pronouncedly manifest by their low energy proton radiation damage which is due to a strong attenuation of the penetration depth of the low energy protons. For film solar cells, therefore, at some energy range, the radiation damage could occur in the critical region of the photovoltaic electron-hole generation, and the consequence will be a catastrophic deterioration. On the other hand, bulk solar cells operate on electron-hole pair generation from extended spatial regions and the radiation damage from charged particles of any low energy will not strongly effect the resultant cell performance. We will elaborate on this point later when we discuss some specially fabricated drift field solar cells, because for technological reasons, drift field solar cells might manifest in some aspects the radiation damage of the film solar cell type.

Drift Field Solar Cells-Historical Review and Theoretical Problems

The physical mechanism of creating a drift field in semiconductors by introducing an impurity concentration gradient and its effect on the acceleration of minority carriers is well known¹, and the particular applications of this concept to solar cells has been documented by Wolf.² Experimental samples of drift field solar cells have been fabricated by Electro-Optical Systems, Inc.³ The method used was a double diffusion of concentration gradients on both the front and back of a very thin Si p-type single crystal a few hundred microns thick. The initial result bears out the "slow decay" of the relative power output versus logarithmic integration flux of electron radiation. This is in agreement with that expected from the drift field mechanism. By relative power, we mean the power at any accumulated flux damage divided by the initial power.

From a theoretical standpoint, as well as in practical application, we have to discuss the absolute power-or in a colloquial and not in a precisely described term-the efficiency. The early measurements, due to the scarcity of samples, also have not been extensive insofar as different energies and the types of charged particles are concerned. Probably the most practical limitation, however, is the very low yield resulting from the particular fabrication techniques.

By the summer of 1963, the most natural avenue of furthering this work became obvious: introducing the drift field by epitaxial growth of Si on a Si substrate with vastly different impurity concentrations. The magnitude of concentration differences is in the order of 10^4 to 10^6 . The resultant voltage V is from¹,

$$V = kT \log \frac{N_1}{N_2}, \quad (1)$$

where N_2 is the concentration at the place x_2 where the drift field is initiated; x_2 is not necessarily equal to x_j , the distance from the surface to the np junction. We take the value of x at the surface to be the origin, N_1 is the concentration at the end of the drift field x_1 , and, again, x_1 is not necessarily the thickness of the solar cells except in the case of the original EOS solar cells.³ From (1),

$$\begin{aligned} V &= 0.20 \text{ eV. for } N_1/N_2 = 10^4 \text{ to} \\ &= 0.30 \text{ eV. for } N_1/N_2 = 10^6 \end{aligned}$$

In the design of solar cells, it is more important to consider

$$E = \frac{\partial V(x)}{\partial x}$$

where

$$V(x) = kT \log \frac{C_1(x)}{C_2(x)}$$

and $C_1(x_1) = N_1$, $C_2(x_2) = N_2$. The exact form of $C_1(x)$ and $C_2(x)$ is the so-called concentration profile. In discussing the present status of drift field solar cells, we should first point out that there is no satisfactory method for experimental determination of the concentration profile.

Assuming $C(x)$ has been determined, and furthermore, the mobility and the diffusion coefficient are constant throughout the appropriate (n or p) regions, then the short circuit current of the solar cell can be calculated from a steady state transport equation. Wolf² has solved this equation for cases involving the range of numerical values of parameters considered above. But in reality, these parameters are spatial variables, and thus the nature of the differential equation does not guarantee the validity of an interpolation. Kaye⁴ and our own group are presently studying the solution of the transport equation of the minority carriers with variable parameters.

A limitation on the confidence of the solution of the transport equation is not a theoretical one, but is caused by the present lack of data on the optical absorption coefficient of Si in the region from 0.4 to 1.1, for heavily doped Si. All the current calculations make a tacit assumption of the validity of the early results of Dash and Newman⁵ and of Braunstein, et al.⁶; the former were measured on Si of low impurity concentration (20 ohm-cm) and the latter on pure Si. Only an experimental verification of this assumption can make the present theoretical calculation meaningful. In fact, if the concentration dependence of the optical absorption is appreciable, we have an inhomogeneous system where the experimental decay of the intensity also will not be valid.

Finally, treating the mathematical results presently available as quantitatively satisfactory, we then can proceed to design drift field cells with special radiation resistance. In this respect, we should note that the crude empirical formula⁷

$$\frac{I}{\tau} = \frac{I}{\tau_0} + K\phi$$

does not describe well the behavior of the decay of the short circuit current in the course of the accumulation of radiation flux, and we will discuss this point again when considering the experimental results.

Drift Field Solar Cells - Experimental Problems

We have mentioned central problems of drift field cells; namely, introducing a concentration profile in the ordinary np solar cells. The elementary division of different procedures of preparation are:

1. Single crystal front, epitaxial back,
2. Reverse of the above.

The shallow np junction and the drift field will be located on the front. The source or the sink of the impurity can be either the epitaxial or the single crystal. The physical principle is clear but the fabrication problems are multitudinous. It will not be possible to make a concise description without undermining technological complexities. Therefore, we should refer to the latest technical report⁸.

At present, on the one hand, the efficiency and the uniformity of the product does not warrant a report of the numerical values of the characteristic parameters attained; on the other hand, there are already many alternatives or remedies to the present deficiencies. It seems realistic to hope within

the next six months that drift field solar cells of sufficient quality and quantity to attain our theoretical expectations will become available.

Drift Field Solar Cells ... on Damage Experiments

At present, criteria which could be used to study the effectiveness of the drift field solar cells, are

1. An improvement in the quantum yield at long wavelengths; and
2. Relative reduction of the quantum yield due to the radiation damage in long wavelength regions should not be excessive in comparison with that in short wavelength regions.

We shall explain the physical basis for these two qualitative criteria in the following.

Criterion 1. The basic mechanism of the drift field is to accelerate the minority carriers created in the base region (i.e., electrons in the case of np solar cells) to reach the junction for collection. In ordinary solar cells, if the product of the diffusion mobility and the lifetime of the minority carrier is shorter than the distance from the location of electron-hole pair creation to the np junction, the minority carrier will be unable to reach the junction, and therefore, it cannot contribute to the photovoltaic current. The drift field is designed to improve the probability of collection for these minority carriers with a short lifetime. Figure 1 illustrates this point: the broader distribution of the quantum yield at the long wavelength as exhibited by a drift field solar cell. However, there is a mechanism to invalidate our criterion: the minority carrier lifetime decreases as the impurity concentration increases. The net effect of this mechanism has not been considered.

Criterion 2. In ordinary cells, the radiation damage results in a decrease of the quantum yield only in long wavelength regions, as illustrated in Figure 2a. Now, if the drift field is functioning, we should expect the damage not to be excessively selective with regard to wavelength, at least for wavelengths which have a corresponding optical absorption coefficient smaller than the reciprocal of the distance from the surface to the base side of the np junction. This feature seems to be supported by the experimental data of Figure 2b.

An important observation is the large decrease of the open circuit voltage in the drift field solar cells due to the electron radiation damage (Figure 3). The data of Figure 3 is taken with a xenon arc lamp with 100 mw/cm² illumination. We observe an initial decrease of short circuit

current after $5 \times 10^{14}/\text{cm}^2$ electrons of 1 Mev, but the rate of the decrease on further radiation is lessened, and there is an indication of reaching the saturation of the damage, or in some instances, even a recovery at least in certain wavelength regions, indicating an initiation of annealing. This should be expected to occur in the case of a very high concentration of defects. The disheartening effect is the decrease of the open circuit voltage, worse than the case of the ordinary np cell, as illustrated in the accompanying sketch (Figure 3). One possible explanation of this phenomenon is the localization of the defects. For example, these defects occur in the region where the np junction field effect has tapered off and the effect of the drift field has not commenced. Typically, this region is from 5 to 25μ in width. This explanation is in line with the radiation damage of low energy protons as discussed in the Introduction.

Conclusion

We have described, in the present paper, our present knowledge of the drift field solar cells and offered some interpretations of the problems. In doing so, we have attempted to retain basic physical concepts, and to avoid some heuristic assumptions and nonessential simplifications. As we have seen, present knowledge of the drift field solar cells, or even all solar cells in general, is not sufficient to make an evaluation or a prediction. The immediate program remains a large experimental effort on preparing solar cell specimens, and on careful theoretical analysis.

The drift field solar cells used in the present studies were produced by Electro-Optical Systems, Inc., Heliotek, and Texas Instruments, Inc., under a NASA contract with Goddard Space Flight Center. We take this opportunity to express our appreciation for their enthusiastic cooperation and many illuminating discussions. We would like to acknowledge the help of Mr. W. Gialla in our experimental work. This work is being carried out under the guidance and with the encouragement of Mr. M. Schach. The cooperation of the Insulation Section of the Naval Research Laboratory, under Mr. Emanuel Brancato, is gratefully acknowledged.

U212

References

1. E. Spenke, Electronic Semiconductors, New York: McGraw-Hill, 1958, p. 77.
2. M. Wolf, Proc, IEEE 51, 674 (1963).
3. M. Cheslon and S. Kaye, "Feasibility Study Toward Development of Radiation Resistant Solar Cell" Final Report, Contract NAS 7-92, 28 Feb. 1963, Electro-Optical Systems, Inc.
4. S. Kaye, "Development of an Improved Radiation Resistant Solar Cell," Semi-annual Report, Contract NAS-3560, May 1964, Electro-Optical Systems Inc.
5. W. C. Dash and R. Newman, Phys. Rev. 99, 1151 (1955).
6. R. Braunstein, A. R. Moore and F. Herman, Phys. Rev. 109, 695 (1958).
7. G. W. Simon, J. M. Denney and R. G. Downing, Phys. Rev. 129, 2454 (1963).
8. "Development of Epitaxial Structure for Radiation Resistant Silicon Solar Cells," Semi-annual Report, May 1964; Contract NAS 5-3559, Texas Instruments Inc.
"Development of Improved Radiation Resistant Solar Cell," Semi-annual Report, May 1964 Contract NAS 5-3558, Heliotek.
See Ref. 4.

FIG. 1 QUANTUM YIELD VS λ
1 Mev ELECTRON RADIATION

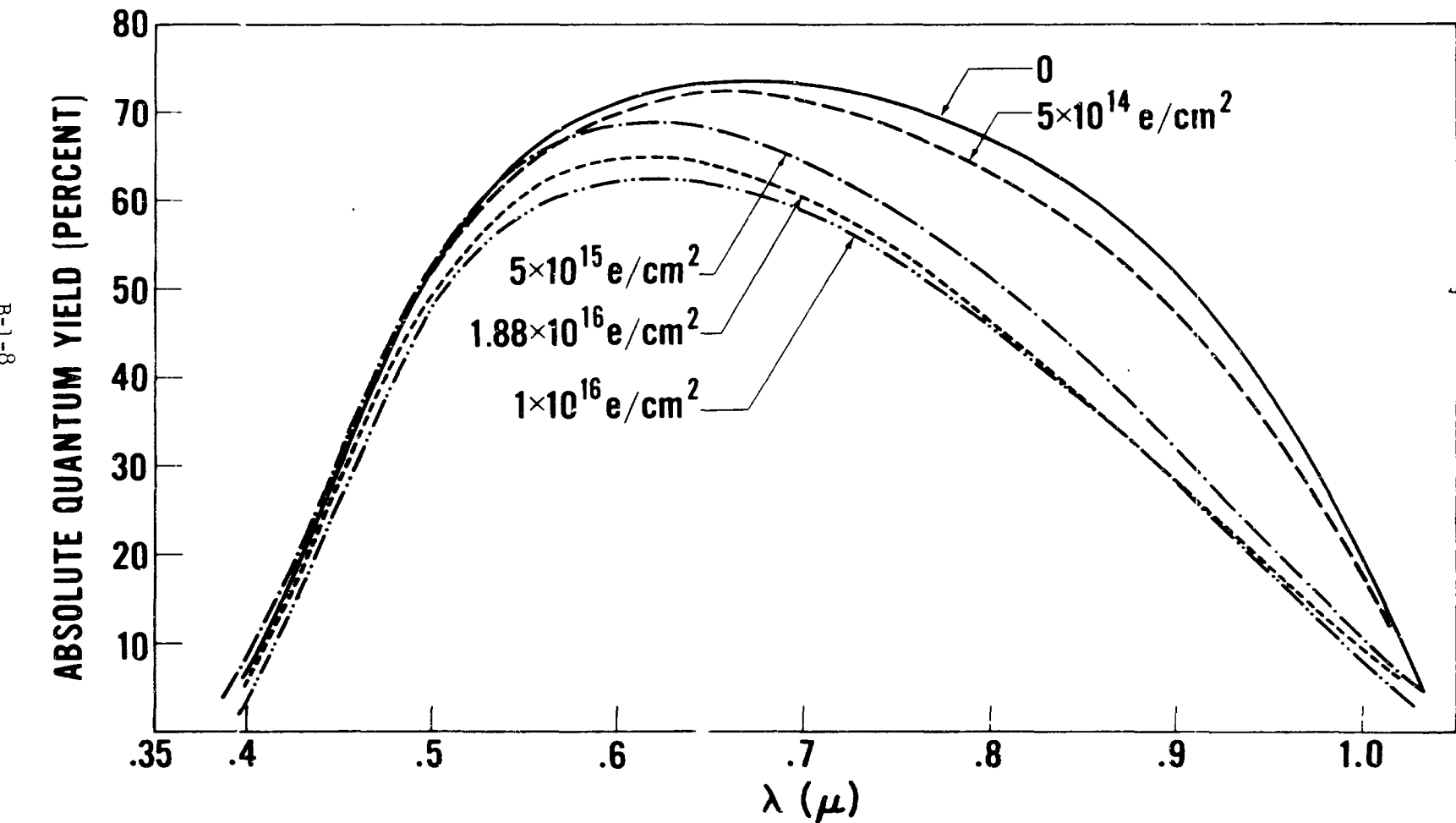
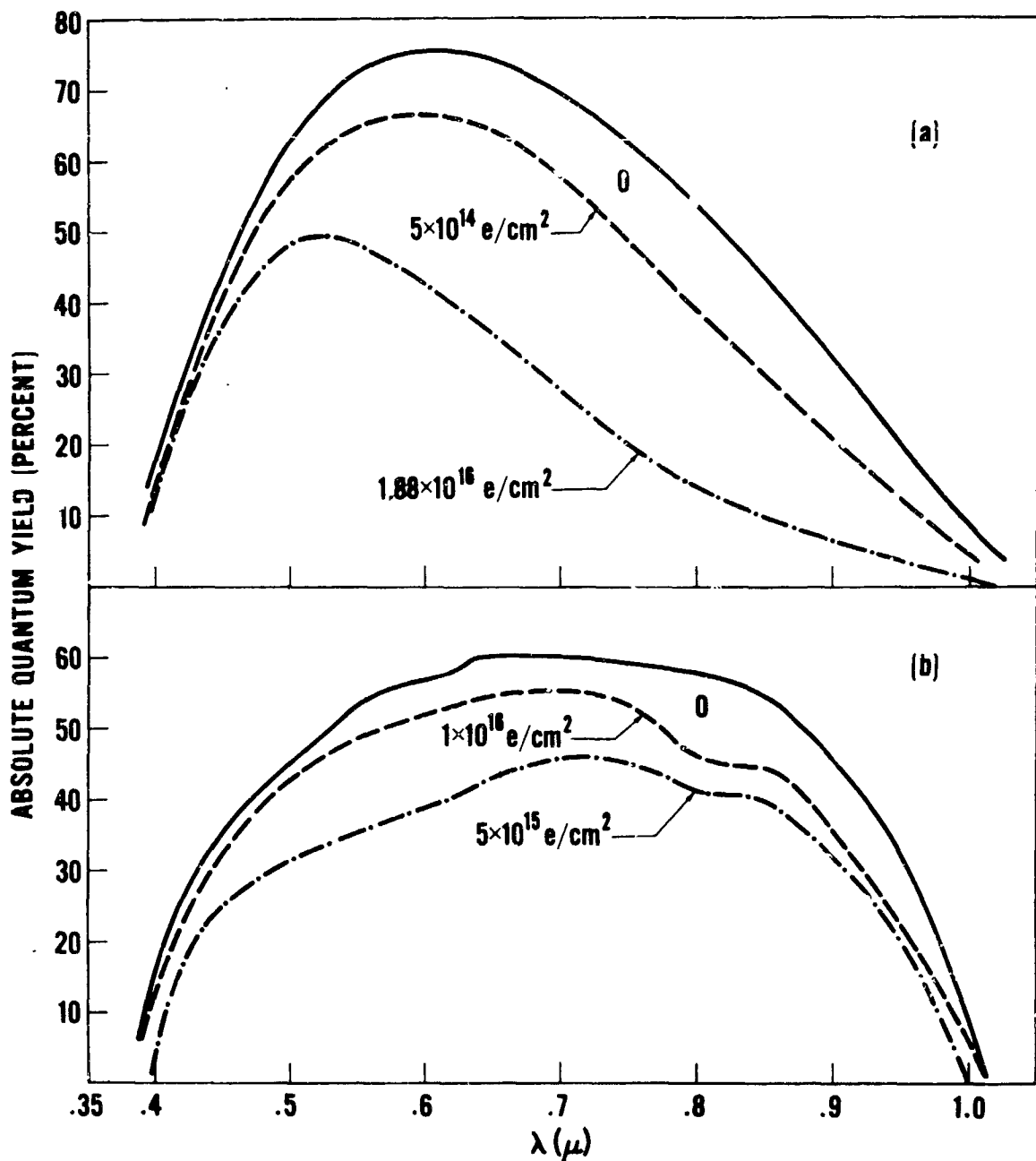
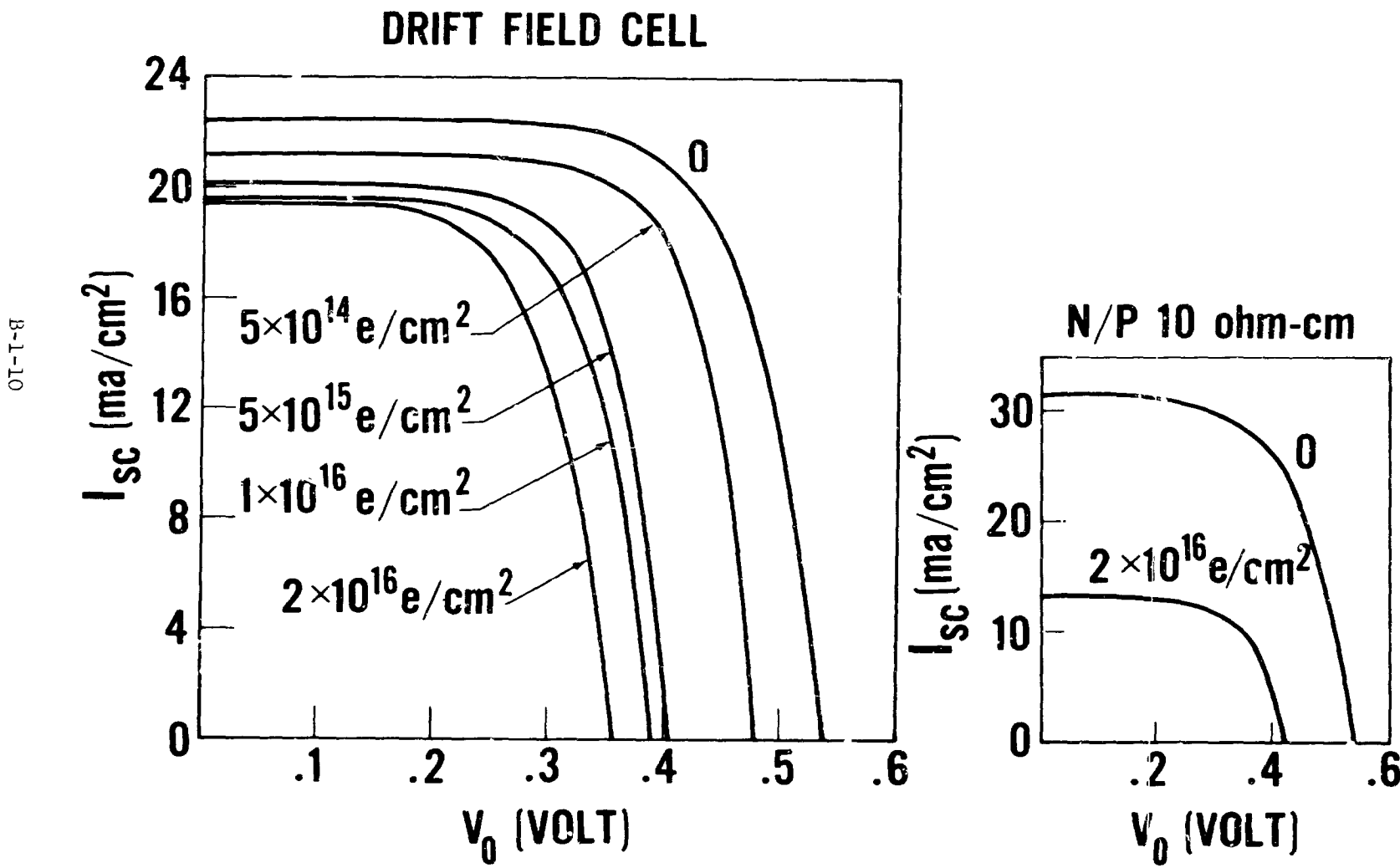


FIG. 2 1 Mev ELECTRON RADIATION



**FIG. 3 I-V CHARACTERISTIC CURVE
1 Mev ELECTRON RADIATION**



DISCUSSION

TARNEJA-WESTINGHOUSE: In your last slide what was the light intensity? 140 milliwatts?

DR. FANG: The intensity was 100 milliwatts per square centimeter.

SOLAR CELLS PRODUCED BY ION IMPLANTATION DOPING

Presented by

W. J. King

Ion Physics Corporation

Burlington, Massachusetts

2 June 1964

N64-29164

29164

Abstract

Fabrication of "controlled-junction" solar cells by implantation of appropriate doping ions into bulk silicon has been demonstrated using a Van de Graaff accelerator. Boron ions of energy 100 keV to 1.5 MeV (0.35 to 2.3 microns junction depth respectively) were used to form P-type surface layers while phosphorus ions of 300 keV energy (0.51 microns junction depth) were used for N-type layers. After being passed through an analyzing magnet to obtain a spectroscopically pure beam, the accelerated ions were scanned by electrostatic deflection plates to obtain uniform irradiation of the samples. Doping concentration could be varied as a function of depth in the crystal by programmed rotation of the slices about an axis perpendicular to the beam. In this manner it is possible to arbitrarily insert a "drift-field" in the surface region to study the effect on carrier collection efficiency and radiation damage resistance.

This technique is being studied as a means of producing high efficiency single-crystal cells and as a method for forming junctions in thin-film polycrystalline silicon cells. The state-of-the-art for these applications is discussed in terms of factors affecting cell efficiency, drift-field effects, radiation damage and annealing effects, and thin film deposition techniques.

(cont'd)

SOLAR CELLS PRODUCED BY ION IMPLANTATION DOPING

W. J. King and J. T. Burrill

Ion Physics Corporation
Burlington, Massachusetts

1. INTRODUCTION

This paper presents the results of an investigation in which radiation, or more exactly a beam of accelerated particles, has been used to make rather than destroy solar cells. The investigation was initiated three years ago by IPC and has been supported for the last eighteen months by the Research and Technology Division of the United States Air Force. Basically, the objective of the program is the development of an ion implantation technique for economically fabricating high efficiency, high yield single crystal silicon cells. It is anticipated that higher efficiencies may be obtained by inserting a drift field immediately adjacent to the surface to overcome high surface recombination velocity and increase collection efficiency at shorter wavelengths. This may be accomplished without exposing the cell to temperatures greater than 800°C, thereby maintaining bulk lifetime and red response.

Additionally, the program is directed at achieving a more controlled doping of silicon layers during deposition for thin film cells. The object is to provide a mating of techniques, yielding the ability to deposit thin film cells with a drift field in the bulk region for better collection efficiency and radiation resistance.

Currently the program is divided into two completely separated sections; ion implantation doping and thin film silicon deposition. This discussion is limited primarily to the former since the deposition techniques are in an early stage of development.

In principle, the major technical advantage of the ion implantation technique lies in the capability of accurately producing the required impurity concentration distribution in a reproducible manner. The main energy loss mechanism for heavy charged particles in matter is the process of ionization.¹ Elastic nuclear scattering becomes important only at the end of the range where the ions are moving slowly, and for this reason heavy ions have discrete ranges. It is precisely this property that makes implantation appealing as a "controlled" doping technique. This discrete range characteristic occurs in amorphous or polycrystalline materials and in single-crystal materials along most directions. By a suitable choice of ion species and implantation parameters, it is possible to dope n- or p-type in silicon or, in principle, in other semiconductor materials.

2. EXPERIMENTAL APPARATUS AND TECHNIQUE

Figure 1 shows schematically the general apparatus and procedure used in making solar cells by this technique. A high energy (50 keV - 2 MeV) Van de Graaff electrostatic accelerator is used to accelerate boron or phosphorus ions from an RF ion source to the energy corresponding to the junction depth desired. The beam is passed through an analyzing magnet to remove all contaminating ion species. This spectroscopically pure beam is then scanned vertically and horizontally to a uniform cross-section larger than the sample area. Finally, it impinges on a silicon slice mounted in the target position in such a way that it can be rotated continuously from a position normal to the beam to a position parallel to the beam. Since the ions have discrete ranges independent of incident angle, the distance below the silicon surface at which the ions come to rest is determined by the angle; i.e.,

$$X_p = R_E \sin \theta \quad (1)$$

where X_p ≡ penetration depth perpendicular to surface

R_E ≡ range of the incident ions in Si at energy E

θ ≡ angle between incident direction and Si surface.

By rotating the sample continuously while the beam energy is held constant, a continuous implantation of ions is obtained from the surface to a deptl. corresponding to the maximum range. During implantation, beam current is held constant. Since the incident flux rate decreases with θ a servo system is used to control the speed of sample rotation and therefore integrated flux at any given depth below the surface. A variable program controlling the servo system controls the concentration gradient and can be used to vary junction profiles. The entire sample irradiation chamber is enclosed in a clean bench to prevent channeling caused by dust particle beam shadowing. The latter was found to be one of the limiting factors in producing devices by this technique. If dust particles of size larger than twice the ion range are present on the sample surface during implantation, small channels beneath the particles do not become properly doped and leakage channels result. If the channel or channels occur beneath the front contact they can markedly affect the cell characteristics.

In the general procedure, the slice are first lapped to a 5.0μ finish and then etched to a smooth surface in a 3:1:1, nitric, hydrofluoric, acetic acid etch. All final pre-implantation cleaning operations on the samples are performed in the clean bench area at the machine, the cells then being transferred directly into the implantation chamber. To remove dust particles, the best procedure found was a surface scrub with

a trichloroethylene dipped cotton swab followed by a trichloroethylene vapor degreasing. After post-implantation annealing Ti-Ag contacts are applied.

In addition to inserting doping atoms into the crystal lattice, the implantation process also creates a high degree of radiation damage. Temperatures required for annealing this damage are normally in the 300°-600°C range as shown by reflection electron diffraction studies of lattice structure. Cells are, however, typically annealed at 800°C for 16 hours in vacuum since these higher temperatures have been found empirically to give higher efficiency cells. This latter result has been tentatively ascribed to an activation energy required to transfer implanted atoms from interstitial positions to lattice sites.

At the present time ion energies are in the 300 keV range although values as high as 1.5 MeV have been studied. Optimization of cell characteristics is expected to reduce the maximum required energy to <100 keV, a value where relatively inexpensive air insulated accelerators may be used. Van de Graaff accelerators have proven very useful in this type of investigation because of their inherent control of beam current, energy and energy spread. The latter is controlled to better than 1 keV which represents a spread of only .33% at 300 keV corresponding to a range spread for P³¹ ions of approximately 13 Å in 4,000 Å. Any straggle in junction definition is primarily due to statistical variations in ion range, and impurity movement during annealing. All of these factors can be controlled to give a junction depth control of better than 0.1 microns.

Figure 2 shows angled sections of two typical junctions. The upper one is a microphotograph of a 500 keV B¹¹ implanted sample with a junction .76μ deep following the surface unevenness exactly. The lower

one is an interference micrograph of a more highly polished sample implanted with 300 keV P^{31} ions to give a very flat .51 μ deep junction.

Figure 3 gives a summation of the accumulated range-energy data compiled at IPC from junction depth measurements on silicon samples implanted with B^{11} and P^{31} ions. These data agree fairly well with those found by more conventional techniques and are useful in predicting ion energies required for different junction depths and profiles.

3. CELL CHARACTERISTICS

The electric drift field in a given region due to an impurity concentration gradient is given by²

$$E = \frac{kT}{q} \cdot \frac{1}{\Delta x} \cdot \ln \frac{\left| N_A - N_D \right|_{x_1}}{\left| N_A - N_D \right|_{x_2}} \quad (2)$$

where k \equiv Boltzmann constant

T \equiv absolute temperature

q \equiv electronic charge

N_A \equiv density of ionized acceptors

N_D \equiv density of ionized donars

x_1, x_2 \equiv layers 1 and 2 in sample, respectively

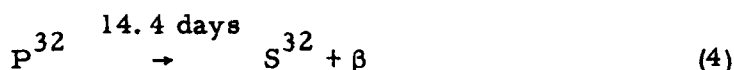
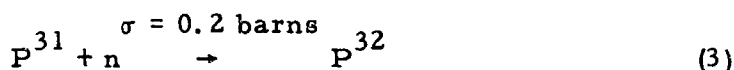
Δx \equiv distance between layers x_1 and x_2 .

Typical concentration profiles suggested for studies on drift field effects in this program are shown in Fig. 4. These are linear, 10:1, 100:1 and 100:1 - linear impurity concentration gradients from the surface to the junction with steeper gradients being available if necessary. Since the program involves development of an entirely new technique, it was

found that other effects, such as leakage, were masking drift field effects and consequently most cells have been arbitrarily implanted with profile A. This profile, if present in a 0.5μ deep junction introduces a drift field of approximately 4,700 volts/cm from the surface to a point 0.25μ below the surface. Fields are, of course, proportionately lower for deeper junctions; i. e., the same absolute concentration variation then appears over a more extended region. It should be noted that the results of Tannenbaum³ and Iles and Leibenhaut⁴ indicate that the actual profile in a shallow diffused junction is flat near the surface with a sharp fall-off at the junction. Such a profile does not give an effective drift field right at the surface where it is most required. The present technique has the capability of investigating what might be called a true surface field.

Initial efforts were concerned with p on n cells using B¹¹ as the implanted species. Although the highest efficiency obtained in these early investigations was 8.5% (2800°K tungsten - 140 MW/cm^2) some of the results were interesting as trend indicators. This is particularly true of spectral response curves as shown in Fig. 5. In this figure, a very marked "blue shift" with reduced implantation energy and therefore reduced junction depth, may be seen. Efficiencies of the various cells were taken under 2800°K tungsten light and solar simulator (Spectrosun) illumination at 140 MW/cm^2 and the drop-off vs. implantation energy is shown in Fig. 6. Spreads in measured values are shown as vertical bars with single value points having no bar. From this graph, it appears possible to manufacture cells by this technique which are almost as efficient under solar illumination as under tungsten illumination. The problem is one of decreasing ion energy and junction depth while maintaining the series resistance at a low value by increased doping.

At this point the program was switched to n on p cells using P³¹ as the implanted ion species. One of the primary objectives has been a determination of the profiles of physically implanted and electrically active ions. The actual concentration distribution of implanted ions was determined by implanting a cell with P³¹, then irradiating with thermal neutrons to develop P³² which decays with a 14.4 day half-life generating a 1.7 MeV beta particle; viz



The profile was determined by measuring the amount of activity remaining after successive 400 Å layer removals by anodization and etching. Figure 7 shows the distribution found for a 100:1 - linear profile implanted at 800 keV. It was found that anodization was extremely difficult due to the radiation damage resulting from the neutron irradiation and it was necessary to anneal at 930°C for 5 minutes before the experiment could be carried out. This was in addition to the standard 800°C anneal and almost certainly affected the distribution through radiation enhanced diffusion effects, especially in the region removed just after anneal. The general profile, however, still corresponds to that implanted. The error bars are representative, getting progressively larger as the counting rate gets lower while the dashed line represents a sudden drop to a very low value at the junction.

The profile of electrically active phosphorus was obtained for a similar 100:1 - linear implanted and annealed sample. This was accomplished by a more or less standard technique of measuring sheet

resistivity by the 4-point probe technique, combined with successive anodization and etching procedures.

Figure 8 shows the results with the error bars again showing representative values. The general profile is similar to that obtained for the physically present ions but the initial 100:1 drop is not reproduced. This is believed to result from radiation enhanced diffusion effects during the radiation damage anneal causing a marked out-diffusion from the implanted region to a non-implanted 1,000 Å surface layer. The latter occurs because the programmed sample rotation covers only the angles 5° - 90° between the incident beam direction and the sample surface. Implantation is stopped at 5° since rotation through decreased angles effectively causes a decrease in flux density for a constant total beam. Speed of rotation is programmed to compensate for this decrease but as the angle approaches 0°, the required implantation time approaches infinity. For practical reasons, rotation is stopped at 5°. This effect is avoidable at lower energies by programming machine energy rather than sample rotation. At the present time this out-diffusion is being avoided by implanting through a 1,000 Å oxide layer which is removed prior to annealing, but profiles for these cells are not yet available.

The profile studies presented were for the profile arbitrarily used in most of the IPC cells. A study of the change in cell characteristics with variations in the implanted profile is just beginning. Using the 100:1-linear profile, current cell efficiencies are in the 10-11% range under tungsten illumination and 7.6-8.1% under solar illumination. One of the most striking features is the consistency of the process. As improvements in cell performance are made it is notable that almost all cells come off with the same increased efficiency, although this is partially due to the individual care they receive.

A typical spectral response for one of the later cells is shown in Fig. 9. If the same blue shift occurs with decreased implantation energy as occurred for the p on n cells, and if the anticipated efficiency increases are achieved with decreased depth, improved profiles and increased doping, it should be possible to produce cells which are 10-12% solar efficient by this process with a very high yield. Reductions in implantation energy should result in an economical process since a low priced, high current air insulated voltage supply could be used for ion acceleration.

Another possible application of this technique is in fabricating drift field thin film solar cells. The objective here is a process in which a layer of polycrystalline silicon is deposited and simultaneously or alternately implanted to give the desired doping level. Layers could gradually be built up giving the required concentration profiles and p - n junction. Appropriate drift fields would greatly improve radiation damage resistance. For this purpose IPC has been studying two possible deposition techniques. The first of these involves a process in which substrates are immersed in a SiHCl_3 fed plasma source. Electron bombardment dissociation of the SiHCl_3 produces Si^+ ions which impinge randomly on the substrate and become attached at nucleation sites. The basic premise of the program is that random velocity ions have an enhanced probability of satisfying the requirements of all "open" positions in a growing lattice, particularly if the substrate is heated to give the ions additional surface mobility. This plasma deposition process can economically be applied to film areas larger than 200 cm^2 . Si films up to 10μ thick with grain size > 1 micron have been grown by this method. At the present time, film contamination and inadequate grain size preclude the fabrication of useful cells. With a useful base layer, the ion implantation technique could be used to make the p - n junction with some assurance of control.

The second technique involves high vacuum sputtering, high vacuum being 10^{-6} torr or less. Since this program is in an early stage and involves a proprietary IPC process no further comment will be given at this time.

4. SUMMARY

In summary, ion implantation looks promising as a highly controlled technique for manufacturing silicon solar cells. Through proper manipulation of implantation parameters it appears possible to make high solar efficiency cells under high yield conditions. Assuming a developed technique for depositing useful thin film silicon layers it should prove useful as a doping technique to provide drift fields for better collection efficiency and radiation damage resistance.

REFERENCES

1. Evans, R. D., The Atomic Nucleus, McGraw-Hill Publishing Co., Inc., New York, Chap. 22, 1955.
2. Shockley, W., "Electrons and Holes in Semiconductors," D. Van Nostrand Co. Inc., New York, N.Y., 1950.
3. Tannenbaum, E., Solid-State Electronics, 2, p. 131, 1961.
4. Iles, P. A., and Leibenhaut, B., Solid-State Electronics, 5, p. 331, 1962.

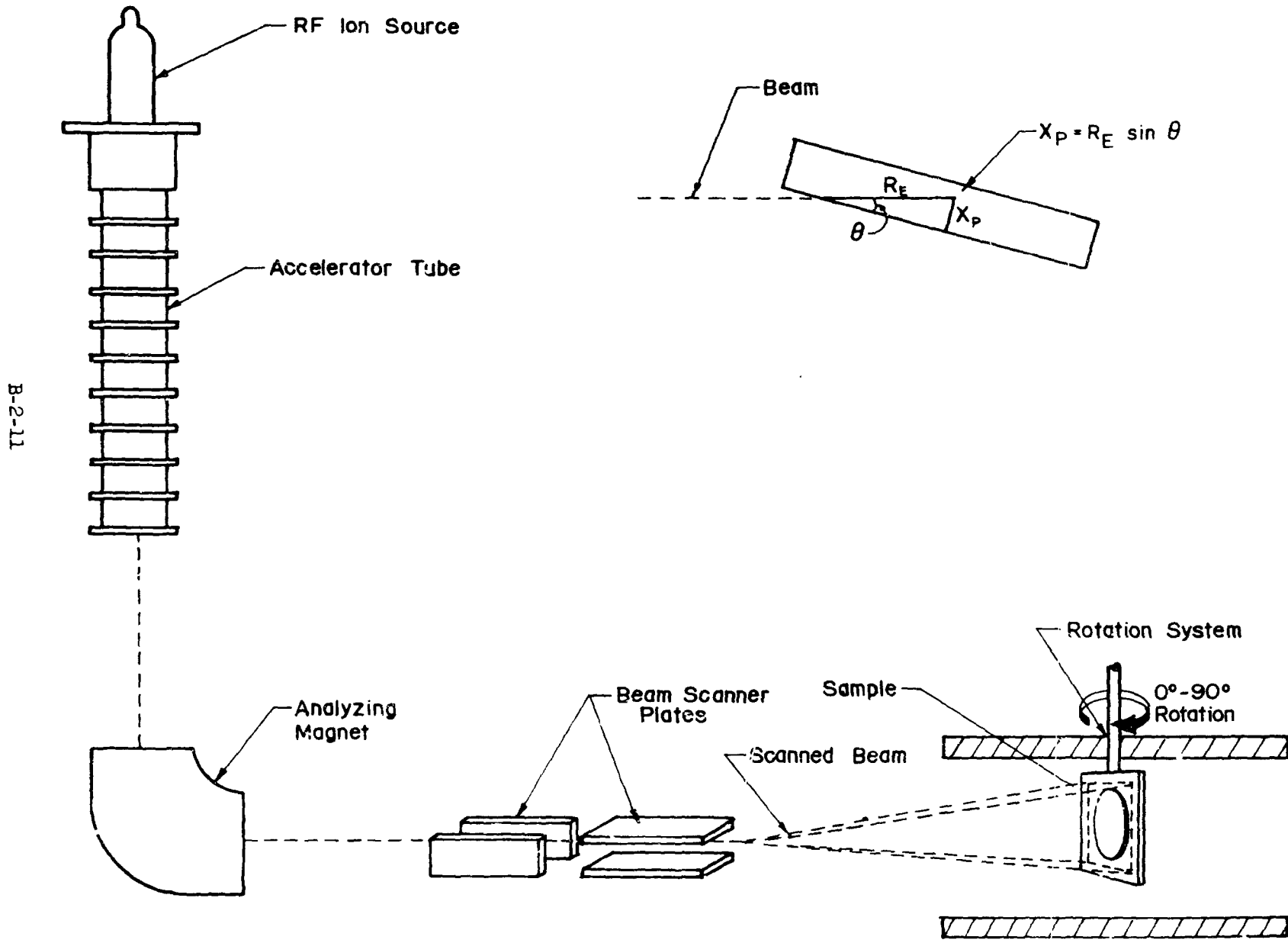
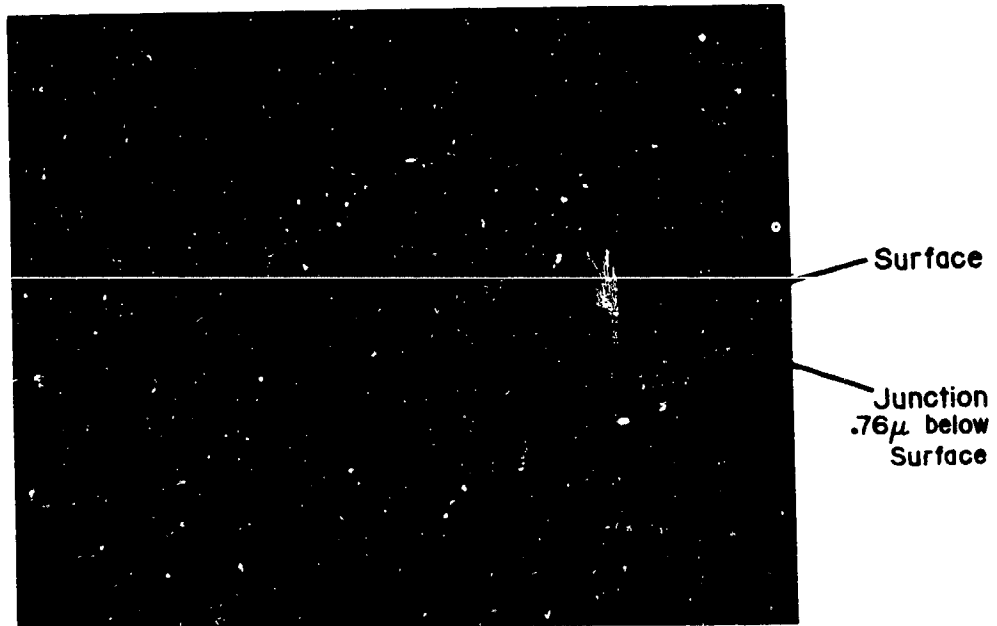
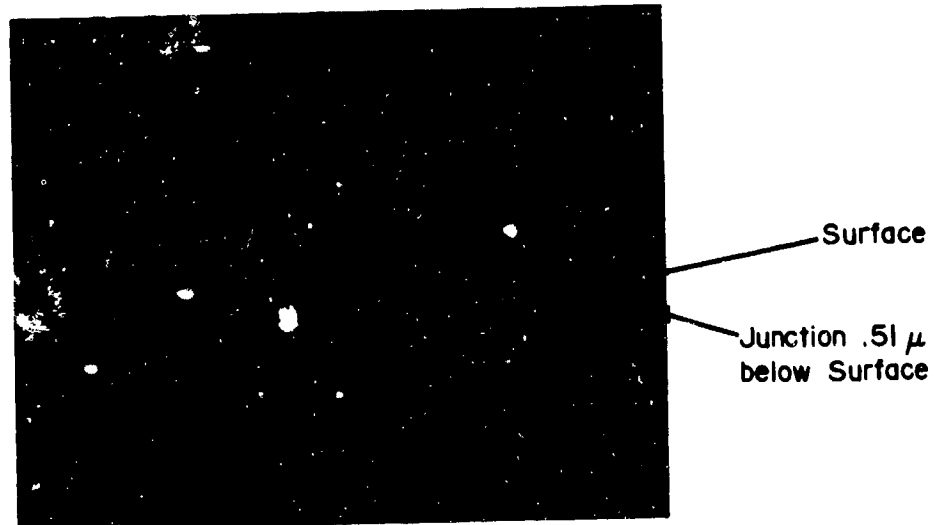


FIG. 1 IMPLANTATION APPARATUS

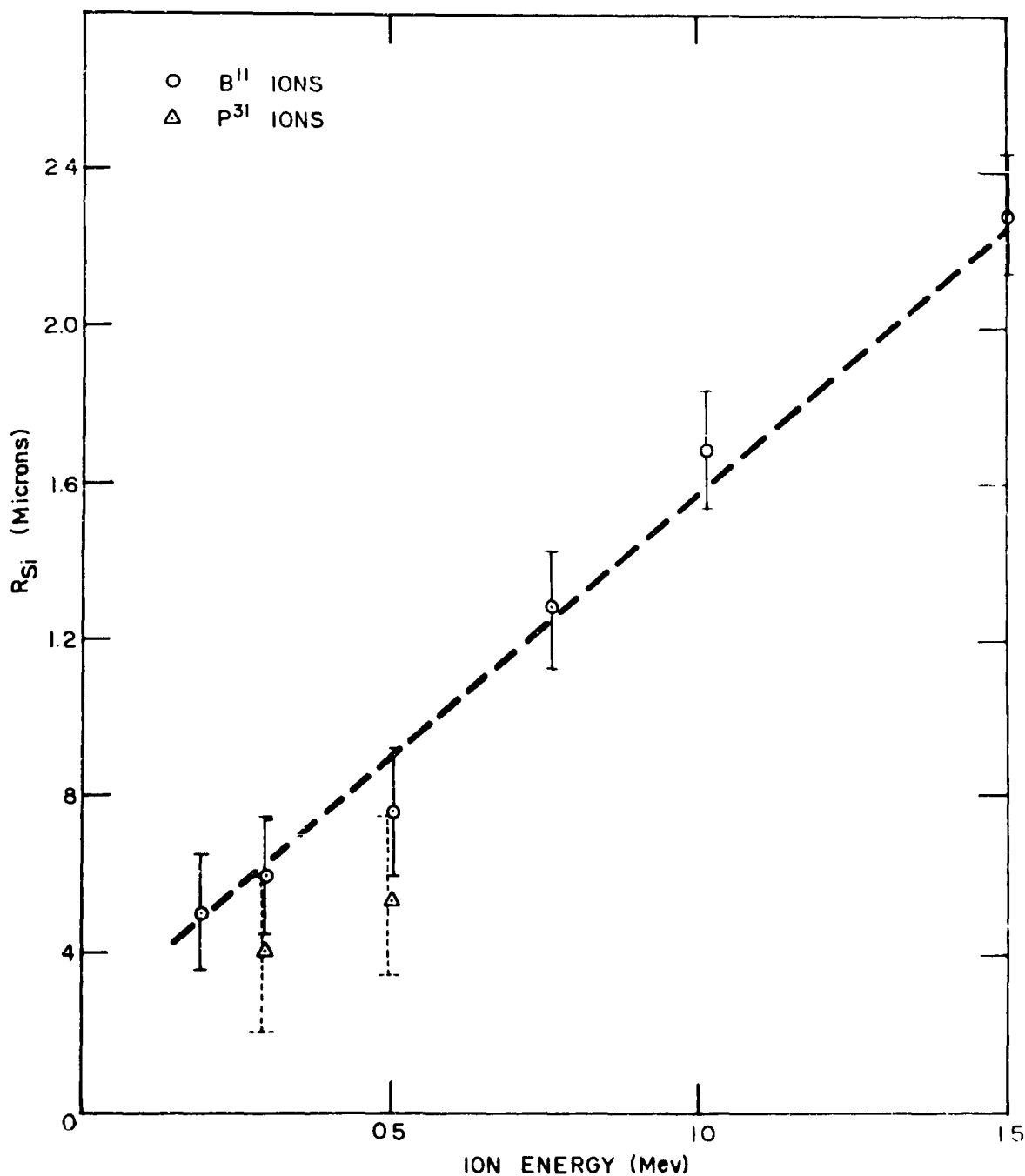


(A) 500 Kev B¹¹ Sample
(1° angle bevel, magnification 200 X)



(B) 300 Kev P³¹ Sample
(1° angle bevel taken with 5080 Å light)
(Magnification 130 X)

FIG. 2 ANGLE SECTIONS

FIG. 3 - RANGE OF B^{11} AND P^{31} IONS IN SILICON

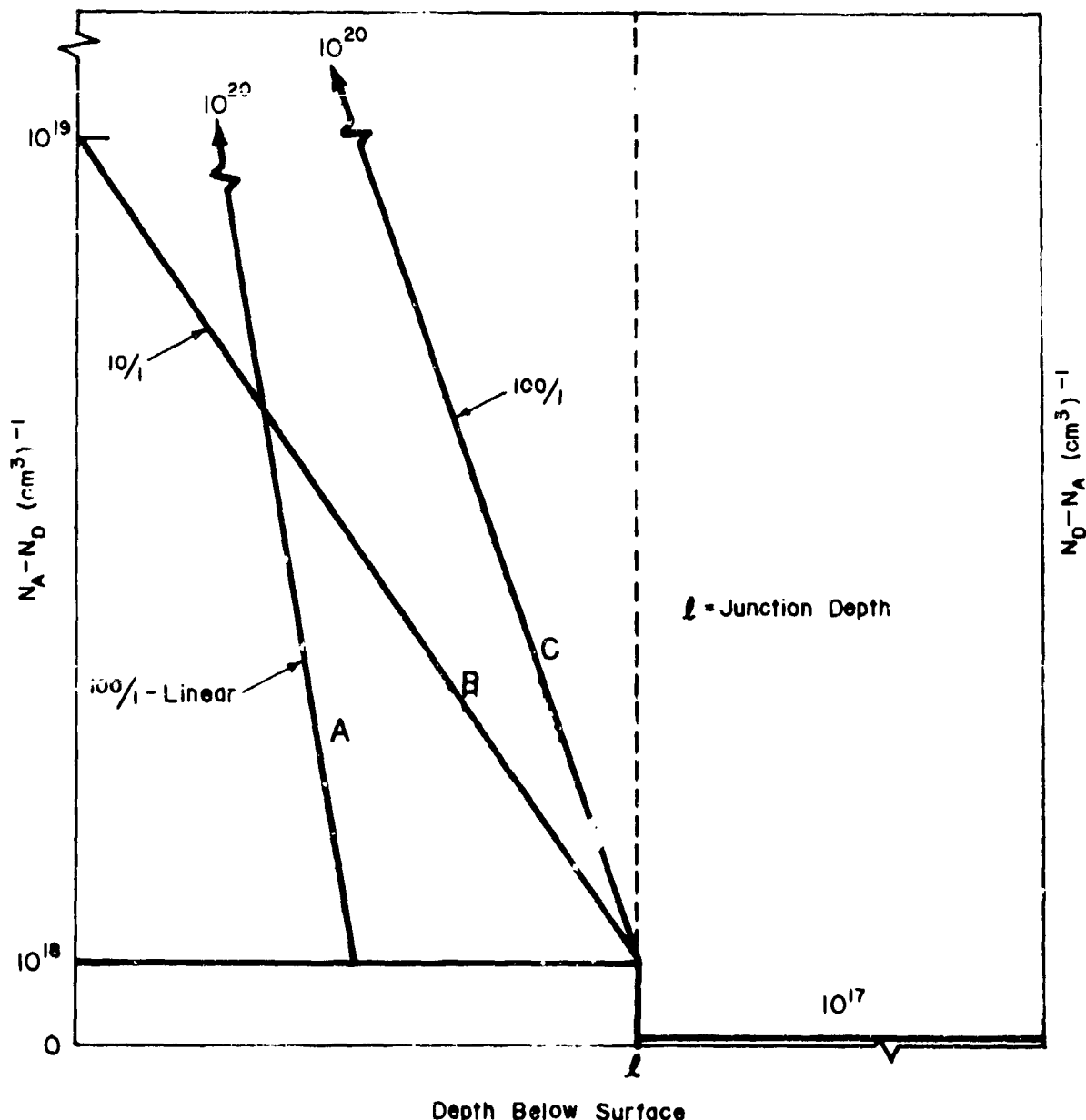


FIG. 4 - TYPICAL PROFILES

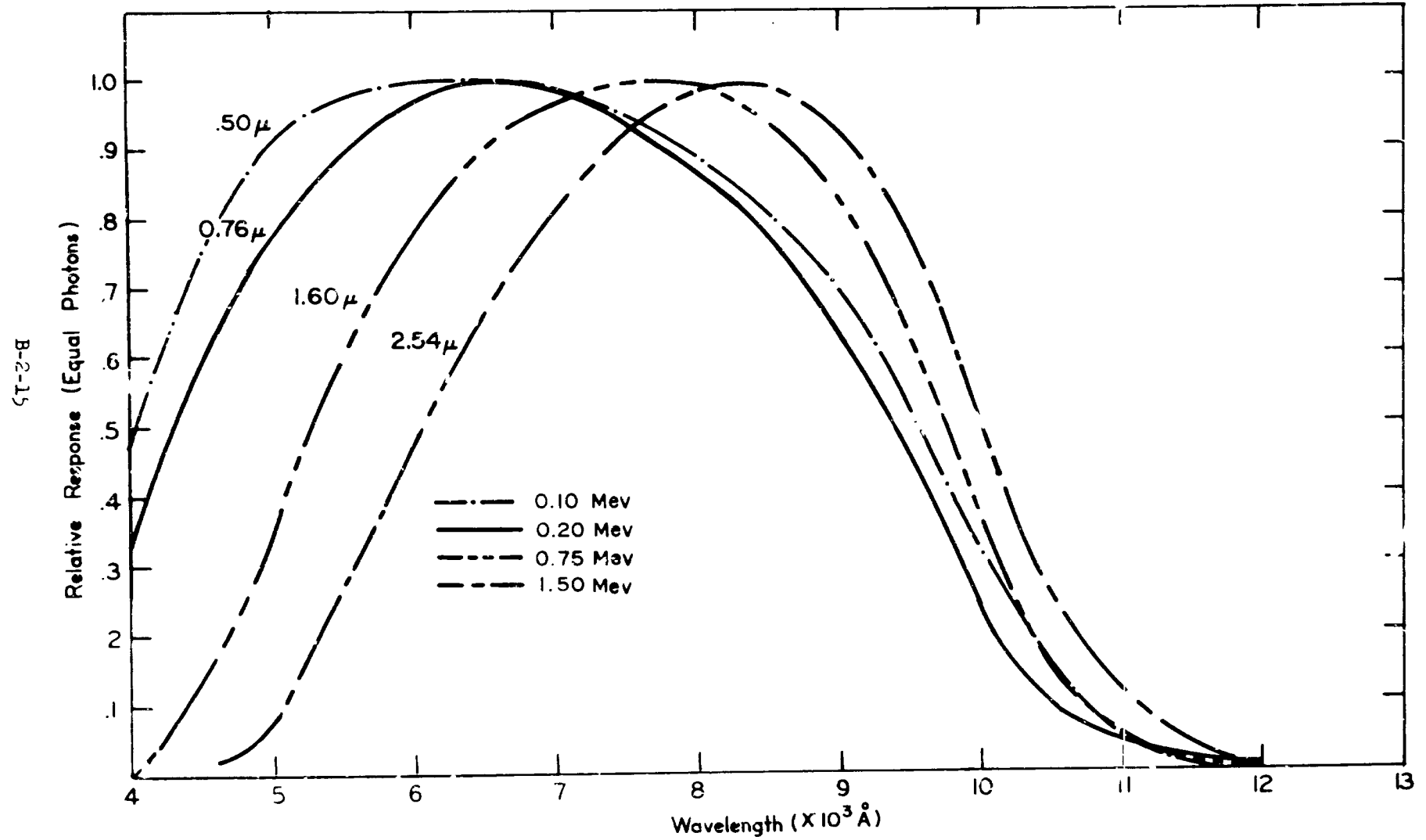


FIG. 5 - SPECTRAL RESPONSE OF I.P.C. CELLS

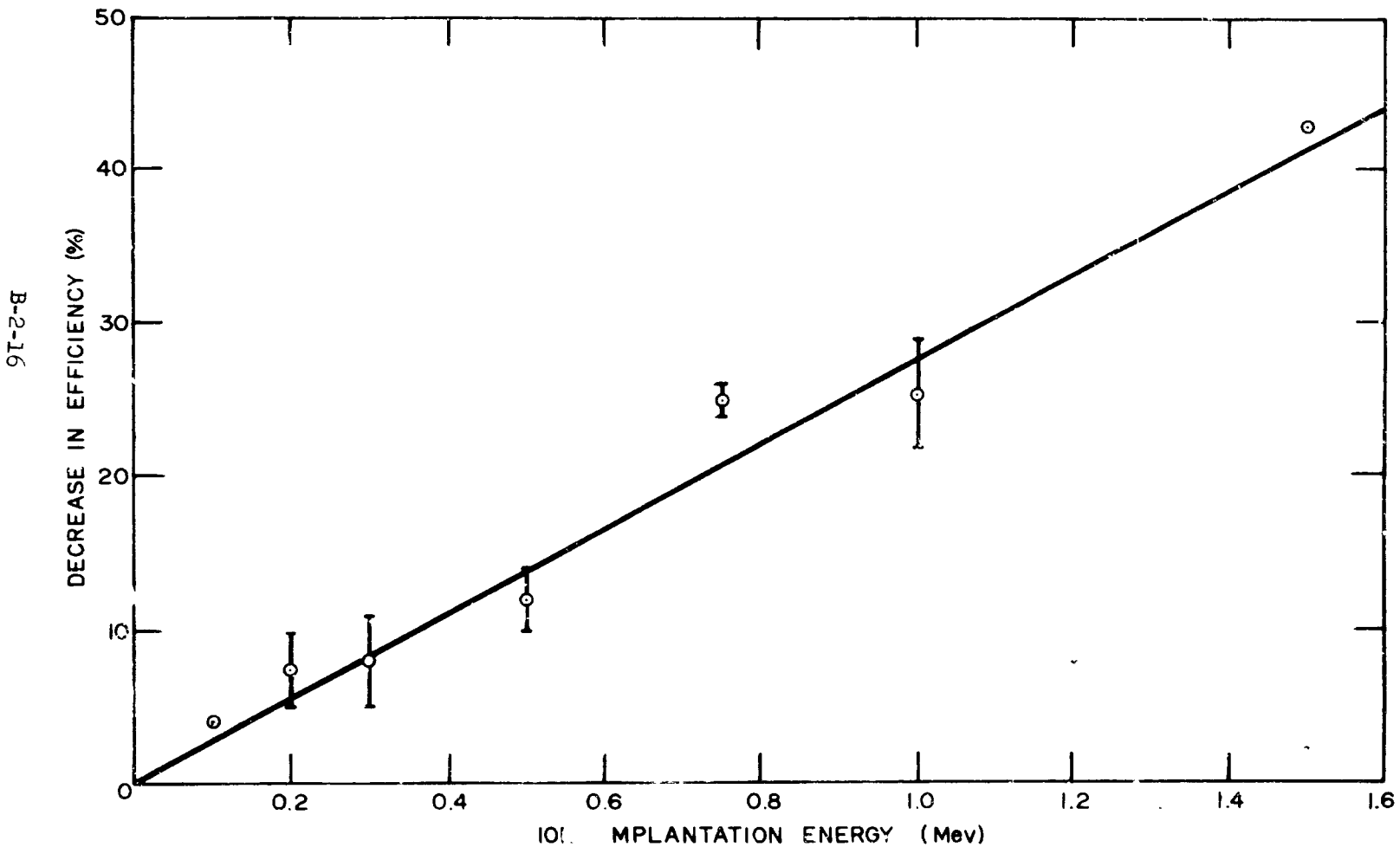


FIG 6 - TUNGSTEN TO SOLAR EFFICIENCY DECREASE
FOR B'' IMPLANTED CELLS

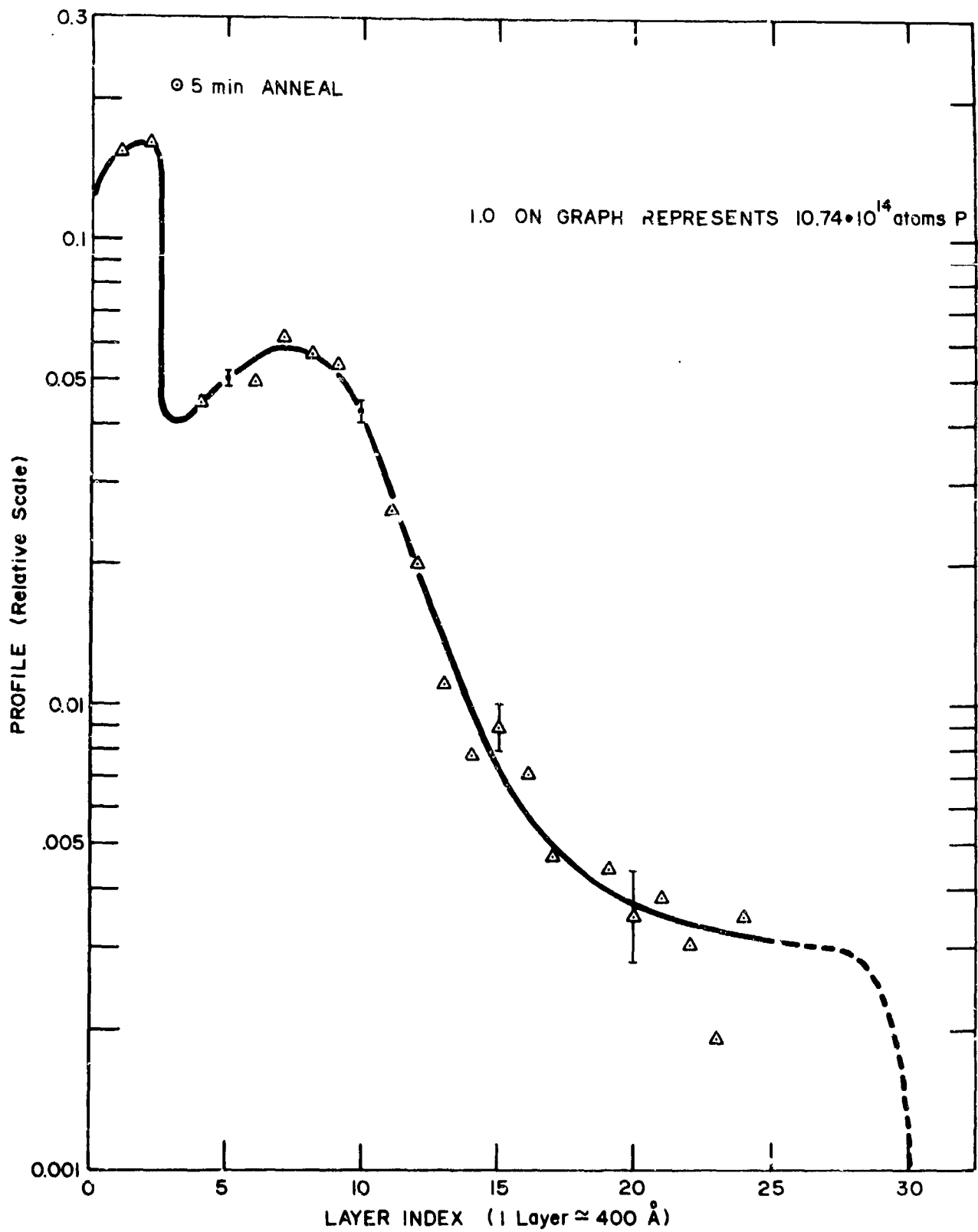


FIG 7 IMPURITY PROFILE, 100/I - LINEAR

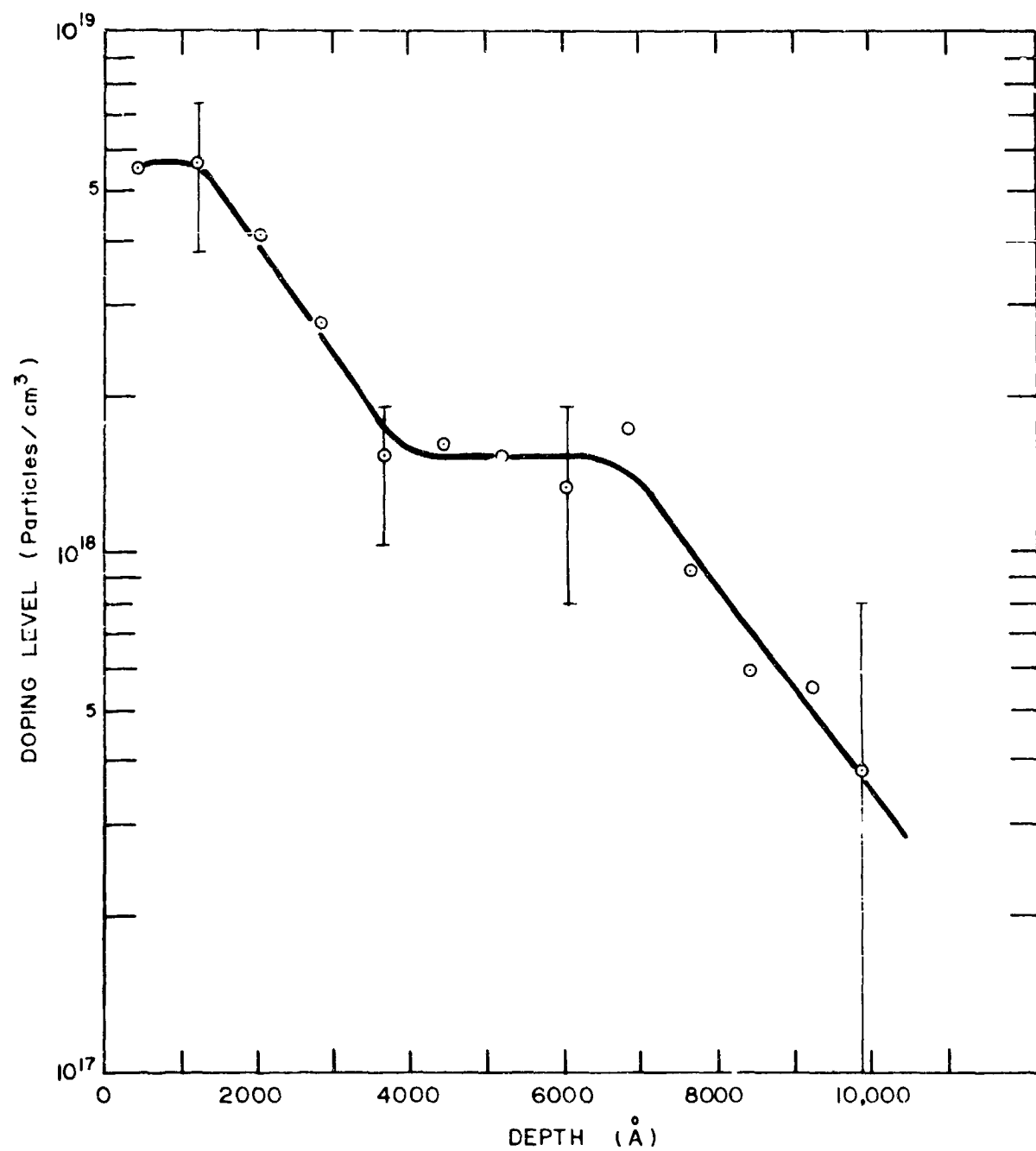


FIG. 8 - IMPURITY PROFILE 100/1 - LINEAR

B-2-18

GT-2-19

PIC-SOL 209/5

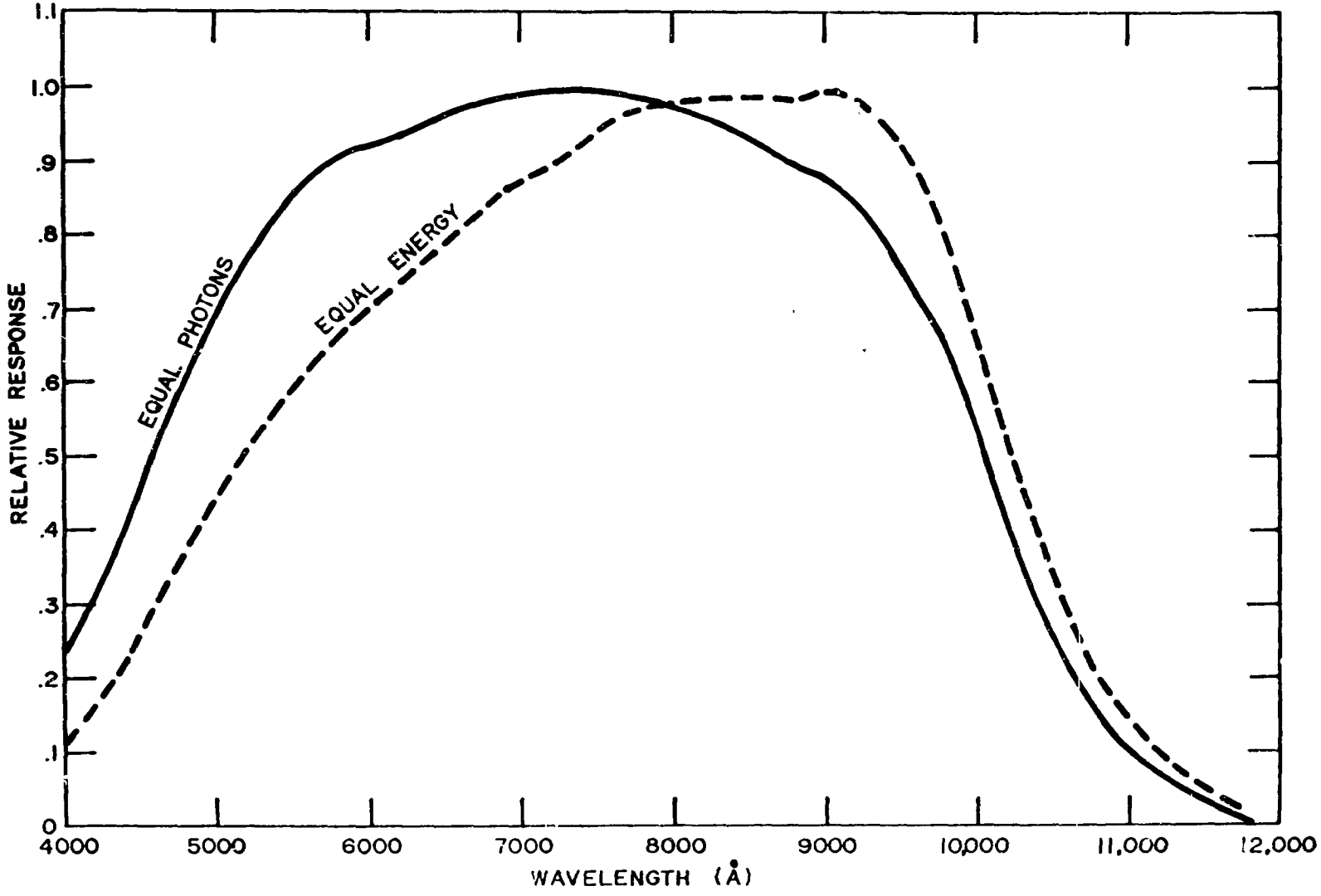


FIG. 9 SPECTRAL RESPONSE OF SAMPLE No. 42

DISCUSSION

BOURKE - ALLISON: In your measurement of junction depth how did you say you removed a layer at a time?

MR. KING: We used anodization etching procedure developed by Tannebaum at Bell Labs. I'm not sure of the solution, I think it was a sodium borate-boracic acid solution. I don't know what the voltage was off hand. You can tell by the interference colors what the thickness is.

BOURKE - ALLISON: What were the best efficiencies you observed for your cell?

MR. KING: 10 to 11 percent under tungsten, 7.6 to 8.1 under solar illumination.

GOLDSTEIN - RCA: What are typical values for the bombarding currents of phosphorous and boron?

MR. KING: Very low. This is one of our main problems at the present time. 1 to 10 microamperes both for boron and phosphorous.

GOLDSTEIN - RCA: Why are the currents so low?

MR. KING: We use a Van De Graaff because it is very effective for this type of investigation. We have problems with the ion source. However, there are ion sources which could be used with an air insulated machine to give 100 microamps up to milliamps rather than microamps. In other words if we reduce the energy to the 100 kilovolt range, we can make an economical process out of it.

GOLDSTEIN - RCA: Would you anticipate that your sample might get unduly hot under those conditions?

MR. KING: No, I don't think so. As a matter of fact we irradiate them cold in liquid nitrogen.

GOLDSTEIN - RCA: There was a point I missed about your 80°C 16-hour anneal. Did you mention that this did have some effect on the implanted impurity distribution?

MR. KING: I think it does but I'm not absolutely positive. It appears to vary at different times depending on the material we get. It appears to be an enhanced diffusion effect. We are now keeping the temperature at 750° and we don't see any of these effects. We can control it to something like a tenth of a micron.

GOLDSTEIN - RCA: Even with the 16-hour anneal?

MR. KING: Yes, with phosphorous 31 and 300 kilovolts we get a half micron deep junction and very flat. We have done 100 kilovolts and gotten a quarter of a micron, also flat.

ROSENZWEIG - BELL TELEPHONE LABS: Can you tell us what areas of devices you have made and what the VI characteristics are like forward and reverse?

MR. KING: You mean the solar cells. They are conventional 1 by 2 centimeter size, and the characteristics are almost identical to silicon cells made by conventional techniques.

ROSENZWEIG - BELL TELEPHONE LABS: What were the reverse currents?

MR. KING: I can't really remember but I would say that they were in the tens of microamp range. In this regard, we have made radiation detectors by the same technique with reverse leakage currents in the fractional microamp range. The difference is in the doping level and in the bombardment.

KAYE - EOS: I would like to point out that my colleagues at EOS have made some cells using low voltage cesium ions at around 5 kev. This was reported in Applied Physics Letters. It hasn't been necessary to do any annealing at all to get short circuit currents equivalent to those obtained from ordinary solar cells, although our efficiencies weren't as good, due to the high sheet resistance.

MR. KING: These efficiencies were quite low weren't they?

KAYE - EOS: Efficiencies were quite low because of a high sheet resistance. But, of course, this is a long way from an optimum bombardment. I wonder if you have done any work with low voltage bombardments?

MR. KING: We are coming down. We are approaching you from the other end. The difference in the two techniques is that you are relying on a channeling mechanism which occurs in single crystals along a certain direction. This is a secondary mechanism. We deliberately avoid channeling by taking a 111 crystal and implanting at an angle of 7°. This avoids implantation along any major crystallographic axes. This way you avoid channeling and you get discrete range effects. You can control the profile, rather than take what the channel gives you.

ROSS - HOFFMAN ELECTRONICS: I noticed on the last slide that the spectral response was not very good in the blue by comparison with other cells. I believe I noticed something like 30 percent at 5000 angstroms. Would you clarify as to whether this was one of the 100 to 1 linear implantations?

MR. KING: It was. It was done at 300 kilovolts, the junction is a half a micron deep, and these are fairly recent cells. I'm not sure why the

difference is. We are just not going to lower energies to see whether or not there is a concomitant blue shift as we go to 200-100 kilovolts.

ADDIS - RCA: All your work was done on single crystal silicon. Do you have any idea what effect a grain boundary would have on the implantation process?

MR. KING: I think, although I have no real proof on this, that it would have none at all. Do you mean on the depth of implantation or on the cell characteristics?

ADDIS - RCA: On the depth first and then on the cell characteristics.

MR. KING: In that case, no effect at all because the range versus energy in polycrystalline silicon is a much better behaved function than it is in single crystal material.

ROSENZWEIG - BELL TELEPHONE LABS: What about the annealing process after implantation?

MR. KING: Then you might get diffusion along the grain boundaries.

GUMMEL - BELL TELEPHONE LABS: Do you have any idea what the lifetime is in your front layer?

MR. KING: No, we really haven't worked it out. I do know for the p-on-n cell that we have calculated diffusion lengths. For the cases where the fall off under solar light is very small, the diffusion length is almost equal to the junction depth. This is quite important, and I think it's something that has not been considered in diffused cells. There exists a dead layer on the surface from which there is no charge collection. This is quite apparent when you work with radiation detectors where this dead layer is quite important. Normally the dead layer in a diffused cell is half the diffusion depth. In radiation detectors, you measure this by measuring the fall-off in collection efficiency as you bring an alpha particle beam into the glancing angle.

PIC-SOL 209/5
Section B-3

N64-
29165

PHOTOVOLTAIC EFFECT AND SURFACE STATES
ON SILICON-METAL INTERFACES

Presented by

G. Rupprecht

Tyco Laboratories, Inc.

Waltham, Massachusetts

2 June 1964

N64-29165

PHOTOVOLTAIC EFFECT AND SURFACE STATES
ON SILICON-METAL INTERFACES

by

G. Rupprecht and A. H. A. Pampanini
Tyco Laboratories, Inc.
Waltham, Massachusetts

Introduction

When a metal and a semiconductor are brought into contact, an initial transfer of charge must occur, in accordance with the difference in work functions, to align the Fermi levels in both materials. This is equivalent to the statement that, in equilibrium, the charge transfer is determined by the condition which establishes zero total current through the interface. In the metal, the transferred charge stays at the surface because of the large electrical conductivity. In the semiconductor, however, an equal charge of opposite sign will be distributed spatially over the space charge region which develops near the semiconductor surface and among possible surface states at the interface.

In reality, semiconductor-metal interfaces, as used in this investigation, exhibit an additional complication which is introduced by the presence of a thin oxide film between metal and semiconductor. Although this oxide layer can be neglected in some respects, it was noticed that its thickness was important to the charge transfer properties through the interface. It is so much so that a small change in thickness made the difference between a reasonably efficient photovoltaic device and an inefficient one. The data obtained with Au on n-type silicon suggest that the charge separation which occurs at the interface, when illuminated under short circuit conditions, is due to a tunneling of charge carriers through the oxide layer.

In spite of the dominating role of the oxide layer at the interface for the charge transfer, it was noticed that the observed open circuit voltage did qualitatively agree with previously reported work function data in so far as Au on n-type silicon and Al on p-type silicon proved to be useful combinations for photovoltaic devices, while the combinations Au on p-type silicon and Al on n-type silicon exhibited only a negligible photovoltaic effect at room temperature.

In order to study the cause of the photovoltaic effect at a metal-semiconductor interface, the space charge capacity with and without illumination was measured together with the open circuit voltage. It was found that the open circuit voltage is connected with the change in barrier height under

illumination in a one to one relationship, although, in the case of illumination, one deals with a non-equilibrium situation. This provides the basis for determining the position of the Fermi level at the semiconductor-metal interfaces from the open circuit voltage alone. Since the position of the Fermi level at the interface is dominated by the presence of surface states, its temperature dependence, together with the behavior of the short circuit current, provides information about the surface states at the metal-semiconductor interface and their role in the charge separation process during illumination.

Sample Preparation and Experimental Arrangement

Single crystals of n-type and p-type silicon of different resistivities were cut to provide circular samples about 1 cm in diameter and 0.5 mm thick. One side of each slice was nickel-plated to provide a large area ohmic contact; the other side was carefully etched to minimize the oxide thickness and was coated immediately after etching with a thin layer of gold or aluminum. A narrow, thicker ring of the same metal was deposited around the periphery of the sample as a current-collecting electrode. The thickness of the metal film was monitored during vacuum deposition. The evaporation was stopped when the film had a transmission of about 27% for the radiation of a tungsten lamp since it was found, as shown in Fig. 1 and 2, that the photovoltaic effect was nearly optimum under this condition. The resistance per square of a goldlayer on silicon vs. transmission is shown in Fig. 3. It varies from about $10 \Omega/\square$ to $60 \Omega/\square$, as the transmission varies between 25% and 30%.

The sample was mounted with silver paste to a copper heat sink in a vacuum chamber; this prevented condensation of water vapor when the sample was cooled, but had no effect on the experimental results. During the photovoltaic measurements, the thinly-coated region within the current-collecting electrode was illuminated under normal incidence with the radiation from a tungsten lamp, providing for a radiation density of 80 mw/cm^2 .

The effect of thin anti-reflection layers of magnesium fluoride and silicon monoxide upon the photovoltaic effect was studied. Degradation of the electrical properties was noticed in all cells in which the electrodes were coated with magnesium fluoride, but appreciable improvements were observed in those coated with silicon monoxide.

The optimum silicon monoxide film thicknesses was determined empirically. Six n-type gold-on-silicon photovoltaic cells with uniform characteristics were prepared and coated with silicon monoxide layers of varying thicknesses. The short-circuit current, I_0 , before and, I_1 , after coating is used to define the percentage deviation

$$p \text{ as } p = \frac{I_1 - I_0}{I_0} \times 100, \text{ which is shown in Fig. 4 as a function of the thickness}$$

of the anti-reflective coating. Accordingly for radiation from a tungsten source, the optimum silicon monoxide film thickness is 2400 Å. However, all the samples used in the course of this investigation were without coating, since it was felt that an increased short circuit current would not contribute to the basic-understanding of the photovoltaic effect.

Some experiments were carried out to investigate the influence of the oxide layer between metal and semiconductor upon the photovoltaic properties. For this purpose, silicon slices from the same single crystal with one side unpolished and the other side polished and etched were exposed at 550°C to flowing oxygen for various periods of time. The additional oxide thickness produced by this procedure was estimated using Attalla's formula:

$$x^2 = 8.4 \times 10^{10} p_{O_2}^{4/5} t \exp [(-1.7q)/kT] \quad (1)$$

where x is in Å, p in atmospheres, t in minutes and kT/q is in electron volts (eV). After oxidation, the unpolished surfaces of the samples were lapped and nickel plated to provide for an ohmic-contact. A gold film and a collecting electrode were evaporated onto the oxidized surface as described above. The samples were then ready for use in photovoltaic measurements, in particular, of the short circuit current which will be described below. Since care was taken to treat these samples under as close to identical conditions as possible, the oxidation time was the only parameter which discriminated them.

Influence of the Silicon Oxide Interface Layer upon the Photovoltaic Properties

As described above, a dozen n-type silicon samples were exposed for different time intervals to a thermal oxidation treatment at 550°C and the additional oxide thickness of each sample calculated. Even if equation (1) did not hold accurately in this very low thickness range, the estimate of the additional oxide thickness should still yield the right order of magnitude. Thus, at least the relative thickness should be meaningful. With this qualification, the result of photovoltaic measurements at room temperature on this series of samples is shown in Fig. 5. Since the varying oxide thickness has little influence upon the open circuit voltage, the short circuit current is shown as a function of oxide growth. It can be seen that the short circuit current density is drastically reduced at first and then decreases more gradually as the oxide film grows thicker. The sample without additional thermal treatment yielding 10 mA/cm² is not shown in Fig. 5 since it would fall outside the graph. The same is true for a sample point which was obtained in a completely different way as follows. In a vacuum system capable of about 10⁻⁶ mm Hg, a silicon slice was cleaved during gold evaporation. The short circuit current density of this sample was ≈ 20 mA/cm². Since the abscissa for this point is not known (but should probably be negative) it also has not been included in Fig. 5.

A somewhat more revealing display of the same data is shown in Fig. 6 where the reciprocal of the short circuit current density is plotted vs. the additionally grown oxide film thickness. For thick oxide layers, j_{sc}^{-1} seems to follow a linear relation. If one extrapolates back to the intercept with the abscissa, one obtains about (-7) Å. One is tempted to interpret this as the original thickness of the oxide layer prior to the thermal treatment. The extrapolation may be justified on the ground that an oxide layer of thickness λ acts similar to an ohmic resistance with respect to the short circuit current, j_{sc} .

From the relation

$$\frac{d(j_{sc}^{-1})}{dx} = \frac{\rho}{V} \quad (2)$$

one obtains a value for the resistivity ρ of about $4 \times 10^9 \Omega\text{-cm}$ when the driving voltage V is equated to the open circuit voltage V_{oc} . This value for ρ is considerably smaller than the values quoted for bulk quartz, but it is sufficiently large to identify the grown oxide film as an insulator. According to this reasoning, a new origin for the thickness scale should be used which is shifted by (-7) Å. It is also apparent that j_{sc}^{-1} , deviates from Ohm's law below a critical oxide thickness of about 10 Å, as seen in Fig. 6. This observation is interpreted as a tunnelling process of charge carriers through the oxide film which is the essential mechanism of charge separation under short circuit current condition.

Therefore, the proper condition for an efficient photovoltaic device of this kind is a sufficiently thin oxide interface. The dividing line between a sensitive and an insensitive cell is apparently quite narrow and may be characterized by a critical oxide thickness.

Identification of the Open Circuit Voltage

When the surface of a barrier photocell is irradiated, an open circuit voltage V_{oc} between the metal and semiconductor and a simultaneous change of the cell capacity from C_0 to C , are observed. The cell capacity and its variation can easily be measured in a bridge circuit. It seems to be closely related to the open circuit voltage V_{oc} and other known parameters of the system. It is the purpose of this section to establish this connection experimentally without unnecessary conjectures. Without light, the system is in thermal equilibrium. With illumination, it is in a stationary state with two quasi-Fermi levels, one for holes and one for electrons. Nevertheless, one may describe the space charge capacity at the semiconductor surface, even in the stationary state, by the relation

$$C = (\epsilon \epsilon_0 q^2 N / 2kT)^{1/2} \frac{|e^Y - 1|}{(e^Y - Y - 1)^{1/2}} \quad (3)$$

Here N is the impurity concentration, ϵ is the bulk dielectric constant, $C_0 = 8.9 \times 10^{-12}$ amp sec/volt-m, Y is the bending of the energy bands at the surface in units of kT , and q is the electronic charge. For any given capacity per unit area, the bending of the bands in equilibrium is uniquely determined without an adjustable parameter. Therefore, if C_0 and C_i are the capacity values of the space charge layer in the dark and under arbitrary but constant illumination, respectively, one can calculate unambiguously two values, Y_0 and Y_i , which describe the space charge region in the semiconductor provided that surface states do not contribute to the capacity value. Their contribution can be avoided by measuring at a sufficiently high frequency. The difference, $Y = Y_0 - Y_i$, is then characteristic of the change in electrostatic potential under illumination. A comparison of ΔY with the observed open circuit voltage, V_{oc} , is given in Table I for a number of different temperatures. The measured values of capacity per unit area, C_0 and C_i , for a gold on n-type silicon cell indicate that the values of C under illumination are considerably larger than for those in the dark. In the last column in Table I the measured open circuit voltage V_{oc} is expressed as Y_{oc} in units of kT , ($Y_{oc} = V_{oc} q/kT$).

It can be seen that the ΔY values calculated from capacity data agree fairly well with the directly measured values of V_{oc} expressed by Y_{oc} . Thus, we draw the conclusion that to a good approximation $kT\Delta Y/q$ can be identified with the open circuit voltage. Hereby it is assumed that the capacity of the oxide layer between the metal and the semiconductor is large compared to the space charge capacitance and can therefore be neglected. The validity of this assumption can be readily confirmed. The position of the Fermi level at the semiconductor surface F_s can now be determined. For an n-type sample, for instance, it is $E_c - F_s = [(E_c - F) + qV_{oc} + kT \approx Y_i]$, where E_c is the energy at the bottom of the conduction band, and F is the Fermi level in the bulk. When the open circuit voltage is saturated at a sufficiently high level of illumination, Y_i becomes quite small, and the position of the Fermi level at the surface can be determined approximately from the bulk Fermi level and the observed open circuit voltage alone.

This simplified procedure was used to determine the Fermi level at the surface for a series of samples as a function of temperature.

The Fermi Level at the Metal Semiconductor Interface

Gold on n-type Silicon

The Fermi level at the interface between gold and n-type silicon was obtained as a function of temperature for three samples of different resistivities by the method described in the previous paragraph. Accordingl, the surface Fermi level can be found to a good approximation at $(E_c - F) + V_{oc}$ eV below the conduction band. The experimental results are shown

in Figs. 7, 8 and 9. In the lower part of these figures the photovoltaic data, short circuit current, and open circuit voltage are plotted as a function of temperature. In the upper part, pertaining to the same temperature scale, the positions of bulk and surface Fermi level are shown.

In all three cases it is apparent, that the surface Fermi level F_s is locked in a fixed position below room temperature, then breaks away from this position to approach a new level at elevated temperature. This temperature behavior of F_s suggests the existence of two discrete surface states at the interface, 0.52 eV and about 0.3 eV below the conduction band. They are indicated by the dashed lines in Figs. 7, 8 and 9. In a previous study of oxide covered n-type silicon surfaces by pulsed field effect, a prominent surface level was consistently found 0.52 eV below the conduction band and was identified as an acceptor state. This is in agreement with the present observation: only an acceptor state at the interface can keep the Fermi level locked below it. The energy position of the surface state, which is suspected to exist at about 0.3 eV below the conduction band, can be identified somewhat more accurately from the data shown in Fig. 7. An extrapolation of F_s to higher temperatures suggests an energy value close to 0.27 eV for this level. A value of 0.28 eV may be estimated from the abrupt change of the short circuit current shown in Fig. 7, when one makes the conjecture that the surface Fermi level sweeps across this surface state at about 430 K.

Aluminum on p-type Silicon

A series of measurements was performed with p-type silicon of different resistivities onto which aluminum had been evaporated. The results on one sample, which are representative for all the others, are shown in Fig. 10. Here the photovoltaic data are exhibited as a function of temperature in the upper part of Fig. 10, whereas in the lower part the position of the bulk Fermi level and the Fermi level at the metal - semiconductor interface are shown in respect to the valence band. The temperature behavior of F_s is more complicated than was the case in Au on the n-type silicon cells. At low temperature, F_s seems to be locked to a surface state approximately 0.37 eV above the valence band. As the temperature rises, F_s moves towards the middle of the energy gap and seems to return to the 0.37 eV level at elevated temperature. In this case, however, the surface states cannot be identified as easily. Therefore, an additional experiment was performed. The capacity of this sample was measured at different frequencies under a series of forward bias conditions. The results are shown in Fig. 11. For reasons of comparison, the lower part of Fig. 10 is reproduced again in Fig. 11. In the upper part of this figure, the measured space charge capacity is shown as a function of temperature with frequency and forward bias as parameters. The relation between the maxima of the apparent space charge capacity and the crossing of surface states by the Fermi level F_s is indicated by dashed lines. It is apparent that at sufficiently low frequency and high enough bias, the presence of the surface states manifests itself as an increase in

apparent space charge capacity when the Fermi level at the surface crosses the 0.37 eV level and another level herewith identified at 0.54 eV above the valence band. This level too has been found on oxide covered silicon surfaces and was identified as a donor level.

Conclusion

29165

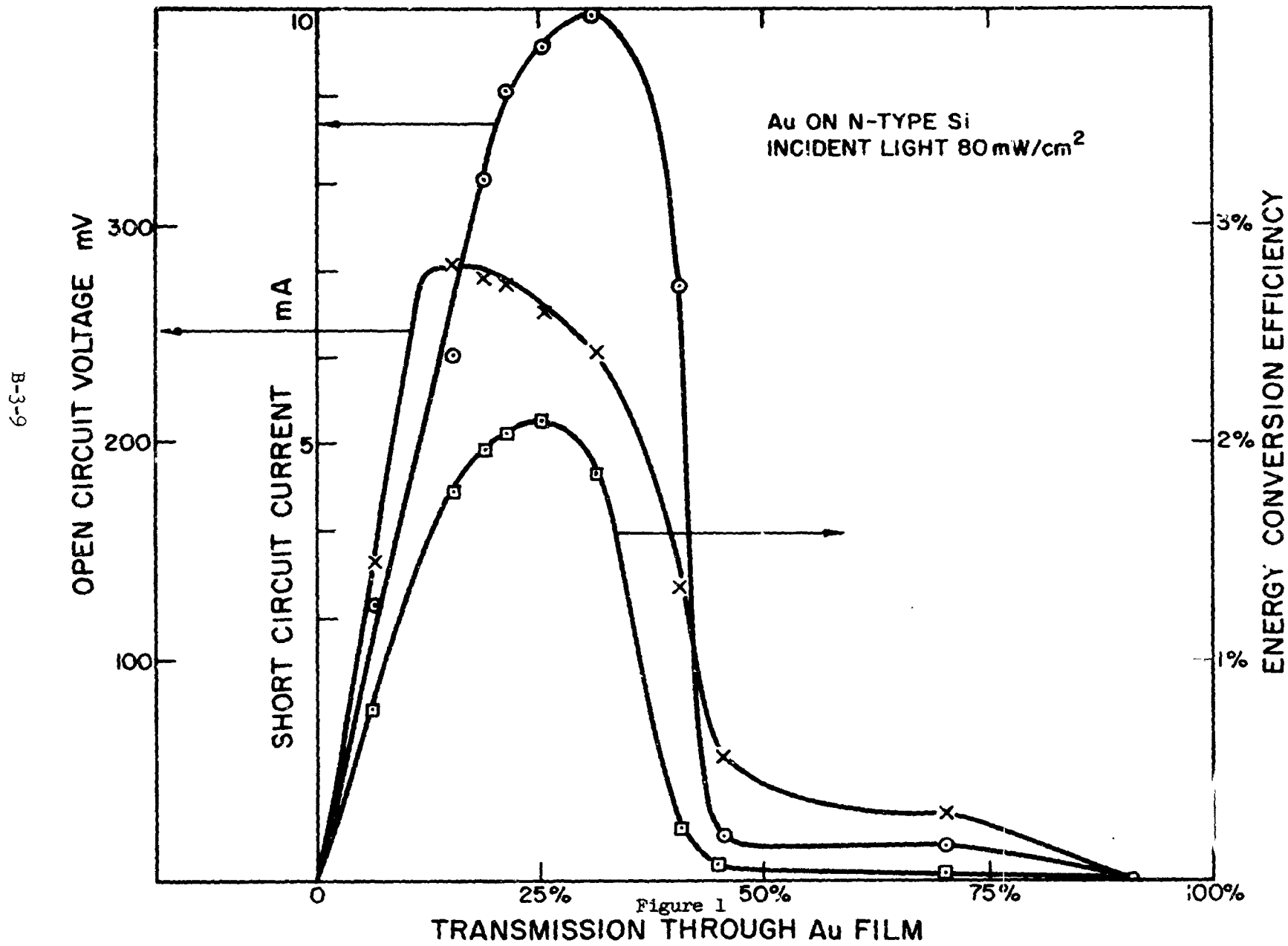
The photovoltaic effect which is observed at the interface between a metal and a semiconductor in the presence of a thin oxide interface can be interpreted as the consequence of the charge transfer characteristic of the thin oxide film, and the effect of surface states at the oxide-semiconductor interface. Since the position of the surface Fermi level F_s is determined, to a large extent, by the surface states, the open circuit voltage V_{oc} is directly related to the surface state structure. Four surface states have been identified: $E_1 = 0.37$ eV and $E_2 = 0.54$ eV above the valence band and $E_3 = 0.52$ eV and $E_4 = 0.28$ eV below the conduction band.

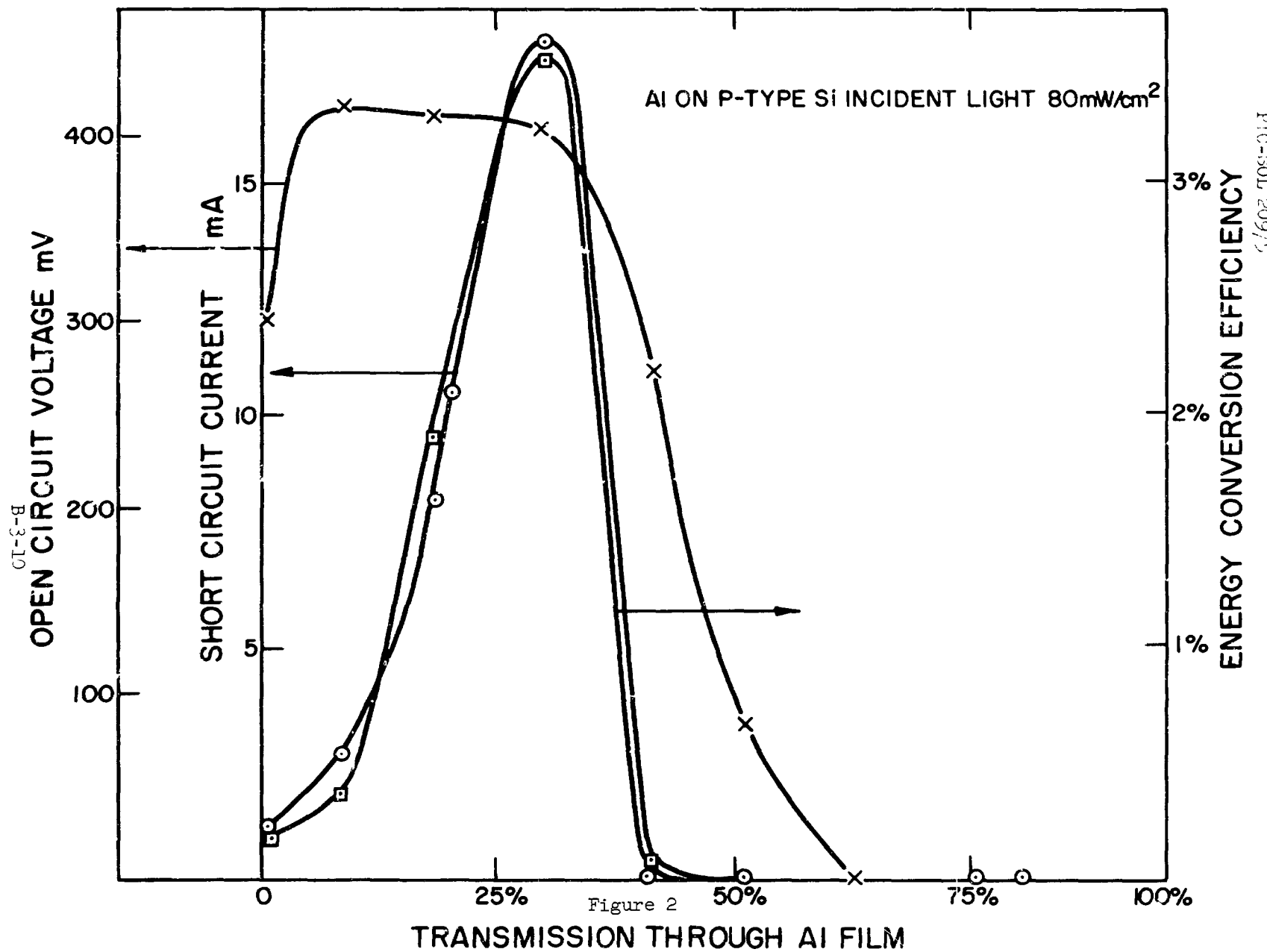
Author

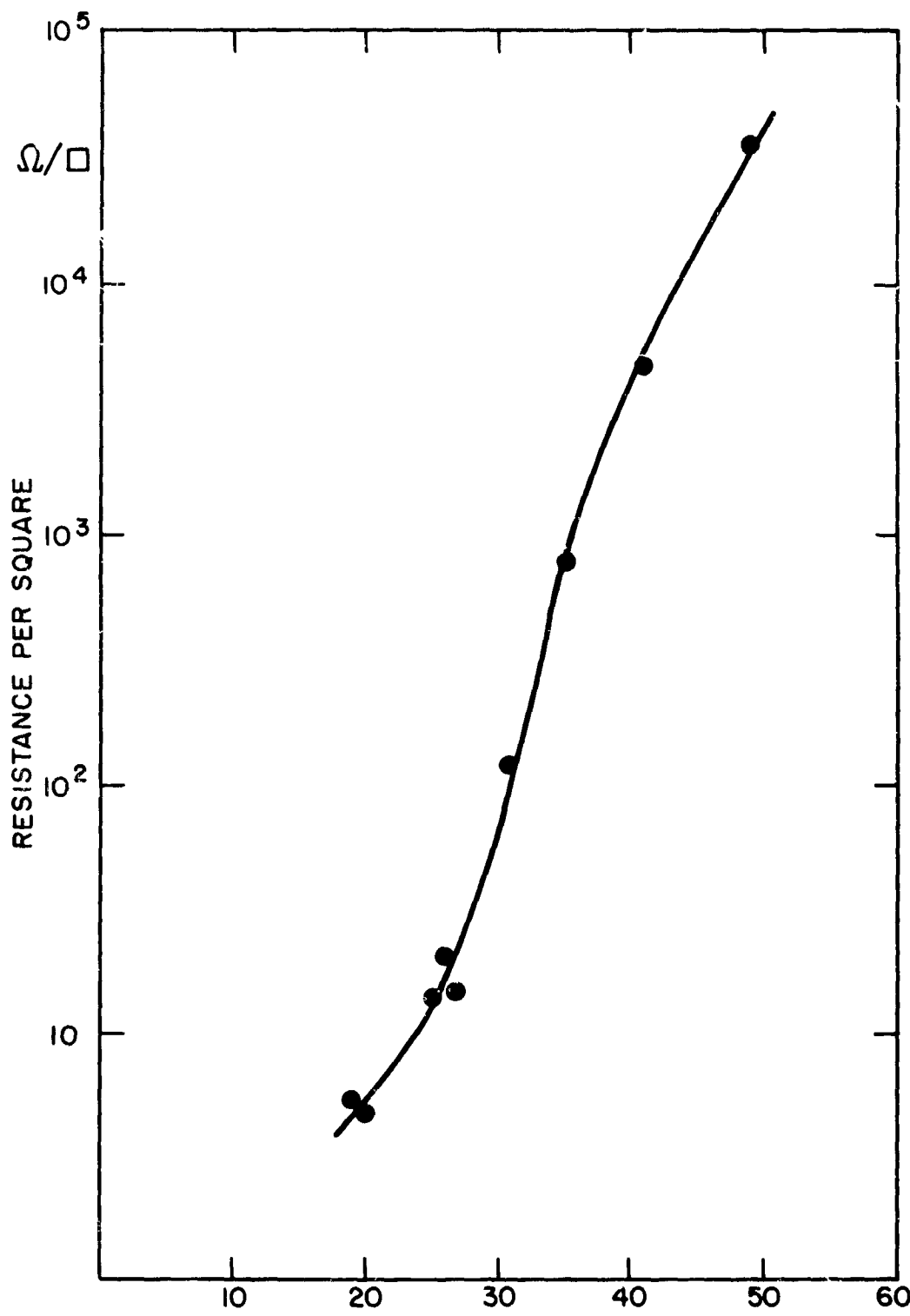
TABLE I

Space Charge Capacity and Open Circuit Voltage as a
Function of Temperature

Temp. (°K)	$\frac{C_i}{(F/cm^2)} \times 10^{-8}$	$\frac{C_o}{(F/cm^2)} \times 10^{-8}$	V (Volts)	γ_i	γ_o	$\Delta\gamma$	$\gamma_{oc} = V_{oc}/kT$
155	9.5	1.7	0.388	2.4	33.4	31.4	29.4
189	9.6	2.1	0.350	2.2	25.1	22.9	21.7
219	10	2.3	0.312	1.9	18.3	16.4	16.7
247	12.5	2.5	0.274	1.5	14.0	12.5	13.0
260	14.2	2.6	0.236	1.4	12.4	11.0	10.6
273	16.8	2.9	0.200	1.3	9.7	8.4	8.6
285	14.8	3.0	0.188	1.32	8.8	7.5	7.7







RESISTANCE OF THIN GOLD FILMS DEPOSITED
ON A SILICON SUBSTRATE

Figure 3

B-3-11

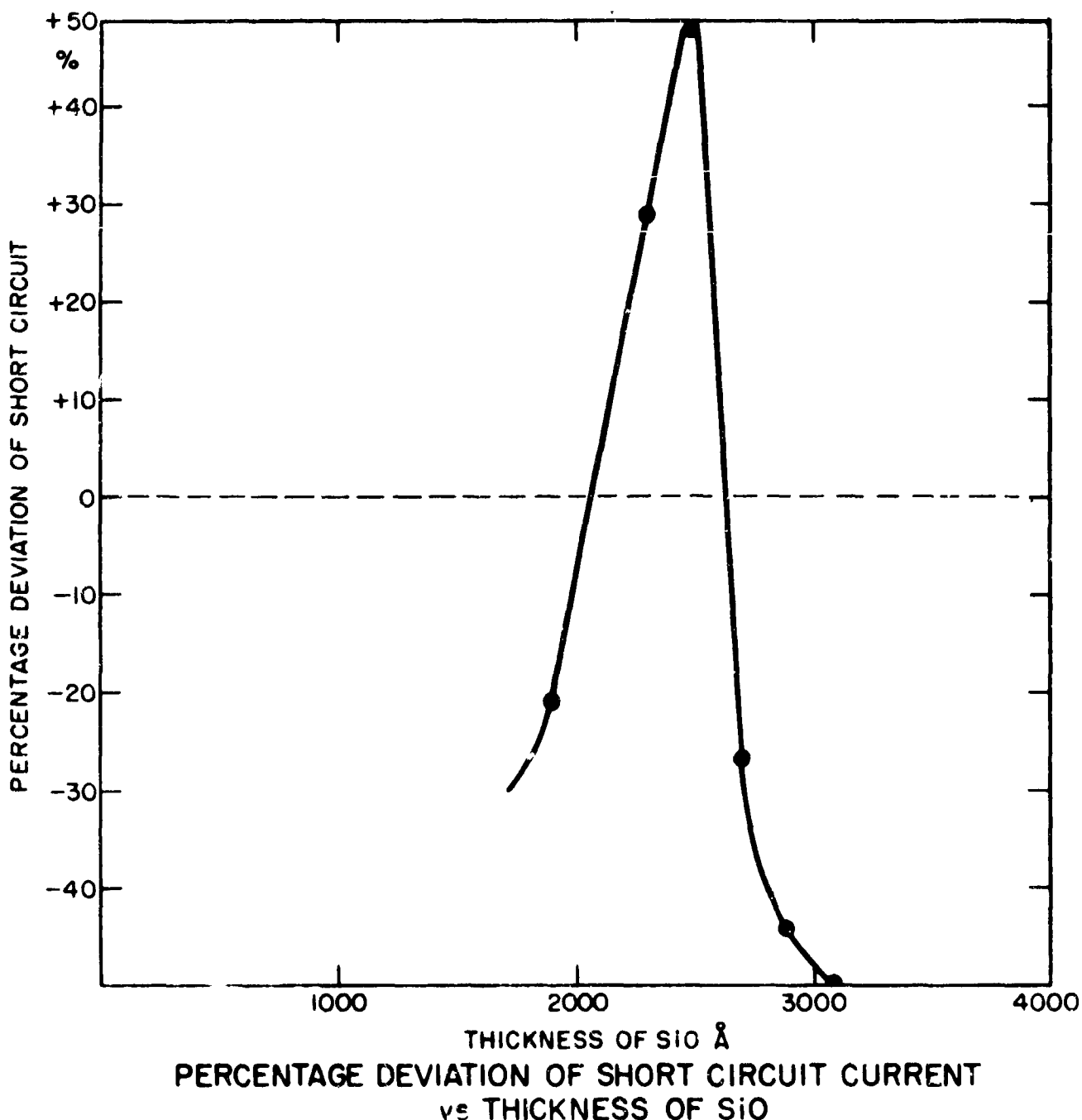


Figure 4

B-3-12

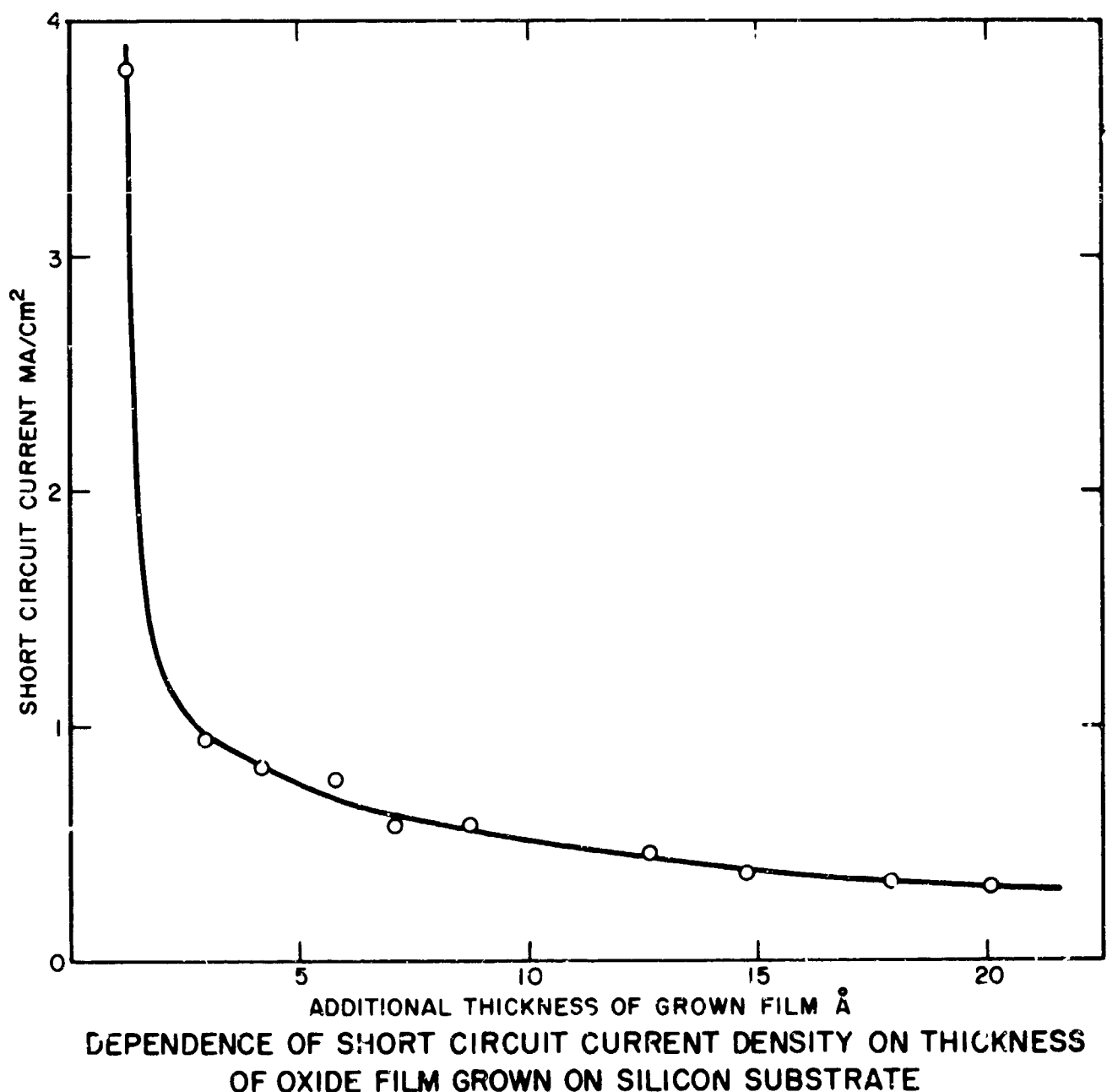
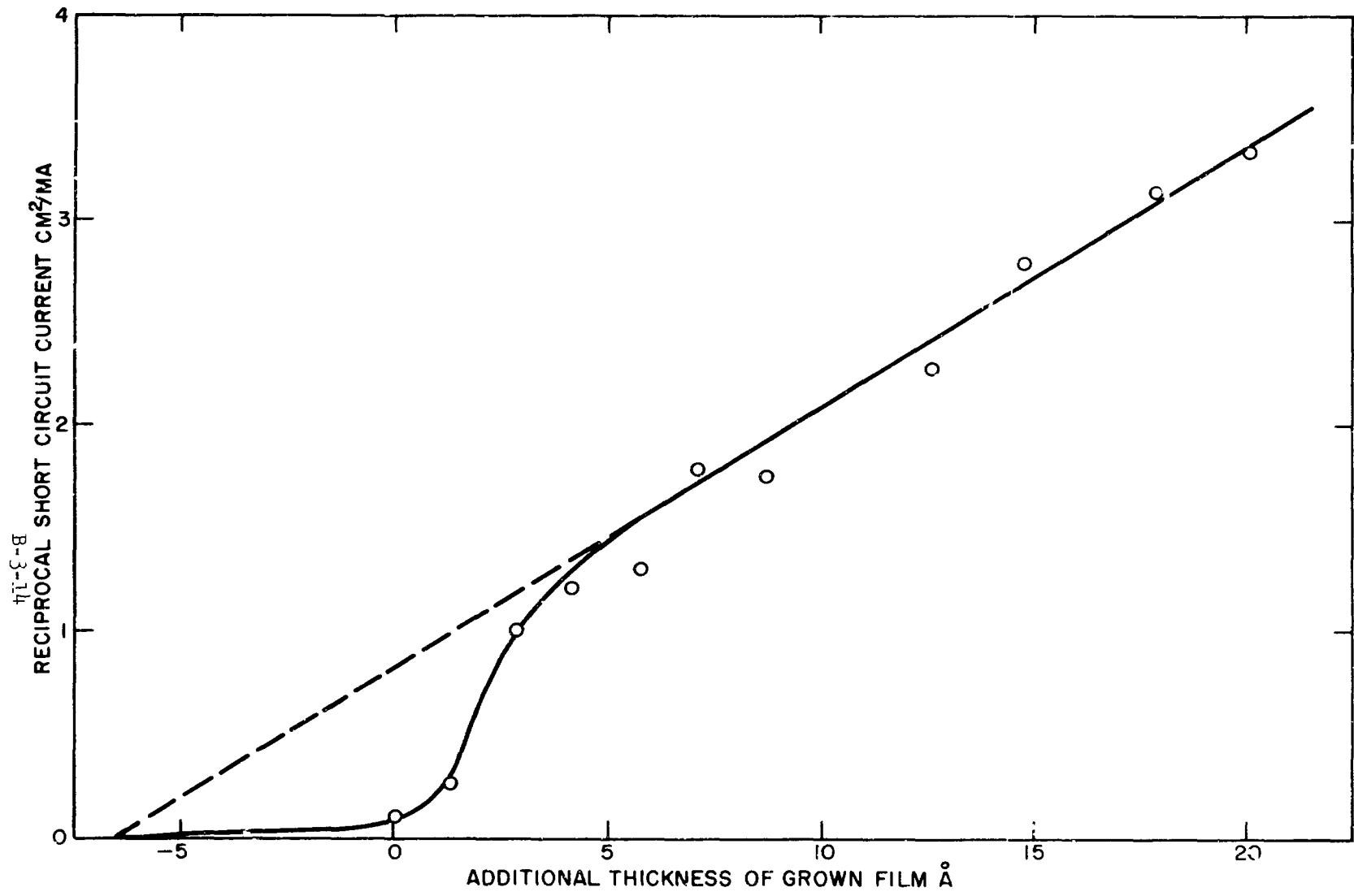


Figure 5

B-3-13



DEPENDENCE OF SHORT CIRCUIT CURRENT DENSITY ON THICKNESS
OF OXIDE FILM GROWN ON SILICON SUBSTRATE

Figure 6

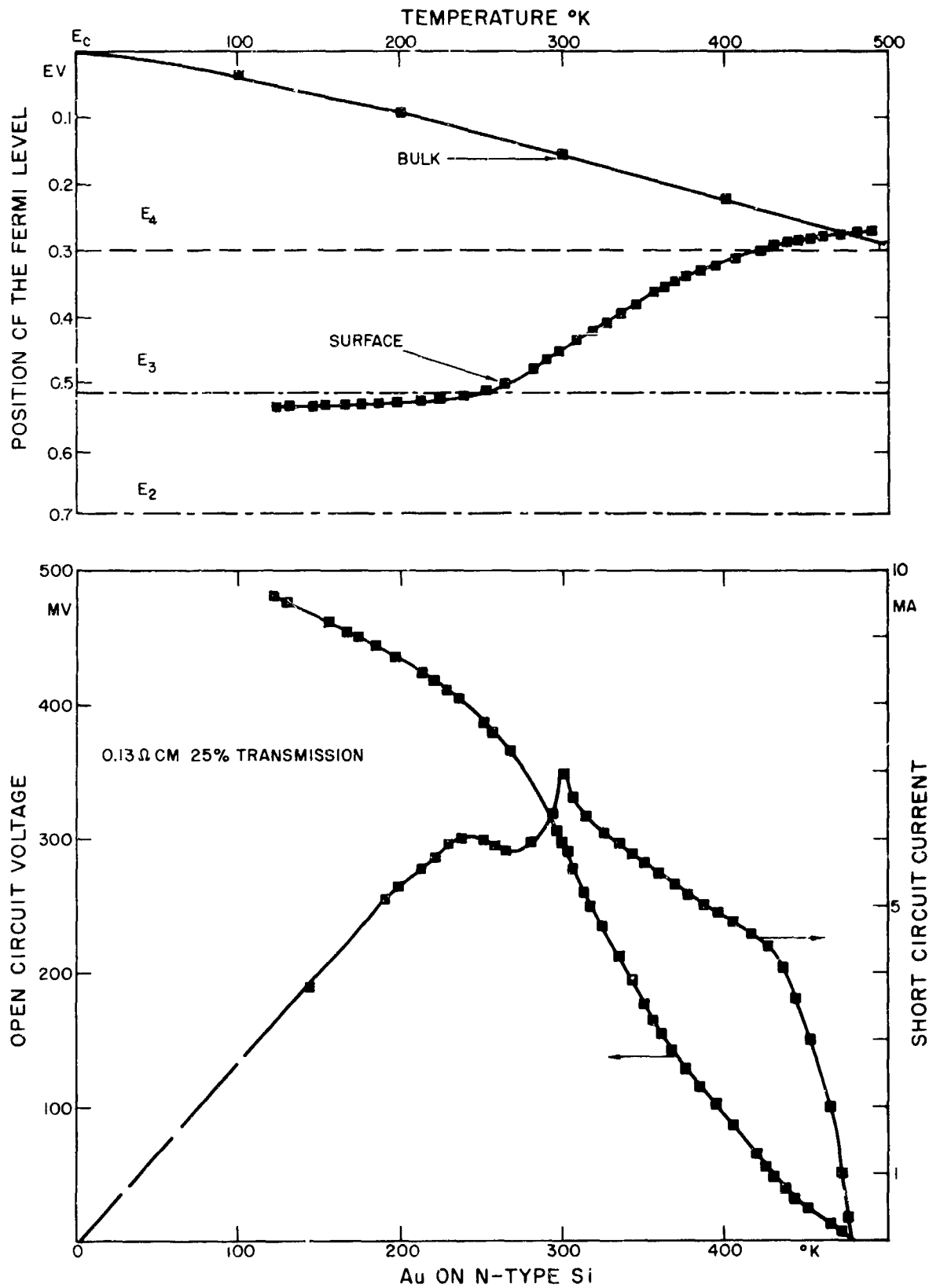


Figure 7

B-3-15

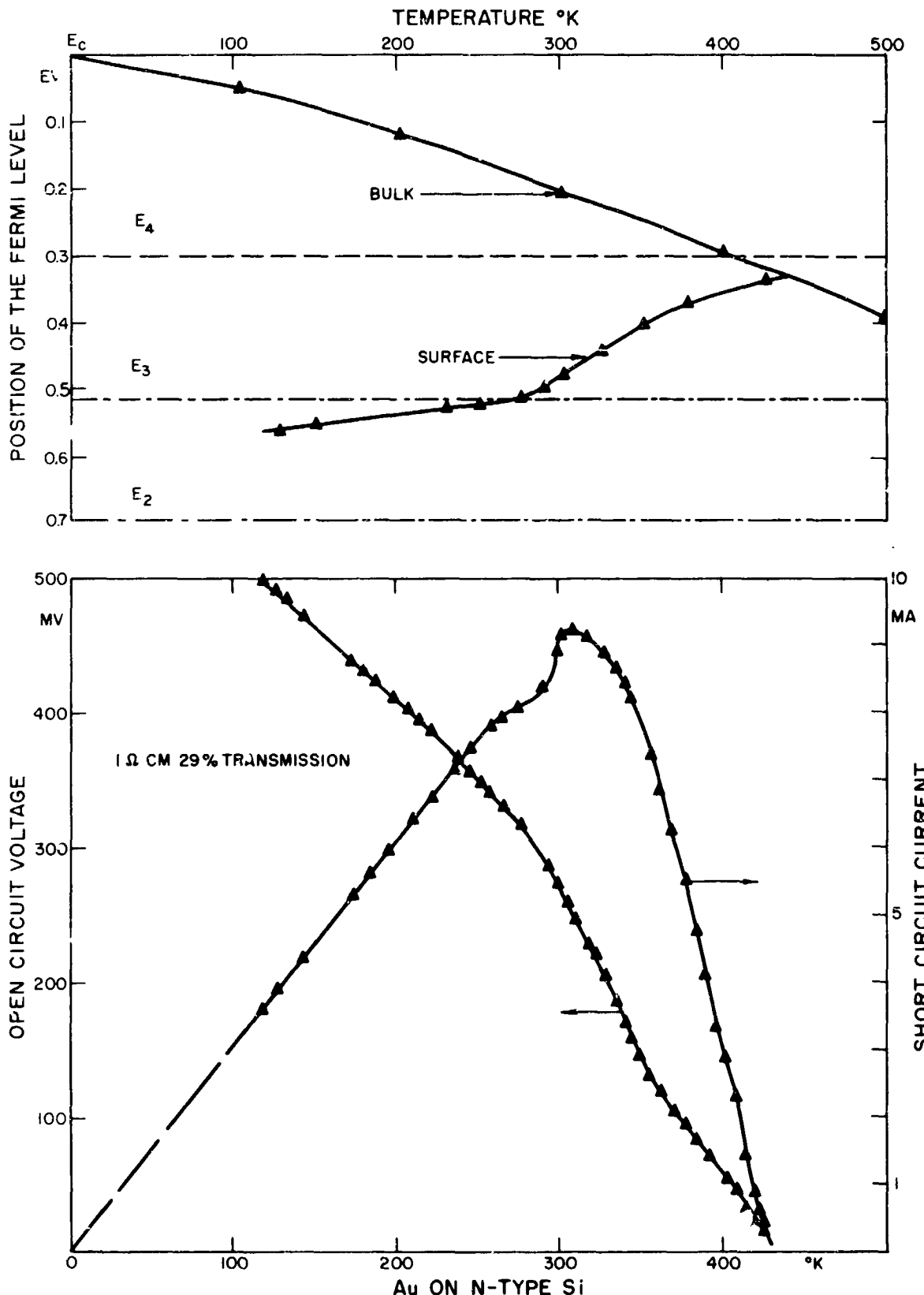


Figure 8

B-3-16

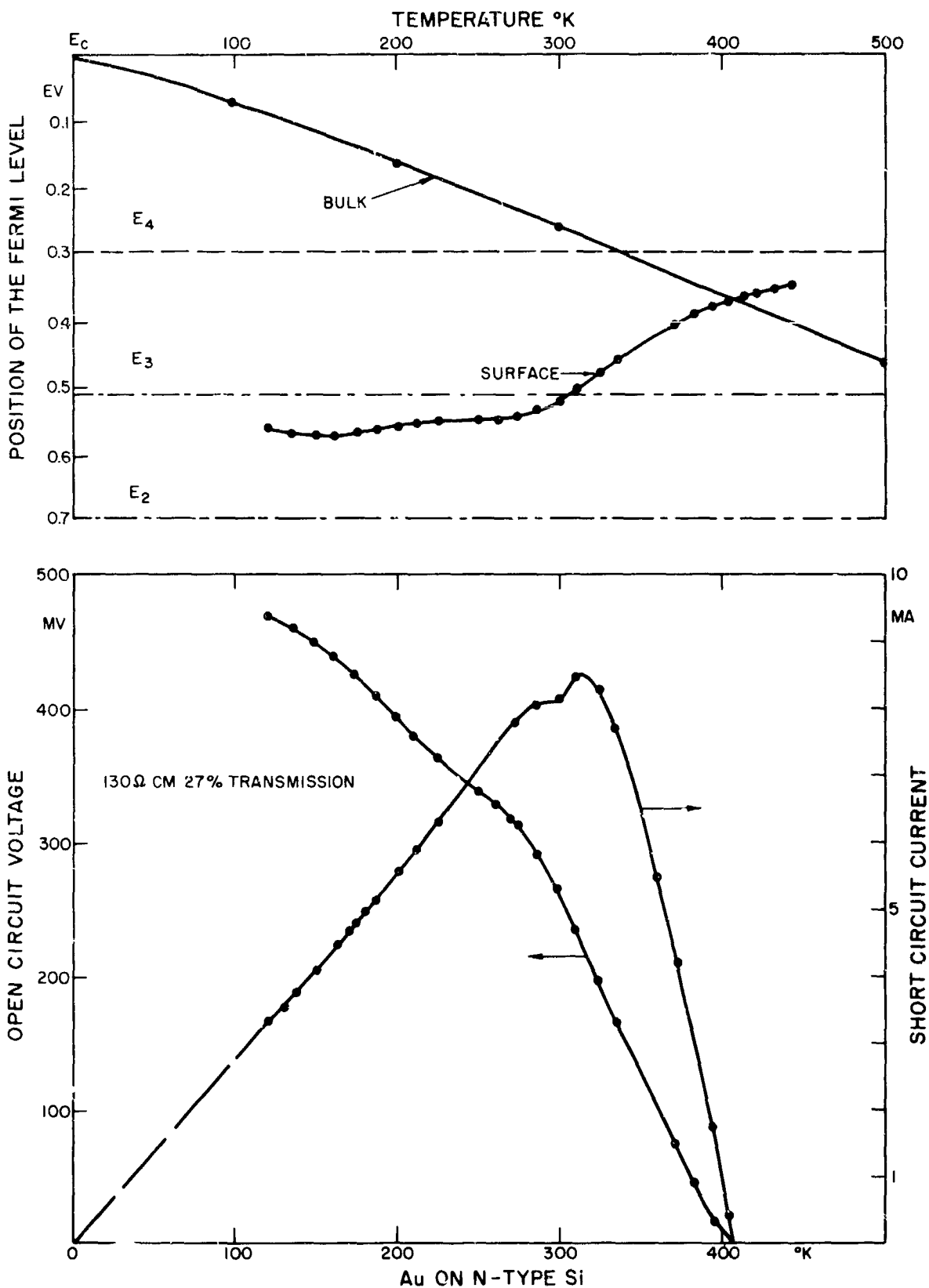


Figure 9

B-3-17

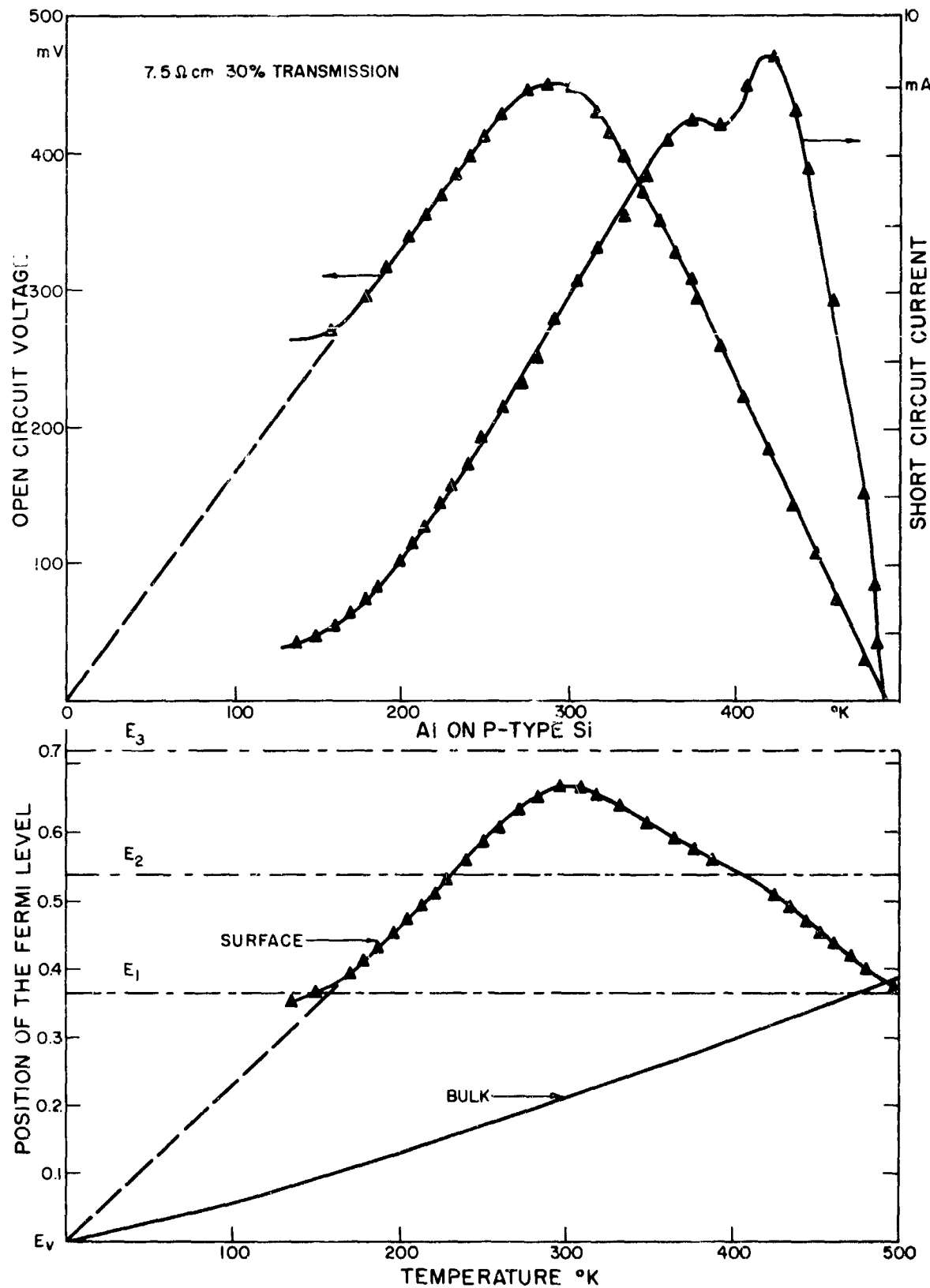


Figure 10

B-3-18

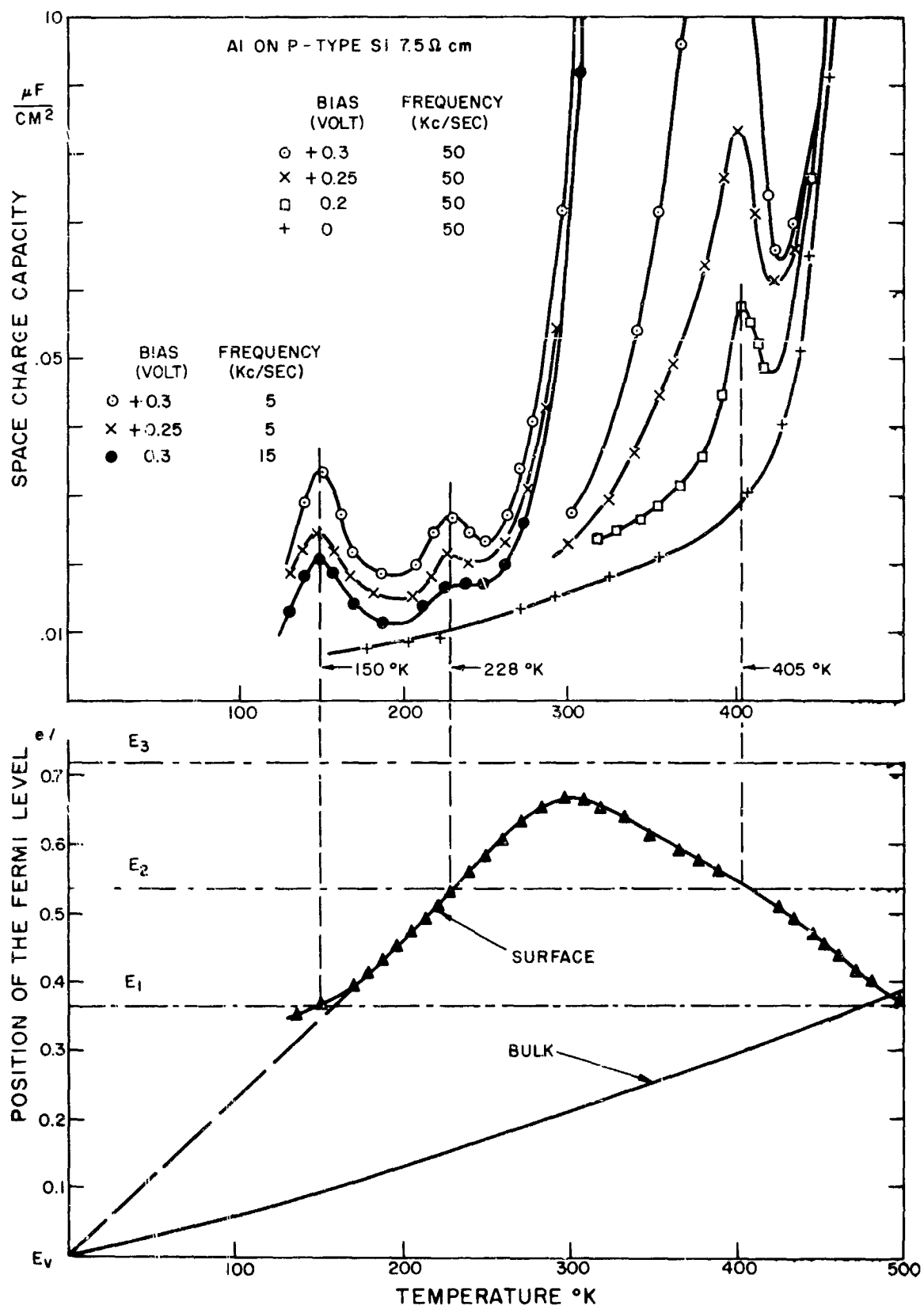


Figure 11

B-3-19

DISCUSSION

GUMMEL - BELL TELEPHONE LABS: I think that the structure that you have is a Schottky barrier layer type diode. Frequently, one assesses the quality of the diode one has by making a semi-log plot of current versus voltage and observing what value of the exponential one has. From this, you can calculate the value of n in the $\frac{qV}{nT}$ term. What value of n did you find?

MR. RUPPRECHT: I don't remember now the n values but I think that they were of the order of 2, perhaps 1.8.

GUMMEL - BELL TELEPHONE LABS: How did you clean your surfaces?

MR. RUPPRECHT: They were etched with a CP-4 solution, I think. It was white etch or something like that. It was nothing special.

GUMMEL - BELL TELEPHONE LABS: What was resistivity of the substrate?

MR. RUPPRECHT: I had three resistivities. One was 0.13 ohm centimeter, one was 1 ohm centimeter, and the other was 130 ohm centimeter. I have also studied aluminum on p-type silicon of three widely different resistivities.

PERKINS - RCA: Concerning the curves showing the reciprocal of short circuit current versus film thickness, was there a portion on the lower part of the curve where there is a deviation from linearity? Were you able to make this nonlinear portion move in the reverse direction with applied voltage, such that you might be able to see the effects of tunneling due to the high field across the oxide film?

MR. RUPPRECHT: No, in these series of experiments we have observed only photovoltaic effects. A photovoltaic effect happens only when you have the separation of charges before they have a chance to recombine at the surface. The effect of separation in this case is that the holes are tunneled through the oxide layer into the metal.

PERKINS - RCA: Under conditions of tunneling through the oxide layer wouldn't you expect that the resistance would vary linearly with voltage at low voltages across the oxide layer, but would decrease approximately exponentially at higher voltages?

MR. RUPPRECHT: Yes, I think this is theoretically to be expected.

ACAMPORA - NASA, LEWIS: Does the oxide layer lie between the metal contact and the surface of the semiconductor?

MR. RUPPRECHT: Yes, the semiconductor has been heat treated to about

550° for different amounts of time in oxygen. This forms the oxide layer. Then you evaporate gold on top of it, such that the transmission through the gold is about 30%.

ACAMPORA - NASA, LEWIS: Have you ever noticed oxide formation between the metal contact and semiconductor surface without removing the metal contact?

MR. RUPPRECHT: Yes, we have made some observations concerning this. There is a time dependence of the properties of these cells, which can be explained as an increase in oxide layer thickness with time. There may be oxidation of the silicon going on through the thin metal film.

29166
SINGLE CRYSTAL GALLIUM PHOSPHIDE SOLAR CELLS*

Presented by

A. S. Epstein

Central Research Department

Monsanto Company

St. Louis, Missouri, 63166

2 June 1964

* Performed under NASA Contract NAS 3-2776

SINGLE CRYSTAL GALLIUM PHOSPHIDE SOLAR CELLS

A. S. Epstein and W. O. Groves
Central Research Department
Monsanto Company
St. Louis, Missouri 63166

Introduction

Photovoltaic energy converters are of interest for space utilization. Silicon has been the most widely used material for these applications. In recent years consideration of optimum energy-gap materials has led to the study of gallium arsenide for photovoltaic utilization. Since higher temperature operation of solar cells is desired there has also been increasing interest in higher energy gap III-V compounds such as GaP. This report is concerned with some optical, electrical and thermal characteristics of experimental solar cells fabricated from epitaxially grown single crystal GaP.

Experimental ProceduresMaterial Preparation and Properties

Single crystal gallium phosphide was synthesized from the elements by vapor transport and epitaxial deposition on single crystal gallium arsenide substrates. The transport gas* was a dilute mixture of hydrogen chloride in hydrogen. The reaction was carried out in a 20 mm I. D. quartz tube in a furnace system having three individually controlled zones. Phosphorus* was evaporated into the gas stream at temperatures from 400° to 450°; gallium* was held at temperatures from 890° to 975° with the substrates between 790° and 870°. Temperature gradients in the deposition zone ranged from 3°C/cm to 25°C/cm. Typically, the total gas flow was 300 cc/min with a hydrogen to hydrogen chloride volume ratio of 150, although in some experiments hydrogen flow rates were varied from 155 cc/min to 800 cc/min and hydrogen chloride flow rates in the <100> direction ranged from 0.1 to 0.2 microns/cc HCl but fell as low as 0.03 microns/cc HCl at lower H₂/HCl ratios and at the lowest phosphorus pressures. The growth rate depends on both temperature and on temperature gradient in the deposition zone.

* Purified hydrogen and anhydrous hydrogen chloride were obtained from the Matheson Company. Red Phosphorus of semiconductor grade from the American Agricultural Chemical Company or from L. Light and Co., Ltd. Gallium of 99.999% purity was obtained from Alcoa.

The thicknesses of the single crystal epitaxial GaP varied from about 10 microns to about 200 microns with the majority of the GaP material having thicknesses of the order of 40 microns.

The surfaces of the gallium phosphide layers were generally poor, containing many bumps and other defects, however, no effect on solar cell properties has yet been detected. The best surfaces were prepared at lower growth rates. Surface appearance depends on substrate surface preparation, orientation and run conditions. A significant improvement was achieved by pretreating the substrate at 1000°C in phosphorus vapor carried by hydrogen just prior to deposition of gallium phosphide.

Electrical properties of the layers were obtained by measurement of Hall constant and resistivity of Hall bars located adjacent to the wafers during deposition. Typical values for mobility and net carrier level of "undoped" <100> grown material were $100 \text{ cm}^2 \text{ volt}^{-1} \text{ sec}^{-1}$ and $2 \times 10^{18} \text{ cm}^{-3}$ respectively. A total ionized impurity level in the 10^{17} range is indicated in all samples.

Sample Preparation and Cell Fabrication

The sample areas were typically of the order of 0.2 to 0.5 cm^2 and rectangular with the epitaxial GaP layers having n-type conductivity. Shallow p-n junctions of the order of 1μ or less were formed by zinc diffusion (with phosphorus added) in closed tubes at approximately 800°C for short times. Following the diffusion, the junction depth was determined by cleaving and etching delineation techniques and the surface concentration deduced from Hall effect measurements. The back surface was lapped back. A contact of Au-Sn-Ni was used on the back surface and silver was evaporated on to the p surface while the sample was held at 200°C for the p surface contact. The cells were lapped, cleaned and etched to remove any shorting paths around the edges.

Electrical Measurements

The conversion efficiency of circuit voltage and short circuit current measurements were made in bright sunlight using secondary standard silicon solar cells for light intensity calibration. Preliminary electrical measurements however were usually made with a nominal 2800°K tungsten light source filtered through three inches of water. The voltage was measured with an Applied Physics electrometer. Currents were measured with a Hewlett Packard Microvoltammeter Model No. 425A. The cell area was determined from its length and width which were measured with a traveling microscope.

Optical Measurements

The spectral response measurements were made on a Bausch and Lomb

monochromator Cat. No. 33-86-40 with a plane circular grating blazed for 0.5μ .

The experimental procedure followed was a standard method. The source used was a tungsten lamp. The solar cell was mounted so that it was in the exit beam of the monochromator. A constant slit of 2 mm was held during the entire scan for the solar cell and a Reeder thermocouple in the wavelength interval of 0.35 to 0.9μ . The scan was made first with the solar cell and then with the thermocouple as a detector with all other conditions held constant. A ratio was then taken between the response of the solar cell and the thermocouple and plotted as relative response.

Thermal Measurements

The solar cell, for temperature measurement of the electrical parameters, was mounted in a cell holder of lavite with provisions for Chromel-Alumel thermocouples under and near the solar cell. The cell holder was inserted into a cylindrical muffle furnace. The source used was either a tungsten source or sunlight. In the case of the tungsten source, it was mounted directly on the furnace and focused through an opening in the cell holder on the solar cell. The tungsten source used was a G. E. projector spotlight 150 PAR/SP.

Results and Discussion

Two main types of solar cells have resulted in this investigation: (1) an extrinsic cell having its main spectral response at room temperature in a broad band roughly centered at about 0.75 microns, (2) an intrinsic cell having its principal response at about 0.45 microns. The typical spectral response curves for these cells are shown in Figure 1.

The differences in electrical, optical and thermal characteristics of the two classes of cells are shown in Table I for cells NA31 and NA22 SC21-3 which are examples of the intrinsic and extrinsic cells respectively.

The extrinsic cell is characterized by about half the open circuit voltage and about three times the short circuit current density thus far found for the intrinsic cell. The short circuit current density of the intrinsic cell increases with temperature, doubling at about 275°C , whereas the extrinsic cell shows little change in short circuit current until about 200°C where it decreases rapidly. The open circuit voltages of both cells show the characteristic decrease with increasing temperature and the temperature coefficients are not appreciably different, being of the order of 3 mv/deg. However, at 150°C the voltage of the extrinsic cell has decreased to less than .1 volt. At higher temperatures the intrinsic cell is far superior to the extrinsic cell.

A conversion efficiency of about 1% in bright sunlight at room temperature has been obtained for the intrinsic cell. Somewhat higher values, 1.6%, have been noted for the extrinsic cell.

An E-I power curve taken in sunlight for a solar cell of the intrinsic type, NA31, SC34-3, at $t = 23^{\circ}\text{C}$ is shown in Figure 2 with an input of 0.4 mw/cm^2 as deduced using a standard silicon solar cell. An efficiency of about 1% has been obtained.

Open Circuit Voltage vs. Temperature

A parameter of interest is the temperature coefficient of the open circuit voltage, β . The temperature coefficient of the intrinsic cells is found to be about 3 mv/deg for most of the samples. This agrees with that calculated from solar cell theory, assuming an ideal junction and with the energy gap assumed to provide the main variation with temperature. In Figure 3 we have indicated the calculated V_{oc} vs. temperature curve and the experimental results obtained for GaP. It is noted that the absolute value of V_{oc} for the best cell is about 0.3 volts below that calculated from simple theory and this difference holds true throughout the temperature range shown in Figure 3. The difference cannot be easily accounted for in terms of lifetime or diffusion length as permitted by simple theory. Additional effects such as recombination type currents, etc., as pointed out by Wysocki and Rappaport⁽¹⁾ are in the right direction as expected.

At lower temperatures ($<150^{\circ}\text{C}$) there appears to be some deviation from a straight line in the experimental open circuit voltage-temperature curves. This bending is generally noted around room temperature. It could be related to surface effects, although this has not been established.

With improved material and fabrication processing it is hoped that better agreement in V_{oc} between experiment and theory can be achieved as noted for silicon and GaAs. The three materials and the theoretical and experimental data for the open circuit voltage with temperature are shown in Figure 4⁽²⁾. It is of interest to note the difference in magnitude of open circuit voltage between the extrinsic and intrinsic cells as a function of temperature. The slopes of these curves are however similar and about 3 mv/deg. A comparison of the two types of cells is shown in Figure 5.

Short Circuit Current Density vs. Temperature

The short circuit current density of the intrinsic GaP solar cell increases with temperature following a relationship which can be expressed as

$$J_{sc} \sim e^{-\frac{\Delta E}{kT}}$$

where ΔE the activation energy is of the order of 0.05 ev.

In the case of the extrinsic cell the short circuit current density is independent of temperature of 200°C , decreasing after that.

Typical curves for both types of cells are shown in Figure 6.

Effect of GaAs Substrate

With the thin (40 micron) epitaxial layers and the relatively large areas desired, the GaAs substrate has been retained as a support. The possible effect of the GaP-GaAs interface on the GaP solar cell has been examined.

The procedure involved was to etch out a portion of the GaAs from zinc diffused GaP cells to provide a window directly to the back of the GaP n layer. The GaAs was masked with black wax except for the portion to be etched away. The etch used was 1 HF : 3 HNO_3 : 2 H_2O . This etch attacks GaP only negligibly.

A sketch of the sample with contacts is shown in Figure 7. Contact 2 is the original back contact of Au-Sn-Ni, contact 3 to the GaP, is made in the same manner. Contact 3 is, as can be seen, smaller than the "window". The top contact 1 employs evaporated silver.

If a photovoltage is developed at the GaP-GaAs interface, open circuit voltages and short circuit currents measured between contacts 1 and 2, which include this interface, should differ from those measured between contacts 1 and 3, which do not. No differences have been noted on making the measurements under a variety of conditions including normal solar cell testing conditions both with our standard test apparatus and in sunlight and with a microscope light using both front and back illumination. These results seemed to indicate that with our method for making material the GaP-GaAs interface does not play a significant role in determining the characteristics of the GaP solar cell.

Diffusion Length Measurements

Using the method of Logan and Chynoweth⁽³⁾, room temperature measurements of diffusion length have been made on mesas of some of the solar cells. From a plot of $1/C/A$ ($\text{capacitance}/\text{area}$)⁻¹ vs. J (photo current density of the cell with reverse bias) the minority carrier diffusion length can be determined. Such a plot is shown in Figure 8, for sample NAL6 SC13-6 (from the plot, $L_D = 150 \text{ \AA}$). The values obtained by this method for some of our samples range from about 150 \AA to about 5000 \AA . Using a carrier diffusion constant of $2.5 \text{ cm}^2/\text{sec.}$, the values of the diffusion length correspond to values of minority carrier lifetime varying roughly from 10^{-12} to 10^{-10} sec.

Capacity-Voltage Measurements

The junctions prepared from the epitaxial GaP material with our procedure generally seem to follow a $1/C^3$ law dependence. We have been able to fit our capacity-voltage data with expressions of the following type:

$$V_a + V_i = \frac{-qa}{12\epsilon} \quad \left(\frac{\epsilon}{C/A} - W_I \right)^3$$

or

$$V_a + V_i = \frac{-qa}{12\epsilon} \quad \left(\frac{\epsilon}{C/A} - W_I \right)^2 \left(\frac{\epsilon}{C/A} + \frac{W_I}{2} \right)$$

where V_a is the applied reverse voltage, V_i is the built in voltage of GaP, q , the electronic charge, ϵ , the dielectric constant, C the capacity of the junction, a , is a concentration gradient, A the cross sectional area of the junction. (W_I) has been introduced into the equations following Logan and Chynoweth⁽³⁾, to fit our data. It signifies as expected that the space charge layer of the junction is extremely wide and that in actuality our p-n junction can be better represented by a p-I-n structure. The I layer or W_I is found to vary for our cells from about 150 Å to about 10,000 Å.

I-V Characteristics

From D. C. current-voltage characteristics at 23°C , the factor n in the expression $I = I_0 \exp \frac{-ev}{nkT}$ for a p-n junction is found to be > 2 ($n = 4$) for cells which have their main spectral response at 0.45μ whereas for 0.7μ cells, $n = 2$. The latter suggests from the work of Sah, Noyce, and Shockley⁽⁴⁾ that recombination center mechanisms may predominate in the extrinsic cells.

Current-voltage characteristics taken on a Tektronix Oscilloscope No. 536 are shown in Figure 9. These are the best traces obtained for a 0.45μ solar cell and a 0.7μ cell.

 0.7μ Extrinsic Solar Cell

While it is believed that the mechanism leading to current generation in the 0.7μ cells must likely involve a two step excitation consisting either of two optical steps or one optical and one thermal step, the nature of the centers responsible for the 0.7μ response in the epitaxial GaP is unknown. The 0.7μ response has been found to occur as a major response, however, when a low hydrogen flow rate is used in the growing of epitaxial GaP.

Since the background level of ionized impurities in our material is 10^{18} cm³ with net carrier levels of 10^{16} , self compensation is suggested. To achieve the close compensation noted in many of the samples which still remain n-type, it is suggested that a deep donor which could correspond to the 0.7μ level could be present. If this is so, it could be the same as the 0.4 ev donor postulated by Gershenzon and Mikulyak⁽⁵⁾ and thought to be due to oxygen. This model remains to be verified.

Acknowledgment

The authors would like to express their appreciation to Dr. Robert A. Ruehrwein for many interesting and helpful discussions of the problems. They acknowledge the assistance of J. F. Caldwell, C. A. Lowther and J. W. Sharp in making many of the measurements and E. Pittenger and J. Reynolds for construction of some of the equipment.

References

- (1) J. J. Wysocki and P. Rappaport, J. Appl. Phys., 31, 571 (1960).
- (2) The experimental data for Si and the calculated curves for Si and GaAs were taken from Ref. 1; the experimental data for GaAs was taken from A. R. Gobat, M. F. Lamorte, G. W. McIver, IRE Trans. Mil. Electronics, p. 20, Jan., 1962.
- (3) R. A. Logan and A. G. Chynoweth, J. Appl. Phys. 33, 1649 (1962).
- (4) C. T. Sah, R. N. Noyce and W. Shockley, Proc. IRE, 45, 1228 (1958).
- (5) M. Gershenson and R. M. Mikulyak, Solid State Electronics, 5, 313 (1962).

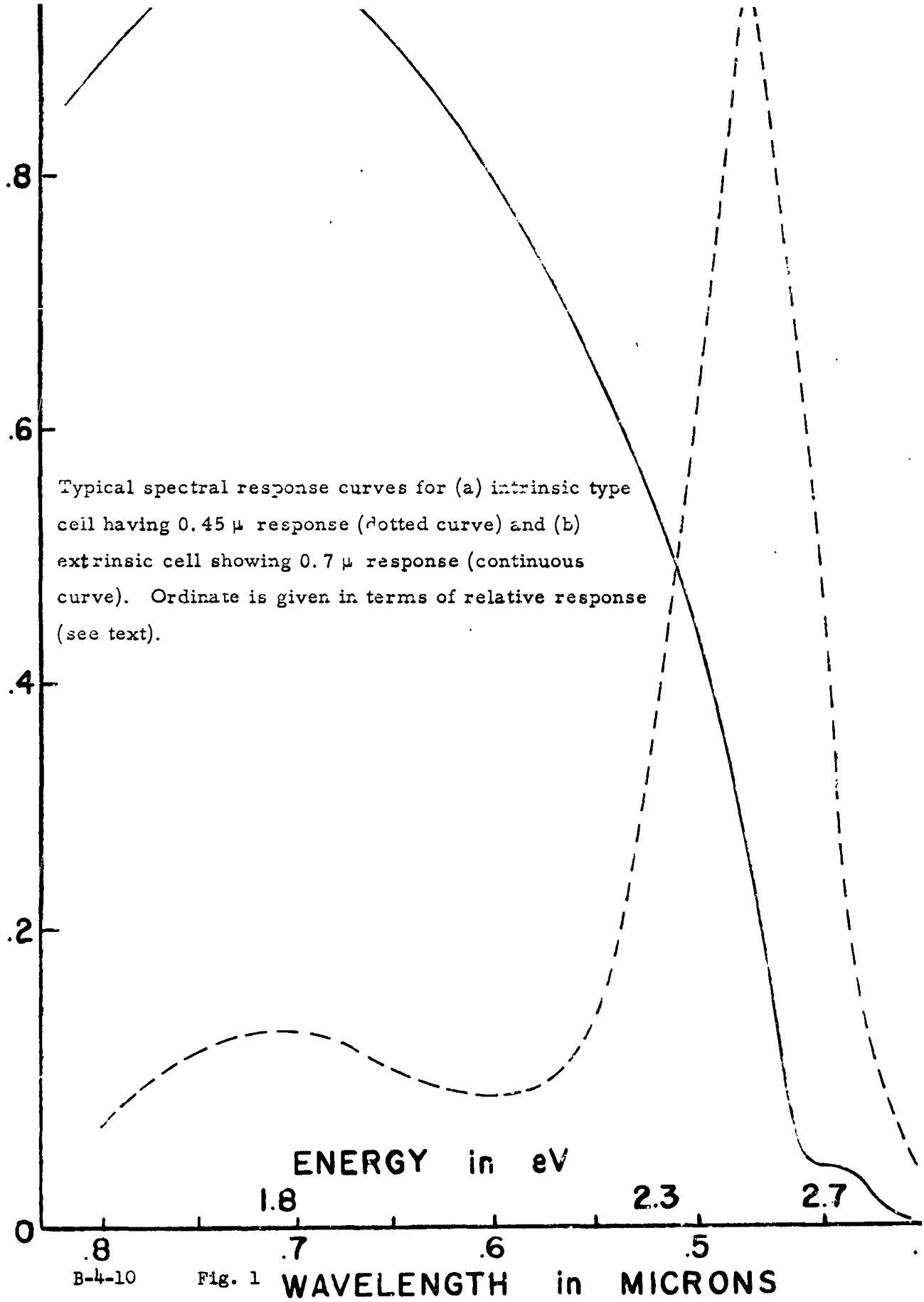
Table ICharacteristics of Extrinsic and Intrinsic GaP Solar Cells

Type:	<u>Intrinsic</u>	<u>Extrinsic</u>
Sample:	NA31 SC34-3	NA22 SC21-3
<u>Electrical:</u>		
V_{oc} (volts)	1.35	0.58
J_{sc} (ma/cm^2)	1.4	4.0
Efficiency (measured in sunlight)	1.1*	1.6±
<u>Optical:</u>		
Spectral Response Peak (μ)	0.45	0.75 (broad)
<u>Temperature:</u>		
Slope J_{sc} vs. $1/T$ (ev)	.06	0 (to $200^{\circ}C$) J_{sc} decreases after $200^{\circ}C$
V_{oc} vs. T, β (mv/deg)	3.5	2.8
V_{oc} at $300^{\circ}C$	0.23	~ 0
D. C. $I_f - V_f$, $I_o \exp^{eV/nkT}$:	$n = 4$	2

* Based on solar intensity as measured with silicon solar cell of 94 mw/cm^2 .

± Based on solar intensity as measured with silicon solar cell of 74 mw/cm^2 .

RELATIVE RESPONSE



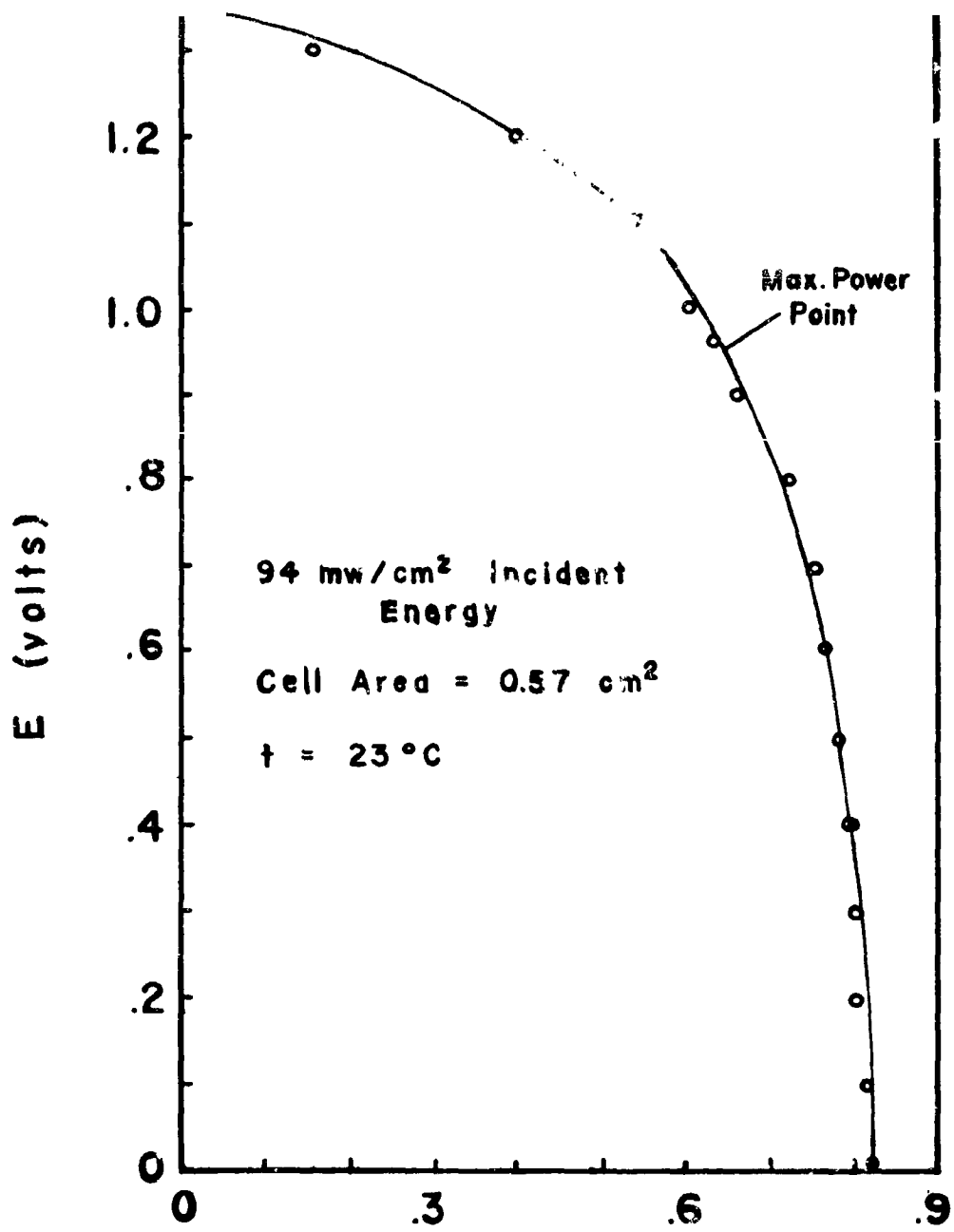
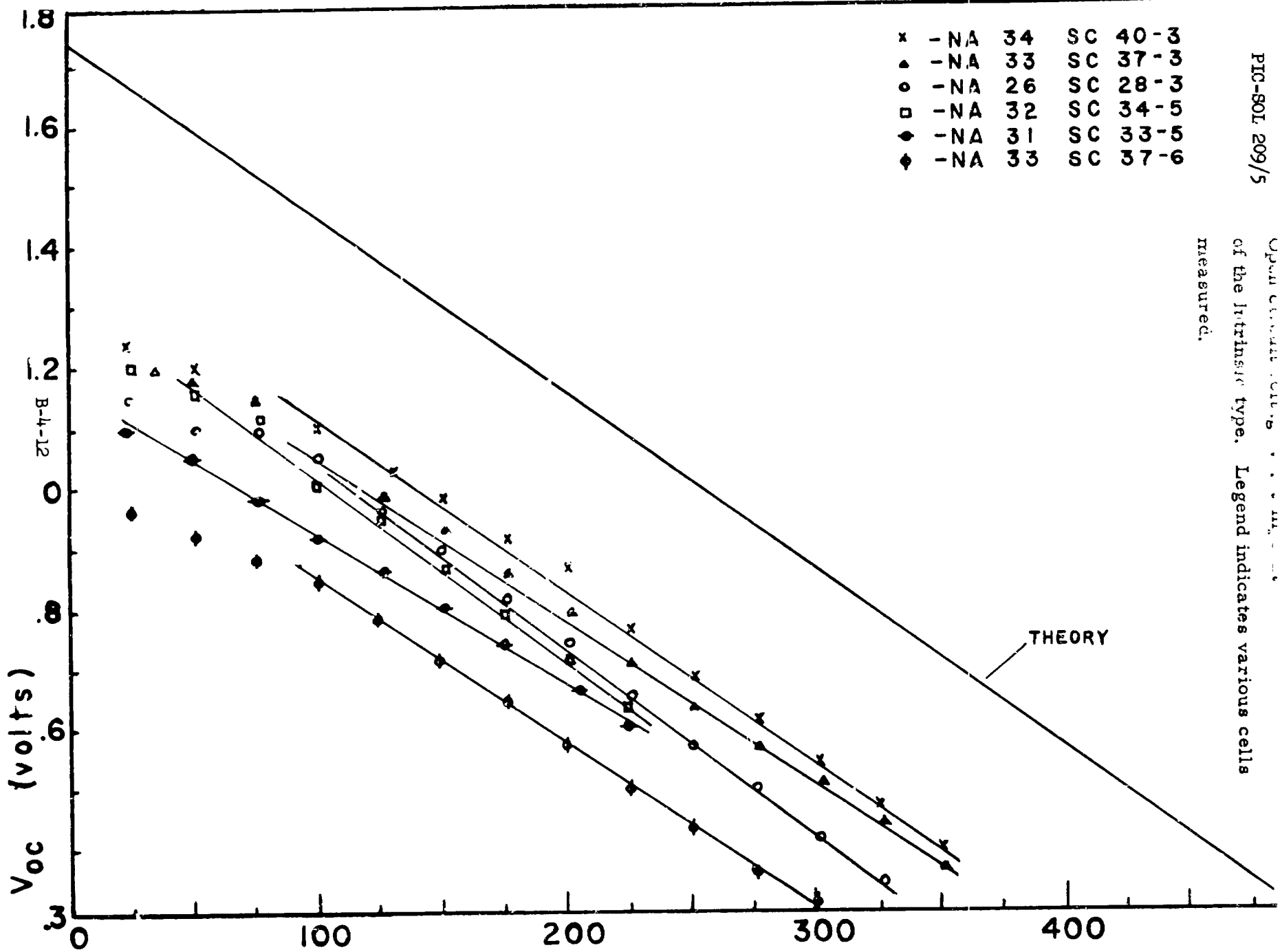


Fig. 2 I (ma)

Representative E-I curve taken in sunlight for sample NA31 SC34-3. Sample exhibits main spectral response at 0.45 μ . Maximum power point is at 0.608 mw. Efficiency is about 1%. Temperature of measurement was 23° C.

of the Intrinsic type. Legend indicates various cells measured.



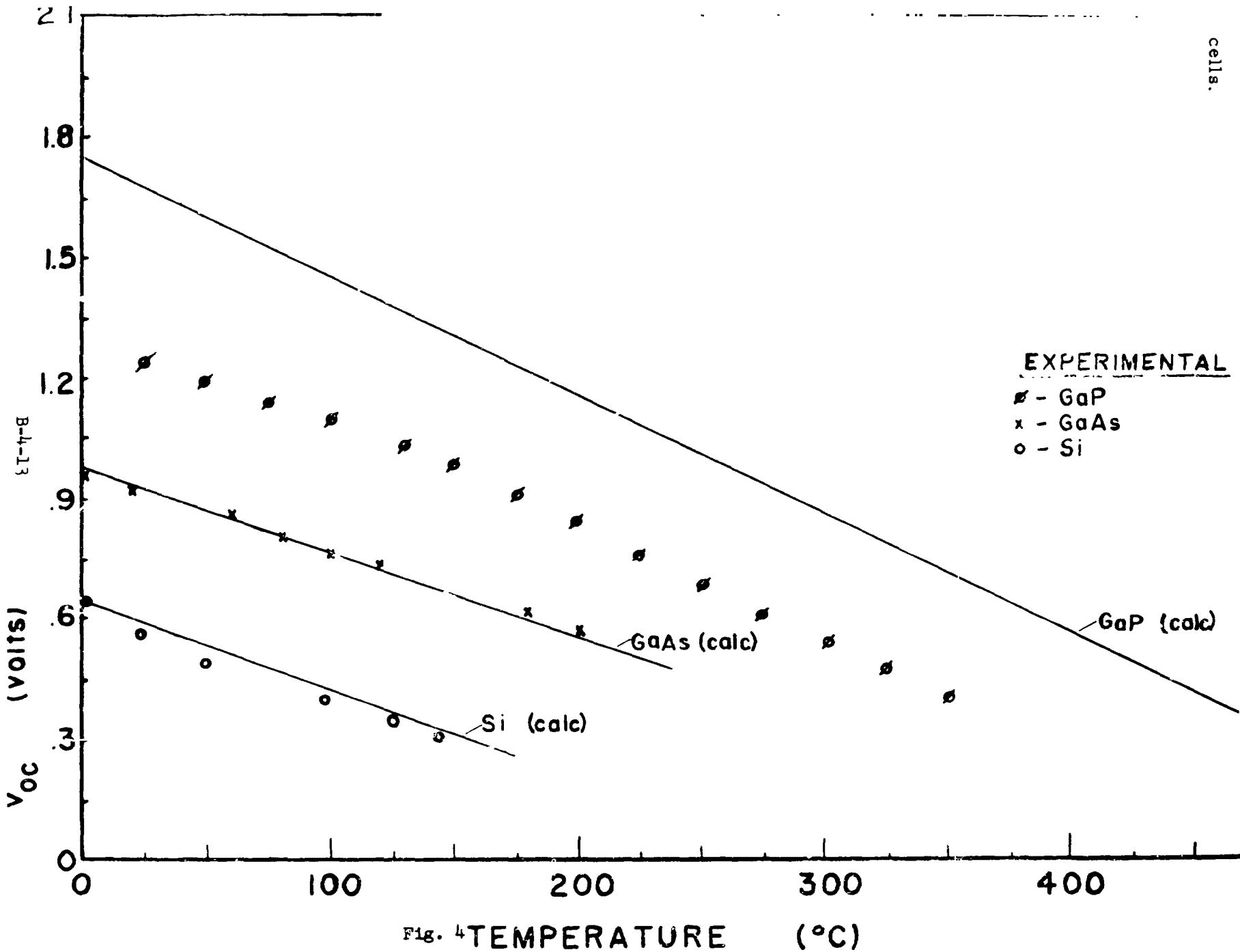
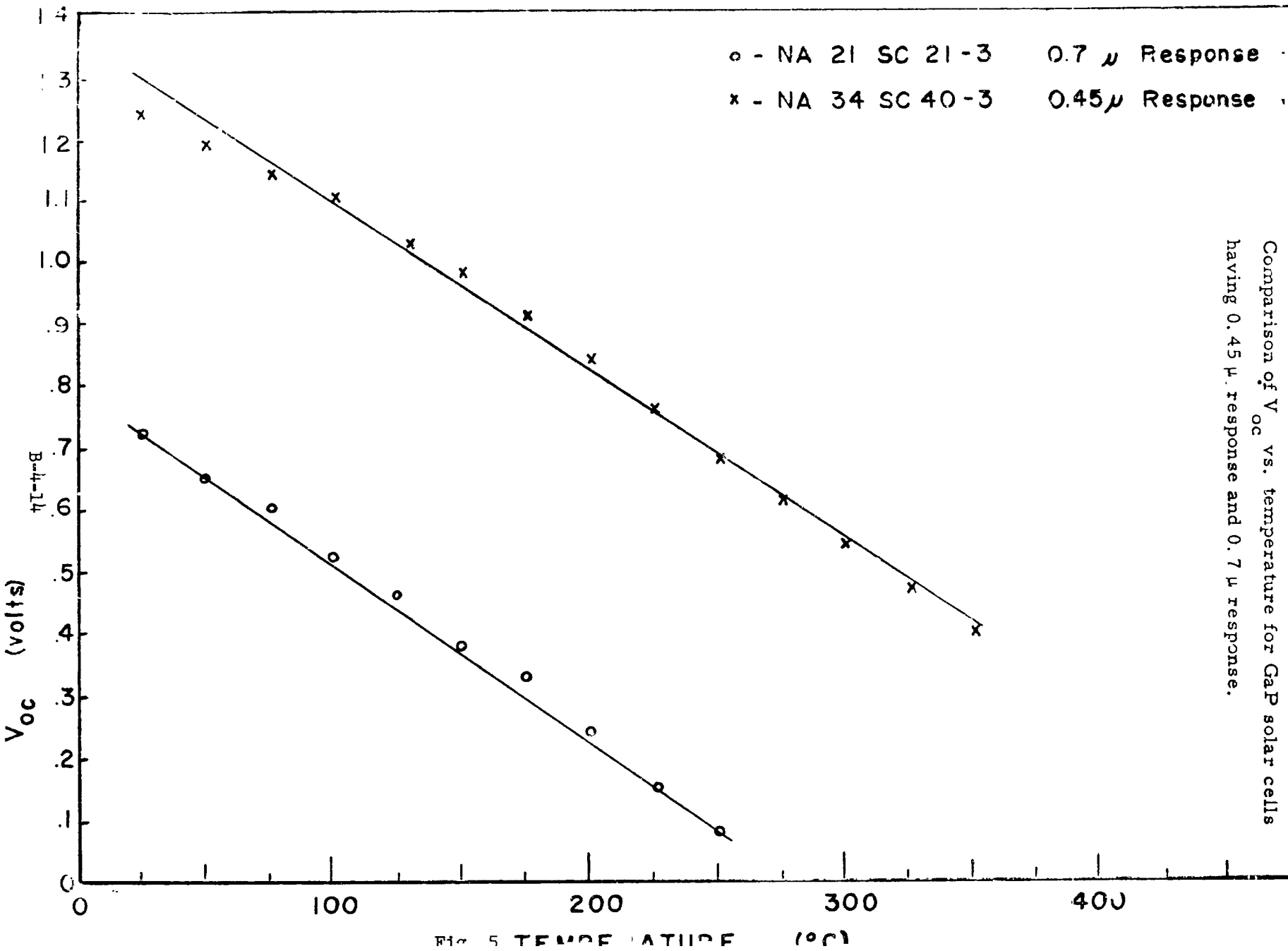
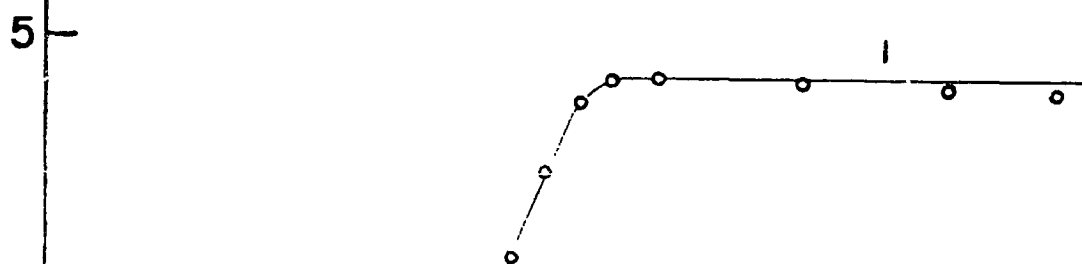


Fig. 4 TEMPERATURE (°C)

Comparison of V_{oc} vs. temperature for GaP solar cells having 0.45μ . response and 0.7μ response.



3 NA 25 SC 25-3 .04 0.15
 4 NA 21 SC 20-3 .05 0.45



Typical curves of short circuit current density vs.
temperature for both 0.45μ and 0.7μ response cells.

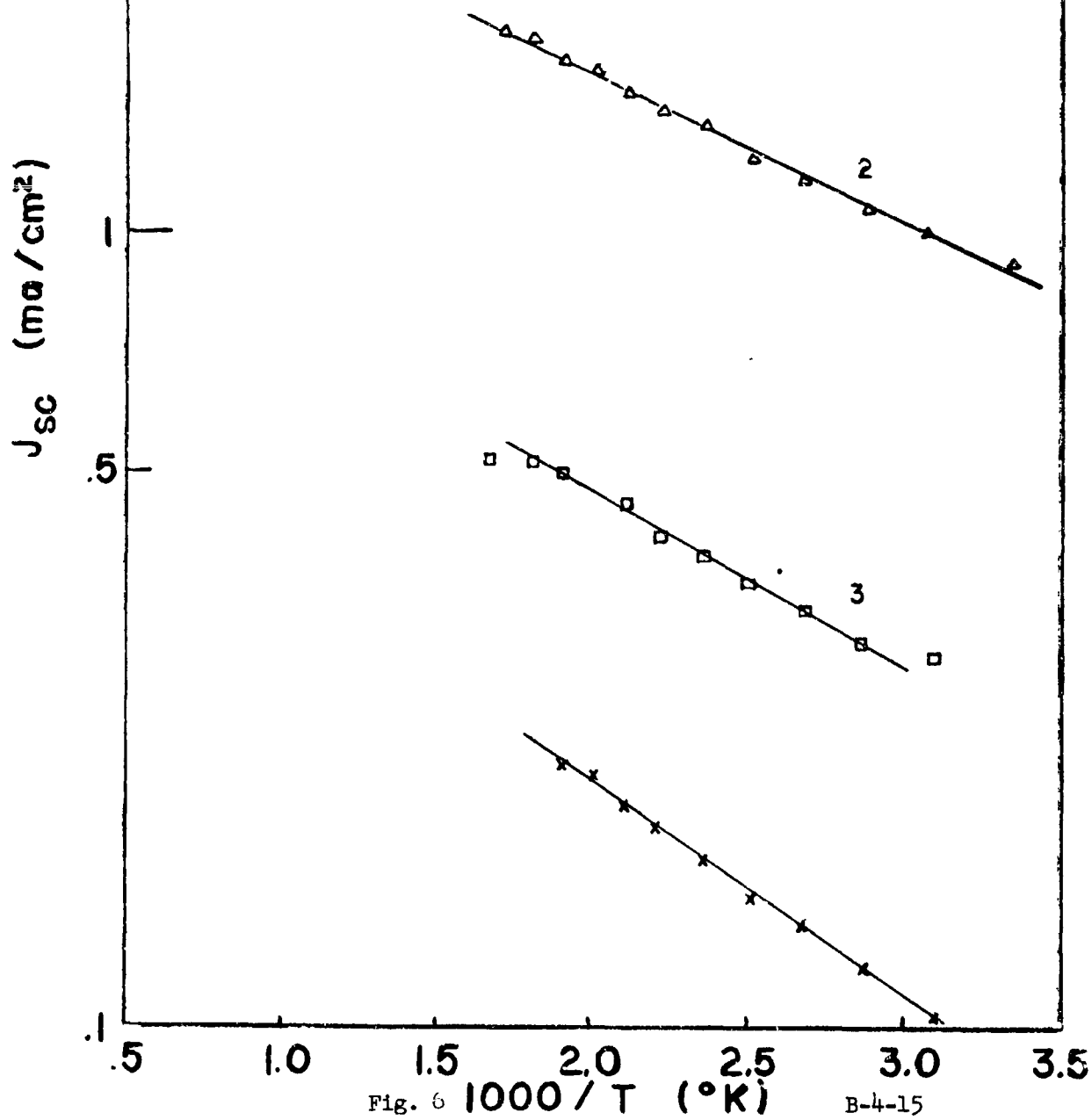
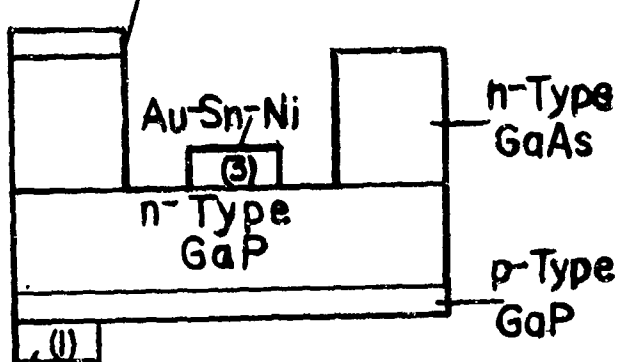


Fig. 6 $1000/T$ ($^{\circ}\text{K}$)

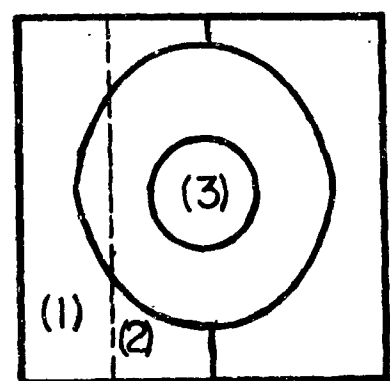
B-4-15

Au-Sn-Ni Contact (2)



Ag Contact

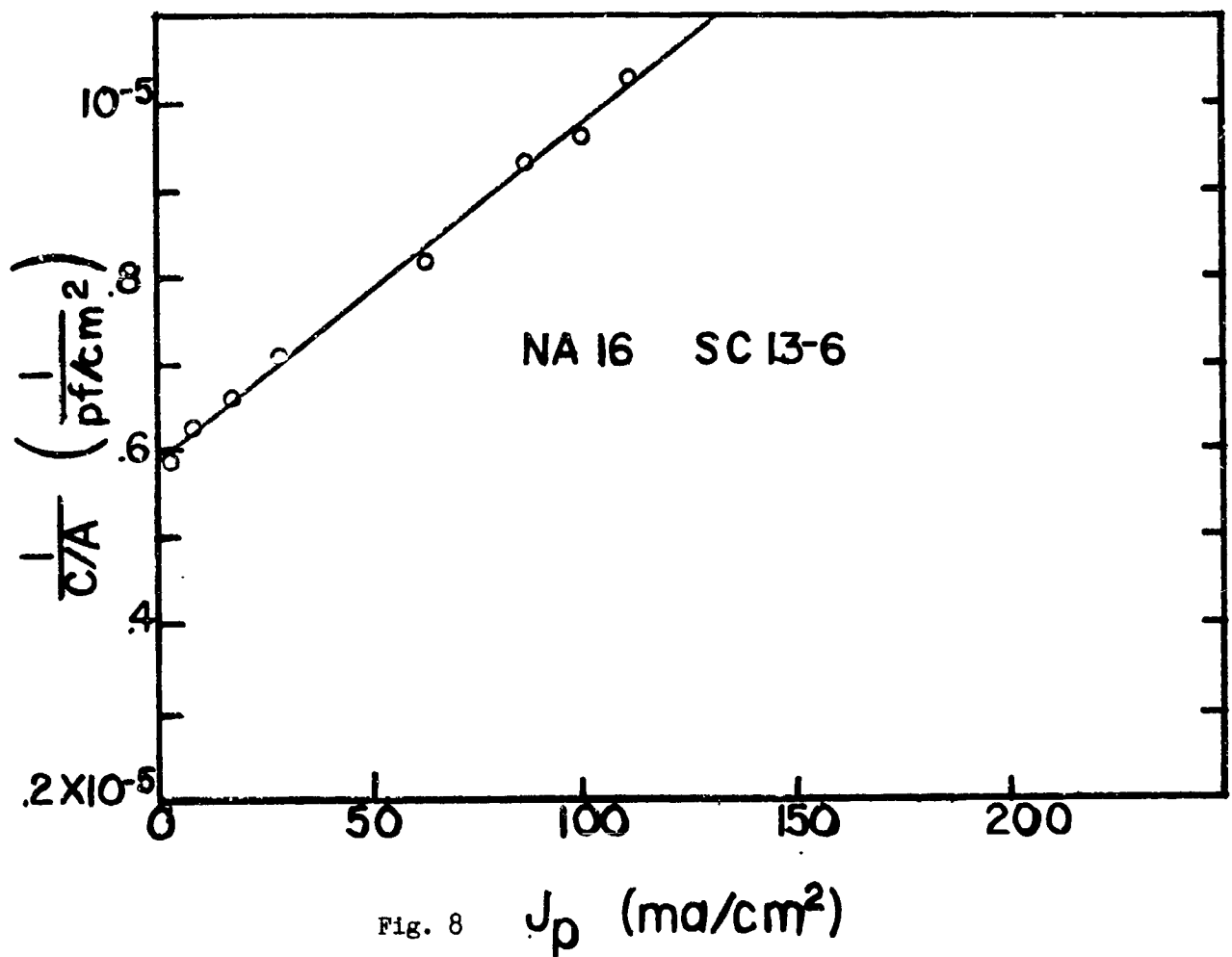
CROSS SECTION



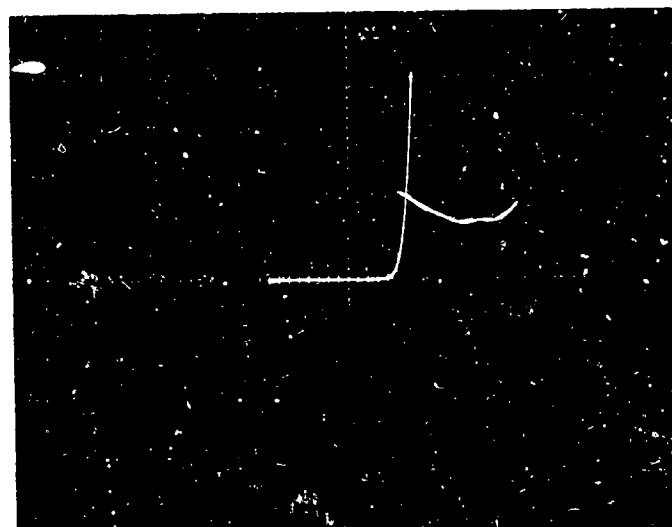
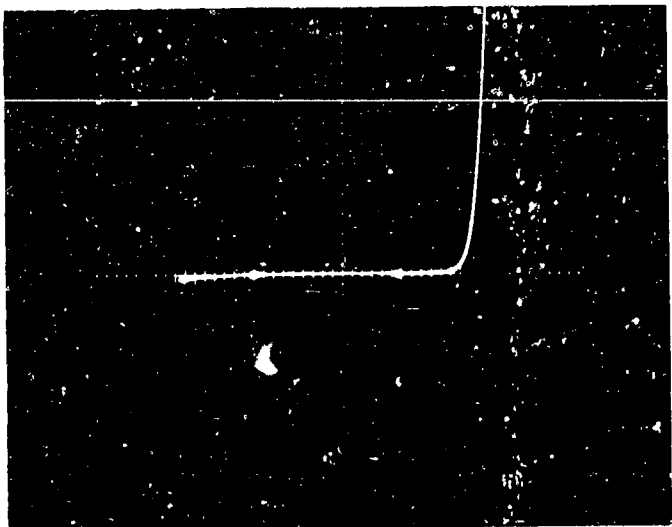
BOTTOM VIEW

Fig. 7

Experimental arrangement for checking effect of GaP-GaAs interface.



Sample of plot used for determining minority carrier diffusion length (from plot, $L_D = 150 \text{ } \overset{\circ}{\text{A}}$).



Best current-voltage traces obtained for a 0.45μ cell and a 0.7μ cell. Current, vertical axis, 0.2 ma/cm ; Voltage, horizontal axis, 0.5 volts/cm for both traces. Top trace, sample NA32 SC34-5, represents a 0.45μ cell. Lower trace, sample NA22 SC21-3, represents a 0.7μ cell.

Fig. 9
B-4-18

DISCUSSION

CHAMBERLIN-NATIONAL CASH REGISTER: Was the cell for which you etched away the GaAs layer, a .7 or .5 micron type?

MR. EPSTEIN: It was a .45 type.

CHAMBERLIN-NATIONAL CASH REGISTER: Did you measure spectral response with both front and back illumination?

MR. EPSTEIN: Yes, we did. They were both the same.

CUSANO-GENERAL ELECTRIC: Grimmeisen did some work on gallium phosphide, and he got efficiencies comparable to yours. He felt that there were series resistance effects, and that an efficiency of 7% could eventually be realized if you could eliminate the series resistance. Do you feel that this is a realistic estimate?

MR. EPSTEIN: Yes, I think it's reasonable.

CUSANO-GENERAL ELECTRIC: Was series resistance a limiting factor in your cells?

MR. EPSTEIN: No, but there was a great deal of it, as I implied from the capacity voltage curves.

QUESTION (NO NAME): Do you have any information about the crystalline imperfections present in your epitaxial layers?

MR. EPSTEIN: There are many imperfections. Also, the surfaces are not very smooth on the material that we have been making. In addition, there is a great deal of strain in the material resulting from the unequal thermal expansion coefficients of GaAs and GaP.

WOLF-HELIOTEK: You explained the 0.7 micron response by a two-step excitation process. If this is the case, how can you explain the low open circuit voltage associated with this cell?

MR. EPSTEIN: I'd rather not comment on that.

PERLMAN-RCA: I was wondering about the GaP layers. After you have grown them on the gallium arsenide, what preparation do you make of the surface prior to diffusion?

MR. EPSTEIN: We have tried a very light etch with hydrogen peroxide and sulphuric acid and water. We haven't found the most suitable etch yet.

PERLIN-RCA: Is the resulting surface finish matte or polished?

MR. EPSTEIN: It's not polished and it's not matte. It's somewhere in between.

GOLDSTEIN-RCA: To continue the line of trying to find an explanation for the difference between 0.7 and 0.45 micron cell, I am wondering if you ran impurity analyses on your grown gallium phosphide material?

MR. EPSTEIN: No, we didn't have enough material. This is one of the things we are trying to do now.

W64-2916A

EFFECT OF THICKNESS ON SHORT CIRCUIT CURRENT

Presented by

Martin Wolf

Heliotek, Division of Textron Electronics, Inc.

Sylmar, California

2 June 1964

2916A

Abstract

Reduced weight is still a desired feature for photovoltaic solar energy conversion systems for space vehicles. One approach to weight reduction is a decrease of the solar cell thickness. It has been found that the parameters of present high performance N/P silicon solar cells are such that even small reductions in the thickness of the cells result in noticeable decreases of the short circuit current due to lower collection efficiency at long wavelengths. Theoretical and experimental results of an investigation into the change of short circuit current as function of thickness are discussed. This effect is studied in dependence on the spectral distribution of the irradiating light for three commonly used types of light source as well as on the minority carrier lifetime and mobility in the base region of the solar cell. It is noteworthy that the differences in short circuit current are eliminated by moderate damage due to nuclear particle radiation.

Walter

EFFECT OF THICKNESS ON SHORT CIRCUIT CURRENT

by

M. Wolf and E. L. Ralph

Heliotek, Division of Textron Electronics, Inc.

Introduction

A reduction in the weight of photovoltaic energy conversion systems for space vehicles is still a desirable objective, even in view of the availability of boosters of higher thrust ratings. One approach to such weight reduction is through a decrease of the thickness of the silicon solar cells. Since the skills in handling fragile semiconductor devices have improved, this latter approach has gained renewed interest. In the process of fabricating solar cells of somewhat reduced thickness and of experimenting with cells of even further reduced thickness, it was found that the short circuit current and correspondingly the maximum available power output of the thinner cells were generally lower than those of thicker cells. This effect was especially noticed in tests carried out by use of tungsten filament light sources of 2800° Kelvin color temperature, but was less pronounced in tests performed in sunlight on Table Mountain and in a sunlight simulator. As a consequence of these early observations, an experimental and theoretical investigation of the problem was undertaken, the results of which are described in the following paragraphs.

Theoretical Considerations

Reference to data published earlier by Elliott¹⁾ (see Fig. 1) did not explain the recent experimental findings. The author's earlier curve²⁾ showing the ratio of the energy absorbed in silicon wafers of varying

-
- 1) J. F. Elliott, V. F. Meikleham, and C. L. Kolbe, "Large Area Solar Solar Cells", Academic Press, New York, Progress in Astronautics and Rocketry, Vol. III, Energy Conversion for Space Power, 1961
 - 2) M. Wolf, "Advances in Silicon Solar Cell Development", Academic Press New York, Progress in Astronautics and Rocketry, Vol. III, Energy Conversion for Space Power, 1961

thickness to that available in the air mass zero sunlight spectrum between .4 and 1.15μ (see Fig. 1), which was used for a quick estimate of the upper limit for thin film silicon solar cell performance, was too coarse an approximation to be applicable for the present problem.

In consideration of the collection mechanism of a solar cell, plotting that portion of photons available in the source spectrum which is absorbed in a silicon layer of given thickness as a function of this thickness might have yielded a better approximation. However, Fig. 1 indicates, that actual average collection efficiency curves do not parallel the curve for absorption of available photons. The reason is that the base region thickness considerably exceeds the diffusion length of minority carriers, thus making the excess portion of the wafer ineffective. At decreasing base region thicknesses, however, the back contact which represents a plane with extremely large surface recombination velocity, is brought in progressively closer proximity of the p-n junction. The closer proximity of this "sink" reduces the average minority carrier density in the base region and with it the collection rate at the p-n junction.

To gain better insight into the effect of thickness, the collection efficiencies and the resulting short circuit currents from the base region of silicon solar cells of varying thickness were calculated using the formulism developed earlier.^{3) 4)} The parameters entered into the calculation for 10 ohm centimeter p-type base material were an electron mobility of $1300 \text{ cm}^2 \text{ Volt}^{-1} \text{ sec}^{-1}$ and minority carrier lifetimes of 6, 12, and 24 microseconds, since minority carrier lifetimes measured in the bases of such solar cells range mostly from 10 to 25 microseconds. Added to the base region collection efficiency was the contribution from the diffused layer which was assumed to be identical to that found earlier for P/N

3) M. Wolf, "Limitations and Possibilities for Improvement of Photovoltaic Solar Energy Converters, Considerations for Earth's Surface Operation" Proc. IRE, vol. 48, pp. 1246-1263; July, 1960

silicon solar cells⁴⁾. This contribution corresponds to an n-region thickness of 0.5 microns with a minority carrier lifetime of 5×10^{-10} seconds, a hole mobility $10 \text{ cm}^2 \text{ Volt}^{-1} \text{ sec}^{-1}$, and a surface recombination velocity of $5 \times 10^3 \text{ cm per second}$.

Obtained from these calculations were curves of collection efficiency as function of wavelength, such as that shown in Fig. 2 for solar cells with an electron lifetime in the base of 24 microseconds and with base region thicknesses of 0.05 cm (0.020 inches) and 0.02 cm (0.008 inches) respectively. These collection efficiencies were multiplied for each wavelength interval with the photon flux of the corresponding interval in the spectrum of the light source considered, and the products were totalled. Division of this sum by the total number of photons yields an average collection efficiency which is weighted by the photon distribution of the light source. Figure 1 contains several curves of weighted average collection efficiency as function of base region thickness for three light sources considered: sunlight of airmass 0⁵⁾, sunlight of airmass 1 similar to that received on Table Mountain, California,⁶⁾, and light from a tungsten filament bulb of 2800° Kelvin color temperature. Also included in Fig. 1 is a curve for a low resistivity N/P silicon solar cell with a base region electron mobility of $800 \text{ cm}^2 \text{ Volt}^{-1} \text{ sec}^{-1}$ and an electron lifetime of three microseconds. The figure illustrates the differences in the effect of thickness on weighted average collection efficiency caused by variations of minority carrier lifetime and mobility, but also indicates that these differences are vanishing at base region thicknesses below .01 centimeter. The curve also verify the observation of a larger effect of base region thickness on weighted average collection efficiency in light with a higher relative content of low energy photons and the expectation of a diminishing of the effect in solar cells with low base region minority carrier lifetime and mobility.

-
- 4) M. Wolf, "Drift Fields in Photovoltaic Solar Energy Converter Cells," Proc. IEEE, vol. 51, pp.674-693; May 1963
 - 5) F. S. Johnson, "The Solar Constant," J. Meteorology, vol. 11, pp. 431-439, December 1954
 - 6) P. Moon, "The Scientific Basis of Illuminating Engineering" Dover Publications, New York, pp. 117-126; 1961

Experimental Results and Comparison with Theory

To substantiate and to expand beyond the early observations, which were made on cells in the thickness range of 0.033 to 0.046 cm (0.013 to 0.018 inches), several groups of N⁺/P silicon solar cells with 10 ohm centimeter base resistivity and diffused regions of about half micron thickness were prepared with evaporated titanium-silver contacts, except for two groups of 0.020 cm (0.008 inches) and 0.046 cm (0.018 inches) thickness, which were prepared with the older type plated gold-nickel contacts (represented by symbol "+" in Fig. 3). The preparation of the groups with plated contacts resulted from the earlier observations on cells with this older type of contact, which showed a larger change of short circuit current as function of thickness than could be explained by theoretical considerations. It had been hypothesized that the sandblasting of the wafer, which takes place before deposition of the back contact in the process of applying the plated contacts, might cause penetrating damage to the crystal structure and thus result in an effective thickness smaller than the actual thickness of the cell. In the preparation of the cells with evaporated contacts, silicon was removed prior to the contact application by an etching process, which was not expected to cause penetrating damage. The experimental data, however, did not confirm the hypothesis since the evaporated contact cells showed the same large change of short circuit current with thickness as the plated contact cells (Fig. 3).

Cells were prepared both in the 1x2 cm and in the 2x2 cm sizes in a number of batches of varying quantities in order to obtain sufficient statistical data, since it has to be remembered that investigations of this kind are afflicted with a certain spread of data caused by the large number of process variables. The short circuit currents measured in light from three types of sources, namely from tungsten filament bulbs of 2800° Kelvin color temperature, from sunlight approximating air mass one as received on Table Mountain, California, and from the Spectrosun Solar Simulator were averaged for the various thickness groups. These averages

were then expressed as ratios to the average of the corresponding group of largest thickness and normalized so that the averages of the groups of largest thickness coincide with the theoretical curves. This data is presented in Fig. 3 as experimental points represented by various symbols for the different types of cells and light sources used. Each set of experimental data points was normalized to both sets of theoretical curves for 12 microseconds and 24 microseconds minority carrier lifetime, with the first normalization indicated by hollow symbols and the latter by identical, but filled symbols.

Also shown in Fig. 3 are calculated curves of the relative short circuit current, expressed as a ratio of short circuit current at solar cell thickness d to the short circuit current of a 0.1 cm thick solar cell, both for air mass zero sunlight and for light from a tungsten filament source of 2800° Kelvin color temperature, and for minority carrier lifetimes of 6, 12, and 24 microseconds in 10 ohm centimeter N/P cells. Comparison of the experimental points with the theoretical curves indicates that the fit is good above 0.03 cm of thickness. However, below this value the experimentally observed short circuit currents decrease with thickness nearly at twice the rate of the calculated currents. In order to obtain a better match between the calculated and the experimental data, much larger base region minority carrier lifetimes would have to be assumed. Direct measurements of base region minority carrier lifetimes let such an assumption appear unreasonable.

Figure 4 shows the calculated normalized spectral responses for four solar cells, having base region thicknesses of .05 cm and .02 cm, and base region minority carrier lifetimes of 24 microseconds and 6 microseconds. While the collection efficiency curve, Fig. 3, showed no effect of base region thickness on the short wavelength portion of the curve - and would similarly have shown no effect of change in minority carrier lifetime - but indicated considerable change in the long wavelength portion of the curve, the normalization performed on the spectral

response curve results in a small variation of the short wavelength portion of the curve and a slight reduction of the effect on the long wavelength portion of the curve. It is interesting to note that changes of minority carrier lifetime and changes of base region thickness both have similar effect on the change of the spectral response curve, although a slight difference in the shape of the long wavelength portion of the curve will be observed between the thickness change and the minority carrier lifetime change.

Also shown in Fig. 4 are experimental spectral response points obtained from two typical N/P 10 ohm centimeter base silicon solar cells of 0.045 cm and 0.019 cm base region thickness. For both cells, the experimental spectral response points were extrapolated to zero reflection, using measured spectral reflectance data⁷⁾. The shape of the experimental spectral response curves of the two cells deviates considerably from that of the calculated spectral response curves, but the difference between the two experimental curves agrees very well with the difference of the calculated curves. Correspondingly, calculation of the short circuit currents in air mass one sunlight and light from a tungsten filament bulb (2800° Kelvin color temperature) using the unnormalized experimental spectral response curves of the two cells, which were measured on an identical, although otherwise unknown, absolute base, resulted in experimental points (symbol "x" in Fig. 3) extremely close to the calculated curves although the measured short circuit currents of these two cells were very close to their group averages. The deviation in shape between the experimental and the theoretical spectral response curves is such as to indicate considerably smaller minority carrier mobility or lifetime in the base region than used in the calculation. Such an assumption would be contrary to the previously mentioned assumption needed to obtain better fit to the measured effect of thickness on short circuit current (normalized to the 12 microsecond minority carrier lifetime curves).

7) E. L. Ralph and M. Wolf, "Effect of Anti-reflecting Coatings and Coverglasses on Silicon Cell Performance," presented at the 4th Annual Photovoltaic Specialist's Conference, Cleveland, Ohio; June 2nd and 3rd, 1964

Of interest to the measurement of silicon solar cell performance and to the application are the so-called "tungsten light to air mass one degradation factor" and the "air mass one to air mass zero extrapolation factor." The "tungsten light to air mass one degradation factor" expresses the ratio of short circuit current measured on any particular solar cell in air mass one sunlight to the short circuit current measured on the same solar cell under light from a tungsten filament source of 2800° Kelvin color temperature set to an arbitrary, but carefully maintained constant light intensity. This "tungsten light to air mass one degradation factor" is a function of the spectral response of the solar cell tested. This factor has been calculated for the 10 ohm centimeter N/P silicon solar cell with 24 microsecond minority carrier lifetime in the base region, but of varying base region thickness. The data have been normalized to a "tungsten light to air mass one degradation factor" of .95 for the 0.05 cm base region thickness, a value which is typically observed in cells of this type. The resulting theoretical curve shown in Fig. 5 illustrates that with decreasing thickness of the base region the degradation turns into an appreciation, all other solar cell parameters being constant. Also entered into the plot have been experimental points which indicate a much more rapid increase of the degradation factor with decreasing base region thickness. This observation corresponds with the comments made with respect to Fig. 3.

Also shown in Fig. 5 is the "air mass one to air mass zero extrapolation factor" which is the ratio of short circuit current expected to be obtained under air mass zero sunlight irradiation to the short circuit current obtained under air mass one sunlight irradiation. Although the irradiance of air mass zero sunlight is larger by a factor of 1.40 than the irradiance of standardized air mass one sunlight, the overall collection efficiency of a solar cell is smaller for air mass zero sunlight than it is for air mass one sunlight (compare Fig. 1), since the two types of sunlight have a different spectral distribution. Only a

small variation of the "air mass one to air mass zero extrapolation factor" with a change of solar cell spectral response will be expected. This change of "air mass one to air mass zero extrapolation factor" is plotted as a function of base region thickness in Fig. 5. It may be observed that the extrapolation factor shown here is very close to most other calculated values, although it is larger by as much as 5% than the values obtained by high altitude balloon flight calibrations and other various experimental methods for determining solar cell output in air mass zero sunlight. The difference may be in a scale factor, but could also be based on a difference in the spectral distributions on which the calculations are based. In the latter case, a variation of the calculated "air mass one to air mass zero extrapolation factor" as a function of base region thickness might occur.

Base Region Thickness and Radiation Resistance

Since the reduction of base region thickness affects only the long wavelength portion of the solar cell spectral response, and since the effect of decreased base region thickness is similar to that of reduced minority carrier lifetime, it is reasonable to expect a decreased effect of nuclear particle radiation on the short circuit current of silicon solar cells of reduced thickness. Calculations for change of short circuit current with irradiation by 1 MeV electrons analogous to those described in reference 4) have been carried out for 10 ohm centimeter N/P silicon solar cells of .05 centimeter and .015 centimeter base region thickness, respectively. Figure 6 presents the resulting data. It shows the difference in short circuit current density in air mass zero sunlight between the normal and the reduced thickness solar cells before the onset of radiation damage and verifies expectation of a less severe effect of moderate integrated fluxes of 1 MeV electrons on the thinner cell. The result is that both types of cells exhibit equal short circuit current densities at integrated fluxes of more than 10^{14} 1 MeV electrons cm^{-2} .

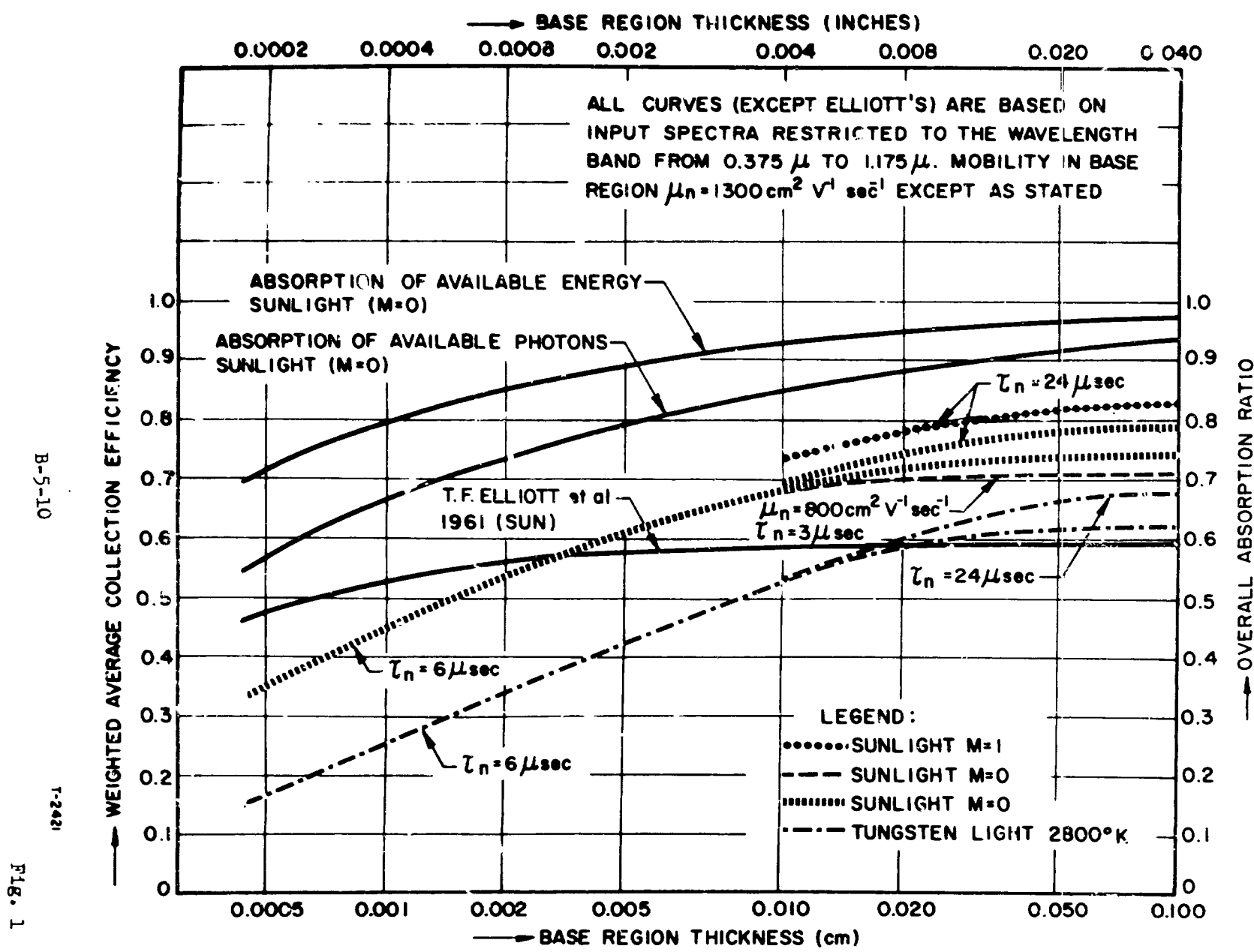
Thus reduced thickness of the solar cell base region has the interesting side effect of decreased sensitivity to high energy particle radiation. This effect will be welcomed in all those cases, where the dissipation of excess power during the early part of the space vehicle mission creates problems. The effect will be considered undesirable, however, in those cases where the additional power provided by the thicker cells would be needed during the early portions of the space vehicle life.

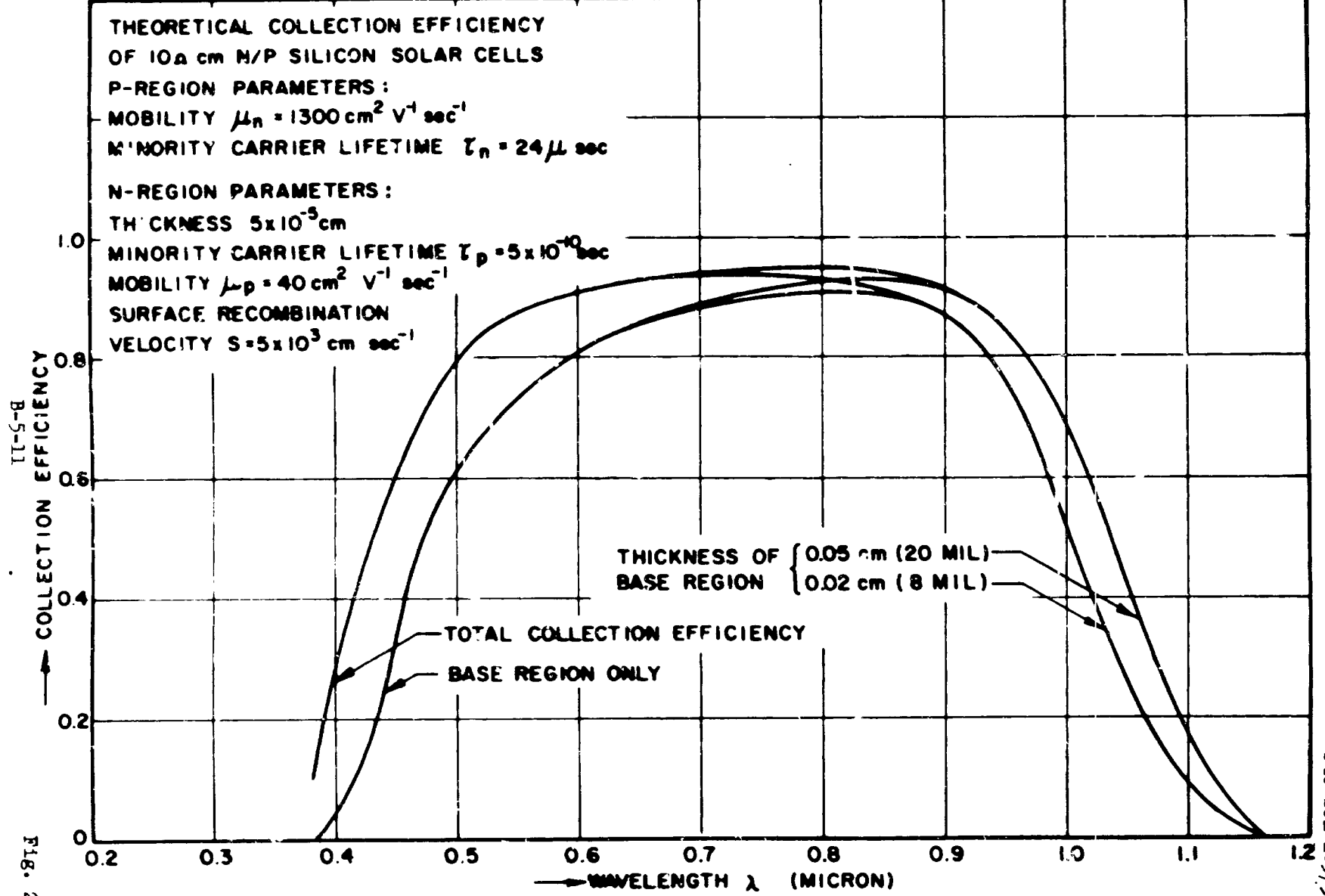
Conclusion

A decrease of short circuit current density with reduced thickness of silicon solar cells has been observed. This decrease is explainable by theory and could have been expected. Discrepancies between experimental and theoretical data have, however, been found, which are not yet resolved and are being investigated further. An interesting side effect is the decreased radiation sensitivity of the thinner solar cells, which in some cases may be desired as much as the reduced weight.

Acknowledgement

The authors wish to express their thanks to numerous coworkers, but especially to Mr. R. L. Oliver for bringing attention to the effect through his early observations and to Mr. W. von der Ohe, for the preparation of the samples and for various measurements.





B-5-12

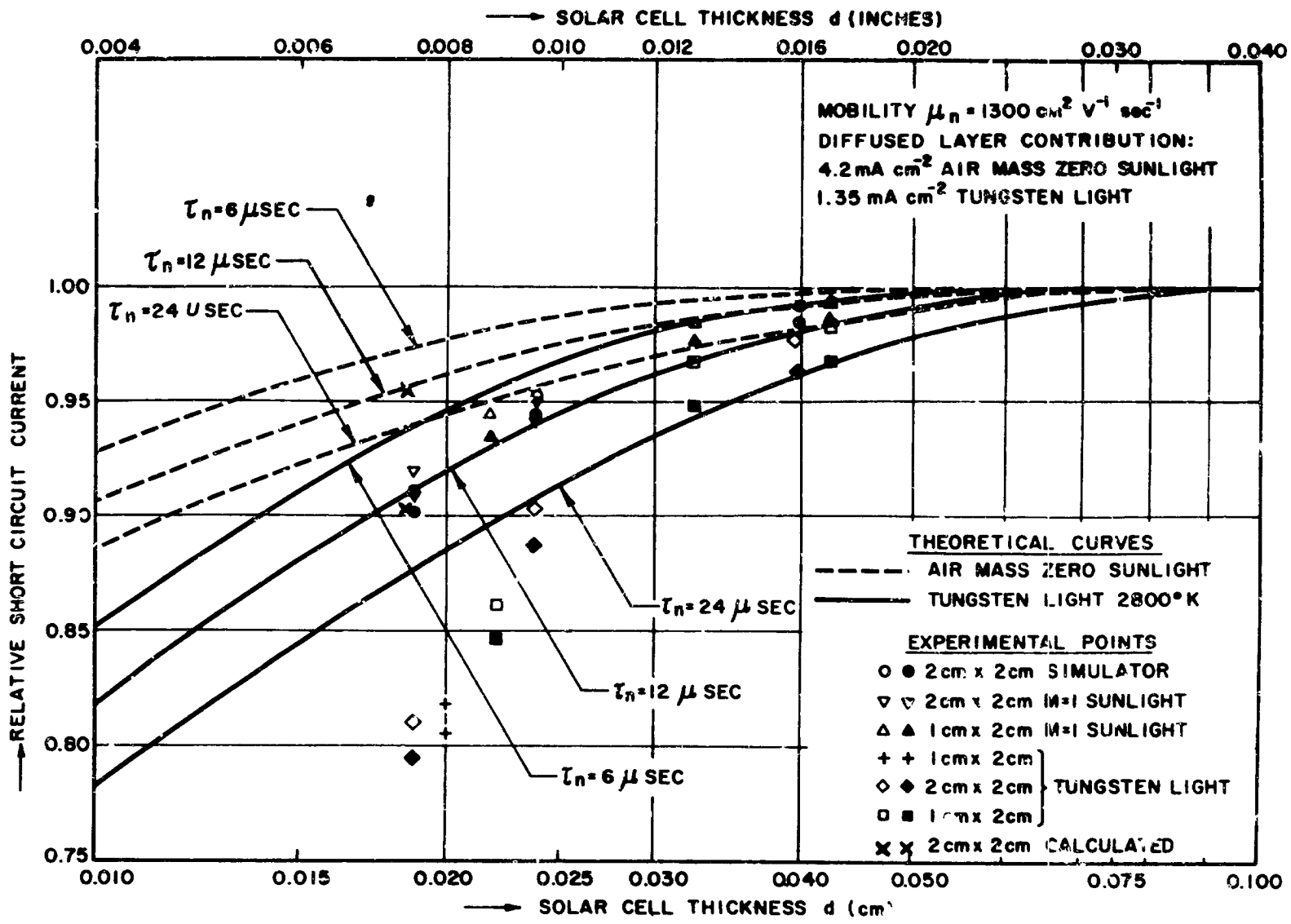


FIG. 3

B-5-13

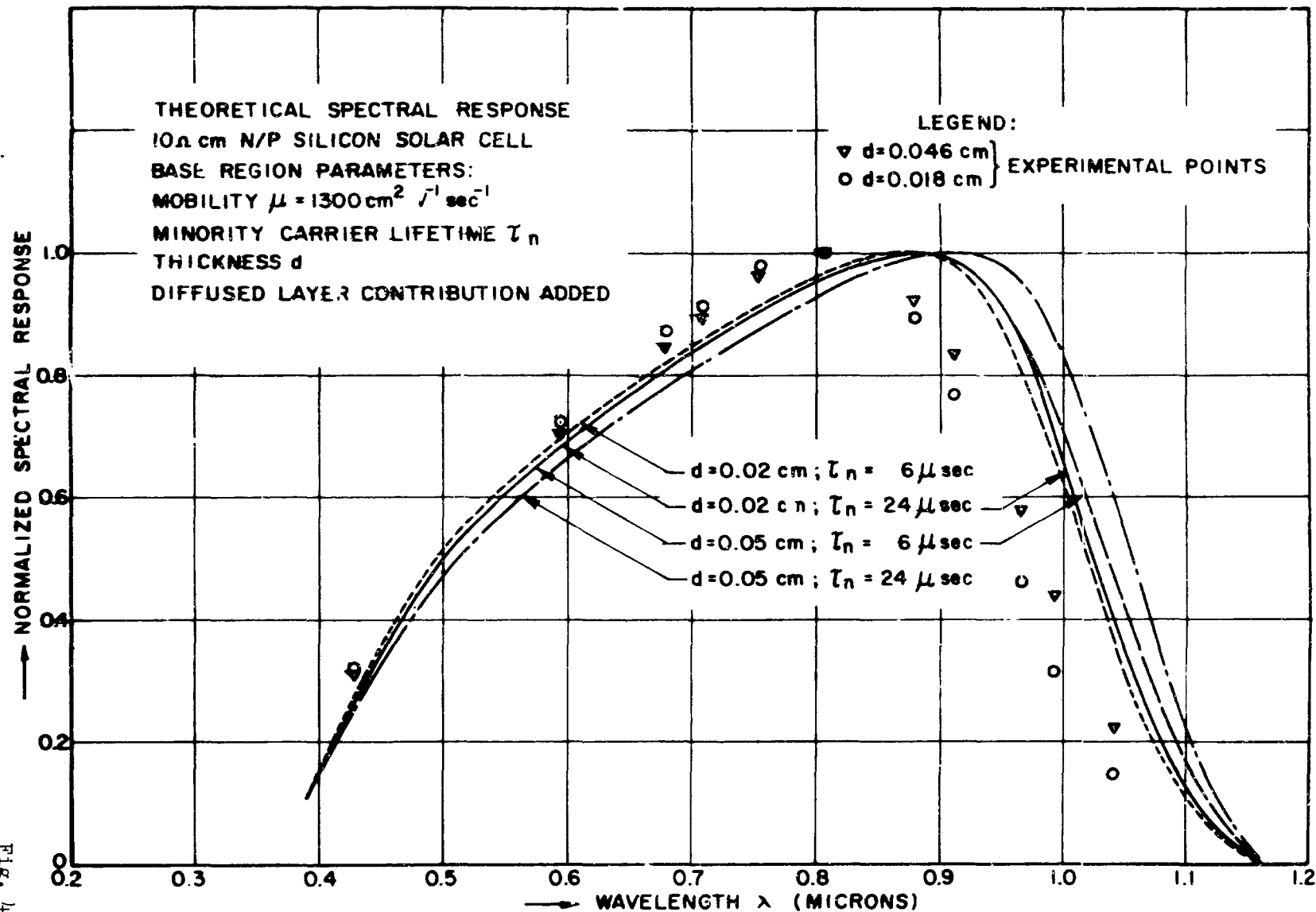
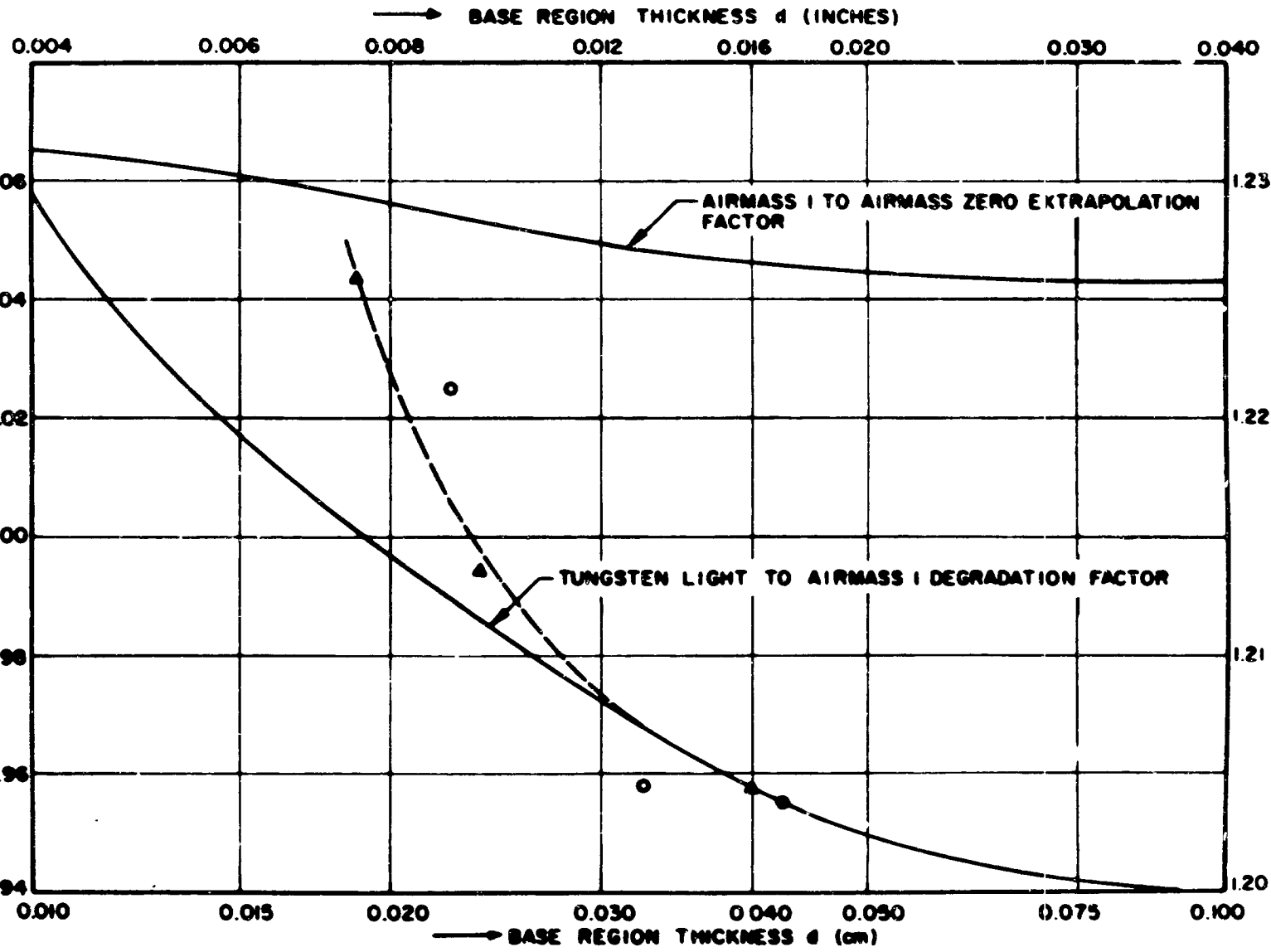


FIG. 4

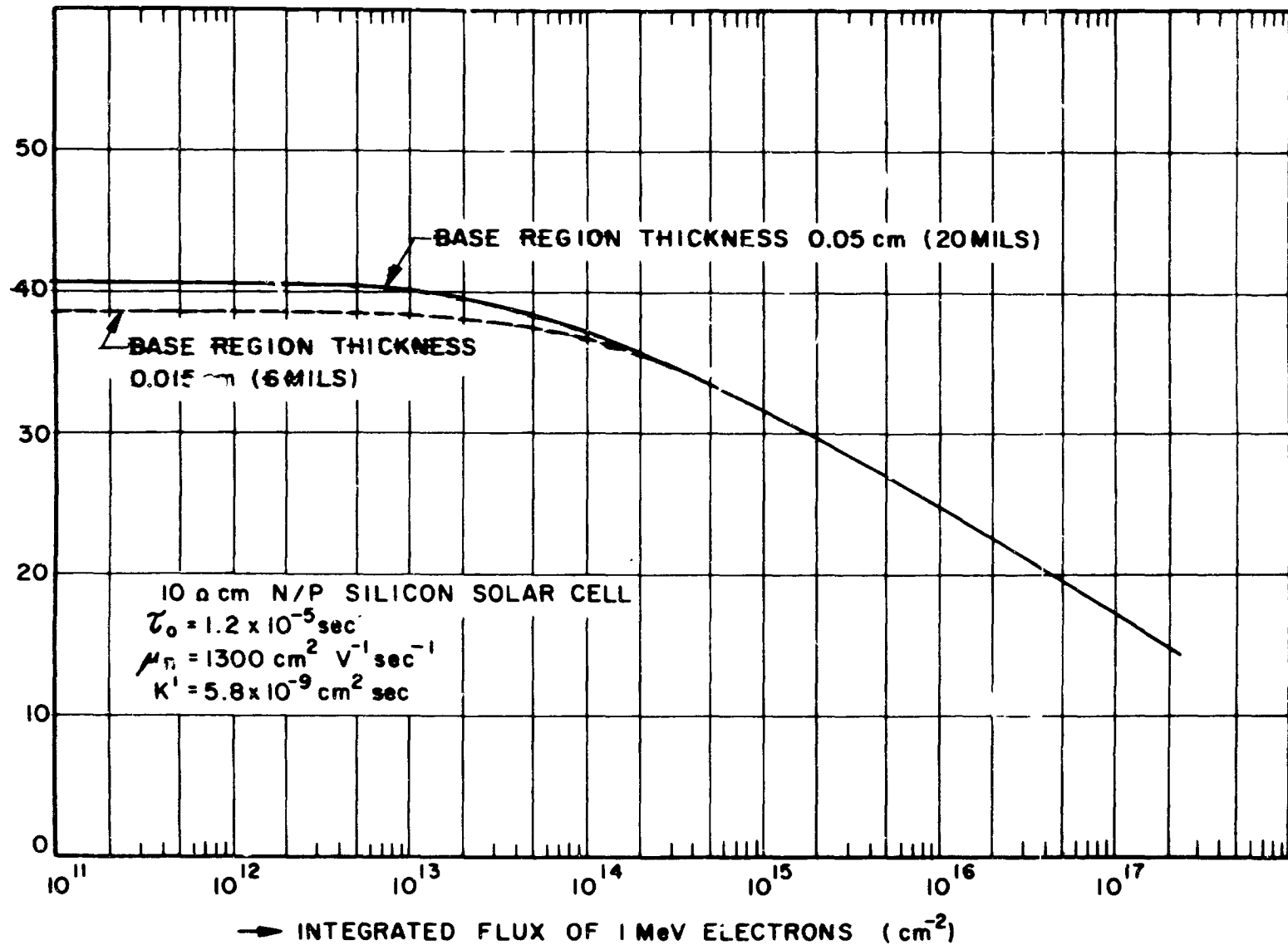
→ TUNGSTEN LIGHT TO AIR MASS I (TABLE MOUNTAIN) DEGRADATION FACTOR



PIC-SOL 209/5

FIG. 8T-8

→ SHORT CIRCUIT CURRENT DENSITY (mA cm⁻²)
(AIR MASS ZERO SUNLIGHT)



Page intentionally left blank

DISCUSSION

KAYE - FOS: Could you say what assumptions you made about the nature of the back contact? What was the value of the surface recombination velocity?

MR. WOLF: Infinite surface recombination velocity.

KAYE - EOS: Did you consider the effect of noninfinite surface recombination velocity on the shapes of your curves? It might explain the discrepancy between experiment and theory.

MR. WOLF: No, it would not explain the difference.

MANDELKORN - NASA, LEWIS: We are making cells without etching of the order of 6 to 8 mils in thickness. Our results under our simulator show that, for approximately 150 micron base diffusion length, we lose absolutely no current for the 8 mil thickness and for the 6 1/2 mil thickness we lose only about 5 percent. We feel that the 6 mil thickness is good to stick with in terms of radiation damage, while the 8 mil gives you absolutely no loss of current.

MR. WOLF: The 150 micron diffusion length comes close to the case calculated here for a 6 microsecond minority carrier lifetime. This was considerably flat down to the region of thickness you are speaking about.

MANDELKORN - NASA, LEWIS: Increasing the diffusion length from 150 microns to 200 microns gives hardly any increase in the short circuit current. This is why we achieve great uniformity of short circuit current in our 10 ohm centimeter cell, because we are always above where the diffusion lengths have any great influence on the short circuit current.

PIC-SOL 209/5
Section B-6

SOLAR CELL PERFORMANCE AT HIGH TEMPERATURES

Presented by

Jacob D. Broder

NASA-Lewis Research Center

Cleveland, Ohio 44135

2 June 1964

N64-29168

SOLAR CELL PERFORMANCE AT HIGH TEMPERATURES

by Jacob D. Broder, Harold Kautz, Joseph Mandelkorn,
Lawrence Schwartz, and Robert Ulman

Lewis Research Center
National Aeronautics and Space Administration
Cleveland, Ohio

Various space missions can be envisioned which would subject the solar cells of a space vehicle to temperatures higher than 75°C. Questions arise as to what performance to expect of silicon solar cells, and what, if any, substitute cells can be used to better advantage at these high temperatures.

In this paper, the temperature behavior of various resistivity, unbombarded and bombarded silicon cells and unbombarded and bombarded GaAs cells will be discussed and compared. The characteristics to be discussed are: the open circuit voltage, the maximum power output, and the curve power factor, which is defined as the maximum power output divided by the product of the short-circuit current and open-circuit voltage.

$$\text{CPF percent} = \frac{P_0}{V_{OC} \times I_{SC}} \times 100$$

Table I shows typical outer space characteristics of unbombarded cells at 25°C. These are the values that can be achieved at the present time

TABLE I. - EQUIVALENT OUTER SPACE CHARACTERISTICS

	V_{OC} , V	R_C , Ohms	I_{SC}/cm^2 , ma/cm ²	P_0/cm^2 , MW/cm ²	V_{MP} , V	CPF, per- cent	Efficiency $1\text{ cm} \times 2\text{ cm}$ percent
GaAs	0.9	0.3	11	7.2	0.7	73	5.1
GaAs	.9	.3	16	10.0	.7	70	^a 7.1
Si:							
1 Ohm cm	.57	.3	32	12.6	.43	69	9.0
10 Ohm cm	.54	.3	36	14.0	.44	72	10.0
50 Ohm cm	.49	.4	36	11.5	.42	65	8.2
100 Ohm cm	.43	.7	36	8.5	.3	55	6.0

^aManufacturer's quoted sunlight efficiency, 10.5 percent.

for various resistivity n on p silicon solar cells. In going from 1-, to 10-, to 50-, to 100-ohm-cm cells, the open-circuit voltage decreases. The small increase in short-circuit current for 10-ohm-cm cells occurs because of the longer diffusion lengths in 10-ohm-cm cells. The short-circuit current remains at this value for the higher resistivity cells since the processing reduces the diffusion lengths to approximately equal values.

The curve power factors of the 10-ohm-cm cells are better than the 1-ohm-cm cells because junctions with better characteristics can be made in 10-ohm-cm material. However, as the resistivity increases, the maximum power output decreases due to both the lower open-circuit voltage and the increasing bulk parasitic resistance. Maximum efficiencies are achieved for 10-ohm-cm cells.

Considering the two categories of GaAs cells (Table I), the 5 percent cells were procured commercially and the 7 percent cells were obtained through the courtesy of the U.S. Air Force, Wright Development Center. The efficiencies quoted are based on airplane measurements that agree with Lewis simulator measurements.

Figure 1 shows the change in open circuit voltage as a function of temperature for various resistivity silicon solar cells. There is a 0.2 mv/ $^{\circ}$ C difference between the coefficients for 1- and 10-ohm-cm cells; a negligible difference between 10- and 20-ohm-cm cells and a significant difference of 0.6 mv/ $^{\circ}$ C between the coefficients of 1- and 80-ohm-cm cells. Similar temperature coefficients of open-circuit voltage were obtained for solar cells doped to equivalent resistivities with either aluminum, gallium, indium, or gadolinium.

Another important factor in the temperature degradation of solar cells is the change of curve power factor with temperature as shown in Figure 2. The curve power factor of 10-ohm-cm cells degrades faster than that of 1-ohm-cm cells, and that of 80-ohm-cm cells degrades most rapidly with increasing temperature. This decrease of curve power factor occurs because junction losses increase with increasing temperature.

The degradation of open circuit voltage and of curve power factor leads to degradation of maximum power output as shown in Figure 3. For these measurements the short-circuit current was maintained constant for all temperatures at a value equivalent to 25 $^{\circ}$ C outer space current. A measure of the power degradation is indicated by the temperature at which the power has fallen to half that at 25 $^{\circ}$ C and is given by the coefficient expressed as percent-power-lost per $^{\circ}$ C. As the resistivity of the base material is increased, the half-power point occurs at lower temperatures. For 1-ohm-cm cells, the half-power point occurs at about 135 $^{\circ}$ C; for 10-ohm-cm cells it is about 20 $^{\circ}$ lower; and for 80-ohm-cm cells, it occurs below 100 $^{\circ}$ C. The same values of half-power point have been found for silicon doped with materials other than boron.

From the above considerations it is apparent that the 1-ohm-cm cell would be the most useful for high temperature applications.

One- and 10^{18} ohm-cm silicon cells were subjected to an electron bombardment of 1.5×10^{18} -1 Mev electrons per cm^2 . The open circuit voltages were measured at various temperatures below 100°C with the illumination level such that the short-circuit currents were equivalent to those the cells would have in outer space. There is no observable change in the temperature coefficient of open-circuit voltage after this level of bombardment. The same is true for proton-bombarded cells, bombarded to a dose of 3.9×10^{12} -10 Mev protons per cm^2 , which is equivalent in damage production to approximately 1×10^{18} -1 Mev electrons per cm^2 .

Figure 4 is a plot of curve power factor versus temperature for 1- and 10-ohm-cm, unbombarded and bombarded cells. Since the plots are straight lines in this temperature range, a coefficient can be determined. There is a significant change in the rate of decrease of the curve power factor with temperature for bombarded cells. The same behavior is also found for proton-bombarded cells. The change in power output degradation of bombarded cells also depends upon the variation of short-circuit current with temperature. Bell Laboratories reports (private communication) that the short-circuit current increases with temperature at a rate of 0.2 percent per $^\circ\text{C}$ for heavily bombarded cells. Based on our measurements and calculations, the half-power point and temperature coefficient of power output for bombarded cells will be similar to those of unbombarded cells.

The power supplies of satellites are usually designed for constant-voltage operation. Therefore, bombarded solar cell power output was studied as a function of temperature for various constant-voltage conditions. Figure 5 shows the power output for 1- and 10-ohm-cm electron-bombarded cells. For maximum power output at 55°C , the voltage for constant-voltage operation should be 0.3 V for 1-ohm-cm and 0.25 V for 10-ohm-cm cells. For operation at 75°C , the voltages are 0.325 V for 1-ohm-cm cells and 0.2 V for 10-ohm-cm cells. Between 75°C and 100°C maximum power output under constant-voltage operating conditions is attained by operating 10-ohm-cm cells at 0.15 V. The power output in the constant-voltage condition depends on the operating temperature and the bombardment dose. In all cases, 10-ohm-cm cells maintain considerably higher power output than do 1-ohm-cm cells, as shown in Figure 5.

For temperatures above 150°C , the 1-ohm-cm cell is preferable to the 10-ohm-cm cell. GaAs solar cells have also been proposed for operation between 150° to 200°C . Figure 6 compares the open-circuit voltage degradation with temperature for typical GaAs cells and 1-ohm-cm silicon solar cells. GaAs cells have a temperature coefficient of 2.5 mv/ $^\circ\text{C}$ as compared to 2.1 mv/ $^\circ\text{C}$ for 1-ohm-cm silicon cells. However, because of the initially higher open-circuit voltage of the GaAs cell, its open-circuit voltage at 200°C is 0.43 V as compared to 0.22 V for the silicon cell. It should be realized that the ultimate limitation in the use of cells made from high-energy-gap semiconductor materials

is the temperature at which the open-circuit voltage approaches zero. If the curve for GaAs cells is extrapolated, the voltage will fall to zero at a temperature of about 375°C . This should be contrasted with reported open-circuit voltages for GaP experimental cells of 0.4 V at 350°C .¹

Figure 7 is a plot of curve power factor for 1-ohm-cm silicon cells and for GaAs cells. In general, the curve power factor of silicon cells decreases more rapidly than that of GaAs cells, the decrease becoming more rapid at temperatures above 125°C .

The variation of maximum power output with temperature is shown in Figure 8 for both high and low efficiency GaAs cells and for 1-ohm-cm silicon cells. The half-power point occurs at about 165°C for GaAs cells as compared to 135°C for silicon cells. This is reflected in the lower degradation factor for GaAs, $0.35\%/\text{C}$, as compared to $0.45\%/\text{C}$ for silicon. However, since the silicon cell has twice the short-circuit current under citer space illumination as does the high-efficiency GaAs cell both cells have the same power output at 175°C . At 200°C there is a 2-milliwatt difference in power output. However, the power output of the 1-ohm-cm silicon cell equals that of the commercially available, lower efficiency, GaAs cell at 200°C . The choice of either silicon or GaAs cells for 200°C operation depends on the factors of reliability, availability, cost, and minimum power output requirements. Based on these considerations, the present commercial 1-ohm-cm silicon cells are not surpassed for operation at 200°C by any other type of commercial cell presently available.

Figure 9 is a plot of the product of open-circuit voltage and short-circuit current versus temperature for high efficiency GaAs cells and 1-ohm-cm silicon cells. The significance of this plot is that, if the curve power factor of the 1-ohm-cm silicon cell can be raised sufficiently at room temperature, then its power output will be greater than that of the high-efficiency GaAs cell for all temperatures up to and including 200°C . Recent information on the effects of impurities indicates that this improvement may now be possible.

Just as in the case of silicon solar cells, GaAs cells bombarded to a dose of $3.9 \times 10^{12} - 10$ Mev protons/cm² show no change in the temperature coefficient of open-circuit voltage. Curve power factor degradation increases after bombardment in a manner similar to the silicon case. A degradation coefficient of $0.12\%/\text{C}$ in the temperature range from 50° to 100°C is found for bombarded cells as compared to $0.10\%/\text{C}$ in the same temperature range for unbombarded cells.

At present, the performance of any available solar cell is marginal at 200°C . GaP is therefore being considered for use in the range above 200°C . The current status of GaP solar cells has been mentioned in a previous paper; however, it should be pointed out that, if the anticipated open-circuit voltage of 1.5V can be achieved, then operation of these cells to temperatures of 500°C would be possible. The low short-circuit currents of GaP cells would not necessarily eliminate them from consideration since these cells would be expected to operate where solar intensities are many times those in earth space.

References

1. Graves, W. C. and Epstein, Arnold S., "Single Crystal Gallium Phosphide Solar Cells." These proceedings, Section B-4.

V_{OC} VS TEMPERATURE FOR VARIOUS RESISTIVITIES

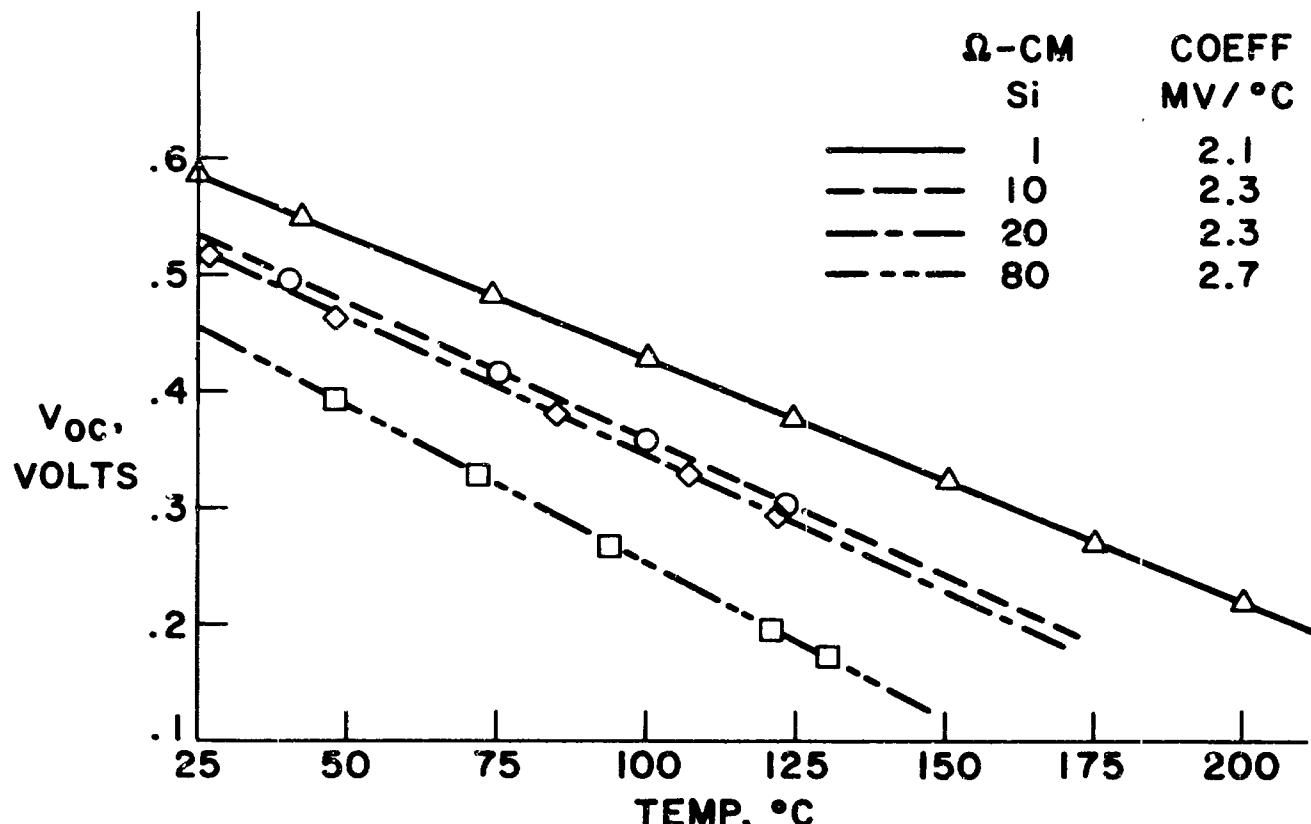


Figure 1.

CURVE POWER FACTOR VS TEMPERATURE

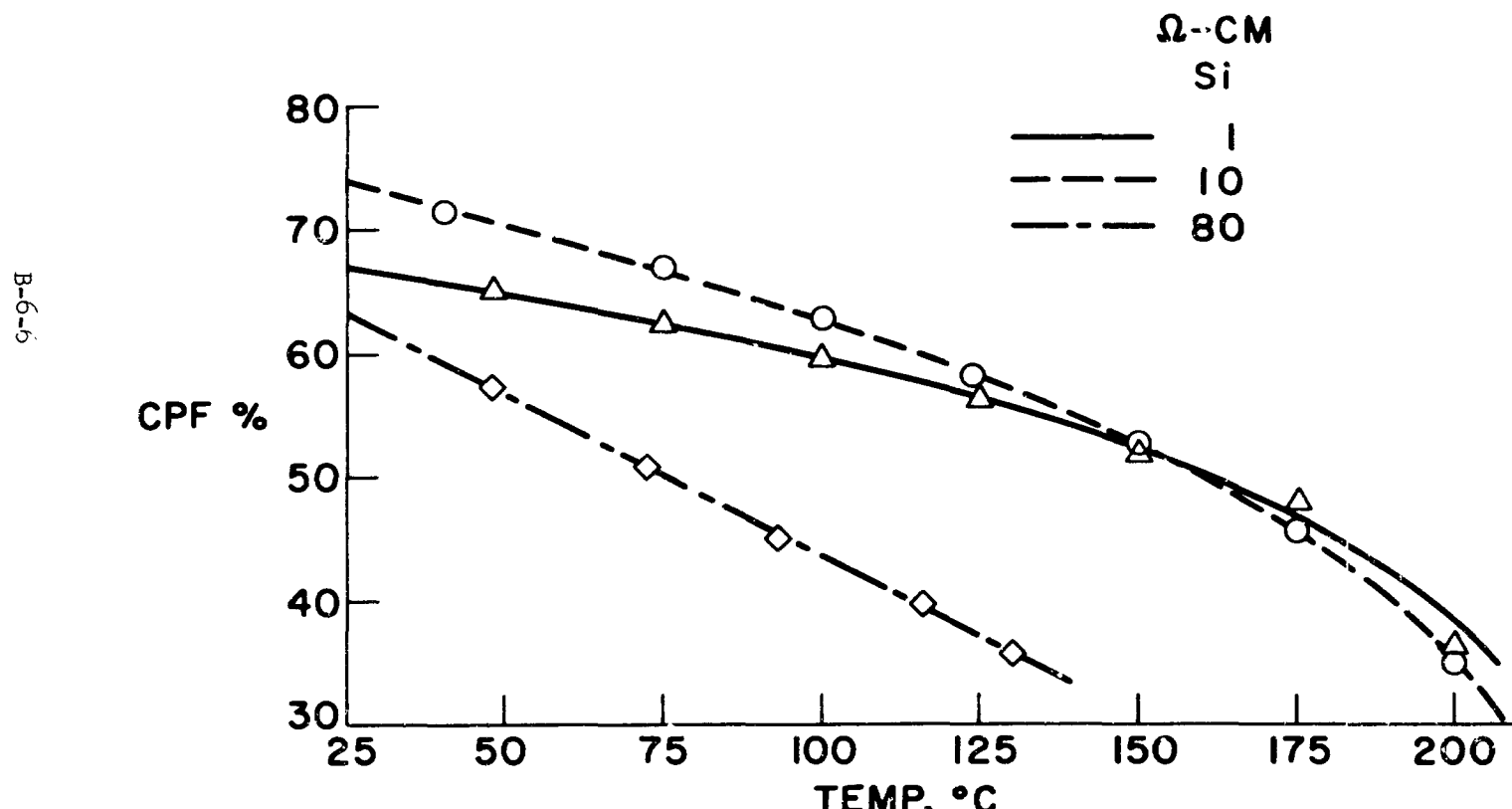


Figure 2.

MAXIMUM POWER VS TEMPERATURE

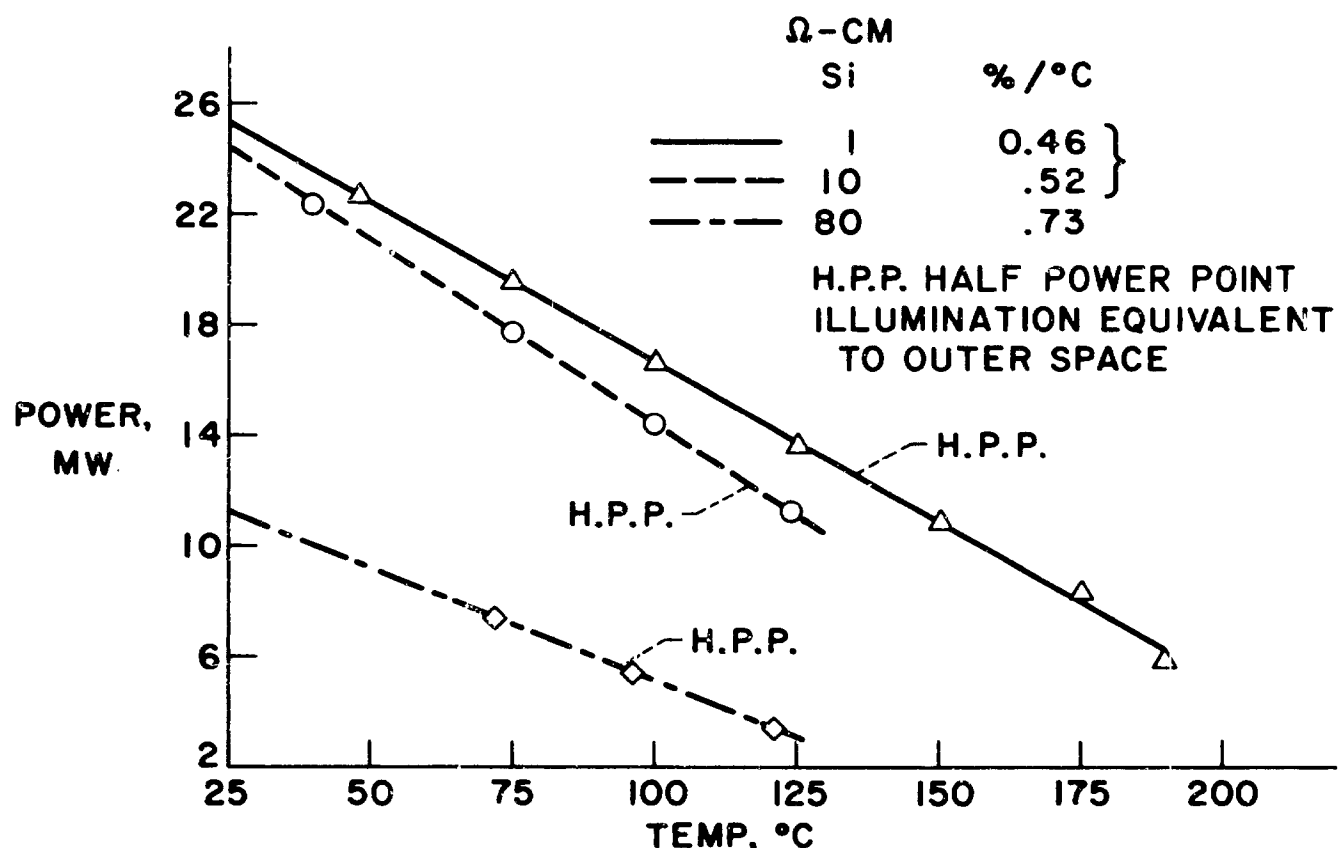


Figure 3.

CURVE POWER FACTOR VS TEMPERATURE

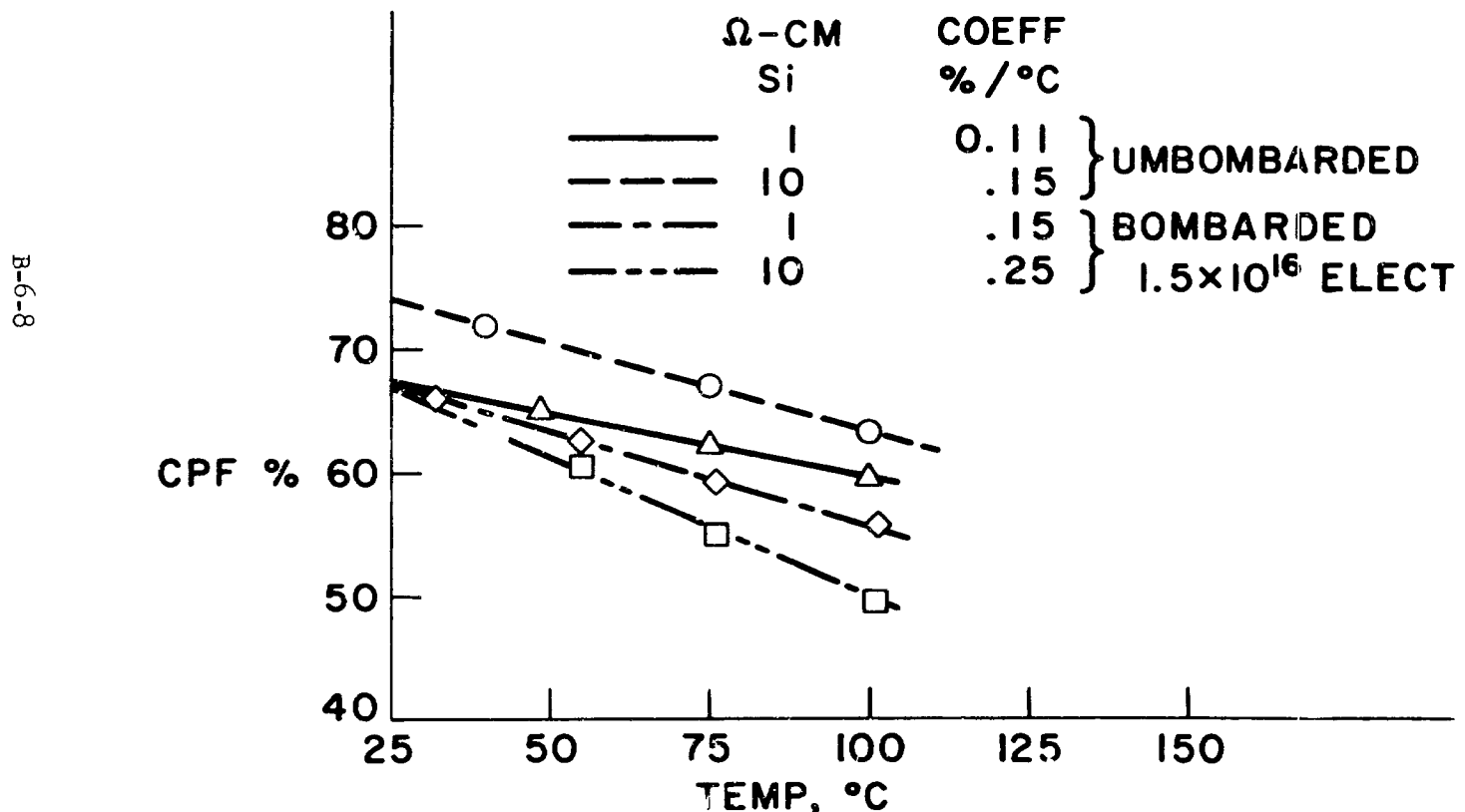


Figure 4.

B-6-9

PIC-SOL 209/5

POWER OUTPUT FOR CONSTANT VOLTAGE OPERATION VS TEMPERATURE

BOMBARDMENT LEVEL 1.5×10^{16} 1 MEV ELECTRONS

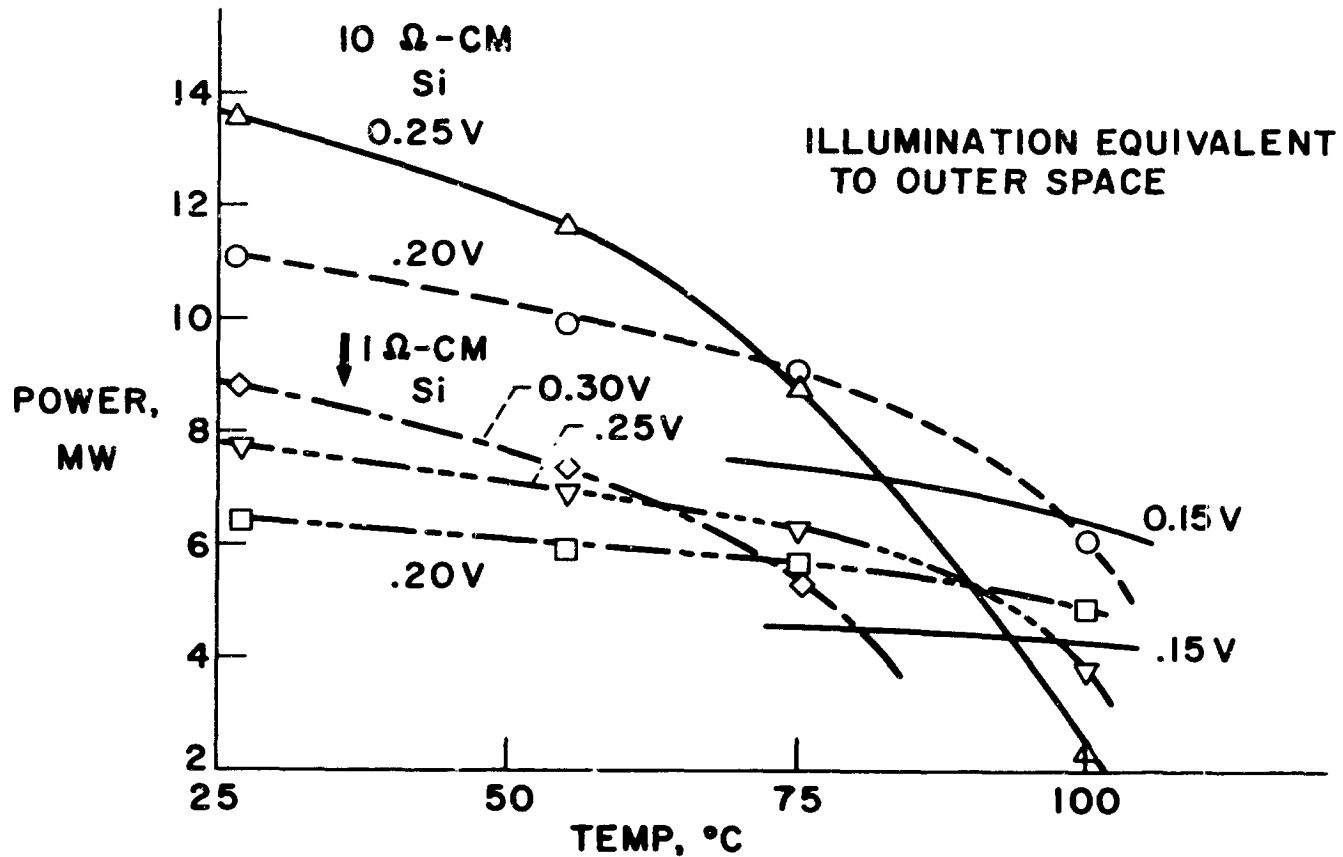


Figure 5.

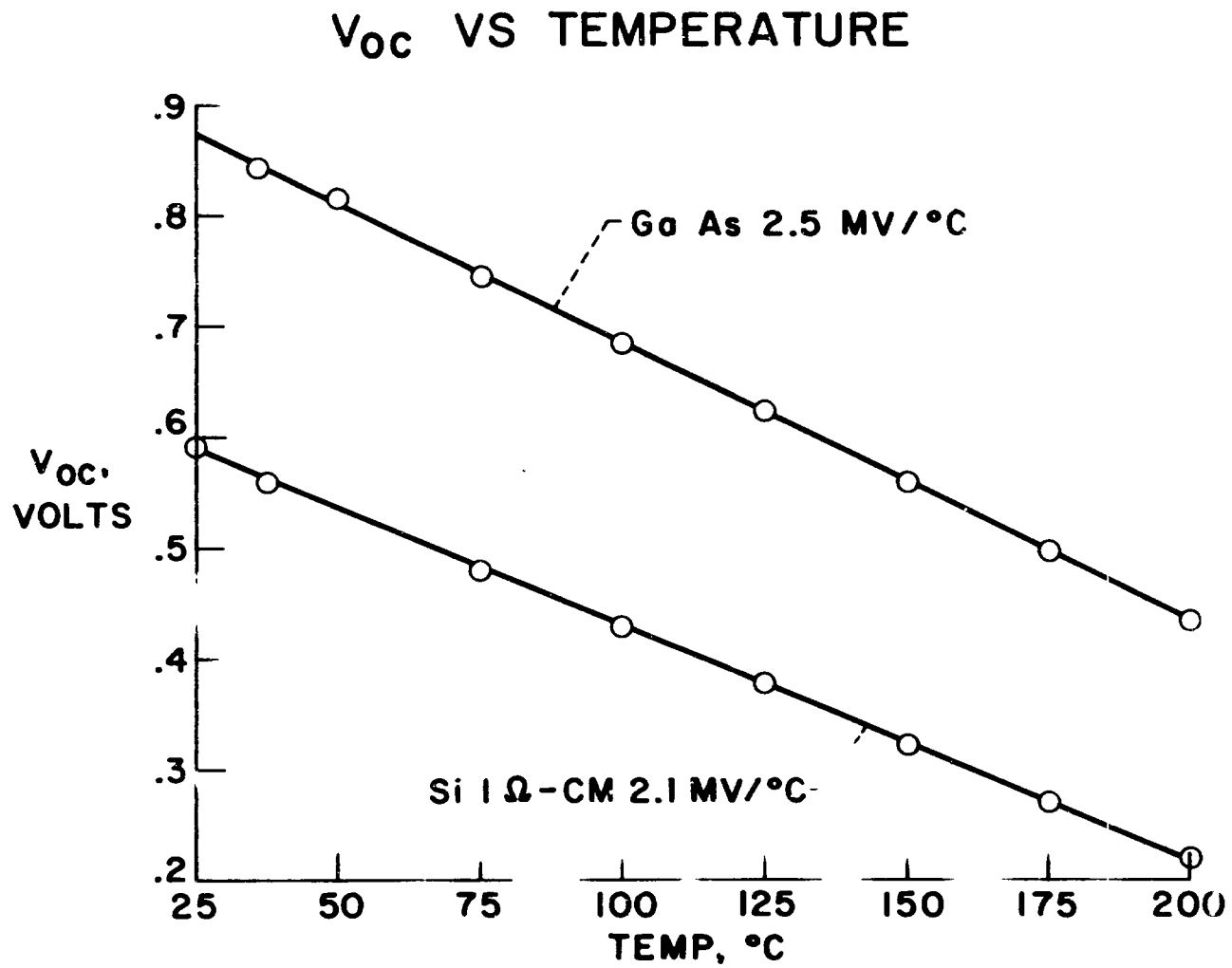


Figure 6

CURVE POWER FACTOR VS TEMPERATURE

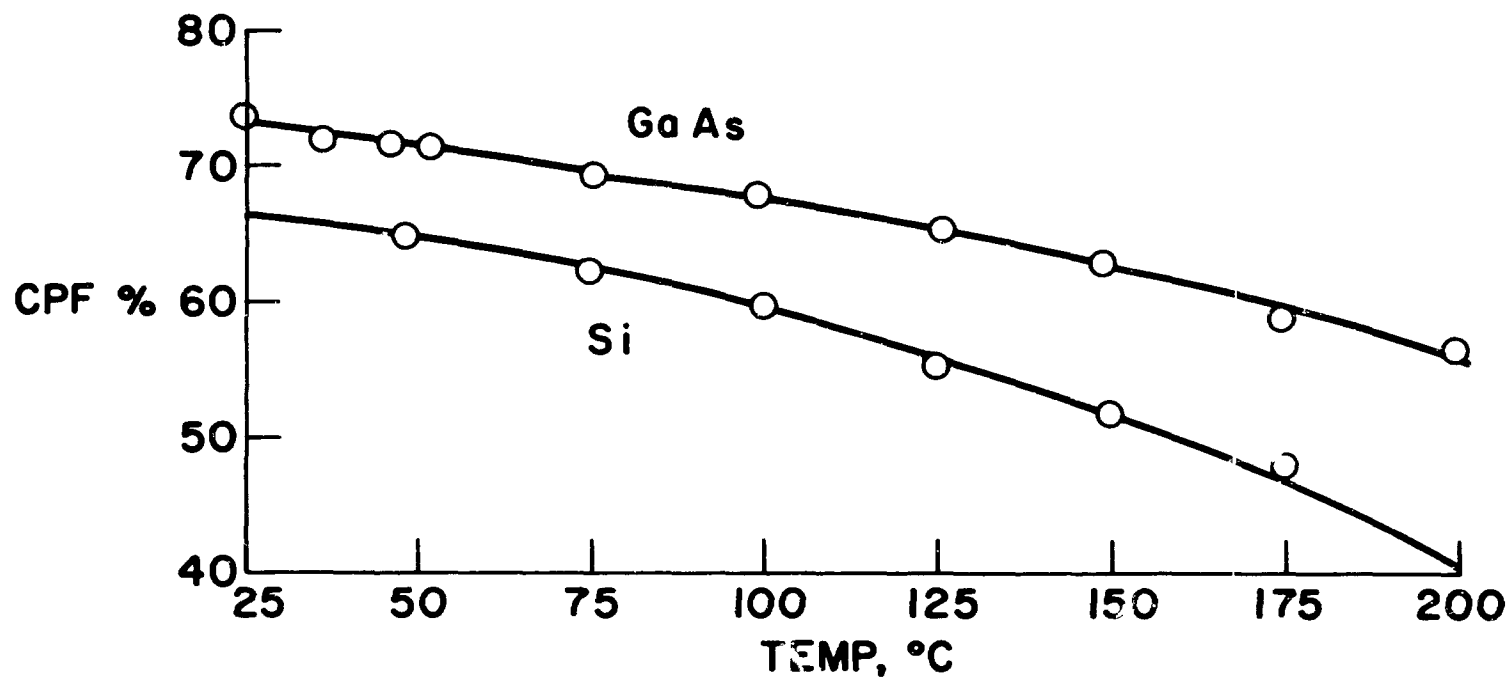


Figure 7.

B-6-112

MAXIMUM POWER VS TEMPERATURE

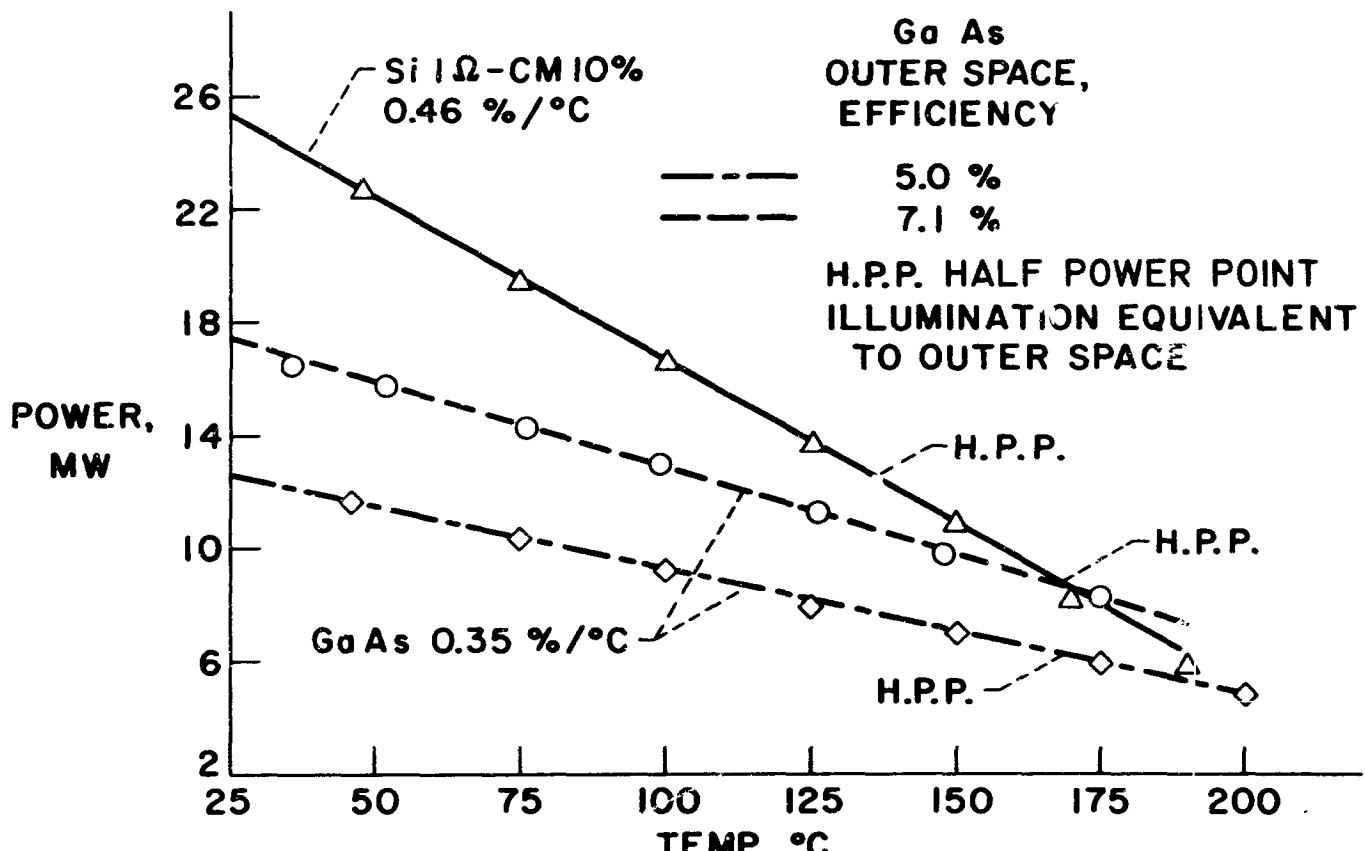


Figure 8.

$V_{oc} \times I_{sc}$ VS TEMPERATURE

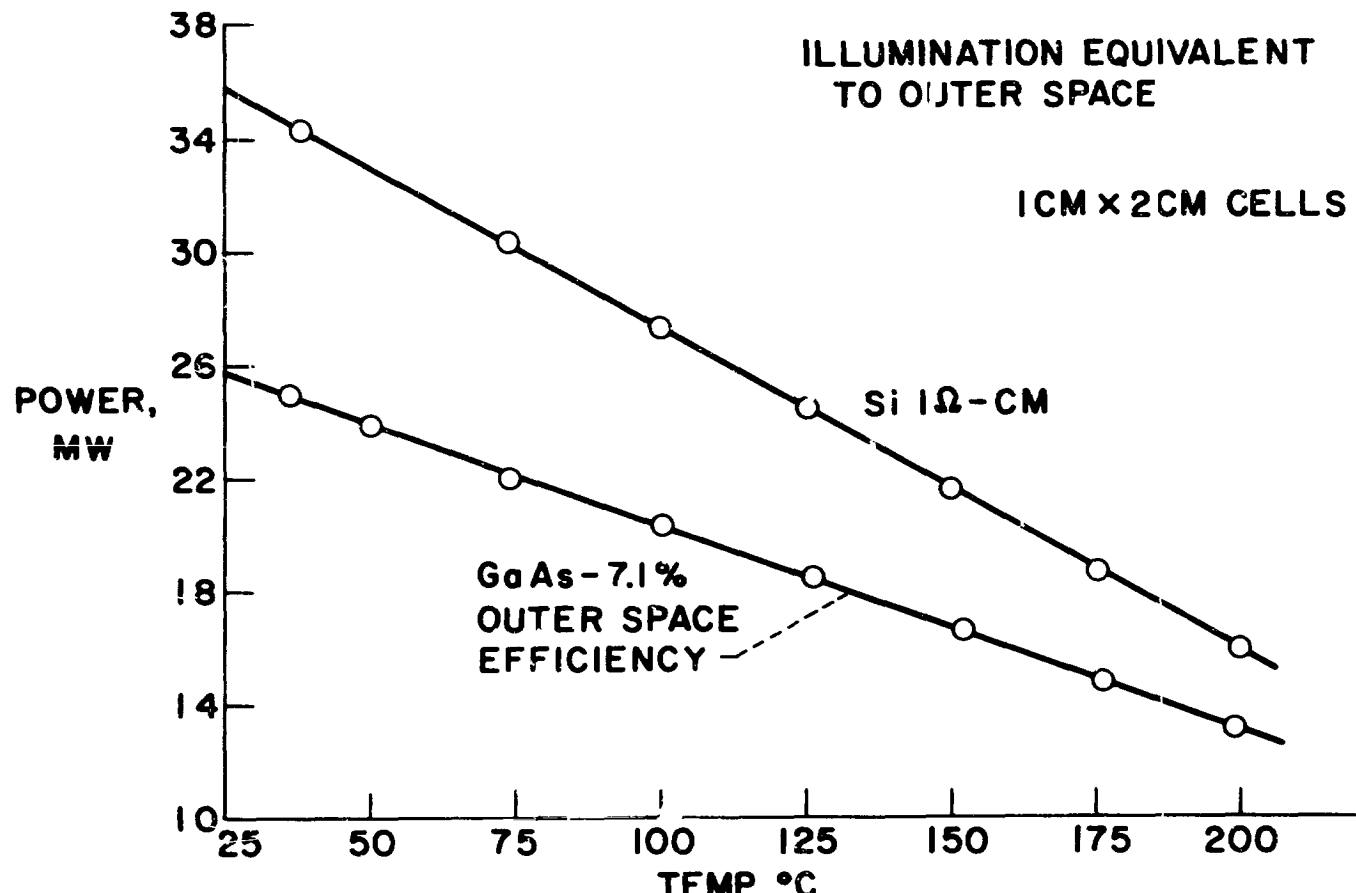


Figure 9.

DISCUSSION

JOHNSTON-NASA AMES: What sort of commercial solder did you use on your solar cell? Did many of your contacts fail at high temperatures?

MF. BRODER: We used a gold plated base for the maximum area contact. The top contact was a platinum sheathed knife edge pressed down on the top contact. The solder did not run away. The gallium arsenide had a high temperature alloy for the top contact, and we had no trouble there at all.

EFFECT OF ANTIREFLECTION COATINGS AND COVERGLASSES ON
SILICON SOLAR CELL PERFORMANCE

N64-29169

Presented by

E. L. Ralph

Heliotek, Division of Textron Electronics, Inc.

Sylmar, California

2 June 1964

99/6A

ABSTRACT

The high reflectivity of the polished silicon surface of the n-e-r N⁺/P silicon solar cells has emphasized the need for properly designed antireflection coatings to obtain improved solar cell performance.

The problem is complicated by the facts, that solar cells are generally tested in air, but are for their final application, covered with a glass or quartz slide which is adhesive-bonded to the cell surface, and further, that solar cells operating in a nuclear particle radiation environment change their spectral response and are frequently to be optimized for performance at the end of design-life.

Experiments have been performed to explore the antireflection characteristics of thin films of silicon monoxide which have been evaporated on the solar cell surface. The effect of the antireflection coating thickness on cell response as a function of wavelength has been determined and the improvement in cell short circuit current for Air Mass Zero space sunlight evaluated.

Included in this study was the evaluation of the antireflection characteristics after the application of a coverglass with adhesive over the antireflection coating. For comparison, coverglasses were also applied to bare cells with no antireflection coating present.

In all cases the various coating comparisons were evaluated based on the cell short circuit current performance in Air Mass Zero sunlight.

July 19

EFFECT OF ANTIREFLECTION COATINGS AND COVERGLASSES ON
SILICON SOLAR CELL PERFORMANCE

by

E. L. Ralph and M. Wolf

Heliotek, Division of Textron Electronics, Inc.

INTRODUCTION

This paper discusses recent investigations into the effect of antireflection coatings on the performance of N⁺/P silicon solar cells. The solar cells studied were evaporated contact type cells with a polish-etched active surface. The evaluation considered evaporated films of SiO as the material deposited on the cell surface to form an interference type antireflection coating. By varying the thickness of a single layer coating it is possible to obtain low reflection over a fairly broad range of wavelengths, and the minimum reflection point can be adjusted so that optimum solar cell performance is obtained for a space solar spectrum. If coverglasses are placed on the cell surface by means of an adhesive the cell absorption characteristics are altered and this effect was studied in an attempt to determine the optimum coatings required for typical space applications.

DISCUSSION

To improve the transmission of photons across the boundary between two materials of differing optical properties, a layer of a suitable third material may be placed at this interface to form an interference type optical coating. The material in this layer has to have the proper index of refraction and a low absorption coefficient. The proper index of refraction η_1 of the material in the interference coating is determined by the relationship:¹⁾

1) "Optical Design" Military Standardization Handbook #141, 5 Oct. 1962, page 20-22.

$$\eta_1 = \sqrt{\eta_o \eta_s} \quad (\text{Eq. 1})$$

where η_o and η_s are the indices of refraction of the materials on either side of the antireflection coating.

In the case studied, essentially pure silicon with an index of refraction of 3.4 to 4.0 in the visible range^{2) 3)} was the material on one side of the boundary, while the second material could be any one of the following: air (normally the case where cells are being tested for acceptance); vacuum (when bare cells are used in space); or the coverglass adhesive (normally the case in space applications). For both air and vacuum the index of refraction is 1.0, but for the adhesive it is typically 1.2. Therefore it is obvious that the optimum material for an antireflection coating would not be identical for the two cases above. Since coverglasses are typically used, the most desirable coating should have an index of refraction of about 1.8 to 2.2. This is a very high value compared to most materials which have the desirable properties of low absorption, high stability and high abrasion resistance. Silicon monoxide has the desirable properties listed above and has an index of refraction of 1.7 to 1.9 (depending on the evaporation process)⁴⁾ which makes it a very suitable coating material even though it may be a compromise in respect to the index of refraction.

Besides having the proper index of refraction the interference type antireflection coating must have the proper thickness. If minimum

-
- 2) "Handbook of Chemistry and Physics" 1943 Edition; Chemical Rubber Publication Co., 1961-63, page 3032.
 - 3) "Journal Optical Society of America" Vol. 47, 244.6, C. D. Salzberg and J. J. Villa.
 - 4) "Triple-Layer Antireflection Coatings on Glass for Visible and Near Infrared", J. J. Cox, et al, Optical Society of America; Vol. 52, No. 9, September 1962, page 969.

reflection is desired at a specific wavelength of light, the optical thickness of the coating must be $1/4$ wavelength, the optical thickness being equal to the physical thickness multiplied by η . Since a single layer antireflection coating typically has low reflection properties over a fairly large wavelength range it is possible to achieve a coating designed for minimum reflection at a specific wavelength (such as about 0.6 micron for space type cells) and simultaneously to obtain good antireflection properties over most of the solar cell response range.

MEASUREMENT EQUIPMENT

To properly evaluate the effects of antireflection coatings on solar cells two measurements are of primary importance. First the cell spectral response can be used to evaluate the coating effect on short circuit current performance as a function of wavelength. This measurement probably is most valuable in antireflection coating analysis since improved short circuit current is the goal of the study and spectral response is a direct measurement of the property being investigated. Second, the reflectance from the cell surface is needed to determine the amount of light being lost. Reflectivity measurements point out the amount of improvement that can potentially be made, and the change of reflectance achieved by the film, while the spectral response shows what improvements in over-all collection efficiency have been made, but do not indicate losses. Having made both of the above measurements one is able to evaluate all of the properties of the antireflection coating and determine both the decrease of reflectance and the losses in the film thus indicating the suitability of the coating design.

For this investigation the spectral response and the reflectance were measured using an electro-optical system as shown in Fig. 1. The light from a tungsten filament source was passed through a narrow band pass filter to obtain a light beam of the desired wavelength. Thirteen filters were used which cover the wavelength range of the solar cell

spectral response, (0.4 to 1.1 micron). To measure spectral response the short circuit current of the cell under test was measured relative to a standard cell thus allowing for calibration on an equal energy basis.

To measure reflectance the light beam was collimated into a small area by means of an optical system. The intensity of the light beam was measured with a solar cell detector which was larger in area than the beam. The cell to be tested was then placed into the beam and the reflected light intensity measured with the same detector by rotating the detector to various angles from the reflecting surface.

EXPERIMENTAL RESULTS

For this study 10 ohm cm N⁺/P solar cells were used. These cells were of the evaporated-sintered contact type and had a polish-etched silicon active surface. Figure 2 shows a spectral response curve (equal energy basis) of a typical bare cell with no antireflection coating, as measured in the equipment described above. Also shown is the spectral response curve of the same cell after application of a near optimum coating of an evaporated film of silicon monoxide. Both curves are relative response curves (i.e., the absolute flux density of the light source is not known), but both curves were taken at identical flux densities. Therefore a change in solar cell spectral response due to the coating gives an actual measurement of the change in the over-all collector efficiency $\gamma(\lambda)$. By taking the ratio of the short circuit current measured at each narrow wavelength band $I_{sc}(\lambda)$ (coated) to $I_{sc}(\lambda)$ (bare) and by applying this ratio and the bare cell spectral response to the Air Mass zero sunlight spectrum, the degree of improvement obtained from the antireflection coating can be evaluated for space applications.

The reflectivity as a function of wavelength for a bare and a coated cell, as measured in the equipment described above, is compared in Fig. 3.

The bare cell reflectivity was found to be essentially wavelength independent with a value of about 32%. The coated cells had a minimum reflection point, which was dependent on the coating thickness, and there the reflectivity attains values of less than 1%. This type reflection curve with the broad range of decreased reflection is typical of single layer anti-reflection coatings and is highly desirable for a broad response device such as the solar cell.

In order to determine the optimum thickness for SiO antireflection coatings a series of cells were made with various coating thicknesses. The short circuit current improvement and reflection losses were measured and are shown in Fig. 4. It can be seen that substantial changes in the antireflection properties of the films were obtained with a slight change in coating thickness. As the film thickness increased the wavelength of the peak current ratio and of the minimum reflection value simultaneously shifted toward longer wavelengths. This data indicated that for a specific light source such as Air Mass Zero sunlight there would be an optimum coating thickness which would give maximum current output. To determine this optimum thickness a numerical integration of the product of spectral response times the Air Mass Zero sunlight energy spectrum was performed. Column 4 of Table I shows the detail and result of this process for the bare cell. Columns 5 through 11 are obtained by multiplying the products of Column 4 for each wavelength interval with the current ratios shown in Fig. 4 (for the various coatings). The relative Air Mass Zero sunlight short circuit currents corresponding to a bare cell and to the various SiO coating thicknesses are shown as summations at the bottom of the Table. Also shown is the coated to uncoated I_{sc} ratio which indicates the improvement in Air Mass Zero sunlight that was obtained. The maximum improvement obtained was 28%, however all of the four thinnest coatings had an improvement of 26% or greater. Therefore any of these coatings would be suitable for space applications assuming the coating terminates in air or vacuum and no other materials were placed at the surface.

Since most solar cell applications require glass coverslips to be applied to the cell surface by means of an adhesive, the above analysis was studied further in respect to this modification. A curve showing the effect of coverglasses on coated and bare cells is shown in Fig. 5. The short circuit current ratio was measured and the coverglass on the coated cell caused an improvement in response in the long wavelength region and a decrease in response at the maximum improvement wavelengths. Since the coverglasses had a 0.410 micron cutoff filter applied there was a substantial drop-off at this wavelength. The effect of applying a coverglass to the bare cell was a relatively uniform improvement of about 13%. This was substantially below the values obtained when coverglasses were applied to SiO coated cells irrespective of the variations in coatings that were studied. Three different SiO coating thicknesses (in addition to the bare cell) were analyzed with and without a cover-glass applied and the integrated $m = 0$ short circuit current values obtained from this experiment along with the first experiment are summarized in Table II. In each case the SiO coated cells decreased slightly after coverglass application, however only the thicker light blue cells (which did not have the optimum design coating) showed more than a 1% decrease. Therefore it appears that the optimum coatings for cells terminating in air or vacuum are only slightly affected by applying coverglasses and a single SiO coating thickness design is satisfactory for space applications with or without coverglasses applied.

CONCLUSIONS

It has been shown that the optical characteristics of evaporated silicon monoxide antireflection coatings on solar cells are highly dependent on the film thickness. By proper design, these coatings can be optimized for maximum solar cell performance in space sunlight applications. Although silicon monoxide coatings are satisfactory and make a substantial improvement in solar cell performance, it should be possible with the proper selection and matching of the index of refraction to obtain

a coating material with decreased losses (i.e., minimum reflection and absorption).

The effect of applying coverglasses with an adhesive to the cell surface was found to be significant at certain wavelengths, however the overall effect on solar cell performance was small and a suitable coating thickness design was obtainable which gave good antireflection properties with or without coverglass applied. It was determined that the use of coverglasses without any antireflection coating present did not give satisfactory cell performance.

ACKNOWLEDGEMENTS

The authors wish to thank Mr. Werner von der Ohe and Mr. D. Irvine for their help in preparing the cells and obtaining data for this study.

TABLE I

Effect of Antireflection Coating Thickness

on N⁺/P Solar Cell Short Circuit Current in Space Sunlight

1 Wavelength Interval Center Point Micron	2 Sunlight m = 0 Energy in 10^{-2} W/cm^2	3 Relative Spectral Response Bare Cell	4 Product (2) (3) Bare Cell Current	5 Pale Blue Coating	6 Light Blue Coating	7 Dark Blue Coating	8 Dark Purple Coating	9 Purple- Red Coating	10 Red- Yellow Coating	11 Yellow- Green Coating
.40	.808	.243	.196	.15	.17	.19	.22	.24	.25	.28
.45	1.035	.337	.349	.31	.36	.38	.44	.47	.48	.51
.50	.998	.420	.419	.41	.48	.50	.56	.59	.59	.59
.55	.965	.499	.482	.52	.60	.61	.66	.67	.67	.67
.60	.903	.575	.519	.59	.67	.67	.71	.72	.71	.70
.65	.812	.641	.520	.61	.69	.68	.70	.69	.69	.68
.70	.721	.702	.506	.62	.67	.65	.66	.60	.65	.64
.75	.647	.760	.492	.61	.64	.63	.63	.62	.62	.61
.80	.563	.797	.449	.56	.58	.57	.57	.56	.55	.54
.85	.502	.796	.400	.50	.51	.50	.49	.49	.43	.47
.90	.448	.752	.337	.41	.42	.42	.41	.41	.40	.39
.95	.402	.588	.236	.29	.29	.28	.28	.28	.28	.27
1.00	.363	.398	.144	.17	.17	.17	.17	.17	.17	.16
1.05	.333	.205	.068	.08	.08	.08	.08	.08	.08	.07
Relative m = 0 Current = Σ = 5.214				5.83	6.33	6.33	6.58	6.65	6.62	6.58
Ratio $\frac{I_{sc} (\text{Coated})}{I_{sc} (\text{Bare})}$ = 1.000				1.12	1.22	1.22	1.26	1.23	1.27	1.26

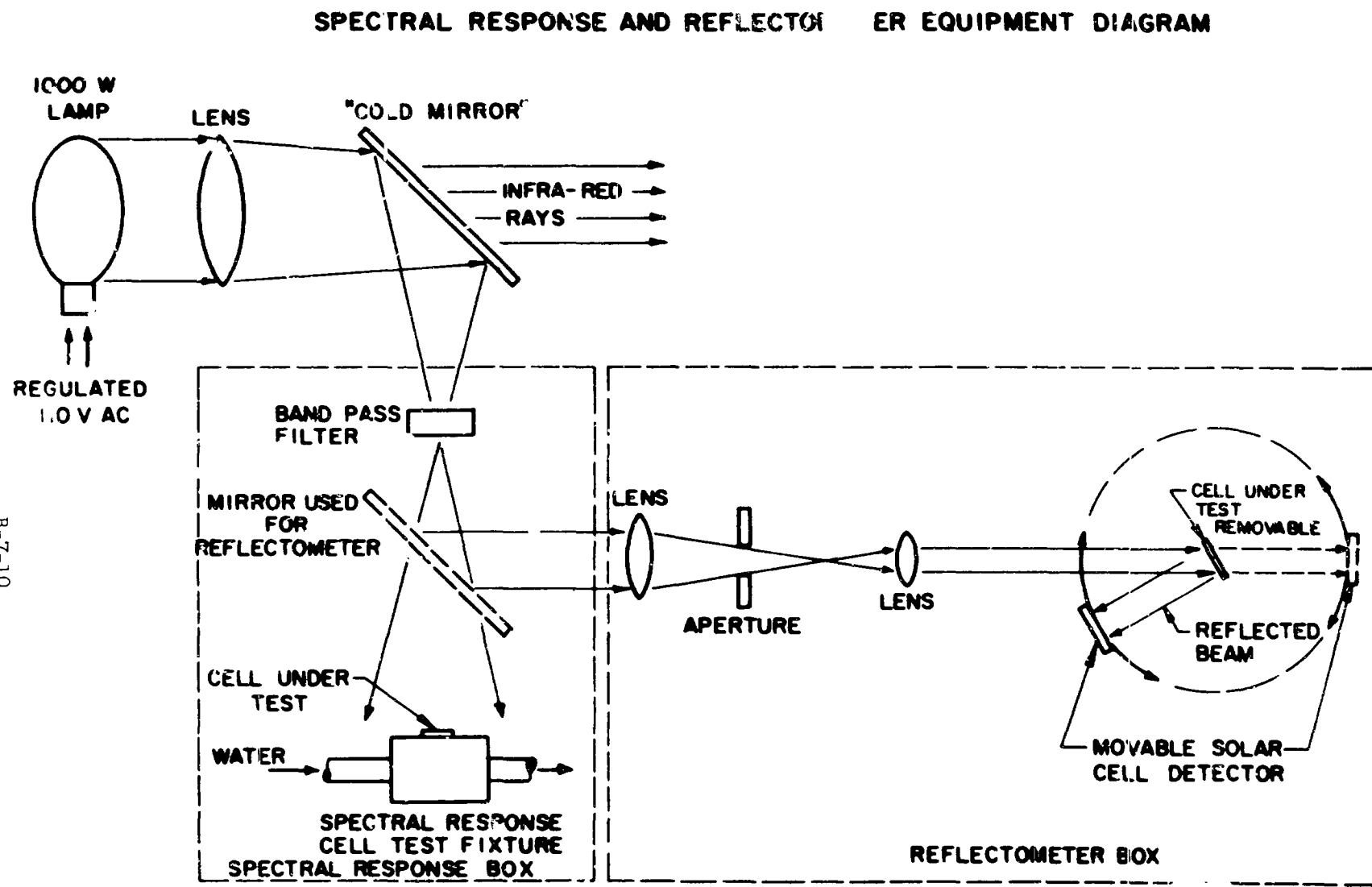
SUMMARY-TABLE II
Effect of Antireflection Coatings and Coverglasses

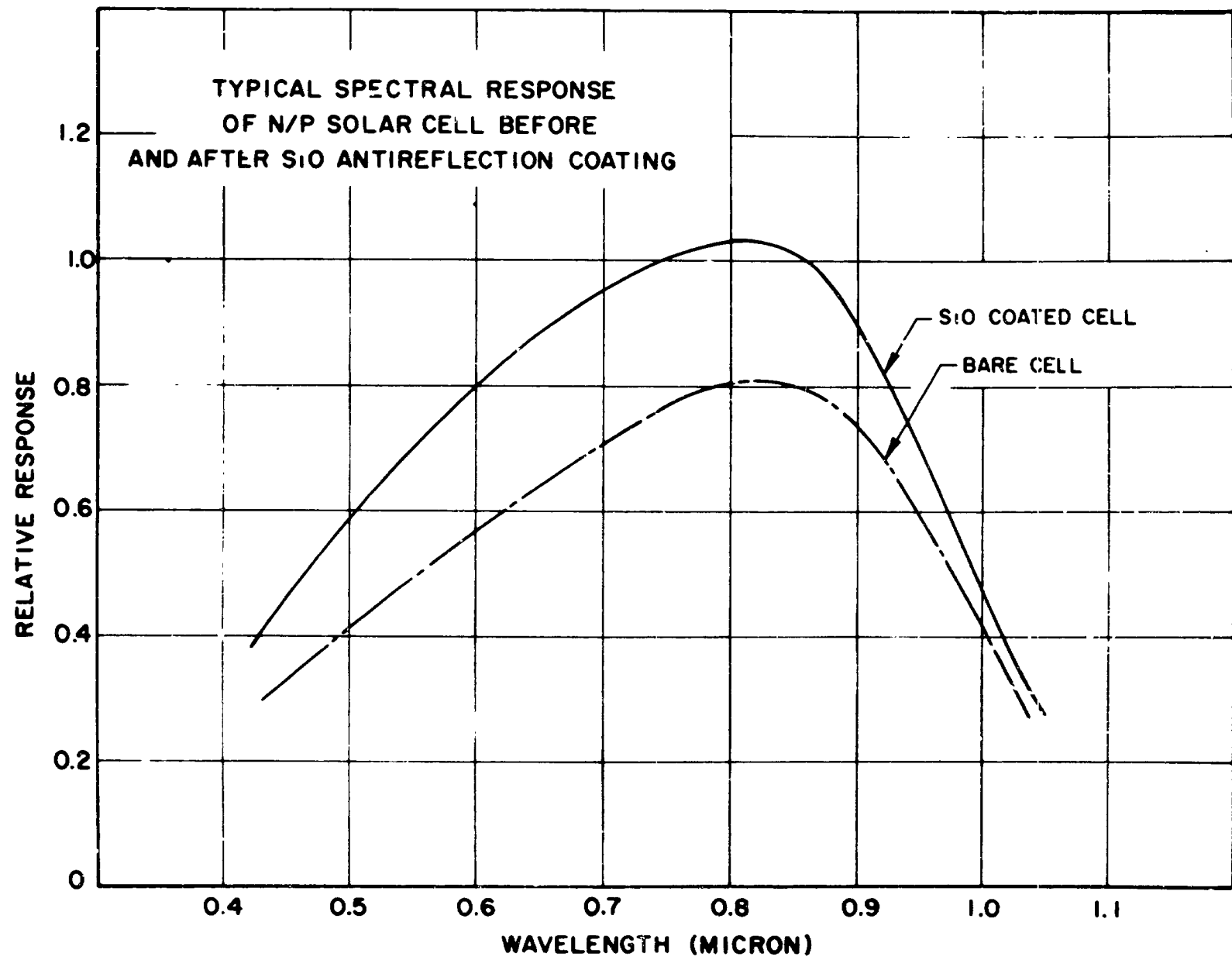
on N⁺/P Solar Cell m = C Current Ratio $\frac{I_{sc} \text{ (Coated)}}{I_{sc} \text{ (Bare)}}$

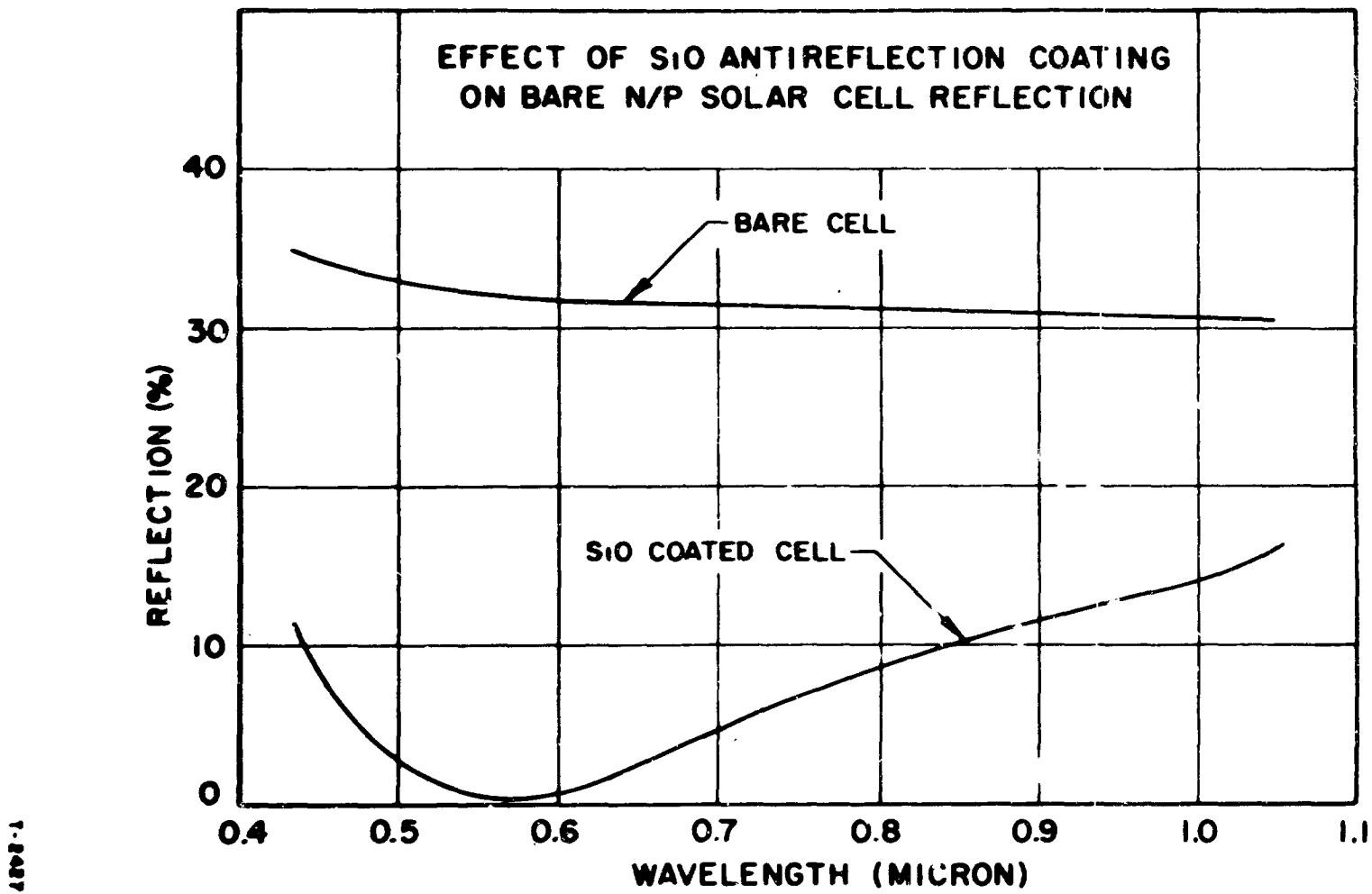
Antireflection Coating Color	First Experiment $I_{sc}(C)/I_{sc}(B)$ SiO Coated Only	Second Experiment $I_{sc}(C)/I_{sc}(B)$	
		SiO Coated Only	After Coverglass Applied
Bare	1.00	1.00	1.13
1. Pale Blue	1.12	--	--
2. Light Blue	1.22	1.25	1.22
3. Dark Blue	1.22	--	--
4. Dark Purple	1.26	1.26	1.25
5. Purple-red	1.28	--	--
6. Red-yellow	1.27	1.24	1.23
7. Yellow-green	1.26	--	--

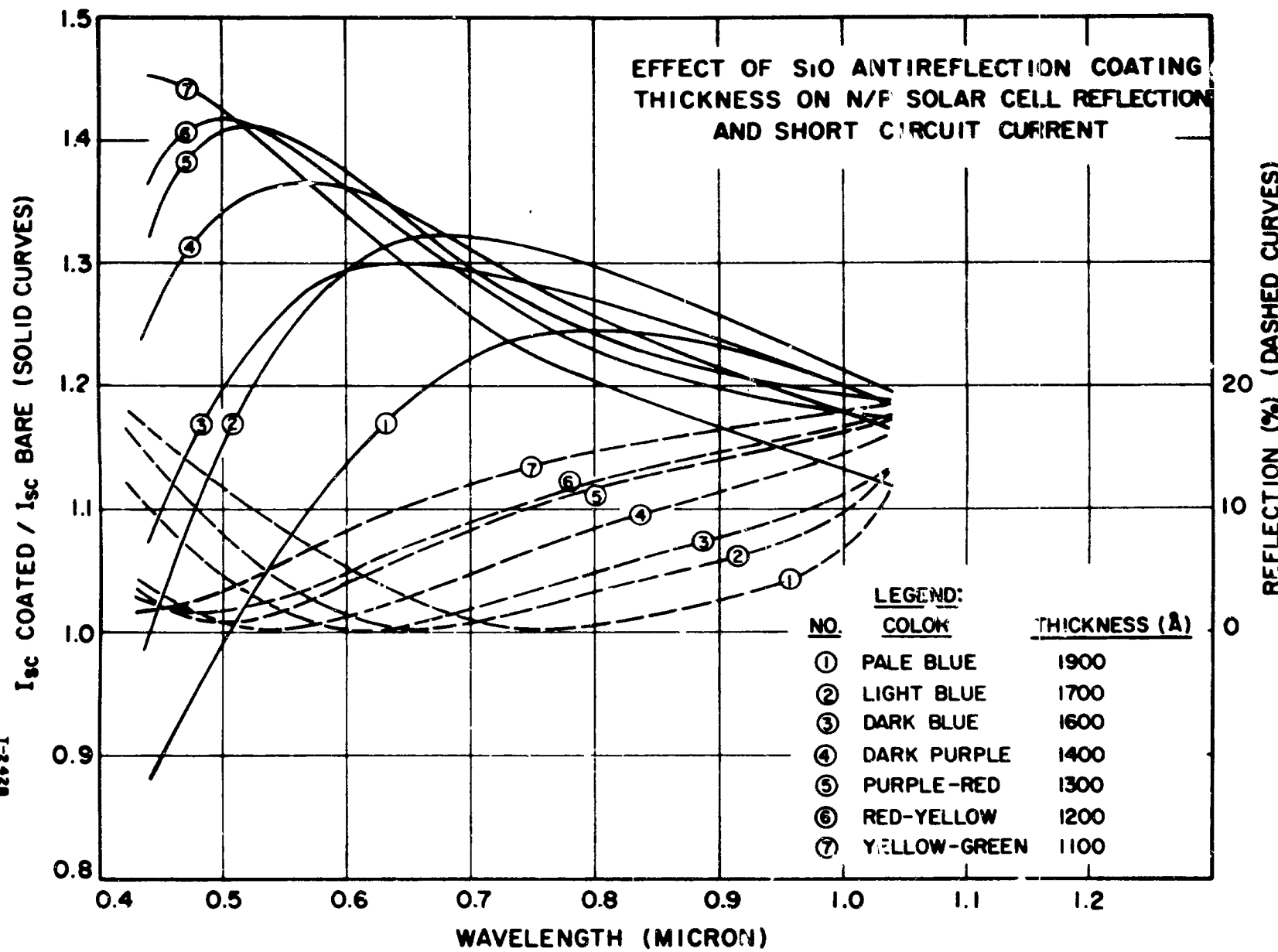
B-7-9

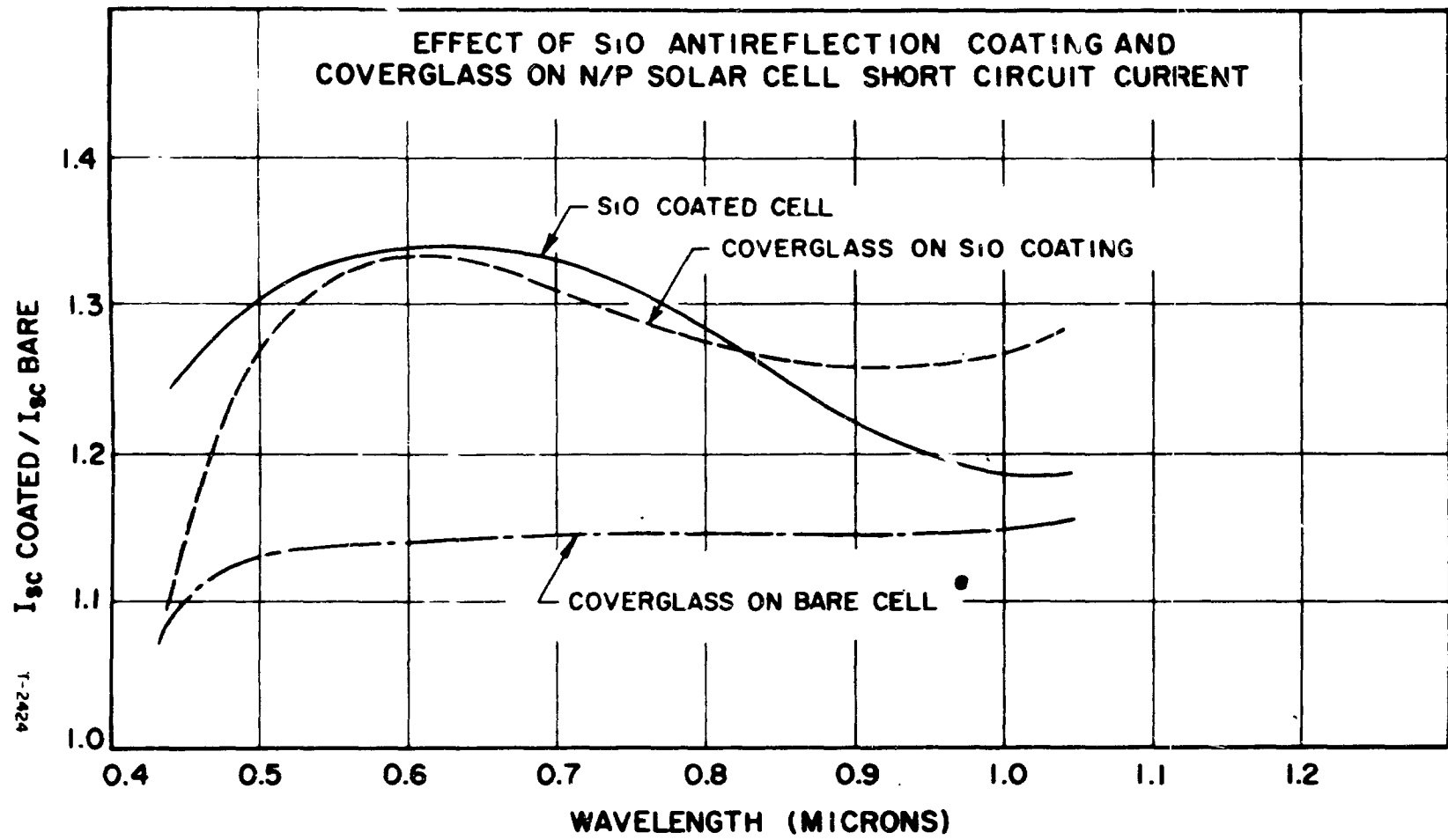
Figure 1











3-7-14

FIG. 5

DISCUSSION

LOFERSKI - BROWN UNIVERSITY: I hope that it's not true that super blue coatings are really purple or yellow green. (LAUGHTER)

AMES - NASA, LANGLEY: Were your slides microsheet Corning 0211?

MR. RALPH: Yes.

AMES - NASA, LANGLEY: A second question. I noticed that you got about 13% increase when you covered a bare cell with the slide. Is that correct?

MR. RALPH: Yes.

AMES - NASA, LANGLEY: Do you have an explanation for this?

MR. RALPH: Why, yes. There is an adhesive that holds the cover glass down, so that there is an adhesive layer on the silicon. This layer has a refractive index of about 1.2, which is not the optimum index for an anti-reflection coating, but it is better than nothing. As a result of the reduction in reflectivity, the output increases.

CUSANO - GE: You are putting material on the surfaces to make them anti-reflecting. Does this have any effect on the surface recombination velocity? Do you see any decrease in collection efficiency?

MR. RALPH: No, you definitely see an increase. Any effects of surface recombination would have been overwhelmed by the increased numbers of photons penetrating into the silicon.

CUSANO - GE: The performance of the cells at maximum absorption conditions is dependent on surface recombination velocity.

MR. RALPH: Yes, but you always have an oxide layer on the surface anyway and you are just putting the anti-reflection layer on top of it. I don't think there would be any effect.

WERTH - GENERAL MOTORS: We put some anti-reflection coatings on germanium and we found an increase in the short-circuit current from about 3.2 amps per cell to about 4.8 amps per cell. This is quite appreciable, but of course the index of refraction of germanium is 4 which is somewhat higher than for silicon at 3.4. You would expect more improvement for silicon than for germanium.

2-ii-70
N64-2917D

DESIGN OF OPTICALLY REFLECTIVE ELECTRODES
FOR GERMANIUM CELLS

Presented by

John Werth

General Motors Corporation

Santa Barbara, California

2 June 1964

**Design of Optically Reflective Electrodes
for Germanium Cells**

John Werth
General Motors Corporation

Germanium photovoltaic cells powered from a 1400°C gray body at 400°C (figure 1) have a potential efficiency (i.e., output/radiant energy absorbed) of 20 to 25%.⁽¹⁾ In order to achieve this level of efficiency, however, a relatively transparent cell backed by an optically reflective electrode must be fabricated. Such a cell acts, in effect, as a second surface mirror for radiation beyond the energy gap of the cell. (figure 2) More than two-thirds of the radiation from a 1400°C gray body lies in this spectral region, hence the importance of reflecting as much of it back to the heat source as possible. In addition, the effective depth of a reflective cell is twice its actual thickness, hence more useful radiation can be absorbed and converted.

To be effective, the back electrode must be designed to meet three criteria: flatness, high total reflectivity, and ohmicity. It must be flat to within a fraction of a degree, for otherwise the light would not return to the source due to the high refractive index of germanium. Its reflectivity must approach the theoretical maximum, given by the equation

$$R = \frac{k^2 + (n_1 - n_2)^2}{k^2 + (n_1 + n_2)^2} \quad (2)$$

where k is the absorption coefficient of the metal electrode and n_1 and n_2 are the indices of refraction of the metal and the germanium.

(1) J. Werth, Proc. 17th Annual Power Sources Conf., pp. 25-26

(2) Concepts of Classical Optics, J. Strong, p. 72

For germanium and gold, theory predicts a maximum reflectivity of 95%. Finally, the electrode must provide good ohmic contact with the germanium. There should not exist a barrier in the direction of cell current flow capable of causing a voltage drop of more than a few percent of open-circuit voltage.

Gold electrodes on 0.1 ohm-cm n-type germanium were fabricated, and measured with respect to the three criteria. The germanium was first electropolished. The electrode was then vacuum-deposited after the germanium surface had been degreased and cleaned with dilute nitric acid. No glow discharge was used; the vacuum was of the order of 10^{-8} millimeters of mercury. A gold leaf was vaporized from a tungsten filament at approximately 2000°C ; the gold condensed on the germanium surface which was being held in the evacuated enclosure at low temperature, facing the tungsten filament.

The resulting samples were then measured for flatness, reflectivity, and ohmicity. Flatness and reflectivity were measured by means of a specially designed goniometer capable of distinguishing between purely specular reflection, angularly displaced specular reflection, and scattered radiation. The measured specular component of reflectivity was $92.7\% \pm 0.5\%$ in the 2 to 10 micron region, showing that the first two criteria could be met - at least for cells with the junction at the front surface and an electropolish at the back surface. Ohmicity was then measured as follows.

Contact was made between a $.03 \text{ cm}^2$ probe and the germanium front surface by means of a gallium-indium eutectic. The gold-coated back surface was placed on a large, flexible copper electrode. The effective resistivity was determined by subtracting from the measured external resistance the measured resistance of the germanium slab (the resistance of the probe contacts was found to be negligible). The results

showed that, for current densities of up to 4 amps/cm^2 in the normal direction of current flow, i.e., from the gold electrode into the n-region, the contact resistance did not exceed 0.001 ohm-cm^2 , and may actually have been smaller. The resulting voltage drop of 4 millivolts or less is only about 1.2% of the open-circuit voltage, and represents a reasonable and acceptable loss.

Before the complete feasibility of a satisfactory reflecting back electrode can be established, the same measurements will have to be repeated for back surfaces that have been etched after electropolishing, since an untreated back surface may give rise to excessive surface recombination. Alternatively, the electrical performance of an unetched, electropolished, electrode-connected back surface would have to be verified.

Also, it would be interesting to repeat the fabrication and measurement steps for germanium slabs with reflecting electrodes next to, instead of opposite, the junction, since there are advantages to cells with the junction at the back surface.

From the measurements made so far, an ohmic electrode of high specular reflectivity can be deposited on an electropolished slab of n-type germanium by conventional vacuum-deposition techniques.

FIGURE 1

THERMO-PHOTOVOLTAIC CONVERTER (CYLINDRICAL CONFIGURATION)

B-8-14

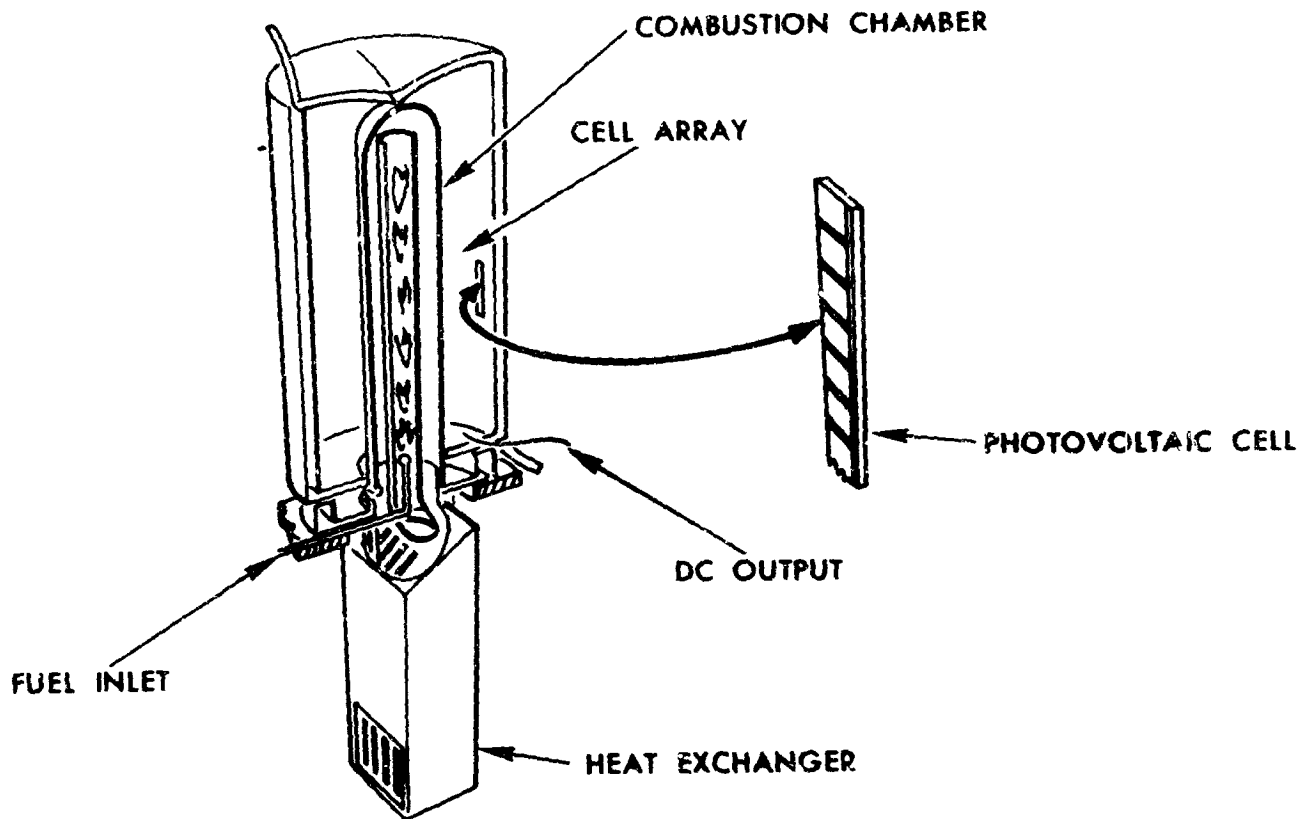
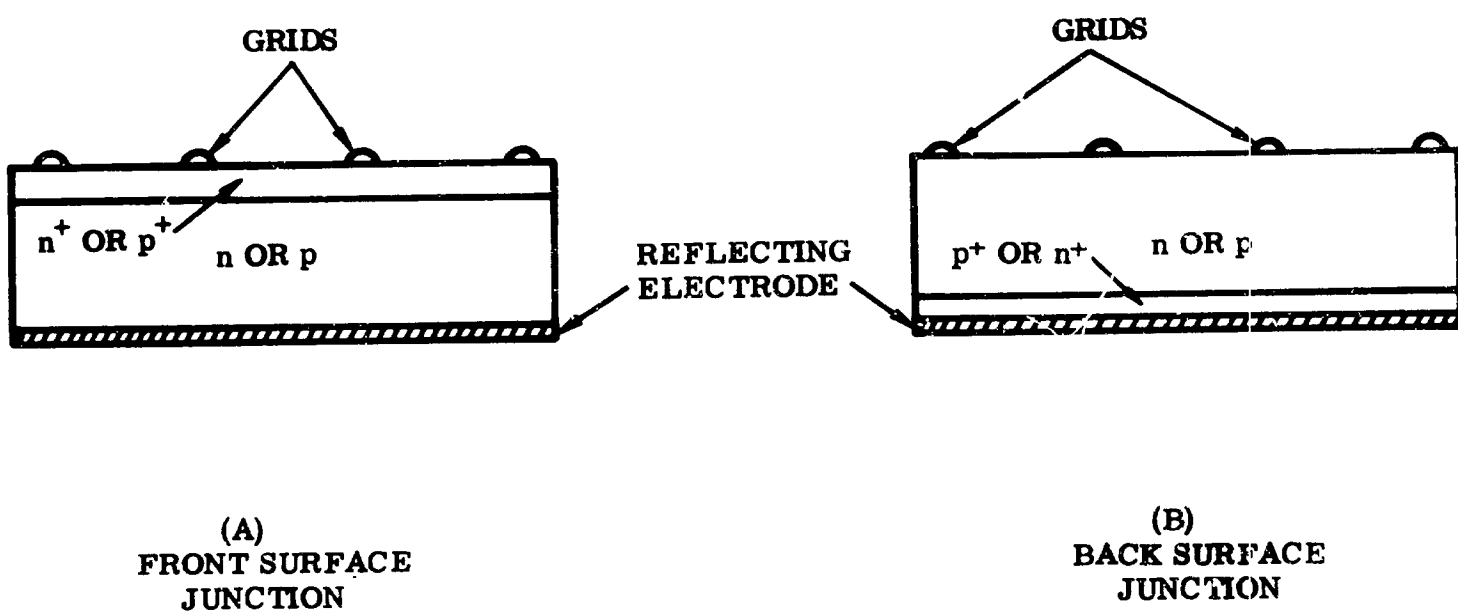


FIGURE 2
MIRROR CELL



Page intentionally left blank

DISCUSSION

LOFERSKI-BROWN UNIVERSITY: You said that the efficiency was about 24%. Is the overall efficiency for the device you are talking about?

MR. WERTH: No, this is not the overall efficiency of the device. This is the potential efficiency of the cell. It is the ratio of electrical power out of the cell to energy absorbed into the cell. It does not take into account the efficiency of the burner, and it does not take into account the amount of power required to keep the cell cool.

LOFERSKI-BROWN UNIVERSITY: What is the overall efficiency?

MR. WERTH: The overall systems efficiency would depend on the size of the device. For a large device, it could approach 15 to 18%. For a small device, a 1 kilowatt or less, it would be less than 10%.

ROSS-HOFFMAN ELECTRONICS: I wonder if the layer that you placed next to the reflecting electrode, namely the side with the diffused in impurity layer, does not degrade your lifetime below the advantage you have gained from the low resistance contact.

MR. WERTH: It may very well be that the optical characteristics of an electrode with an alloyed or diffused junction may not be as good as with a straight slab of germanium.